NUREG/CP–0056
SAND84–1514
R1,RD,RM
Printed August 1984

Proceedings of the Second Workshop on Containment Integrity

Toni Molina and Ruby Cochrell, Editors

Prepared by
Sandia National Laboratories
Albuquerque, New Mexico 87185 and Livermore, California 94550
for the United States Department of Energy
under Contract DE-AC04-76DP00789

Prepared for
U. S. NUCLEAR REGULATORY COMMISSION

Available from

GPO Sales Program
Division of Technical Information and Document Control
U.S. Nuclear Regulatory Commission
Washington, D.C. 20555

and

National Technical Information Service
Springfield, Virginia 22161

NUREG/CP-0056
SAND84-1514
R1,RD,RM

PROCEEDINGS OF THE SECOND WORKSHOP ON CONTAINMENT INTEGRITY

Toni Molina and Ruby Cochrell, Editors

August 1984

Sandia National Laboratories
Albuquerque, NM 87185
Operated by
Sandia Corporation
for the
U.S. Department of Energy

Prepared for
Division of Engineering Technology
Office of Nuclear Regulatory Research
U.S. Nuclear Regulatory Commission
Washington, DC 20555
Under Memorandum of Understanding DOE 40-550-75
NRC FIN No. A1249

PREFACE

The Second Workshop on Containment Integrity was held in Crystal City, Virginia on June 13-15, 1984. The workshop provided a forum for exchanging information on the integrity of containments at nuclear power plants. The behavior of containments during severe accidents was of primary interest to the over 130 participants. Forty-three oral presentations were made at the workshop. Written contributions that correspond to each of the presentations make up the body of this report.

The workshop was hosted by Sandia National Laboratories under the sponsorship of the U. S. Nuclear Regulatory Commission. Principal organizers for the workshop were T. E. Blejwas and W. A. von Riesemann of Sandia, T. D. Molina of Technadyne, and J. F. Costello of the U. S. Nuclear Regulatory Commission.

The questions and answers following each presentation and the open discussion periods were tape recorded. The organizers originally planned to include the transcription of the recordings with these proceedings. However, because of the quality of the recordings and transcriptions, severe editing of the very large volume of transcriptions would have been necessary and significant omissions would have been present. Therefore, the transcriptions are not included. We apologize for any inconvenience or disappointment this may cause.

CONTENTS

CONTENTS (Continued)

CONTENTS (Continued)

SECOND WORKSHOP ON CONTAINMENT INTEGRITY

Hyatt Regency Crystal City
Arlington, Va.

June 13-15, 1984

Hosted by: Sandia National Laboratories

Sponsored by: U. S. Nuclear Regulatory Commission

General Chairman: Thomas E. Blejwas, Sandia National Laboratories
Scientific Chairmen: James F. Costello, U. S. Nuclear Regulatory Commission
Walter A. von Riesemann, Sandia National Laboratories
Conference Coordinator: Toni D. Molina, Sandia National Laboratories

PROGRAM SCHEDULE

Tuesday, June 12

6:30 – 8:00 p.m. Registration

Wednesday, June 13

7:30 – 8:30 a.m. Registration

8:30 – 8:50 a.m. Opening of the Workshop

8:50 – 11:00 a.m. SESSION A
OPERATIONAL EXPERIENCE AND ITS RELATIONSHIP TO CONTAINMENT PERFORMANCE DURING ACCIDENT CONDITIONS

Chairmen: Y. S. Huang – U. S. Nuclear Regulatory Commission
T. E. Renton – Quadrex

"The PWR Integrated Leak Rate Test, A Review Of Experiences And Results"
P. M. Keogh – Ove Arup & Partners, United Kingdom

"Reliability Analysis Of Containment Isolation Systems Project"
P. J. Pelto – Pacific Northwest Laboratory

"Shortened Duration ILRT's Versus ILRT Failure Detection"
T. E. Renton, C. L. Larsen – Quadrex Corporation

"On-Power Containment Integrity Monitoring In CANDU Multi-Unit Stations"
G. D. Zakaib – Ontario Hydro, Canada

"Determination Of As Found Containment Integrated Leakage Rate"
R. E. Shirk, R. M. Carey – Gilbert/Commonwealth

"Containment Integrity And Leakage Evaluation"
E. C. Tarnuzzer – Yankee Atomic Electric Company

11:00 – 11:30 a.m. Discussion

11:30 – 12:50 p.m. Lunch

12:50 – 2:20 p.m. SESSION B
CONTAINMENT ENVIRONMENT AND LOADING CONDITIONS DURING SEVERE ACCIDENTS

Chairmen: J. Rosenthal – U. S. Nuclear Regulatory Commission
S. Hodge – Oak Ridge National Laboratory

"Impact Of The HDR Tests On The Modeling Of Containment Loads"
K. Almenas, K. Scholl, L. Valencia – University of Maryland

"CONTAIN Calculations Of Containment Loading Of Dry PWR's"
K. D. Bergeron, D. C. Williams, T. Zimmerman – Sandia National Laboratories

"Combustion Induced Containment Loads In Large-Dry PWR's"
F. E. Haskin, V. L. Behr, L. Smith – Sandia National Laboratories

"HECTR Results For Ice-Condenser Containment Standard Problem"
F. E. Haskin, V. L. Behr, A. L. Camp – Sandia National Laboratories

2:20 – 2:50 p.m. Discussion

2:50 – 5:00 p.m. SESSION C
CONTAINMENT INTEGRITY AS PART OF RISK ASSESSMENT"

Chairmen: M. Cunningham – U. S. Nuclear Regulatory Commission
R. Denning – Battelle, Columbus Laboratories

"Computer Aided Probabilistic Assessment Of Containment Integrity"
J. C. Tsai, R. A. Touchton – Westinghouse Electric Corporation

"A Hierarchical Goal Tree Structure For Containment Integrity"
M. L. Roush, R. N. Hunt – University of Maryland

"Thermodynamic Consequences Of Leakages In A Double Containment During Severe Accidents"
M. Tiltmann – Geseilschaft fuer Reaktorsicherheit, Federal Republic of Germany

"Containment Release Modes, Rainout And Risk"
R. G. Spulak, Jr., B. A. Boughton – Sandia National Laboratories

"Effects Of Hydrogen Burns And Flooded Reactor Cavity On Public Risk"
J. L. Manek – Massachusetts Institute of Technology
D. A. Dube – Northeast Utilities Service Co.

"Uncertainties Associated With Containment Analysis"
L. Greimann, F. Fanous – Ames Laboratory

5:00 – 5:30 p.m. Discussion

6:00 – 7:00 p.m. Reception (Hors d'oeuvres with no-host bar)

Thursday, June 14

8:30 – 11:30 a.m. SESSION D
LEAKAGE OF CONTAINMENTS DURING SEVERE ACCIDENTS

Chairmen: G. Bagchi – U. S. Nuclear Regulatory Commission
T. M. Brown – Wiss, Janney, Elstner & Associates

"Failure/Leakage Predictions Of Concrete Structures Containing Cracks"
Y. C. Pan, A. H. Marchertas, J. M. Kennedy – Argonne National Laboratory

"Aerosols And Leaking Concrete Containment Walls"
J. F. van de Vate – Netherlands Energy Research

"Structural Aspects Of Leakage In Reinforced Concrete Containments-- Experimental Approach"
P. D. Moncarz, J. D. Osteraas – Failure Analysis Associates

"Limit Load Analysis Of Actual Spherical Containments Subjected To Static Internal Pressure & Temperature"
J. Jeschke – Kraftwerk Union, Federal Republic of Germany

"Containment Leakage During Severe Accident Conditions"
C. H. Hofmayer – Brookhaven National Laboratory
G. Bagchi, V. S. Noonan – U. S. Nuclear Regulatory Commission

"Determination Of Containment Large Opening Penetrations Leakage During Severe Accident Conditions"
T. Bridges – EG&G, Idaho

"Numerical Studies Of Large Penetrations And Closures For Containment Vessels Subjected To Loadings Beyond The Design Basis"
R. F. Kulak, B. J. Hsieh, J. M. Kennedy, J. E. Ash, G. A. McLennan – Argonne National Laboratory

"Containment Penetration Elastomer Seal Test"
B. L. Barnes – EG&G, Idaho

11:30 – 12:00 noon Discussion

12:00 – 1:20 p.m. Lunch

1:20 – 3:30 p.m. SESSION E
PROGRAMS ON CONTAINMENT INTEGRITY

Chairmen: J. F. Costello – U. S. Nuclear Regulatory Commission
H. T. Tang – Electric Power Research Institute

"The KfK/PNS Research Program On PWR Steel Containment Behavior Under Accident Conditions"
W. Gulden – KfK/PNS, Federal Republic of Germany

"Concrete Containment Integrity Program At ERPI"
R. K. Winkleblack, Y. K. Tang, H. T. Tang – Electric Power Research Institute

"Procedures And Objectives For Testing A 1/8th Scale Model Of A Steel Containment"
L. N. Koenig – Sandia National Laboratories

"Plans For A 1/6th Scale Reinforced Concrete Containment Model"
J. Jung – Sandia National Laboratories

"Integrity Of Containment Penetrations Under Severe Accident Conditions"
C. V. Subramanian – Sandia National Laboratories

"ANL Survey Of LWR Containment Penetrations – A Progress Report"
T. R. Bump, R. W. Seidensticker – Argonne National Laboratory

3:30 – 4:00 p.m. Discussion

4:00 – 5:30 p.m. SESSION F
TESTING/ANALYSIS OF CONTAINMENT STRUCTURES

Chairmen: C. P. Tan – U. S. Nuclear Regulatory Commission
J. J. Ucciferro – United Engineers

"Computer Modelling Of The Sealing Behaviour Of Gaskets In Flanged Joints"
B. S. Nau – BHRA, United Kingdom

"Nonlinear Analysis Of Concrete Containments Under Static Pressurization – Evaluation Of The Risk Of Leakage"
A. Combescure, A. Hoffmann, P. Jamet, A. Millard – CEA-IRDI/DEDR.DEMT, France
R. Avet-Flancard, B. Barbe –DEA-IPSN/DAS, France

"Full Scale Leak-Rate Tests Of Concrete Containment Wall Elements"
D. M. Schultz, N. W. Hanson – Portland Cement Assoc.

"Liner Integrity In Overpressurized Post-Tensioned Concrete Containments"
C. N. Krishnaswamy, R. Namperumal – Sargent & Lundy

Friday, June 15

8:00 - 11:40 p.m. SESSION F (continued)
TESTING/ANALYSIS OF CONTAINMENT STRUCTURES

Chairmen: C. P. Tan – U. S. Nuclear Regulatory Commission
J. J. Ucciferro – United Engineers

"Structural Behavior Of Penetrations In Reinforced Concrete Secondary Containment Vessels"
R. N. White, W. Kim – Cornell University

"Nonlinear Failure Analysis Of A Reinforced Concrete Containment Under Internal Pressure"
S. K. Sharma, Y. K. Wang, M. Reich – Brookhaven National Laboratory

"Recent Results On The Evaluation Of The Overpressure Response Of Concrete And Steel Containments"
R. S. Dunham, Y. R. Rashid – ANATECH Corporation
Y. K. Tang – Electric Power Research Institute

"Thermal Stresses In PWR-Containments Under Loss Of Coolant Accidents"
B. Goller, G. Hailfinger, R. Krieg – KfK-IRE, Federal Republic of Germany

"Behavior Of Spherical PWR-Containments Close To Reinforced Sections Under Excessive Internal Pressures"
B. Goller, R. Krieg, G. Messemer – KfK-IRE, Federal Republic of Germany

"Failure Internal Pressure Of Spherical Steel Containments"
S. R. Idelsohn, A. Cordona, V. Sonzongi – Instituto de Desarrollo Tecnologico para la Industria, Argentina
G. Sanchez Sarmiento – Empresa Nuclear Argentina de Centrales Electricas S.A., Argentina

"Experimental And Analytical Results Of Steel Containment Tests"
D. S. Horschel – Sandia National Laboratories

"Analysis Of A 1/8th Steel Containment Model Subject To Internal Static Pressurization"
D. B. Clauss – Sandia National Laboratories

"Fragility Curves For Steel Containments With Internal Pressure"
F. Fanous, L. Griemann – Ames Laboratory

11:40 – 12:10 p.m. Discussion

12:10 – 12:30 p.m. Closing Comments

SECOND WORKSHOP ON CONTAINMENT INTEGRITY

Hosted by SANDIA NATIONAL LABORATORIES

Washington, DC
June 13-15, 1984

LIST OF ATTENDEES

Thomas J. Ahl
Chicago Bridge & Iron Co.
800 Jorie Blvd.
Oak Brook, Il 60521

Kazys D. Almenas
University of Maryland
College Park, MD 20742

Gunter Arndt
U.S. Nuclear Regulatory Commission
Office of Research
Mail Stop NL5650
Washington, DC 20555

Hans Ashar
U.S. Nuclear Regulatory Commission
Mechanical/Structural Engr. Branch
Mail Stop 217 NL
Washington, DC 20555

Dr. Goutam Bagchi
U.S. Nuclear Regulatory Commission
Equipment Qualification Branch
Mail Stop P-234
Washington, DC 20555

Wilfred E. Baker
Wilfred Baker Engineering
218 Edgewood Pl.
San Antonio, TX 78209

J. Ball
U.S. Nuclear Regulatory Commission
Region V
1450 Maria Lane
Suite 210
Walnut Creek, CA 94596

Bernard Barbe
Cea
Dentra D'Etudes Nuclearies
De Fontenay
92260 Fontenay-Aux-Roses
France

Bert Barnes
EG&G, Idaho
P. O. Box 1625
Idaho Falls, ID 83415

V. L. Behr
Sandia National Laboratories
Division 6411
Albuquerque, NM 87185

Kenneth Bergeron
Sandia National Laboratories
Division 6449
Albuquerque, NM 87185

Steve Blazo
Bechtel Power Corp.
15740 Shady Grove Rd.
Gaithersburg, MD 20877

Thomas Blejwas
Sandia National Laboratories
Division 6442
Albuquerque, NM 87185

Lloyd L. Bonzon
Sandia National Laboratories
Division 6442
Albuquerque, NM 87185

Tom Bridges
EG&G, Idaho
P. O. Box 1625
Idaho Falls, ID 83415

Ted M. Brown
Wiss, Janney, Elstner
Associates, Inc.
330 Pfingsten Rd.
Northbrook, Il 60062

Tom Bump
Argonne National Laboratory
Bldg. 308
9700 Cass Ave.
Argonne, Il 60439

Dr. J. J. Burns
U.S. Nuclear Regulatory Commission
Structural Engineering Section
Division of Engineering Technology
Washington, DC 20555

S. B. Burson
U.S. Nuclear Regulatory Commission
Mail Stop 1130 SS
Washington, DC 20555

Robert M. Carey
Gilbert/Commonwealth
P. O. Box 1498
Reading, PA 19603

James Carp
Volumetrics
P. O. Box 2084
3025 Buena Vista
Paso Robles, CA 93447

Pei-Ying Chen
U.S. Nuclear Regulatory Commission
Mail Stop 516
Systematics Evaluation
Program Branch
Washington, DC 20555

Roger I. Chen
Ontario Hydro
700 University Ave.
Toronto, Ontario H17F27
M5G 1X6 Canada

Thomas M. Cheng
U.S. Nuclear Regulatory Commission
7920 Norfolk Ave.
Bethesda, MD 20014

David Clauss
Sandia National Laboratories
Division 1523
Albuquerque, NM 87185

Scott Close
Bechtel Power Corp.
15740 Shady Grove Rd.
Gaithersburg, MD 20877

Dr. James Costello
U.S. Nuclear Regulatory Commission
Mechanical/Structural Eng. Branch
Mail Stop NL5650
Washington, DC 20555

Mark Cunningham
U.S. Nuclear Regulatory Commission
Washington, DC 20555

Dirk Dahlgren
Sandia National Laboratories
Division 6440
Albuquerque, NM 87185

Marwan Daye
Bechtel Power Corp.
15740 Shady Grove Rd.
Gaithersburg, MD 20877

Richard Denning
Battelle Columbus Laboratory
505 Ding Ave.
Columbus, OH 43201

Patrick Dillon
EBASCO Services, Inc.
640-13 Tete L'ours Dr.
Mandeville, LA 70448

Donald A. Dube
Northeast Utilities
Service Co.
P. O. Box 270
Hartford, CT 06141

Robert S. Dunham
ANATECH
334. N. Torrey Pines Ct., #320
La Jolla, CA 92037

A. R. Edwards
United Kingdom Atomic
Energy Authority Safety and
Reliability Directorate
Wigshaw Lane, Culcheth,
Warrington Cheshire,
England WA34NE

Peter Eisert
Gesellschaft fuer
Reaktorsicherheit
Schwertnergasse 1
D 5400 Koln 1
West Germany

Fouad Fanous
Ames Laboratory
Iowa State University
Ames, IA 50010

Paola Fasoli-Stella
Reactor Safety Program
Projects Directorate
Joint Research Center of
the CEC
Ispra Establishment
21020 Ispra (Varese) Italy

N. Foster
TVA
400 Summit Hill Dr.
Knoxville, TN 37921

P. J. Fulford
NUS
910 Colpper Rd.
Gaithersburg, MD 20898

Michael J. Gahan, III
Baltimore Gas & Electric Co.
P. O. Box 1475, Rm. 923
Baltimore, MD 21203

Phillip J. Galanti
Bechtel Power Corp.
P. O. Box 3965
San Francisco, CA 94119

James Glynn
U.S. Nuclear Regulatory Commission
Division of Risk Analysis
Nickolson Lane
Rockville, MD 20852

Lowell Greimann
Ames Laboratory
Iowa State University
Ames, IA 50010

Timothy Griesbach
EPRI
3412 Hillview Ave.
P. O. Box 10412
Palo Alto, CA 94303

Werner Gulden
Kernforschungszentrum Karlsruhe
GmbH Projekt Nukleare Sicherheit
Postfach 3640
D-7500 Karlsruhe,
Federal Republic of Germany

Lars Gunsell
Swedish State Power Board
S-16287 Vaellingby
Sweden

Orhan Gurbuz
416 Beryl Cove Way
Seal Beach, CA 90740

A. Hadjian
Bechtel Power Corporation
12400 E. Imperial Highway
Nowalk, CA 90650

L. P. Harrop
United Kingdom Atomic Energy
Authority
Safety & Reliability Directorate
Wigshaw Lane, Culcheth Warrington
Cheshire, England WA5 4NE

F. Eric Haskin
Sandia National Laboratories
Division 6411
Albuquerque, NM 87185

Edwin A. Hiltunen
Wisconsin Public Service Corp.
700 N. Adams St.
Green Bay, WI 54305

Stephen A. Hodge
Oak Ridge National Laboratory
P. O. Box Y, Bldg. 9104-1
Oak Ridge, TN 37813

Charles H. Hofmayer
Brookhaven National Laboratory
Structural Analysis Division
Bldg. 129
Upton, NY 11973

Daniel S. Horschel
Sandia National Laboratories
Division 6442
Albuquerque, NM 87185

A. Huber
Motor-Columbus Consulting
Engineers, Inc.
Parkstrasse 27
CH-5400 Baden
Switzerland

Ian Hunter
Ontario Hydro
700 University Ave.
Toronto, Ontario, Canada
M5G1X6

Toshikuni Isozaki
Japan Atomic Energy Research
Institute Department of
Nuclear Safety Research
Tokai-Mura, Ibaraki-Ken, 319-11
JAPAN

Philippe Jamet
Commissariat A L'Energie
Atomique Centre d'Etudes
Nuclearies de Saclay
DEMT/SMTS/LAMS
F-91191 Gif Sur Yvette Cedex
France

F. Jape
U.S. Nuclear Regulatory Commission
Region 2
101 Marietta St NW, Suite 2900
Atlanta, GA 30023

Jochen Jeschke
Kraftwerk Union Aktiengesllschaft
Hammerbacherstr 12+14
P. O. Box 3220
8520 Erlangen
West Germany

Joseph Jung
Sandia National Laboratories
Division 1524
Albuquerque, NM 87185

R. M. Keanneally
U.S. Nuclear Regulatory Commission
Mechanical/Structural Eng. Branch
Mail Stop 113055
Washington, DC 20555

Peter M. Keogh
Ove Arup & Partners
13 Fitzroy Street
London WIP 6BQ
United Kingdom

Don Kirkpatrick
U.S. Nuclear Regulatory Commission
Office of Inspection & Enforcement
Washington, DC 20555

Larry Koenig
Sandia National Laboratories
Division 6442
Albuquerque, NM 87185

Rolf Krieg
Kernforschungszentrum Karlsruhe
GmbH
Institute fuer Reaktorentwicklung
Postfach 3640
7500 Karlsruhe
Federal Republic of Germany

C. N. Krishnaswamy
Sargent & Lundy Engineers
Structural Engineering
Specialist Division
55 East Monroe St.
Chicago, IL 60603

Ronald Kulak
Argonne National Laboratory
9700 South Cass Ave.
Argonne, IL 60539

P. T. Kou
U.S. Nuclear Regulatory Commission
Section B
Structural & Geotechnical Branch
Division of Engineering
Washington, DC 20555

Carl L. Larsen
Quadrex Corp.
4500 S. Garnett, Suite 500
Tulsa, OK 74016

Dan Lurie
U.S. Nuclear Regulatory Commission
Cost & Management Support Branch
Mail Stop 7602 MNBB
Washington, DC 20555

Joy Maneke
MIT
Building 38-182
Cambridge, MA 02139

Al Marchertas
Argonne National Laboratory
9700 South Cass Ave.
Argonne, IL 60439

Federico Maura
U.S. Nuclear Regulatory Commission
799 Roosevelt Rd.
Glen Ellyn, IL 60137

Craig McWhorter
Southern Co. Services
P. O. Box 2625
Birmingham, AL 35202

J. Metcalf
Stone & Webster
245 Summer St.
Boston, MA 02107

Piotr D. Moncarz
Failure Analysis Associates
2225 E. Bayshore Rd.
Palo Alto, CA 94303

Ken Muramatsu
Sandia National Laboratories
Division 6423
Albuquerque, NM 81785

R. Namperumal
Sargent & Lundy Engineers
Structural Engineering Specialist
Division
55 East Monroe St.
Chicago, IL 60603

Bernard S. Nau
BHRA
Cranfield, Bedford, MK43 OAJ
England

S. J. Niemoyk
UCS
Suite 1101, 1346 Connecticut Ave, NW
Washington, DC 20036

T. K. Niyogi
U.S. Nuclear Regulatory Commission
Mail Stop NL5650
Division of Risk Analysis &
Operation
Washington, DC 20555

Paul Norian
U.S. Nuclear Regulatory Commission
Generic Issues Branch/DST
7920 Norfolk Ave.
Bethesda, MD 20814

P. O. O'Reilly
NUS Corporation
910 Colpper Rd.
Gaithersburg, MD 20878

Yen Pan
Argonne National Laboratory
9700 South Cass Ave
Argonne, IL 60439

Peter J. Pelto
Pacific Northwest Laboratory
P. O. Box 999
Richland, WA 99352

Giuseppe Pino
ENEA-DISP
Via Vitaliano Brancati, 48
00144 Rome - Italy

Harold Polk
U.S. Nuclear Regulatory Commission
Mail Stop P1022
Washington, DC 20555

Dale Powers
U.S. Nuclear Regulatory Commission
Suite 100
611 Ryan Plaza Dr.
Arlington, TX 76011

C. Radens
University of Cincinnati
Cincinnati, OH 45224

J. Rashid
Anatech
3344 N. Torrey Pines Ct #320
La Jolla, CA 92037

Terrence E. Renton
Quadrex Corp.
4500 S. Garnette, Suite 500
Tulsa, OK 74016

Frank Rinaldi
U.S. Nuclear Regulatory Commission
Washington, DC 20555

Jack Rosenthal
U.S. Nuclear Regulatory Commission
Office of Nuclear Reactor Regulation
Washington, DC 20555

Marvin L. Roush
University of Maryland
Chemical & Nuclear Engineering Dept.
College Park, MD 20742

G. Sanchez-Sarmiento
ENACE S. A.
Av. L. N. Alem 712
Buenos Aires, Argentina

Ray Schneider
Combustion Engineering, Inc.
1000 Prospect Hill Rd.
Windsor, CT 06095

Donald M. Schultz
Portland Cement Assoc.
5420 Old Orchard Rd.
Skokie, Il 60077

Ralph Seidensticker
Argonne National Laboratory
9700 S. Cass Ave.
Argonne, Il 60439

Robert E. Shirk
Gilbert/Commonwealth
P. O. Box 1498
Reading, PA 19603

Larry Shao
U.S. Nuclear Regulatory Commission
Division of Eng. Technology
Mail Stop NL5650
Washington, DC 20555

N. Sivarpragasom
Taylor Woodrow Construction Limited
345 Ruislip Southhall
Middlesex, England

R. Spulak
Sandia National Laboratories
Division 6411
Albuquerque, NM 87185

Ronald Staniforth
Atomic Energy Establishment
Bldg. A32
Minfrith, Dorset
Dorchester DT2 8DH
England

M. Stetson
Stone & Webster
P. O. Box 2325
Boston, MA 02107

E. P. Stroube
Technology for Energy Corp.
One Energy Center
Pellissipi Parkway
Knoxville, TN 37822

Tsung-Ming Su
U.S. Nuclear Regulatory Commission
Mail Stop 268
Washington, DC 20555

C. V. Subramanian
Sandia National Laboratories
Division 6442
Albuquerque, NM 87185

William M. Suslick
Duke Power Co.
P. O. Box 33189
Charlotte, NC 28242

C. P. Tan
U.S. Nuclear Regulatory Commission
Structural & Geotechnical Branch
Division of Eng.
Washington, DC 20555

H. T. Tang
EPRI
3412 Hillview Ave.
Palo Alto, CA 94304

Y. K. Tang
EPRI
3412 Hillview Ave.
Palo Alto, CA 94303

Edmund Tarnuzzer
Yankee Atomic Electric Company
1671 Worcester Rd.
Farmingham, MA 01701

Frank V. Thome
Sandia National Laboratories
Division 6446
Albuquerque, NM 87185

G. Thompson
Union of Concerned Scientists
26 Church St.
Cambridge, MA 02238

Manfred Tiltmann
Gesellschaft Fur Reaktorsicherheit
(GRS) Schwertnergasse 1
D 5000 Koln 1
West Germany

John Tsai
1906 Woodleight Dr, W.
Jacksonville, FL 32211

K. R. Turnbull
TVA
WIUAIOC-K, 400 Summit Hill
Knoxville, TN 37921

Joseph Ucciferro
United Engineers & Constructors, Inc.
Structural Analysis Group
30 S. 17th St.
Philadephia, PA 19101

J. F. Van de Vate
Netherlands Energy Research
Foundation
P. O. Box 1
1755 ZG Petten
The Netherlands

H. J. van Grol
Netherlands Energy Research
Foundation
112 Scheveninseweg
The Hague, The Netherlands

Walt von Riesemann
Sandia National Laboratories
Division 6442
Albuquerque, NM 87185

Dr. Tom Walker
U.S. Nuclear Regulatory Commission
Mail Stop 1130SS
Experimental Fast Reactor
Safety Research Branch
Washington, DC 20555

Y. K. Wang
Brookhaven National Laboratory
T129
Upton, NY 11973

Richard White
Hollister Hall
Cornell University
Ithaca, NY 14853

Karen Whittlesey
U.S. Nuclear Regulatory Commission
Region IV
611 Ryan Plaza, Suite 1000
Arlington, TX 76011

Carlo Zaffiro
ENEA-DISP
Via Vitaliano Brancati, 48
00144 Rome - Italy

Gary D. Zakaib
Ontario Hydro
700 University Ave.
Toronto, Ontario, Canada
M5G1X6

SESSION A

OPERATIONAL EXPERIENCE AND ITS RELATIONSHIP TO CONTAINMENT PERFORMANCE DURING ACCIDENT CONDITIONS

THE PWR INTEGRATED LEAK RATE TEST, A REVIEW OF EXPERIENCES AND RESULTS

P. Koegh
Ove Arup and Partners
13 Fitzroy Street
London W1P 6BQ

Abstract

This paper reviews the Integrated Leak Rate Test as carried out in the USA and as reported in papers for European countries. The methods of analysis of test results are discussed and it is recommended that only the mass point method be permitted. The reliability of the instruments used in a test are described and the care needed during a test is identified. The use of a preliminary zero pressure test is recommended as a necessary part of the test to counter any instrument inaccuracies, to identify any unwanted temperature gradients, and to ensure that no ingress of water or air is taking place at the start of a test.

Valves are identified as the major leak source during tests with about 40% of tests being adversely affected by their performance. Recommendations are given to improve the reported integrity of the valves.

The use of the part pressure test is discussed and for various reasons it is recommended that only full pressure tests (at design accident pressure) be permitted. The lack of correlation between full and part pressure tests is considered to be due to gas absorption/release of internal concrete and the behaviour of steam generator equipment giving greater leaks at higher pressures.

Secondary effects of diurnal influences and the use of the ideal gas laws in place of more accurate Van de Waals state equation are discussed.

1.0 BACKGROUND

For a number of years, Ove Arup and Partners have been providing assistance to HM Nuclear Installations Inspectorate (NII) on a wide range of topics related to the containment structure of pressurised water reactors (PWR). As part of this continuing work, a review has been made of the integrated leak rate test (ILRT). Some of the main points of the review are described in this paper. The review is reported in full in reference 14.

The author wishes to thank the NII for their assistance and support in the preparation of this paper. The views cxpressed in this paper do not necessarily represent those of the NII.

2.0 SCOPE

The initial objective of the review was to evaluate containment integrity degradation, should it exist, to gain an appreciation of the general performance of PWR containments with respect to integrity and to evaluate the main aspects of the ILRT. It has been necessary to consider the testing programme in the USA since current practices there are likely to be adopted by the Central Electricity Generating Board (CEGB) for use in the United Kingdom (UK).

The research was conducted via a literature search, by discussion with other interested engineers, and by examination of copies of ILRT reports. These reports were obtained from the Public Document Room (PDR) of the Nuclear Regulatory Commission (USNRC) and some were kindly given by the Oak Ridge National Laboratories.

The results of 53 tests were examined. These tests were not selected on a systematic basis except that only concrete containments were considered, as this type of structure is proposed for Sizewell in the UK, and ice condenser PWRs were excluded in view of their lower design accident pressure. The reports examined revealed a wide spectrum of events and features to an extent that gave assurance that efforts to obtain more reports were not justified for this project.

3.0 STANDARDS

The fundamental purpose of an ILRT is to give a global test of the containment integrity and to show that the assumptions made in the offsite consequence calculations for radioactivity releases following a reactor accident are still valid. The maximum permitted leak rate for a containment structure is given in the technical specifications for the plant and is derived from the requirements of 10CFR100 (4) and the methods of TID 14844 (5). The current regulations are described in 10CFR50, Appendix J (1) which refers to the 1972 standard (2). Efforts are being made at this time to modify 10CFR50 so that it contains only the technical requirements of the test. The specifications for the test would then be described in a Regulatory Guide which, initially at least, would refer to the 1981 standard (3). This arrangement will allow greater flexibility and a better ability to respond to new information or technical developments.

The NRC have reservations regarding the 1981 standard and some of these are described in reference 15. Some of those reservations are amplified in this paper and other reservations are made. Some of the evidence supporting changes made from the 1972 to the 1981 standard is also identified.

4.0 ANALYSIS METHODS

Of the two physical methods available, the reference vessel method is not now used and had practical difficulties associated with it (7, 15). The absolute method, in which the internal mass of the atmosphere held in the containment is estimated from the temperature and pressure readings of the containment, is now widely used. There are various methods of deriving the estimated leak rate from the collected data and these are described here. Reference 10 also discusses this topic.

4.1 Total Time Method

The total time method evaluates the leak rate at successive time points based on the mass of air contained at the first time point compared to that at the latest time point.

These successive values of estimated leak rate are then evaluated by regression analysis. The intercept of the least squares fit straight line with the time at the end of the test is deemed to be the calculated leak rate. It can be shown that this method is relatively sensitive to the first calculation for the contained air mass. An example is given in Table 1 in which the actual leak rate is zero but the first point is perturbed, perhaps by instrument variations, giving an apparent leak rate initially. The result in Table 1 shows that the normal total time method gives a significant error in the result. The 1981 standard (3) recommends (in Appendix A, A3.2.1) that the data should be weighted in accordance with the time interval associated with each calculated leak rate. It may be seen from Table 1 that this method improves the result in that the sign is correct and the result is of smaller magnitude, but the achieved error for a 10 hour test may still be regarded as significant, compared with a permitted leak rate of 0.1%/day, for example.

4.2 Point to Point Method

The point to point method is similar to the total time method except that the leak rate data items are based on the contained air mass between successive points only. The result may be indicated either as an intercept from a regression analysis, or as an average of the leak rate results calculated

over the test. The results of these two methods are shown in Table 1. Here the errors are generally smaller but of the same magnitude as the two total time methods. For accuracy, the time intervals between data sets must be equal.

4.3 Mass Point Method

The mass point method relies upon a regression analysis applied to the calculated contained mass of air with respect to time. The leak rate is determined from the ratio of the slope to the intercept of the line with the start of the test and is expressed as a percentage per day. The results in Table 1 show that the method is not sensitive to errors in the first, or indeed any one data point.

Table 1

Results of computations using different analysis methods.

Example

Relative mass at first reading (t_o)	1.0001
Relative mass at all subsequent readings (t_i)	1.0000
Time interval between readings	15 mins

Method	Variation of method	Test length (hours)	Calculated result (%/day)
Total Time	intercept at end of test	10	-0.0649
		24	-0.0436
	including weighting	10	+0.0167
		24	+0.0068
Point to Point	intercept at end of test	10	-0.0444
		24	-0.0194
	average of results	10	+0.0240
		24	+0.0100
Mass Point		10	+0.0033
		24	+0.0006

In the calculation process for the mass point method, it is found to be convenient to express the contained atmosphere relative to the initially contained air. This results in calculated masses in the region of 1.0 and makes the presentation and understanding of the results easier. It has no effect on the accuracy of the final result.

A further point to note is in respect of the equations for "S", which is used in the calculation for the upper confidence limit, given in Appendix B of the 1981 standard. The equation given in B3, apparently intended to reduce truncation errors, in fact gives greater potential for truncation errors than the formula given in B2 (Equation B.4). The reason for this is that the equation B4, viz

$$S = \left\{ \frac{\Sigma (Wi - \hat{W}i)^2}{(n-2)} \right\}^{\frac{1}{2}}$$

is based on an aggregate of small values where the alternate formula in B3 involves the difference of large numbers to arrive at the relatively small number "S". The parameters S_A, S_B, and S_{AB}, also used in the upper confidence limit calculation, should then be derived via the parameter "K" as described in B2 of the appendix.

It is recommended that only the mass point method of data analysis is used in the evaluation of leak rates and that the total time and point to point methods should not appear in any UK ILRT documents which might be proposed.

5.0 INSTRUMENTATION

The instruments used in the test are for pressure, temperature and for water vapour pressure. The test reports and the certification documents they contain indicate that the instruments are sufficiently sensitive to give an accurate result after an appropriate length of time (16).

The pressure transducers used appear reliable. Failures were noted in three of the tests examined.

1)	Robert Emma Ginna, 1982.	Both gauges replaced.
2)	Fort Calhoun 1, 1976.	A gauge was recalibrated.
3)	Zion 1, 1981.	One sensor abandoned.

The temperature sensors, typically resistance gauges, are a little less reliable than the pressure gauges, five of the tests showed problems with the gauge itself. The failure causing possibly the most difficulties was at Beaver Valley 1, 1978. One of the temperature gauges was moved prior to the test to a location where it was influenced by the heat output from a motor which operated intermittently. The test itself was a marginal pass but failed on the verification procedures, which are described in reference 2.

After eliminating the gauge from the test and after other repairs, the test was completed satisfactorily.

The 1981 standard calls for various parameters to be plotted as the test proceeds. It is suggested here that the data acquisition system be also capable of giving plots of the performance of individual gauges compared to say the average of that type of instrument. In the particular case given here, had such a system been available, the errant gauge would have been found earlier. This proposal is also relevant to the water vapour pressure instruments.

The dew cells or dew point detectors are the least reliable of the instruments used and some care and attention is needed with them. 12 of the tests examined had problems with the sensors directly (23% of all the tests). In addition, one of the tests required the containment to be depressurised as the detector had not been saturated with lithium chloride before the test started. This had to be attended to manually. An interesting case was at Indian Point in 1976. In this test, the mass point plot drawn from the recorded data showed a significant deviation from the final regression line during the test. Between 4 and 13 hours from the start of the test, the local best fit straight line indicated a leak rate of -0.07%/day. Between 14 and 21 hours, the local best fit line indicated a leak rate of +0.10%/day, which is the limiting leak rate for the plant. The overall result was calculated as virtually zero for the 24 hour period of the test. Examination of the test report revealed that the water vapour pressure varied significantly during the test and the water vapour pressure/time curve was similar to that achieved by the mass point plot. The implication was that the water vapour, which is normally fairly constant during a test, was measured incorrectly by the instruments and this had a marked affect on the result.

6.0 ZERO PRESSURE TEST

In view of the possibility of the instruments drifting during a test, or to a malfunction in them by other causes, it is suggested here that a period of time be spent at the start of a test with the containment sealed but not under pressure. The result of the leak rate calculation should, of course, indicate a zero leak rate. This will test out the overall accuracy and dependability of the instrumentation and data acquisition system. Where deficiencies are identified, a significant time saving may be gained by a utility since entry to the containment can be effected immediately. Delay due to depressurisation and repressurisation is avoided. There are other advantages of the test.

The period of zero pressure can usefully give an indication of the accuracy of the weighting given to the various temperature gauges. This is considered (16) to be a cause of some error if uniform temperatures are not achieved in the containment. The means of achieving uniformity of

temperatures may also be verified and corrected if need be, before the containment is pressurised. The need for more gauges may be indicated.

The zero pressure test will also give an assurance that no unintended ingress of water of gas is taking place. There are several examples of this in the tests examined, some are described here.

1) Salem 1, 1979. Adjustments were needed to allow for a change in water inventory during the test. The leakage was estimated to add 0.016%/day to the ILRT result.
2) Indian Point 3, 1975. After the test, the containment recirculation sump had about 8 inches of water due to a leakage from an accumulator line which was vented to the containment.
3) Zion 2, 1980. After the test, the containment sump was full of water to 1 inch over the top. This was thought then to be the cause of the negative leak rate found during the test. The isolation valves for this water supply were shut off during the test.
4) Arkansas Nuclear One 2, 1981. 16500 gallons of water were inadvertently pumped into the containment, but this was outside the period of the test so no allowance for it was necessary.

The 1981 standard (3) requires that free water surfaces are monitored during the test. It would appear desirable to also establish that no water or gas is flowing into the containment before the test starts.

It is reported (6) that France and Italy carry out the zero pressure test procedure before leak rate tests.

It is recommended here that this procedure be adopted in the UK as part of the PWR test procedure.

7.0 SOURCES OF LEAKS - VALVES

The isolation valves for the containment are the largest single source of containment leaks. Table 2 shows the reported performance of isolation valves in the reports examined. The terms used in the table are described here.

Table 2 Valve Performance Reported

Type of Test	Number of tests reporting:			
	Misaligned Valves	Large Leaks In Valves	Small Leaks In Valves	No Valve Leaks
Pre-operational (11 tests)	2 (18%)	1 (9%)	5 (45%)	4 (36%)
In-service (42 tests)	11 (26%)	15 (36%)	5 (12%)	17 (40%)
All (53 tests)	13 (25%)	16 (30%)	10 (19%)	21 (40%)

"Misaligned" valves are those which are open when they should be shut. Because of valves being used in series, an incorrectly aligned valve need not lead directly to a loss of containment integrity, but it should be noted that the cases discussed here were all found as a result of unacceptable leaks initiating more detailed examination of the containment.

The misalignment of valves may be caused by human error and the omission of these valves from the operating schedule for the test was a common event where misalignment had occurred. Alternately, there may be a fault in the valve, valve mechanism or the valve motor. Examples of misalignment are given here.

1) Oconee 1, 1976. During the test, air was discovered coming from a 3/4" pipe leading to the emergency personnel hatch equalisation valve. This was closed before the test continued.
2) Surry, 1981. At a containment pressure of 4.8 psig, a valve was found leaking at a calculated rate of about 3000 cubic feet of air per minute (compared to 5.16 cu.ft/min permitted). It was found to be partially open.

3) Three Mile Island 1, 1974. Valves were found to be misaligned. This was due to earlier efforts to find a dc ground.
4) Zion 2, 1980. A purge valve was leaking at low pressure causing the exhaust fan to run backwards. It was cranked down but continued to leak.
5) Maine Yankee, 1982. One isolation valve failed to auto close as the pressure built up and had to be isolated manually.

Valves with "Large" leaks are those which caused tests to initially fail or were major contributors to an initial failure. The reported performances of these are shown in Table 2. It must be noted that the identification of these cases involves some subjective interpretation of the written text in the reports. Actual leak rates through the faulty valves were generally not quoted in the reports. As a guide, it was judged that the leaks were a significant proportion of the permitted leak rate or greater. Differences here with reference (12), which showed a 5% loss of integrity for PWRs are thought to be due to the size of leak being considered.

"Small" leaks in valves in Table 2 were cases where leaks were identified, often in access hatch valves, but these did not appear, from the text of the report, to be the main cause of the leak rate being unacceptable or the cause of delay.

It may be judged that the reported performance of the valves in the relatively controlled condition of an ILRT reflects on the condition that might be found in a plant should a loss of coolant accident occur. This is a matter which is still being considered.

Consideration has been given as to whether the reported performance is changing with time. An attempt has been made to answer this by looking at the percentages of tests made in each year which have significant valve leaks or misaligned valves. This is shown in Table 3.

A weighted regressional analysis of the figures in table 3 indicates that the failure rate, as such, is generally in the range 40% - 45%. There does not appear to be any strong variation with time shown by these results.

It would appear desirable that the reported valve integrity should be improved upon. The occurrence of misalignment of valves can only be improved by management procedures. The effectiveness of the isolation valves in new plants such as that proposed for Sizewell may be helped by modifying older specifications or quality assurance procedures to take advantage of the information gained from valve performances to date.

The 1981 standard requires that valves be tested at intervals not exceeding two years. The valve integrity reliability will be improved by shorter intervals between type C tests and, where this is practical, consideration should be given to this.

Table 3 Valve Leaks Related to Time

Year	No. of Tests	F	F%
1971	2	0	0%
1972	1	0	0%
1973	2	0	0%
1974	4	2	50%
1975	3	1	33%
1976	4	4	100%
1977	4	2	50%
1978	5	2	40%
1979	4	0	0%
1980	7	4	57%
1981	7	3	43%
1982	8	4	50%
1983	2	0	0%
	53	22	42%

The table shows the number of tests (F) in which valves were misaligned or had significant leaks.

Proposals have been made (9), for the Netherlands, that a short ILRT be carried out at each outage of the plant. It is possible that this may be a quicker, and more efficient, way of confirming that no gross leaks exist since the ILRT does not rely on management procedures as part of its assurance of leak integrity. This short test has been referred to as a Blunder test. Certainly, consideration should be given to this being adopted in the UK testing programme.

8.0 SOURCE OF LEAKS - STEAM GENERATORS

During the test, the steam generators are not under pressure. Some features such as manways and hand holes are subject to pressures in the reverse direction for which they are designed. Occasionally this may lead to significant leaks, which since they occur usually only at higher pressures, these leaks can be difficult to locate.

This type of leak was found on a number of the tests examined, and its significance needs to be considered. During a LOCA, leakage can occur through a lifted manway if the isolation valves of the secondary loop leak outside the containment or there is another leak source outside the containment. There is an apparently unresolved probabilistic argument attached to the likelihood of this occurring. Irrespective of the probabilities involved it would appear desirable to show that the leak which might occur through such features is not significant. This can be shown by testing at full pressure. This is referred to later under partial pressure testing.

9.0 SOURCES OF LEAKS - RESILIENT SEALS AND CONTAINMENT LINER

The seals of locations such as the plant access hatch and the personnel access hatches appear to give rise to only small leaks in the tests examined. The liner appears not to be a problem at all. In all the tests there was only one reference to a leak through the liner. This was at Surry 1 in 1975; leaks from welds to penetrations were measured at 0.345 ft^3/minute (compared with 2.75 ft^3/minute permitted). These welds were not repaired at the time of the test.

10.0 PROBLEMS CAUSED BY PRESSURE

The pressure used to test the containment leak rate places significant load on various parts of the equipment inside the structure. For example,

1) Fort Calhoun 1980, A rupture disc failed.
2) Indian Point 1971, The unvented box girder for the polar crane was buckled.
3) Millstone 2, 1979, One of the fans was declared inoperative since the power required to move the dense air was causing overheating.

The accident pressure applied also ensures that the various isolation valves, as installed and as maintained, are still functionally capable of resisting the pressure.

11.0 PART PRESSURE TESTS

The 1972 standard (2) and 10CFR50 Appendix J(1) currently permit the use of a part pressure test where the part pressure is not less than half the design accident pressure. This test requires a reliable correlation to be established between the leakage at the part pressure and at the full design accident pressure. Those tests reviewed have been examined and the cases were two pressures were utilised were used to draw the graph shown in figure 1. This figure should show points close

to the straight line for the correlation indicated in the 1972 standard (2) to be applicable. The graph does not indicate any correlation.

There are several reasons for this lack of correlation. Features such as the steam generator may leak at a significantly greater rate at higher pressures, valves may vary their leak rate with pressure upwards or downwards. Another factor, not recognised by the 1972 code, is that of gas absorption by the internal concrete. Toossi (13) states that this effect can be significant. A good example of the phenomenon was at Indian Point 2 in March 1971. At the end of the test, when the containment was entered, the floor was expelling bubbles through the water puddles. The ability of concrete to absorb/transmit gas is also described by Asmis (17).

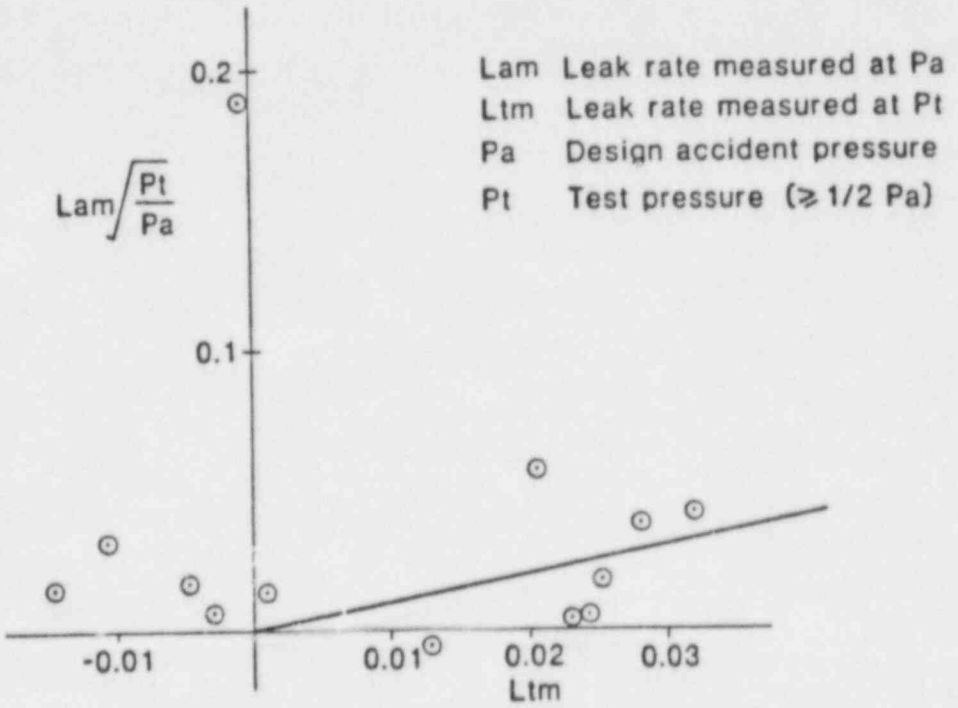

Figure 1 Relationship of Leak rates at pressures Pa and Pt

The 1981 standard (3) now requires that if the pressure in the containment has exceeded the test pressure previous to the ILRT, the pressure must be held at 85% of the test pressure, or below, for 24 hours before the ILRT is commenced. This goes some way to ensuring that the effect of gas absorption by the concrete, if any, is to increase the apparent leak rate which is conservative.

In view of the lack of correlation between half pressure tests and full pressure tests, it is not possible to say from a half pressure test what a subsequent full pressure test might indicate. The half pressure test will certainly indicate any gross leaks that might exist but will it give assurance of leak integrity at higher pressures ? It appears that this cannot be said either. At Calvert Cliffs December 1973, the leak rate at 25 psig was about 0.01%/day, which is good compared to the 0.2%/day required. However, at 50 psig, the leak rate was found to be 0.5%/day due to leaks through the steam generator manways. At Arkansas Nuclear One, #2, in October 1977, a feedwater check valve bonnet (to steam generators) leaked at pressures greater than 14 psig. The resistance to this pressure level was due to the water head in the steam generators. Had this bonnet been fitted tighter, it is credible that it would not leak under a low pressure test but would leak under higher pressures.

With regard to the half pressure test it may be summarised that this test gives no indication of the leak rate that may be achieved at higher pressures nor does it give assurance that the containment plant and safety equipment, such as fans and rupture discs, or new valves, will operate effectively at higher pressures. It is suggested here that the part pressure test is not used in the UK test programme and reliance is placed only on the full design accident pressure for the ILRT.

12.0 DIURNAL EFFECTS

It is considered (11) that diurnal effects may influence the leak rate of steel containments. Reference is made in the 1972 American Standard to the need to allow for weather conditions. There was very little evidence found that significant diurnal effects exist for concrete containments. At Robinson 2 plant in March 1982 a leak rate of 0.01% per day was established and this jumped to 0.02% per day. Searches and enquiries could not establish the cause. It was thought that the morning sunshine had affected the purge valves.

At another plant, in April 1977, the test had been running for some time and excess leakage was indicated. At 1600 hours the leak rate changed, favourably and then went to a satisfactory conclusion. There was no satisfactory explanation of the behaviour observed. The test had been in progress for several days.

It would be of interest to plot out the calculated contained air mass for a number of tests which went on for long periods to see if diurnal influences can be found. This was done for some of the tests examined, for other reasons, but no diurnal influences could be seen. This is an area where further research is required.

13.0 VAN DE WAALS EQUATION

The ILRT analysis is based on the ideal gas laws, which assume that each gas molecule is a point mass without volume and that cohesion and adhesion forces can be neglected. The Van de Waals state equations allow for these effects. The air used in the ILRT is of course a real gas and calculations have been made to evaluate the effect these considerations would have on a calculated leak rate.

Analysis shows (9) that the error in not using the Van de Waals equations is governed by the relative changes of temperature and pressure over the period of the test. Sample calculations have shown that for concrete containments, the temperature and pressure changes are typically not sufficient to show significant error when using the ideal gas laws.

It is noted however that the 1981 standard (3) does not place a limit on the absolute magnitude of the temperature change which may occur over the period of a test and that might be a useful addition. For tests examined the temperature was found to be fairly constant within one or two degrees over the period of the test.

REFERENCES

1. 10CFR50 Appendix J

   Code of Federal Regulations, Title 10 - Energy, Part 50 Primary Reactor Containment Leakage Testing for Water-cooled Power Reactors.

2. ANS-7.60/N54.4-1972 (16th March 1972)

   American National Standard
   Leakage Rate Testing of Containment Structures for Nuclear Reactors

3. ANSI/ANS-56.8-1981 (19th February 1981)

   American National Standard
   Containment System Leakage Testing Requirements

4. 10CFR100

   Code of Federal Regulations, Title 10-Energy, Part 100 Reactor Site Criteria (USA)

5. TID 14844
Technical Information Document 14844
Reactor Technology
Calculation of Distance Factors for Power and Test Reactor Sites
Division of Licensing and Regulation
US Atomic Energy Commission

6. Significant Aspects concerning the leakage tests of the safety containments: Operational experience evaluation
CSNI specialist meeting on Water Reactor Safety,
Toronto, Canada,
Paper 29, Grimaldi
October 1983

7. Experimental Study of Accuracy of Leak Rate Test for Reactor Containment
Yamaguchi Hisayoshi, Yutaka
Technical Review, Mitsubishi Heavy Industrial Ltd.

8. Integral Leak Rate Tests of Containments
Engel, Siefart, Walter
Kerntechnik 20, Jahragang (1978) No. 3.

9. Considerations with respect to procedures and measuring methods for containment leak rate tests
Domselaar, Pruimboom, Wieringen
CSNI Specialist Meeting on Water Reactor Containment Safety,
October 1983

10. Containment, Leak Rate Testing, Why Mass Point Method is Preferred
Fleshwood
Power Engineering
February 1976

11. Experience in Integrated leak rate measurements
Shirk
Proceedings of the Workshop for Containment Integrity
June 1982

12. Integrity failure experiences with reactor containments
Weistein
Proceedings of the Workshop for Containment Integrity

13. Air ingress to internal concrete members of a reactor containment building during leakage rate tests
Toossi
ACI Journal Feb. 1984

14. The Integrated Leak Rate Test, A Review
Ove Arup and Partners
March 1984 ref. IOE 84-44

15. NUREG/CR-3549, Evaluation of Containment Leak Rate Testing Criteria.
JR Dougan, March 1984

16. EPRI NP-3400 Project 1393-5
Criteria for determining the Duration of Integrated Leakage Tests of Reactor Containments
Quadrex Corporation

17. A small study of air vapour permeability of concrete
K. Asmis
Proceedings of the Workshop for containment integrity
June 1982

RELIABILITY ANALYSIS OF CONTAINMENT ISOLATION SYSTEMS

P. J. Pelto and C. A. Counts
Pacific Northwest Laboratory
Richland, WA 99352

ABSTRACT

The Pacific Northwest Laboratory (PNL) is reviewing available information on containment systems design, operating experience, and related research as part of a project being conducted by the Division of Systems Integration, U. S. Nuclear Regulatory Commission. The basic objective of this work is to collect and consolidate data relevant to assessing the functional performance of containment isolation systems and to use this data to the extent possible to characterize containment isolation system reliability in terms of leakage area versus leakage probability for selected reference designs. This paper summarizes the results from initial efforts which focused on collection of data from available sources and briefly describes detailed review and analysis efforts which commenced recently.

INTRODUCTION

This paper is a summary of results to-date from work undertaken on the Reliability Analysis of Containment Isolation Systems Project (RACISP). Work in this project was divided into two major tasks: 1) Document Survey and 2) Detailed Review and Analysis. Efforts thus far have primarily focused on the Document Survey Task with the objective of collecting and consolidating data relevant to functional performance of containment isolation systems (CIS). Data collected in the Document Survey Task will be used in a recently initiated Detailed Review and Analysis Task to characterize CIS reliability in terms of leakage area versus leakage probability for selected reference nuclear power plant designs.

Research efforts for the Document Survey Task were focused by establishing four specific objectives.

1. Make a search for sources of CIS performance data.

2. Review and retain data that have potential uses.

3. Organize the data so that it can be used for detailed review and analysis.

4. Provide comments on general CIS performance trends recognized during an initial review of the data.

To accomplish these objectives, the task was divided into three work areas: a design review, an operating experience review, and a related research review. Sources of information in each of these areas were reviewed in the context of the task objectives.

In the design review, Final Safety Analysis Reports (FSARs) were reviewed for five nuclear power plants that utilized the main types of CIS design. This review resulted in compilation of penetration and isolation valve parameters that are common to various designs. Guidelines and standards governing CIS design and performance were also surveyed for relevant information (e.g., penetration/valve testing frequency). This information was used to develop a data classification scheme. In the operating experience review, data related to CIS operating experience was collected. The primary source of this type data were the Licensee Event Reports (LERs). Data extracted from the LERs were assembled into a computer data base for use in the subsequent detailed review and analysis task. A limited review of Integrated Leak Rate Test (ILRT) reports was also undertaken and NRC inspectors were interviewed as potential sources of information. Information resulting from related research programs and from the technical literature was also collected.

Following are summaries of the results from the three work areas of the Document Survey Task and a brief description of the recently commenced detailed review and analysis.

DESIGN REVIEW

As noted by Blejwas (1982), there are at least 11 different combinations of containments using different combinations of reinforced concrete, steel and tendons in a variety of geometric configurations. The use of such design options as ice condenser, subatmospheric, and inerted containments further increases the number of different containment types. A brief review of the different types of containment designs was performed as one of the initial steps of the RACISP. A review of guidelines and standards related to CIS design and performance was also conducted. The basic objectives of this design review were to identify major differences in containment isolation system design; to develop potential groupings of containment types; and to develop information to assist in developing a data classification scheme for use in the operating experience review.

Seven containment types were selected as representative of the main type of CIS design. These include: large dry, ice condenser, dual, subatmospheric, Mark I, Mark II, and Mark III. Of these seven, FSARs were reviewed for the following plants:

Plant	Containment Type
Palisades (PWR)	Large Dry
Sequoyah 1 (PWR)	Ice Condenser
St. Lucie 2 (PWR)	Dual
Surry 1 (PWR)	Subatmospheric
Peach Bottom 2 (BWR)	Mark 1

Available information on valve and penetration size, type, and normal, shutdown and accident status (e.g., open or closed) was cataloged.

This review indicated that similarities exist for the penetrations and valve designs for the above containment types. For example, they all contain such large penetrations and valves as equipment hatches, personnel air locks, and purge/vent valves. However, many differences are noted, particularly, between PWR and BWR designs.

The simplest grouping of containment design is a PWR category and a BWR category. This grouping may be useful for general reliability comparisons. More specific reliability comparisons and consideration and of potential improvements (e.g., continuous containment pressure monitoring systems) would require more containment type specific and even plant specific analyses. The Detailed Review and Analysis Task will further investigate differences in performance of the different containment designs.

In support of this design review, applicable standards and guidelines related to CIS design and performance were identified and reviewed. A summary compilation was made of these standards and guidelines to provide background information for the operating experience review task.

OPERATING EXPERIENCE REVIEW

The primary sources of information concerning operating experience with containment isolation systems were the Licensee Event Reports (LERs). Additional information was gathered from NRC inspectors, containment leakage testing reports, and the technical literature. The Nuclear Safety Information Center (NSIC) data base was screened for failures of containment isolation valves and penetrations as recorded in the LERs. Using a cutoff date of May 1983, approximately 3000 entries were

identified which could be of potential interest. LER abstracts were reviewed for these incidents and a classification scheme was developed. Figure 1 provides an example of the coding form used for data extracted from the LER abstracts. This information was assembled into a computer data base using the d-BASE II program and an IBM-PC. This section provides discussion of the general findings from the various sources of information on CIS operating experience.

Trends Observed In Reviewing LER Abstracts

Of the 3100 LER (and Abnormal Occurrence Report) abstracts from April 1965 through May 1983 reviewed for failures related to CISs, approximately 2000 were found to be applicable, i.e., relating to failures to isolate and/or excessive leakage. Since some LERs describe multiple failure incidents, the total number of applicable CIS failure incidents extracted from these abstracts is approximately 3000. Thus, for every three LERs classified as CIS-related in the Nuclear Safety Information Center data base, one can expect two to address CIS failures to isolate and/or excessive leakage.

Failure Trends For Isolation Valves

Valve failures accounted for approximately 70% of all applicable CIS failures. Leakage was observed to be the most frequent type of isolation valve failure in the LER Review. Most often, seat damage due to foreign material was the cause of the leakage. Seat corrosion, general seat wear, and packing leakage were other frequently observed failure causes. Failures of isolation valves to close were usually found to be caused by the following:

Valve operator failure/problems

Packings (generally too tight, thereby causing torque switches to kick out before full closure)

Interruption of valve operator power/air supply

Figure 1. EXAMPLE LER CODING FORM

Identification Information

Data Base # 0013 LER # 83-005 Revision # 0

Accession # 181872 Failure # 1

Component Information

Type: Main V Sub-1 B Sub-2 __

Location A Manufacturer L200

Reactor: Name VY1 Type B NSSS Vendor G

System: Primary 29 Secondary 05

Emergency Boilder Feed Pump Steam Line

Failure Information

Date 02/ 03/ 83 Power Level 87% Failure Mode B

Cause: Parimary 10 Secondary 09

Duration 1/ 12/ 0-A Containment Isolated? ____

Discovery N Corrective Actions B,A

Related LERs 82-015m 83-001

Comments

Failure of isolation valves V-16-20-20 and V-16-20-22B discovered due to high nitrogen makeup flow. Valves closed after several remote actuations. Failures were common-cause due to collection of ferrous metal particles on magnet of valve position indicator. Particles came from corrosion on inside of carbon steel piping. Fix = installation of Y-strainer with magnetic insert upstream of valves.

The valve operator problems accounted for approximatley 40% of the failures to close, with air solenoids and limitorque operators comprising the majority of these. In the case of air-operated solenoid valves, the solenoid failure was often caused by contaminated air. In several incidents, less clean service air was bled into the cleaner instrument air supply. Solenoids have shown a tendency to stick due to baking of oil contained in the air supply. The Zion plants have been especially susceptible to these air-operated solenoid valve problems.

Failure Trends For Penetrations

Penetration failures accounted for approximately 30% of all CIS failures. Approximately 90% of the penetration failures in the LER Reveiw were attributable to personnel air lock (PAL) problems. Primary failure causes were as follows:

Leakage past door seal gaskets

Leakage due to foreign material on seals

Failures to close due to interlock mechanism failures or maladjustment

PAL failures accounted for the majority of failures to isolate (as opposed to excessive leakage).

Failure Trends In BWRs

Primary containment failure/problems for BWRs are most often related to valve failures to close or excessive leakage. Leakage past MSIVs was especially frequent (much more than in PWRs), often involving as many as 15 valves leaking in excess of technical specifications. MSIV failures to isolate were rarely reported, although the number of MSIVs usually reported as being involved in an incident leads one to speculate that pairs of valves (inboard and outboard) may have been involved.

Failures to close were most often attributable to valve operator problems, closing on foreign materials, and separation of the valve disk from the valve stem (a mechanical control parts failure). Other BWR valves experiencing problems include vacuum breaker valves, containment vent valves, and traversing in-core probe valves.

Failure Trends in PWRs

PAL leakage dominated the CIS failures in PWRs, accounting for approximately half of the LERs for PWRs. PAL seal problems were caused primarily by dirt, again, and foreign material damage. Failures of one or both of the PAL doors to close and latch were also reported frequently. Often, one of the doors would not latch. When the operator opened the other door, the pressure differential would cause the unlatched door to swing open. This type of failure was almost always caused by problems with the interlock mechanism. However, many of the incidents involving simultaneous opening of PAL doors were attributed to "operator error." Also noteworthy is that PAL failures often occurred while the plant was at or near full power.

Remaining problems in PWRs involved valve leakage and/or failures to close. Although much less frequent than in BWRs, MSIV leakage incidents were reported for the PWRs. These incidents followed the same trends as discussed for the BWR MSIVs. Excessive leakage through large purge isolation valves was another prevalent type of valve failure at the PWRs. Environmental degradation of the valve seat was often responsible for the leakage.

Trends in Operator/Personnel-Induced Failures

Both BWRs and PWRs experienced CIS failures attributed to plant personnel. Such occurred relatively uniformly at both plant types. Common incidents involved the following:

Operators forgetting to close valves after testing or power transitions

Maintenance personnel incorrectly wiring or installing valves

Construction personnel damaging valves and penetrations during plant modifications or repairs

Incidents such as the above were often traceable to procedural deficiencies. Several incidents were also reported where holes were drilled through containment and left unsealed until discovered during an ILRT. These were attributed to personnel error.

General Reporting Trends in LERs

With reference to the information extracted from the LER abstracts for the LER Coding Form, the following data were found to usually be reported [>2/3 of the time].

Component identifier

System (in which located)

Failure mode and causes

Discovery mode

Corrective actions

The following data were sometimes reported [1/3-2/3 of the time]: Component type, location (relative to containment), and manufacturer.

Usually not reported [<1/3 or the time] were the following data:

Failure duration

Whether or not containment was isolated

Leak rates

LER abstracts on valve leakage tended to provide the least information, primarily due to a tendency to address several leak rate test failures in a single LER.

LER (and Abnormal Occurrence Report) abstracts from April 1965 through May 1983 were reviewed. From 1965 through mid-1977, the abstracts contained only general information about the incidents. Little of the specific information sought for the LER Coding Forms was provided. No definite numbering system for the incident reports was evident. Event dates and reactor power levels were reported inconsistently. The event descriptions provided in the abstracts were general, providing little specific information such as leak rates and valve types, locations, sizes, and manufacturers.

From mid-1977 through 1981, the quality of the abstracts improved. More detailed incident descriptions were provided. More of the specific information sought for the LER Coding Forms was found. However, some relapse in the reporting quality seems to have occurred with the most recent LER abstracts (1982-3). Sufficient information was still provided to permit completion of most of the items on the LER Coding Forms. However, this information was less complete than that found in the mid-1977 through 1981 LER abstracts.

Failures Resulting In High Leak Rates

In reviewing the LER data base several incidents were noted which had the potential for very high leakage rates. Since limited information was provided on leak rates or leak areas, a brief review was performed of failures involving valves and penetrations with a large leak potential. Three types of events are of interest: large penetration failures (e.g. airlocks); large valve failures (e.g. purge/vent valves); and direct breach of containment (e.g. drilling holes).

Many instances of failure of one airlock door or seal appear in the data base. A smaller number of failures of both doors or instances of leaving both doors were noted. The following incident is a typical example:

Date	Reactor	Cont Type	Event	Leak Rate
12/18/78	Arkansas Nuclear 1	Large Dry	Emergency hatch outer and inner doors left open	Leak rate function of hatch area but corrective action taken in seconds

Although the potential leak area is large for these type of events, airlock or similar penetration failures may not be of major concern due to the short failure duration and frequent testing interval. The large number of failures do indicate some design problems which should be investigated.

Failures of large valves have resulted in large leak rates. The data base contains a large number of single valve failures but failure of two valve is required for a large leak rate. Purge valves and vent valves are of interest because of their size and failure rates. Selected incidents are described below:

Date	Reactor	Cont Type	Event	Leak Rate
1973	Oconee 1	Large Dry	3 isolation valves open	No information
(Data Base #40205)				
1974	Ft. Calhoun	Large Dry	Vent valve failure	No information
(Data Base #30334)				
1974	Dresden 2	Mark I	Failure of 2 purge valve seats	No information
(Data Base #40203)				
1974	Dresden 3	Mark I	Failure of 2 purge valve seats	No information
(Data Base #40204)				
1976	Ft. Calhoun	Large Dry	2 purge valves leak	42 inch valves
(Data Base #30334)				
9/14/79	Palisades	Large Dry	2 cont exhaust by-pass valves left open	3 inch valves
(Data Base #40219)				

Based upon this cursory review, several valve failures with potentially large leak rates have occurred. The LER data base describes the failure mechanism but gives little or no information on the leak rates. The next section discusses another source of leak rate information, Integrated Leak Rate Test (ILRT) reports.

A quick search of the data base revealed no events in which containment was directly penetrated by events as inadvertent drilling. At least two such instances have been documented in ILRT reports (San Onofre 1 in 1977 and Surry 2 in 1980). These events did not appear in the LER data base which indicates they did not get written up as LERs or that the data base missed them. If either is true, additional support is lent to examining ILRT reports.

Summary Of Results Of NRC Inspector Survey

A number of NRC Senior Inspectors for containment systems were contacted and asked to relate their experience with CIS performance. Their experiences provide information regarding both hardware and procedural influences on CIS performance usually as indicated by the results of Type A, B and C tests. From a hardware standpoint, the most commonly noted problems concerned leakage in BWR MSIVs and PWR large purge isolation valves. Common causes of isolation valve leakage included seating problems, dirt/debris, and packing problems.

Procedures used in conducting tests appear to cause a variety of problems that could be interpreted as poor CIS performance. Some inspectors identified seat deformation as the main cause of leakage during testing of PWR large purge isolation valves (butterfly type). The inspectors also noted that, if these type valves are left open for a few hours prior to a test, the valve seats deform sufficiently to allow excessive leakage upon closing and immediate testing. Often, about an hour in the closed position is required before a valve seat will return to its normal configuration and seal sufficiently to pass the leakage test.

All the inspectors mentioned that reported leakage rates often do not represent true leakage rates. Utilities are generally allowed to perform some minor repair on a valve prior to recording its "as-found" condition for a leakage test. Similarly, major repair (such as completely rebuilding a valve) is permitted prior to recording that valve's "as-left" condition at the end of its leakage test. Type B and C tests are also performed before Type A tests, enabling repairs to be made so that the Type A tests can be passed easily.

In addition to the NRC inspector contacts, American Nuclear Insurers was contacted regarding their CIS performance related work that has been reported in the technical literature (Weinstein 1980). The goal of their work was to estimate an upper bound on the availability of containment integrity, and conversely, a lower bound on the unavailability of containment integrity. In developing their data base from a screening of LERs and integrated leak rate test reports, only those incidents where a definite leakage path was established through containment were considered. Certain classes of large valves were of particular interest (e.g., purge valves, vent valves, and MSIVs) since these valve types often fail in pairs, enabling leakage to exceed the allowed maximum. The American Nuclear Insurers containment integrity failure file currently includes incidents that have occured through 1982.

Potential Uses of Integrated Leak Rate (ILRT) Data

A review of reports resulting from ILRTs conducted at eighteen nuclear power plants during the period 1973 through 1983 was undertaken to determine the potential of these type reports as sources of data for use in the detailed review and analysis task. ILRT reports for the following nuclear power plants were reviewed. The reactor and containment types and the year during which the ILRT was conducted are presented in parenthesis.

- Millstone 1 (BWR, Steel Mark-1, 1973)
- Prairie Island 1 (PWR, Steel. Double, 1973)
- Arkansas Nuclear 1 (PWR, Prestressed Concrete, 1974)
- Brunswick 2 (BWR, Reinforced Concrete Mark-1, 1974)
- Calvert Cliffs 1 (PWR, Prestressed Concrete, 1974)
- Brunswick 1 (BWR, Reinforced Concrete Mark-1, 1976)
- Kewaunee (PWR, Steel Double, 1976)
- Donald C. Cook 1 (PWR, Reinforced Concrete Ice Condenser, 1978)
- McGuire 1 (PWR, Steel Ice Condenser, 1979)
- Donald C. Cook 2 (PWR Reinforced Concrete Ice Condenser, 1981)
- Sequoyah 2 (PWR, Steel Ice Condenser, 1981)
- Surry 1 (PWR, Reinforced Concrete Subatmospheric, 1981)
- Surry 2 (PWR, Reinforced Concrete Subatmospheric, 1981)
- Calvert Cliffs 2 (PWR, Prestressed Concrete, 1982)
- Maine Yankee (PWR, Reinforced Concrete, 1982)
- St. Lucie 1 (PWR, Steel Double, 1983)
- Crystal River 3 (PWR, Reinforced Concrete, 1983)
- Fort Calhoun 1 (PWR, Reinforced Concrete, 1983

The focus of these reviews was to develop an understanding of the type of information contained in the ILRT reports and ideas about how the information could be used in the process of evaluating containment performance under various accident conditions.

General Description Of ILRT Data Relevant To RACISP

The purpose of ILRTs is to demonstrate that leakage through primary reactor containment and systems and components penetrating the primary containment is less than the allowable leakage rates specified in the plant's technical specifications. Demonstration of containment integrity is accomplished by successful performance of local leak rate tests first and then the integrated primary containment leak rate test.

Local leak rate tests are performed individually on components which seal or penetrate the primary containment (Type B tests) plus all primary containment isolation valves (Type C tests). The integrated primary containment leak rate test (Type A test) is performed by pressurizing the entire containment structure and measuring the overall integrated leakage rate.

Generally, the ILRT reports reviewed contained some information about results of the Type A, B and C tests; however, the degree of detail available varied considerably. Narrative summaries describing the conduct of the Type A tests (including descriptions of test equipment, instrumentation used and analytical techniques used to compute leakage rates), initial plant conditions, a chronology of events occurring during the test (including the discovery of leaks), analysis of the Type A test data and a statement about successful completion of the tests were generally included in all the reports reviewed. Detailed numerical data about the Type A test were generally included in the reports in various forms (i.e., tabular and/or graphically).

Data from the Type B and C tests varied considerably in the degree and form in which it was reported. The report resulting from an ILRT conducted at Maine Yankee in 1982 contained data from Type B and C tests conducted in 1980 and 1981. This data was presented in two tables making it easy to compare leakage rates found for given systems or component during that two-year time period. A similar reporting format was used in the St. Lucie 1 ILRT report. Other reports provided some data from previously conducted Type B and C tests but in less convenient formats, while others provided only limited data from conducted in conjunction with the ILRT being reported. In some reports the system or component tested was identified by title; while in other reports, systems or component identification was by a code or number which would require referring to the plant FSAR for further specification.

Various other types of information such as system drawings, procedure change descriptions, test checklists, computer code descriptions, and measuring equipment calibration certifications were also included in the ILRT reports reviewed. This type of information is probably not very useful to the objectives of RACISP.

Information Available in ILRT Reports

Basically the information contained in ILRT reports that may be useful to RACISP appears to be the narrative descriptions of the Type A and the numerical data resulting from the Type A, B and C tests.

The narrative descriptions provide information concerning leaks that are discovered during pressurization of primary containment. Discovery of a leak during pressurization for the ILRT was reported in many of the reports reviewed. In every case pressurization was halted while the source of leakage was identified and either repaired or isolated. After repair or isolation, pressurization contained and the ILRT proceeded until it successfully concluded. In some cases the leakage rate and the system or component are specifically identified in the narrative.

The numerical data resulting from the Type A, B and C tests described in the ILRT Reports can provide useful information on the overall condition of containment integrity. As previously indicated, the LER data base contains little information on leak rates and duration times. Information from the over 300 ILRT reports which have been generated can supplement the LER data base and provide essential information on leakage areas. Several organizations have performed report reviews of ILRT reports. Oak Ridge National Laboratory (ORNL) (Dougan 1984) reviewed selected ILRTs in support of the Appendix J revision. Quadrex (Rowley et al. 1983) reviewed a large amount of Type A tests to study testing time reduction. Stone and Webster (Frank et al. 1982) reviewed selection ILRTs and assisted in developing improved test procedures. However, none of these reviews have examined the ILRTs to extract leakage rate data. It is recommended that the RACISP program perform a more detailed review of available ILRT reports and use this inforation to supplement the LER data base.

RELATED RESEARCH REVIEW

A search was conducted for information on current projects and documents from completed projects which were directly related to the RACISP. Brief descriptions of each of the projects were prepared. The projects were summarized under two headings: "Current Projects" and "Completed Projects". Each project description includes, where available: project title, performing organization, project manager, objectives, major activities, and comments. Major pertinent documents already published in the project are included. Examples of projects reviewed include ongoing work on containment integrity at Sandia National Laboratories; the ongoing containment leak rate estimation program being coordinated by the Idaho National Engineering Laboratory; and the completed containment systems experiment program performed by Pacific Northwest Laboratory.

Some additional studies with particular relevance to FACISP include: the ORNL (Dougan 1984) review of ILRT reports in supprot of the Appendix J revision; the Quadrex (Rowley et al. 1983) review of Type A test results in support of ILRT testing time reduction; and the Stone and Webster (Frank et al. 1982) review of selected ILRTs to assist in developing improved test procedures.

DETAILED REVIEW AND ANALYSIS

The data discussed in the previous sections form the basis for the Detailed Review and Analysis Task. The objective of this task is to characterize to the extent possible containment isolation system reliability in terms of leakage area versus leakage probability for selected reference designs. Work was recently initiated using the approach discussed below.

St. Lucie 2 and Peach Bottom 2 were selected as a reference PWR and BWR. The major penetrations and valves were categorized for each plant. Failure frequency estimates are being generated from the LER data base. These values are also being compared to predicted frequency estimates using reactor safety data bases (e.g., WASH-1400). Leakage rate/area estimates are being generated from available data. The LER data base has provided only limited information on leakage rates and failure durations. Predictive models and information from selected ILRT reports are being used to supplement the LER data base. These estimates of leakage probability and leakage area for each of the major penetrations and valves will be combined to generate preliminary plots of probability of leakage versus leakage area for the reference PWR and BWR.

REFERENCES

Blejwes, T. E., et al. 1982. Background Study and Preliminary Plans in a Program on the Safety Margins of Containments. NUREG/CR-2549, Sandia National Laboratories, Albuquerque, New Mexico.

Dougan, J. R. 1984. Evaluation of Containment Leak Rate Testing Criteria. NUREG/CR-3549, Oak Ridge National Laboratory, Oak Ridge, Tennessee.

Frank, S., B. C. Kueckler, and H. J. Kunkel. 1982. Containment Integrated Leak-Rate Testing Improvements. EPRI NP-2726, Stone and Webster Engineering Corporation, Boston, Massachusetts.

Rowley, C. W., T. E. Renton, and K. Martin. 1983. Criteria for Determining the Duration of Integrated Leakage Tests of Reactor Containments. EPRI NP-3400, Quadrex Corporation, Tulsa, Oklahoma.

Weinstein, M. B. 1980. Primary Containment Leakage Integrity Availability and Review of Failure Experience. Nuclear Safety 21(5): 618-632.

SHORTENED DURATION ILRT'S VERSUS ILRT FAILURE DETECTION

Carl L. Larsen and Terrence E. Renton
Quadrex Corporation
4500 S. Garnett, Suite 500
Tulsa, OK 74146

ABSTRACT

The shortened duration ILRT (e.g., less than 24 hours) has always been of significant interest to the nuclear utility industry. Not surprisingly, this interest is due to the fact that most ILRT's are typically conducted on the critical path of an outage. The key requirment for a shortened impact on the critical path is a method to determine the minimum number of hours after stabilization that would accurately represent containment leakage. Compounding the issue of shortened duration test methodology is the existence of three different analytical techniques to reduce the data. These techniques are known as: point-to-point, total time and mass point.

The purpose of this paper is to present an argument favoring shortened duration testing and illustrating that the EPRI criteria (as contained in EPRI NP-3400) can be used to determine the duration of an ILRT. The essential element in the arguments presented is that performing a shortened duration ILRT does not prevent reliable ILRT failure detection.

INTRODUCTION

The basis for this paper is taken from research performed by Quadrex Corporation for EPRI which was culminated by the issuance of a report (EPRI NP-3400) entitled "Criteria for Determining the Duration of Integrated Leakage Rate Tests of Reactor Containments", and subsequent independent research. As a result of these efforts over 90% of all domestic ILRT reports and several international ILRT reports have been obtained as a data base. This data base and the subsequent analysis have allowed tabulation of the ILRT's as either successful or unsuccessful. These two tabulations were then categorized by time expired as to when the ILRT results first gave indications of successfully or unsuccessfully meeting the allowable leakage rate criteria. For those ILRT's which were successful, the EPRI criteria

were used to determine the earliest time at which the test could be considered successful in accordance with the applicable termination criteria. For those ILRT's which were unsuccessful, the believed failure causes and remedies were tabulated and analyzed.

BACKGROUND

The primary purpose for an ILRT is to provide continued assurance that in the event of a design basis accident the containment structure will properly function to control the release of radioactivity to the environment within established limits and thereby provide for protection of the health and safety of the public. The detailed regulatory requirements pertaining to an ILRT (and associated local leak rate testing) are provided in 10CFR50, Appendix J.

Guidance from the USNRC relating to shortened duration testing is not included in the Commission's rules and regulations, except as provided by reference to ANS N45.4-1972. This standard provides little guidance and methodology which can be used to determine both the time of stabilization and the minimum number of hours after the test that will permit accurate determination of containment leakage. Instead, the standard and the USNRC Staff (except as addressed by Bechtel Topical Report BN-TOP-1) arbitrarily establish a test duration of 24 hours which typically results in tests lasting upwards of 4 to 5 days from pressurization to depressurization.

The only methodology currently sanctioned by the USNRC for use in a shortened duration test is that contained in BN-TOP-1. This report, however, uses the total-time technique for data reduction and includes extremely conservative acceptance criteria which may lead those attempting to utilize this method to ultimately perform a 24 hour test. The more accepted mass point technique for data reduction, contained in ANSI/ANS 56.8-1981, is not addressed by this report, which results in a major disconnect in sanctioned methodology versus accepted industry practice.

The EPRI criteria, developed by Quadrex Corporation, provides the needed connection between accepted industry practice and reasonable (reliable) methodology. This criteria provides the nuclear industry with a methodology

for shortened duration ILRT's that incorporates commonly accepted and utilized technical criteria.

DISCUSSION

As discussed in EPRI Report No. 3400, Quadrex has proposed seven (7) criteria for determining the completion of an ILRT. These criteria are:

1. Use the absolute method, mass point technique.
2. The containment must be adequately modeled (e.g., sensors and weighting factors).
3. The 95 percent upper confidence level leakage rate must be zero or a positive value.
4. The calculated LSF leakage rate must be less than 75 percent of the plant's allowable leakage rate criteria at test pressure.
5. The calculated 95 percent upper confidence level must be less than 75 percent of the plant's allowable leakage rate criteria at test pressure.
6. The calculated least squares fit leakage rate as a function of time shall have stabilized with a negligible positive or negative slope.
7. The calculated 95 percent upper confidence level leakage rate shall be converging with the LSF leakage rate.

As postulated, when all seven (7) criteria are met concurrently, the test can be terminated and can be considered completed successfully. Continuing the test beyond this point should not significantly affect the test results unless a significant physical change occurs.

A total of 247 ILRT reports have been reviewed in preparation for this paper. Of the 247 reports reviewed, 171 had sufficient information regarding test duration of direct use. Table 1 provides a listing, by plant, of all test reports reviewed and indicates the reported duration for the ILRT (Type A). Of the 247 reports, 53 were subjected to the EPRI criteria. In 47 of these tests the EPRI criteria would have permitted a shorter duration in the test. The average test duration of these 47 tests using the EPRI criteria would have been approximately nine hours versus the average actual test duration of 20 hours. Table 2 provides a comparison of the actual final reported duration and LSF leakage rate to the EPRI

criteria duration and reported LSF leakage rate at the respective termination times.

In those instances where the actual test only marginally met the termination (acceptance) criteria, the EPRI criteria did not permit any reduction in test duration. In a recent ILRT conducted by Quadrex Corporation, the EPRI criteria proved to be particularly responsive to even small perturbations in the sensor data. While the EPRI criteria were not used as test termination criteria, this test did provide substantiation that the EPRI criteria are responsive and conservative in predicting test termination.

In 96 of the 247 ILRT reports, or approximately 39% of the total, the Type A test possibly failed or was unsuccessfully completed. The failures were recognized and the Type A test was interrupted or aborted before the Type A phase had begun. Test failure is likely to be detected early, and therefore a change in methodology will create little impact. The causes of Type A test failure or unsuccessful completion were predominately due to valve failures. Over 60%, or 58 out of 96 test failures were attributed to valve and penetration problems (e.g., lineup, error, leakage, failure, etc.). The vast majority of these failures should have been discovered as a part of the local inspection program (pre-Type A test inspection) or as part of the Type B and C local leakage rate test (LLRT) program. Proper administrative control, procedure compliance and full recognition of the importance of the LLRT program could have conceivably prevented a large number of these "failures". In each case, however, when failure occured it was very early into the Type A test program; frequently during pressurization or stabilization.

The desirability of shortened duration ILRT's is intuitively obvious. Assuming a net replacement cost value of 3 cents per kilowatt-hour generated and an 800 megawatt plant, the net savings would be $24,000 for each hour that the test was shortened. Using the results of the investigation presented above, the 11 hour savings in test duration could produce a savings, per plant, of $264,000; far in excess of the cost of the test itself. Further, assuming that on the average there are 15 ILRT's performed

in the U.S. each year, such an average reduction in test duration could result in a savings of nearly $4 million to the nuclear industry.

REGULATORY PERSPECTIVE

The Code of Federal Regulations, Title 10, Part 50, Appendix J, (Reference 1) endorses ANSI N45.4-19072. Proposed changes to this regulation endorse ANSI/ANS 56.8 (through a proposed Regulatory Guide); however, substantial regulatory position statements reduce the true effectiveness of this endorsement. Nevertheless, this change will result in the long awaited formal sanction of the mass point technique by the USNRC Staff.

CONCLUSION

On the basis of the information and data presented above and in the EPRI Report NP-3400, it is obvious that a need exists to fully investigate recent advancements in the methodologies applicable to shortening the duration of a nuclear power plant ILRT. The driving force is certainly more than a reduction in the total duration of the test; it is the economic incentive.

Work performed by Quadrex Corporation clearly indicates that there is no reasonable doubt as to the viability and validity of the EPRI criteria. In addition, increased emphasis needs to be placed on Type B and C testing due to their obvious connection with early Type A test failures. It is our conclusion that such a program of improved Type B and C testing along with the use of a proven (and reasonable) shortened duration Type A test criteria (such as the EPRI criteria) can produce effective containment testing. Tne overall objective is minimize the duration of ILRT's, thus improving plant economics by reducing critical path outage time, while maintaining an acceptable and technically accurate approach.

REFERENCES

1. 10 CFR 50, Appendix J, Primary Reactor Containment Leakage Testing for Water-Cooled Power Reactors, as amended.

2. ANSI N45.4-1972, Leakage Rate Testing of Containment Structures for Nuclear Reactors, American Nuclear Society through American Nuclear Standards Institute, 1972.

3. BN-TOP-1, Testing Criteria for Integrated Leakage Rate Testing of Primary Containment Structures for Nuclear Power Plants, Bechtel Corporation, 1972.

4. ANSI/ANS 56.8-1981, Containment System Leakage Testing Requirements, American Nuclear Society through American Nuclear Standards Institute, 1981.

5. Electric Power Research Institute, EPRI NP-3400, Criteria for Determining the Duration of Integrated Leakage Rate Tests of Reactor Containments, prepared by Quadrex Corporation, 1983.

Table 1

PLANT SUMMARY OF TESTING TIME DURATIONS

PLANT NAME	YEAR	DURATION IN HOURS
ANO 1	1973	8.5
ANO 1	1978	24
ANO 1	1981	10
ANO 2	1977	8
ANO 2	1981	8
BEAVER VALLEY 1	1975	24
BEAVER VALLEY 1	1978	24
BIG ROCK POINT	1974	--
BIG ROCK POINT	19	24
BROWN'S FERRY 1	1973	24 FULL/24 HALF
BROWN'S FERRY 1	1976	26
BROWN'S FERRY 1	1980	27.05
BROWN'S FERRY 2	1974	25 FULL/24 HALF
BROWN'S FERRY 2	1983	13.5
BROWN'S FERRY 3	1979	24
BRUNSWICK 1	1976	24 FULL/24 HALF
BRUNSWICK 1	1981	24
BRUNSWICK 2	1977	24
BYRON 1	1983	24 FULL/24 HALF
CALVERT CLIFFS 1	1973	9 FULL/8.75 HALF
CALVERT CLIFFS 2	1979	8.15
CONNECTICUT YANKEE	1976	24
CONNECTICUT YANKEE	1980	24
COOK 1	1978	14
COOK 2	1981	24
COOPER	1973	24 FULL/24 HALF
COOPER	1976	NO REPORT
COOPER	1980	14
COMANCHE PEAK 1	1983	25

PLANT NAME	YEAR	DURATION IN HOURS
CRYSTAL RIVER 3	1976	24
CRYSTAL RIVER 3	1980	24
DAEC	1978	10.25
DAEC	1980	8
DAVIS-BESSE	1976	24
DAVIS-BESSE	1980	8
DIABLO CANYON 1	1975	35 FULL/24 HALF
DIABLO CANYON 1	1978	20
DIABLO CANYON 2	1977	24
DRESDEN 1	1975	24
DRESDEN 1	1977	24
DRESDEN 2	1976	25.5
DRESDEN 2	1983	12
DRESDEN 3	1982	24
GINNA	1972	NO REPORT
GINNA	1976	NO REPORT
FARLEY 1	1981	25.25
FARLEY 2	1980	12.5
FITZPATRICK	1978	26
FITZPATRICK	1982	24
FORT CALHOUN	1976	13
FORT CALHOUN	1980	24
GRAND GULF 1	1982	8
HATCH 2	1978	8
INDIAN POINT 2	1971	24
INDIAN POINT 2	1976	24
INDIAN POINT 2	1979	24
INDIAN POINT 3	1975	24 FULL/24 HALF
INDIAN POINT 3	1978	24
KEWAUNEE	1974	--
KEWAUNEE	1980	24

PLANT NAME	YEAR	DURATION IN HOURS
LaCROSSE	1975	24
LaCROSSE	1978	24
LaCROSSE	1979	24
LaCROSSE	1980	24
LaSALLE 1	1982	26.18
MAINE YANKEE	1975	24
McGUIRE 1	1979	24
MILLSTONE 1	1970	--
MILLSTONE 1	1973	--
MILLSTONE 1	1976	8
MILLSTONE 1	1981	41
MILLSTONE 2	1975	--
MILLSTONE 2	1979	57
MONTICELLO 1	1980	8.20
NINE MILE POINT	1979	71.5
NORTH ANNA 1	1981	26
NORTH ANNA 2	1979	24
OCONEE 1	1971	10
OCONEE 1	1976	10
OCONEE 1	1980	65
OCONEE 2	1973	11 FULL/10 HALF
OCONEE 2	1977	10
OCONEE 2	1980	14.5
OCONEE 3	1974	10
OCONEE 3	1978	24
OCONEE 3	1981	20
OYSTER CREEK	1978	24
OYSTER CREEK	1980	24
PALISADES	1974	24
PALISADES	1978	--
PALISADES	1982	--

PLANT NAME	YEAR	DURATION IN HOURS
PEACH BOTTOM 2	1976	8
PEACH BOTTOM 2	1980	8
PEACH BOTTOM 3	1977	--
PEACH BOTTOM 3	1981	8
PILGRIM	1980	34
PILGRIM	1982	24
POINT BEACH 1	1970	24 FULL/24 HALF
POINT BEACH 1	1977	12
POINT BEACH 1	1981	8
NINE MILE POINT 1	1981	24
NINE MILE POINT 1	1983	8.75
PEACH BOTTOM 3	1974	24 FULL/9.5 HALF
POINT BEACH 2	1971	24 FULL/24 HALF
POINT BEACH 2	1978	12
POINT BEACH 2	1982	12
PRAIRIE ISLAND 1	1973	24 FULL/24 HALF
PRAIRIE ISLAND 1	1977	--
PRAIRIE ISLAND 1	1980	10.?
PRAIRIE ISLAND 2	1977	24
PRAIRIE ISLAND 2	1981	NO REPORT
QUAD-CITIES 1	1976	24
QUAD-CITIES 1	1979	24
QUAD-CITIES 2	1980	24
RANCHO SECO	1974	24 FULL/24 HALF
RANCHO SECO	1977	24
RANCHO SECO 1	1983	10.75
ROBINSON 2	1978	24
ROBINSON 2	1982	24
SALEM 1	1979	24
SALEM 1	1980	--
SAN ONOFRE 2	1980	24
SAN ONOFRE 3	1982	8

PLANT NAME	YEAR	DURATION IN HOURS
SEQUOYAH 1	1979	NO REPORT
SEQUOYAH 2	1981	24
SHOREHAM 1	1982	24
ST. LUCIE 1	1975	24 FULL/24 HALF
ST. LUCIE 1	1979	24
SURRY 1	1981	33.51
SURRY 2	1972	24
SURRY 2	1976	24
SURRY 2	1980	12
SURRY 2	1981	63.99
THREE MILE ISLAND 1	1974	24 FULL/24 HALF
THREE MILE ISLAND 1	1978	44.5
THREE MILE ISLAND 1	1981	24
THREE MILE ISLAND 2	1981	17
TROJAN 1	1975	9 FULL/8.75 HALF
TROJAN 1	1979	24.5
TURKEY POINT 3	1972	NO REPORT
TURKEY POINT 3	1975	24
TURKEY POINT 3	1979	8
TURKEY POINT 3	1982	24
TURKEY POINT 4	1973	NO REPORT
TURKEY POINT 4	1976	24
TURKEY POINT 4	1980	41
VERMONT YANKEE	1974	24
VERMONT YANKEE	1978	37
VERMONT YANKEE	1979	24
VERMONT YANKEE	1980	--
YANKEE ROWE	1974	24 FULL/26 HALF
YANKEE ROWE	1977	NO REPORT
YANKEE ROWE	1980	31
ZION 2	1977	40
ZION 1	1981	215
ZION 2	1980	26

DATA SUMMARY

Test Duration	Number Tests	% of Total No.
< 8 HRS.	13	7.6%
> 8 AND < OR = 12 HRS.	22	12.9%
> 12 AND < OR = 16 HRS.	6	3.5%
> 16 AND < OR = 20 HRS.	2	1.2%
> 20 AND < 24 HRS.	0	N/A
= 24 HRS.	83	48.5%
> 24 HRS.	26	15.2%
DURATION NOT SHOWN/NO REP:	19	11.1%
TOTAL NUMBER OF TESTS:	171	100.0%

TABLE 2

COMPARISON OF ACTUAL vs CRITERIA TEST DURATION AND REPORTED LEAKAGE RATE

	DURATION OF TESTS IN HOURS			LEAKAGE RATE REPORTED		
	Actual	Allowed by Criteria	Difference	Actual	Allowed by Criteria	Absolute Value
1. ARKANSAS NUC UNIT 1 1981	9.75	6.75	3.00	.0382	.0361	.0021
2. ARKANSAS NUC UNIT 2 1981	10.00	9.25	.75	.0271	.0292	.0021
3. BEAVER VALLEY 1 1978	24.00	13.00	11.00	.0305	.0414	.0109
4. BROWN'S FERRY 3 1979	24.23	2.67	21.56	.1576	.2410	.0834
5. BRUNSWICK 2 1977	25.00	7.67	17.33	.3054	.2845	.0209
6. CALVERT CLIFFS 2 1979	8.25	4.75	3.50	.0523	.0380	.0143
7. COOPER 1980	13.67	10.67	3.00	.4209	.4115	.0094
8. CRYSTAL RIVER 3 1980	24.00	21.00	3.00	.1333	.1420	.0093
9. DAVIS-BESSE 1 1980	8.00	3.25	4.75	.0642	.0883	.0241
10. FARLEY 1 1981	25.25	17.25	8.00	.0441	.0768	.0327
11. FARLEY 2 1980	24.00	6.00	18.00	.0331	.1053	.0722
12. FITZPATRICK 1978	26.00	13.00	13.00	.2914	.2938	.0024
13. FITZPATRICK 1982	24.00	9.00	15.00	.2004	.2210	.0206
14. GRAND GULF 1982	8.00	2.75	5.25	.0736	.1038	.0302
15. LASALLE 1982	26.18	8.84	17.34	.3780	.3805	.0025
16. MILLSTONE 1 1976	24.00	8.00	16.00	.6128	.7767	.1639
17. MILLSTONE 1 1981	24.50	11.25	13.25	.2979	.5774	.2984
18. MILLSTONE 2 1979	15.25	3.25	12.00	.0622	.0020	.0602
19. NINE MILE POINT 1975	24.75	14.00	10.75	.7439	.8046	.0607
20. NORTH ANNA UNIT 1 1981	24.10	7.23	16.87	.0111	.0306	.0195
21. NORTH ANNA UNIT 2 1979	24.00	18.00	6.00	.0331	.0451	.0120
22. OCONEE UNIT 1 1980	24.00	8.75	15.25	.0220	.0377	.0157
23. OCONEE UNIT 2 1980	15.00	2.75	12.25	.0537	.0413	.0124
24. OCONEE UNIT 3 1981	14.92	9.92	5.00	.0307	.0228	.0079
25. PALISADES 1978	24.00	17.00	7.00	.0084	.0028	.0056
26. PALISADES 1982	23.00	8.00	15.00	.2001	.1103	.0898
27. PEACH BOTTOM UNIT 2 1981	8.00	4.50	3.50	.0113	.1246	.1133
28. PILGRIM 1980	28.00	8.67	19.33	.4170	.2992	.1178
29. PILGRIM 1982	23.00	11.00	12.00	.2002	.1855	.0147

TABLE 2 (continued)

	DURATION OF TESTS IN HOURS			LEAKAGE RATE REPORTED		
	Actual	Allowed by Criteria	Difference	Actual	Allowed by Criteria	Absolute Value
30. POINT BEACH UNIT 1 1981	12.00	8.75	3.25	.0804	.0967	.0163
31. POINT BEACH UNIT 2 1982	12.00	10.00	2.00	.0480	.0390	.0090
32. QUAD-CITIES UNIT 1 1979	22.75	15.00	7.75	.0054	.0002	.0052
33. QUAD-CITIES UNIT 2 1980	23.75	10.00	13.75	.4369	.5136	.0767
34. H. B. ROBINSON 2 1982	23.60	12.60	11.00	.0186	.0001	.0185
35. SAN ONOFRE UNIT 2 1980	24.00	9.25	14.75	.0576	.0614	.0038
36. SAN ONOFRE UNIT 3 1982	8.00	5.50	2.50	.0157	.0254	.0097
37. SEQUOYAH UNIT 1 1979	27.38	3.50	23.88	.0005	.0019	.0014
38. SEQUOYAH UNIT 2 1981	25.67	7.33	18.34	.1380	.1488	.0108
39. SURRY UNIT 1 1981	13.00	12.00	1.00	.0328	.0339	.0011
40. SURRY UNIT 2 1980	15.67	5.00	10.67	.0353	.0424	.0071
41. SURRY UNIT 2 1981	12.00	9.00	3.00	.0187	.0155	.0032
42. THREE MILE ISLAND 1978	44.50	17.00	27.50	.0607	.0343	.0264
43. THREE MILE ISLAND 1981	24.00	9.30	14.70	.0230	.0402	.0172
44. TROJAN 1975 HALF PRESSURE	9.00	9.00	-0-	.0007	.0007	-0-
45. TURKEY POINT UNIT 3 1979	12.00	6.00	6.00	.0975	.1207	.0232
46. TURKEY POINT UNIT 3 1981	12.00	5.25	6.75	.0314	.0358	.0044
47. TURKEY POINT UNIT 4 1980	15.67	6.33	9.34	.0318	.0414	.0096
48. YANKEE ROWE 1980	30.50	13.75	16.75	.0477	.0734	.0257
AVERAGES	19.67	9.22	10.45	.1278	.1354	.0315

DATA SUMMARY

Duration Time with use of Criteria:

< or = 8 hrs:	20	42%
Between 8 and 10 hrs:	13	27%
Between 10 and 12 hrs:	5	10%
Between 12 and 16 hrs:	4	8%
Between 16 and 20 hrs:	6	13%
TOTAL	48	100%

ON-POWER CONTAINMENT INTEGRITY MONITORING IN CANDU MULTI-UNIT STATIONS

G. D. Zakaib
Ontario Hydro
700 University Avenue
Toronto, Canada

ABSTRACT

Based on a general review of current on-power test methods and experience in CANDU multi-unit containments, it is concluded that such tests make a significant contribution to plant safety. In particular continuous monitoring at low pressure differentials merits further development and more widespread application.

Current on-power tests include individual component testing, quarterly reduced pressure tests (typically at -15 kPa (g)), and continuous pressure trend monitoring at normal operational pressure of -3 kPa(g). A continuous monitoring concept is outlined which consists of a periodically updated mass balance. Instrument error uncertainty for this technique was estimated to be on the order of a 1 cm hole. However systematic fluctuations (often attributable to physical causes) dominate the error analysis in on-power tests. With precautions on sampling interval, a moving regression may be used to generate a leakage rate time series such that the fluctuations can be bounded or eliminated.

Experience to-date has indicated that most containment boundary impairments are detectable by component tests or continuous monitoring. On-power tests methods are capable of addressing a significant portion of the containment failure mode spectrum. Station risk assessment and regulatory testing requirements are identified as means by which these methods can be creditted in demonstrating containment integrity.

INTRODUCTION

The provision of a physical barrier to mitigate the potential release of radionuclides represents a fundamental safety requirement at nuclear electric generating facilities. Implicitly this containment boundary must maintain a high degree of leak tightness during both normal operation and accident conditions. Leakage rate testing is the primary means of demonstrating this requirement is being met over the plant life.

The purpose of this paper is to indicate the type and quality of information that is available from on-power leakage rate tests and continuous monitoring of containment parameters.

System Description

The layout of a typical CANDU multi-unit station is illustrated in Figure 1. The cornerstone of the containment concept in such a station is the Vacuum Building. This large post-tensioned concrete structure is maintained at very low pressure (about 7 kPa abs (1 psia)). In the event of a pressure excursion (i.e. LOCA) in any unit, pressure activated relief valves open, enabling the Vacuum Building to rapidly draw containment pressure subatmospheric. A pressure activated water spray system in the Vacuum Building condenses any steam present, thus aiding the pressure reduction. Containment overpressures are therefore of low magnitude and short duration.

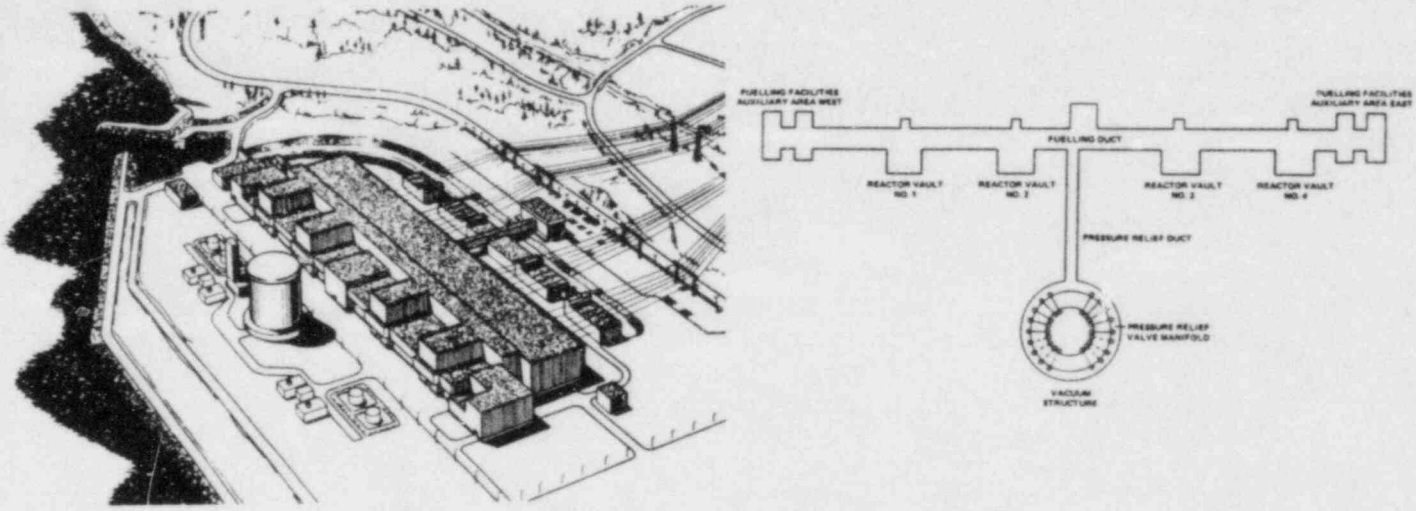

Figure 1. Example of Multi-Unit Containment Layout (Darlington GS)

The resultant effect is lower containment design pressures and less stringent leakage rate targets than other containment systems. Table 1 provides containment design parameters for multi-unit stations operated by Ontario Hydro. The design target leakage rate for all stations is based on 1 percent per hour of the contained air mass at the positive design pressure.

Two 'types' of containment are used. In earlier stations a unitized concept is employed, wherein a low pressure relief panel provides for atmospheric separation of the buildings. The shared containments are connected during normal operation by the fuelling machine ducts.

The reactor buildings and ducts are thick walled (typically 4 ft) conventionally reinforced concrete structures. Epoxy liners are the norm in the early stations with steel lining prevalent at the Bruce and Darlington stations.

Table 1 - Containment Parameters

Station	Reactors (Net Output)	Type	Volume	Positive Design Pressure
Pickering A & Pickering B	8-520 Mw(e)	Unitized	51,000 m^3 per reactor bldg	41 kPa(g) (6 psig)
Bruce A	4-750 Mw(e)	Shared	95,000 m^3 (Station)	69 kPa(g) (10 psig)
Bruce B	4-750 Mw(e)	Shared	95,000 m^3 (Station)	84 kPa(g) (12 psig)
Darlington	4-880 Mw(e)	Shared	150,000 m^3 (Station)	96 kPa(g) (14 psig)

CURRENT ON-POWER TEST METHODS

In keeping with the system-wide goal of achieving high station availability, information on containment integrity status is collected on-power. The methods employed may be grouped into the following categories.

1. Component Testing - This includes periodic pressure testing of airlocks, containment isolation dampers and penetration seal plate interspaces. Test periods vary from one month to five years. Active components such as airlock seals and isolation valves are tested more frequently than passive components.

   We can also include in this category periodic visual inspection (which may reveal incipient failures) and lab tests of non-metallic components.

2. Low Pressure Leakage Rate Tests - Typically performed four times annually, there are currently two types of tests in use. In the unitized containment concept, there is a significant amount of instrument air in-leakage for control valve operation. With containment isolation valves closed, analysis of the rate of pressurization indicates the presence of leakpaths for each building. The test is terminated in several hours, prior to approaching reactor trip setpoints. Constant power operation is maintained during the test interval.

   In the shared containment concept, the Vacuum Building is used to draw all the reactor buildings and associated ducts significantly below atmospheric pressure in a controlled manner. Once at pressure, typically -15 kPa(g) (-2 psig), leakage rate analysis is performed with measured instrument air in-leakage subtracted.

In order to interpret low pressure in-service test results a comprehensive commissioning program is undertaken. Leakage rates are measured over a complete range of pressures between the positive and negative design pressures. A good example is the results for Bruce A, illustrated in Figure 2. These results provide strong evidence for a reproducible laminar leakage assumption [1].

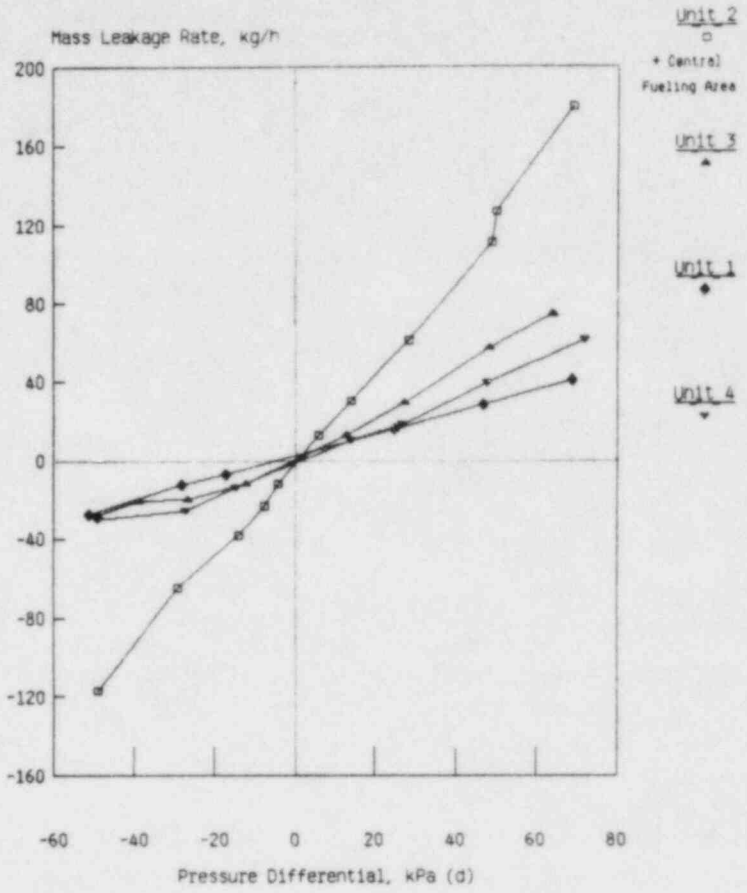

Figure 2. Bruce 'A' Commissioning Leakage Rate Data

3. Continuous Monitoring - The shared containments are continuously operated at about -3 kPa(g) (-0.5 psig) with continuous pressure trend monitoring. An abrupt change in containment integrity status is diagnosed by a change in computer generated pressure trend or a high containment pressure alarm (-1 kPa(g)) depending on severity. This capability along with exhaust flow metering represents a practical first approximation to the ideal continuous monitoring concept.

Leak tightness in the Vacuum Building is even more readily monitored since it continuously must operate at its design pressure differential. Not only is the pressure trend monitored between pumpdown phases, but vacuum pump running hours are also recorded. As well, atmosphere separation between the main vacuum chamber and a smaller upper chamber (required for spray system activation) is monitored. Integrity is confirmed by maintaining the two chambers about 3 kPa apart. The Vacuum Building will be excluded in future references to "continuous monitoring".

CONTINUOUS MONITORING CONCEPT

The continuous monitoring concept is illustrated in Figure 3. A purge fan connected to the heavy water Vapour Recovery System is the means by which the containment boundary is maintained subatmospheric. The Vapour Recovery System is normally used to maintain the reactor vault dew point very low (about -20°C) to conserve costly heavy water vapour and to minimize radiological hazards (i.e. tritium) for workers.

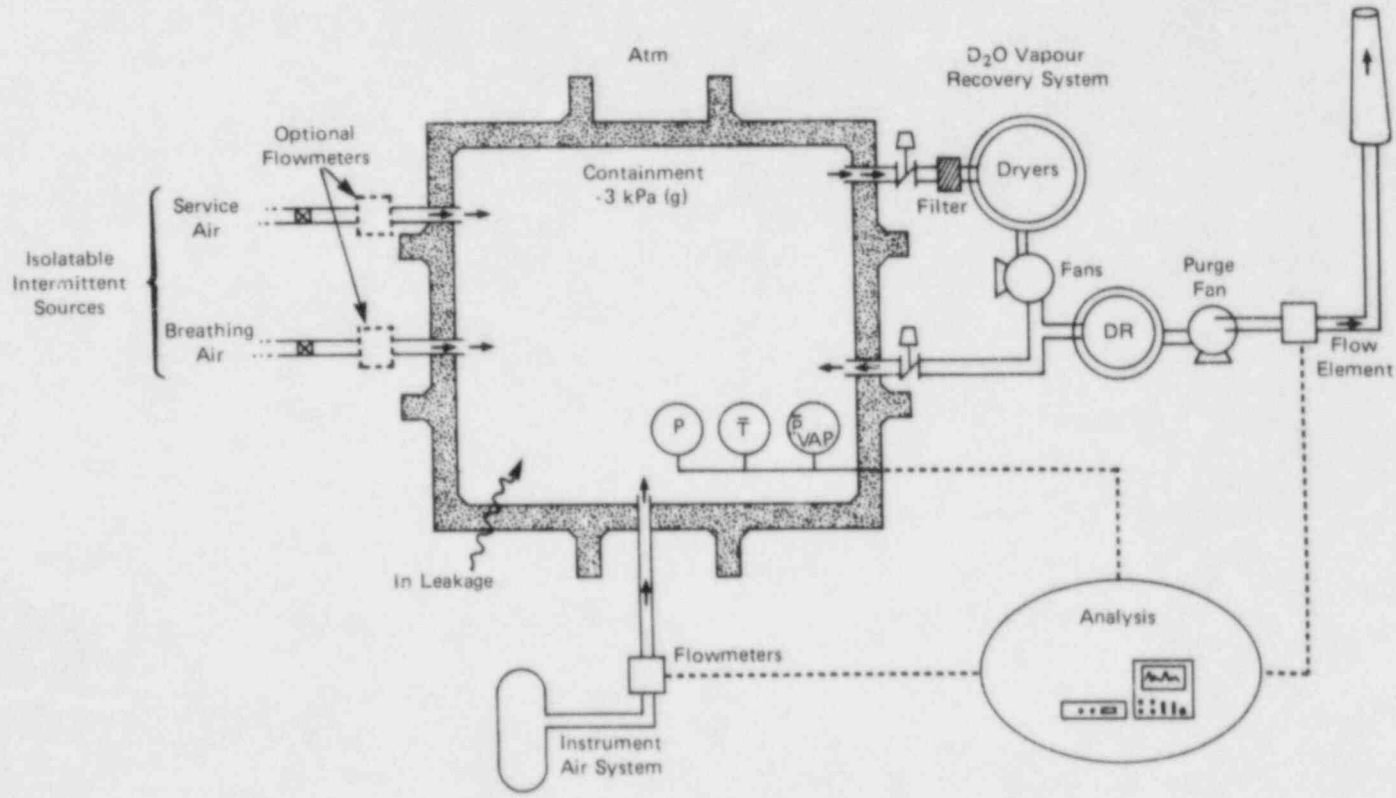

FIGURE 3
Continuous Monitoring Concept

The principle underlying an absolute measurement of containment leak tightness is that of continuously updated form of the mass conservation equation, integrated over a sampling interval.

$$\text{Rate of Mass Outflow} - \text{Rate of Mass Inflow} = \frac{dM}{dt}, \qquad (1)$$

where,

Mass Outflow = Measured outflow rate
Mass Inflow = Measured inflows + structural leakage rate

$\frac{dM}{dt}$ = Rate of change of air mass in containment as determined by regression analysis of mass vs time data using leakage rate instrumentation and ideal gas laws.

The outflow is measured by a hot wire-type flowmeter in the 20 cm (8 in) exhaust duct although other methods are being investigated. Each unit has an exhaust fan, but only one is needed to maintain containment pressure subatmospheric. Inflows may be monitored by rotameters on the smaller instrument air lines but in-line integrating gas meters are preferred. Whereas some instrument air is always required for control functions, service air and breathing air sources are intermittent (required during maintenance activities).

With readily available instrument errors and quarterly in-service leakage rate results we can estimate a target uncertainty for this technique. Flowmeters of the aforementioned types have accuracies better than 5 percent of scale and a typical in-service leakage rate may produce a result with an error bar of $\pm$ 10 kg/h for a 4 hour test. With these assumptions, and considering only random instrument errors for a 4 hour mass balance at -3 kPa(g), an uncertainty on the order of the leakage rate through a 1 cm hole is projected.

Non-random systematic errors, however, must also be taken into account. These errors can dominate and include factors such as thermal stability in an operating unit, process air in-leakage fluctuations, volume changes, etc.

ERROR ANALYSIS

Leakage rate analysis by the "Mass Plot" method is now widely accepted [1,2]. In this method the leakage rate is defined as the rate of change of contained air mass,

$$L = \frac{dM}{dt}, \text{ kg/h}. \qquad (2)$$

The best estimate of slope is the result of a linear regression applied to the mass vs time data. The mass is given by the ideal gas law,

$$M = \frac{(P - P_V)\ V}{R \quad T} \ , \text{kg} \qquad (3)$$

where,

P = absolute containment pressure, kPa(a)
P_V = water vapour partial pressure, kPa(a)
V = net free volume of containment, m^3
R = gas constant for air = 0.2871 kPa m^3/kg (air) °K
T = volume weighted average containment temperature, °K

Regression theory gives the following confidence interval for the leakage rate (slope). In computational form,

$$\delta = \tau_{95} \left[\frac{\Sigma M^2 - a\Sigma(Mt) - b\Sigma M}{(N-2)\ (\Sigma(t^2) - \frac{(\Sigma t)^2}{N})} \right]^{\frac{1}{2}} \qquad (4)$$

where a and b are the slope and intercept of the regression line respectively. τ_{95} is the value of the "Student's T" distribution for the 95 percentile with N-2 degrees of freedom.

However, it is necessary to recall some of the assumptions associated with a valid linear regression result. In particular,

(i) The errors should be normally distributed random errors with a mean of zero and a constant variance for all times, t.

and (ii) The errors are independent, such that the error at time t has no effect on the errors at time t+ Δt.

We have found that these assumptions are often violated during on-power tests with the consequences that the error estimate, given by Equation (4), is not credible. This is due to the presence of "systematic" errors or non-random fluctuations. They are often the result of actual physical variations in containment conditions such as those previously mentioned.

An example of this behaviour is shown in Figure 4A for a recent Pickering test. The residuals of the linear regression do not satisfy the aforementioned assumptions. This does not preclude obtaining a useful result however so long as sufficient time is allowed to bound the fluctuations. All fluctuations, regardless of cause, must vary within bounds which can be delineated or analyzed.

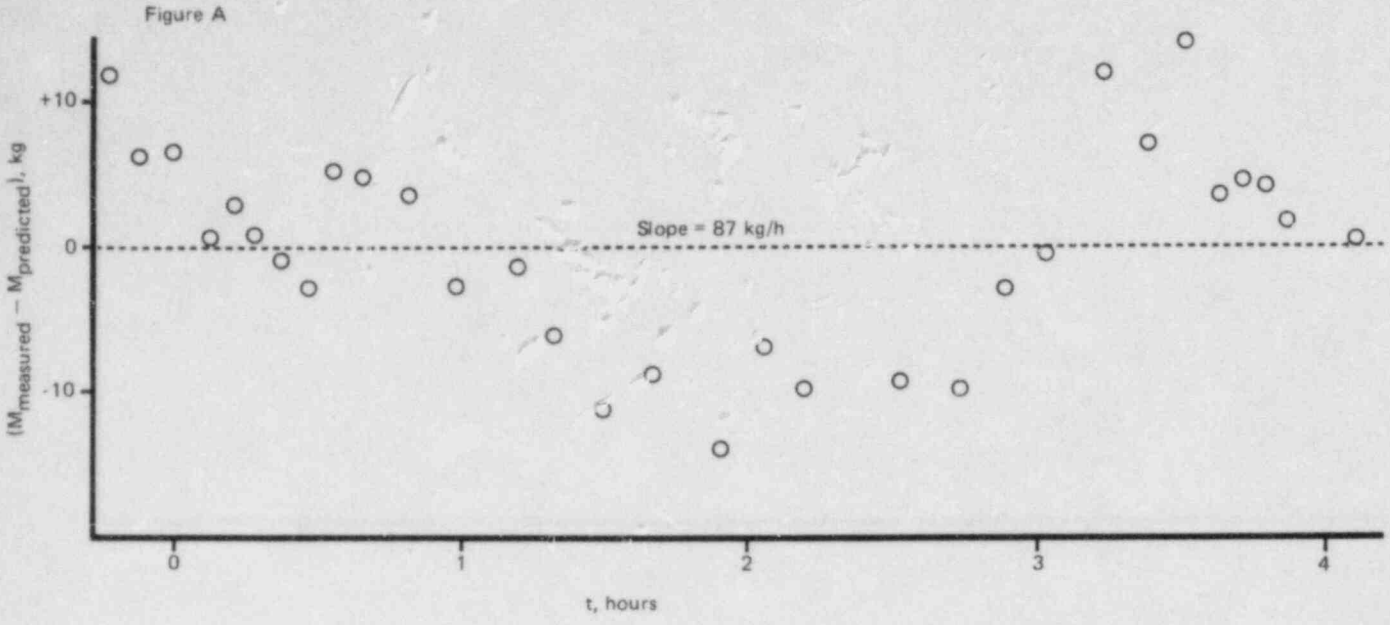

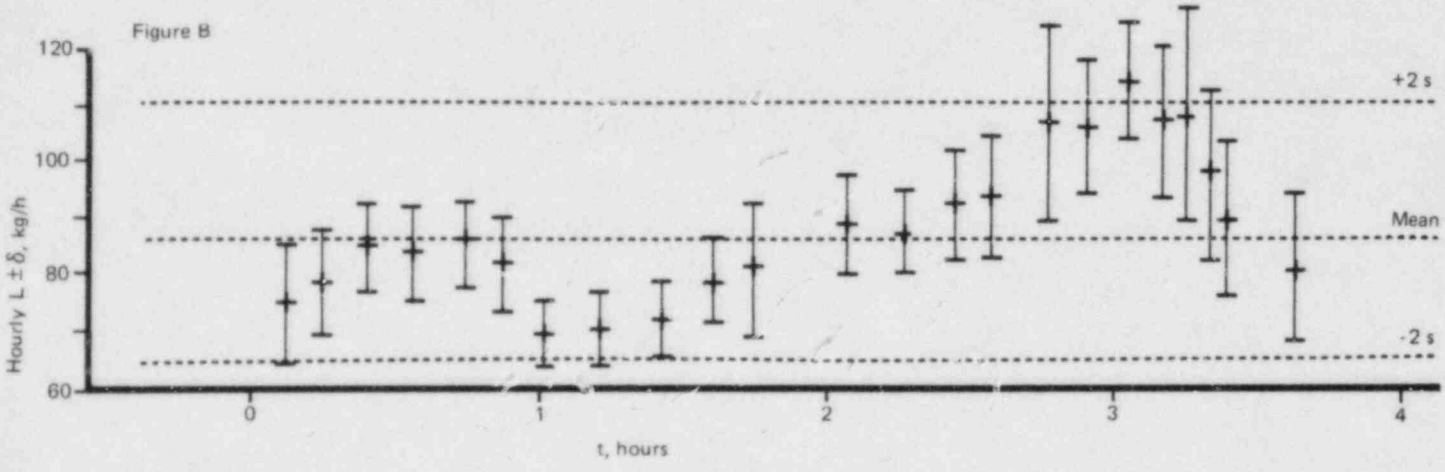

FIGURE 4
Example of Leakage Rate Test Results
with Systematic Fluctations

(A) Residuals Plot from Linear Regression Analysis (Mass Plot)

(B) Moving Regression Leakage Rate Results Based on Hourly Sampling
(Error Bands = 95% Confidence Intervals)

Test Conditions:
Pickering A, Sept. 1983
V = 51 000 m^3
Decay heat removal; all coolers
and driers operational.
ΔP = 13.8 kPa (g) (+2 psig)
Quartz manometer, 13 Pt RTC's

Techniques used in TIME SERIES ANALYSIS and short-term forecasting can be applied in these cases. The general approach is to decompose a time varying function Y(t) into trend, periodic (or seasonal) and random components.

$$Y = T \times P \times R \qquad (5)$$

The long-term trend (or mean value) can be determined by regression over the longest possible time period and divided out of Equation (5). Similarly the periodic component, if present, may be eliminated by computing the average peak to mean ratio over a number of cycles and dividing it out. Recall that for leakage rate evaluation we require a statistical bound on the analysis results. The residual random error from the decomposition process can be readily quantified statistically. More advanced techniques are available which make use of autoregression theory [3] and require computer analysis.

This method has been successfully applied when a periodic fluctuation due to daily volume changes or a seasonal fluctuation due to temperature effects has been diagnosed. For many cases however, the fluctuations will not be periodic or attributable to a known cause. Figure 4B shows how such a situation may be treated. Regression analysis is performed for subintervals of the total test time, and the regression is moved along as more data comes in, thereby tracking the fluctuations. The moving regression "averages" out the noise and minor fluctuations in the mass plot providing a reasonable accurate "view" of leakage rate with time. Note that in the process, information at either end of the test period is lost. Although Figure 4B shows the 95 percent confidence intervals for each data point, only the mean values of independent hourly samples are used to obtain the variance of the fluctuation. A 95 percent prediction interval, about $\pm$ 2 standard deviations in size, can then be created. The trend or mean slope is reasonably constant at about 87 kg/h in this case.

The key means of treating systematic error is sufficient time or a sufficient number of repeated measurements to bound or preferrably characterize the leakage rate-time spectrum. This point is illustrated in Figure 5A for the case of a hypothetical sinusoidal fluctuation of amplitude A and period T.

It is evident that the "error" declines with time and that the maximum error is approximately 2A/t. Hence the time required to reduce the error to less than 10 percent of the leakage rate is

$$\frac{2A}{t} \leq 0.1\ L\ . \qquad (6)$$

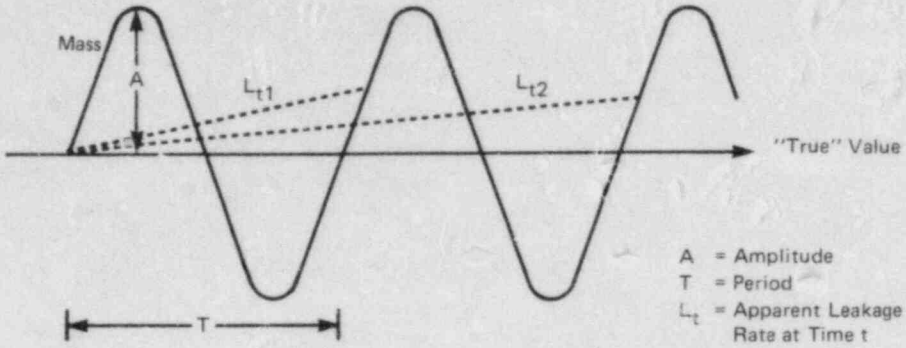

FIGURE 5a
Systematic 'Error' Modelled as Sinusoidal Fluctation
in Containment Mass vs. Time

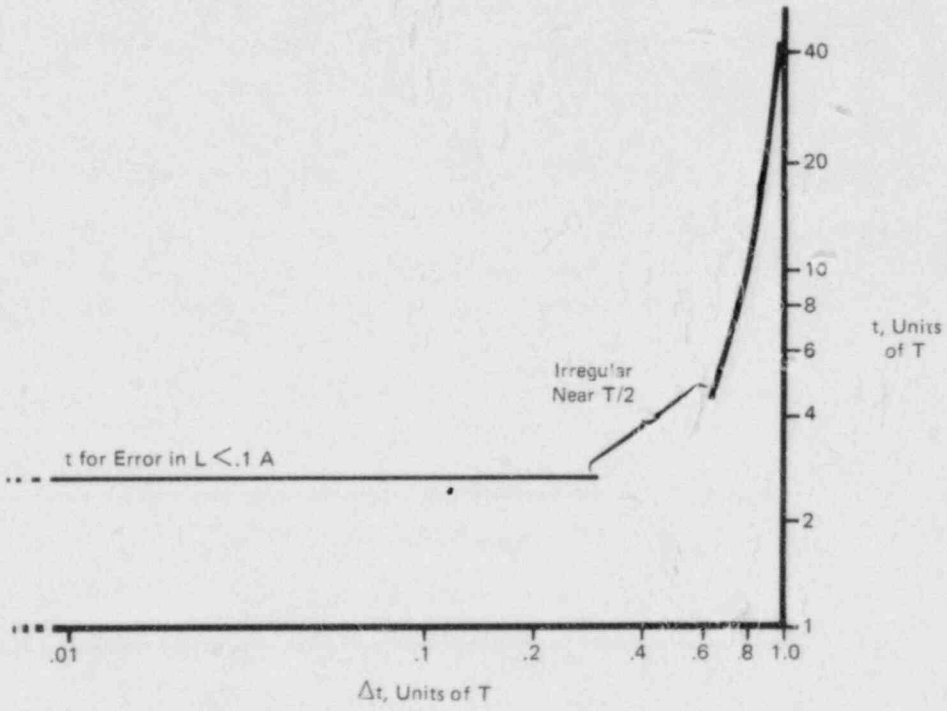

FIGURE 5b
Approximate Test Time (t) Required to Reduce Error
to Less than 10% of A vs. Sampling Interval (Δt)

Notes: Unit Value = 1 Represents Period T

$$L = \frac{1}{N} \Sigma \frac{\Delta M}{\Delta t}, \; t = N \Delta t$$

For the case illustrated in Figure 4 with A = 15 kg, the time required would be about 3.5 hours. L in Equation (6) could have been the target leakage rate if we were only interested in confirming a result below target. The minimum time is, of course, T/2 or two turning points in order to have even the possibility of bounding the error. Independent repeated measurements at different times can also give this information.

One exception to the above criterion is if the sampling interval is selected near the fluctuation period. Figure 5B illustrates this effect, again using a hypothetical sinusoidal fluctuation. It indicates the specific case where we wish to know how long it takes to reduce the maximum deviation to 10 percent of the amplitude. Any sampling interval below about 0.3 T enables bounding of the fluctuation in the shortest possible time (about 2.5 cycles in this case). Near T/2, T and multiples thereof, a non-converging series of results may occur. This can introduce oscillations in the results which may not really exist. To avoid this problem the following approaches should be considered (in order of preference):

(i) If the series shows a repeatable period, divide it out (e.g. diurnal fluctuations). This is the preferred approach.

(ii) Use more than one sample period and compare analysis results. If the fluctuation is real it will appear in both sets of results.

(iii) Select random sample periods within prescribed limits.

In summary, with the above precautions on sampling period, leakage rate results are convergent with time. This is a necessary and important consideration in the feasibility of continuous monitoring at reduced pressure levels. For continuous monitoring we must trade-off the desirability of having frequently updated information on containment status against the improved accuracy of the result if we sample for longer times before updating the mass balance.

EXPERIENCE

Quarterly on-power tests in the latest stations have been able to measure the leakage rate with accuracies a small fraction of operational targets. Their main use is diagnosis of trends, but any apparent increase in long-term leakage trend to-date has been small enough that it is not considered statistically significant at a high confidence level.

Individual test results often show the presence of systematic errors as discussed above. However, with the large number of results acquired over the years, the true error for any given test result has been estimated. In addition the presence of a seasonal component has been noted with results in winter up to 20 percent higher than the mean value now anticipated. This is particularly evident in Vacuum Building results and may be a sign of concrete shrinkage.

As mentioned previously, Vacuum Building leakage has proven to be relatively easy to monitor. Problems diagnosed so far have generally not been due to structural leakage but pressure relief valve seat leakage or vacuum pump problems.

Experience in conducting verification tests at low pressures has shown that it is preferable to input a metered amount of air from the station compressed air system rather than to superimpose an orifice. The test can be completed quickly with a small gas meter and involves no breach of containment with units on-power.

Almost all of the few containment impairments experienced to-date have been detected by our components tests, visual inspection or continuous pressure trend monitoring. Figure 6 is a particularly interesting example of continuous monitoring during a reported event at the Bruce A station. The abnormal slope of the computer generated pressure trend was readily detectable by operators. Their efforts to maintain containment pressure is evident. Simple equations fitted to the slope of the pressure rise indicated that an 8 cm (3.3 in) impairment existed when modelled as a idealized orifice. In actual fact, a promptly called leak search revealed that a nominal 10 cm (4 in) airlock equalizing valve represented the leakpath.

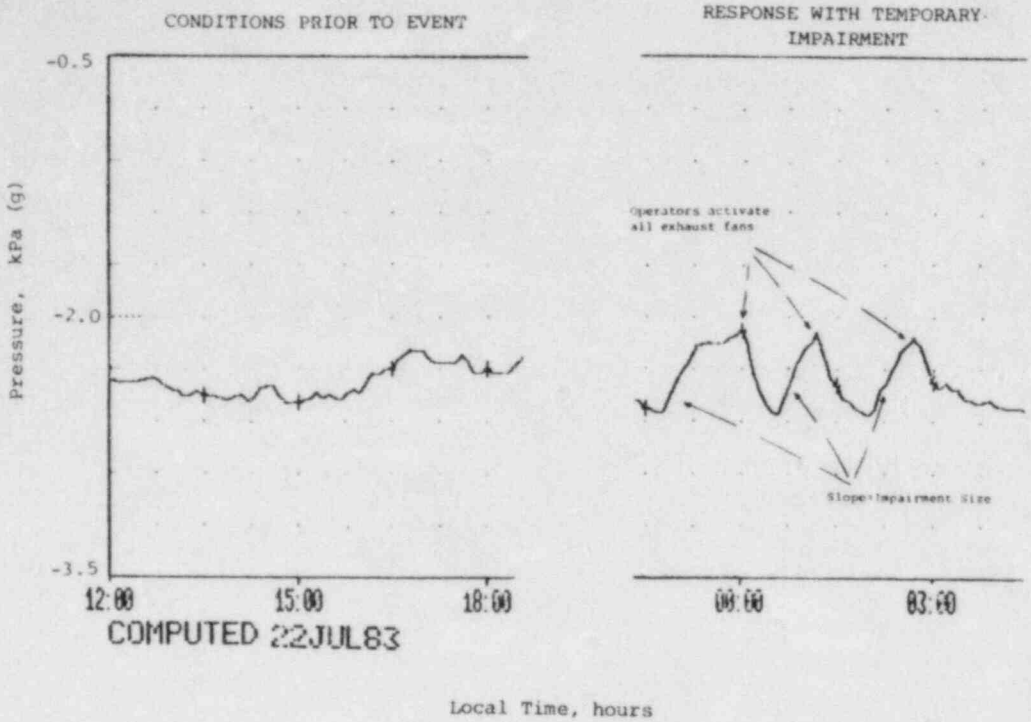

FIGURE 6. EXAMPLE OF CONTINUOUS PRESSURE TREND MONITORING OF CONTAINMENT

RELATED INVESTIGATIONS

Concomitant with the process of detecting abnormal leakage during overall leakage rate tests or continuous monitoring, is the problem of prompt location of the leak site. In large complex containments this is a non-trivial problem. Containment operation at negative gauge pressures makes the task even more difficult because of the flow direction of the leakage.

To assist leak search efforts, assessment and development programs are now underway in the following areas:

(i) Ultrasonic detectors. These hand held units provide for remote leak site identification and have directional capability.

and (ii) Tracer gases. SF_6 is the currently preferred tracer because it is odourless, non-toxic and is detectable in parts per billion. This sensitivity is important for tests at low pressure differentials.

It is hoped that these techniques may supplement the current approach which usually consists of a pre-planned leak search starting with known leak-prone components (e.g. airlocks).

APPLICATION TO RISK ASSESSMENT

In order to gain widespread acceptance and to merit further development, continuous monitoring and other on-power tests must have a quantifiable benefit. One means is in probabilistic risk assessments if containment event trees are designed to discriminate failure modes. Failure modes may be categorized by size, as well as by time of occurrence,

In the size category we can have leakages,

(1) On the order of design target values,
(2) Corresponding to hole sizes that result in siting guide release limits being exceeded,
and (3) Resulting from significant structural or large component failures.

Depending on the station there may be up to an order of magnitude difference in the leakages for these categories and hence in their release consequences.

By time of occurrence we have,

(A) During normal plant operation,
(B) Caused by LOCA,
(C) Long-term post-LOCA.

Continuous monitoring has the potential for making the probability of undetected Type A failure modes zero. The larger, more significant failures or those due to active components (airlock seals, isolation valves) or human misoperation are the most readily detectable, even on-power at low pressures.

Potential Type B failures, of all sizes, can only be detected by pressure testing at accident pressure levels. Integrated full pressure tests are almost always costly to undertake, hence test frequencies should be traded off against the incremental benefit as experience accumulates.

Type C failure modes are addressed by laboratory LOCA qualification tests and aging tests.

Regulatory authorities have an important role to play in encouraging or discouraging implementation or improvements to in-service test methods. Proposed regulatory guide C-7 by the Canadian Atomic Energy Control Board permits the period between full pressure leakage tests to be twice as long if successful reduced or negative pressure tests are frequently performed. Flexibility in this direction is considered appropriate since it recognizes the safety benefits of in-service tests and gives the owner incentive to develop a credible integrity monitoring program.

CONCLUSION

On-power integrity monitoring makes an important contribution to the safety of CANDU multi-unit containments. Continuous monitoring is technically feasible using instruments commonly available for periodic pressure tests. Although at present it may only detect larger failure modes occurring during routine station operation, this portion of the failure mode spectrum is considered significant enough to warrant further development. More widespread implementation or retrofitting requires that credit be given for the improved assurance of containment boundary integrity in station risk assessments and regulatory testing requirements.

REFERENCES

1. Zakaib, G.D., "Interpretation of Leakage Rate Data For Vacuum Containment Structures", Proceedings of Third Annual Canadian Nuclear Society Conference, C-31, ISSN 0227-1907, Toronto, Canada, June 9, 1982.

2. American National Standard ANSI/ANS-56.8-1981, "Containment System Leakage Testing Requirements", American Nuclear Society, La Grange Pk, Illinois, USA.

3. Box, G. and Jenkins, G., "Time Series Analysis: Forecasting and Control", Holden-Day, San Francisco, California, 1976.

DETERMINATION OF AS FOUND CONTAINMENT INTEGRATED LEAKAGE RATE

Robert E. Shirk and Robert M. Carey
Gilbert/Commonwealth
Post Office Box 1498
Reading, Pennsylvania 19603

ABSTRACT

Section III.A.1(a) of Appendix J to Title 10, Code of Federal Regulations, Part 50 (10CFR50) states the following:

"During the period between the initiation of the containment inspection and the performance of the Type A test, no repairs or adjustments shall be made so that the containment can be tested in as close to the "as is" condition as practical."

and further:

"During the period between the completion of one Type A test and the initiation of the containment inspection for the subsequent Type A test, repairs or adjustments shall be made to components whose leakage exceeds that specified in the technical specification as soon as practical after identification."

Most utilities perform local leakage rate testing (Type B and C), including necessary repairs and retests, from the start of the refueling outage until the Type A test containment inspection. Although this does not appear to conflict with the 10CFR50, Appendix J, requirement due to the time frames involved, it does not allow an evaluation of the containment integrated leakage rate in an "As Found" condition, prior to local leakage rate tests and repairs. The word of the law is met, but not the intent.

Meeting both the word and intent of the law would entail performing the Type A test prior to performing any repairs or adjustments, i.e., at the beginning of the outage. Recognizing the economic penalties which would exist, the Nuclear Regulatory Commission (NRC) has not prohibited the practice of conducting local leakage rate tests (and subsequent repairs) prior to the Type A test. Instead the NRC is interpreting Section III.A.1(a) of 10CFR50, Appendix J, to require an evaluation of the "As Found" condition of the containment to assess the extent of containment deterioration that may have occurred since the last Type A test.

INTRODUCTION

Background

The purpose of the periodic integrated leak rate test (ILRT) is to measure the total degradation which has occurred to the containment boundary system. In assuring that this degradation has not caused the containment leakage to exceed certain acceptance criteria, continued containment boundary integrity is assumed. Local leakage rate testing (LLRT) is performed at each refueling outage to help ensure the continued integrity of the containment boundary between periodic ILRT's. Local leak rate tests are also used to identify, measure and document sources of containment boundary degradation prior to an ILRT for possible repair. The repairs performed to the containment boundary before an ILRT improve the performance of the containment system during the ILRT but tend to mask the actual amount of degradation the containment barrier suffers between ILRT's.

Section V.B.3 of Appendix J to 10CFR50 requires that "For each periodic test, leakage test results from Type A, B and C tests shall be reported. The report shall contain an analysis and interpretation of the Type A test results and a summary analysis of periodic Type B and Type C tests that were performed since the last Type A test". As Appendix J of 10CFR50 allows local leakage rate testing between ILRT's and the reporting format is specified, the NRC has been deriving data for an "As Found/As Left" analysis of the containment boundary from information supplied in the present test report format.

Definitions

"As Left" Containment Leakage

The leakage measured during the ILRT is considered by the NRC to be the "As Left" leakage of the containment, i.e., leakage after the repairs to containment barrier components, initiated because of Type B & C tests, resulting in an improvement of overall containment performance.

"As Found" Containment Leakage

The containment boundary system leakage prior to repairs, i.e., what the leakage measured during an ILRT would have been if it had been performed prior to Type B & C testing and subsequent repairs.

Current NRC Position

The NRC had been deriving its own "As Found" analysis from the ILRT results and the pre-repair/post-repair local leakage rate test results reported with the ILRT. Currently, the NRC is requesting (read "requiring") that an evaluation of the local leakage rate tests be performed to determine the total leakage savings achieved through repairs and retests. The NRC is considering altering the ILRT Test Report format to require the reporting of containment leakage in the "As Found" and "As Left" conditions.

METHODOLOGY

Local Leakage Rate Testing

Local leakage rate testing is performed as surveillance testing each refueling outage to meet the requirements of the license's technical specifications. The results of these

tests are reported with the Type A test results, and if these local leakage rate tests indicate excessive leakage, repairs are performed, and the post-repair leakage rate is also reported. When possible, each containment isolation valve in a penetration pathway is tested separately, and the results are reported separately. In many cases, the containment isolation valves in a penetration pathway are not individually testable, so the valves' leakages are determined and reported together as a total pathway leakage.

Minimum Pathway Leakage

As previously discussed, the NRC is requiring that an evaluation of the local leakage rate test results be performed to determine the total leakage savings achieved through repairs and retests. This evaluation is performed based on minimum pathway leakage. Minimum pathway leakage is the minimum leakage value that can be quantified through a penetration leakage path (e.g., the smallest leakage of two valves in series). This is consistent with the results of the Type A test, which would reflect the lowest leakage of two containment isolation barriers in series. For example, in Figure 1A, barrier one (V1) had a leakage rate of 500 sccm and barrier two (V2), in the same penetration path (penetration 1) and in series with barrier one, had a leakage rate of 1,500 sccm. The Type A test results would reflect only the leakage from barrier one. Therefore, the minimum pathway leakage for that penetration would be the 500 sccm of barrier one.

Leakage Savings

Leakage savings are realized when containment isolation valve repairs result in a lower minimum pathway leakage than that measured prior to valve repairs or adjustments. Figure 1B illustrates the results of post-maintenance local leakage rate testing on the penetration path shown in Figure 1A. Repairs to barrier two (V2) resulted in a post-maintenance leakage rate of 200 sccm. The minimum pathway leakage for penetration 1 is now 200 sccm, a net savings of 300 sccm. Note that if the repairs on V2 had resulted in a leakage rate of 500 sccm or above, the minimum pathway leakage for penetration 1 would not have changed and no "savings" or improvement in penetration leakage rate performance would have been realized.

Calculating the As Found Leakage Rate

The "As Found" containment leakage is derived as follows:

(1) Type B and C test results are analyzed.

- The lowest pre-repair barrier leakage for each penetration is considered the pre-repair minimum pathway leakage and is the basis for determining penetration leakage performance improvements for the "As Found" analysis.

- In the case of penetrations in which valve repairs have been performed, the lowest post-repair leakage rate represents the minimum pathway leakage for that penetration.

- The post-repair minimum pathway leakage is compared to the pre-repair minimum pathway leakage. If the post-repair pathway leakage is smaller, a leakage savings has been realized for that penetration (Figures 2A and 2B).

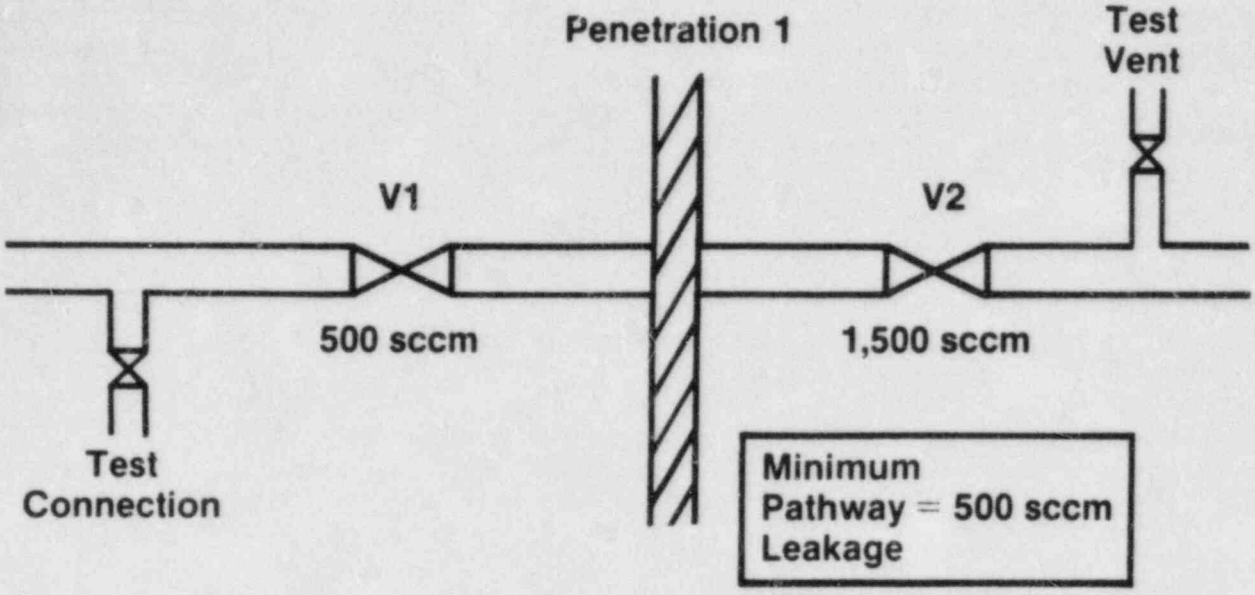

Pre Maintenance Local
Leakage Rate Testing
Figure 1A

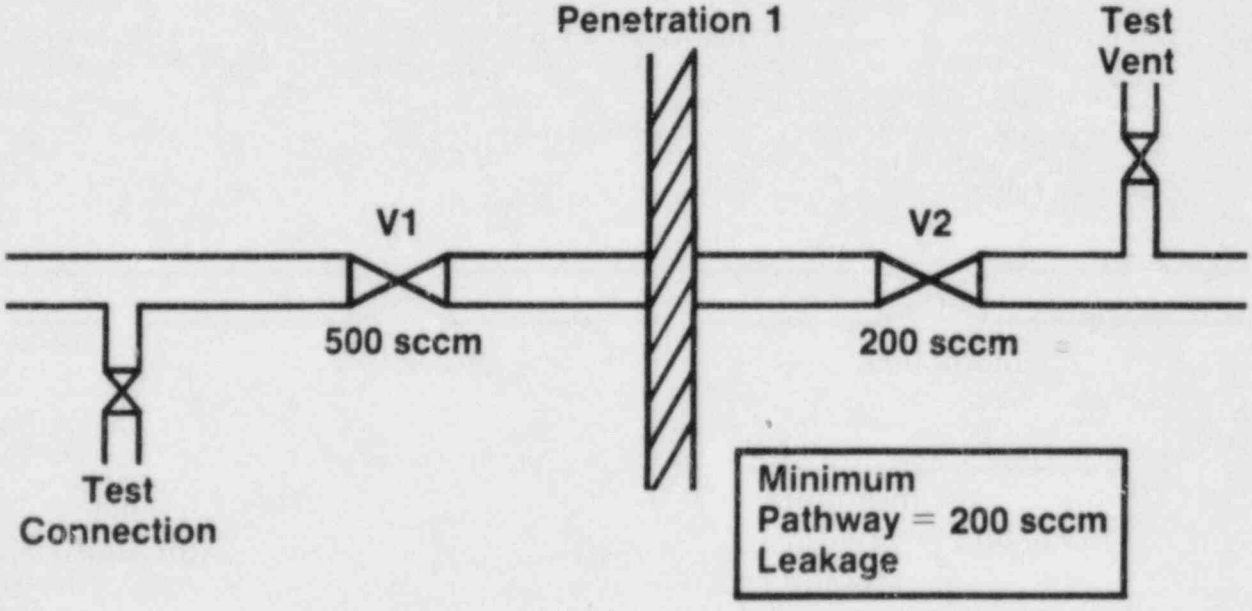

Post Maintenance Local
Leakage Rate Testing
Figure 1B

- If the post-repair minimum pathway leakage is equal to, or larger than the pre-repair minimum pathway leakage, no leakage saving has been realized for that penetration, and no contribution is made by that penetration to the "As Found" condition of the containment (Figures 3A and 3B).

(2) The total of all improvements, or leakage savings realized from repairs, is applied to the reported Type A leakage to determine the "As Found" condition of the containment.

Table 1 is a sample Pre-Maintenance Minimum Pathway Leakage Analysis, using the penetrations and leakages illustrated in Figures 1A, 2A and 3A. Table 2 is a sample Post-Maintenance Minimum Pathway Leakage Analysis using the same penetrations as Table 1 but with the post-maintenance test results shown in Figures 1B, 2B and 3B. Table 3 compiles the pre-maintenance and post-maintenance minimum pathway leakages in tabular form for a Determination of Leakage Savings. These leakage savings are applied to the reported Type A leakage to determine an "As Found" containment leakage rate in Example 1.

EXAMPLE 1

Assume an ILRT was performed subsequent to the local leakage rate testing illustrated by the preceeding figures, with a resultant "As Left" containment integrated leakage rate of 0.056 percent by weight per day at the upper 95 percent confidence interval. The initial weight of the air in the containment, determined by least squares fit analysis, was 389,403 pounds. The "As Found" containment integrated leakage rate is determined as follows:

A. Convert the total leakage savings from sccm to pounds per day:

$$4{,}300 \frac{\text{scc}}{\text{m}} \times (3.531 \times 10^{-5}) \frac{\text{scf}}{\text{scc}} \times .07517 \frac{\text{lbs}}{\text{scf}} \times 1440 \frac{\text{m}}{\text{day}} = 16.44 \text{ lbs/day}$$

B. Convert lbs/day to percent by weight per day:

$$\frac{16.44}{389{,}403} \times 100 = .004 \text{ wt.\%/day}$$

C. Add the leakage savings to the "As Left" containment integrated leakage rate:

0.056%/day + 0.004%/day = 0.060%/day

The 0.060%/day number represents the "As Found" containment integrated leakage rate.

As Found/As Left Leakage Rates Acceptance Criteria

The acceptance criteria for the "As Found" and "As Left" integrated leak rate tests is as follows:

- "As Found" leakage = La
- "As Left" leakage = 75% La

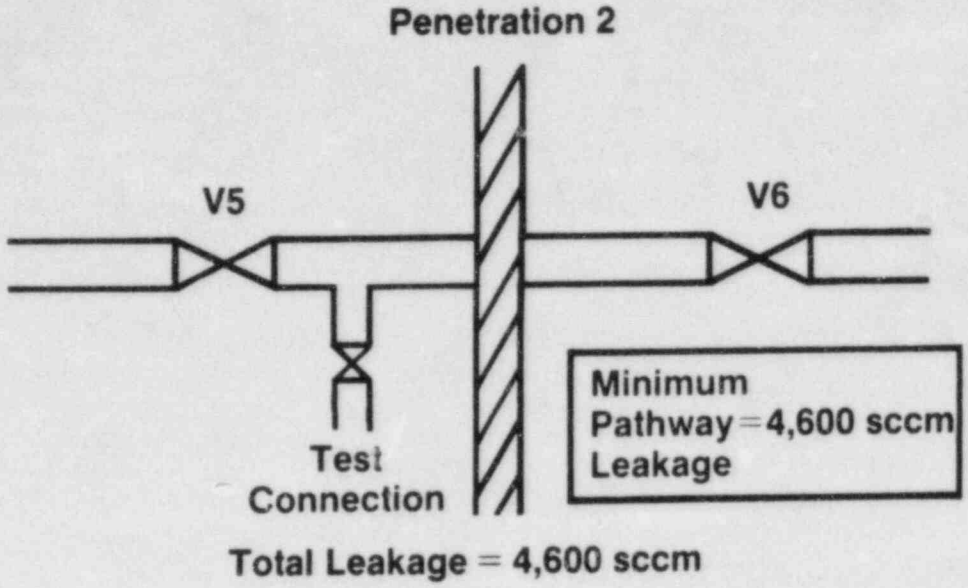

Pre Maintenance Local
Leakage Rate Testing
Figure 2A

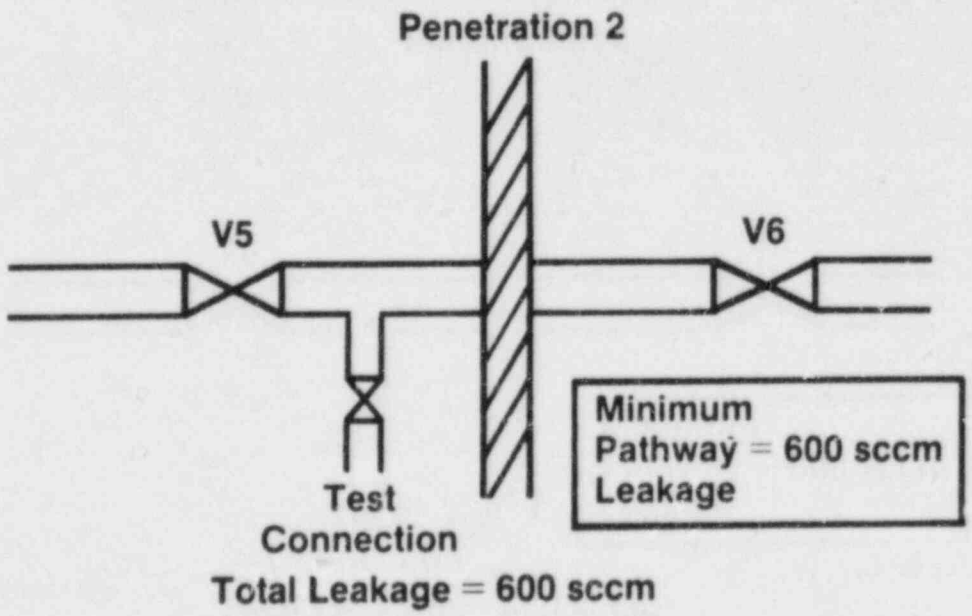

Post Maintenance Local
Leakage Rate Testing
Figure 2B

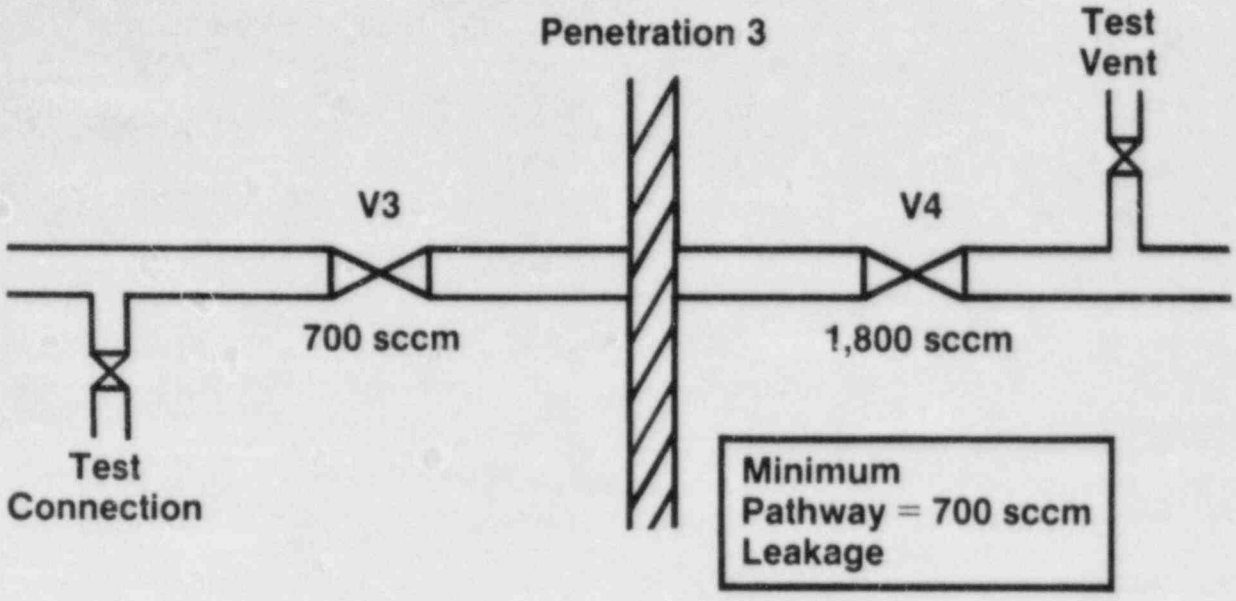

Pre Maintenance Local
Leakage Rate Testing
Figure 3A

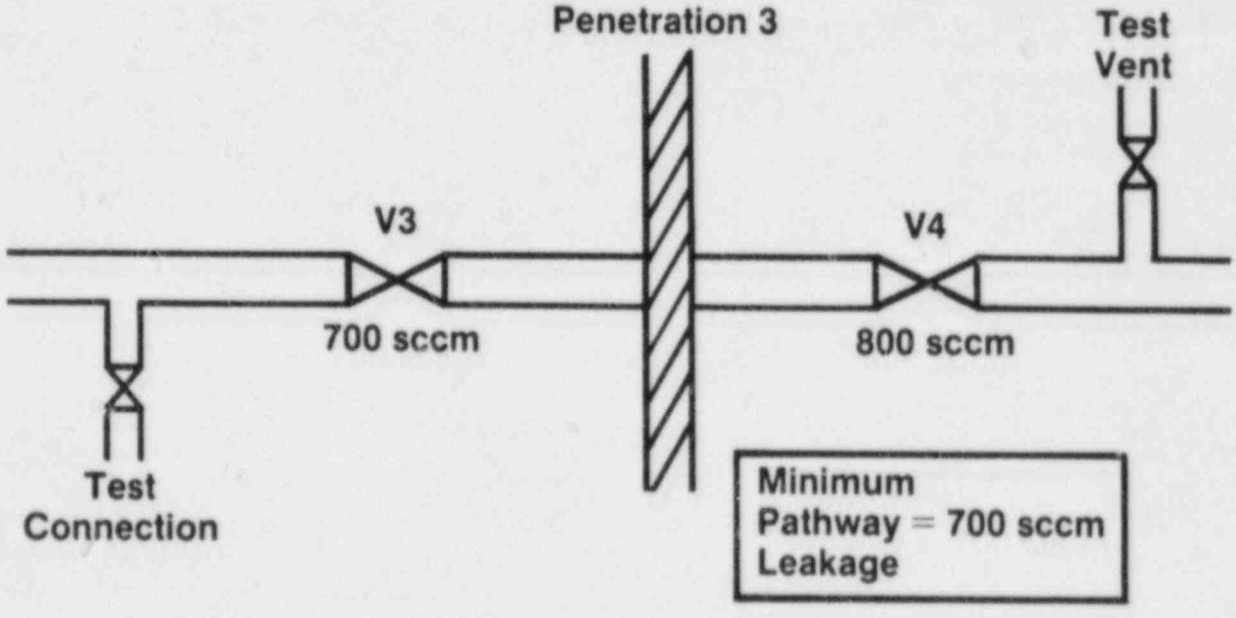

Post Maintenance Local
Leakage Rate Testing
Figure 3B

An "As Found" leakage greater than La would indicate that containment degradation between Type A tests is unacceptable, and a Corrective Action Plan would have to be developed. The NRC can require a Corrective Action Plan presently (even though a change in the reporting format has not been endorsed) due to the wording in 10CFR50 Appendix J requiring testing the containment in as close to the "as is" condition as possible.

IMPACT ON UTILITIES

Pre-Maintenance Local Leak Rate Testing

The vast majority of pre-repair and post-repair leakage rates included in the Type B and C test results summary portion of the Type A test report were historically the results of repairs identified as necessary by the Type B and C test programs. Technical specification requirements to perform local leak rate testing on containment isolation valves prior to maintenance vary widely throughout the industry. The NRC realized in their early "As Found" assessments that without pre-maintenance leak rate data on containment isolation valves prior to any maintenance which might affect their leakage characteristics, an accurate "As Found" assessment of the containment was not possible. Therefore, in order to provide the necessary data for calculating leakage savings for the "As Found" analysis, the NRC requires that a utility must perform pre-maintenance local leakage rate tests to establish the "As Found" (pre-maintenance) leakage rate. Pre-maintenance local leakage rate tests are performed prior to any scheduled maintenance on a containment isolation valve. After the maintenance has been performed, an additional local leakage rate test must be performed to determine the "As Left" (post-maintenance) leakage rate. This has increased the amount of testing required during an outage and therefore results in increased manhours and schedule (read "increased cost").

Design Considerations

In addition to the impact of the requirement for pre-maintenance local leakage rate testing, many of the older plants, per Appendix J design, do not have the design features necessary to test containment isolation barriers in series. This imposes an additional penalty in that it is often not possible to determine the leakage rate of individual valves, and therefore, as in the Figure 2A, the measured leakage rate becomes the minimum pathway leakage (even though the leakage could be mostly, or entirely, from one valve).

CONCLUSIONS

Based on the limited data available, the determination of "As Found" containment integrated leakage rates has not shown any significant degradation of containment integrity since the performance of the last Type A test. One question which must be asked is whether the approach described is valid for determining "As Found" containment integrated leakage rates. Another is that since containment isolation valves have historically been the major contributor to containment leakage and these valves are tested at each refueling outage, will containment integrity be improved by determining "As Found" containment leakage rates based only on the performance of these valves in leakage tests just prior to the Type A test, or is a broader perspective called for? Improvements in containment performance can only be achieved by paying the proper attention to problem areas such as containment isolation valve design and operation. Will determination of "As Found" containment integrated leakage achieve this?

Table 1
Minimum Pathway Leakage (MPL) Analysis—Pre Maintenance

Pen. No.	Inboard CIV Leakage (sccm)	Outboard CIV Leakage (sccm)	MPL (sccm)
1	500	1,500	500
2	—	—	4,600
3	700	1,800	700

Table 2
Minimum Pathway Leakage (MPL) Analysis—Post Maintenance

Pen. No.	Inboard CIV Leakage (sccm)	Outboard CIV Leakage (sccm)	MPL (sccm)
1	500	200	200
2	—	—	600
3	700	800	700

Table 3
Determination of Leakage Savings

Pen. No.	Pre Maint. MPL (sccm)	Post Maint. MPL (sccm)	Leakage Savings (sccm)
1	500	200	300
2	4,600	600	4,000
3	700	700	0

Total Savings: 4,300 sccm

CONTAINMENT INTEGRITY AND LEAKAGE EVALUATION

Edmund C. Tarnuzzer
Yankee Atomic Electric Company
Framingham, MA

ABSTRACT

As part of a Probabilistic Risk Assessment (PRA) of the Yankee Atomic Electric Company plant at Rowe, MA, an evaluation was made of the ultimate pressure capability of the reactor containment structure. Design features of the structure that had the potential to limit the ultimate capability were investigated in detail. Data was not available to calculate the capability of electrical penetrations and a test program to qualify these components is described. The ultimate capability is determined to be approximately three times the design pressure.

An evaluation is presented for leakage characteristics at pressures in excess of design. The leakage rate at the ultimate pressure is extrapolated and data from previous tests up to the design pressure is compared to the developed extrapolation curve.

Yankee Atomic Electric Company has completed a Probabilistic Risk Assessment (PRA) on its Rowe plant. This is one of the older nuclear units in the country, having been in operation since completion of construction in 1960. As a part of the PRA, an evaluation was made of the containment pressure capability and leakage characteristics at pressures in excess of design. The primary containment consists of a 125 ft. diameter, free standing, bare steel sphere, elevated 25 ft. above grade and supported at the equator by 16 3-1/2 ft. diameter columns. The nominal design conditions of the structure are: 34.5 psig and 250°F and a leakrate of 0.1%/24 hr. It was constructed by Chicago Bridge & Iron using the rules of Section VIII of the ASME Boiler and Pressure Vessel Code, 1956 Edition.

The concept behind Section VIII is the "design by rule" approach, wherein the basic vessel (in this case a sphere) is designed for specific pressure and temperature conditions and penetrations such as pipe nozzles, hatches, and the like are "designed by rule" to have strength properties at least equal to the basic vessel. The basic vessel shell thickness is 7/8 in. Several thickness plates were used in construction and they range from 7/8 in. to 3 in. The thicker sections being around the major penetrations and the equator support area.

In order to determine the pressure capability of the structure, the minimum shell thickness was assumed along with 90 percent of the minimum yield strength from all heats of the 7/8 in. plate material used in fabrication of the shell. Under these assumed conditions, vessel failure is calculated to occur at 84 psig, almost 3 times the nominal design pressure. This result is in agreement with other industry studies and consistent with recognized factors of safety inherent in the ASME code.

The above analysis assumed an uncomplicated, simple spherical structure. Three design features of this containment structure had the potential to limit the ultimate strength.

First, stainless steel expansion bellows are provided between the shell and a set of eight columns that support the inner shielding structure and reactor primary and secondary systems. These bellows mechanisms are necessary to provide for differential movement of the two separate structures. Sufficient documentation was available to demonstrate through calculations that the bellows seal assemblies would not limit the containment pressure capability.

Second, two purge air lines and several pipe lines penetrate the shell and provide potential leakage paths. Valves are located in these lines and form the pressure retaining boundary. As a minimum, these valves are standard commercial units with ANSI 125 pound pressure rating and, as such, will not limit the pressure rating of the structure.

Third, electrical cables and instrument signals cross the shell boundary through penetrations that are sealed against leakage by double O-rings on the bolted flange and two sets of seal fittings around each conductor. Documentation was not sufficient to immediately qualify these penetrations and I will shortly describe the test program undertaken to do so.

The only other penetrations not previously described are the following:

> A 14 ft. diameter equipment hatch closed with a single grooved seal, bolted flange connection. The hatch cover is inside the structure, bowed inward such that increased internal pressure will flatten the seal and result in metal-to-metal contact.
>
> A 7 ft. diameter personnel air lock in which the inner door opens inward. Each door flange contains a single grooved seal and hydraulic breach lock. Increased containment pressure increases sealing pressure on the inner door.

Three bolted flanged manways used during construction now closed with seal-welded diaphragms. The bolted flanges are rated at 150 pounds.

The spent fuel chute to the fuel pit is closed by a blind spectacle flange at the containment end and a 125 pound rated valve at the spent fuel pit end.

ELECTRICAL PENETRATION QUALIFICATION

Electrical penetrations consist of piping penetrations welded to the containment shell and containing a flanged, bolted, double O-ring end seal. The electrical cartridge consists of a smaller diameter pipe section containing two end seal plates, through which the electrical conductors pass, and a mating bolt flange.

Three basic types of penetrations were originally installed: one for the 2400 V reactor coolant pump power supply and for the 480 V power and control supply, one for the coaxial and triaxial instrumentation cables, and one for the thermocouple cables. A brief description of each is as follows.

For 2400 V conductors, a solid copper rod with 5 kV Buna insulation is used for the conductor through the penetration. The solid copper rod serves to stop any leakage through the cable stranding. A sonolastic (pourable synthetic rubber sealing) compound is used in the seal in addition to the high temperature rubber seal furnished with the gland seal. After completion of the cartridge assembly by shop bench methods, the assembly was cured and leak tested.

Mineral insulated cable (MI) is used for power and control penetration under 600 V except for coaxial cables. A cartridge of similar construction to the 2400 V cartridge is used, except the gland seal closely fitting the cable is potted with sonolastic sealing compound. Coaxial and triaxial cables pass through primary containment penetrations in a cartridge similar to those used for power and control cables, except connectors filled with epoxy are inserted in the coaxial and triaxial strands to prevent air passage.

Thermocouple cables are magnesium oxide insulated with an overall cold drawn steel sheath. A gland seal with metalic seal ring and potting compound around the cable is tapped into the end flanges of the electrical cartridge similar to the 600 V type of fitting.

Initial prototype testing and subsequent periodic testing did not verify that these penetration cartridges had the capability to withstand pressures in excess of 40 psig and temperatures in excess of approximately 250°F. A detailed test program was devised to verify the ability of these penetration cartridges to withstand conditions exceeding the original design. This test program was as follows.

TEST PROGRAM

A series of five tests were conducted of a Type IB MI insulated, 600 V power cable penetration cartridge that had been removed from service and replaced. The tests were devised to be of increasing severity to determine the conditions resulting in failure. The initial test was at ambient temperature and 35 psig, which is representative of the periodic test conditions for all penetrations. Temperature and pressure were increased as the testing progressed, with the final test conditions being 100 psig and approximately 360°F.

TEST RESULTS

No leakage was measured across the bolted, flange connection during any testing. All measured leakage from inside containment to outside containment was acceptably low. Conditions that would cause the penetration to fail were not discovered. Pressure was limited to the capacity of the service air compressor discharge, approximately 100 psig. No attempt was made to adjust any of the mechanical connectors prior to the test, so that testing was the "as found" condition and would be representative of the existing penetrations in the primary containment.

A random electrical penetration that had been removed from service and replaced was selected for testing at elevated pressure and temperature. The penetration selected was a Type IB, containing three mineral insulated cables. The penetration was tested in the "as found" condition with no attempt to check any of the cable fittings. New flange O-rings were installed to replace those damaged when the penetration was removed from service.

The test device consisted of a 40 in. section of 8 in. pipe, blanked at one end and flanged at the other end to match the flange of the electrical penetration. The pipe section was wrapped with four 1000 W and four 500 W electrical strip heaters and covered with an insulating blanket. A test tap with an isolation valve and a test gauge permitted pressurization of the test chamber. A thermocouple installed on the outside of the test chamber near its flange provided temperature indication.

A series of five tests--two at ambient temperature, and three at elevated temperature--were conducted to demonstrate the ability of a typical electrical penetration to withstand without failure, the postulated accident conditions and beyond. In preparation for testing, one electrical penetration was selected from those that had been replaced and had not yet been discarded. Preliminary examination indicated that the original O-rings had possibly been cemented into the grooves in the electrical penetration prior to their initial installation in 1960.

Parts of both O-rings had pulled away and loose rust particles were evident as a result of its removal. The old O-rings were removed and all loose rust was removed in the area of the two grooves. New O-rings were obtained from stock and installed in their respective grooves with only friction holding them in place. The penetration was mated to the test device and each of the eight flange bolts were torqued to 50 ft. lbs., which was estimated to be the original requirement.

The first test was conducted at 35 psig and ambient temperature to determine (1) that the test device did not leak, and (2) that the penetration assembly could meet the current testing requirement for electrical penetrations on the primary containment structure.

The second test was conducted at 85 psig and ambient temperature to determine the ability of the components to withstand such pressure without failure as well as to measure the leakage rate.

Prior to the third test the heaters were energized and heated the insulated test chamber to a surface temperature in excess of 300°F. The test pressure was 35 psig. Upon completion of the third test, the pressure was increased to 85 psig for the fourth test. A fifth test was conducted at a later date to both check the repeatability of the test procedure, as well as to qualify the penetration at a pressure of about 100 psig.

The primary purpose of the testing program was to determine the ability of the selected penetration to withstand without failure, a postulated containment transient with a peak pressure at 85 psig and 270°F. The fifth and final test was conducted at 100 psig after the temperature had stabilized at over 300°F. All tests were successful, giving reasonable assurance that the existing electrical penetrations will withstand a minimum of 85 psig without failure.

The only leakage observed during any testing was a maximum of 0.1 lb. mass per hour from the test chamber to the inside of the penetration cartridge. This leakage

decreased with time as the pressure within the test chamber and the inside of the cartridge equalized. The time to equalize was approximately 40 minutes. This indicated that one or more of the three gland nuts around the inner conductors leaked slightly. However all three gland nuts surrounding the outer conductors were leaktight and no leakage occurred between the inner containment and the outside.

CONTAINMENT LEAKAGE CHARACTERISTICS AT ELEVATED PRESSURES

The primary containment structure leakage characteristics were evaluated based upon past Type A integrated leakage test results. Based upon these test results, a conservative extrapolation of containment leakage at pressures in excess of calculated peak accident pressure has been made.

The previous evaluation has determined that gross containment failure will not occur below about 85 psig. The current Technical Specification limit on overall containment leakage is 0.20%/24 hours at a calculated peak accident pressure of 31.6 psig. All of the containment leakage tests have been conducted at 32 psig or less, and all test results have been less than 50% of the allowable limit. The four most recent test results were examined to determine a realistic extrapolation factor for pressures in excess of design, that still would be conservative. The potential flow regimes of leakage from this containment include orifice, turbulent, laminar and molecular flows, or a combination of these. Orifice flow has been disregarded as not being realistic as it would represent a large (relative to the allowable leakage) opening and most certainly would have been detected by the operating continuous leakage monitoring system (CMS) and repaired. Molecular flow can also be disregarded for even if it does exist, it can only make a very small contribution to the overall leakage rate. Turbulent and laminar flow represent the most reasonable flow regimes for this type of containment. The total leakage is composed of a series of small diameter leaks that have defied detection in over 20 years of operation. They most likely consist of long leak paths (when compared to path diameter) and exhibit laminar flow characteristics, especially at the lower end of the pressure spectrum. In this situation, one would predict the flow regime would shift from predominantly laminar to turbulent flow as the pressure differential increases. Assuming a laminar flow model for all pressures is conservative.

The available data consists of the results of two tests--one at 16 psig and one at 32 psig--that exhibit pure laminar flow. Published data on leakrate tests run at elevated temperatures and pressures and with steam-air atmospheres indicate a reduction in measured leakage rates due to swelling of resilient seals and plugging of leakage pathways, when compared to test results run at ambient temperatures. We, therefore, are quite confident that our model will produce conservative results and that even under extreme accident conditions, beyond those previously analyzed, the off-site consequences will not exceed those specified in 10CFR Part 100.

BIBLIOGRAPHY

IN-1399 Final Results of the CVTR Containment Leakage Rate Tests, G. E. Bingham, Idaho Nuclear Corp., 1970.

BNWL-1495 Leakage Rate Tests on the CSE Containment Vessel with Heated Air and Steam-Air Atmospheres, M. E. Witherspoon, Battelle-Pacific Northwest Laboratories, 1970.

ORNL-NSIC-5 US Reactor Containment Technology, W. B. Cottrell and A. W. Savolainen, Eds., NSIC, 1965.

--------- Yankee Nuclear Power Station Probabilistic Safety Study, Energy Inc. and YAEC, 1983.

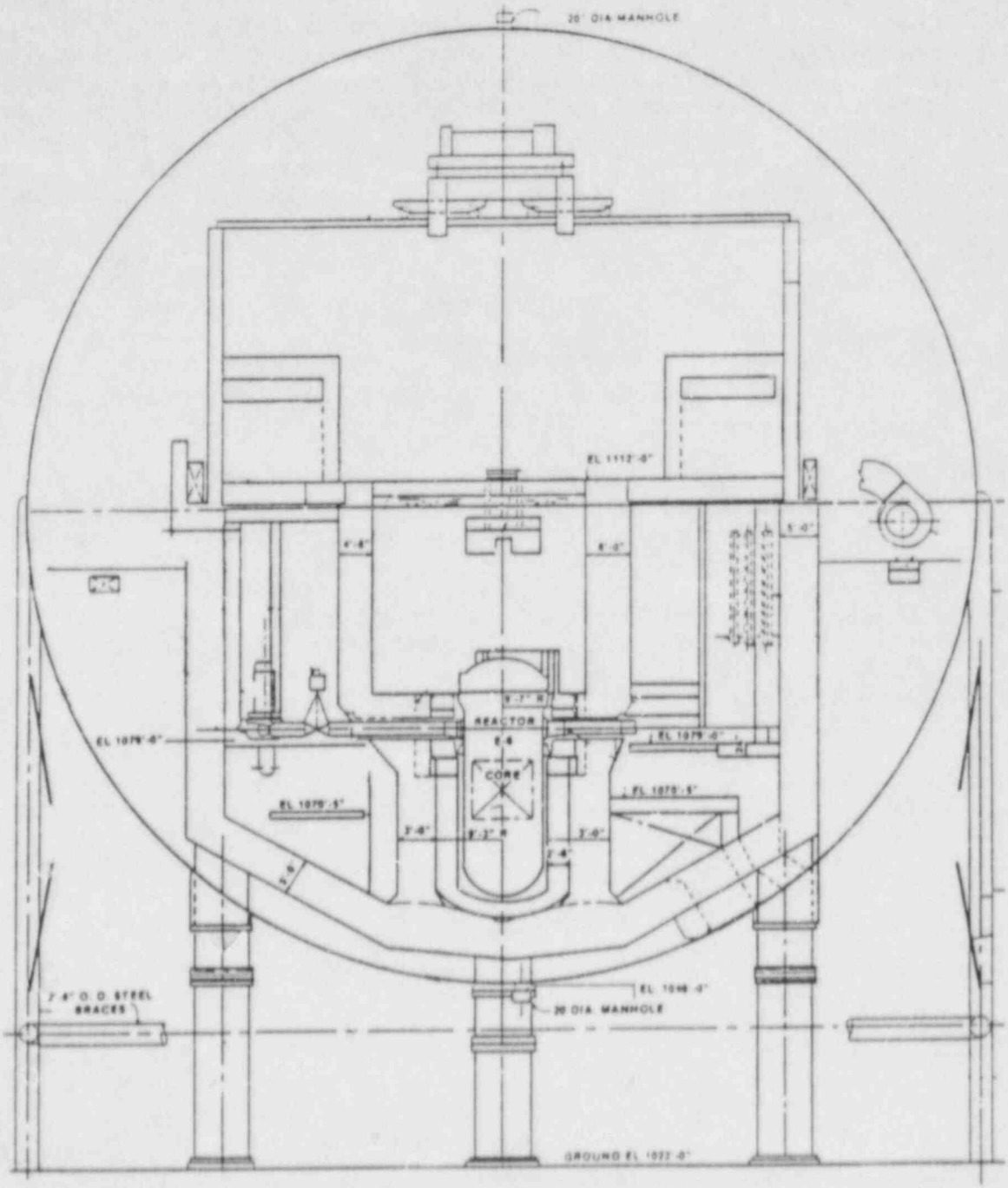

Figure 1. Cutaway View of Reactor Containment

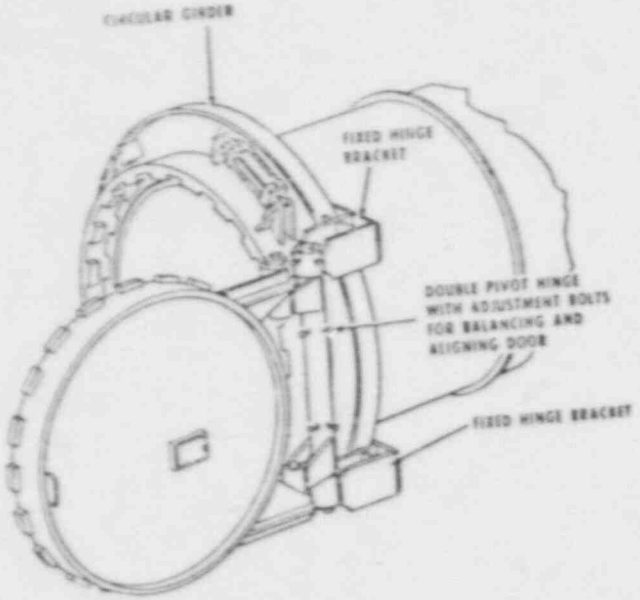

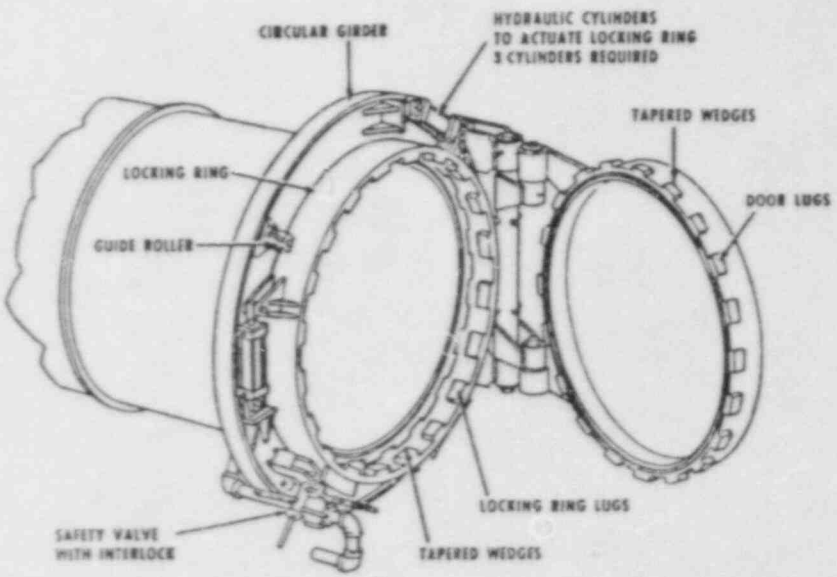

Figure 2. Breech-Lock Type of Quick-Opening Door
(From Chicago Bridge & Iron Company)

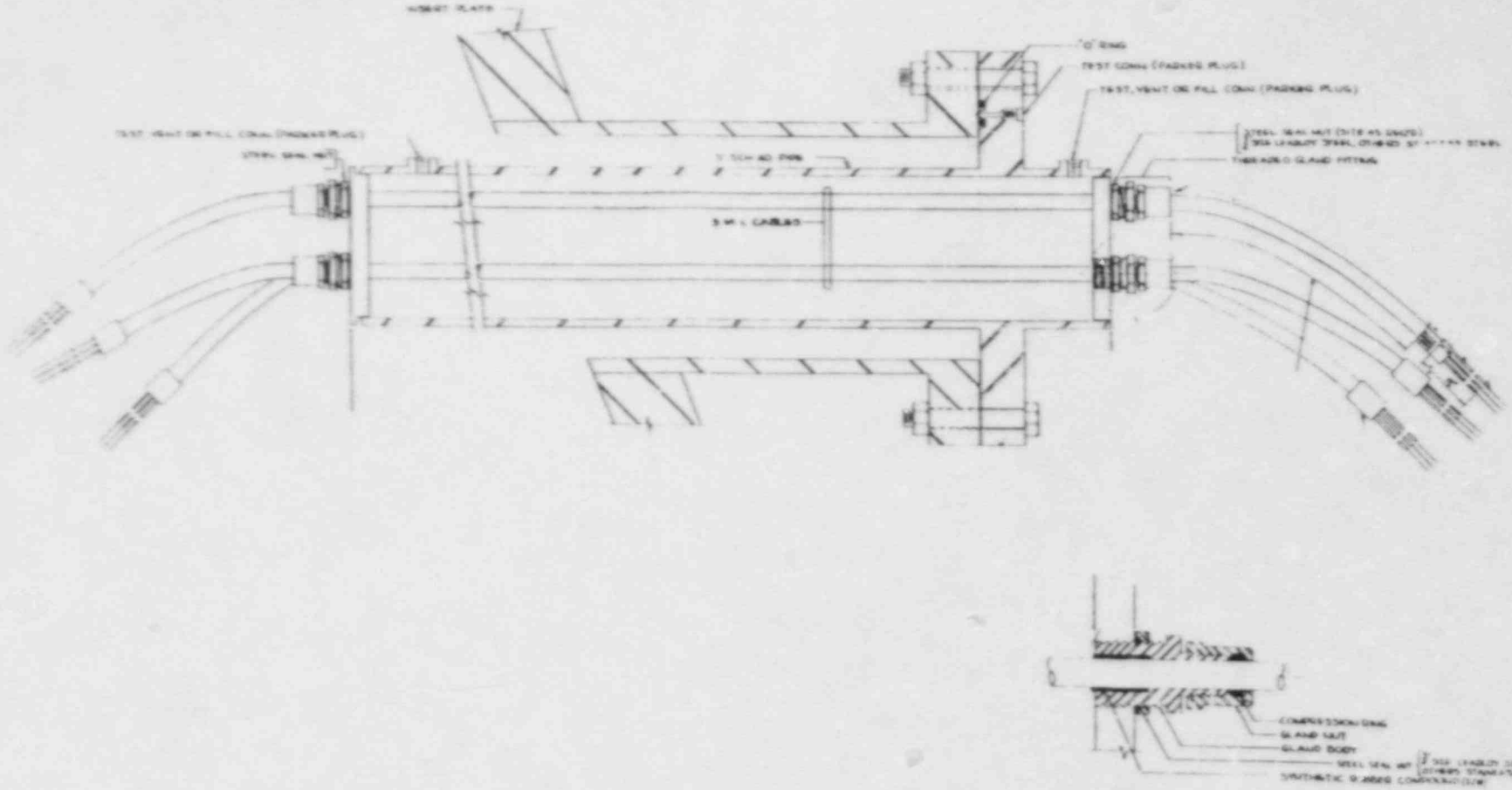

Figure 3

YANKEE NUCLEAR POWER PLANT	ELECTRICAL PENETRATIONS

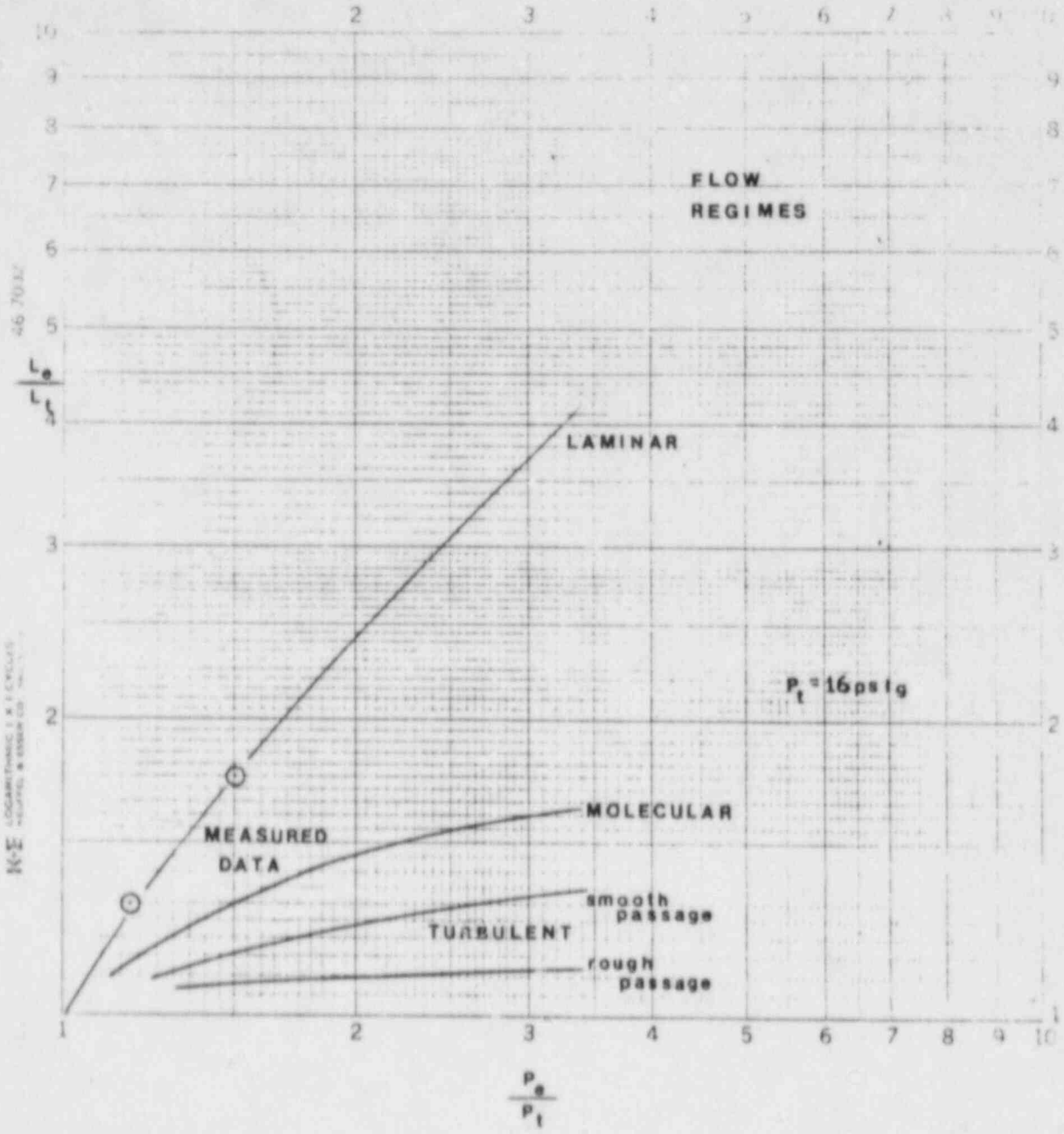
FLOW
REGIMES
LAMINAR
MOLECULAR
MEASURED
DATA
TURBULENT
smooth
passage
rough
passage
P_t = 16 psig
$\frac{L_e}{L_t}$
$\frac{P_e}{P_t}$

Figure 4

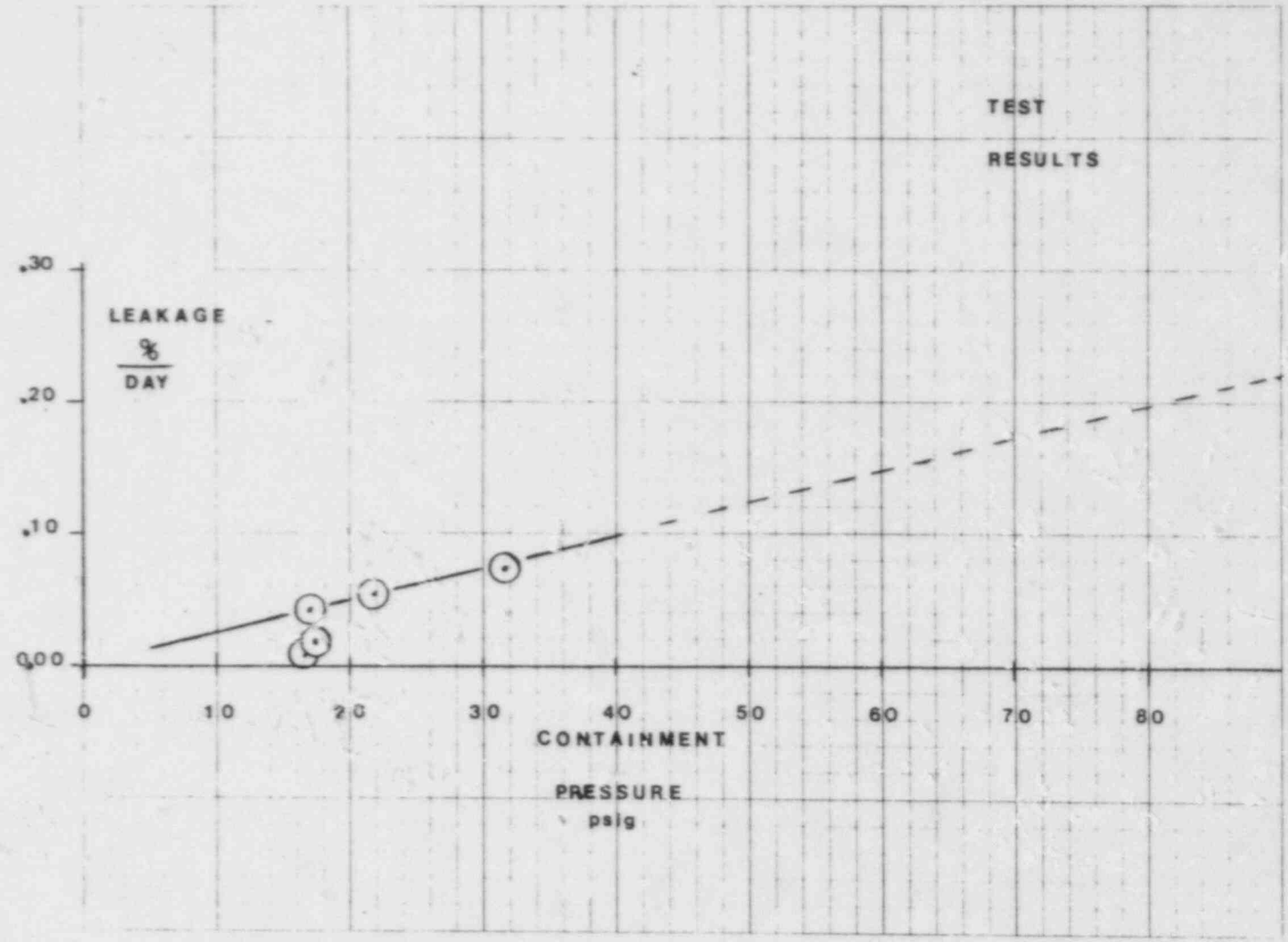
TEST
RESULTS
.30
.20
.10
0.00
LEAKAGE
%
DAY
0
10
20
30
40
50
60
70
80
CONTAINMENT
PRESSURE
psig

Figure 5

SESSION B

CONTAINMENT ENVIRONMENT AND LOADING CONDITIONS DURING SEVERE ACCIDENTS

IMPACT OF THE HDR TESTS ON THE MODELING OF CONTAINMENT LOADS

K. Almenas
Chemical and Nuclear Engineering Department
University of Maryland
College Park, MD 20742

K. Scholl and L. Valencia
Kernforschungszentrum Karlsruhe (K.F.K.) Germany

ABSTRACT

Experimental data having a direct applicability for nuclear power reactor containment design has been limited. The experiment serie conducted at the HDR facility (Karlstein, Germany) have brought a welcome and needed addition to this data base. The type of thermal-hydraulic data measured during the tests is reviewed and placed into context. The impact of this new data on containment design is summarized.

OVERVIEW

The experimental data base having a direct applicability to nuclear power reactor containment design has been limited. That is understandable. Power reactor containments are large structures and consequently full or near scale experiments are expensive and difficult. Until a year ago basically only two sets of experiments were available. A repetetive and sparsely instrmental test at the CVTR containment (1) and two series of well instrumented tests performed at the scalled Battele-Frankfurt facility (2). The tests performed at Marvikken are of limited applicability since that is a pressure supression containment.

This relatively narrow data base has now been broadened by 6 blowdown tests perfcrmed in the HDR facility at Karlstein, Germany. The tests were conducted in an actual containment which in terms of overall scale is quite close to containments of large, modern power plants (the linear scale ratio is $\sim$ 1.6 to 1). The Battele-Frankfurt experiments were performed in a carefully scaled specially built test facility. A qualitative illustration of scale for these facilities is shown in Fig. 1.

The data obtained from these two test series complement each other in an important way. The Batt-Fr. data is distinguished by its comprehensiveness. It covers a broad range of blowdown intensities which approaches, and in some respects exceeds, the conditions that could be expected in the event of loss-of-coolant accident. The facility is especially built for experimental pur-

poses, therefore for some runs the experimental conditions (i.e. geometry, flow channels) could be idealized in order to facilitate the analysis of specific physical phenomena. The HDR tests cover a spectrum of blowdowns of similar intensity but they extend the range of the data base in two respects.

1. The containment is larger and more complex therefore a wider variety of local test conditions are present.

2. As already noted, this is a containment built to house a nuclear power plant. As a consequence the compartments have irregular geometries, they are connected not by idealized openings, but by doors, stairwells, pipe penetrations and elevator shafts. They are packed with pipes, heat exchangers, stairs, railings and other structures.

The later, seemingly obvious point is emphasized since it determines both the strength and the drawbacks of the HDR data base. Real containments are complex therefore it is true that in several respects it is not easy to analyze the measured data. Internal flow fields are unknown, flow geometries can not be idealized and flow resistance coefficients can not be found even in such comprehensive compilations as Idelchiks. It is difficult to represent the bewildering variety of structures in terms of a finite number of analytically tractable analogues. Both the data and the analytical model employed to analyze it are therefore subject to a wider uncertainty margin. However, this wider uncertainty also incorporates essential design information. It is a mirror of the actual design and operation reality. Thus the HDR test results have provided an opportunity to check how effectively the available knowledge could be utilized to reproduce physical processes taking place in a containment under accident conditions. With the addition of the HDR test results, the data base chain available for containment analysis is now complete. It consists of basic heat and mass transfer data obtained from small scale experiments, data measured in large, scaled experimental facilities and data obtained in an actual containment.

TYPE OF DATA

The HDR test series encompasses a wide range of disciplines, including structural mechanics, earthquake effects, thermal schock tests and others (13,17). In this review we confine our attention to those measurments which are relevant to the calculation of loads generated by the pressure, temperature and composition changes of the confined containment atmosphere.

The data is made available in its entirety through a series of reports which are issued shortly after the completion of individual tests (3-7). Evaluation of various measurement categories and their comparison with analytically obtained results has been presented in a number of studies (8-11). The volume of this new data base is sizable. In order to provide an overview, representative samples

IMPACT OF THE HDR TESTS ON THE MODELING OF CONTAINMENT LOADS

K. Almenas
Chemical and Nuclear Engineering Department
University of Maryland
College Park, MD 20742

K. Scholl and L. Valencia
Kernforschungszentrum Karlsruhe (K.F.K.) Germany

ABSTRACT

Experimental data having a direct applicability for nuclear power reactor containment design has been limited. The experiment series conducted at the HDR facility (Karlstein, Germany) have brought a welcome and needed addition to this data base. The type of thermal-hydraulic data measured during the tests is reviewed and placed into context. The impact of this new data on containment design is summarized.

OVERVIEW

The experimental data base having a direct applicability to nuclear power reactor containment design has been limited. That is understandable. Power reactor containments are large structures and consequently full or near scale experiments are expensive and difficult. Until a year ago basically only two sets of experiments were available. A repetetive and sparsely instrmental test at the CVTR containment (1) and two series of well instrumented tests performed at the scalled Battele-Frankfurt facility (2). The tests performed at Marvikken are of limited applicability since that is a pressure supression containment.

This relatively narrow data base has now been broadened by 6 blowdown tests performed in the HDR facility at Karlstein, Germany. The tests were conducted in an actual containment which in terms of overall scale is quite close to containments of large, modern power plants (the linear scale ratio is $\sim$ 1.6 to 1). The Battele-Frankfurt experiments were performed in a carefully scaled specially built test facility. A qualitative illustration of scale for these facilities is shown in Fig. 1.

The data obtained from these two test series complement each other in an important way. The Batt-Fr. data is distinguished by its comprehensiveness. It covers a broad range of blowdown intensities which approaches, and in some respects exceeds, the conditions that could be expected in the event of loss-of-coolant accident. The facility is especially built for experimental pur-

poses, therefore for some runs the experimental conditions (i.e. geometry, flow channels) could be idealized in order to facilitate the analysis of specific physical phenomena. The HDR tests cover a spectrum of blowdowns of similar intensity but they extend the range of the data base in two respects.

1. The containment is larger and more complex therefore a wider variety of local test conditions are present.

2. As already noted, this is a containment built to house a nuclear power plant. As a consequence the compartments have irregular geometries, they are connected not by idealized openings, but by doors, stairwells, pipe penetrations and elevator shafts. They are packed with pipes, heat exchangers, stairs, railings and other structures.

The later, seemingly obvious point is emphasized since it determines both the strength and the drawbacks of the HDR data base. Real containments are complex therefore it is true that in several respects it is not easy to analyze the measured data. Internal flow fields are unknown, flow geometries can not be idealized and flow resistance coefficients can not be found even in such comprehensive compilations as Idel'chiks. It is difficult to represent the bewildering variety of structures in terms of a finite number of analytically tractable analogues. Both the data and the analytical model employed to analyze it are therefore subject to a wider uncertainty margin. However, this wider uncertainty also incorporates essential design information. It is a mirror of the actual design and operation reality. Thus the HDR test results have provided an opportunity to check how effectively the available knowledge could be utilized to reproduce physical processes taking place in a containment under accident conditions. With the addition of the HDR test results, the data base chain available for containment analysis is now complete. It consists of basic heat and mass transfer data obtained from small scale experiments, data measured in large, scaled experimental facilities and data obtained in an actual containment.

TYPE OF DATA

The HDR test series encompasses a wide range of disciplines, including structural mechanics, earthquake effects, thermal schock tests and others (13,17). In this review we confine our attention to those measurments which are relevant to the calculation of loads generated by the pressure, temperature and composition changes of the confined containment atmosphere.

The data is made available in its entirety through a series of reports which are issued shortly after the completion of individual tests (3-7). Evaluation of various measurement categories and their comparison with analytically obtained results has been presented in a number of studies (8-11). The volume of this new data base is sizable. In order to provide an overview, representative samples

are chosen for illustration purposes.

o Total Pressure

One of the most important parameters measured during a containment blowdown test is the buildup and decay of the total pressure. Fig. 2 shows the time dependent pressure during the first 3 minutes for tests V-44 and V-45. The tests differ in the total amount of primary water available for blowdown and in the size of several internal flow openings. The energy available in this primary system for the above tests is sufficient to increase the containment pressure to above 4 bars in an adiabatic transient. As seen, the actual maximum pressure reached barely touches 2.4 bars. This is a direct illustration of the importance of energy transfer to structures in an actual containment. Data of this nature can be used as part of a check verifying integral energy transport models.

o Pressure Differences

The HDR facility is extensively instrumented. Thus, for example, typically pressures are measured at $\sim$ 20 locations differential pressures at $\sim$ 9. This has the advantage that a reasonably complete pressure history can be established for the entire containment. A typical direct pressure difference measurement is shown in Fig. 3. It represents the pressure difference between the break and an adjoining compartment for tests V-44 and V-45. As seen, for this parameter the test results are distinctively different. The V-45 pressure difference is lower because an additional flow area out of the break compartment was opened for this test. Of interest also is the time variation of the measured ΔP values. As seen, a broad maximum exists at $2 \leq t \leq 3.5$ sec. The maximum blowdown rate occurs before 2 sec, the inertial resistance of the break compartment atmosphere has decayed in less than 1 sec, consequently the observed peak must be caused by other physical phenomena. It must be due to changes in the suspended water content or possibly also due to its physical state (droplet size).

o Temperature Distribution

Atmospheric temperatures are measured at over 30 locations. Besides providing a comprehensive picture of the temperature history within the containment, these measurements can be used to estimate atmosphere composition (in conjunction with pressure data) and to infer direction of the main atmospheric currents. A small part of this data obtained for test V21.1 is plotted in Fig. 4. It illustrates the atmospheric temperature history at various elevations within the containment for the initial 20 min. Observe that during the first few minutes the temperatures at the middle elevations (where the break compartment is located) climb to a nearly uniform maximum. After blowdown is terminated a gradual adjustment of temperatures and elevations take place. The stratification reached in $\sim$ 10 minutes is quite large (over 40°C) and remarkably stable.

o Heat Transfer Coefficients

A total of 11 instrumented metal and concrete blocks were employed to measure local heat fluxes. The heat flux measurement in conjunction with a near by (usually ∿ 20 cm) atmospheric temperature is then used to infer time dependent heat-transfer coefficients. Most of the blocks are distributed at various levels within the containment, but three of them are grouped in close proximity (within ∿ 2.5 m). The measurements obtained from these blocks for test V-44 are shown in Fig. 5. The figure includes also the data obtained from a 2 thermocouple heat flux measurement device which produces reliable measurements only at relatively high heat flux rates.

Several points of interest can be noted. During and immediately after the blowdown period when steam concentrations and turbulence levels are high, extremely large heat transfer coefficient values can be present. For comparison purposes, the heat transfer coefficients shown exceed the maximum values of the widely used Uchida correlation (18) by a factor of ∿ 5. The exceedingly high values measured for the steel block can be ascribed to differing turbulence levels. The steel block is placed directly in the path of a stream exciting from the break compartment while the remaining measurement surfaces are built flush with a wall and are therefore somewhat shielded.

o Atmospheric Velocities

The measurements listed up to now are available also from previous test series. The HDR project has developed and installed also some unique instrumentation. A particularly welcome addition are 3 multibeam infrared sensors built into flow channels connecting containment subcompartments (12). Under ideal operating conditions these instruments should be able to measure steam air and droplet density, droplet velocities and to infer an average droplet size. Conditions have not been that ideal, however some reliable measurements have been obtained. In particular droplet velocities have been measured. An example of this data is presented in Fig. 6. It shows droplet velocities in a channel leading from the break compartment. The velocities are seen to be surprisingly high. For the first 3 sec they exceed 300 m/s and thus approach sonic velocities for two phase flow.

o Atmospheric Composition

The new instrumentation includes also 3 infrared beam attenuation devices for the measurement of local steam concentrations. For all of the tests conducted up to now saturation conditions prevailed in the containment. Atmospheric composition can then be determined also from the more numerous local pressure and temperature measurements. The infrared devices then merely provide an independent check. The time dependent infered atmospheric composition for test V-43 is shown in Fig. 7 (from ref. 10). It

illustrates the extreme ranges of steam concentration that will exist for large scale blowdowns. As shown, the break and near break zone contain almost pure steam while the composition of the lower containment regions changes very little.

IMPACT OF THE NEW DATA

Development of computational models typically goes through several stages. In the initial stages when little directly applicable data exists, models are developed which usually fit the limited data base in an examplary fashion. As the amount of experimental data grows and covers a wider range of operational conditions, various shortcomings in the initial models become apparent. This, in general describes the present situation in containment analysis.

It is worth noting that we are talking about modeling shortcomings and not outright errors. Containment thermal analysis methods rest upon the solid foundations of time dependent mass, energy and momentum balances. This approach remains sound. However improvements are required in the modeling of some transfer rates and in the degree of spatial and atmosphere component resolution.

The models involved are complex. A listing of the observed experiment to analytical result differences and an analysis of the probable causes is beyond the scope of this review. Selected modeling areas are studied in references 8 to 17. This work is still ongoing. Here we will only note the main thermo-hydraulic areas for which the new HDR experimental data have had an appreciable impact.

o Total Pressure-integral Heat Transfer

For a condition where the energy source term (the blowdown) is reasonably well known, the calculation of the time-dependent total pressure depends primarily on an accurate modeling of energy transfer into structures. This in turn requires the ability to calculate proper local atmospheric conditions and to determine reasonable averaged heat transfer coefficients. The HDR experiments constitute a severe test for both of these modeling aspects. The elongated shape of the HDR containment favors the establishment of strongly stratified atmospheric conditions (see Figs. 4 and 7). The large number and variety of internal structures emphasizes the difficulties of grouping the structures into a finite number of heat transfer surfaces. Averaged heat transfer coefficients must then be calculated which reflect both the local conditions and surface variety.

Pre and post test calculations of the HDR experiments exposed weaknesses in both modeling areas. They showed that few node representations of the containment could not be used for best estimate pressure transient computations, that more flexible heat

transfer correlations are required and that in order to calculate the long term pressure behavior natural circulation effects must be accounted for (8,9,10).

o Pressure Differences-Intercompartment Mass Transfer

The largest direct impact of the HDR experiments probably has been in this area. Pre test calculations and subsequent experiment to model comparison clearly showed that the models employed were unsatisfactory (13,14). Further analysis showed that this is not merely a question of a more accurate evaluation of integral input parameters such as flow resistance coefficients. Rather the tests demonstrated that the transfer of a two phase fluid between large compartments through irregular flow channels is a complex physical process which can not be represented by over-simplified models. The models will have to be able to consider (or at least approximate) the effect of:

Internal atmospheric currents,

Amount and relative velocity of suspended water,

Flow resistances of internal structures.

These phenomena are interrelated. The data provided by the HDR experiments served to highlight their importance. A satisfactory resolution will require additional analytical work and in all probability additional experimental data.

o Equipment Qualification-Local Heat Transfer

A companion concern of containment analysis is the assurance of survivability of safety related equipment under accident conditions. This requires the determination of local (rather than averaged) energy rates. Fortunately, this is a parameter which can be measured directly and as already noted, during the HDR tests local heat transfer coefficients were measured in up to 11 positions. The test sites covered the entire range of potential ambient conditions, from pure steam and very high atmospheric turbulance down to almost all air and low turbulence. Significantly, though in several locations extremely high heat transfer coefficients were measured (see Fig. 5), heat fluxes were limited by the circumstance that the atmospheres remained saturated.

o Thermal Stresses-Atmospheric Stratification

The HDR experiments have shown convincingly that under loss of coolant conditions substantial temperature gradients will be established and maintained in the containment atmosphere (Fig. 4). The same phenomenon was observed for the CVTR tests (1), however, in that case steam was released at a moderate rate into the main body of the containment. In the HDR tests blowdown intensity was higher and the blowdown was directed into relatively enclosed compartments. Nevertheless, after an initial period in

which the steam concentrations (and temperatures) were higher in the mid level break zone, buoyancy forces established an elevation based, stable atmospheric temperature stratification. It was pointed out by Jansky (17) that such quasi steady state temperature differences can lead to thermal stresses in the containment steel shell.

o Margin of Uncertainty

The traditional engineering design method consists of a best estimate calculation adjusted by a safety factor which covers the uncertainties inherent in the design parameters and operational conditions. Regretably, for the most part this methodology has not been used in past containment designs. Rather, a 'conservative' approach was usually imposed in which each computational step is biased in a 'conservative' direction. It is recognized that such a procedure compounds and amplifies to arrive at a result for which the actual safety margin is unknown. The justification for this procedure has been that the available data base is inadequate to establish realistic safety margins. At a time when only the CVTR measurements were available, it was difficult to oppose this argument, however the situation is altered now. With the extensive and complementary data base generated by the Batt.-Fr and HDR test series, containment design methodology can rejoin the traditional engineering disciplines. Now we can establish not only what we know, but we can also quantify the uncertainty margins which bound our knowledge.

In the final analysis this will probably be the most significant impact of the HDR data.

REFERENCES

1. Schmitt, R.C., et al., "Simulated Design Basis Accident Test of CVTR", IN-1403 (1970).
2. Kanzleiter, T., "RS-50 Modellcontainment Versuche Abschlusbericht", BF-RS 50-01 (Dec. 1980).
3. Versuchsprotokoll Blowdown-Versuch V-42 (19/08/82) PHDR 3.32/82.
4. Versuchsprotokoll Blowdown-Versuch V-44 (09/9/82) PHDR 3.329/82.
5. Versuchsprotokoll Blowdown-Versuch V-44 (07/10/82) PHDR 3.333/82.
6. Versuchsprotokoll Blowdown-Versuch V-21.1 (10/5/83) PHDR 3.376/83.
7. Versuchsprotokoll Blowdown-Versuch V-21.3 (07/6/83) PHDR 3.380/83.
8. Almenas, K., "Comparison of Measured and Calcuated Heat Transfer Coefficients for the HDR Containment Experiments", (March 1983) PHDR-Arbeitsbericht Nr 3.364/83.

9. Wolf, L., Valencia, L. and Kanzleiter, T., "Overview of the HDR-Containment Tests", 11th Reactor Safety Research Meeting, NUREG/CP.0048 (Oct. 1983).

10. Almenas, K., "Containment Related Tests at HDR Energy Transfer to Structures" 11th Reactor Safety Research Meeting, NUREG/CP.0048 (Oct. 1983).

11. Valencia, L. and Kanzleiter, T., "Blowdown-Untersuchungen in einem Reaktorcontainment" Techn. Fachbericht PHDR 38-83 (May 1983).

12. Jansen, K., "Auswertebericht Wassermitrißmessungen V-42, V-43 and V-44" PHDR Nr. 3.378/83.

13. "Statusbericht des Projektes HDR-Sicherheits program, 1983" PHDR-Asbeitsbericht 05.18/83.

14. Almenas, K., "Comparison of Experimental and Calculated Pressure Differences in the HDR Containment" PHDR-Asbeitsbericht Nr. 3.388/83 (Aug. 83).

15. Burkett, M.W., et al., "Comparison of BEACON and COMPARE Reactor Cavity Subcompartment Analysis", April 1984 NUREG/CR-3305.

16. Thurgood, M.J., "COBRA-NC Post-Test Predictions for HDR Containment Steam Blowdown Test V-44", May 1984, NUREG/CR-3749.

17. "Statusbericht des Projektes HDR-Sicherheits program 1982", PHDR-Arbeitsbericht 05.12/82.

18. Uchida, et al., "Evaluation of Post Incident Cooling Systems of Light-Water Power Reactors", 3rd Geneva Conf. (A/Conf. 28/P. 436).

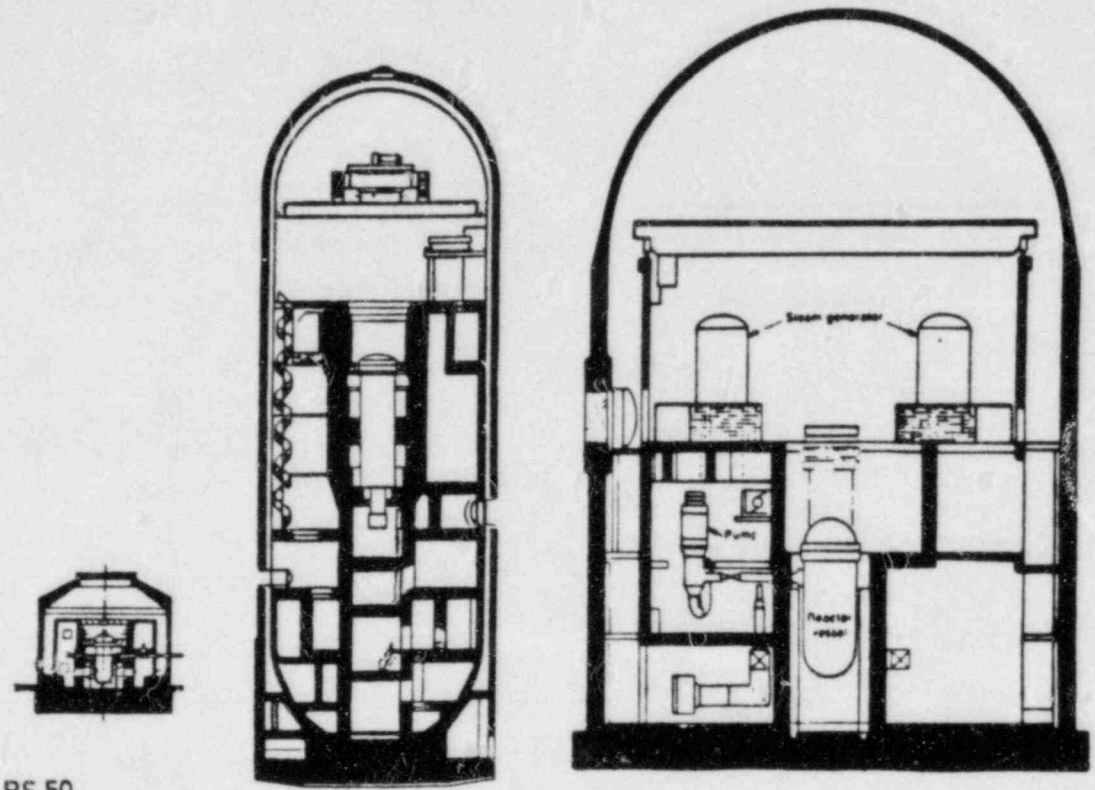

Figure 1. Relative Scale of Experimental and Actual Containments

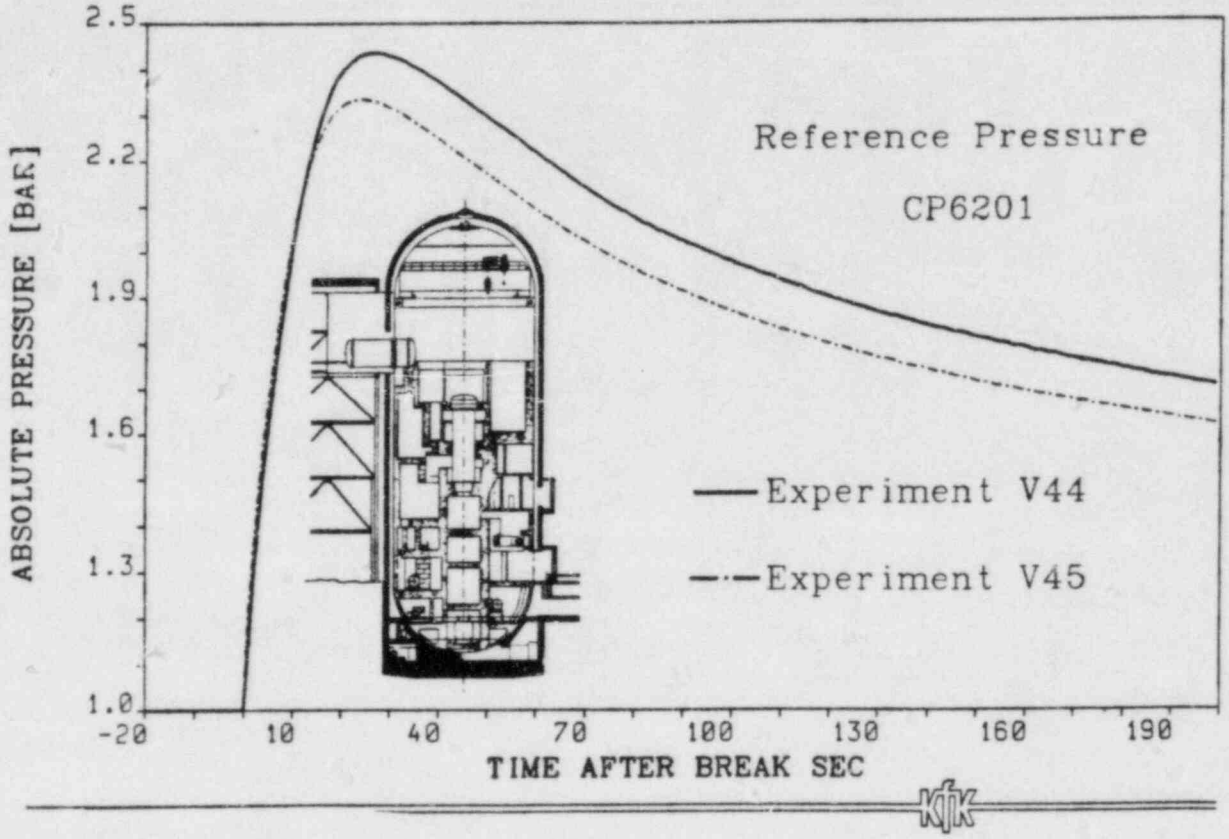

Figure 2. Time Dependence of Total Pressure

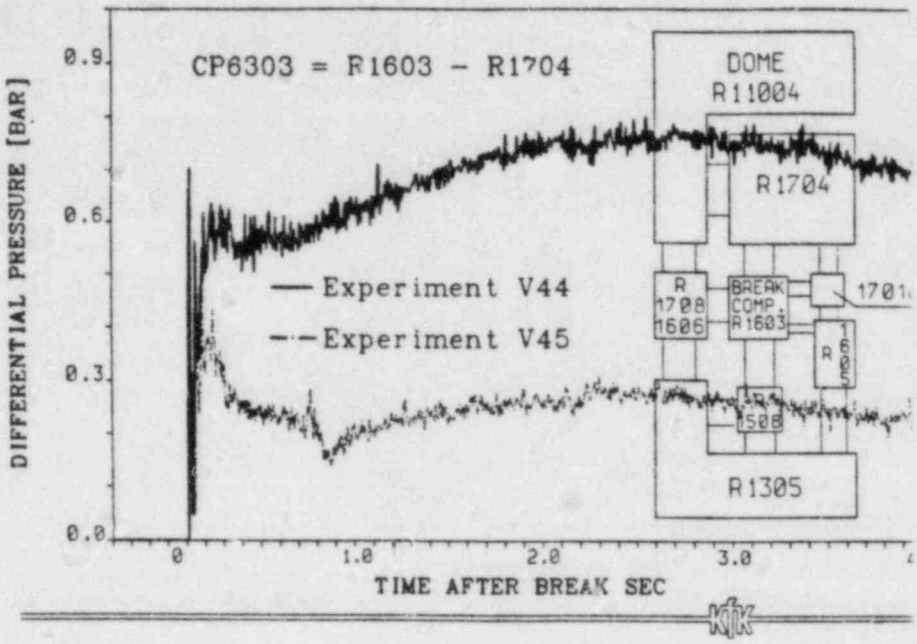

Figure 3. Pressure Difference Between Break and Adjoining Compartment

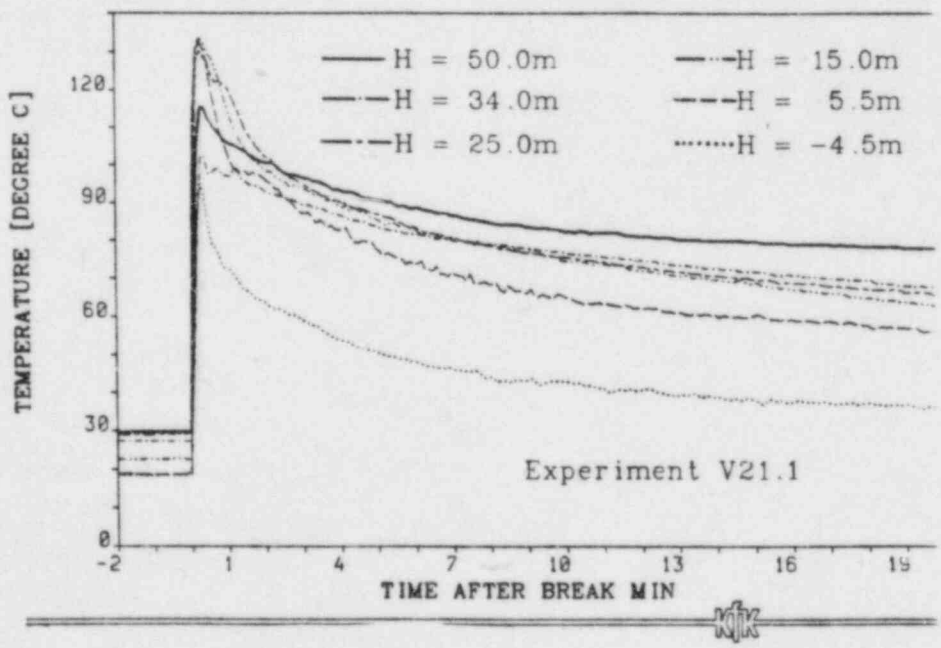

Figure 4. Vertical Atmospheric Temperature Distribution

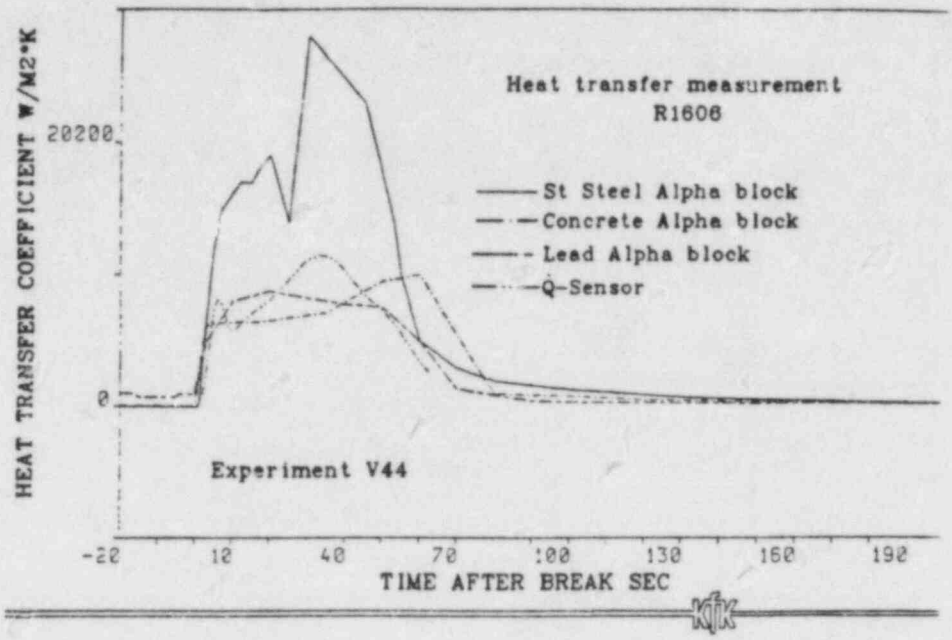

Figure 5. Measured Heat-Transfer Coefficients in Break Near Zone

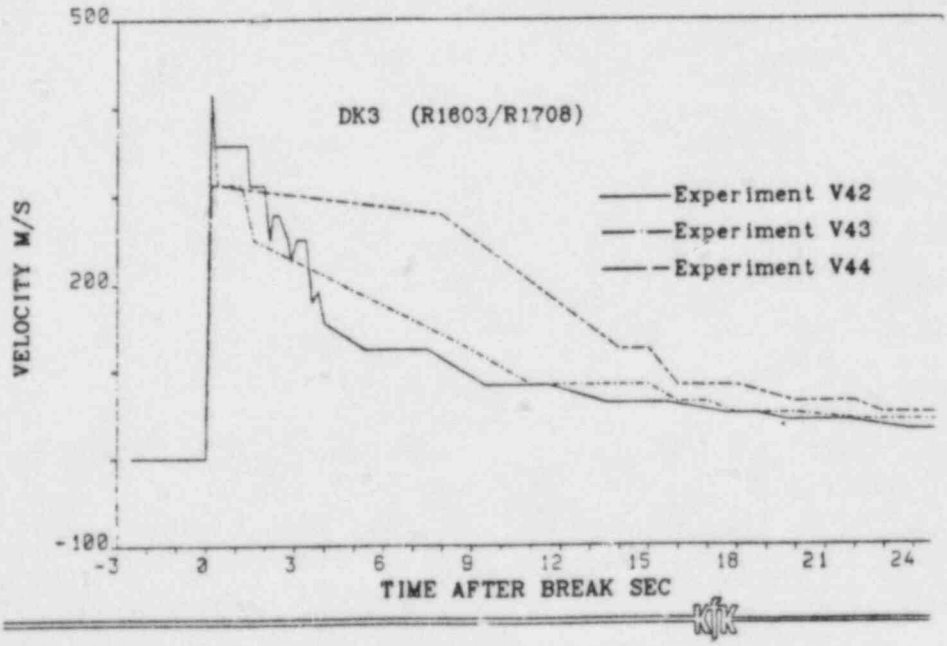

Figure 6. Droplet Velocities in Channel Leading from Break Compartment

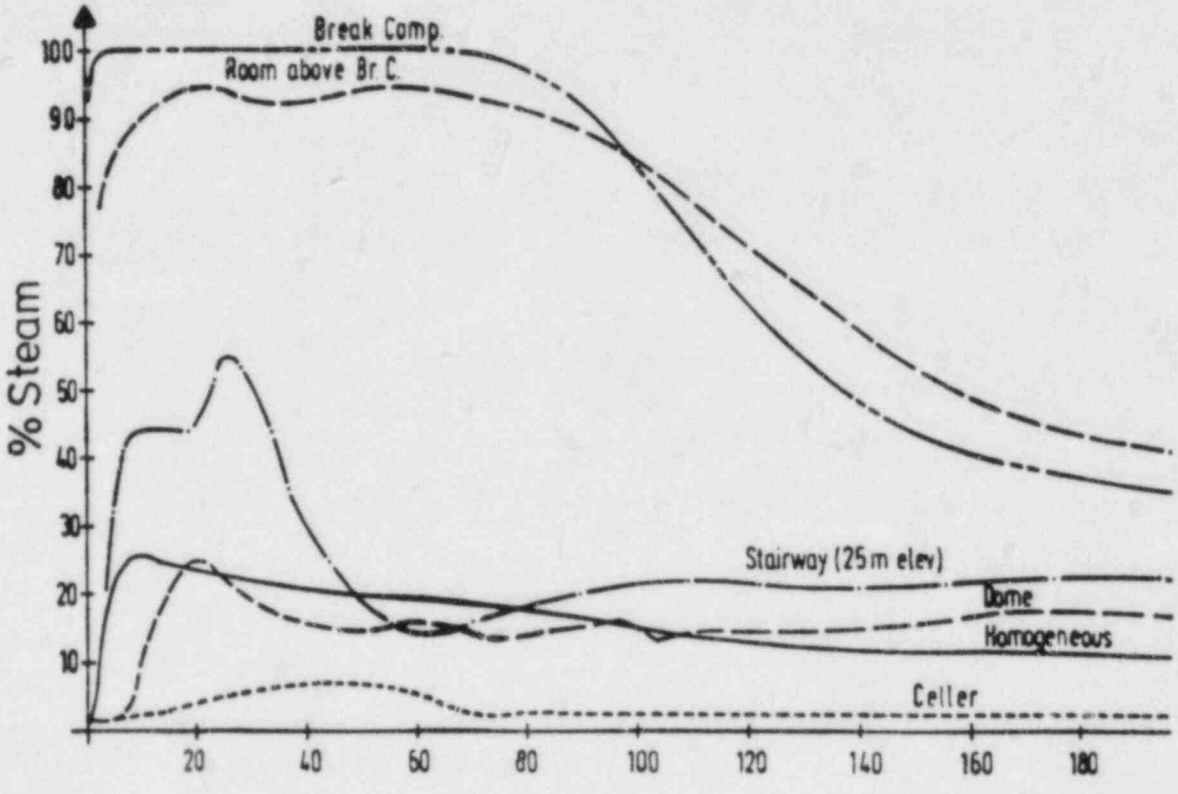

Figure 7. Weight Fraction of Steam for Test V-43

CONTAIN CALCULATIONS OF CONTAINMENT LOADING OF DRY PWRS*

K. D. Bergeron, D. C. Williams
Sandia National Laboratories
Containment Modelling Division 6449
Albuquerque, NM 87185

ABSTRACT

As part of the NRC's effort to re-evaluate the severe accident source term, two experts' groups have been formed to consolidate information and assess the state of the art in key phenomenological areas. These are the Containment Performance Working Group (CPWG), and the Containment Loads Working Group (CLWG). The CONTAIN code has been used extensively in support of the latter group to calculate pressure and temperature loads for a variety of phenomenological scenarios for core melt accidents at two reference plants, subject to standard problem constraints established by the CLWG. The two plants are a large dry PWR (resembling Zion) and a subatmospheric PWR (resembling Surry). The accident sequence in both cases was TMLB'. The following conclusions have been reached:

1. In terms of uncertainties, adiabatic pressurization due to a steam spike is essentially a one-parameter problem. A useful choice for the independent parameter is the total mass of water boiled. The non-adiabatic steam spike is essentially a two-parameter problem, the second being the time until boiling stops (presumably because of end of contact between debris and water.)

2. For the steam spike cases studied, the effect of heat losses, expressed as a percentage reduction of the pressure rise (compared to the adiabatic pressure rise) is relatively independent of the total mass of water boiled, and depends principally on the boiling time. For example, in the large dry case, for a boiling time of one minute, the pressure rise is reduced by 7% due to condensation on heat sinks, whereas for a boiling time of ten minutes, the reduction is about 20%.

*This work was supported by the U.S. Nuclear Regulatory Commission and performed at Sandia National Laboratories which is operated for the U.S. Department of Energy under Contract Number DE-AC04-76DP00789.

3. Quenching of debris in water, leading to a steam spike, results in peak pressures and temperatures which do not appear to threaten containment integrity for the plants studied. Also, hydrogen burns were suppressed by high atmospheric water content for these sequences early in time (though not necessarily late in time.)

4. Potential heat sinks for the stored and decay heat of the fuel can be ranked according to severity of resulting containment loading in the following order: concrete (least load), water, gas (greatest load). Direct heating of atmospheric gas by all the debris heat results in loads which represent marginal threats of early containment failure.

5. Significant direct heating can only occur if debris is finely dispersed (possibly by high pressure ejection) and has a sufficient residence time in the containment atmosphere. However, if these conditions are met, consideration must also be given to additional heating due to chemical oxidation of metals in the debris. Adequate chemical energy exists in the gas and metal inventories to severely challenge any containment, so more analysis and experiment is warranted to determine the likelihood of this phenomenon.

1. THE CONTAIN CODE FOR SEVERE ACCIDENT CONTAINMENT ANALYSIS

CONTAIN has been under development at Sandia National Laboratories for a number of years under the support of the USNRC. It is intended to be the NRC's principal best-estimate calculational tool for calculating the physical and radiological conditions inside the containment building of a nuclear reactor following a hypothetical severe (i.e., core-melt) accident. It is unique among containment analysis codes in that it simultaneously models thermal-hydraulic phenomena, aerosol behavior, and radioisotope transport, decay, and heating. The calculations to be discussed in this paper do not make use of this integrated analysis capability, however, since fission product and aerosol modelling were not required. The principal models used in these calculations consisted of gas-steam-water thermodynamics, condensation on heat sinks, and conduction into heat sinks. The non-thermal-hydraulic features of the code will not be discussed here; the interested reader is referred to Reference 1, or to the CONTAIN User's Manual [2], which will be released in the very near future.

Some of the calculations discussed below make use of a program referred to as DHEAT. This is a short code which was written to run very quickly, in order that large numbers of parameter variations could be considered. DHEAT results were checked carefully against those from CONTAIN over the parameter

ranges of interest, so that CONTAIN's role for these calculations was as a validation, or benchmarking tool.

2. THE CONTAINMENT LOADS WORKING GROUP STANDARD PROBLEMS 1 AND 2

The Containment Loads Working Group (CLWG) is an ad hoc committee formed by the NRC, consisting of researchers from numerous laboratories who are knowledgeable about severe accident containment phenomena. The overall purpose of the group was to illuminate the state of the art of severe accident containment loading analysis, with special emphasis on applications to NRC's source term reassessment studies. The focus of attention was leakage or failure within the first three hours following vessel failure. The mode of operation chosen was to define a number of standard problems which would allow the different analysts to perform calculations and compare results, thus identifying areas of general agreement about severe accident phenomena, as well as areas of disagreement, which could then be discussed at the technical meetings. These standard problems were not intended to be surrogates for all accident sequences, nor can conclusions drawn about containment loadings for these cases be generalized to any particular class of accidents (e.g., risk-dominant, most probable, worst credible, etc.) The principal motivation in specifying the standard problems (which were six in number) was to provide a common basis for discussion by specifying initial and boundary conditions for detailed calculations, with the purpose of revealing current expert thinking about severe accident containment phenomena.

Two of the six standard problems will be discussed in this paper: Standard Problem #1 (SP-1) and Standard Problem #2 (SP-2). SP-1 involves a large dry PWR, with many parameters taken from the Zion plant, while SP-2 was a subatmospheric containment, like the Surry plant. However, no attempt was made in either case to be completely faithful to any particular existing containment. Both problems represented a TMLB' sequence leading to core melt and vessel failure at high pressure. The principal features of the standard problem specifications are the initial containment conditions prior to vessel failure, the mass of molten debris released to the cavity, the temperature and composition of the released debris, the water level in the reactor cavity, and various geometric features of the containment building. Table 1 provides the most important of the standard problem parameter specifications (these are the base cases; a number of parameter variations were also specified, but will not be discussed in this paper.)

It should be noted that although the specification of initial conditions was helpful in focusing attention on specific containment phenomenological issues, it was also a source of some difficulties. For example, those analysts who used containment

Parameter	SP-1	SP-2
Fraction of Core Released	100%	100%
w/o UO2 in Melt	65%	70%
w/o Steel in Melt	17.5%	15%
w/o Zr in Melt	17.5%	15%
Fraction Zr Oxidized	0.5	0.3
Corium Temperature	2533°K	2533°K
Water Level in Cavity	1.5m	0.10m
Containment Pressure	0.4MPa	0.19MPa
Pressure in Vessel	17.0MPa	15.7MPa

Table 1. Key parameters from standard problem specification of conditions prior to vessel failure.

codes which included heat transfer to structures found that it was necessary to run the problem from the beginning of the accident (i.e., the initial blowdown) in order to condition the heat sinks. However, it was found to be difficult or impossible to reproduce the specified containment pressure at vessel failure if realistic blowdown histories were used. Such problems will be discussed in more detail in Section 3.

A wide variety of calculations have been performed for these standard problems, some using CONTAIN, some using other calculational tools. They will be reported in this paper in two sections. Section 3 discusses the two base case problems evaluated for a variety of alternative assumptions about phenomenology, but with no consideration of the possibility that finely particulated debris could directly heat the air, or react chemically with it; these are called "steam spike calculations." Section 4 discusses results obtained when varying degrees of direct heating of the atmosphere are assumed.

3. STEAM SPIKE PARAMETER STUDIES

When the molten debris is ejected from the pressure vessel, it may encounter water in the cavity or in the upper containment (after being swept out of the cavity as a result of ex-vessel steam explosions, or high velocity gas entrainment.) In either case, rapid quenching of the core debris is assumed to be possible. Extensive discussion of the various phenomenological issues among the CLWG resulted in a consensus concerning the reasonable upper bound which should be placed on the fraction of released melt which is quenched immediately after vessel failure. The group consensus was that 100% was the only justifiable upper

bound for the high pressure scenario. The calculations discussed below are based on this assumption. The parameter studies refer primarily to SP-1, but similar results are expected for SP-2.

Many of the calculations reported at CLWG meetings made use of the assumption that no heat transfer occured to structures on the short time scale of the quench. One important purpose of the present work is to report the results of nonadiabatic calculations using realistic heat sinks for SP-1 and CONTAIN's relatively sophisticated model for condensation heat transfer, which has been proven to be successful in predicting experimental results in blind validation exercises (see Reference 3.)

It is quite clear that the adiabatic steam spike question is a one-parameter problem. That is to say, once the initial conditions and containment parameters are specified, we need to know only one quantity to predict the final pressure. The controlling parameter used for our calculations is M_t the mass of water boiled. Adiabatic calculations are quite simple, and can be performed by hand. The nonadiabatic case is more difficult, and requires a code to deal with the nonlinearities of condensation heat transfer into the heat sinks. In this case, the problem is best understood as a simple two-parameter problem. Again, M_t is important, but a time parameter must also be considered. For the second parameter, t_o, the boiling time, is used. This is the time between melt release and the end of boiling (due to physical separation of the debris and water.) A matrix of calculations was performed for these two parameters, and results are presented in Table 2.

Case	M_t	t_o	Adiabatic Pressure Rise	Non-Adiabatic Pressure Rise	Change
1	5.6E4	60	2.8E5	2.6E5	7%
2	5.6E4	600	2.8E5	2.3E5	16%
3	5.6E4	3600	2.8E5	1.7E5	39%
4	2.8E4	60	2.0E5	1.8E5	7%
5	2.8E4	600	2.0E5	1.6E5	18%
6	2.8E4	3600	2.0E5	1.1E5	46%

Table 2. CONTAIN steam spike calculations: two-parameter matrix.

It was difficult in these calculations to match the initial conditions specified in SP-1. In order to preheat the heat sinks, the calculation had to be run from the beginning of the accident. All the calculations presented correspond to the high pressure (TMLB') case, and the CONTAIN sample problem for the Zion TMLB' was used to generate the initial conditions. This calculation is based on the same sources and heat sinks as were used in NUREG-0850 [4]. It proved impossible, using realistic blowdown sources and heat sink data, to obtain a total pressure at vessel failure time of 0.4 MPa (the specified value in Table 1.) so a case was selected with a peak pressure before failure of 0.4 MPa, which decayed to a pressure at vessel failure of 0.3 MPa. This difference is not considered important to the results in Table 2, since these deal with pressure rises only. However, in later discussions which are presented in terms of peak pressure, this difference of one atmosphere must be kept in mind.

The percent change indicated in the last column in Table 2 is the reduction in the pressure rise for the nonadiabatic case, compared to the adiabatic case. It is interesting that the percent reduction in the pressure rise due to heat loss effects (last column in Table 2) is relatively independent of M_t. Thus we can say, based on these calculations, that heat losses reduce the pressure rise by about 7% when the water limit is reached at one minute, and by about 20% when it is reached at ten minutes.

Two additional runs, designated Cases 7 and 8, were made in order to determine whether there is a dependence on the time to complete the initial quench. This time, t_q, should be distinguished from the boiling time, t_o, which is the time at which boiling stops because of loss of contact between water and debris. Between t_q and t_o, water continues to boil due to decay heating. In Case 7, the debris is quenched in one minute, but the decay heat continues to generate steam for the full hour. In Case 8, the quench takes one hour, and decay heating adds to the steam generated by quenching. Figure 1 shows the results. The final pressure is virtually the same in Cases 7 and 8. The fact that peak pressures are essentially the same for the one-minute and one-hour cases is strong support for the two-parameter hypothesis (both cases have the same t_o = 1 hour.)

4. PARAMETRIC STUDIES INCLUDING DIRECT HEATING

If vessel failure occurs at high pressure, the high velocity steam-hydrogen gas stream which would follow the melt out of the vessel and into containment could entrain the molten debris in the cavity region, and transport it into the larger containment volume. Recent experiments at Sandia and Argonne indicate that this process can occur with reasonable efficiency, and moreover, that significant fragmentation of the melt occurs in the process. An issue of recent concern is the possibility that if such finely fragmented debris is thrown into the containment building

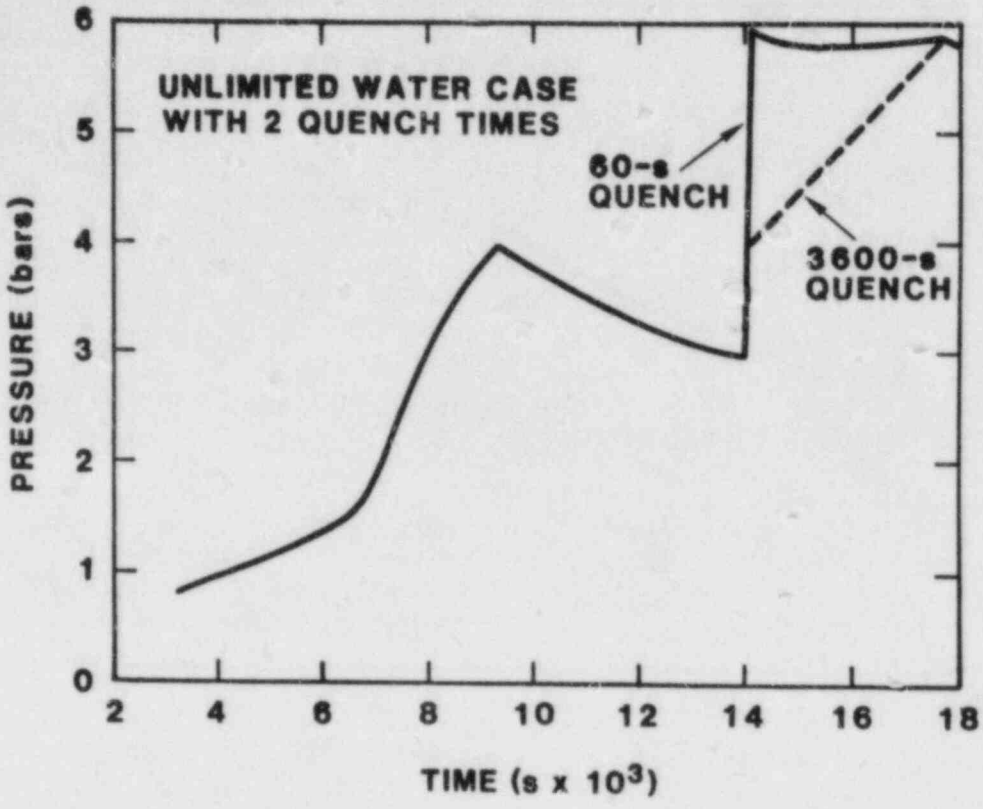

Figure 1. CONTAIN Results for two cases with the same total steam generation, but different rates of production.

atmosphere, it could give up its heat directly to the gas, resulting in higher pressurization than for the steam spike case with the same amount of heat transferred. However, more important for the direct heating scenario is the fact that the unoxidized metal in the debris can react chemically with the oxygen and/or steam in the atmosphere, resulting in a signficant increase in the total heat transferred.

In this section, a number of calculations are described which explore the magnitude of the various effects of interest. These calculations are not intended to represent either central or limiting estimates of the pressures that might result from the specified scenario, since considerable uncertainty exists concerning how much direct heating might actually take place.

CONTAIN Calculations

A series of nonadiabatic CONTAIN calculations was performed for each standard problem in order to determine the pressure and temperature rises to be expected for certain hypothetical limiting cases as well as for other cases as noted below. In each case, a sixty second input of steam and direct heating energy was assumed. For SP-1, the pre-failure history assumed was that of the CONTAIN sample problem for the Zion TMLB' sequence. For SP-2, the pre-failure history was that calculated for the base case Surry TMLB' sequence in the QUEST program 5 . Following vessel failure, the blowdown was assumed to be from the RCS volume filled with steam saturated at the system operating pressure, as was specified in the standard problem definitions. In addition, the SP-2 blowdown included 8800 kg of saturated primary system water, as had been calculated by the MARCH code in the QUEST base case noted above.

Calculations performed for the QUEST program showed that gases and vapors from core-concrete interactions (as calculated by CORCON) would not be nearly enough to reverse the pressure decline due to condensation on structures during the first few hours following vessel failure. Hence, core-concrete interactions need not be considered in any of the cases discussed in this report.

After vessel failure, the atmosphere is typically about 80% water vapor, much more than the 50-60% which is usually assumed to suppress hydrogen combustion in the sense of self-sustaining flame propagation through a relatively cold gas mixture. Hence, it is usually argued that energy release due to hydrogen combustion can be ignored in sequences of this kind. However, it should be pointed out that this argument neglects the very high temperatures which can be developed in direct heating scenarios, as will be seen below. At these temperatures, hydrogen and oxygen might react even if conditions for self-sustaining flame propagation through a cold gas mixture are not satisfied. Direct heating scenarios necessarily imply the presence of a large amount of particulate with a high aggregate surface area suspended in the containment atmosphere at the time of maximum temperature. These particulate surfaces could catalyze the hydrogen-oxygen recombination. In all the calculations presented in this report, any energy released by hydrogen-oxygen recombination has been neglected.

Results of the CONTAIN calculations are summarized in Tables 4 and 5 for SP-1 and SP-2, respectively. The tables also include results obtained with the adiabatic DHEAT code which will be discussed below. In each table, the first line gives the prefailure conditions within containment, and the next line gives the pressure resulting from only the blowdown, with no steam spike generation or direct heating. In each case, the blowdown

yields a pressure rise of approximately 1 bar (1E5 Pa). The third line in each table gives the pressure resulting if 100% of the core mass is quenched by boiling water to yield a steam spike. The steam spike yields pressure increases of slightly under 2 bars for both problems, relative to what the blowdown alone gives.

The fourth line in each table shows results obtained assuming that all the core participates in direct heating (DH), with the full core mass coming into thermal equilibrium with the containment atmosphere. The resulting pressure increases, over and above the blowdown pressure increase, are about 5 bars in SP-1 and somewhat more than 5 bars in SP-2. Thus, core energy deposited in the atmosphere as direct heating is between 2.5 and 3 times as effective in producing a pressure rise as is the same amount of energy deposited in water to generate steam. In fact, if we consider that concrete, water, and gas are the three possible depositories for the corium heat in containment, it is found that for the same heat transferred, gas (i.e., direct heating) gives a greater pressure rise than water (i.e., steam generation), which in turn gives a greater pressure rise than concrete (i.e., core-concrete interactions.) Even so, with 100% direct heating, the pressure in SP-1 is 1 bar less than the assumed failure pressure; with more realistic fractions of the core participating in direct heating it is unlikely that a serious threat would exist. For SP-2, the results exceed the assumed failure pressure by over a bar. Even so, it is not clear that more than a marginal threat to this system would exist for realistic core fractions, provided direct heating is from the core thermal energy alone.

By far the severest threats arise when it is assumed that the corium constituents can react with oxygen in the containment atmosphere. In the SP-1 base case, the atmosphere contains more than enough oxygen to oxidize all corium zirconium metal to ZrO_2, all iron to FeO, and all UO_2 to U_3O_8. In SP-2, oxygen supply is sufficient to oxidize all the Zr and Fe, but only slightly less than half the UO_2 present could be oxidized. However, in all calculations presented in this report, it was assumed that UO_2 would not be oxidized and only metal oxidation was considered. Hence, oxygen supply was never a limiting factor in any of these calculations.

The sixth case in each table shows the results obtained if it is assumed that 100% of the core participates in direct heating with 100% of the metal (but no UO_2) being oxidized. The pressure increase is more than doubled, relative to that obtained when only the core thermal energy is assumed available. The increase would be still larger were it not for the fact that the heat capacity of the containment atmosphere increases substantially (by almost 50%) at the very high temperatures that

Case	CONTAIN P 10^{+5}Pa	CONTAIN T (K)	DHEAT P 10^{+5}Pa	DHEAT T (K)
1. Pre-Failure	2.99	394	2.97	392
2. Blowdown	4.07	406	3.97	405
3. 100% Steam Spike	5.97	423	5.78	422
4. 100% DH 0% Oxidation	8.85	875	9.01	920
5. 90% DH 10% SS 90% Oxidation	13.9	1342	(14.53	1426)
6. 100% DH 100 Oxidation	14.79	1463	15.11	1543

Table 4. Phenomenological Parameter Study, SP-1.

Case	CONTAIN Results P 10^{+5}Pa	CONTAIN Results T (K)	DHEAT Results P 10^{+5}Pa	DHEAT Results T (K)
1. Pre-failure	2.79	452	2.48	386
2. Blowdown	3.80	405	3.60	403
3. 100% Steam Spike	5.69	423	5.57	422
4. 100% DH	9.14	962	9.38	1047
5. 54.2% DH 42.% Oxidation 45.8% Steam	12.05	1045	12.42	1138
6. 100% DH 100% Oxidation	15.96	1744	17.21	1922
7. 100% DH, 100 Ox. (Adiabatic)	17.93	1850	17.61	1861

Table 5. Phenomenological Parameter Study, SP-2

are achieved in these cases. This effect reduces the temperature rise, and hence the pressure rise, relative to what would be obtained if one assumed a constant heat capacity.

The fifth line in the tables gives results for intermediate "mixed" cases, in which it is assumed that the specified fractions of the core participate in thermal direct heating, chemical reaction, and steam generation. No special significance is to be ascribed to the fractions specified in these cases.

In all the cases in Tables 4 and 5 which involve steam generation, only the core thermal energy is assumed to be available for boiling water. No allowance is made for additional energy which might be available due to Zr-water reaction.

DHEAT Calculations

Figures 2 and 3 show the peak pressures and temperatures for the entire range of direct heating assumptions. These calculations were performed not with CONTAIN but with a simpler computational model (designated DHEAT) developed expressly for parameter studies involving direct heating. The principal difference between CONTAIN and DHEAT was that the latter code neglects heat transfer to structures. Numerous comparisons of DHEAT and CONTAIN results have been performed, across the entire range of the parameter space of interest, and differences between the predictions were found to be small. (See Tables 4 and 5.) Several assumptions were made about the energy available and its disposition for the calculations shown in Figures 2 and 3. In all cases, it was assumed that the fraction of potential metal oxidation energy going to direct heating was equal to the fraction of the core that contributed its thermal energy to direct heating. The remaining thermal energy was assumed to go to steam generation, without any augmentation by metal-water reaction.

The curves for the pressure show a distinct curvature, with the slope decreasing as the direct heating fraction increases. One major reason for this effect is the increase in heat capacity with temperature that was noted previously. Another reason is that, after thermal equilibration with the atmosphere, some energy still resides in the corium that participates in the direct heating process. As the direct heating fraction increases, both the corium mass involved and the temperature increase. Hence, the fraction of the total system energy that resides in the corium at equilibrium increases with increasing direct heating. For 100% direct heating, about 17% of the energy remains in the corium at equilibrium in SP-1, and about 21.5% in SP-2. Thus the effect is not large, but neither is it entirely negligible. The effect becomes very important in limiting the influence of direct heating if it is assumed only a small fraction of the containment atmosphere is available to receive

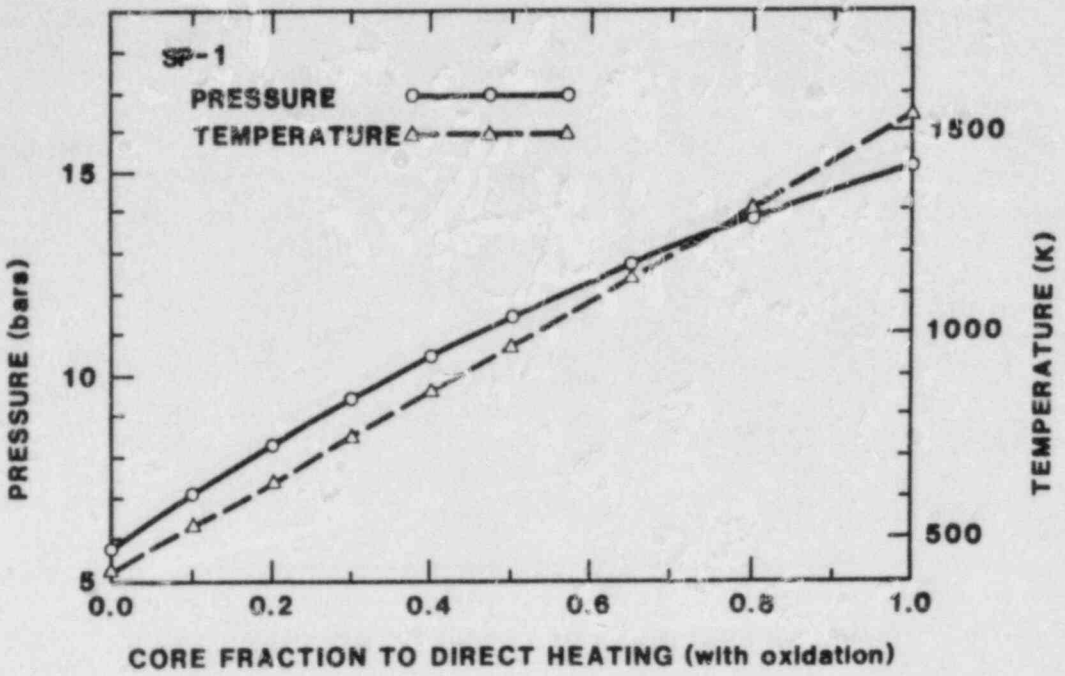

Figure 2. DHEAT predictions of peak containment pressure and temperature over the range of direct heating fractions for SP-1.

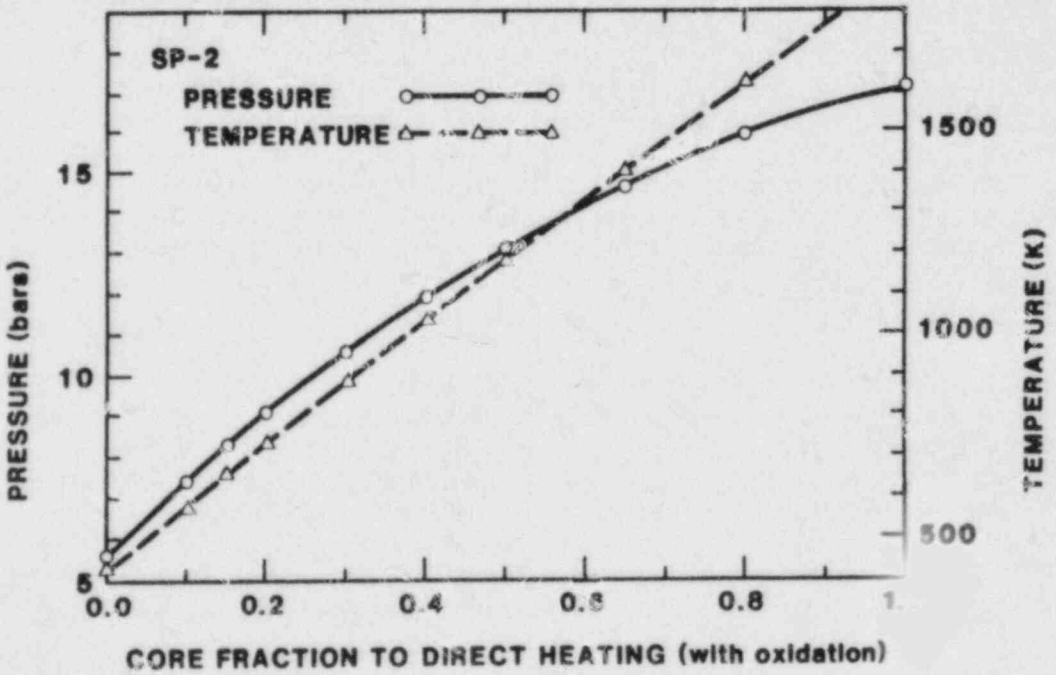

Figure 3. DHEAT predictions of peak containment pressure and temperature over the range of direct heating fractions for SP-2.

energy from the corium. The plot of final temperature versus direct heating fraction is almost linear for both SP-1 and SP-2. Evidently, the effects noted above in connection with the pressures are largely compensated for by the reduced steam generation as the direct heating fraction increases. This effect, in turn, permits a larger temperature rise for a given energy input.

CONCLUSIONS

A number of parameter studies have been performed with the CONTAIN code, and with a simpler code which has been successfully validated by CONTAIN. These calculations are based on the two standard problems specified for the CLWG for a large dry containment and a subatmospheric containment. A number of conclusions can be drawn from these results:

1. Once containment volumes and heat sinks are specified, the peak pressure in the adiabatic steam spike problem depends essentially on one parameter, while the non-adiabatic problem depends on two; a convenient choice is the mass of water boiled and the time to the end of boiling.

2. For both SP-1 and SP-2, peak pressures and temperatures remain well below their nominal failure values for the first few hours following vessel failure when the pressurizing mechanism is steam generation. Hydrogen burns are suppressed for the accident sequence considered, and non-condensible gas generation due to corium-concrete interactions are not an important pressurizing mechanism on this time scale.

3. If it is assumed that, because of fragmentation and dispersal of the melt, chemical reactions between atmospheric oxygen and unoxidized metal in the debris can occur, and that the atmospheric gas can be heated directly by the debris, then the early pressure and temperature loads on containment can be very severe. Whether such direct heating might occur, and what fraction of the ejected melt might participate remains highly uncertain; additional experimental and analytical research would be required to reduce this uncertainty.

REFERENCES

1. K. D. Bergeron et al., "An Overview of the CONTAIN Code for Severe Accident Analysis", Eleventh Water Reactor Safety Research Information Meeting, Gaithersburg, MD, Oct. 24-28, 1983.

2. K. D. Bergeron et al., "User's Manual for CONTAIN, A Computer Code for Severe Nuclear Reactor Accident Containment Analysis", (Draft) SAND 84-1204, Sandia National Laboratories, to be published.

3. K. K. Murata et al., "CONTAIN: Recent Highlights in Code Testing and Validation", Proc. Intl. Mtg. on LWR Severe Accident Evaluation, Cambridge, MA (8/28/83 - 9/1/83), p. 5.4-1.

4. "Preliminary Assessment of Core Melt Accidents at the Zion and Indian Point Nuclear Power Plants and Strategies for Mitigating Their Effects," NUREG-0850, v. 1, U. S. Nuclear Regulatory Commission, November, 1981.

5. D. C. Williams, K. K. Murata, and J. L. Tills, "Phenomenological Uncertainties in the Suspended Radionuclide Concentrations in Containment During Severe LWR Accidents," to be presented at ANS Fission Product Behavior and Source Term Research Meeting, July 15-19, 1984, Snowbird, Utah.

COMBUSTION-INDUCED LOADS IN LARGE-DRY PWR CONTAINMENTS

F. Eric Haskin, Vance L. Behr
Sandia National Laboratories
Albuquerque, NM 87185

Lanny N. Smith
Science Applications, Inc.
Albuquerque, NM 87185

ABSTRACT

The potential for combustion-induced failures of containment must be considered when estimating the risk associated with nuclear power plants. Some large-dry PWR containments are sufficiently strong that it is difficult to envision scenarios in which combustion events alone would challenge their ultimate capacities. On the other hand, the ultimate capacities of other, weaker, large-dry containments are more easily challenged by combustion events. Recently, analyses have been performed to investigate the range of possible containment loadings that could be produced due to combustion events during severe accidents in large-dry PWR containments. Calculations are presented for typical atmospheric and sub-atmospheric containments. Various accident scenarios are examined and key parameters influencing potential combustion-induced loads are identified.

INTRODUCTION

In this paper we discuss the factors which control combustion-induced, pressure-temperature loads in large-dry PWR containments during postulated severe accidents. These loads, in turn, influence the potential for pressure-temperature-induced containment leakage or large-scale structural failure of containment. We discuss pressure-temperature loads in three time regimes: 1, before the reactor pressure vessel is breached and core debris is discharged to containment, 2) shortly following vessel breach, and 3) longer times after vessel breach. Our observations are based, in part, on analyses performed recently for the Containment Loads Working Group organized by the US Nuclear Regulatory Commission.

*This work was supported by the US Nuclear Regulatory Commission, Office of Nuclear Regulatory Research, and performed at Sandia National Laboratories which is operated for the US Department of Energy under Contract Number DE-AC04-76DP00789.

Large-dry PWR containments share some common design features which can influence combustion-induced loads. For example, most are relatively open steel-lined concrete structures which permit rapid mixing of gases throughout their free volumes. All large-dry PWR containments utilize containment sprays for removing heat and radionuclides from their atmospheres. Deliberate ignition systems are not currently installed in large-dry PWR containments.

There are also some important differences among large-dry PWR containments. The subatmospheric containments tend to have lower estimated ultimate capacities; however, this is somewhat compensated for by their lower pre-accident operating pressures. Some large-dry containments have safety-grade fan coolers which provide an alternate means of heat removal; whereas, others only have containment sprays. Some containments are designed to permit overflow of water from the floor of containment to the reactor cavity (so-called wet-cavity designs); whereas, others do not (so-called dry-cavity designs).

Quantitative analyses presented in this paper are based on the plant parameters presented in Table 1. These parameters are used to characterize pressure-temperature loadings in the Zion[1] and Surry[2] containments. Zion and Surry are representative atmospheric and subatmospheric containments, respectively. The results presented herein should not be applied to large-dry containments having significantly different design parameters.

Table 1
Zion and Surry Parameters.

	Zion	Surry
Containment Design Pressure, psig	47	45
Estimated Failure Pressure[1,4], psig	134	85
Containment Free Volume, ft^3	2,715,000	1,800,000
Conditions at Containment Isolation		
Temperature, F	100	100
Pressure, psia	14.7	10
Percent Relative Humidity	100	40
Amount of Zirconium in Core, lbs	47,671	36,300
H_2 from 100% Zirconium Oxidation, lbs	2,107	1,604
Safety-Grade Fan Coolers	5	None
Overflow from Floor to Reactor Cavity	Yes	No

COMBUSTION EVENTS BEFORE VESSEL BREACH

There are two possible causes of pressure-temperature loads in large-dry PWR containments prior to vessel breach and the discharge of core debris from the reactor coolant system. First, steam and hydrogen blowdown from the reactor coolant system can pressurize and heat the containment atmosphere, particularly if containment heat removal systems are not operating. Second, combustion events are possible, provided sufficient hydrogen from in-vessel zirconium oxidation is released to containment and steam concentrations in containment are not high (combustion is precluded when steam mole fractions exceed 0.5 to 0.6).

Primary System Blowdown

Large-dry PWR containment heat removal systems are designed to keep the containment pressure below the design pressure following a large pipe break in the reactor coolant system, even when the worst conceivable single failure of electrical systems is postulated, usually disabling about 50% of the containment heat removal capacity. Thus, in severe accident scenarios in which containment heat removal systems operate, there is little challenge to containment due to primary system blowdown alone. In fact, with full containment heat removal capability, containment pressures, in the absence of combustion events, can usually be kept under about 25 psia. Steam concentrations will not be high enough to preclude combustion events before vessel breach in such accidents.

In accident scenarios in which containment heat removal systems are not operating, steam blowdown from the reactor coolant system rapidly results in "steam inerting" (i.e., a steam mole fraction in excess of 0.60) which precludes combustion events. In many such scenarios, blowdown from the reactor coolant system is limited to the initial coolant inventory with some conversion of water to hydrogen due to in-vessel zirconium oxidation. With this limited blowdown, the containment ultimate capacity is rarely challenged and the containment atmosphere will still be steam inerted (with pressures typically in the 40 to 60 psia range) just before vessel breach. If additional reactor coolant system blowdown is generated as a result of limited or full emergency core coolant flow, decay heat will effectively be transferred to the containment atmosphere and large-scale structural failure of containment could occur due to steam over-pressure.

Hydrogen Combustion

In severe accident scenarios in which containment heat removal systems operate to condense steam, combustion events may occur. Factors which would determine the actual magnitude of combustion induced loads and the threat to containment integrity which they pose include:

1. Steam and hydrogen releases to the containment over the course of the accident,

2. The containment design, particularly its ultimate capacity, free volume, and compartmentalization,

3. The survivability and performance of containment ESFs which act to reduce pre-burn pressures and, in the case of containment sprays, the pressure rise associated with a burn,

4. Pre-burn transport and mixing of gases released to containment,

5. The point in time and space at which ignition occurs,

6. The burn time, and

7. The completeness of combustion.

Figure 1 shows adiabatic, constant-volume hydrogen burn (deflagration) pressures for Zion and Surry as a function of both the pre-burn hydrogen mole fraction (ranging from 0.04 to 0.14) and the corresponding pre-burn hydrogen mass in containment. The pre-burn containment atmosphere is assumed to be steam saturated. Combustion is assumed to be complete. Results are shown for pre-burn pressures of 20, 30 and 40 psia for Zion and 15, 25, and 35 psia for Surry. In addition, results are shown for pre-burn conditions bounding the onset of steam inerting (steam mole fractions ranging from 0.50 to 0.60).

The burn pressures shown in Figure 1 are upper bounds. They depend primarily on the pre-burn pressure and the quantity of hydrogen burned. Table 1 includes the initial conditions at containment isolation which were used to develop Figure 1. Less water vapor in the atmosphere at the time of containment isolation would increase the air mole fractions, but this would shift the adiabatic burn curves in Figure 1 only slightly higher. For the assumed initial conditions, Zion has roughly 2.0 times and Surry roughly 1.5 times as much oxygen as would be required to burn the hydrogen from 100% zirconium oxidation.

Actual peak pressures would be less than shown in Figure 1 due to the time available for heat transfer from the burning gases and the possibility of incomplete burning. For example, Figure 2 shows typical results for the pressure suppression achievable due to containment sprays as a function of burn time[3]. As a point of reference, the TMI-2 burn time has been estimated as 0.13 minutes.

The estimated ultimate capacity of the Zion containment is 149 psia[1]. Accepting this estimate, Figure 1 shows that containment failure due to hydrogen deflagrations is not plausible at Zion before vessel breach.

The ultimate capacity of the Surry containment is estimated to be 100 psia (with a large uncertainty band)[4]. Figure 1 shows that 100 psia due to a hydrogen deflagration before vessel

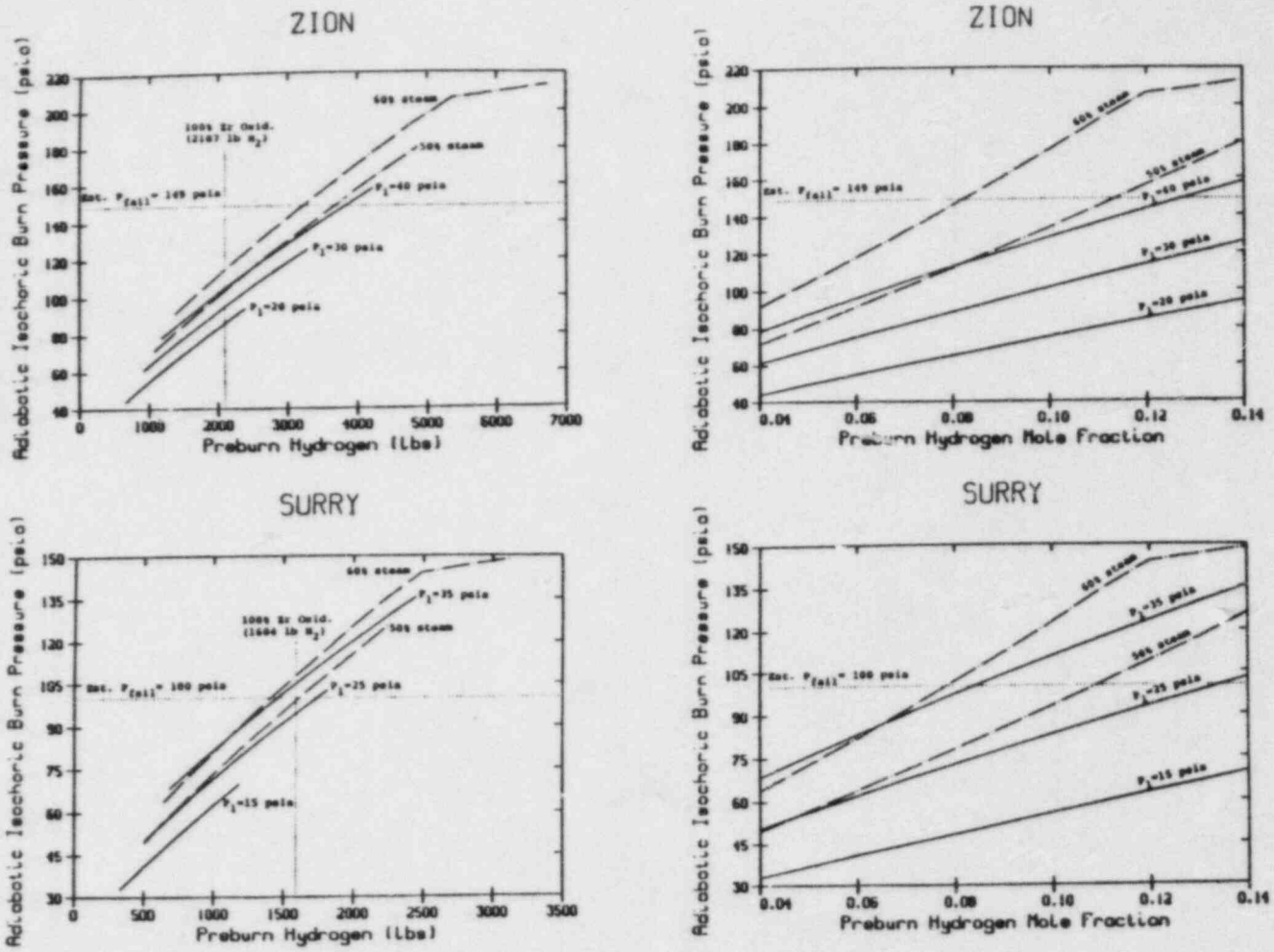

Figure 1 Adiabatic Isochoric Burn Pressures for Complete Deflagrations Ignited at Saturated Conditions in the Zion and Surry Containments.

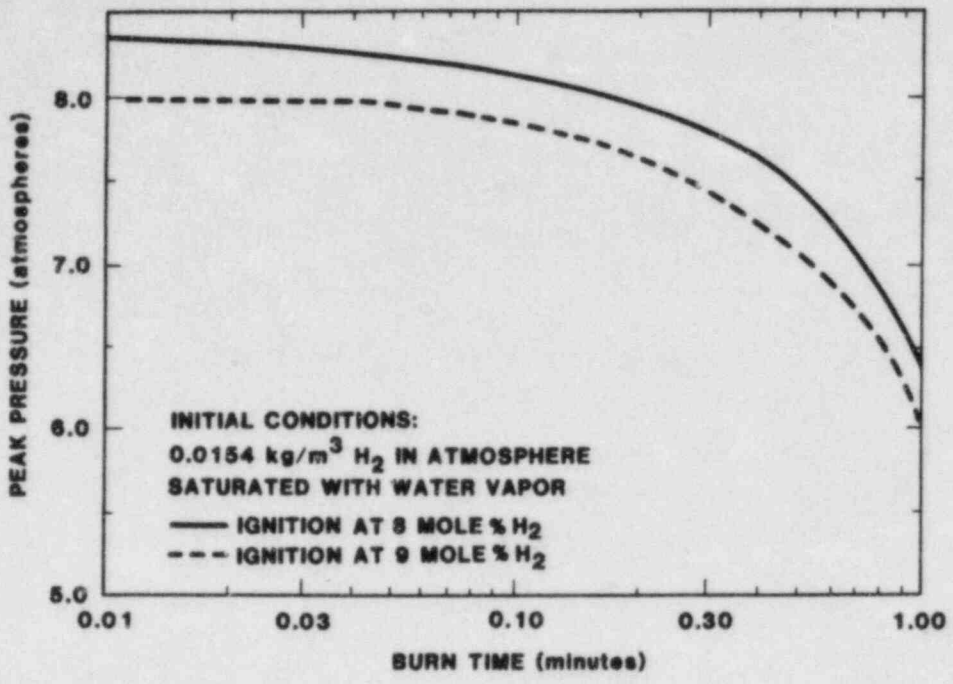

Figure 2. Effect of Burn Time on Peak Pressures

breach at Surry would only be possible if approximately 100% zirconium oxidation occurred, all the hydrogen were released to containment before vessel breach, the containment heat removal systems were performing marginally so that a high (but not high enough to be steam inerted) pre-burn pressure existed, and there was a very rapid and complete deflagration.

Given the uncertainty in the containment failure pressure for Surry, it is instructive to use Figure 1 to see what kind of burn would be required to reach the proof pressure (67 psia). With containment sprays operating, containment pressures prior to vessel breach are typically less than 25 psia. From Figure 1, to reach 67 psia at Surry due to a burn initiated at 25 psia would require the hydrogen from approximately 60% zirconium oxidation to be released to containment and ignited.

Hydrogen mole fractions greater than 0.041 (conventional limit for upward flame propagation) are certainly achievable prior to vessel breach at Surry. Hence, burns prior to vessel breach could occur at Surry. Without a deliberate ignition system, combustion would depend upon ignition from other sources such as sparks from electrical equipment. Thus, the point in time and space where ignition would occur (if it occurred) is uncertain. If burns do occur prior to vessel breach they could have detrimental effects on equipment operability or containment penetration seals. On the other hand, such burns would reduce the possibility of subsequent containment failure by reducing the hydrogen and oxygen inventories.

Local Detonations

A local detonation may be possible if hydrogen accumulates in certain areas and the geometries are such that a detonation can propagate. Detonations have been observed in hydrogen-air mixtures containing 13.8% hydrogen[5]. For most postulated severe accidents in large-dry PWR containments, steam and hydrogen blowdown from the primary system would be directed to one (or both) of the steam generator compartments prior to vessel breach. Pockets of high hydrogen concentration would be difficult to achieve in accidents in which sprays were operating because strong mixing would be induced by the sprays. Detonations also require fairly strong ignition sources or a transition from a deflagration to a detonation. Finally, even if a local detonation were to occur, the secondary shield walls which enclose the steam generator compartments are usually 3 to 4 feet thick and might serve to isolate the containment from the local detonation. In spite of the above arguments it is not possible, at this time, to state with certainty the threat to large, dry PWR containments posed by possible local detonations.

PRESSURE-TEMPERATURE LOADS SHORTLY FOLLOWING VESSEL BREACH

After the reactor vessel has been breached and the core debris discharged into containment, there are five sources of energy available to heat and pressurize the containment atmosphere:

1. Internal energy of steam, hydrogen, and water in the reactor coolant system just prior to vessel breach.
2. Combustion energy associated with hydrogen in the containment and reactor coolant system.
3. Internal energy of the core debris.
4. Chemical energy potentially available via oxidation of the core debris.
5. Decay heat which will be released by the core debris.

The internal energy of steam, hydrogen, and water in the reactor coolant system will be added to the containment as the reactor coolant system depressurizes following vessel breach. There are four principal methods for transferring portions of the other energy sources to the containment atmosphere:

1. By vaporizing available water.
2. By direct heating, that is, heating due to direct contact between finely dispersed debris and the containment atmosphere.
3. By combustion events.
4. By interactions between debris and structures (e.g., the concrete basemat). Such interactions can indirectly transfer energy to the containment atmosphere.

During the hour following vessel breach, vaporization, direct heating, and combustion are capable of imposing high pressure-temperature loads. The potential loads which could result from combustion events alone are adequately covered by Figure 1. Combustion events coincident with steam spikes and direct heating are discussed below.

Steam Spike

The term "steam spike" refers to the phenomena which would occur in containment shortly after vessel breach if the hot debris expelled from the vessel were quenched by water in the reactor cavity. The associated rapid production of steam can, in certain instances, threaten containment integrity due to steam over-pressure. In order for this phenomena to occur, there must be water present with the debris in the reactor cavity and the debris must be fragmented sufficiently to provide ample heat transfer area. Water can be available in the reactor cavity from at least two sources, either due to overflow from the containment sump earlier in the accident or due to accumulator discharge at the time of vessel breach. The debris can be fragmented by the ejection process itself or by interactions with water in the reactor cavity.

The US Nuclear Regulatory Commission devised standard problems for the Containment Loads Working Group to quantify the potential containment pressure-temperature loadings due to "steam spikes" in large dry containments such as Zion and Surry. Analyses of these standard problems have shown that for very rapid (one minute or less) quenching, the pressure rise attributable to quenching may be treated adiabatically, and, as a first approximation, is independent of the containment pressure prior to vessel breach. That is, the containment pressure-temperature loads due to a steam spike alone are determined by two parameters: the amount of water vaporized and the time interval over which it is vaporized. Steam spike pressure rises of 25 to 30 psi are conceivable at both Zion and Surry. The additional pressure rise due to reactor coolant system depressurization following vessel breach will depend on the reactor coolant system pressure but can be as high as 15 psi. These two effects combined are insufficient to challenge either the Zion or Surry containments.

Steam Spike Coincident with Combustion

We cannot preclude the possibility of combustion events occuring coincident with a steam spike. For example, consider an accident in which the primary system is above the accumulator set point and the reactor cavity is either dry or only partially full of water just before vessel breach. If there is a combustible mixture in containment, hot debris initially ejected from the vessel could serve to ignite the mixture before steam inerting could be achieved during the subsequent quenching of ejected debris by accumulator water and/or pre-existing water in the reactor cavity. If the debris is quenched by pre-existing water in the reactor cavity, the quench could produce steam inerting

before any release of hydrogen from the vessel, and combustion coincident with the steam spike would be limited to the hydrogen present in containment before vessel breach. If the debris is quenched by accumulator water, substantial hydrogen could be released from the vessel before the accumulator dump (and associated steam spike), and this hydrogen could participate in combustion.

Table 2 provides adiabatic estimates of the peak pressures (P_2) which could result from a deflagration coincident with a steam spike. The values presented in Table 2 are consistent with those in Figure 1, with P_1 now being interpreted as the containment pressure which would result from vessel depressurization and the steam spike without coincident combustion. The effect of postulating ignition just before the steam spike is to effectively negate steam inerting so that resultant pressures higher than those shown in Figure 1 for 60% steam become plausible.

Table 2
Adiabatic Loadings for Combustion Coincident with Steam Spike

Containment	Zr Oxid.	H2 (lb)	P_1 (psia)	P_2 (psia)	T2 (F)
Surry	25%	401	35	55	640
			45	65	573
			55	74	532
			65	84	507
	50%	802	35	73	1018
			45	83	875
			55	93	785
			65	102	722
	100%	1604	35	106	1714
			45	116	1437
			55	126	1257
			65	136	1131
Zion	25%	527	40	58	550
			50	68	509
			60	77	483
			70	87	468
	50%	1054	40	75	852
			50	84	754
			60	94	690
			70	104	647
	100%	2107	40	105	1412
			50	115	1215
			60	124	1083
			70	134	988

In the absence of direct heating (see next section), the values in Table 2 are upper bounds. Timing would determine the actual peak loadings following vessel breach. The key timing questions are:

1. When would combustion begin?
2. How much hydrogen would be burned?
3. What would the burn time be?
4. When would quenching begin?
5. How much debris energy would be quenched?
6. What would the rate of quenching be?

Longer burn times and slower quenching rates would tend to reduce the peak loads. Similarly, time separation between burning and quenching would reduce the peak loads. While currently the possibility of containment failure due to coincident quenching and burning in containments like Zion can be excluded, it cannot for containments like Surry.

A local detonation may be possible at the time of vessel breach. Ejection of melt from the reactor cavity could provide the required ignition source. The comments made in our discussion of local detonations before vessel breach still apply. Again, the likelihood of a detonation would depend on geometry and mixing dynamics, and it is not clear that a local detonation would substantially increase the loads imposed on the containment shell.

Direct Heating

Recent efforts by the Containment Loads Working Group have focused on so-called direct heating scenarios in which hot debris ejected from a pressurized reactor coolant system at vessel breach escapes the reactor cavity as finely fragmented particles. Experimental evidence has been obtained in the 1:20th scale SPITS experiments and the 1:10th scale HIPS experiments at Sandia to confirm the possibility of such scenarios[6]. However, there is considerable uncertainty regarding the fraction of hot core debris which could participate in direct heating in full scale reactor accidents. Some investigators feel that as much as 50% of the debris thermal energy and 50% of the available chemical energy could be transferred to the atmosphere in direct heating. Others feel that physical barriers coupled with simultaneous ejection of water from the reactor cavity would limit direct heating to 2% of the debris thermal energy with the remaining debris energy being water quenched or proceeding to core-concrete interactions. Direct heating scenarios have also been questioned on the grounds that the reactor coolant system pressure boundary may fail due to high temperature even before the core melts. The resultant reactor coolant system depressurization would remove the driving force for the particularizing and ejection of debris into the containment atmosphere at the time of vessel breach.

Bergeron, Williams, and Zimmerman[7] have performed extensive parametric calculations of the possible containment loads associated with direct heating. Their results indicate that core energy deposited in the atmosphere by direct heating is between 2.5 and 3 times as effective in producing pressure rise

as is the same amount of energy deposited in water to generate steam. For example, if water quenching 100% of the debris gave a steam spike pressure increase of 30 psi, a 50:50 split between water quenching and direct heating would give a pressure rise of approximately 56 psi. Thus, direct heating involving thermal energy alone would not challenge the estimated ultimate capacity of the Zion containment but could, depending on the containment pressure just prior to vessel breach, challenge the ultimate capacity of the Surry containment.

The chemical energy available for direct heating will depend primarily on the amount of un-oxidized zirconium in the ejected debris. At 40% in-vessel zirconium oxidation, the available chemical energy is roughly twice the available thermal energy, assuming a debris temperature of 4100 F. The heat of the reaction $Zr+O_2 \rightarrow ZrO_2$ is -258 kcal/mole. The heat of the reaction $2H_2+O_2 \rightarrow 2H_2O$ is -115.6 kcal/mole. Thus direct oxidation of zirconium with oxygen in the containment atmosphere would add roughly 2.2 times as much energy to the containment atmosphere as in-vessel zirconium oxidation followed by combustion of the resultant hydrogen (since the heat of reaction associated with oxidation of zirconium in-core to produce hydrogen primarily remains with the core). If both chemical and thermal energy are directly transferred to the containment atmosphere, involvement of only modest fractions of the core debris (10 to 35%) could generate severe threats to containment integrity even for Zion.

Hydrogen combustion concurrent with direct heating can be precluded if the extent of direct heating is mild (<2% of core debris involved) and the containment atmosphere is steam inerted prior to vessel breach. If the containment atmosphere is not steam inerted, a single hot particle could serve as an ignition source. The loads presented previously in Table 2 are roughly applicable for the mild direct heating scenarios, since non-adiabatic effects would tend to compensate for the small additional heat input due to direct heating. If large fractions of the core are involved in direct heating, the resulting temperatures can be high enough to permit recombination of hydrogen and oxygen in the containment atmosphere even in the presence of high steam concentrations. However, as noted above, the dominant uncertainty is not that associated with whether concurrent hydrogen recombination will occur. Rather, the dominant uncertainty is whether large fractions of core debris can participate in direct heating.

LATE PRESSURE-TEMPERATURE LOADS

Steam and Non-condensible Gases

There are two factors which combine to determine to potential for significant combustion-induced loads late in the accident. First, the status of the debris will determine the amounts of gases available for combustion. If the debris assumes a coolable configuration and sufficient water is available to

keep the debris cooled, the decay heat will be removed from the debris in the form of steam released to the containment atmosphere. If the debris is not coolable, concrete attack is inevitable. When basemat concrete is decomposed due to contact with molten debris, steam and carbon-dioxide are released. When the steam and carbon-dioxide pass through the overlying molten debris, they can react chemically with metallic species in the molten debris. These chemical reactions release combustible carbon monoxide and hydrogen to the containment atmosphere.

Second, the status of containment heat removal systems will strongly influence whether the containment will be steam inerted. If containment heat removal systems are not operating or fail due to conditions in the containment atmosphere, steam from debris-liquid and/or debris-concrete contact as well as from the heating and degassing of unlined concrete walls can induce or maintain steam inerting. If concrete attack by the hot debris takes place while the atmosphere is steam inert, hydrogen and carbon-monoxide will accumulate in the containment atmosphere. If the steam mole fraction is subsequently reduced below the level required for steam inerting, these combustible gases would be available to participate in combustion events. This scenario is discussed further below. Of course, without containment heat removal system, the containment may fail by over-pressurization while steam inerted.

Late Combustion With Continuous Containment Heat Removal

If containment heat removal systems operate continuously throughout the scenario, late combustion-induced loads can potentially be higher than combustion induced loads before vessel breach. More combustible gases are available after vessel breach than before. Additional hydrogen is released to containment as the reactor coolant system depressurizes,and hydrogen and carbon monoxide are released via ex-vessel oxidation of metallic debris. The molar combustion energy for carbon monoxide is approximately 10% higher than that for hydrogen. More importantly, however, carbon monoxide tends to increase the flammability limits. For example, the classical, downward flammability limit increases monotonically[8] from a combustible mole fraction of 0.09 for hydrogen to a combustible mole fraction of 0.15 for carbon monoxide. This means that, when carbon monoxide is present, proportionately more energy has to be released per unit volume to sustain global burning. The release of non-condensible gases following vessel breach will also tend to raise the baseline pressure for late combustion events. On the other hand, carbon dioxide released from core concrete interactions acts (like steam) to inhibit burning and, given a burn, acts to reduce peak pressures somewhat due to its relatively high molar heat capacity.

In spite of the above considerations, the adiabatic results presented in Figure 1 are, to a first approximation, applicable to combustion after vessel breach if: 1)the total combustible mole fraction of hydrogen and carbon monoxide is used in lieu of

the hydrogen mole fraction, 2)the combined steam and carbon dioxide mole fraction is used as an inerting indicator, and 3)the threshold for ignition is adjusted upward in accordance with Reference 8. Finally, the total amount of burning is ultimately limited by the amount of oxygen present in containment. In scenarios in which containment heat removal is continuously available, it is much more likely that the oxygen would be consumed in a series of burns initiated at 7-10% combustible gas than it is for the combustible gas to accumulate to the point where one large burn would consume all the oxygen.

Late Combustion Following De-inerting

The question of combustible gas accumulation is appropriate for accidents in which steam inerting occurs early, but sufficient steam is condensed late in the accident to bring the containment atmosphere back into the combustible region. Substantial combustion induced loads then become plausible. Figure 3 illustrates the effect of such a delayed ignition for a postulated (TMLB') accident at Zion. The accident is initiated by loss of AC power. Vessel breach occurs at about 2.5 hours, and power is restored to permit containment heat removal by sprays and/or fan coolers six hours into the accident. Note that the time required to de-inert the atmosphere (at least 30 min.) would also allow a large amount of fission product removal from the containment atmosphere in this scenario.

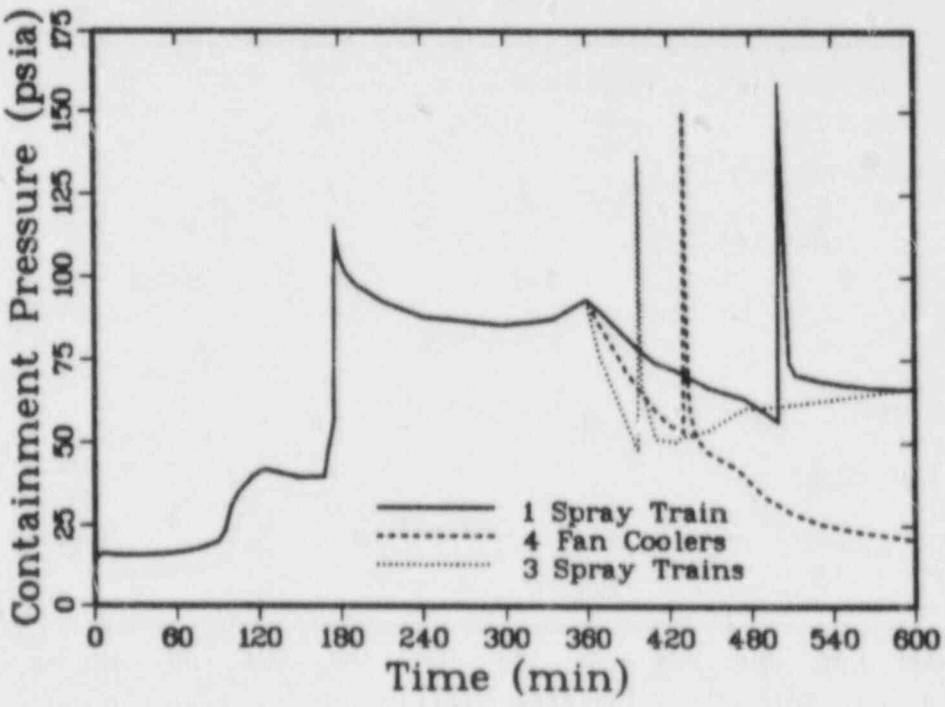

Figure 3.
Combustion Induced Loads at Zion Following De-Inerting

There are two factors which might tend to reduce or prevent combustion induced loads following de-inerting. First, ignition and complete combustion tend to be more difficult to achieve when steam mole fractions approach the levels required for inerting. Second, pressure-temperature induced leakage could occur before de-inerting thereby depleting the inventories of hydrogen, carbon monoxide, and oxygen in containment.

Continuous Recombination in the Reactor Cavity

It has been postulated that during core-concrete interactions the temperature of the reactor cavity atmosphere would be high enough to allow the hydrogen and carbon monoxide released to spontaneously recombine with oxygen. This would be a continuous recombination as opposed to a combustion event, and, because of the high temperatures it is postulated that the recombination could occur in spite of the very high steam concentrations which would exist due to degassing of unlined concrete walls of the reactor cavity. Such recombination would eliminate the threat to containment due to global combustion late in the accident. There are two key questions here. First, will sufficient oxygen be present in the reactor cavity atmosphere to support continuous recombination in the reactor cavity? The postulate is that natural convection currents between the reactor cavity and the rest of containment will be sufficiently strong to provide the required oxygen. While it is reasonable to expect some natural convection, it is not clear that it will be adequate to supply the required amounts of oxygen. Second, will the recombination reaction occur in spite of the locally high steam concentrations? It is not clear that it will, and if not, the comments on combustion in the previous sections still apply.

CONCLUSIONS

In scenarios in which operating containment heat removal systems preclude high steam concentrations in the containment atmosphere, combustion events in large dry PWR containments are plausible before vessel breach, immediately after vessel breach, or later in the accident. Before vessel breach, combustion induced loads by themselves are sufficiently limited by the available hydrogen that they will not challenge typical estimated failure pressures for atmospheric or sub-atmospheric large-dry PWR containments. Combustion occurring coincident with vessel depressurization and a steam spike cannot be precluded. The pressure loads resulting from such coincident events could conceivably challenge containments with relatively low failure pressures such as Surry; however, stronger containments such as Zion would not be challenged. Late combustion could challenge the ultimate capacity of either containment if hydrogen and carbon monoxide accumulated during periods when containment heat removal systems were inoperable, but burned after containment heat removal systems were restored, thereby de-inerting the containment atmosphere. In any of the above scenarios, the potential impact of combustion-induced loads on equipment operability and penetration seals should be considered.

REFERENCES

1. "Zion Probabilistic Safety Study," Commonwealth Edison Company, September, 1981.

2. Final Safety Analysis Report, Surry Power Station Units 1&2, Virginia Electric and Power Company, 1970.

3. F. E. Haskin, J. L. Darby, W. B. Murfin, "Analysis of Hypothetical Severe Core Damage Accidents for the Zion Pressurized Water Reactor," NUREG/CR-1989, SAND81-0504, Sandia National Laboratories, Albuquerque, New Mexico, October, 1982.

4. Reactor Safety Study, WASH-1400 (NUREG-75/014), U. S. Nuclear Regulatory Commission, 1975.

5. J. Lee, et. al., "Hydrogen Air Detonations," Second International Workshop on the Impact of Hydrogen on Water Safety," Albuquerque, NM, October, 1982.

6. D. A. Powers, J. E. Brockmann, D. R. Bradley, and W. W. Tarbell, "The Role of Ex-Vessel Interaction in Determining the Severe Reactor Accident Source Term for Fission Products," Proceedings of Int. Mtg on Light Water Reactor Severe Accident Evaluation, Cambridge, Mass., August, 1983.

7. K. D. Bergeron, D. C. Williams and T. Zimmerman, "CONTAIN Calculations of Containment Loading of Dry PWR's," Second Workshop on Containment Integrity, Arlington, Va., June, 1984.

8. H. F. Coward, C. W. Carpenter, and W. Payman, Journal of Chemical Society, 115, 27, 1919.

HECTR RESULTS FOR ICE-CONDENSER CONTAINMENT STANDARD PROBLEM

F. Eric Haskin, Vance L. Behr, and Allen L. Camp
Sandia National Laboratories
Albuquerque, NM 87185

ABSTRACT

We have performed calculations to study the Ice-Condenser Containment Standard Problem for the NRC Containment Loads Working Group (CLWG). This problem is based on a TMLB' accident sequence. TMLB' denotes a transient-initiated accident in which there is total failure of both AC power and feedwater to the steam generators. We used MARCH 2 and CORCON Mod2 to predict the steam, hydrogen, carbon dioxide, and carbon monoxide sources. We employed HECTR to predict the containment pressure temperature response. The results of our calculations include quantitative indications of the sensitivity of containment pressure-temperature loadings to the gas source terms, the ignition criteria, and the magnitude of the steam spike following vessel breach.

STANDARD PROBLEM DESCRIPTION

To generate the steam-hydrogen source term, we employed MARCH 2[1] and an input deck provided for the standard problem by Battelle Columbus Laboratories (BCL). Table 1 summarizes the key events predicted by MARCH 2 prior to vessel breach for the base case input deck provided by BCL. Natural circulation through the steam generators permits removal of decay heat by boiling and relief of steam through the atmospheric dump valves on the secondary side until 3885 s when the steam-generators boil dry. The primary system then rapidly heats up and the primary system relief valves open, discharging primary coolant to the containment. Core uncovering is predicted to begin at 5550 s. This is followed by core heatup, melting, slumping into residual water in the bottom head, and bottom head heatup and failure. While one can postulate events which would depressurize the primary, the standard problem did not consider these and the primary system is predicted to remain pressurized at the relief valve setpoint until vessel breach at 9465 s.

---

*This work was supported by the U.S. Nuclear Regulatory Commission, Office of Nuclear Regulatory Research, and performed at Sandia National Laboratories which is operated for the U.S. Department of Energy under Contract Number DE-AC04-76DP00789.

Most of the hydrogen generated from Zr oxidation is predicted to remain in-vessel until vessel breach. Upon vessel breach, MARCH 2 discharges the steam and hydrogen remaining in the primary system in a single timestep (15 s as specified by BCL). As a result, the steam and hydrogen sources for the base case have very large spikes at the time of vessel breach as indicated in Figures 1 and 2.

Table 1. MARCH 2 Base Case (Q Case) Chronology

Event	Time (s)
Steam Generator Dryout	3885
Begin Uncovering Core	5550
Start Core Melting	7350
Core Slump	8640
Start Bottom Head Heatup	8745
Vessel Breach	9465

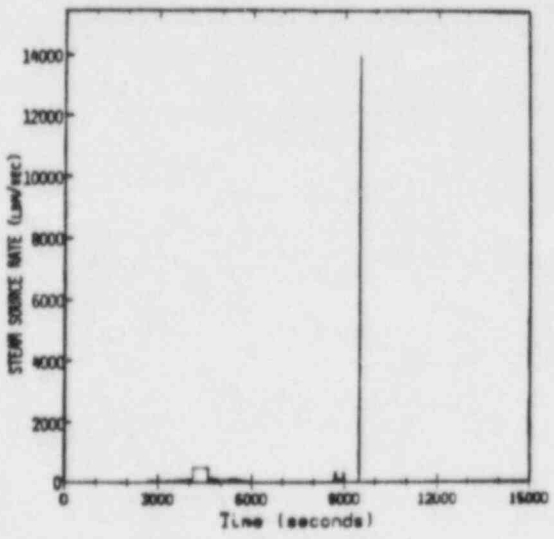

Figure 1
Steam Source for Q Cases

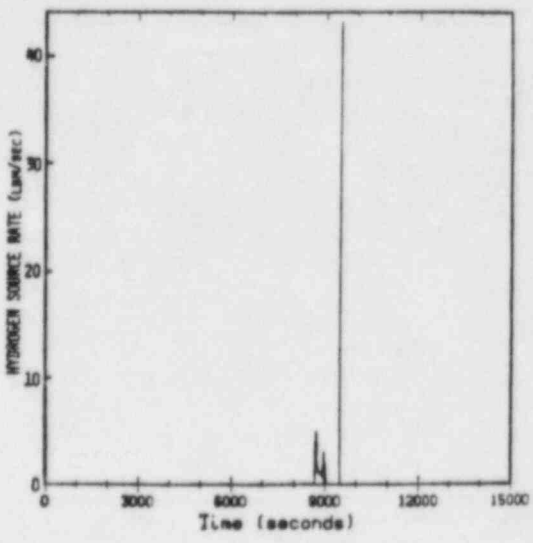

Figure 2
Hydrogen Source for Q Cases

The standard problem statement requests peak containment loadings during the hour following vessel breach. The modeling of events following vessel breach is left to the discretion of each analysis group, with three constraints. First, geometry and heat sinks characteristic of the Sequoyah containment are to be used. Second, the containment is specified to have zero leakage and an unlimited structural capacity. Third, the properties of the basemat concrete are specified to be the default properties from MARCH 1.0[2] -- a limestone concrete.

CODES AND MODELS

BCL Version 111 of MARCH 2 was used to provide the steam-hydrogen sources to containment. We replaced the INTER core-concrete-interactions subroutine in MARCH 2 with CORCON Mod2[3]; however, this change had little impact since gases generated from core concrete interactions have a negligible impact on containment loadings during the first hour following vessel breach.

We used HECTR[4] to predict containment pressure-temperature loadings. HECTR is a lumped volume code developed specifically to compute containment pressure and temperature loadings associated with hydrogen deflagrations (detonations are not modeled). HECTR models for intercompartment gas flows, combustion, heat transfer, containment sprays, and the ice-condenser are more mechanistic than corresponding MARCH models. HECTR has been shown to agree well[5] with two other lumped volume codes of comparable complexity (CLASIX and COMPARE) in predicting ice-condenser containment loadings for a small-break LOCA.

The nodalization of the ice-condenser containment for our HECTR calculations is shown in Figure 3. The nine compartments include the dome; the lower compartment (which contains the reactor coolant system); an annular, dead-ended compartment; the ice-condenser upper and lower plenums; and four ice regions of the ice-condenser. HECTR includes models for the recirculation fans and containment sprays; however, both are inoperable due to failure of AC power in TMLB' accidents. The models used for the ice-condenser lower-plenum and intermediate-deck doors block downward flow through the ice-condenser. However, there is a small "bypass" flow area around the intermediate deck doors which (coupled with finite door closing times) permits downward burn propagation and limited downward flow.

We employed HECTR default values for 1) inerting due to high (>55%) steam and carbon-dioxide mole fractions, 2) inerting due to low (<5%) oxygen mole fraction, 3) flame speed, 4) burn completeness, and 5) burn propagation (4.1% upward, 6.0% horizontal, 9.0% downward).

CASE DESCRIPTIONS AND RESULTS

In order to examine the sensitivity of the containment pressure-temperature loadings with respect to variations in source term, ignition criteria, and steam spike magnitude, we examined twenty cases. Each case has been assigned an identifier consisting of a single letter prefix and a two digit suffix. Each distinct prefix denotes a different steam-hydrogen source term obtained with a different set of MARCH inputs chosen to vary such things as the amount of Zr oxidation and magnitude of the steam spike. Parameters affecting combustion and intercompartment flows were varied by changing HECTR inputs thus, each case required a separate HECTR run. Results for all cases are compiled in a table at the end of the paper. Specific sensitivities indicated by these results are discussed below.

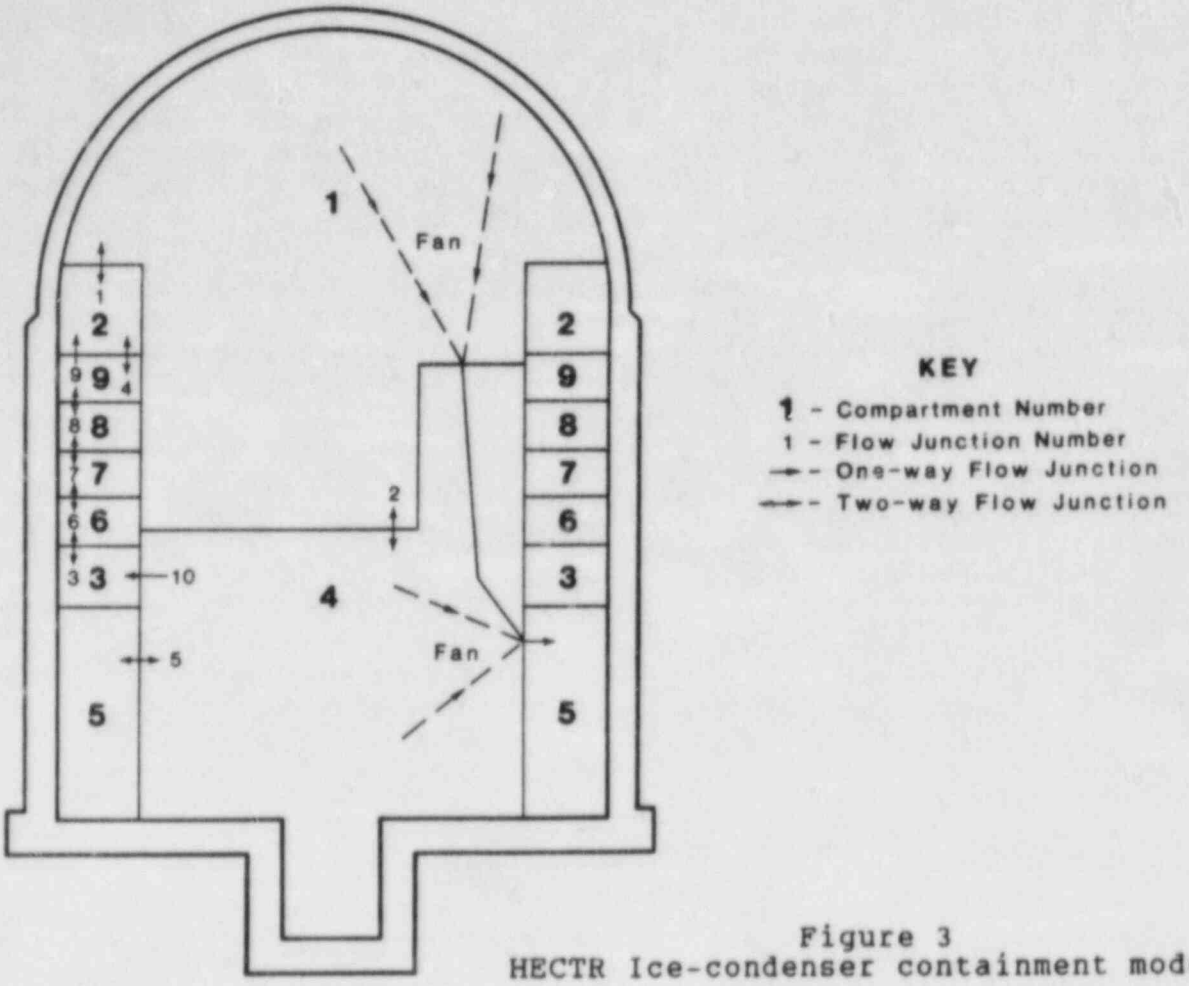

Figure 3
HECTR Ice-condenser containment model.

LOADINGS WITHOUT COMBUSTION

In order to better understand the containment loadings for different combustion scenarios, it is helpful to first analyze the containment response with combustion precluded. This is a possible scenario because the failure of AC power in the TMLB' accident sequence would eliminate many sources of ignition, including the AC-dependent deliberate ignition (DI) systems currently planned for or installed in ice-condenser containments. Since the steam-hydrogen source is dominated by the spike at the time of vessel breach, we plot results for the no-combustion case over the 60 s interval beginning 5 s before vessel breach.

Figure 4 shows the pressure in Compartment 1, the dome. The pressures in all compartments are essentially equal. The peak pressure during the hour after vessel breach is 339 kPa (48 psia) and occurs ~ 30 s after vessel breach. During primary system depressurization and the subsequent steam spike, steam is released to the lower compartment too rapidly to permit total condensation in the ice regions. Figures 5, 6, and 7 show the steam, hydrogen and oxygen mole fractions in the dome.

Steam and hydrogen accumulate in the dome thereby decreasing the oxygen mole fraction. However, inerting does not occur in the dome at any time either due to high (>55%) steam or low (<5%) oxygen mole fractions. By 3 s after vessel breach upward burn propagation into the dome becomes possible (>4.1% hydrogen).

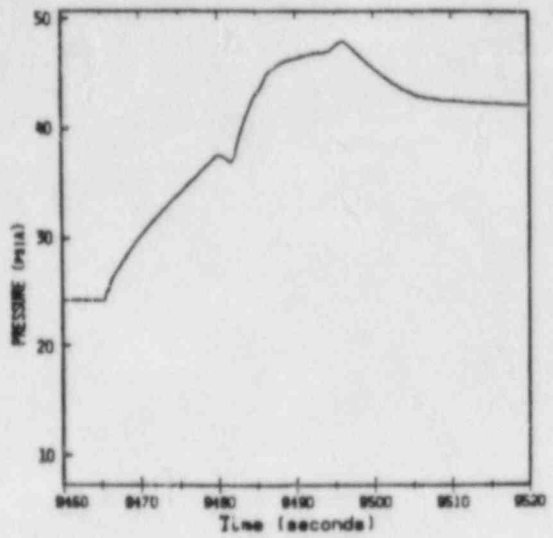

Figure 4
Dome Pressure, Case Q.06

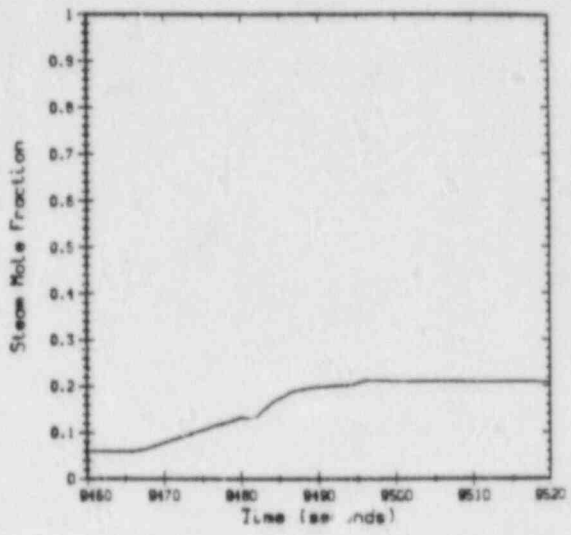

Figure 5
Dome Steam, Case Q.06

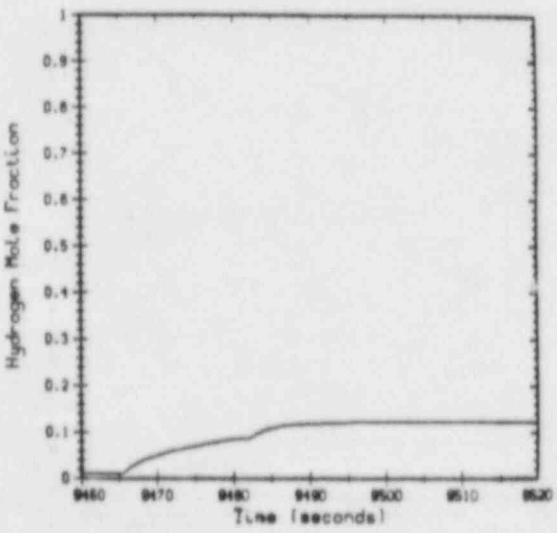

Figure 6
Dome Hydrogen, Case Q.06

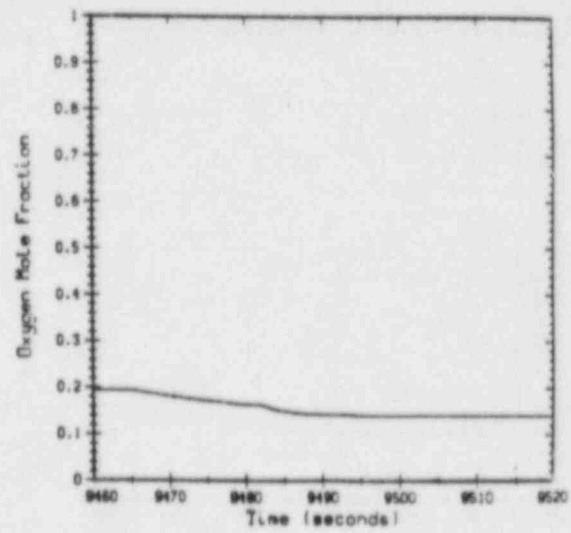

Figure 7
Dome Oxygen, Case Q.06

Figure 8 shows the temperature in the lower compartment which initially receives the steam and hydrogen from the primary system and from the steam spike. The peak temperature in containment in the absence of combustion occurs in the lower compartment. The peak during the first hour following vessel breach is 440 K (330 F).

Figures 9, 10, and 11 show the steam, hydrogen, and oxygen mole fractions in Compartment 2, the ice-condenser upper plenum. Figure 10 shows that there is always ample hydrogen in the upper plenum to permit combustion; however, by 17 s after vessel breach the upper plenum contains insufficient (<5%) oxygen to support combustion, and by 18 s after vessel breach the upper plenum is also steam inerted (>55% steam).

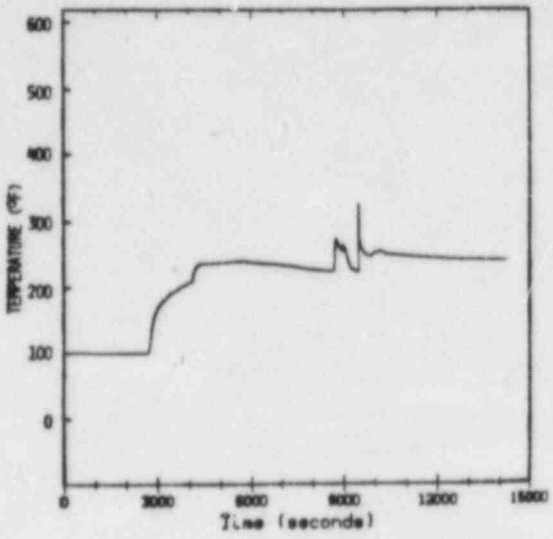

Figure 8
Lower Compartment
Temperature, Case Q.06

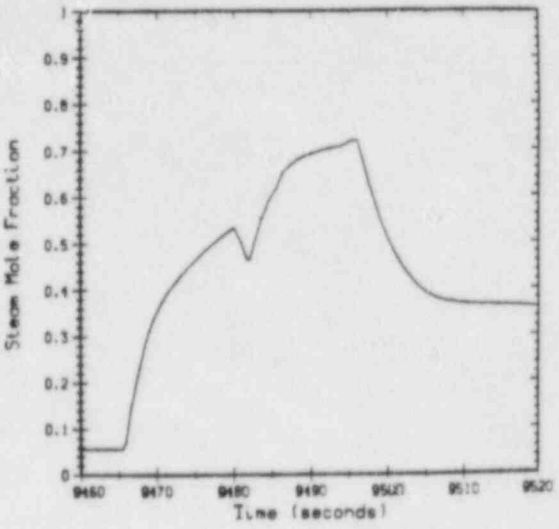

Figure 9
Upper Plenum
Steam, Case Q.06

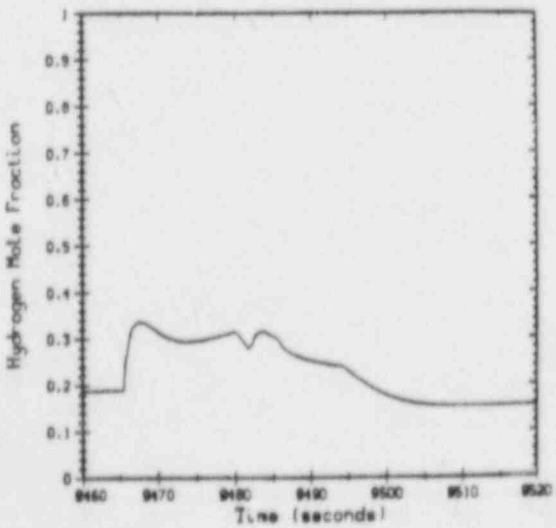

Figure 10
Upper Plenum
Hydrogen, Case Q.06

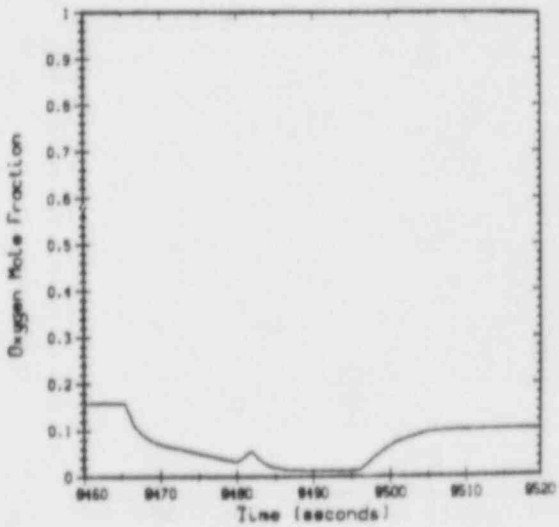

Figure 11
Upper Plenum
Oxygen, Case Q.06

Results for the upper ice regions, Compartments 8 and 9, are similar to those for the upper plenum. Prior to vessel breach, detonable concentrations occur in Compartments 8 and 9; however, following vessel breach these compartments rapidly inert. Table 2 summarizes the combustibility conditions in all of the compartments following vessel breach.

Table 2. Inerting During the Hour Following Vessel Breach (VB), Case Q.06--No Burning

Compartment	Time Period During Which There is <5% O_2	>55% H_2O	<4.1% H_2
1 Dome	None	None	<VB+ 3s
2 IC Upper Plenum	>VB+ 17s	>VB+ 18s	None
3 IC Lower Plenum	>VB- 720s	>VB-5300s	>VB+18s
4 Lower Compartment	>VB-5330s	>VB-5920s	>VB+18s
5 Dead-ended Region	None	None	<VB
6 Bottom Ice Region	>VB- 720s	>VB- 720s	>VB+19s
7 Next-To-Bottom Ice Region	>VB- 660s	>VB- 660s	>VB+21s
8 Next-To-Top Ice Region	>VB+ 1s	>VB+ 3s	None
9 Top Ice Region	>VB+ 6s	>VB+ 10s	None

Note that the lower a compartment is in the ice-condenser, the more rapidly it inerts. Compartment 8 is inerted within one second, Compartment 9 within six seconds, and Compartment 2 within 17 seconds of vessel breach. The lower compartment (Compartment 4), the lower plenum (Compartment 3), and the lower ice regions (Compartments 6 and 7) are inert both before and after vessel breach. The dead-ended region (Compartment 5), although not inert, has a relatively low (<5.3%) hydrogen concentration at all times.

IGNITION FOLLOWING VESSEL BREACH

Currently planned or installed deliberate ignition systems for ice-condenser containments are powered by the AC systems which fail by definition in TMLB' accident scenarios. Failure of the AC power systems might also preclude other ignition sources, that is, electrical discharges from operating equipment inside containment. It is, therefore, not unreasonable to postulate that ignition could be delayed until after vessel breach. The ejection of hot gases or particles during vessel depressurization might serve as a source of ignition. Alternatively, ignition might be delayed indefinitely.

Based on Case Q.06 in which combustion was precluded, we developed several cases to examine the sensitivity of containment loading to the timing and threshold for ignition following vessel breach. Table 3 summarizes the sensitivity of containment loading to the timing of ignition. Ignition was assumed to be possible starting at the times indicated and was precluded again 30 s later. An ignition threshold of 8% hydrogen was

assumed. There was no ignition in the dead-ended region because it contained less than 5.3% hydrogen following vessel breach.

Table 3. Ignition Timing Sensitivity

Case No.	Ignition Time	Limit $\%H_2$	Preburn Dome Press.& Hydrogen kPa (psia)	$\%H_2$	Peak Pressure kPa (psia)	Peak Temperature K (F)
Q.07	VB	8.0	466 (68)	4.1	620 (90)	2110 (3330)
Q.08	VB+5s	8.0	228 (33)	6.1	540 (78)	1300 (1890)
Q.09	VB+10s	8.0	250 (36)	8.0	690 (100)	1460 (2170)
Q.10	VB+20s	8.0	298 (43)	11.0	850 (120)	1500 (2250)
S.02	VB+1hr	8.0	246 (36)	22.7	1500 (210)	2370 (3800)

Case Q.07 postulates ignition at the time of vessel breach; that is, 9465 s after accident initiation. At this time, the mixtures in the upper plenum (Compartment 2) and the upper ice regions (Compartments 8 and 9) are ignited. The initial burn in Compartments 8, 9, and 2 acts to retard the buildup of hydrogen in the dome and inert Compartments 8 and 9 due to low (<5%) oxygen. Two subsequent burns are ignited in the upper plenum (Compartment 2) and propagate upward into the dome. The first upward propagating burn occurs when the dome pressure is 260 kPa (37 psia) and the dome hydrogen concentration reaches 4.1%. The second upward propagation occurs when the dome pressure is 470 kPa (68 psia) and the dome hydrogen concentration again reaches 4.1%. This later burn results in a peak pressure of 620 kPa (90 psia). The peak temperature of 2110 K (3340 F) occurs in Compartment 2 during the first burn.

Case Q.08 postulates ignition 5 s after vessel breach. As indicated in Table 2, Compartment 8 is inerted by this point in time. Ignition occurs in Compartments 9 and 2. Sufficient hydrogen has accumulated in the dome to permit upward propagation from the upper plenum. When upward propagation occurs, the dome contains 6.1% hydrogen, but the pressure is only 230 kPa (33 psia). The resulting peak pressure is 540 kPa (78 psia) which is lower than for Case Q.07 due to the lower pressure preceding burning in the dome. The burning in the dome forces sufficient oxygen back into the ice-condenser to permit additional burns in Compartments 8, 9, and 2, but these burns do not affect the peak loadings. The peak temperature of 1300 K (1890 F) occurs in Compartment 2, during the first burn.

Case Q.09 postulates ignition 10 s after vessel breach. As indicated in Table 2, ice compartments 8 and 9 are inerted at this time; however, 8% hydrogen has accumulated in the dome so that the initial burn is ignited simultaneously in the dome and the upper plenum. This initial burn starts at a baseline pressure of only 250 kPa (36 psia); however, it forces oxygen

back into the ice-condenser permitting simultaneous burns in Compartments 8 and 9. The pressure resulting from the initial dome burn and concurrent burns in Compartments 2, 8, and 9 is 690 kPa (100 psia). The peak temperature of 1460 K (2170 F) occurs in Compartment 8.

Case Q.10 postulates ignition 20 s after vessel breach. As indicated in Table 2, all of the compartments in the ice-condenser (including Compartment 2, the upper plenum) are inerted at this time. However, 9.8% hydrogen has accumulated in the dome and is ignited. The baseline pressure at ignition is 300 kPa (43 psia). The burn in the dome forces enough oxygen back into the ice-condenser to permit simultaneous and subsequent burns in Compartments 2, 9, and 8. The peak pressure of 850 kPa (120 psia) results from the initial burn in the dome. The peak temperature of 1300 K (1890 F) occurs during the first burn in Compartment 2.

The maximum load we can conceive of during the hour following vessel breach would occur if ignition were delayed until the end of this one hour time interval. The longer the delay until ignition, the more hydrogen will accumulate in the dome. The source term considered for Case S.02 postulates 100% in-vessel Zr oxidation. With ignition delayed until one hour after vessel breach, the dome mixture at time of ignition is composed of 22.7% hydrogen, 14.5% oxygen, and 7.9% steam. This is clearly a detonable mixture; however, HECTR treats only deflagrations. The HECTR-predicted peak loadings for Case S.02 are 1459 kPa (212 psia) and 2369 K (3804 F) in the dome. A detonation of the same mixture would result in even more severe loadings.

Based on the preceding discussion, the results in Table 3 can be explained as follows. If ignition is delayed until after vessel breach, the peak loadings will be sensitive to the time interval between vessel breach and ignition. The peak loadings are, in general, determined by the dome hydrogen content and the pressure prior to burning in the dome. For early ignition (near the time of vessel breach) burning in the dome will not occur until the dome hydrogen mole fraction is sufficient to permit upward propagation (4.1%). Early burning in the ice-condenser can delay the buildup of hydrogen in the dome while increasing the pressure. Thus, ignition at vessel breach (Case Q.07) yields higher peak loadings than ignition which is delayed 5 s (Case Q.08). However, with more delay (Cases Q.09, Q.10) the hydrogen content in the dome begins to dominate the resulting peak loads, and, for an indefinite delay, detonable mixtures can be achieved in the dome (Case S.02).

IGNITION THRESHOLD

Table 4 shows the effect of reducing the ignition threshold from 8% to 4.1% for cases in which ignition follows vessel

breach. Recall from Table 3 that, by reducing the ignition threshold from 8% hydrogen to 4.1% hydrogen, initial burning will occur in the dead-ended region (Compartment 5) as well as in the upper regions of the ice-condenser and possibly the dome. Thus, in Table 4 the peak temperature in Compartment 5 increases when the ignition threshold is changed from 8% to 4.1% hydrogen. The addition of burning in the dead-ended region has only a slight impact on the peak loadings predicted for ignition at vessel breach (Case Q.05 versus Case Q.07). For ignition at vessel breach plus 5 s (Case Q.00 versus Case Q.08), the impact on the peak pressure is more significant due to the higher preburn pressure and the addition of more hydrogen to Compartment 5 before ignition.

Table 4. Sensitivity to Ignition Threshold When Ignition Follows Vessel Breach

Case No.	Ignition Time	Limit $\%H_2$	Peak Pressure kPa (psia)	Peak Temperature, K (F) Compt. #2	Compt. #5
Q.05	VB	4.1	620 (90)	2100 (3330)	641 (694)
Q.07	VB	8.0	620 (90)	2110 (3330)	475 (395)
Q.00	VB+5s	4.1	600 (87)	1400 (2060)	546 (523)
Q.08	VB+5s	8.0	540 (78)	1300 (1890)	475 (395)

DELIBERATE IGNITION

As mentioned earlier, ignition in a TMLB' accident is unpredictable because the failure of AC power implies failure of the deliberate ignition system and other potential sources of electrical discharge. One might attempt to achieve non-random ignition with a deliberate ignition (DI) system designed to be independent of AC power. Table 5 summarizes the sensitivity of peak loadings to deliberate ignition. Two igniter configurations were considered. In Case Q.01 igniters were located in all compartments except the ice-condenser lower plenum and the ice compartments (DI ex IC) similar to actual designs currently installed or planned. In Case Q.02 igniters were located in all compartments including the ice regions (DI all). By inducing burns before vessel breach, the deliberate ignition systems raise the baseline pressure for burns after vessel breach. As a result, higher peak pressures are predicted with deliberate ignition. However, deliberate ignition precludes the possibility of a detonable mixture in the dome. Adding igniters to all compartments, including the ice-condenser lower plenum and the ice compartments, lowers the predicted loadings (Case Q.02 versus Case Q.01), and also precludes the possibility of local detonations. Containment pressure responses for Cases Q.01 and Q.02 are shown in Figures 12 and 13.

Table 5. Sensitivity to Deliberate Ignition (DI)

Case No.	Ignition Type	Limit $\%H_2$	Peak Pressure kPa (psia)	Peak Temperature K (F)
Q.01	DI ex IC	8.0	730 (110)	1628 (2470)
Q.02	DI all	8.0	570 (83)	1177 (1660)
Q.08	VB + 5s	8.0	540 (78)	1305 (1890)

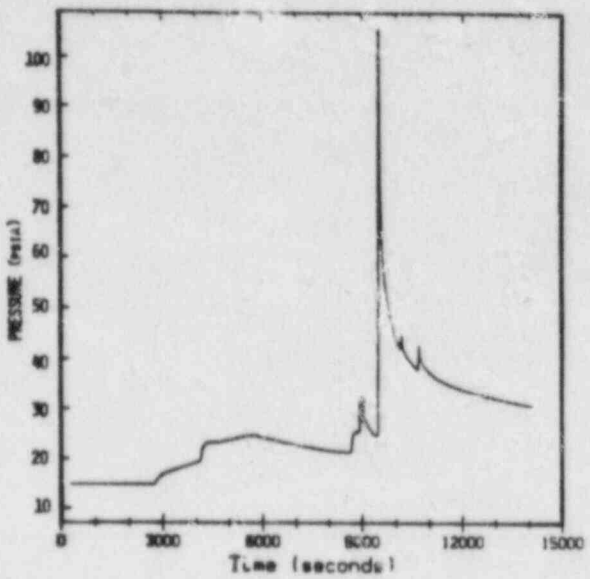

Figure 12
Dome Pressure for Case Q.01

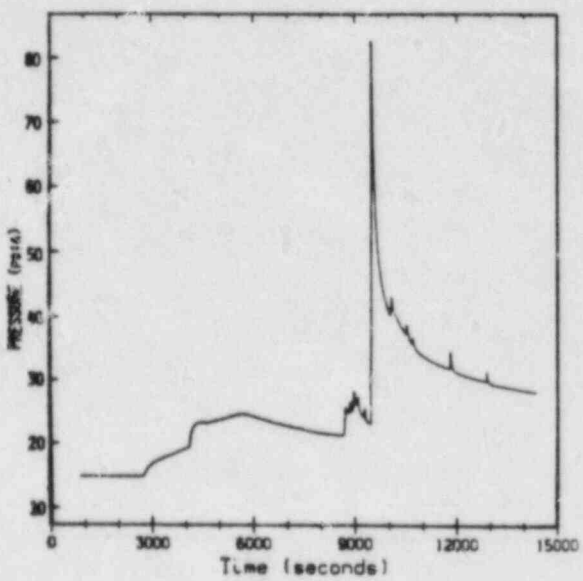

Figure 13
Dome Pressure for Case Q.02

NONMECHANISTIC IGNITION THRESHOLD

To permit comparisons with results obtained by others, in four cases (Q.00o, Q.01, Q.02o, and Q.03o) ignition is assumed to occur whenever the hydrogen mole fraction in non-inerted compartments outside the lower plenum and ice regions reaches an arbitrary threshold. The arbitrary ignition thresholds for these runs are 10%, 8%, 12%, and 30%. Our opinion is that only one of these runs (Q.01 with ignition at 8% hydrogen) has any physical significance. As discussed above, Case Q.01 simulates a deliberate ignition system which is independent of AC power. Such a deliberate-ignition system would most realistically yield ignition at $\leq$8% hydrogen, well before 10%, 12%, or 30% hydrogen. Without deliberate ignition, a single random ignition could certainly occur at 8%, 10%, 12%, or even 30% hydrogen; however, there is no mechanism which would make all subsequent ignitions occur at the same threshold.

There are two reasons for excluding ignition in the ice compartments in Cases Q.00o, Q.01, Q.02o, and Q.03o. First,

Case Q.01 was designed to simulate deliberate ignition independent of AC power and deliberate ignition systems currently planned or installed do not have igniters in the ice compartments. Second, Cases Q.00o, Q.02o, and Q.03o are non-physical, their sole purpose is for comparison to calculations made by others with MARCH which does not compartmentalize the ice region. Hence, there was no point in postulating ignition in the ice compartments for Cases Q.01, Q.00o, Q.02o, and Q.03o. The results for these cases are summarized in Table 6.

Table 6. Sensitivity to Nonmechanistic Ignition Threshold

Case No. (F)	Ignition Type	Limit $\%H_2$	Preburn Dome Press.& Hydrogen kPa (psia)	$\%H_2$	Peak Pressure kPa (psia)	Peak Temperature K
Q.01	DI ex IC	8.0	328 (48)	8.0	730 (100)	1630 (2470)
Q.00o	Nonmech	10.0	305 (44)	6.8	670 (95)	1670 (2540)
Q.02o	Nonmech	12.0	300 (44)	6.6	650 (93)	1770 (2720)
Q.03o	Nonmech	30.0	*	*	350 (50)*	2040 (3220)

*No combustion in the dome

The results presented in Table 6 are somewhat counterintuitive. The peak temperatures increase with increasing ignition threshold, but the peak pressures decrease. This can be explained as follows. The peak temperature for all four cases occurs in the upper plenum (Compartment 2). The more hydrogen burned in a single burn in Compartment 2, the higher the temperature. The peak pressure, however, is determined by burns in the dome (Compartment 1) which, unlike burns in the upper plenum, cannot expand into larger compartments. In Case Q.00o and in Case Q.02o the ignition threshold (10% and 12% respectively) is not reached in the dome, but burns propagate into the dome from the upper plenum of the ice-condenser. The higher the ignition threshold, the fewer upper plenum (and propagated ice region) burns. With fewer ice-condenser burns, the pressure is lower when propagation into the dome occurs and hence the peak pressure is reduced. In Case Q.03o, with the ignition threshold set at 30% hydrogen, burning in the ice-condenser precludes buildup of hydrogen in the dome to a level (4.1%) which would permit upward propagation.

DEPRESSURIZATION PRIOR TO VESSEL BREACH

As indicated in Figures 1 and 2, the base case steam and hydrogen source terms predicted by MARCH are strongly concentrated about the time of vessel breach. This is because MARCH assumes that the primary system will remain pressurized until the time of vessel breach. Cases V.00 and V.01 test the importance of this assumption with respect to predicted containment loadings. In Cases V.00 and V.01 the primary system relief valve (SRV) is assumed to stick open 8640 s into the accident

when MARCH predicts the core will collapse into residual water in the bottom head. Relief through the stuck open relief valve reduces the primary-system pressure to below the accumulator setpoint and delays vessel breach until 10150 s as opposed to 9465 s for the Q cases. Table 7 compares the peak containment loadings predicted by HECTR with and without depressurization prior to vessel breach.

When ignition is postulated shortly after vessel breach (Cases V.00 and Q.08) primary system depressurization prior to vessel breach allows hydrogen to accumulate to significant levels in the dome before ignition. In Case V.00 HECTR predicts 14.5% hydrogen, 15.6% oxygen, and 11.0% steam in the dome at time of initial ignition, 5 s after vessel breach. Obviously, if ignition is postulated shortly after vessel breach, primary system depressurization before vessel breach yields higher loadings (Case V.00 versus Case Q.08). However, early primary system depressurization would also eliminate the high pressure ejection of hot core debris particles which could serve as ignition sources.

Table 7. Sensitivity to Depressurization Prior to Vessel Breach

Case No.	SRV Sticks Open	Ignition Type	Peak Pressure kPa (psia)	Peak Temperature K (F)
Q.02	No	DI all	570 (83)	1180 (1660)
Q.08	No	VB+5s	540 (78)	1300 (1890)
V.01	Yes	DI all	660 (96)	1800 (2790)
V.00	Yes	VB+5s	1050 (150)	1680 (2560)

When deliberate ignition is postulated (Cases V.01 and Q.02), early primary system depressurization shifts both the hydrogen release and associated burning to before vessel breach. In Case V.01, an initial series of burns occurs in Compartments 2, 8, and 9 after the relief valve sticks open at 8640 s. This initial series of burns results in the inerting of Compartments 2, 8, and 9 due to insufficient oxygen. Subsequent ignition occurs when the hydrogen concentration in the dome reaches 8% at 9340s. The dome burn forces sufficient oxygen back into the ice-condenser to result in simultaneous burning in Compartments 2, 8, and 9. The pressure preceeding the dome burn is 270 kPa (39 psia). The peak pressure for Case V.01 is higher than for the corresponding deliberate-ignition case (Case Q.01) with no primary system depressurization prior to vessel breach. In Case Q.01 the dominant dome burn was ignited by propagation from Compartment 2 when the dome pressure was 300 kPa (44 psia) and the dome contained only 5.1% hydrogen.

EXTENT OF IN-VESSEL Zr OXIDATION

Table 8 indicates the sensitivity of peak containment loads to the extent of in-vessel Zr oxidation. In all of the cases in

Table 8 the primary system is assumed to remain pressurized until vessel breach, ignition is assumed to be delayed until 5 s after vessel breach, and the ignition threshold is taken to be 8% hydrogen. In general, the higher the in-vessel oxidation level, the more hydrogen is available to burn after vessel breach and the higher the predicted peak pressures and temperatures. However, for Case R.00 (49.4% in-vessel Zr Oxidation) the peak temperature is 135 K (243 F) less than for Case U.00 (39.4% in-vessel Zr oxidation). In both Cases U.00 and R.00 the peak temperature is predicted in the upper plenum (Compartment 2) and is sensitive to the timing of successive ignitions in this compartment, which in turn depends on the details of the source term. In Case S.01, however, with 100% Zr Oxidation, sufficient hydrogen is released to yield initial ignition in both the dome and the dead-ended region with propagation downward from the dome into the ice-condenser. The peak temperature for Case S.01 occurs in the upper plenum during this initial burn. A higher peak temperature is obtained for Case S.01 than for Cases U.00 or R.00 mainly because for Case S.01 the upper plenum gases cannot escape due to simultaneous burning in the dome.

Table 8. Sensitivity to Extent of In-Vessel Zr Oxidation

Case No.	In-Vessel Zr Oxid.	Peak Pressure kPa (psia)	Peak Temperature K (F)
U.00	39.4%	407 (59)	1440 (2130)
R.00	49.4%	488 (71)	1305 (1890)
S.01	99.8%	704 (102)	2022 (3180)

STEAM SPIKE

Table 9 indicates the sensitivity of peak containment loadings to the magnitude of the ex-vessel steam spike. In Case Q.08 and Case T.01 a large steam spike is postulated by invoking the IHOT=0 option in MARCH to model quenching of all of the debris as particles of 0.5 cm (0.197 in) diameter. In Cases U.00 and R.00, the steam spike is virtually eliminated by setting IHOT=2 to permit only 2 quenching timesteps to be taken by MARCH.

Table 9. Sensitivity to Steam Spike

Case No.	Steam Spike	In-Vessel Zr Oxid.	Peak Pressure kPa (psia)	Peak Temperature K (F)
U.00	Low	39.4%	407 (58)	1440 (2130)
R.00	Low	49.4%	488 (70)	1305 (1890)
T.01	High	39.4%	602 (86)	1440 (2130)
Q.08	High	49.4%	535 (77)	1305 (1890)

In all of the cases in Table 9 the primary system is assumed to remain pressurized until vessel breach, ignition is assumed

to occur in the interval from 5 s to 35 s after vessel breach, and the ignition threshold is taken to be 8% hydrogen. By eliminating the steam spike, the baseline pressure for hydrogen burning and the resulting peak pressures are significantly reduced.

CONCLUSIONS AND CAVEATS

A summary of all the cases and the key results from HECTR can be found in Table 10. For comparison, the estimated failure pressures for ice condenser containments range from 51 psia[6] (a lower bound for Sequoyah) to 155 psia[7] (an upper bound for Watts Bar). The HECTR results discussed above indicate that for TMLB' accidents in an ice-condenser, the peak containment loads are strongly influenced by four factors:

1) The timing of ignition which is difficult to predict due to failure of AC power and consequent failure of present deliberate ignition systems,
2) The extent of in-vessel Zr oxidation,
3) Primary system depressurization prior to vessel breach,
4) The magnitude of any ex-vessel steam spike.

A lower bound to the containment loadings during the hour following vessel breach corresponds to Case U.01 in which a low steam spike is postulated and burning is precluded. An upper bound to the containment loadings during the hour following vessel breach corresponds to Case S.02 in which 100% in-vessel Zr oxidation is postulated and ignition is delayed until one hour after vessel breach to maximize the buildup of hydrogen in the dome prior to ignition. These are very wide bounds of uncertainty and are due largely to the uncertainty in the time of ignition and amount of zirconium oxidation. However, the loads calculated by HECTR for Case S.02 are not absolutely conservative because they are based on deflagrations, whereas a detonation in the dome is possible.

We have no "best guess" as to the containment loading which would actually arise in a TMLB' accident in an ice-condenser containment mainly because of uncertainties regarding the factors (listed above) which strongly influence predicted loadings.

The HECTR predictions show that detonable mixtures could occur in the ice compartments; however, HECTR cannot calculate the loadings which might result from detonations of such mixtures. Independently powered deliberate ignition throughout the containment including the ice regions would virtually eliminate the possibility of detonations and permit a lowering of the upper bound on containment loadings. However, we have not determined that such a deliberate ignition system would be feasible or warranted from a cost-benefit (risk reduction) perspective.

Table 10. Case Descriptions and Summary of HECTR Results

Case No.	In-Vessel Zr Oxid.	Steam Spike	Ignition Type*	Ignition Limit %H2	Number of Burns by Compartment 1	2	3	4	5	6	7	8	9	Peak Loadings Pressure psia (Comp.#)	Peak Loadings Temp. F(Comp.#)	Peak Temp. Comp. #5 F	Preburn Dome Conditions psia	Preburn Dome Conditions %H2
Q.00	49.4%	High	VB+5s	4.1	2	3	0	0	1	0	0	1	4	87 (1-3,6-9)	2060 (2)	523	78	4.1
Q.00o	49.4%	High	Nonmech.	10.0	1	8	0	0	1	0	0	2	2	97 (all)	2540 (2)	1130	44	6.8
Q.01	49.4%	High	DIexIC	8.0	1	7	0	0	1	0	1	2	6	106 (1,2)	2470 (2)	961	48	8.0
Q.02	49.4%	High	DI all	9.0	1	10	0	0	1	0	1	9	17	83 (all)	1660 (2)	968	44	5.1
Q.02o	49.4%	High	Nonmech.	12.0	1	8	0	0	1	0	0	2	4	95 (all)	2720 (2)	1590	44	6.6
Q.03o	49.4%	High	Nonmech.	30.0	0	1	0	0	0	0	0	0	1	51 (all)	3220 (2)	302	--	---
Q.05	49.4%	High	VB	4.1	2	9	0	0	3	0	0	4	9	90 (all)	3320 (2)	695	67	4.1
Q.06	49.4%	High	None	100.0	0	0	0	0	0	0	0	0	0	48 (all)	327 (4)	293	--	---
Q.07	49.4%	High	VB	8.0	2	3	0	0	0	0	0	1	1	90 (all)	3330 (2)	397	68	4.1
Q.08	49.4%	High	VB+5s	8.0	1	2	0	0	0	0	0	1	3	78 (all)	1890 (2)	395	33	6.1
Q.09	49.4%	High	VB+10s	8.0	1	2	0	0	0	0	0	2	2	100 (all)	2170 (9)	462	36	8.0
Q.10	49.4%	High	VB+20s	8.0	1	2	0	0	0	0	0	1	1	123 (1,2)	2250 (8)	440	43	11.0
R.00	49.4%	Low	VB+5s	8.0	1	2	0	0	0	0	0	1	3	71 (all)	1890 (2)	394	33	6.1
S.01	99.8%	Low	VB+5s	8.0	1	3	0	0	1	0	0	2	2	102 (1,2)	3180 (2)	1480	35	8.7
S.02	99.8%	Low	VB+1hr	8.0	1	1	0	0	1	0	0	1	1	212 (1,2)	3800 (1)	2800	36	22.7
T.01	39.4%	High	VB+5s	8.0	2	2	0	0	0	0	0	0	1	87 (1,2)	2130 (2)	386	66	4.1
U.00	39.4%	Low	VB+5s	8.0	1	2	0	0	0	0	0	0	3	59 (all)	2130 (2)	350	32	4.6
U.01	39.4%	Low	None	100.0	0	0	0	0	0	0	0	0	0	37 (all)	300 (4)	251	--	---
V.00	48.3%	High	VB+5s	8.0	0	0	0	0	0	0	0	0	1	152 (1,2)	2560 (1)	451	36	14.5
V.01	48.3%	High	DI all	8.0	1	8	0	0	0	0	0	5	8	96 (1-3,6-9)	2790 (2)	478	34	8.0

*DIexIC --Deliberate Ignition except in Ice Compartments and lower plenum
DI all --Deliberate Ignition in all compartments
VB --Vessel Breach
Nonmech.--Nonmechanistic Ignition

HECTR results presented herein assume that the intermediate-deck doors and the lower-plenum-inlet doors on the ice-condenser would continue to function to block backflow through the ice-condenser. In some cases in which burning occurs in the dome, substantial differential pressures are predicted across these doors when they shut to block backflow. Based on previous calculations, failure of the doors to block backflow would alter predicted containment loadings; however, more complete analyses would be required to firmly establish the significance of door failure.

Finally, we can state that the temperature loadings calculated in the dead-ended region (Compartment 5) do not appear severe when compared to the typical 450 K (350 F) qualification temperature for electrical penetrations located there. Higher atmospheric temperatures are predicted for some cases during burns in the dead-ended regions; however, these temperatures are short-lived (<10 sec) and could not be transmitted to the electrical penetration seals within the time frame of the burns.

REFERENCES

1. R. O. Wooton and P. Cybulskis, MARCH 2 (Meltdown Accident Response CHaracteristics) Code Description and User's Manual, Battelle Columbus Laboratories, October 1983 DRAFT.

2. R. O. Wooten and H. I. Avci, MARCH (Meltdown Accident Response Characteristics) Code Description and User's Manual, NUREG/CF-1711, U.S. Nuclear Regulatory Commission, Washington, D.C., 1980.

3. R. K. Cole, D. P. Kelley, and M. A. Ellis, CORCON-Mod2: A Computer Program for Analysis of Molten Core Concrete Interactions, Sandia National Laboratories, in preparation.

4. A. L. Camp, M. J. Wester, and S. E. Dingman, "HECTR: A Computer Program for Modeling the Response to Hydrogen Burns in Containments," SAND82-1964C, Procedings of The Second International Workshop on the Impact of Hydrogen on Water Reactor Safety, U.S. Nuclear Regulatory Commission, October 1982.

5. A. L. Camp, V. L. Behr, and F. E. Haskin, MARCH-HECTR Analysis of Selected Accidents in an Ice-Condenser Containment, Sandia National Laboratories, in preparation.

6. Safety Evaluation Report related to the operation of Sequoyah Nuclear Plant, Units 1 and 2, NUREG-0011 Supplement No. 6, U.S. Nuclear Regulatory Commission, Draft Copy, November 1982.

7. F. E. Haskin, V. L. Behr, J. Jung, "Containment Management Study for Severe PWR Accidents," SAND82-2120C, Proceedings of Tenth Water Reactor Safety Research Information Exchange Meeting, Gaithersburg, Maryland, October 15, 1982.

SESSION C

CONTAINMENT INTEGRITY AS PART OF RISK ASSESSMENT

COMPUTER AIDED PROBABILISTIC ASSESSMENT OF CONTAINMENT INTEGRITY

J. C. Tsai
1906 Woodleigh Dr., W.
Jacksonville, FL 32211

R. A. Touchton
6367 Hydepark Circle
Jacksonville, FL 32210

1.0 ABSTRACT

In the probabilistic risk assessment (PRA) of a nuclear power plant there are three probability-based techniques which are widely used for event sequence frequency quantification (including nodal probability estimation). These three techniques are the event tree analysis, the fault tree analysis and the Bayesian approach for data-base development. In the barrier analysis for assessing radionuclide release to the environment in a PRA study, these techniques are employed to a greater extent in estimating conditions which could lead to failure of the fuel cladding and the reactor coolant system (RCS) pressure boundary, but to a lesser degree in the containment pressure boundary failure analysis. The main reason is that containment issues are currently still in a state of flux. However, programs are in progress by the nuclear industry and governmental agencies to resolve the containment issues and to provide an improved data base.

In this paper, the authors describe briefly the computer programs currently used by the nuclear industry to do event tree analyses, fault tree analyses and the Bayesian update. The programs have been applied to various projects such as nuclear power plant PRA studies, safety and reliability analysis for defense related missile systems, support for power plant life extension studies and reactor vessel pressurized thermal shock analyses. The authors discuss how these computer aided probabilistic techniques might be adopted for failure analysis of the containment pressure boundary.

2.0 INTRODUCTION

The functional requirement of a steel or concrete containment is to maintain its structural integrity and to provide a leak-tight pressure boundary under specified design basis loadings such as the earthquake load or the pressure load due to a loss-of-coolant accident. For safety evaluation of containments subjected to loadings beyond the design basis, probabilistic risk assessment (PRA) techniques are generally employed to assess the frequencies of accident sequences as well as consequences of containment failures. In the PRA studies performed for nuclear power plants so far, failure criteria for containments were mainly based on ultimate capacities conservatively established from analyses using a deterministic approach. Considerations of leakages through the containment barrier before structural failure were limited in scope because of the lack of established analytical procedures & test data. However, leakages are important in that they are directly related to the radioactivity "release categories" which in turn significantly affect the results of the consequence analysis. The purpose of this paper is to discuss the probabilistic techniques currently used in PRA studies for possible expanded application to the containment integrity issues.

3.0 RISK-BASED DECISION-MAKING TECHNIQUES

In the PRA study of a nuclear power plant, there are three probability-based techniques which are widely used for event sequence frequency quantification (including nodal probability estimation). These three techniques are the event tree analysis, the fault tree analysis and the Bayesian approach for data-base development. In the barrier analysis for assessing radionuclide release to the environment in a PRA study, these techniques are employed to a greater extent in estimating conditions which could lead to failure of the fuel cladding and the reactor coolant system (RCS) pressure boundary, but to a lesser degree in the containment pressure boundary failure analysis. The main reason is that containment issues are currently still in a state of flux (References 1 & 6). As a result, rather large uncertainties are associated with the quantification of containment failure probabilities. More definitive logic diagrams and an improved data base are needed to improve the quantification of containment failure modes and pathways. In the interim, probabilistic techniques which have been successfully applied for estimating the frequency of sequences leading to fuel cladding and RCS pressure boundary failure can begin to be applied for the analysis of containment integrity in a systematic manner (References 2 through 5). Programs are in progress (1984) by the nuclear industry (e.g., IDCOR and EPRI) and the U.S. government (e.g., the DOE and NRC-sponsored research programs at various institutes) to resolve the containment issues and to provide an improved data base.

The following is a brief description of the three probabilistic techniques.

3.1 Event Tree Methodology

An event tree is a logic diagram that tracks the series of subsequent events in an accident sequence. It is made up of a finite number of branching locations, each branch denoting the success or failure of a particular plant system or function. These branch points are referred to as "top events" and require careful selection by the analyst on the basis of their effect on (or significance to) the subsequent course of events. The event tree is drawn horizontally with the initiating event (on the left hand side) as the first top event. The tree is usually made of binary branches with the upper branch at each node (branching point) depicting the success of the corresponding top event and the lower branch denoting its failure. In branches of the tree where the outcome of prior top events obviate the singificance of the top event or where the top event is of no relevance, no branching is modeled for that top event.

The probability of a sequence occurring is the product of individual probabilities (of success or failure as the case may be) for each top event along the sequence. Although the methodology is straightforward, the bookeeping can be extremely cumbersome for large event trees. However, most of the bookkeeping is now handled by the computer. Figure 1 shows a simple event tree model for a fire hazard analysis.

3.2 Fault Tree Methodology

Fault trees are commonly used to evaluate the system unavailabilities (failure probabilities). The fault tree is a deductive logic model used in the PRA for systematic evaluation of physical and human failures. Unlike the event tree, a fault tree is a display from effect to cause of how a system may malfunction. The undesired effect is at the top of the tree with a logic structure beneath, which identifies the credible causes contributing to the top event. Fault trees are developed down to the lowest level for which "data base" information is available. A fault tree is typically constructed and quantified for each system which appears in an event tree in order to provide the probability of failure for that branch point (note that the success probability is 1.0 minus the failure probability for binary branches). Figure 2 is an example fault tree display.

3.3 Bayesian Approach

The Bayesian approach is a well established statistical tool for data reduction. It provides a formal way of explicitly organizing and introducing into the analysis assumptions about prior knowledge (or distribution). This knowledge may be based on past generic industry-wide data and experience, engineering judgement, expert opinion, and so forth, with varying degree of subjectivity. The parameter estimates will then reflect this knowledge. The approach allows the incorporation of belief and information beyond that contained in the observed data and the assigning of a distribution that describes the analyst's belief about the values of the parameter. This distribution is called the prior distribution. The approach also provides a formal way of updating the generic prior distribution when new evidence becomes available, as well as providing a procedure for obtaining plant- or application-specific parameter estimates from the generic prior distribution based on the plant-specific evidence. The updated, or specialized, prior is called the "posterior distribution" because it can be derived only after the evidence is incorporated. The prior reflects the analyst's degree of belief about the parameter before such evidence; the posterior represents the degree of belief after incorporating the new evidence. Plant-specific estimates are then obtained from the posterior distribution.

4.0 RISK BASED DECISION MAKING COMPUTUER CODES

4.1 Event Tree Computer Program

A significant part of the PRA study is the construction and quantification of event tress. Computer programs have been developed to facilitate the task. A typical program such as ETC (Pickard, Lowe & Garrick) or ARBRE (Westinghouse) has the ability to document the construction and quantification of event trees with many branch points and thousands of paths. The significant task performed by the program is the calculation of the end point probability for each

of the sequential paths through the event tree, given the probability of failure or success of each branch point. Branch points may represent systems, operator actions, signal actuations or phenomenological events. One of the major features of the the program is that the failure probability and conditional failure probability input files can be quickly modified such that sensitivity studies can be accomplished expeditiously.

4.2 Fault Tree Computer Graphics System

An inherent part of PRA is the construction and analysis of detailed fault trees. This, too, can be computer assisted, by a program such as GRAP (Babcock & Wilcox) or GRAFTER (Westinghouse) which is a graphics system to efficiently perform fault tree analyses of complex systems. The graphics system provides the analyst with the capability to construct, revise, and prepare for quantification fault trees in an interactive mode at the computer terminal.

4.3 Fault Tree Evaluation Codes

Computer programs have been developed for the qualitative and quantitative evaluation of fault trees. Examples are the "WAM" family series of codes & FTAP/SAMPLE. The GRAP code automatically interface with FTAP & SAMPLE to determine the minimal cutsets and the failure probability distribution function for the top-event of the fault tree.

4.4 Matrix Manipulation Program

CROSS (Pickard, Lowe & Garrick) or BORIS (Westinghouse) is an example computer program that performs the overall risk assembly in PRA. It executes the matrix multiplication process to consolidate the results from the individual phases of the study - Initiating Event Categorization, Plant Analysis, Containment Analysis, and Offsite Consequence Analysis. The output from each phase of the study is a conditional probability matrix. The initiating event vector is successively multiplied by the plant matrix, the containment matrix, and the site consequence matrix. The output from each matrix manipulation can be used to assemble a family of risk curves in the form of complementary cumulative distribution functions for various damage indices. It can also be used to obtain other valuable information such as a list of sequences that dominate risk as well as their frequencies. In addition to the speed of calculation and elimination of computational errors, the use of a computer to perform this function provides for efficient sensitivity calculations and revisions to reflect changes.

5.0 APPLICATION & EXPANSION FOR PROBABILISTIC CONTAINMENT FAILURE ANALYSIS

Existing PRA studies generally include containment event tree development, consequence analysis and failure probability estimation of the containment vessel evaluated as a single component. To

achieve greater confidence in the quantification of containment failure probabilities in light of the leakage issue, more definitive logic diagrams and an improved data base can be developed to improve the quantification. A logical step which can be taken immediately is to do sensitivity analyses to determine the predominant containment failure modes and leakage pathways at the subcomponent level using the fault tree technique. This measure and other related procedures are described in more detail in the following.

5.1 Containment Event Tree Development

A comprehensive PRA must take into account the behavior of the containment. The containment event tree is a systematic tool used for realistically assessing the containment's ability to prevent a radionuclide release during degraded core accidents. The tree provides the bridge between the plant analysis and the consequence analysis and provides a logic structure for assuring that all significant aspects of a core degradation sequence are considered. A detailed core melt progression and containment analysis is performed to determine the fission product release to the atmosphere.

5.2 Consequence Analysis

Consequence to the public resulting from release of fission products from containment is evaluated. A concentrated airborne release would form a "radioactive cloud" which would disperse away from the immediate vicinity of the plant. The dispersion of the cloud would depend on meteorological stability, the intensity of the wind and its direction, rain and settling of fission products on the ground. Since the population distribution around the plant is not uniform, exposure of the population to the cloud would be determined by the wind direction, the population distribution, and evacuation schemes.

5.3 Failure Probability Estimation

Current practice of estimating the containment failure probability based primarily on deterministic containment ultimate capacity can only satisfy part of the PRA requirements. For a more comprehensive PRA study, additional experimental data and failure analysis based on more expanded leakage considerations are required to upgrade the containment failure probability estimation. Initially the test data and analyses will likely need to be developed from specific plant considerations. As more data become available, the Bayesian update can be used to assemble the generic data and to apply the generic data to plant specific analyses. More specific discussion on the subject can be found in Reference 7.

5.4 Subcomponent Failure Mode and Leakage Pathway

From the leakage standpoint, different areas of the containment will respond differently, developing distinct leakage characteristics for the accident sequence being considered. To assess the significance of each local leakage, analyses can be performed to determine

which local failure modes and pathways are the predominant contributors to risk. Subsequent engineering efforts can thus be concentrated on these predominant leakage pathways, thus making more effective use of the industry's risk reduction resources. For application of this local containment evaluation at the subcomponent level, the following subdivisions of the containment pressure boundary are suggested:

a) Cylindrical or conical membrane shell
b) Double curvature membrane shell
c) Base slab
d) Head/cylinder junction
e) Cylinder/base slab junction
f) Equipment access hatch
g) Personnel locks
h) Mechanical penetrations (hot)
i) Mechanical penetrations (cold)
j) Electrical penetrations
k) Containment isolation valves

5.5 Fault Tree Analysis and Sample Model

Most of the containment leakage pathways analyses can be done based on fault tree models developed at the subcomponent level (top event). Situations may arise where component event trees or system event trees may also be needed. As mentioned in previous sections, substantial portions of the event tree and fault tree analyses are now fully automated and thus it is not unreasonable to do several iterations to arrive at the optimal event/fault tree models suitable for the purpose. As more experience is gained and also more test data are developed, greater confidence in the containment failure analysis can be achieved accordingly. Figure 2 gives a sample fault tree model for leakage analyses of a typical containment equipment hatch.

6.0 CONCLUSIONS

PRA techniques which have been applied successfully estimating the frequency of sequences leading to fuel cladding and RCS pressure boundary failure can also be applied for the analysis of containment integrity. In conjunction with industry and governmental efforts to resolve the containment issues and to provide an improved data base, sensitivity studies can be embarked upon based on fault tree methodology and other existing PRA techniques. These studies will help identify important parameters in the containment integrity issues and guide the ongoing and future research programs to focus on the important parameters.

7.0 ACKNOWLEDGEMENTS

The authors gratefully acknowledge helpful suggestions made by their former colleague R.S. Orr of Westinghouse Electric Corporation.

8.0 REFERENCES

1 "Program Definition Report, Containment System Working Group," USDOE Report, October 1982. Edited by D. H. Walker.

2 Cummings, G. E., "Application of the Fault Tree Technique to a Nuclear Reactor Containment System," proceedings of the Conference on Reliability & Fault Tree Analysis, UC Berkeley, September 1974.

3 Carnino, A. & Duban, J., "Determination of Initiating Events & Sequences of Reactor Accidents by a Barrier Analysis," Proceedings of the International Conference on Nuclear Systems Reliability Engineering & Risk Assessment, Gatlinburg, Tennessee, June 1977.

4 Augustin, W., et al., "A Complex Study on the Reliability Assessment of the Containment of a PWR." Transactions of the 4th SMIRT Conference, San Francisco, California, August 1977, Papers J 1/10, J 1/11 & J 1/12.

5 Tsai, J. C. & Orr, R. S., "Probabilistic Failure Modes & Locations in Containments Subjected to Internal Pressurization," proceedings of the Workshop on Containment Integrity, USNRC Report NUREG/CP-0033, October 1982.

6 American Society of Civil Engineers (ASCE), Nuclear Structures & Materials Committee, "Report on Containment Capability," to be published at the Specialty Conference on Structural Engineering in Nuclear Facilities, Raleigh, North Carolina, September 10-12, 1984.

7 Tsai, J. C. & Walker, D. H., "Bayesian Procedure for Evaluation of Containment Capability," to be published at the Specialty Conference on Structural Engineering in Nuclear Facilities, Raleigh, North Carolina, September 10-12, 1984.

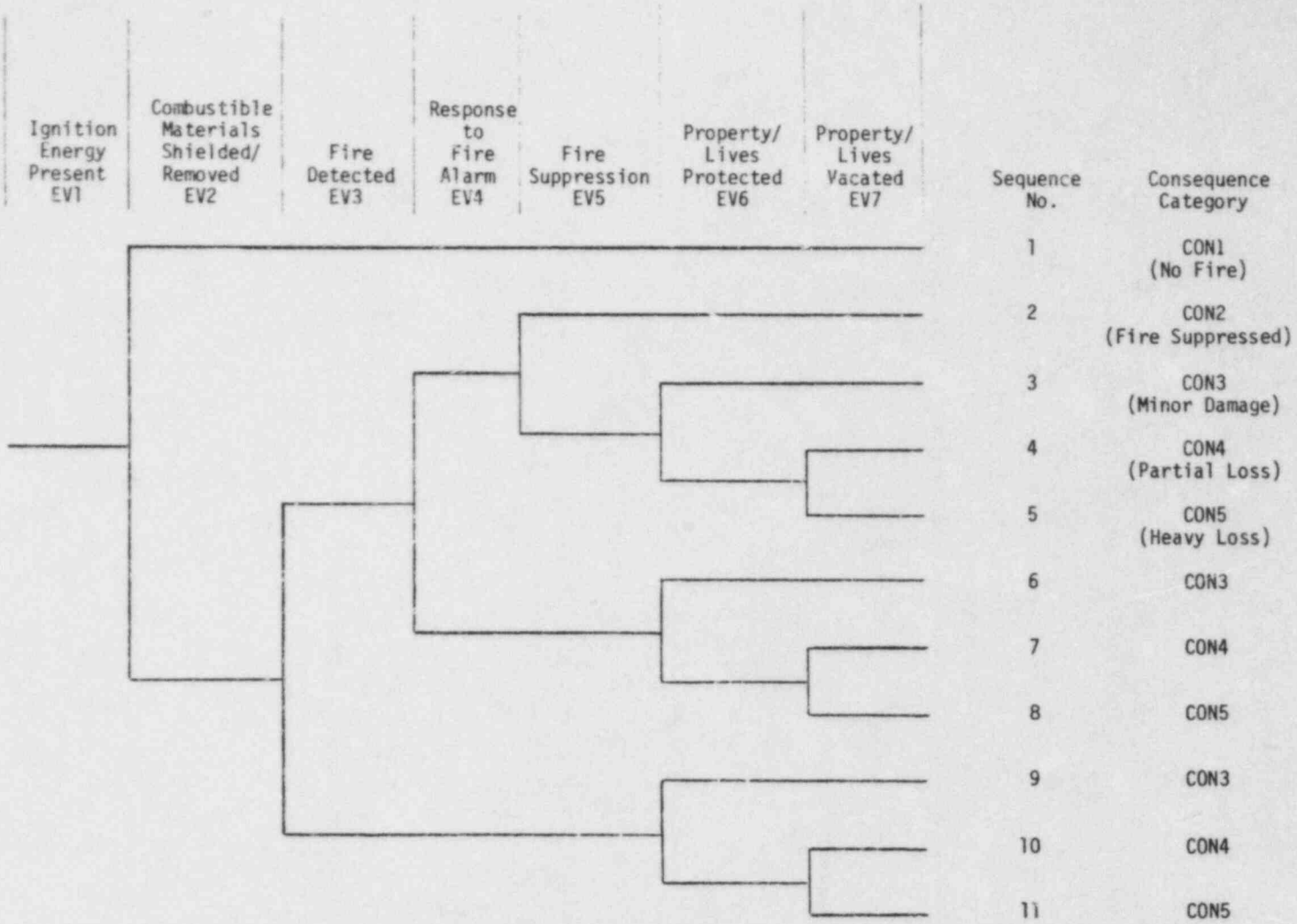

Figure 1. Example Fire Consequence Event Tree

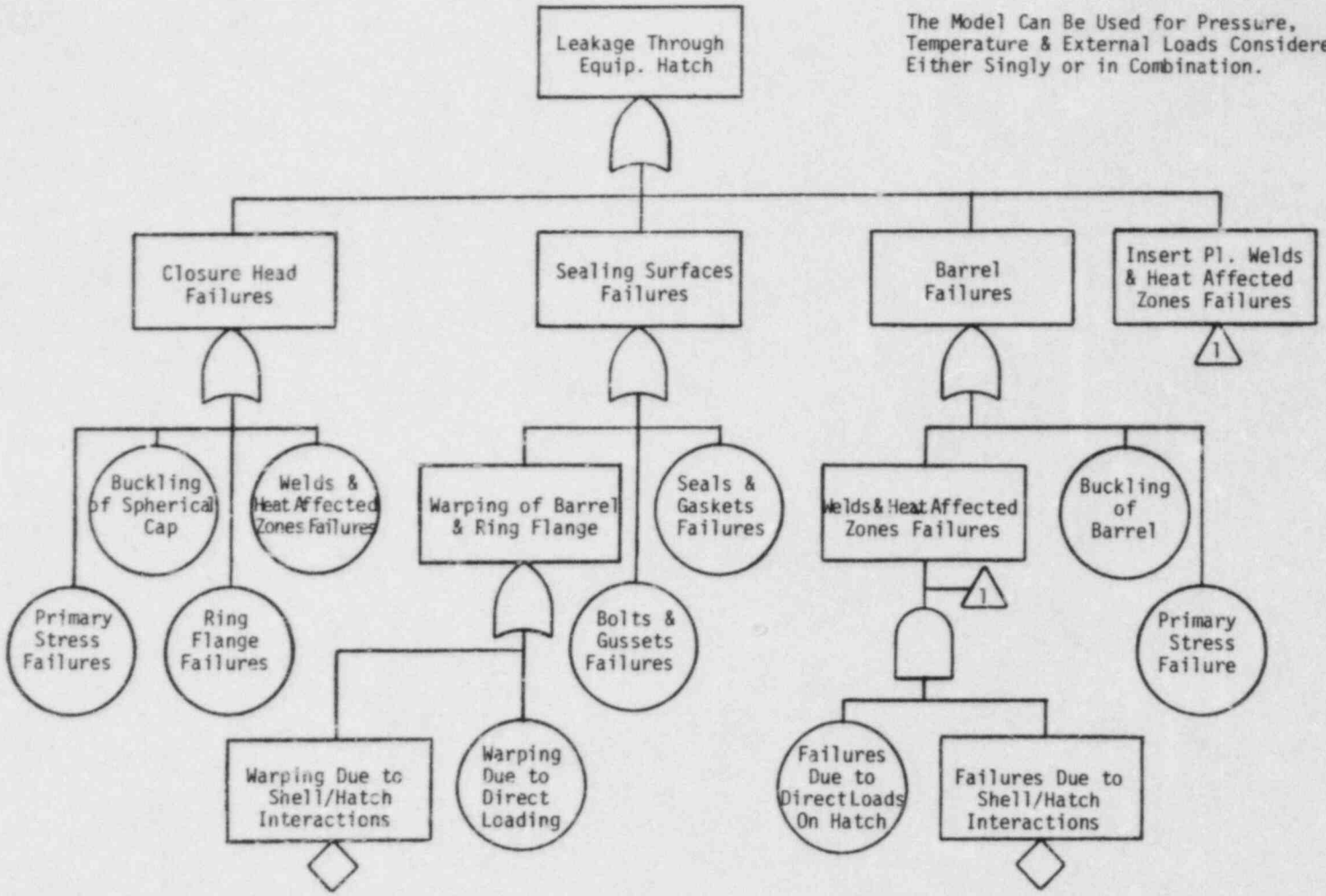

Figure 2. Sample Fault Tree Model For Leakage Through Equipment Hatch

A HIERARCHICAL GOAL TREE STRUCTURE FOR CONTAINMENT INTEGRITY

Marvin L. Roush and Mohammed Modarres
Chemical and Nuclear Engineering Department
University of Maryland
College Park, MD 20742

R. Niall Hunt
Reliability and Availability Engineering Unit
Baltimore Gas and Electric Company
Baltimore, MD 21203

ABSTRACT

A goal tree has been constructed to display the numerous aspects of radioisotope containment in a logical manner which preserves the hierarchy of the various objectives. This goal tree has been examined in terms of potential usefulness as a training aid, as a framework to use as a guide in considering the recovery of containment, and as a framework to examine the adequacy or relevance of various regulations.

INTRODUCTION

In the design and operation of the nuclear plant containment building, assurance of optimal resource allocation hinges upon the designer/owner's understanding of the required design goals and clear definition of their relative importance toward achieving the containment functional objective. To provide the analytical framework within which this "importance" can be recognized, understood, and quantified, it is necessary to develop a containment building model which provides a clear visual representation and analytical integration of all the goals necessary to meet the containment functional objective.

A measure of success for the containment building must reflect the degree of protection it affords the general public should there be a breach of the primary confinement barrier around a high-level radioactive source. Because of the multiplicity of initiating mechanisms and ensuing scenarios involving failure of primary confinement barriers, it is near impossible to define a single measure of success. The challenge to containment is affected by both:

- degree of damage resulting from the initiator of the accident sequence scenario,

and,

- time for which there is a transport path to containment atmosphere,

and various combinations of the two.

Clearly containment must respond in a way so as to minimize the effects on the public from all such postulated scenarios. As a result, success cannot be measured on the basis of a simple "fail/no fail" criterion. For example, if containment is lost, immediately attempts would be made to reestablish the boundary, or minimize transport of radioisotopes through the breach, so that the effects on the general public can be minimized. Considerations similar to the above indicate that analogous goals should be identified explicitly in the design phase and accommodated, if justified economically, in the final containment design.

Identification of all goals, so that each can be addressed in the design phase, must not only be complete, but represent a defined hierarchical structure to allow evaluation of importance for each. Quantification of "importance" for each goal provides the underlying mechanism for optimum allocation of performance requirements in a way that their contribution to the containment function is always satisfied at minimum cost.

To provide a foundation for evaluation of future generic and plant specific containment building analyses, a functionally oriented containment goal tree model has been developed. The end product is both a tool which allows unambiguous definition of the interrelationships between hardware systems and the way in which they contribute to the containment objective, and a rigorously defined analytical model which can be quantified to provide measures of relative "importance" for containment hardware and functions.

It is anticipated that this model can be used both for evaluating the risk significance of events in an operating plant which appear to affect containment performance and for establishing risk benefit criteria for future modifications, or, can be used as a basis for the allocation of performance goals during the design process.

CONTAINMENT INTEGRITY GOAL TREE

The structure presented here is an outgrowth of the Functional Classification presented by D.H. Walker (ref. 1). It also has some features which arise from the Integrated Approach described in reference 2. We have attempted to rigorously structure this tree according to the following simple guidelines:

(1) For each box, one can look "down" and see how that functional objective is attained, and
(2) For each box, one can look "up" and see why that functional objective is required.

The goal tree we have developed for Containment Integrity applies primarily to Pressurized Water Reactors and is displayed in Figures 1 through 3. The top structure of the tree is based upon a recognition that the public health is protected by minimizing the release of radioisotopes, described here as maximizing the containment of radioisotopes. The containment of radioisotopes is accomplished by establishing a rugged shell which is nominally leak-tight, and then minimizing the amount of radioactive material transported across the barrier.

Figure 1 details the considerations which affect the transport of radioisotopes, given some leakage through the containment boundary. This radioisotope transport is kept to a minimum by minimizing both the amount of leakage and the concentration of radioisotopes within the containment atmosphere which is leaking.

Figure 2 provides a continuation of the left-hand side of Figure 1, focusing upon the establishment of a containment envelope around the sources of radioisotopes in a nuclear power plant. We have only developed a detailed consideration for containment of radioisotopes within the reactor core, the most important source. Nuclear plants are constructed with multiple physical barriers to contain fission products during normal operation and particularly in the event of an accident. These barriers include leak-tight cladding of the fuel, the envelope of the reactor coolant system, and the containment vessel. The two goals, "Control All RCS Boundary Penetrations" and "Control All Containment Boundary Penetrations," are not necessarily totally independent. It is of considerable importance to review these two sets of penetrations for common elements since such penetrations have the potential to be common cause failure points for two levels of containment.

Figure 3 provides a continuation from Figure 2 and presents considerations which support the goal of maintaining loads applied to the containment at or below design levels. Consideration is given to loads which arise from explosive combustion, from generation of noncondensible gases, from internal impact loads, and from pressure due to steam. The pressure due to steam at saturation conditions is dependent upon the energy per unit volume in the vapor. One approach to controlling this parameter is to cluster nuclear plants into a power park with an empty containment building available to allow an increase in the effective volume of containment, if needed. The primary approach to pressure control involves design of containment volume so that design pressure will not be exceeded in the short term and provision for energy removal to avoid pressure escalation in the long term.

APPLICATIONS

This goal tree provides a logical display of the various facets which enter into a complete analysis of radioisotope containment. We will look briefly at three applications of such a goal tree.

Use As A Training Aid

The logical layout of the goal tree provides an overview of radioisotope containment requirements. This pictorial model of containment features can lead to a logical approach in response to any unusual challenge that might face a plant operator.

Framework For Prioritizing Recovery Potential

Figure 1, on the right-hand side, focuses upon objectives that become important when the integrity of the containment boundary has been compromised. The potential leakage which would result from failure of a component of the Containment Isolation System can be reduced by rapid diagnosis and response in order to complete the isolation process. The response time can be minimized by providing appropriate sensors to give useful information, by providing automatically controlled response systems where appropriate, and by providing proper training.

If excessive leakage still remains after ensuring that all valves that are part of the Containment Isolation System are in the proper position, efforts would presumably shift to either isolate the leak path through additional valve closure or by some means of mechanically plugging of the leak path. Such an action is unlikely to be possible on a spur of the moment action and since it is such an unlikely requirement at any one site, this item would seem to suggest the development of a single response team on an industry-wide basis. Such a group might have very specialized training and apparatus prepared to deal with the low-probability but important issue of a leaking containment. The many scenarios that might be considered might even include the development of an appropriate device to seal off a "blown out penetration" after the containment has depressurized. For long-term management of such a situation, it might still be valuable to restore the containment integrity.

This same figure also indicates a possible objective of "Filter Radioisotopes From Atmosphere At Point Of Leakage." Again, this might be an accomplishment that could be carried out by a single special response team. The removal of particulates from the escaping gas would seem to have obvious benefit and one might even conceive of situations in which a continuous spray of water might have a desired reduction of escaping iodine levels.

Framework For Prioritizing Regulatory Requirements

The goal tree as it has been demonstrated in Figure 1 can be useful in determining and justifying the adequacy or necessity of a containment system or a regulatory-related backfit for such a system. In this process a required containment system or backfit must in some way improve the performance in meeting one or more of the goals shown in the goal tree. Thus, a determination of the adequacy and extent to which a system satisfies the goal should be made. This would provide a means of systematically and logically evaluating the need and necessity of a system and also provides a means of identifying how well it satisfies or improves the ultimate goal of "Maximize Containment Of Radioisotopes Within Nuclear Plant." A similar approach can also be used to show the impact of new procedures related to containment integrity systems.

As a specific example, let us consider a containment spray system or a modification to such a system. It will affect significantly multiple goals, including "Scrub The Atmosphere," "Minimize Driving Head Across Leak Path" (due to the depressurizing effect of the spray), "Provide Adequate Internal Energy Sink" (the containment spray system usually provides injection of water from an external tank into the containment, water whose considerable heat capacity retards temperature increases), and "Maintain Containment Energy Removal Capability" (many containment spray systems have a heat exchanger aligned during recirculation).

The goal tree provides a mechanism for finding competing risks that may be affected by a single regulation. This structure provides help in identifying negative impacts in one area which result when a "fix" is provided to a specific problem in another area. As an example, a modification to the Containment Spray System could affect the system's ability to meet the various individual objectives, some positively and some negatively. The goal tree can be useful as a part of the decision process in evaluating potential changes.

REFERENCES

1. D.H. Walker, "Definition Of Containment Issues," Proceedings of the Workshop on Containment Integrity, June 1982, NUREG/CP-0033.

2. Combustion Engineering, "An Integrated Approach To Economical, Reliable, Safe Nuclear Power Production," Report ALO-1011, April 1982.

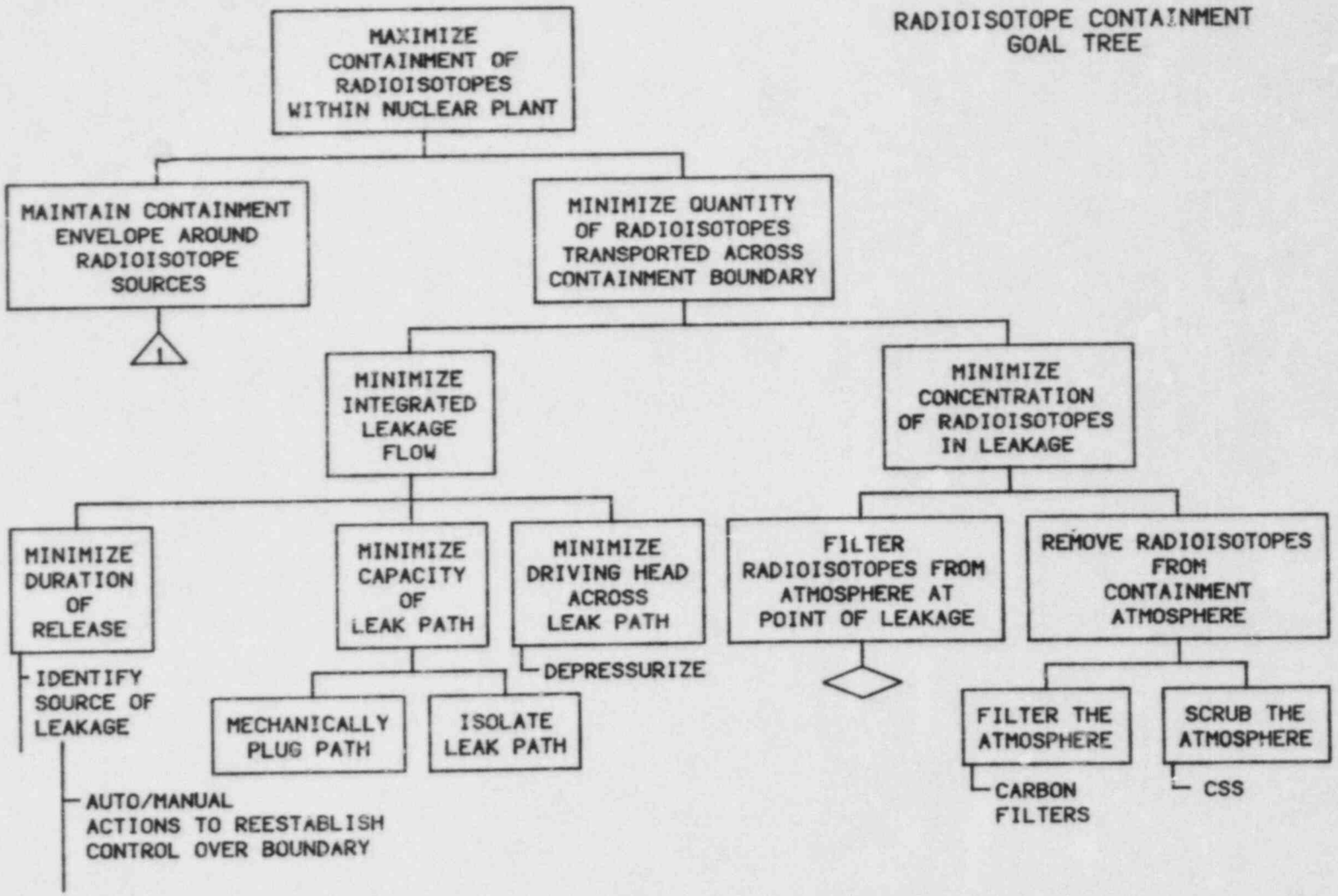

FIGURE 1 TOP OF THE GOAL TREE STRUCTURE FOR RADIOISOTOPE CONTAINMENT

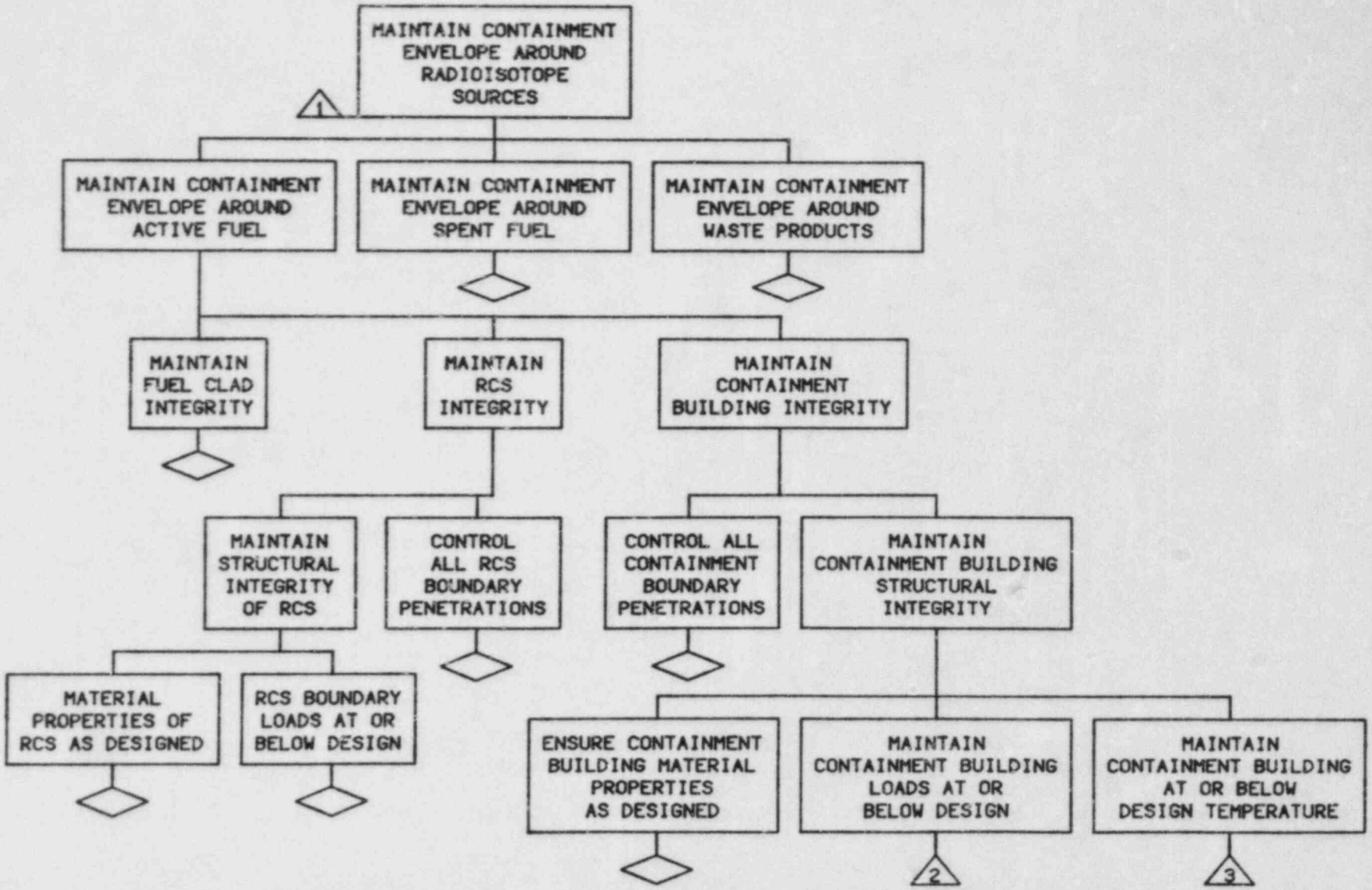

FIGURE 2 CONTINUATION OF THE STRUCTURE IN FIGURE 1

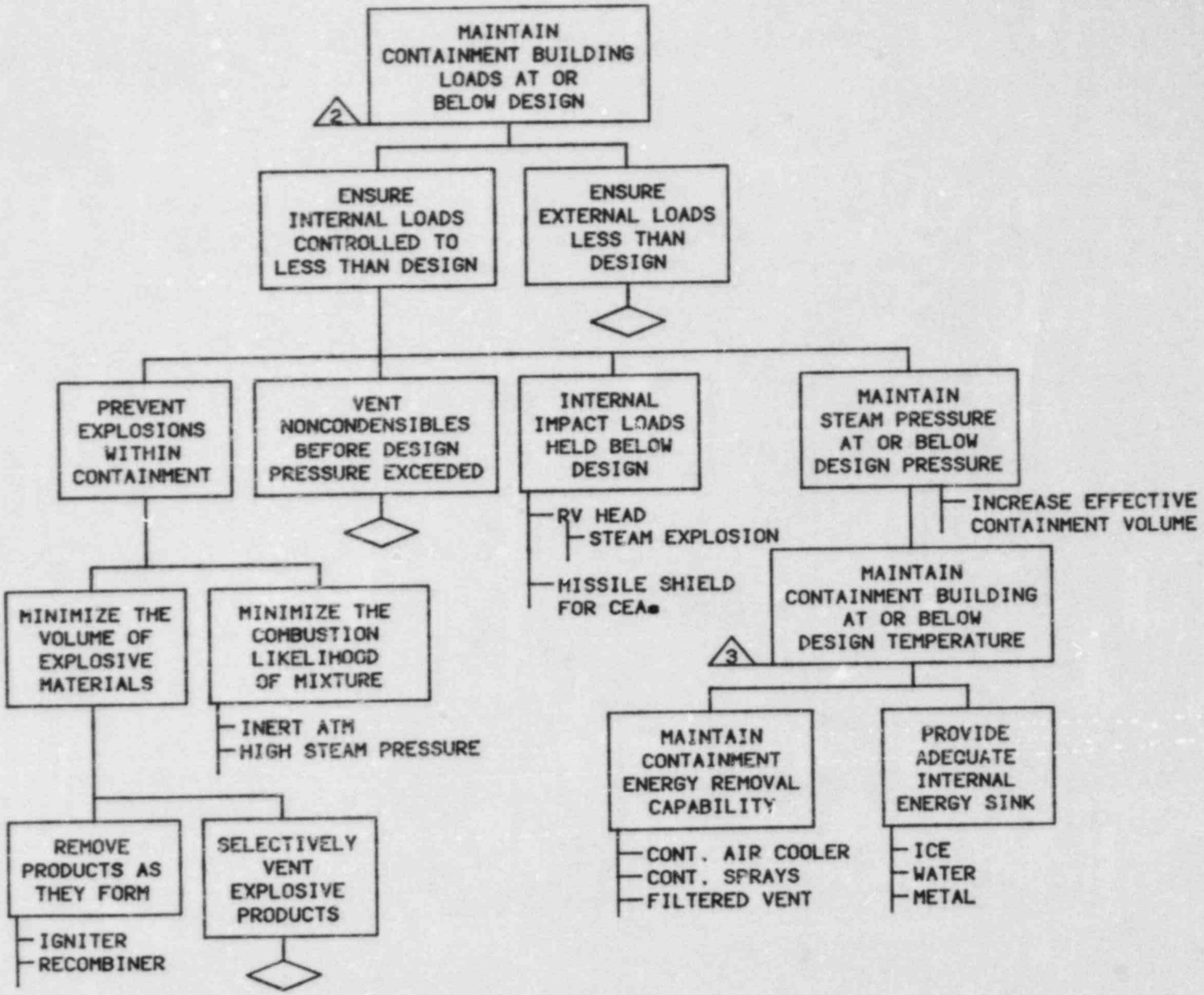

FIGURE 3 CONTINUATION OF THE STRUCTURE IN FIGURE 2.

THERMODYNAMIC CONSEQUENCES OF LEAKAGES IN A DOUBLE CONTAINMENT DURING SEVERE ACCIDENTS

M. Tiltmann
Gesellschaft fur Reaktorsicherheit (GRS) mbH
Cologne, Germany

ABSTRACT

For a large nuclear power plant under normal operating conditions, a leakage rate for the Containment of 0.25 Vol %/day is admissible. During a successfully controlled LOCA, leakages of the containment will be released through filters by the annulus* air exhausting system into the environment. During a core melt accident, a pressurization of the containment has to be expected, which could lead to a failure of the containment due to overpressurization. When openings in the containment steel shell will occur before a catastrophic failure could happen, a depressurization into the annulus takes place. The area of the openings determines the depressurization rate and the thermodynamic conditions in the annulus. Furthermore, the behavior of the components being necessary for accident mitigation is influenced too. This paper discusses the thermodynamic consequences of leaks in the containment shell of a German PWR during a core melt accident. The results of those calculations are the necessary boundary condition for the estimation of fission product retention in the annulus.

Introduction

This paper presents preliminary results of the German Risk Study, Phase B, being sponsored by the Federal Ministry of Research and Technology. The presentation deals with the behavior of a German PWR-Double Containment in case of a typical core meltdown accident which leads to containment failure by overpressurization. According to Reference 1, containment failure due to overpressurization is expected to be the most probable mode for fission product release to the environment. In Reference 1 too, it was assumed, that fission product release caused by leaks in the containment steel shell is directly spread out in the environment without taking into account the retention of fission products in the annulus. In the following, the thermodynamic consequences of leaks in the steel shell of a double containment are discussed for a postulated core meltdown accident in a 1300 MWe

*Annulus between the containment steel shell and the outer concrete shielding.

PWR. Therefore, the concept to the typical German PWR containment is introduced with the reactor building, the annulus, the annulus air exhausting system, and the outer reinforced concrete shielding.

The Typical German PWR Containment

The nuclear power plant containment which retains radioactivity during accidents consists of a gas-tight, spherical steel vessel of 56 m diameter and 30 mm wall thickness. The containment is enclosed by an external reinforced structural shell (the secondary containment), with an air exhausting system for the annulus lying in between. The reinforced structural shell of about 1.5 m thickness protects the reactor system against external events and shields the environment against direct radiation from the containment during accidents, Figure 1.

The secondary containment is not absolutely gas-tight. Normally the untightness is in the range of 2000 - 3000 m^3/h at 4 mbar subatmospheric pressure.

The steel vessel contains a number of pipelines and cable penetrations needed primarily to operate the systems located within the containment. These penetrations are gas-tight and pressure resistant and can be isolated by at least two valves in series.

During an accident with loss of coolant, the reactor protection system closes the building isolation valve. Thus all pipeline penetrations not needed to control the accident are automatically closed off. The annulus of about 2 m width between the containment and the reinforced concrete structure is kept at subatmospheric pressure by means of the annulus air exhausting system. Thus radioactivity release due to smaller leaks from the containment can be detected, monitored, and released through filters and stacks.

Accident Sequence

For the following accident sequence, the availability of electric power is a main assumption. In the event of a loss-of-coolant accident, a double-ended break of a reactor coolant pipe is first followed by a regular emergency coolant injection from the accumulators and low-pressure systems. However, a failure prevents the low-pressure systems from changing over to the sump recirculation mode of operation (approximately 20 minutes after the inception of the accident).

This chain of events leads to a core meltdown at the pressure existing inside the containment and is referred to as low-pressure core meltdown case. At the time when the change-over to the sump recirculation mode fails, the core region in the reactor pressure vessel is assumed to be completely reflooded.

After about 0.7 h, the water level has decreased to the top of the active core as a consequence of the evaporation of the coolant by decay heat. Core meltdown will start about 1.1 h after blowdown. At about 1.4 h, the lower grid plate of the core is assumed to fail. The molten material is expected to slump into the lower plenum of the RPV. Residual water inside the plenum will be evaporated, before about 2.5 h after blowdown. Also the RPV is supposed to fail at the latest due to the attack of molten material.

The failure of the PRV marks the end of the in-vessel-melt phase of the accident.

In the subsequent ex-vessel-melt phase, melt-concrete interaction will decompose thermally the concrete of the foundation of the reactor building. Besides the erosion of the concrete--in FRG predominantly silicious concrete is used--the release of steam and gases like CO_2, CO, and H_2 have to be expected from the melt.

Figure 2 shows the pressure of the containment atmosphere versus time in the "low-pressure case." Additionally, the partial pressures of several components of the containment atmosphere are given in Figure 2.

According to Figure 2, the expected failure pressure of the containment steel shell will be exceeded after about 4.5 days. This time is mainly depending upon the heat transfer from the hot outside of the steel shell to the atmosphere of the annulus. The expected failure pressure will be exceeded after about 3 days by the assumption of an insulated outside surface of the containment steel shell without heat transfer into the annulus. The long-term pressure increase is mainly a consequence of the increase of the partial pressure of steam after the contact between melt and sump water as a result of melt-concrete interaction. This contact occurs when the innermost shield inside the reactor cavity, which initially separates sump water from melt, has been penetrated by the melt. At the expected failure time, the contribution of noncondensible gases (H_2, CO_2, CO) to the pressure of the containment atmosphere is of minor importance.

Results

Investigations of the strength behavior of the containment vessel show that certain leaks may occur at weak points of the containment when the design pressure is exceeded. The causes of leaks in the containment vessel above the design pressure are not discussed in this paper.

Because of their inherent removal of masses and energy, leaks in the containment vessel lead to a pressure reduction in the containment. The gradient of this pressure reduction is determined by the size of the leak.

The plant configurations outside the containment vessel, such as annulus, outer concrete shield and annulus air exhausting system, as well as the environment, are influenced in different ways by the size of the containment leak. The size of the leak also determines the release pathway to the environment. The following basic possibilities exist in this context:

- In the case of small-sized leaks, the annulus air exhausting system working at the upper operating point is not capable of maintaining the subatmospheric pressure in the annulus; the pressure in the annulus is somewhat above the environmental pressure so that (in addition to the filtered material handled by the annulus air exhausting system) unfiltered activities reach the environment through leaks in the outer concrete shielding.

- In the case of medium-sized leaks, the annulus air exhausting system fails (pressure builds up in the annulus 50 mbar), but the openings into the environment and the auxiliary building remain closed.

- In the case of large size leaks in the containment vessel, the sudden pressure builds up in the annulus, which follows the occurrence of a containment vessel leak, may lead to a failure of both the air routing system and the filters or the ventilator. This pressure buildup also exceeds the pressure resistance of the doors leading to the reactor auxiliary building and to the environment. The result is a direct release of containment vessel leakage to the environment. Also compare Figure 3.

The following is a description of the thermohydraulic effects which various leak sizes in the containment vessel have on the pressure and temperature histories inside the containment. It is assumed in this context that the parameterized

leak openings under review inside the containment vessel become effective shortly before the postulated failure pressure of 8.5 bar is reached.

As far as the investigation of containment pressure reductions as a result of leaks in the steel shell is concerned, the most interesting aspect to start with is the minimum size of the containment vessel leak which, on the one hand, prevents the pressure inside the containment from increasing any further and, on the other hand, does not interfere with the function of the subsequent components such as annulus and annulus air exhausting system. The minimum leak size in the containment vessel, which is determined by parameterization, corresponds to a leak diameter of approx. 4 cm ($\hat{=}$ ~14 cm^2 of leak area) with respect to the core meltdown accident outlined before. Although the sudden occurrence of this leak area in the containment vessel, shortly before the overpressure failure, causes a pressure increase in the annulus, this increase remains below the pressure difference of ~50 mbar which leads to a failure of the annulus air exhausting system.

The pressure difference required to open the doors is approximately 100 mbar.

Thus, although the annulus air exhausting system remains operative after the occurrence of the leak, it is not sufficient to produce a subatmospheric pressure again in the annulus, as is indicated in the time range depicted by Figure 4. Beginning at this point in time, in addition to the filtered material discharged through the stack by the annulus air exhausting system, there is also a release of unfiltered material through the leaks in the outer concrete shielding. The time range depicted in Figure 5 shows this unfiltered leakage from the annulus to the environment. The corresponding calculations are based on a cumulated flow area of approximately 300 cm^2 $\hat{=}$ a diameter of 20 cm. The flow rates from the containment vessel and the exhaust rates of the annulus air exhausting system are also depicted in Figure 5. The diagram shows that somewhat more than one half of the escaping masses are filtered by the annulus air exhausting system.

The time range in Figure 6 shows that the pressure inside the containment vessel is maintained at approximately 8 bar after the leak has occurred and that a moderate decrease follows as a result of the decreasing residual heat.

Figure 8 shows the overall pressure history in the containment vessel and the pronounced pressure stabilization after the opening of the leak.

As an example of a large leak in the containment vessel, a 300 cm^2 leak was considered in view of its effects on the annulus, the annulus air exhausting system and the release of activities to the atmosphere. This postulated maximum cross-section leads to such a great pressure buildup in the annulus that it causes a failure of the annulus air exhausting system. Furthermore, this pressure buildup causes the opening pressure difference to be exceeded with respect to the doors leading from the annulus to the environment and to the reactor auxiliary building, so that there is a direct release of the annulus content into the environment.

In this context, Figure 4 shows a certain time range of the pressure history in the annulus where the admissible pressure difference of 0.1 bar at the doors is exceeded. A pressure equalization between annulus and environment is then caused by the large openings of the doors.

Figure 7 shows the masses released from the annulus to the environment. On a long-term basis, they are identical with the outflow rates from the containment vessel.

Within approximately 5 hours, the pressure inside the containment vessel has come to match that previaling in the environment, as is indicated in Figure 6. The relatively fast pressure reduction in the containment vessel through the large leak opening is again depicted in Figure 8 as part of the overall pressure history.

Conclusion

Apart from the existing retention capability of the annulus with respect to fission products, the investigations reveal that, in the event of a core meltdown accident, relatively small leak cross-sections in the containment vessel are already sufficient to prevent a disastrous overpressure failure. The configurations outside the containment vessel, such as annulus, annulus air exhausting system and outer concrete shielding, are not jeopardized as far as their integrity is concerned. Within this range of leaks (approximately 50 cm^2) in the containment vessel, most of the material that is discharged to the environment is thus filtered before.

The above comments constitute a status report. The investigations, and particularly those in the fields of materials, have not yet been completed.

Acknowledgment

This work was supported by the Federal Ministry of Research and Technology (BMFT) of the Federal Republic of Germany as a part of the program RS 576.

References

1. The Federal Ministry of Research and Technology: "The German Risk Study," A study of the Gesellschaft fur Reaktorsicherheit (GRS), Cologne, Germany, 1979.

2. K. Bracht and M. Tiltmann, "Analyses of Containment Loading by Hydrogen Burning During Hypothetical Core Meltdown Accidents," Presentation at the International Meeting on Light Water Reactor Severe Accident Evaluation, August 28 - September 1, 1983, Cambridge, MA, U.S.A.

3. K. Bracht, J. Rohde, and M. Tiltmann, "Thermodynamic Efficiency of Several Additional Measures Against Containment Overpressurization During Hypothetical Core Meltdown Accident," Presentation at the 7th International Conference on Structural Mechanics in Reactor Technology, August 22-26, 1983, "Chicago, IL, U.S.A.

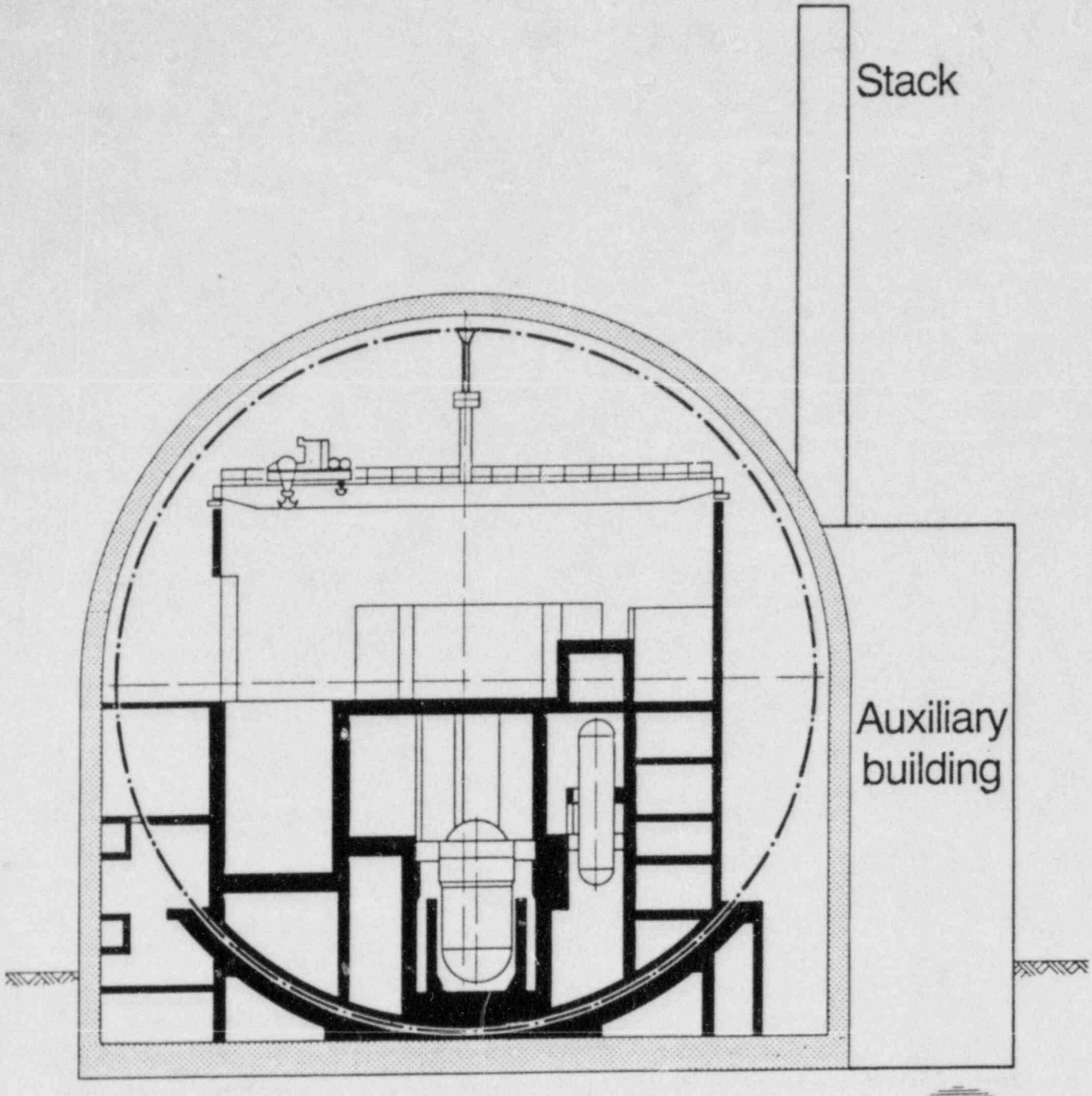

CONTAINMENT 1300 MWe **PWR**
WITH AUXILIARY BUILDING AND STACK

FIGURE 1

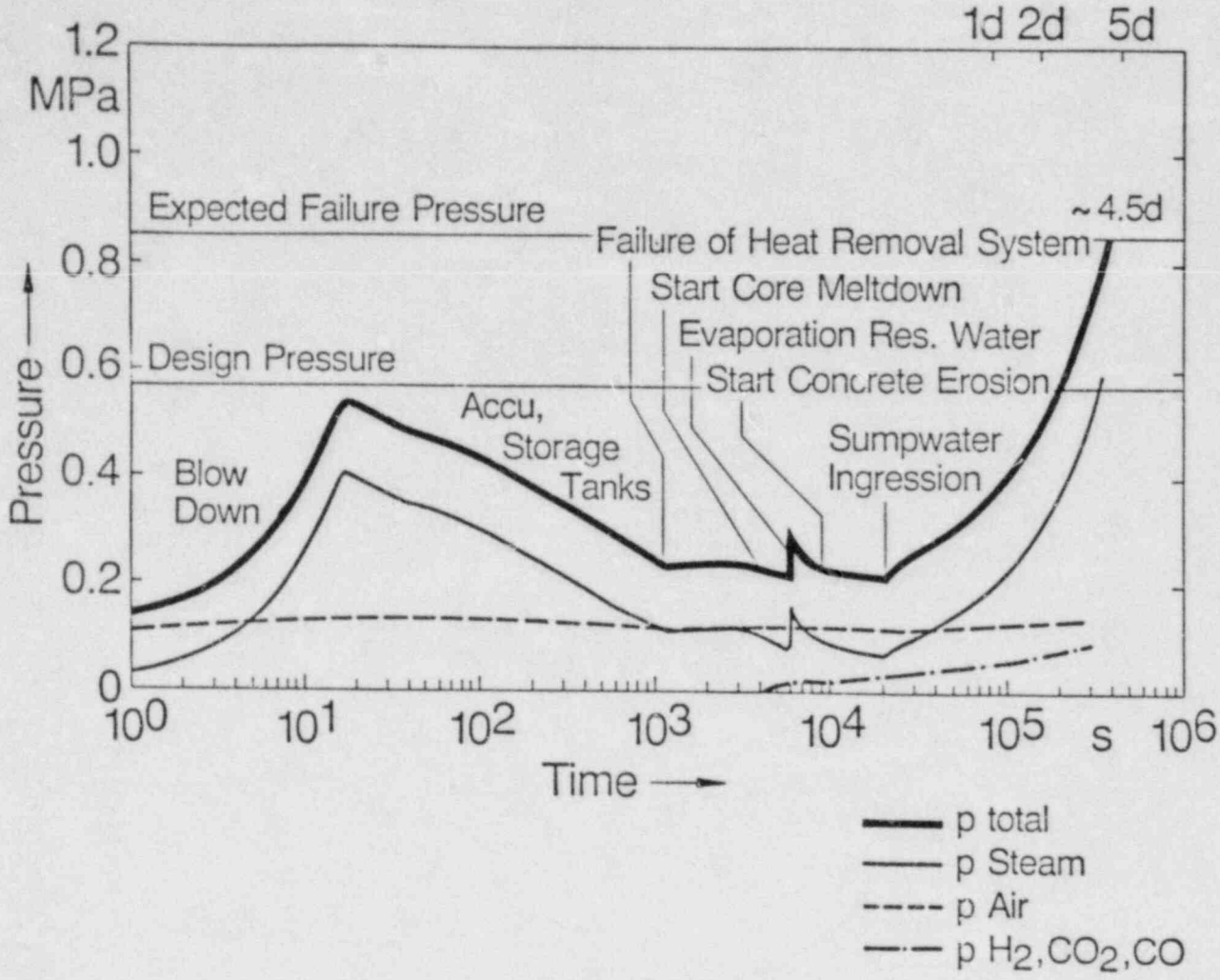

CONTAINMENT PRESSURE-TIME HISTORY (LOW PRESSURE CASE)

FIGURE 2

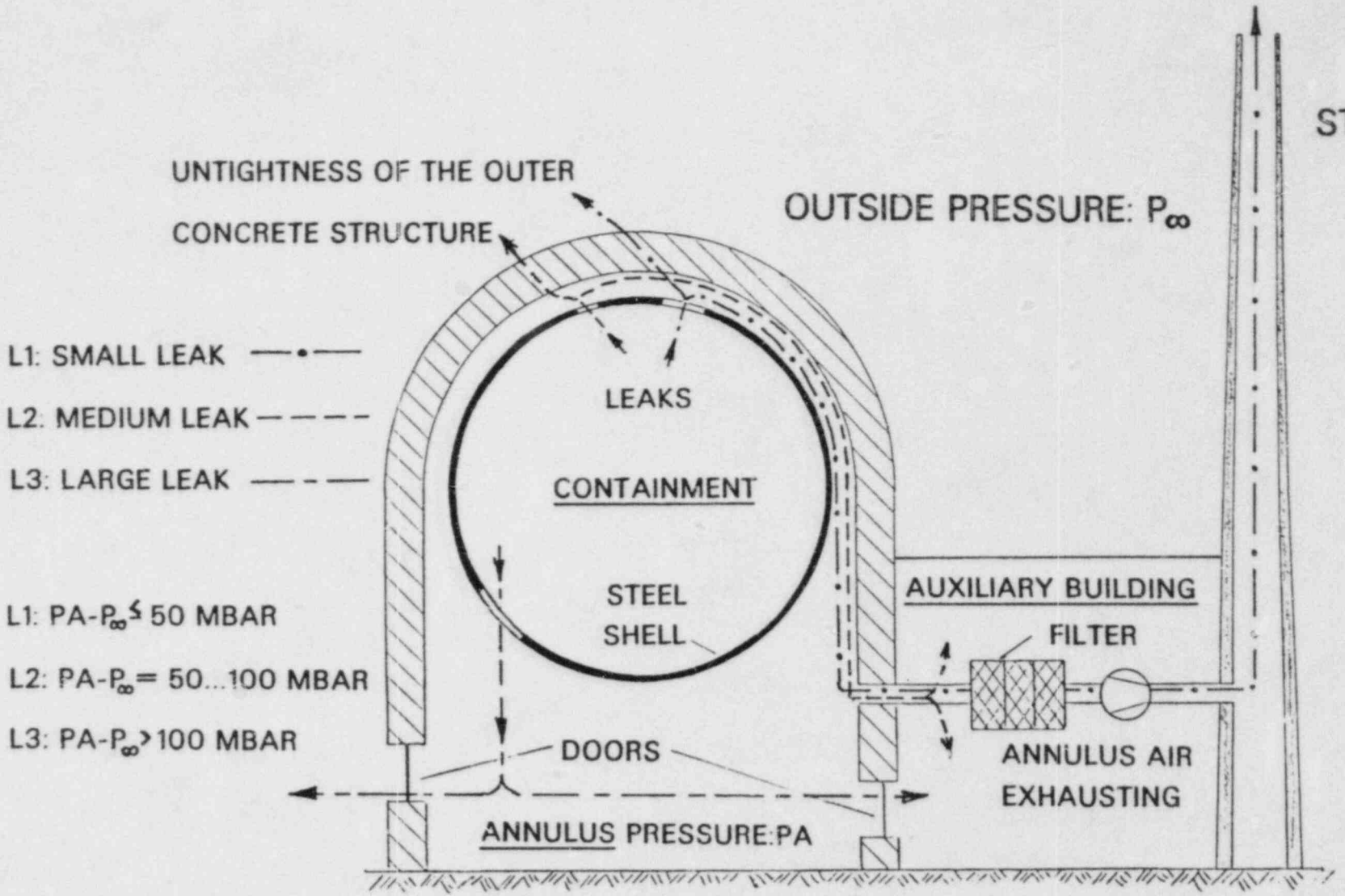

1300 MW PWR

RELEASE PATHES OUT OF THE CONTAINMENT AND ANNULUS DUE TO CONTAINMENT OVERPRESSURIZATION

FIGURE 3

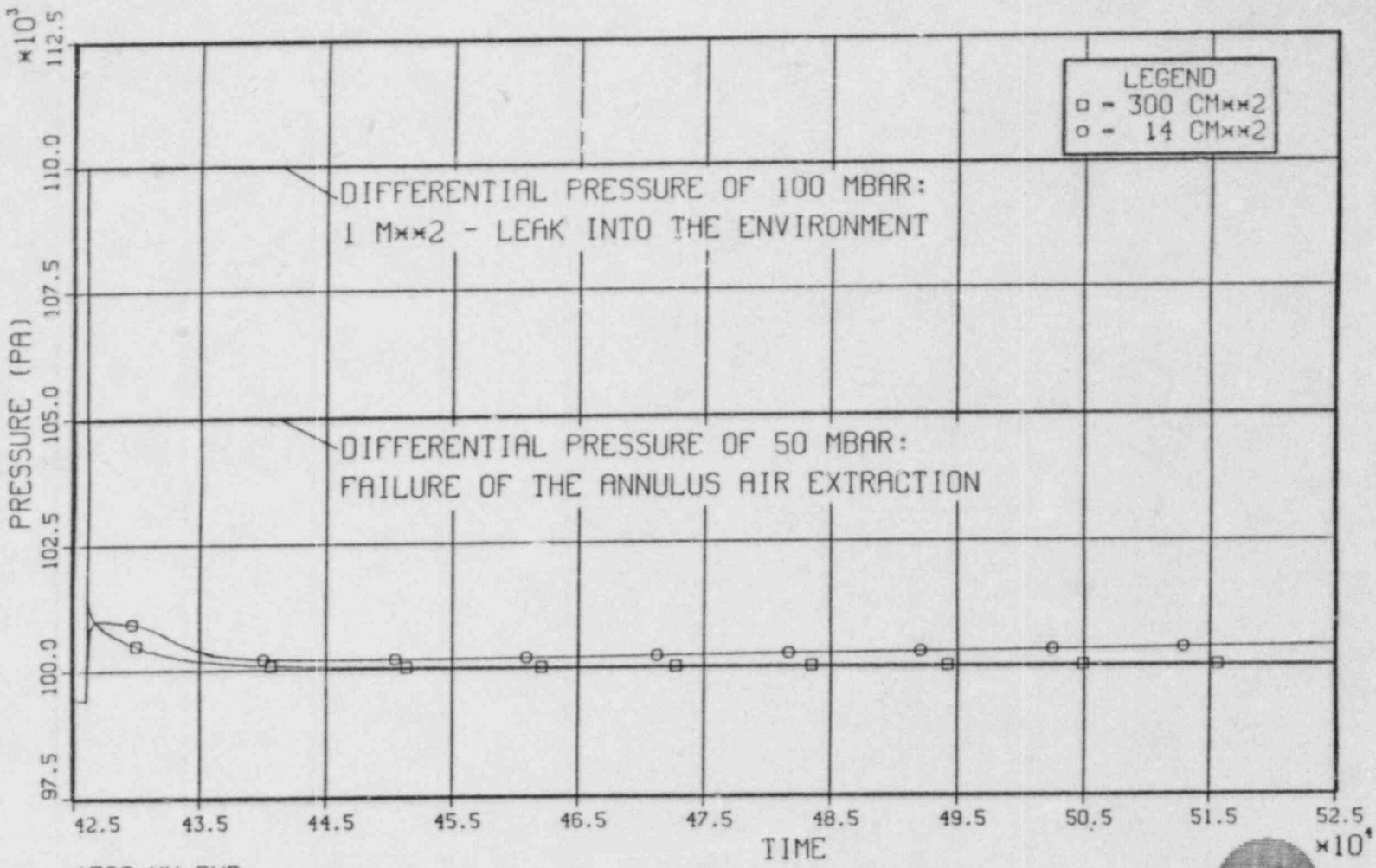

1300 MW PWR
ANNULUS PRESSURE-TIME HISTORY DUE TO LEAKS IN THE STEEL SHELL

FIGURE 4

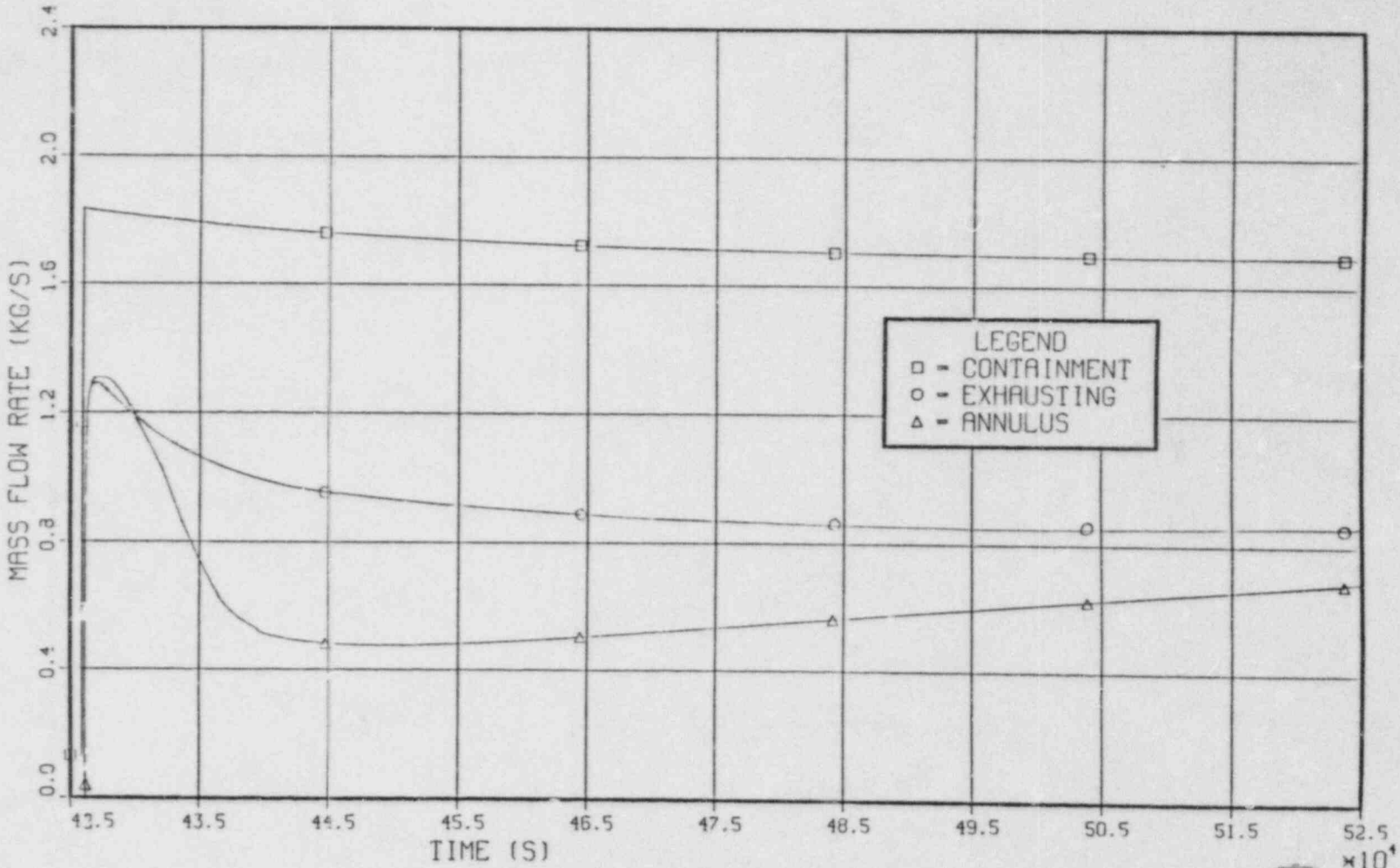

1300 MW PWR
MASS FLOW RATES DUE TO A 14 CM××2-LEAK IN THE STEEL SHELL.

FIGURE 5

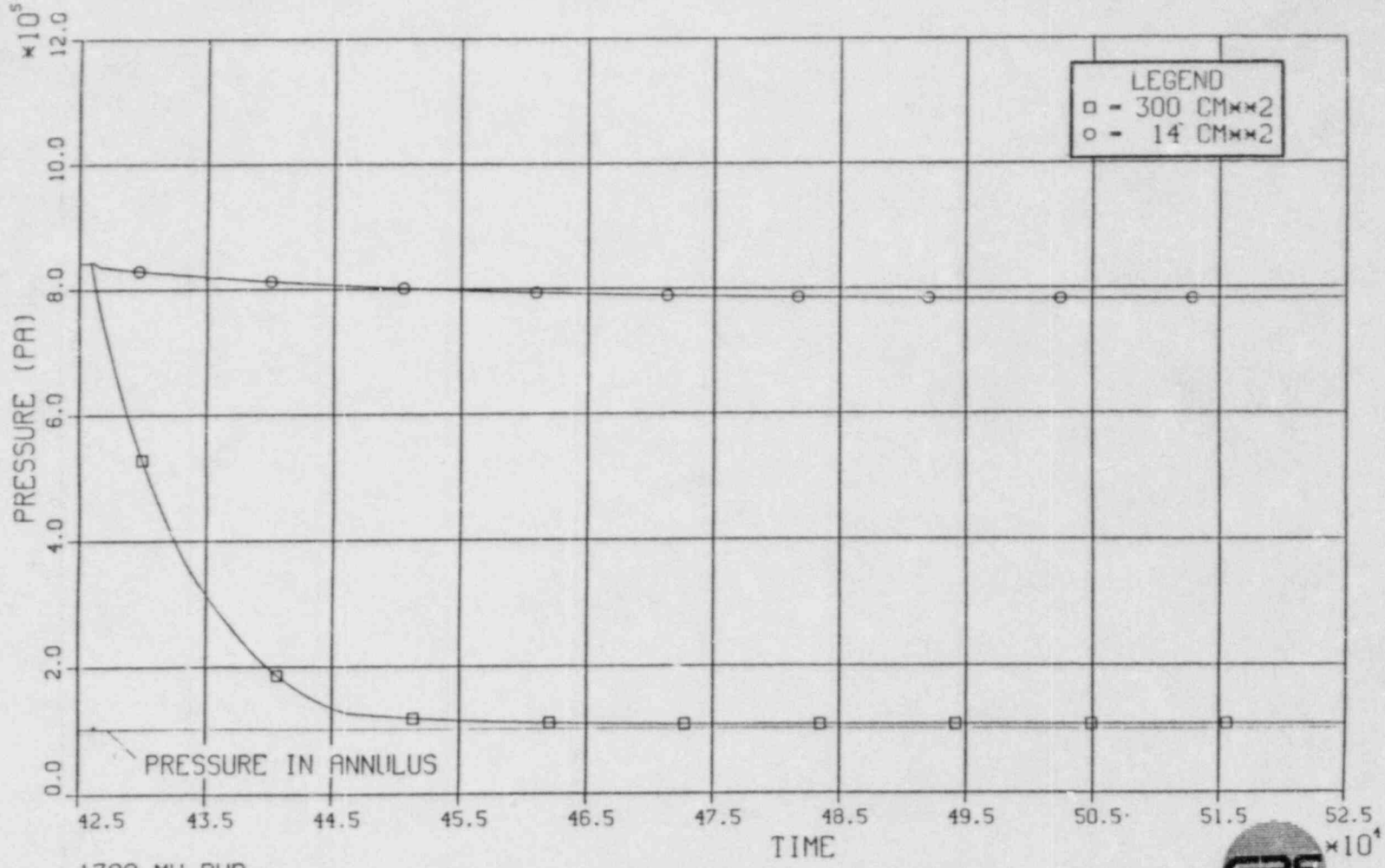

1300 MW PWR
CONTAINMENT PRESSURE-TIME HISTORY DUE TO LEAKS IN THE STEEL SHELL

FIGURE 6

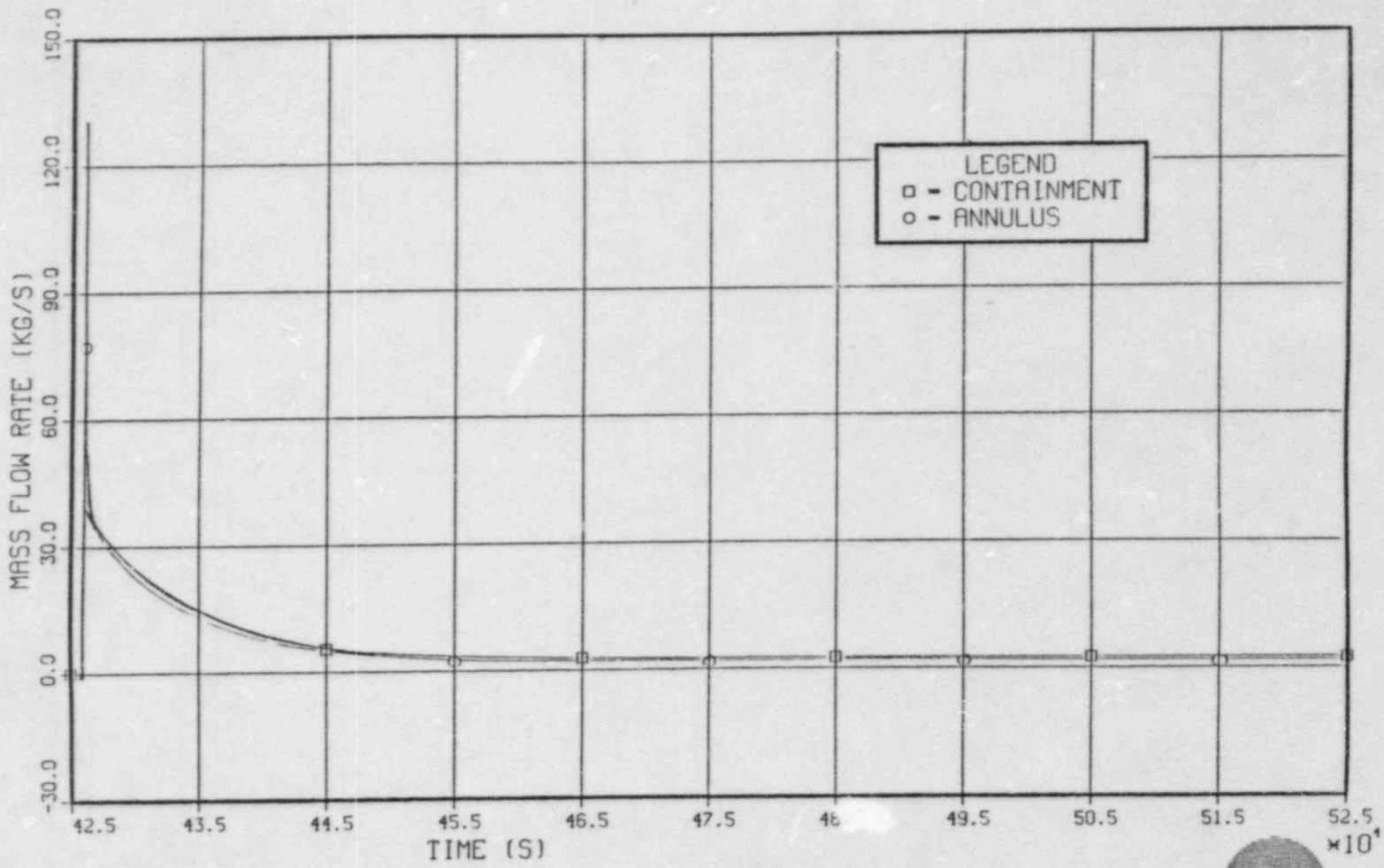

1300 MW PWR
MASS FLOW RATES DUE TO A 300 CM××2-LEAK IN THE STEEL SHELL.

FIGURE 7

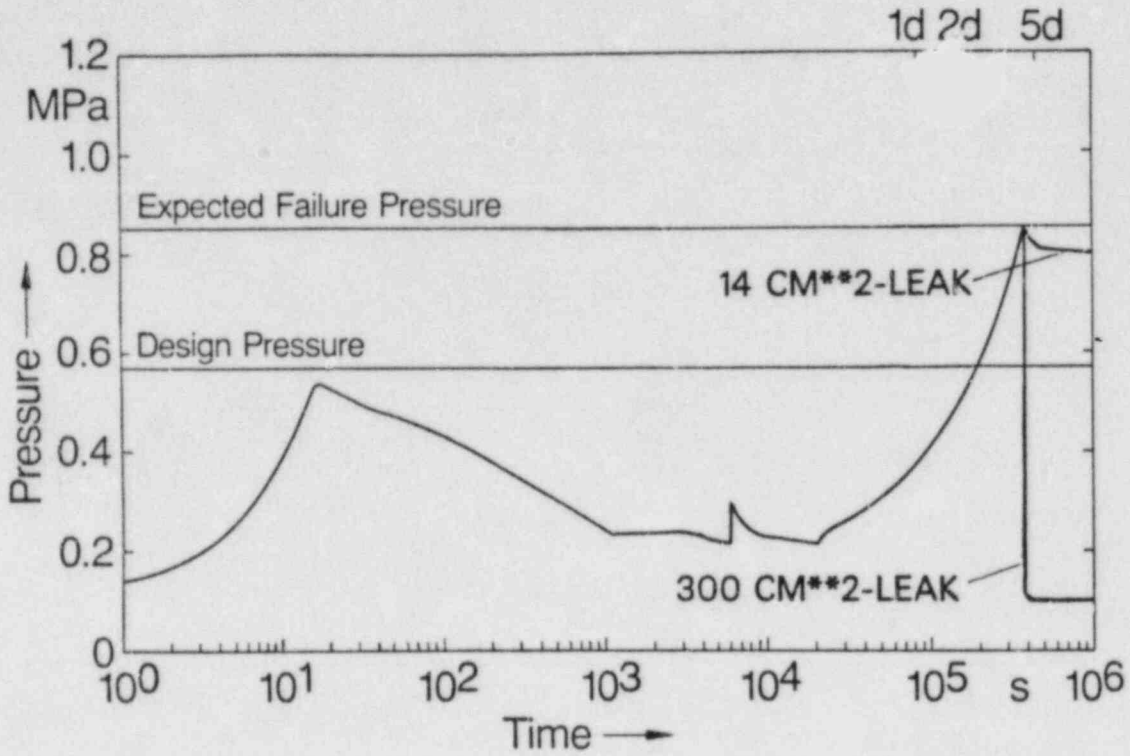

1300 MW PWR
CONTAINMENT PRESSURE TIME HISTORY
DUE TO LEAKS IN THE STEEL SHELL

FIGURE 8

CONTAINMENT RELEASE MODES, RAINOUT, AND RISK*

R. G. Spulak, Jr., and B. A. Boughton
Sandia National Laboratories
Albuquerque, NM 87185

ABSTRACT

Reactor containment failure due to overpressurization (from generation of steam and noncondensible gases or hydrogen burning) after a core-melt accident will result in the release of the contents of the containment atmosphere to the environment. The containment atmosphere at failure typically contains radioactive aerosol particles and a large amount of steam. The steam content of the release has been ignored in ex-plant consequence calculations to date, which model the release as a plume of dry aerosols.

Our research has addressed the possibility that condensation of some of the steam outside the containment could lead to deposition of a significant fraction of the radioactive material near the plant. This "rainout" of radioactive material could drastically alter the calculated consequences of the accident and have dramatic implications for exclusion radii and evacuation and other aspects of emergency planning.

We consider three types of release from the containment: a "puff" from a large-scale rupture, a "jet" from a discrete hole, and release from a "crack" or network of fissures or cracks. The physical details of the exit from the containment is different in each case, possibly leading to a different likelihood of condensation and rainout.

We have modeled each of these releases to the point where the material begins to mix with the ambient air. In addition, we have modeled the jet release from this point through entrainment of ambient air, condensation and agglomeration of water droplets, transition to a plume, and deposition of drops on the ground.

---

*This work is supported by the U.S. Nuclear Regulatory Commission, Office of Regulatory Research, and performed at Sandia National Laboratories which is operated for the U.S. Department of Energy under Contract Number DE-AC04-76DP00789.

The likelihood of rainout in the jet case is most sensitive to the ambient air temperature and to the initial number density of aerosols in the containment. The exact containment failure pressure is relatively unimportant. The puff and crack cases also have the potential to produce rainout, perhaps with different likelihoods and sensitivities. If rainout occurs in a large fraction of accident scenarios, the exact mechanisms by which the containment fails may be important.

INTRODUCTION

In a severe light water reactor (LWR) accident (core-melt), the radioactive material of concern will be in the form of aerosol particles suspended in the containment atmosphere. Present accident consequence predictions model[1] the release from containment as a plume of dry aerosol particles. However, the containment atmosphere will typically consist of a large amount of steam generated by the accident as well as noncondensible gases. The possibility exists that this steam could condense outside the containment during the release and processes related to the condensation could deposit the radioactive particles near the plant. If the effects were large enough, and occur in a large variety of hypothetical accident scenarios, our predictions of risk from nuclear power plants would be altered. In addition, near-plant deposition would have implications for exclusion radii and evacuation planning and other aspects of emergency preparations.

There are four ways in which condensation of steam could affect risk. First, condensation on the dry aerosol particles, agglomeration of the resulting droplets, and later evaporation of the water would result in large solid radioactive particles. This process would affect their dry deposition rates. Second, release of latent heat by condensation would make the plume more buoyant. The effects of plume buoyancy have been considered in past studies.[2] Third, condensation on the aerosol particles would result in a fog of droplets. If this fog encounters surfaces, such as buildings or vegetation, deposition would occur on those surfaces at a rate different than the dry deposition rate. Fourth, the fog droplets could grow and agglomerate to the point where they fall to the ground, taking a significant amount of radioactive material with them. We refer to this process as "rainout."

Rainout appears to have the greatest potential to affect predicted accident consequences. Therefore, we have been performing research to study rainout and quantify its potential effects. This paper focuses on one aspect of this research, the initial release from containment. We present a discussion of three release modes: a "puff," a "crack," and a "jet." We also use results from studies of the jet case, through deposition of drops on the ground, to discuss the possible relative importances of these release modes and why it may be important to know exactly how the containment will fail.

RELEASE MODES

For the purposes of developing models of the release, we have used containment predictions from the Quantitative Uncertainty Estimate for the Source Term (QUEST)[3] study. Specifically, the pressure, temperature, aerosol size distribution, and steam quantity have been taken from the "base case" of that study, a "TMLB'" accident at the Surry nuclear power plant. We have assumed that the containment fails at the time of reactor vessel failure, when a pressure spike occurs due to the release of steam. Containment atmosphere conditions at that time are predicted to be: pressure = 6 atmospheres, temperature = 440K, and 80% steam by mass. (It is not certain that the Surry containment would actually fail at 6 atm.)

An isentropic expansion from 6 atm to 1 atm would condense ~10% of the steam. However, an actual release from containment would not be adiabatic, quasi-static, or reversible, so either more or less steam could condense, depending on the details of the release. We have modeled these details for "puff," "crack," and "jet" releases. In this section, we discuss each in turn. In the next section, we will discuss the implications of the differences between these release modes.

Table 1 defines these release modes. The division into puff, jet, and crack is based on the nature of the compressible flow through the containment wall, which depends on the size of the hole.

Table 1. Definitions of Release Modes

Mode	Definition
Puff	Release through a hole that is large enough that the constriction does not force the flow to sonic speed.
Jet	Release through a hole such that the constriction produces sonic flow at the orifice.
Crack	Release through a crack or network of cracks such that friction keeps the flow below sonic speed.

The puff release was modeled using a two-dimensional hydrodynamic code (CSQ) incorporating water and air equations of

state.(4) This was done by initializing the calculation with ~6 atm of saturated steam in the containment volume, approximately an equal mass (~1.3 x 10^5 kg) of liquid water in the bottom (representing standing water during an accident), a region of ambient air surrounding the containment, fixed boundaries for the containment walls, and no containment roof. Thus, the release was straight up and the size of the hole was extremely large, of the order of the cross sectional area of the containment.

Figures 1a-1c show this release. The density of dots is proportional to the mass density and the solid lines show the boundaries between materials: air, water initially vapor, and water initially liquid. (Note that in this simple geometry, none of the standing water at the bottom of the containment is released.)

The pressure equilibrium time is on the order of the time it would take a sound wave to traverse the system. The sound speed is ~400 m/s and the size of the containment is ~40 m, so the equilibrium time should be extremely short, ~0.1 s. In fact, this calculation shows an equilibration time ~0.3 s, large-scale hydrodynamic motion, and, therefore, high velocities of the released steam, ~300 m/s.

The high velocity leads to two effects. First, a large fraction of the internal energy of the steam is converted into kinetic energy and ~35% of the steam condenses. Second, a great deal of turbulence will be generated. As we will discuss in the next section, insights from more extensive modeling of the jet case indicate that turbulent agglomeration of the water droplets, and, therefore, the presence of turbulence, is probably necessary to produce rainout.

It is hard to interpret the 35% condensation of steam in this calculation since only 10% should condense in an isentropic expansion. Since the specific entropy of steam is greater than the specific entropy of liquid water, and any non-isentropic process must <u>increase</u> the total entropy, a non-isentropic adiabatic expansion should lead to less condensation rather than more. The greater condensation may be a numerical effect. This calculation "cools" the steam within calculational zones by assuming temperature equilibrium between the steam and (cooler) air. Although this is a numerical effect, it is analogous to cooling by turbulent mixing.

The crack case was modeled as a compressible flow with friction assuming equilibrium thermodynamics. The computational method used is described in Reference 5. The friction factor and viscosity used were derived using methods described in References 6 and 7.

The key parameters for this model are the width of the crack, w, the path length through the containment, L, and the

roughness height h. Table 2 gives typical values, for these parameters and the resulting values of exit velocity, u, and exit temperature, T.

Table 2. Flow Through a Crack

w(m)	L(m)	h/w	u(m/s)	T(K)
0.001	2	0.5	190	429
0.001	2	0.1	284	416
0.001	20	0.5	76.3	437
0.0001	2	0.5	37.7	439
0.01	2	0.5	472 (Mach = 1)	

Note that, by our definition in Table 1, a 1 cm crack is shown to be a "jet," with sonic flow. Narrower cracks have enough friction to keep the flow subsonic. The path length, L, represents the true path through the containment wall, not the wall thickness. The exit velocity, u, may be relatively high, ~200 m/s, but this is very sensitive to the details of the structure of the crack. Once again, the prospects for rainout depend on the existence of high velocities leading to turbulent agglomeration. However, in this case there is no condensed water immediately after release. Condensation will occur only after mixing with the cooler ambient air.

We have developed a detailed model of the jet case by treating the release as a one-dimensional compressible flow, using the extensive collection of experimental data on two-phase jets to "benchmark" our analysis.

Initially, the jet expands isentropically from the orifice. This accelerates the flow to greater than Mach = 1. The steam becomes supersaturated because the timescale for the flow is less than the timescale for water vapor to diffuse to the aerosols and condense (and the latent heat to diffuse away). At some critical supersaturation, homogeneous nucleation and condensation occur in a condensation shock[8], which is unaffected by the presence of the aerosol particles[9,10].

After the condensation shock, the flow continues to accelerate and overexpand to a pressure less than 1 atm. To return to 1 atm pressure and less than sonic speeds, the flow passes through a series of barrel shocks which we have modeled as a single normal shock. Shock heating re-evaporates the condensed water so, just as in the crack case, condensation will occur only after mixing and cooling by the ambient air. Figure 2 shows the structure of the jet in terms of steam quality (mass vapor/

total mass H_2O), temperature, and velocity. The first discontinuity is the condensation shock and the second is the normal shock.

INSIGHTS FROM THE JET CASE

We have developed additional models to describe the jet release after the normal shock. As described above, the initial expansion through the containment wall does not result in any condensed water, but the flow is high speed and turbulent. (This may also be true in the crack case, depending on the structure of the cracks.) We have modeled the entrainment of ambient air into the jet, cooling and condensation of the steam onto the dry particles, the evolution of the resulting aerosol droplet distribution due to steam condensation and turbulent agglomeration, the plume behavior, and the turbulent dispersion and deposition of various size drops on the ground due to gravitational settling. Reference (11) describes these models. We will not discuss the models here, but present the results of calculations for discussion with respect to all three release modes.

We have performed sensitivity studies and have found that the amount of condensation is most sensitive to the ambient air temperature. In the absence of agglomeration the final drop size is relatively small, ~5-10 μm.

The deposition calculations indicate that it is necessary to have 200-400 μm drops to get significant rainout. Thus, turbulent agglomeration must act to get drops this large. To ensure large drops, the number of aerosols must be relatively small (2-3 orders of magnitude less than the above number from the QUEST predictions). This gives fewer condensation sites, increases the size of droplets initially formed by steam condensation, and makes agglomeration more effective. The total number of aerosols produced in a core-melt is very uncertain.(11)

Thus, we see that there are three criteria for rainout: low ambient temperature, a relatively small number (but not necessarily small total mass) of dry aerosol particles, and high-speed turbulent flow. The high-speed turbulent flow leads to entrainment, cooling, condensation, and turbulent agglomeration of the droplets initially formed by steam condensation on the dry particles. An interesting point is that the jet release results do not seem to be sensitive to the pressure inside the containment, i.e., the exact containment failure pressure.

All three release modes have the potential to produce high-speed turbulent flow. For some accidents (relatively small total number of aerosols) under some conditions (low ambient temperature) and some containment release modes (those resulting in high-speed turbulent flow), rainout could occur. The questions that must now be addressed are: what are the ranges

of the parameter values that define the region of rainout? How likely or frequently would values of parameters leading to rainout occur? And what are the impacts of the resulting rainout on deposition patterns and consequences? Our current research is attempting to answer these questions.

SUMMARY

We have modeled the initial expansion through the containment wall for three release modes: puff, crack, and jet, including the steam and dry aerosol particle contents of the containment at failure. We have further modeled the entire jet release at a level of detail adequate to estimate rainout as deposition of drops on the ground. Results for the three release modes and insights from the extensive jet model results were used to discuss the three release modes in general terms.

It seems possible that rainout could occur from any of the three release modes. High-speed turbulent flow would result in condensation and agglomeration of drops containing the radioactive material initially released as dry particles. Both the puff and jet cases result in high-speed flow which promotes aerosol agglomeration. The exact intensity and scale of the turbulence depends on the hole size, among other things. The crack case may or may not produce high-speed flow, depending on the details of the crack structure.

The exact containment failure pressure does not appear to affect the likelihood of rainout. However, the ambient air temperature controls whether condensation can occur and the number of aerosol particles determines the final drop size. The number of aerosols produced in a core-melt may vary from accident to accident and is very uncertain.

The likelihood of rainout thus may depend on the details of the release, especially on the intensity and scale of turbulence. Rainout has the potential to drastically alter the predicted consequences of core-melt accidents. If the conditions for rainout are found to coincide with likely accident conditions, it may be more important to know exactly how the containment fails than to know the exact failure pressure.

REFERENCES

1. Ritchie, L. T., Alpert, D. J., Burke, R. P., Johnson, J. D., Ostmeyer, R. M., Aldrich, D. C., and Blond, R. M., "CRAC2 Model Description," NUREG/CR-2552, SAND82-0342 (1984).

2. "PRA Procedures Guide," NUREG/CR-2300, Appendix D2 (1983).

3. Lipinski, R. J., Bradley, D. R., Brockmann, J. E., Griesmeyer, J. M., Leigh, C. D., Murata, K. K., Powers, D. A., Rivard, J. B., Taig, T. A., Tillis, J., and Williams, D. C., "Uncertainty in Radionuclide Release Under Specific LWR Accident Conditions," Draft, Sandia National Laboratories Report (1984).

4. Thompson, S. L., "CSQII-An Eulerian Finite Difference Program for Two-Dimensional Material Response-Part 1, Material Sections," SAND77-1339 (1979).

5. Shapiro, A. H., The Dynamics and Thermodynamics of Compressible Fluid Flow, Ronald Press (1953).

6. White, F. M., Viscous Fluid Flow, McGraw-Hill (1974).

7. Reid, R. C., Prausnitz, J. M., and Sherwood, T. K., The Properties of Gases and Liquids, McGraw-Hill (1977).

8. Wegener, P. O and Wu, B. J. C., "Gasdynamics and Homogeneous Nucleation," Adv. Coll. Inter. Sci., 7, 325 (1977).

9. Oswatitsch, K., "Kondensationsercheinungen in ubershalldussen," z. Agnew. Math. Mech., 22, 1 (1942).

10. Buckle, E. R. and Pouring, A. A., "Effects of Seeding on the Condensation of Atmospheric Moisture in Nozzles," Nature, 208, 367 (1965).

11. Spulak, R. G., Jr., Boughton, B. A., Cummings, J. C., Williams, D. C., Alpert, D. J., Richards, C. N., and Dunn, W. E., "Effects on Consequences of the High Steam Content in LWR Accident Releases: Physics and Preliminary Results," SAND83-2654C, to be presented at the ANS Topical Meeting on Fission Product Behavior and Source Term Research (1984).

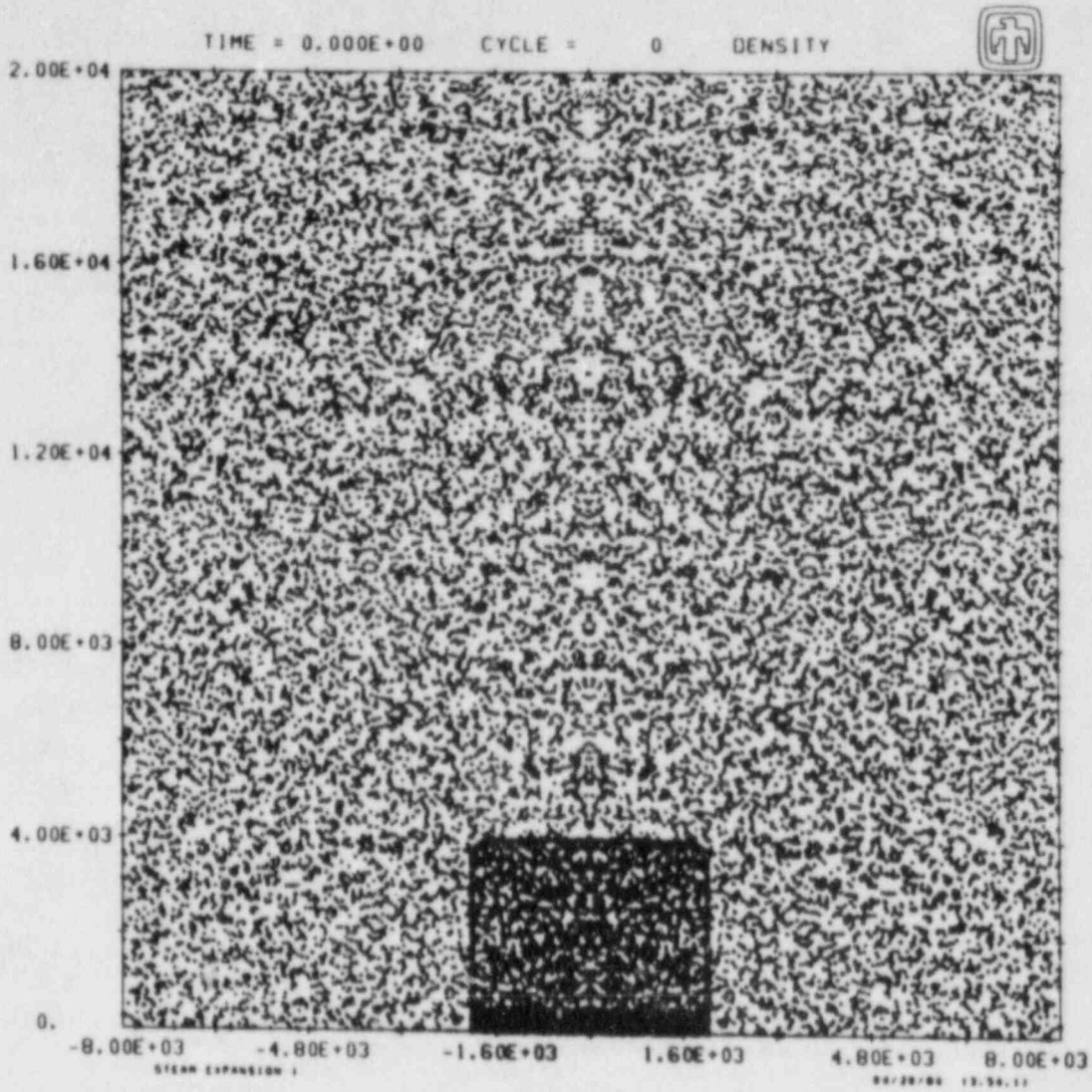

Figure 1a. Initial configuration of puff release calculation. The axes are labeled in cm. The density of dots is proportional to the mass density. The containment is at bottom center and contains ∿6 atm steam and liquid water.

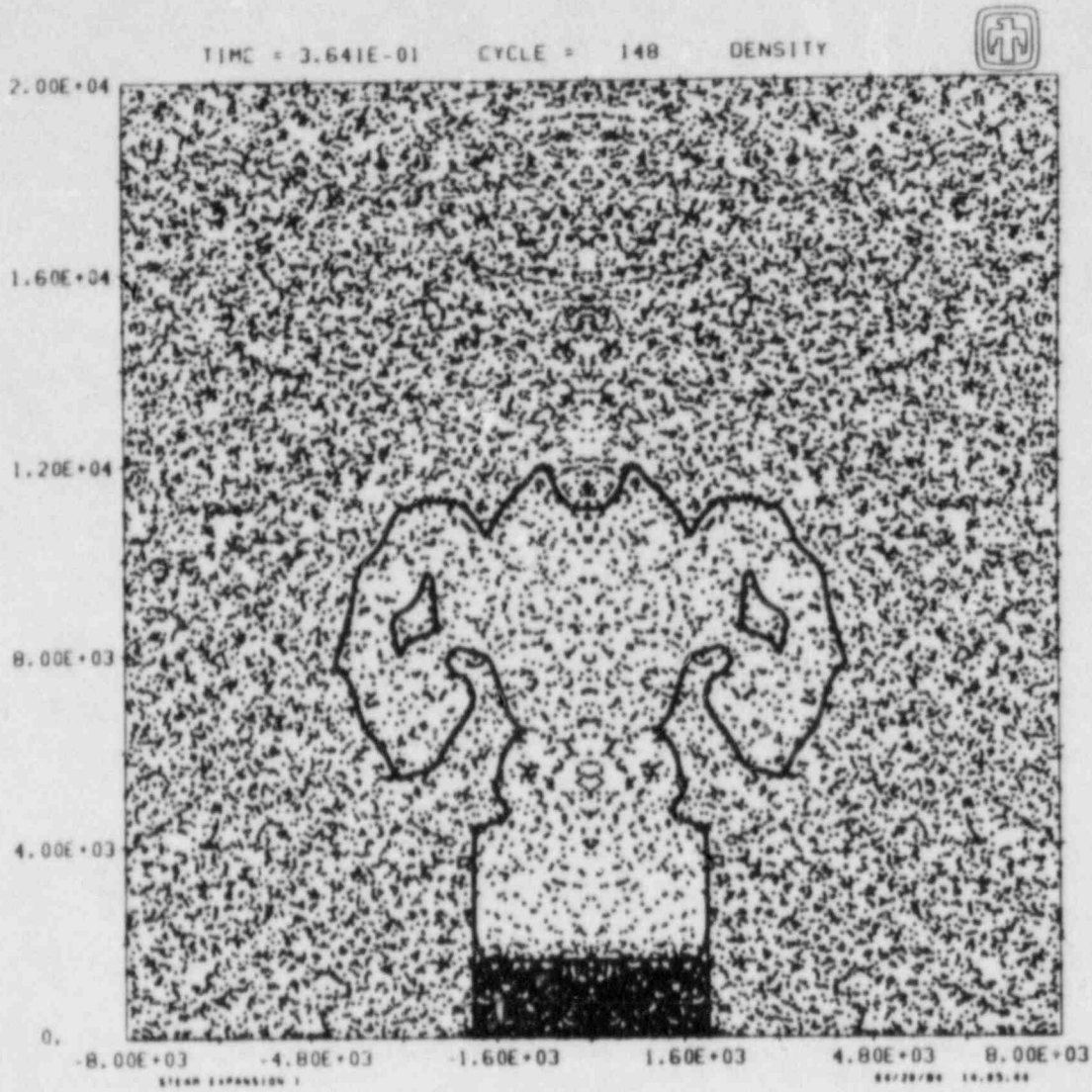

Figure 1b. Expansion of the steam out the top of the containment. Solid lines separate the three materials: air, water initially vapor, and water initially liquid.

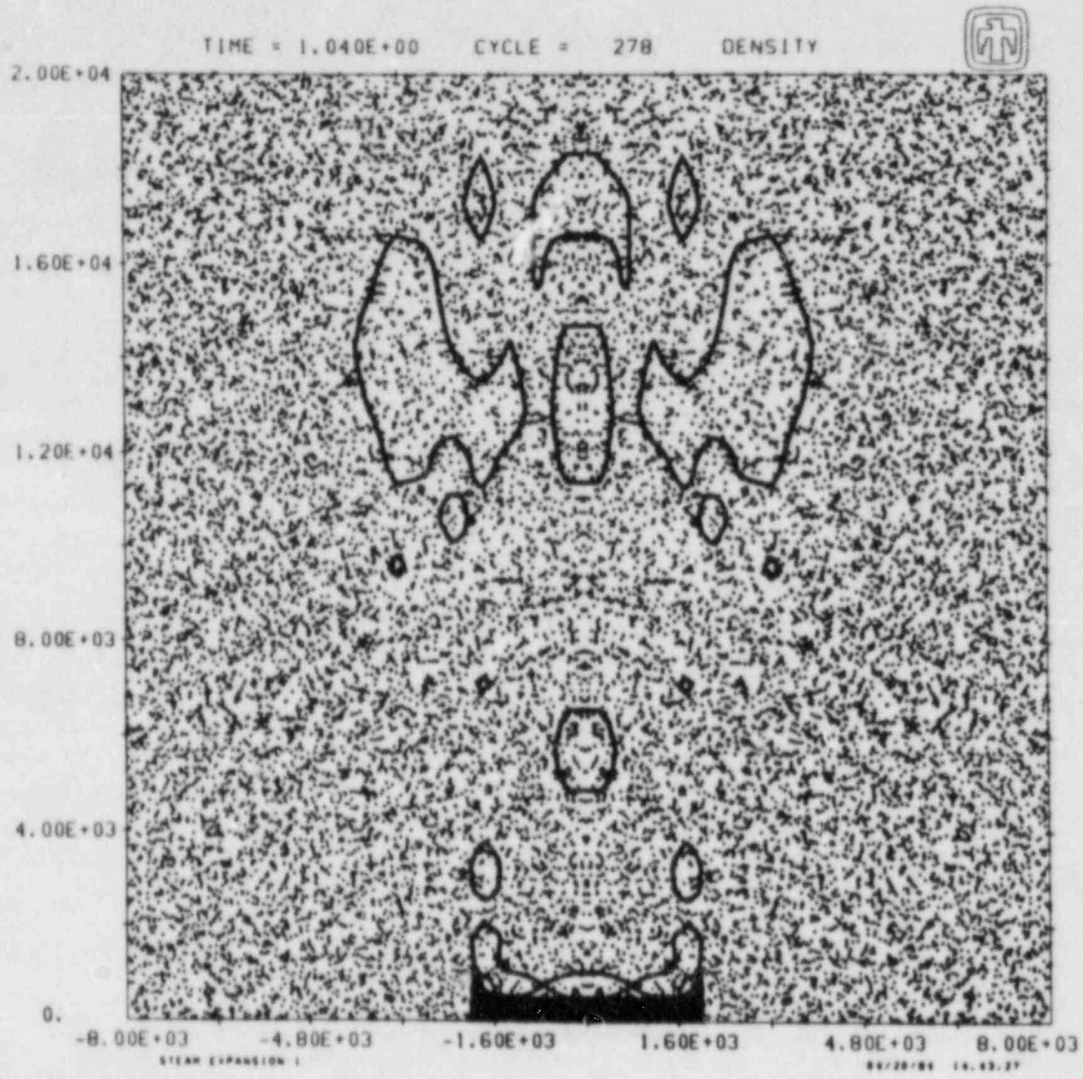

Figure 1c. Puff release after ∿1 s. Note that none of the water initially standing in the bottom was released to the atmosphere.

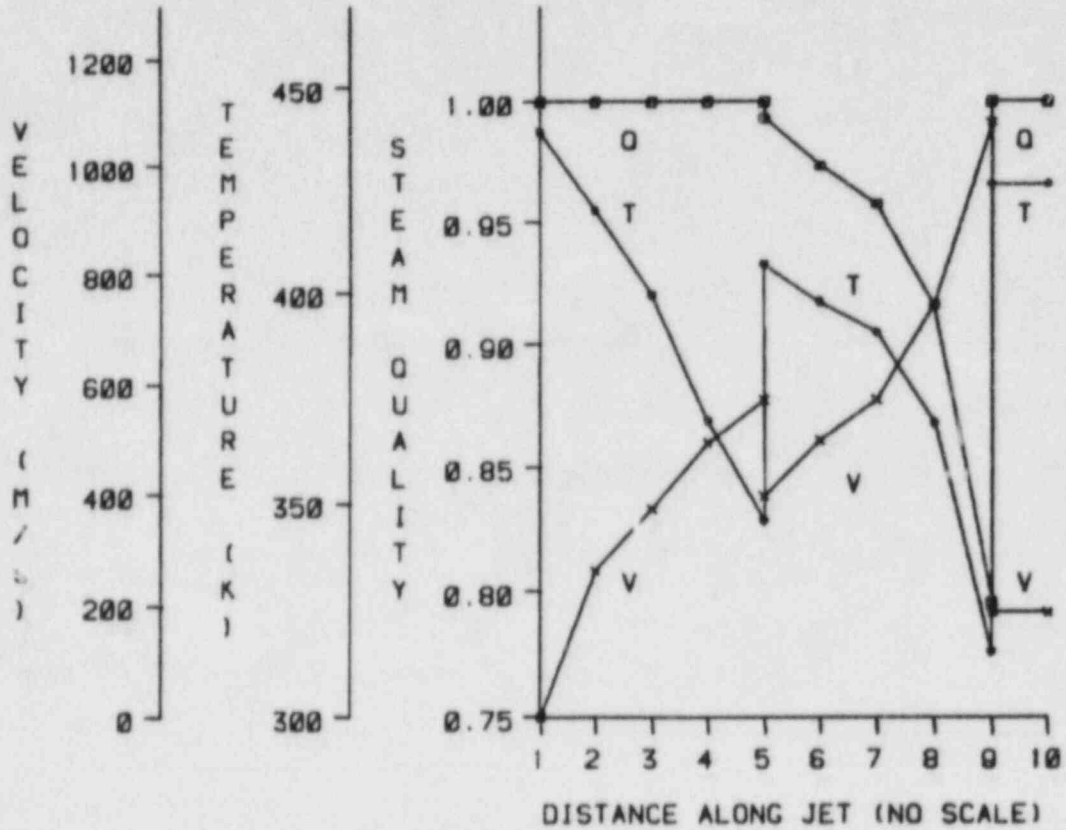

Figure 2. Structure of the jet up to the point where entrainment of ambient air begins. The first discontinuity is the condensation shock and the second discontinuity is the normal shock. Note that there is no condensed water (Q=1) after the normal shock.

EFFECTS OF HYDROGEN BURNS AND FLOODED REACTOR CAVITY ON PUBLIC RISK

J. L. Maneke*
Nuclear Engineering Department
Massachusetts Institute of Technology
Cambridge, MA 02139

D. A. Dube
Northeast Utilities Service Company
Hartford, CT 06141

ABSTRACT

A scoping analysis was performed to compare the risk impact with and without a deliberate hydrogen igniter system and a dry versus a flooded reactor cavity configuration in the Millstone Point Unit 3 containment. A hydrogen igniter system was not found advantageous. Although the igniters would reduce the risk associated with certain low probability sequences, other sequences were identified in which the igniters could conceivably increase the risk to the public. The present, dry cavity configuration was also determined favorable from a risk viewpoint, since vaporization of water in a flooded cavity could lead to earlier containment overpressurization in certain accident sequences.

Conclusions concerning these containment design features were found to be applicable to both internally and externally initiated events. These results were determined not to be sensitive to order of magnitude changes in the values of the dominant accident frequency or the major containment failure mode contribution.

INTRODUCTION

The response of the Millstone Point Unit 3 Nuclear Power Station (MP-3) during core-melt accidents was investigated as part of the Millstone 3 Probabilistic Safety Study (MP-3 PSS) [1]. Preliminary results of this study are summarized in an earlier report [2]. This paper summarizes results from additional analyses performed to discern the risk impact of a flooded cavity configuration or a deliberate hydrogen igniter system.

---

*Work performed at Northeast Utilities

Under construction in Waterford, Connecticut, MP-3 is an 1150 MWe, Westinghouse Electric pressurized water reactor with a Stone and Webster, subatmospheric type containment design. Containment safeguard systems include two diverse spray systems - quench spray and recirculation spray. The pumps in the quench spray system draw water from a 4.5 million liter (1.2 million gallon) refueling water storage tank. No fan coolers are present in the containment.

Certain design features of the MP-3 containment, which could potentially influence the risk impact from severe accidents, were identified in the MP-3 PSS such as:

- A net free volume of 65,140 m^3 ($2.3*10^6$ ft^3) which is relatively low compared to typical large dry PWR containments, and normal containment pressure of 0.7 to 0.8 atmospheres. This results in lower O_2 inventory available for hydrogen burns.

- An estimated mean containment failure pressure of 0.91 MPa (132 psia). Although this value is higher than typical failure pressures for ice condenser or Mark III containments in which hydrogen igniters are being installed, it is lower than other, dry PWR containments which have been investigated in other recently completed PRA studies.

- A basalt concrete composition which is low in calcium carbonate. Hence, the amount of carbon dioxide generated during core-concrete interaction would be lower than the amount generated with a limestone based concrete.

- As shown in Figure 1, up to $4.7*10^6$ liters ($1.24*10^6$ gallons) of water must be present in the containment sump before water spills into the cavity compartment. Thus, in the event of a core melt accident, the cavity would be dry at the time of vessel failure. The cavity design also minimizes the amount of core dispersal under the high pressure conditions which could occur following vessel failure.

- A containment configuration that is "open" with respect to the transport of hot gases, hence reducing the probability of "hydrogen pocketing."

- The existence of a temporary opening (the access plug in the primary shield wall) that could allow a flooded cavity configuration with minimal expense.

An evaluation of these design features led to the decision that the risk impact of a hydrogen igniter system and a flooded reactor cavity design should be further analyzed. Results from this research are presented in this report.

BACKGROUND

A hydrogen igniter and a flooded cavity would produce several effects during a severe core melt accident. Understanding the manner in which these effects interact is necessary to determine the overall risk impact of these features. For this study, a comparison of the containment's thermal response during selected severe accident sequences was utilized to gain insight into the implications of these features.

Dry versus Wet Cavity Phenomena

The concentration of hydrogen and other combustible gases would be higher in a containment with a dry cavity design due to increased core/concrete interaction. The risk of containment failure associated with increased basemat penetration is also higher with the dry cavity configuration. A flooded cavity design has the advantage that the molten corium would quench much faster causing the containment to rapidly become steam inerted after the debris contacts the cavity water. However, the rapid generation of steam also results in high pressures that could threaten containment integrity.

Hydrogen Ignition Phenomena

If hydrogen were to accumulate during a severe core melt accident, it could ignite suddenly and produce a large pressure spike that would threaten containment integrity. A deliberate hydrogen igniter system could reduce the containment hydrogen concentration by burning the gas in a controlled manner over a longer period of time during the accident.

To evaluate the benefit of an igniter system, it is important to determine if the containment atmospheric conditions are such that hydrogen ignition could occur. Specifically, for hydrogen to ignite in a containment atmosphere several criteria must be satisfied. First, the mole fraction of hydrogen in the atmosphere must be greater than about 8 percent for complete combustion to occur. In addition, a molar concentration of oxygen greater than 5 percent is needed. Finally, the molar concentration of steam must be less than 55 percent, since significant hydrogen burning will not occur in a steam inert atmosphere [3] .

Sequence Identification

From the wide spectrum of core-melt accident scenarios examined in the MP-3 PSS, dominant accident scenarios were identified based on their frequency and contribution to containment failure and public risk. In this report, the

following nomenclature is used to identify the accident sequences with three letters as described below:

The first letter refers to the accident sequence type

A - large break LOCA
S - small break LOCA (<5 cm in diameter)
S' - break in the incore instrument line beneath the reactor vessel
T - transient with no break or rupture in the reactor coolant system.

The second letter refers to the timing of core uncovery and melt due to Emergency Core Cooling (ECC) performance

E - loss of ECC injection, leading to early core melt
L - loss of ECC recirculation, leading to late core melt.

The third letter refers to the containment spray systems available

C - both quench and recirculation sprays available
C' - only quench sprays available
C" - only recirculation sprays available
(none) - no sprays available.

For example the SLC' sequence would designate a small break LOCA with ECC injection, but no ECC recirculation or containment recirculation sprays available.

Accident Sequence Selection

Dominant core melt accident sequences, as well as sequences which contribute the most to public risk (early fatalities and latent cancers) for internally initiated events were identified in the MP-3 PSS. Results from the MP-3 PSS indicate that the interfacing systems LOCA (or V-sequence) accounted for over 99 percent of early fatality risk from internally initiated events. Most of the risk of latent cancer fatalities was found to come from two classes of accidents: the V-sequence which accounts for approximately 28 percent of the total and the TE plant damage state that accounts for 60 percent.

Since the V-sequence is unaffected by reactor cavity state, only the TE sequence was used to estimate the difference between the risk associated with a dry and a flooded reactor cavity. The TEC and SLC sequences were also considered in this analysis, since combined, they accounted for approximately 62 percent of the core melt frequency. For the hydrogen igniter studies, the TE, TEC, AE, and AL sequences were investigated. The TE sequence was chosen because it is the dominant contributor to latent fatalities from internal events. The TEC sequence is the most likely of all plant damage states and gives a containment response similar in nature to the SLC sequence. Finally, the AE and

AL sequences were studied because they were identified as being the most challenging to containment integrity, given the accident.

Although no calculations were performed for the SLC', TEC', and SE sequences or any externally initiated events, the effect of cavity design and a deliberate hydrogen igniter system during these transients is also discussed.

Methodology

The containment thermal analysis was performed using the MARCH[4]/MODMESH[5]/CORCON-MOD1[6]/COCOCLASS9[7] series of computer codes. The computational order and some of the phenomena modeled by these codes are shown in Figure 2. Data input for each sequence was developed using data from prior best estimate analysis for the MP-3 PSS. The possible benefit of having a flooded containment cavity was analyzed by comparing the containment's response with water present at the time of vessel failure with dry cavity results for the sequences discussed above. Hydrogen burn sensitivity studies were performed by varying the number, timing, and/or duration of burns in the sequences selected.

There are several limitations to the thermal response calculations performed in this study. The containment's volume is treated as a single node. This limitation would particularly affect the hydrogen ignition studies since neither the igniter location nor hydrogen flow past the igniters is considered.

CONTAINMENT THERMAL RESPONSE

Results from this analysis are summarized in Table 1. In addition, Figures 3 through 6 illustrate the difference in certain parameters for wet and dry reactor cavities. A discussion of the results for each of the sequences studied is presented below.

TABLE 1

RELATIVE RISK IMPACT OF
FLOODED CAVITY AND HYDROGEN IGNITERS
(INTERNAL EVENTS)

ACCIDENT SEQUENCES	FLOODED CAVITY		HYDROGEN IGNITER SYSTEM	
	EFFECT	RELATIVE RISK IMPACT *	EFFECT	RELATIVE RISK IMPACT
AE	EARLIER OVERPRESSURE	INSIGNIFICANT INCREASE	MITIGATE H_2 BURN	INSIGNIFICANT DECREASE
SE	EARLIER OVERPRESSURE	MODERATE INCREASE	MITIGATE H_2 BURN	INSIGNIFICANT DECREASE
AL	EARLIER OVERPRESSURE	INSIGNIFICANT INCREASE	MITIGATE H_2 BURN	INSIGNIFICANT DECREASE
SL	NONE	NONE	MITIGATE H_2 BURN	INSIGNIFICANT DECREASE
TE	EARLIER OVERPRESSURE	MODERATE INCREASE	MITIGATE BURNS DURING RECOVERY	INSIGNIFICANT DECREASE
SLC'	NONE	NONE	NONE	NONE
TEC'	NONE	NONE	NONE	NONE
AEC'/ALC'/SEC'	EARLIER OVERPRESSURE	INSIGNIFICANT INCREASE	NONE	NONE
ALL C* CASES	PREVENT BASEMAT PENETRATION	INSIGNIFICANT DECREASE	NONE	NONE
ALL C CASES	PREVENT BASEMAT PENETRATION	INSIGNIFICANT DECREASE	NONE	NONE
S'L	NONE	NONE	MITIGATE H_2 BURNS	INSIGNIFICANT DECREASE
V	NONE	NONE	NONE	NONE

* INSIGNIFICANT : <1% OF INTERNAL RISK (EARLY FATALITY OR LATENT FATALITY)
MODERATE : 1 - 25%
LARGE : >25%

TE Sequence

A dry cavity configuration was found advantageous for the MP-3 plant. As shown in Figure 3, steam overpressurization with a wet cavity could result in containment failure after 17 hours. Since the molar concentration of steam is estimated to reach the 55% needed for steam inertion within six hours (see Figure 4), the threat of hydrogen burn is negligible. Hence, there is no real need for hydrogen igniters.

In fact, a deliberate hydrogen igniter system could increase the risk to the public in certain situations. In more than half of the TE sequences all AC power would be lost to the igniters and sprays. If AC power were recovered after 1/2 hour, the sprays would condense the steam in the containment, yielding a flammable atmosphere in which a deliberate ignition of hydrogen could produce a pressure spike severe enough to threaten containment integrity.

TEC and SLC Sequences

As shown in Figures 5 and 6, the containment's pressure behavior for the TEC and SLC sequences showed little difference in the flooded cavity and dry cavity configuration due to the containment sprays maintaining the pressure at a relatively low level and the basaltic concrete's relatively low generation rate of non-condensible gases. Although more hydrogen was formed in the dry cavity case, the worst case burn analyzed produced a pressure peak of 0.38 MPa (55 psid) lower than the mean containment failure pressure. The increased probability of containment failure due to basemat penetration in the dry cavity case was also determined negligible compared to the increased contribution to risk with a flooded cavity.

Although a hydrogen igniter system was found to decrease the amount of hydrogen buildup in the containment, the risk reduction is small since pressures produced by worst case burns without hydrogen igniters were not found sufficient to threaten containment integrity.

AE and AL Sequences

In both the AE and AL sequences, a hydrogen igniter system was found beneficial in preventing hydrogen buildup and hence reducing the threat of early/intermediate failure by the pressure increase due to a hydrogen burn. However, the very low probability of either of these accident scenarios would result in the igniters having a negligible impact on risk.

TEC', SLC', and SE Sequences

Although these cases were not specifically analyzed in this study, the results were extended to estimate the effect of a hydrogen igniter system and a flooded cavity design on

the risk. First, the presence of the quench sprays in the SLC' and TEC' sequences would help maintain the containment pressure relatively low and make the containment atmosphere steam inerted until late into the sequence when substantial amounts of hydrogen would be generated. The flooded cavity design would cause:

- o A slightly earlier steam overpressurization due to vaporization occurring after vessel failure.
- o A reduction in hydrogen production due to less core/concrete interaction.
- o No substantial change in risk since the containment failure would occur late in these sequences whether the cavity is flooded or dry.

For the SE case, it is expected that there would be a rapid containment pressurization due to vaporization of the cavity water. There should also be a substantial reduction in the amount of hydrogen produced from core/concrete interaction and a significant reduction in the liklihood of hydrogen burn because of reduced hydrogen, more rapid steam generation, and earlier steam inerting. However, the overall effect of an earlier steam overpressurization should increase the risk from the SE sequence.

Externally Initiated Events

For seismic events, the dominant contributors to risk are the V-3 (crane wall collapse, large LOCA, containment isolation failure), AE, SE, and TE plant damage states. The V-3 sequence, which is in many ways equivalent to the V-sequence for internal events, contributes aproximately 75% of the early fatality risk. The course of events for this accident would be unaffected by a flooded cavity design or hydrogen igniters. Since the AE, SE, and TE plant damage states would likely occur coincidentally with loss of AC power, the existence of a deliberate hydrogen igniter system would provide little benefit. On the other hand, a flooded reactor cavity design may result in somewhat earlier containment overpressure and increase risk.

Summary

Table 1 summarizes the relative risk impact that a flooded cavity or a deliberate hydrogen igniter system would produce.. Of the internally initiated sequences considered, only the TE and SE sequences were significantly affected by a flooded cavity configuration. During both of these sequences, the containment would be expected to fail earlier due to overpressurization from steam production in the cavity.

Although a deliberate hydrogen igniter system was found beneficial for the large break LOCA sequences considered, the

decrease in public risk would be negligible due to the low probability of such accidents. In addition, certain situations could arise in which an igniter system could cause an increase in the risk, such as in the TE sequence discussed earlier.

Hence, neither the flooded cavity configuration nor the existence of a deliberate hydrogen igniter system were found advantageous for the MP-3 containment. These conclusions are considered applicable to both internally and externally initiated events such as fire or seismic related sequences.

QUANTIFICATION OF RISK IMPACT

A thorough assessment of the risk impact of a flooded cavity design or a deliberate hydrogen igniter system with a complete requantification of the containment event trees and risk curves was not deemed necessary for this study. Instead, Table 1 suggests that only the TE and SE sequences need to be re-evaluated in quantifying the risk impact of the flooded cavity and that the existence of hydrogen igniters would not significantly affect the risk to the public for any of the sequences considered. The new release categories were first calculated for the TE and SE sequences based on the predicted earlier over-pressure of the containment. With mean consequence data from the CRAC2 code[8], a percent change in risk between dry and flooded cavity cases could then be determined. For the hydrogen igniters, an upper bound on the risk impact with this design change was calculated assuming that the igniter system eliminated all early/intermediate containment failures due to hydrogen burns.

Flooded Cavity Results

Based on criteria developed in Sections 4 and 5 of the MP-3 PSS, the worst possible change in the release categories would be for the TE sequence to go from an M-7 release category (late containment overpressurization, no sprays) to an M-5 (intermediate failure, late core melt, no sprays). The SE sequence would at most shift from an M-7 to an M-6 (intermediate failure, early core melt, no sprays).

Table 2 shows the values used to arrive at the maximum percent change in risk for the flooded cavity design. At most, a flooded cavity is calculated to produce a 17 percent increase in latent fatalities and a negligible increase in early fatalities for the TE sequence.

These calculations are based on point estimate risk calculations and do not account for the reduction in source term. Since the discrete probability distributions (DPD) are different for the M-5 and M-7 release categories, the relative impact of the flooded cavity on the 50 and 90 percentile risk curves are considerably different. The calculated "effective" source term using the DPD's for the M-5, M-6 and M-7 categories are factors of 0.09, 0.26,

and 0.02 times the unreduced source term. Hence, a shift from M-7 to M-5 would increase the impact on public risk for the median and 90 percent curves. No change is expected for the impact on early fatalities.

TABLE 2

QUANTIFICATION OF MAXIMUM RISK IMPACT OF FLOODED CAVITY (INTERNAL EVENTS/POINT ESTIMATE)

RELEASE * CATEGORY	MEAN EARLY FATALITIES	MEAN LATENT FATALITIES	RELEASE FREQUENCY (YR^{-1}) DRY CAVITY	RELEASE FREQUENCY (YR^{-1}) FLOODED CAVITY	MEAN E.F. PER YEAR DRY	MEAN E.F. PER YEAR FLOODED	MEAN L.F. PER YEAR DRY	MEAN L.F. PER YEAR FLOODED
M-1A	27.0	2790	1.9E-6	1.9E-6	5.1E-5	5.1E-5	5.3E-3	5.3E-3
M-5	0.05	3050	2.4E-8	4.8E-6	1.2E-9	2.4E-7	7.3E-5	1.46E-2
M-6	0.28	3150	9.0E-9	1.2E-7	2.5E-9	3.4E-8	2.8E-5	3.8E-4
M-7	0.0	2380	5.7E-6	0.8E-6	0	0	1.36E-2	1.9E-3
TOTAL			7.6E-6	7.6E-6	5.1E-5	5.1E-5	1.90E-2	2.22E-2

MAX. % CHANGE IN EARLY FATALITY FOR FLOODED: < 1% INCREASE
MAX. % CHANGE IN LATENT FATALITY FOR FLOODED: 17% INCREASE

* ALL OTHER RELEASE CATEGORIES EITHER HAVE VERY LOW PROBABILITY OR VERY LOW CONSEQUENCES

Hydrogen Igniters

Table 3 illustrates how the upper bound on risk reduction was calculated for internally initiated events. No significant risk reduction was calculated to occur for either early or late fatalities. These calculations are also based on point estimate risks, although including the DPD's in the source terms for the system would not reduce the 50 and 90 percent curve fatalities by more than a few percent.

TABLE 3

QUANTIFICATION OF MAXIMUM RISK IMPACT OF HYDROGEN IGNITER SYSTEM (INTERNAL EVENTS/POINT ESTIMATE)

RELEASE CATEGORY	MEAN EARLY FATALITIES	MEAN LATENT FATALITIES	RELEASE FREQUENCY (YR^{-1}) NO IGNITERS	RELEASE FREQUENCY (YR^{-1}) IGNITERS	MEAN E.F. PER YEAR NO IGNITERS	MEAN E.F. PER YEAR IGNITERS	MEAN L.F. PER YEAR NO IGNITERS	MEAN L.F. PER YEAR IGNITERS
M-1A	27.0	2790	1.9E-6	1.9E-6	5.1E-5	5.1E-5	5.3E-3	5.3E-3
M-5	0.05	3050	2.4E-8	0.0	1.2E-9	0	7.3E-5	0
M-6	0.28	3150	9.0E-9	0.0	2.5E-9	0	2.8E-5	0
M-7	0.0	2380	5.7E-6	5.73E-6	0	0	1.36E-2	1.36E-2
TOTAL			7.63E-6	7.63E-6	5.1E-5	5.1E-5	1.90E-2	1.89E-2

MAX. % CHANGE IN EARLY FATALITY FOR IGNITER SYSTEM: <1% DECREASE
MAX. % CHANGE IN LATENT FATALITY FOR IGNITER SYSTEM: <1% DECREASE

Sensitivity of Results to PSS Findings

Calculations in this analysis utilized certain findings from the PSS such as the frequency of the V-sequence and the contribution of hydrogen burn as a containment failure mode. The sensitivity of results from this analysis to these assumptions was tested by assuming:

1. The V-sequence's frequency was reduced by 1/10.

2. The contribution of hydrogen burn as a containment failure mode was increased by a factor of 10.

The new calculations showed that the results were not very sensitive to either of these assumptions.

CONCLUSIONS

In summary, the present, dry cavity Millstone Unit 3 containment with no deliberate hydrogen igniter system was found advantageous from a risk standpoint. The threat of steam overpressurization with a flooded cavity was found to outweigh any reduction in risk due to the decrease in hydrogen generation or basemat penetration with a dry cavity design. Although the existence of a deliberate hydrogen igniter system reduced the concentration of hydrogen in certain sequences, the reduction in risk was found negligible due to the low probability of these accidents. In addition, sequences were identified in which the igniters could increase the risk to the public by forcing a burn in the containment after the atmosphere returned flammable. These conclusions were determined to be valid for not only internally initiated events, but also externally initiated events associated with fire and seismic accidents. The results were not significantly affected by order of magnitude changes in MP-3 PSS results such as the frequency of the dominant risk contributor (the V-sequence) and the contribution of hydrogen burn as a containment failure mode.

REFERENCES

1. Millstone Unit 3 Probabilistic Safety Study, Northeast Utilities, August 1983.

2. D.A. Dube and R.J. Lutz, Jr., "Containment Response during Severe Accidents at Millstone Unit-3," Presented at the International Meeting on LWR Severe Accident Evaluation, Cambridge, MA, August, 1983.

3. J.C. Cummings, et al, "Review of the Grand Gulf Hydrogen Igniter System," NUREG/CR-2530, SAND82-0218, March 1983.

4. R.O. Wooten and H.I. Avci, "MARCH (Meltdown Accident Response CHaracteristics) Code Description and User's Manual," NUREG/CR-1711, BMI-2064, Batelle's Columbus Laboratory, October, 1981.

5. "MESH Code," NS-CCCCA-82-423, Westinghouse Electric Nuclear Technology Division, October, 1982.

6. J.F. Muir, et al., "CORCON-MOD1: An Improved Model for Molten-Core/Concrete Interactions," NUREG/CR-2142, SAND80-2415, Sandia National Laboratories, July, 1981.

7. "COCO: COntainment Pressure Analysis COde," WCAP-8327, Westinghouse Electric Company, Nuclear Technology Division.

8. L.T. Ritchie et al., "Calculations of Reactor Accident Consequences Version 2 CRAC2: Model Description," NUREG/CR-2552, SAND82-0342, Sandia National Laboratories, March 1984.

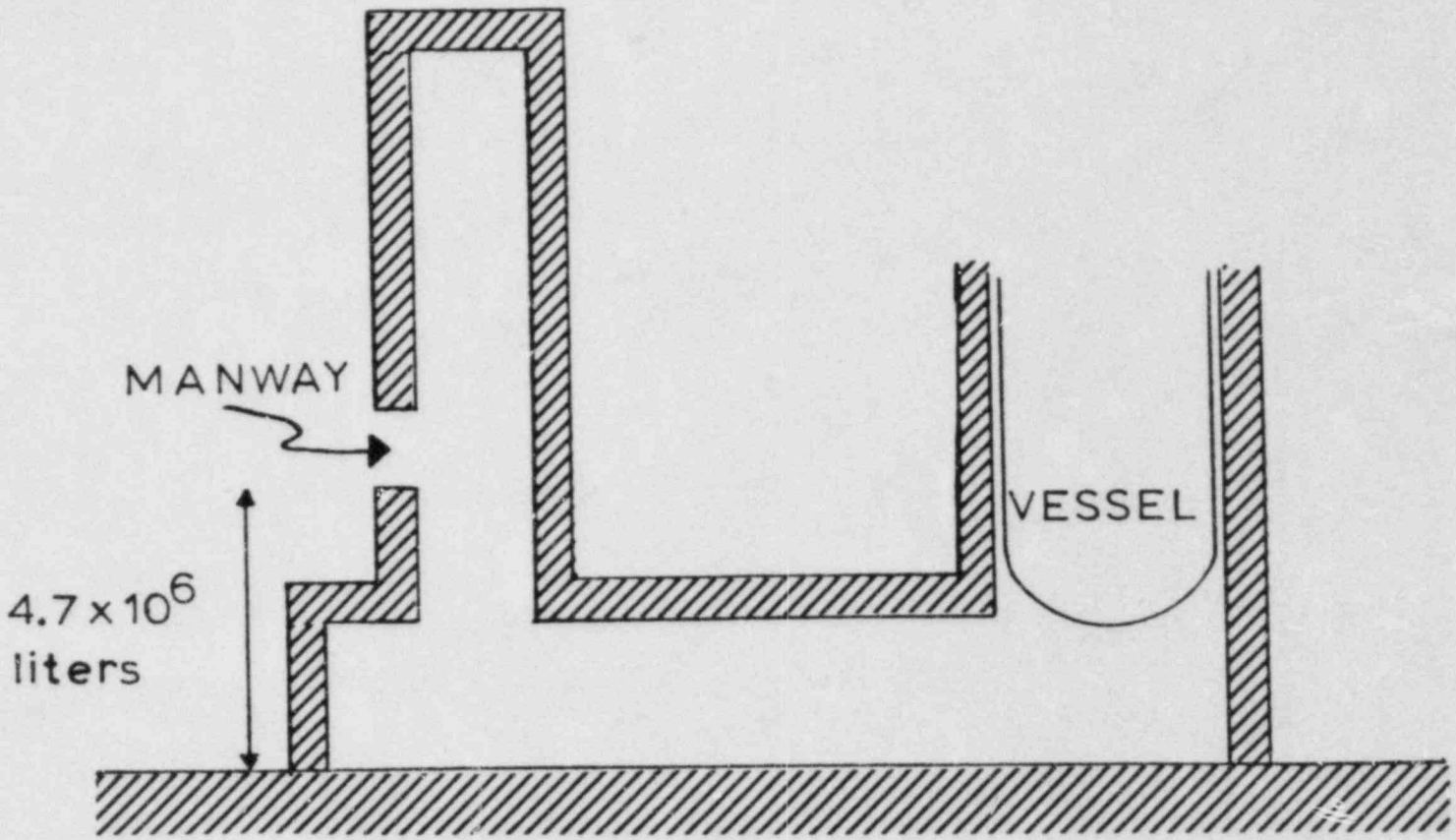

Figure 1. Millstone-3 Reactor Cavity Design

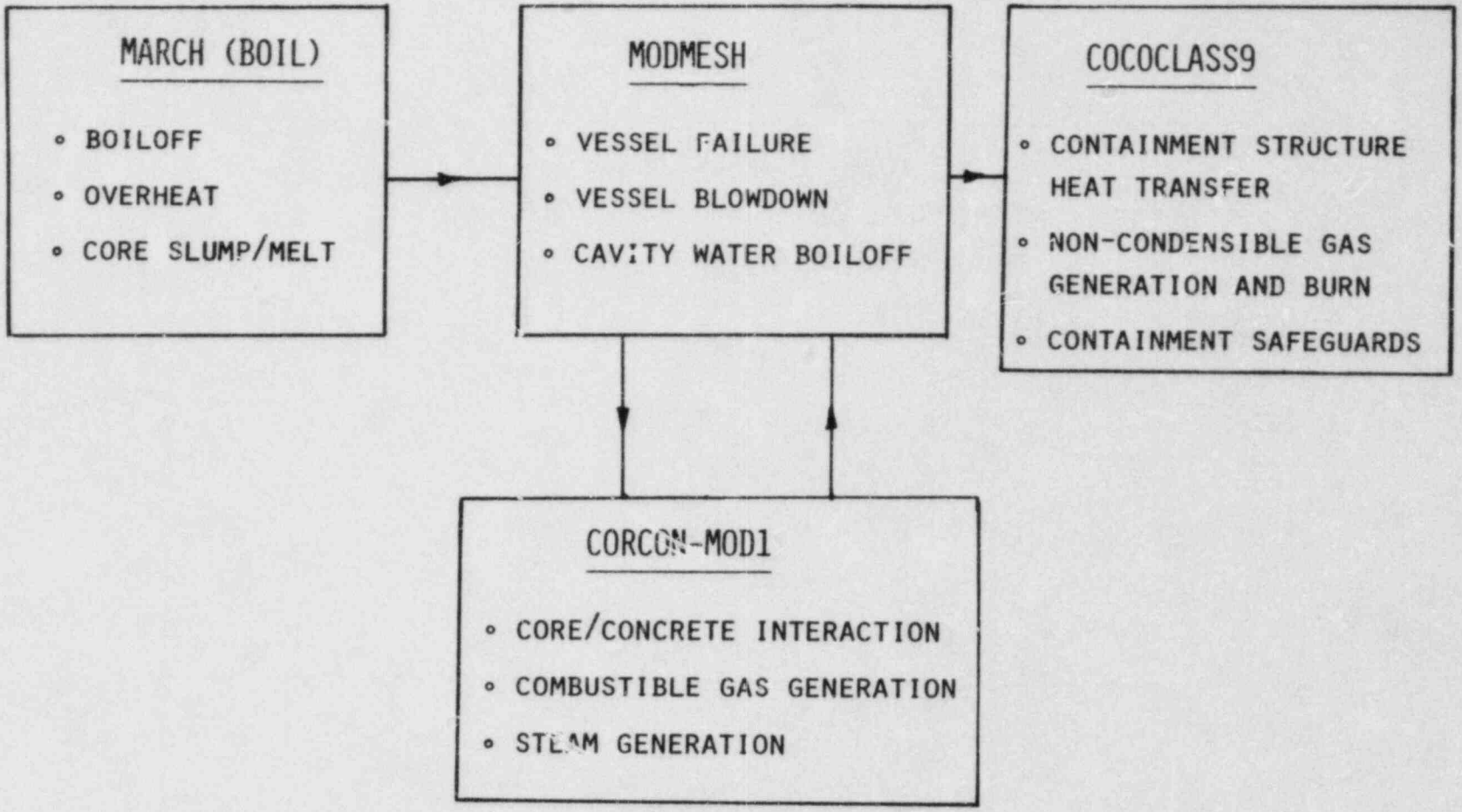

Figure 2. Severe Accident Analysis Code Flow Diagram

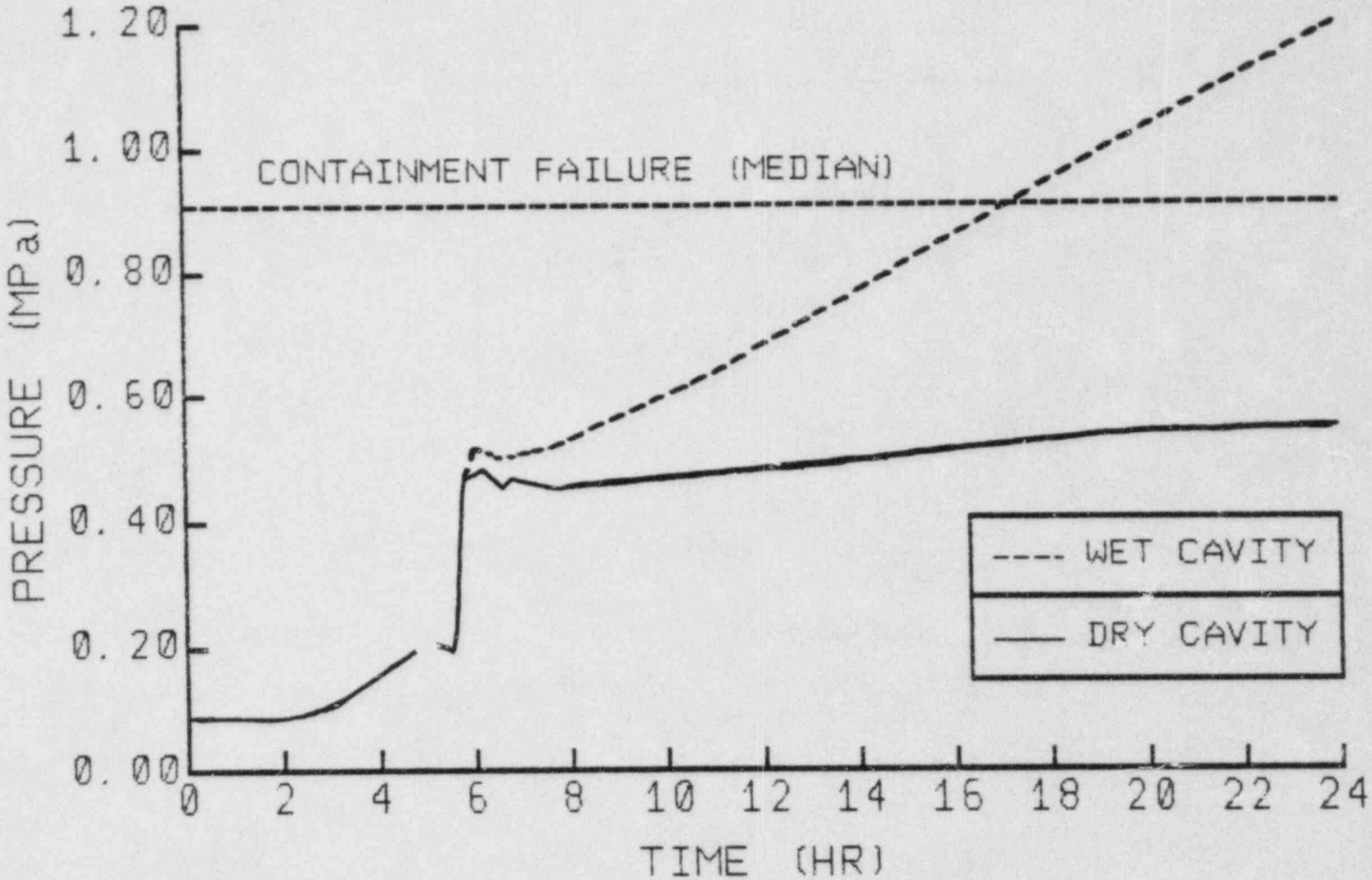

Figure 3. Containment Pressure During a TE Sequence

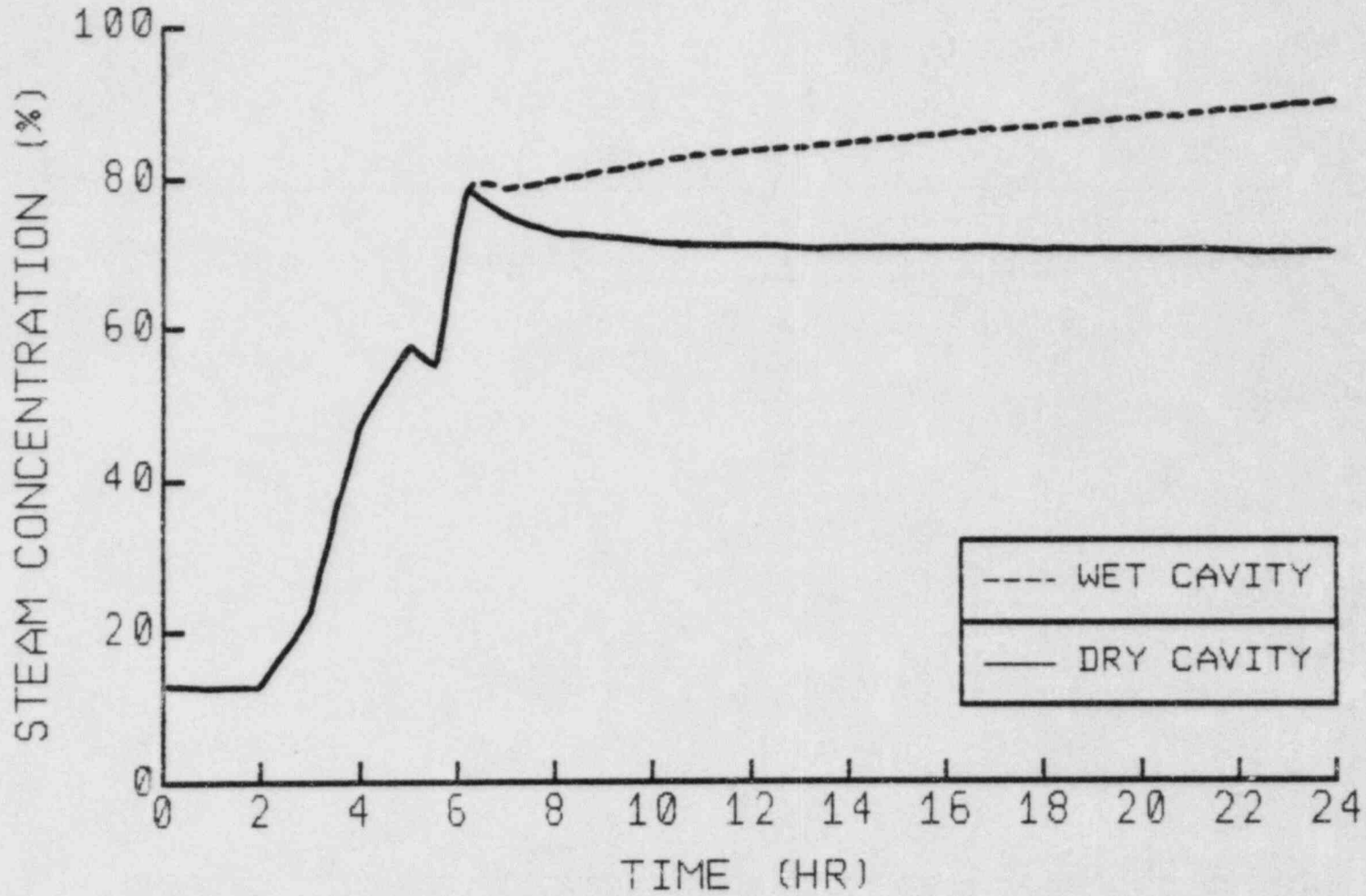

Figure 4. Steam Concentration During a TE Sequence

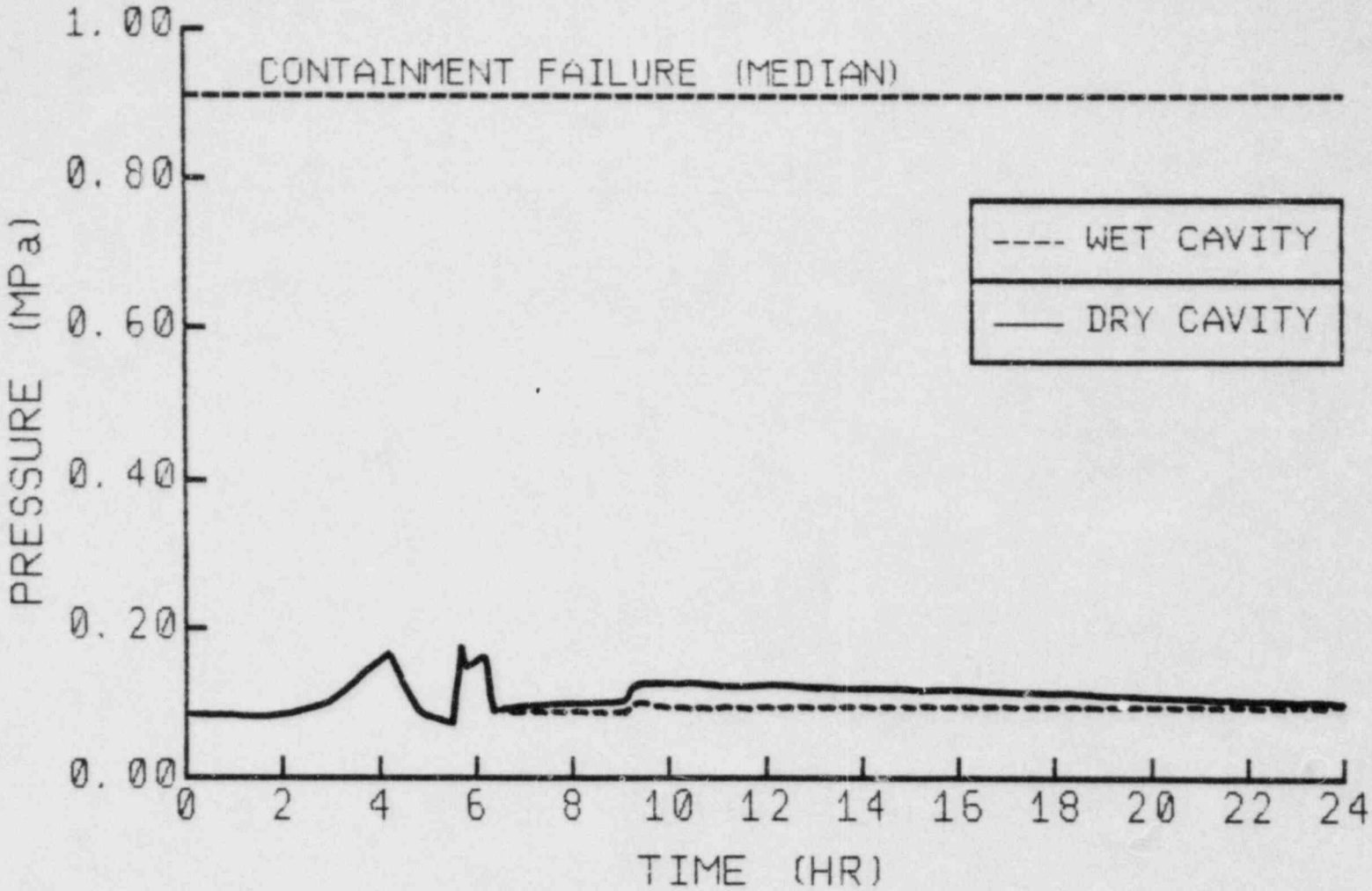

Figure 5. Containment Pressure During a TEC Sequence

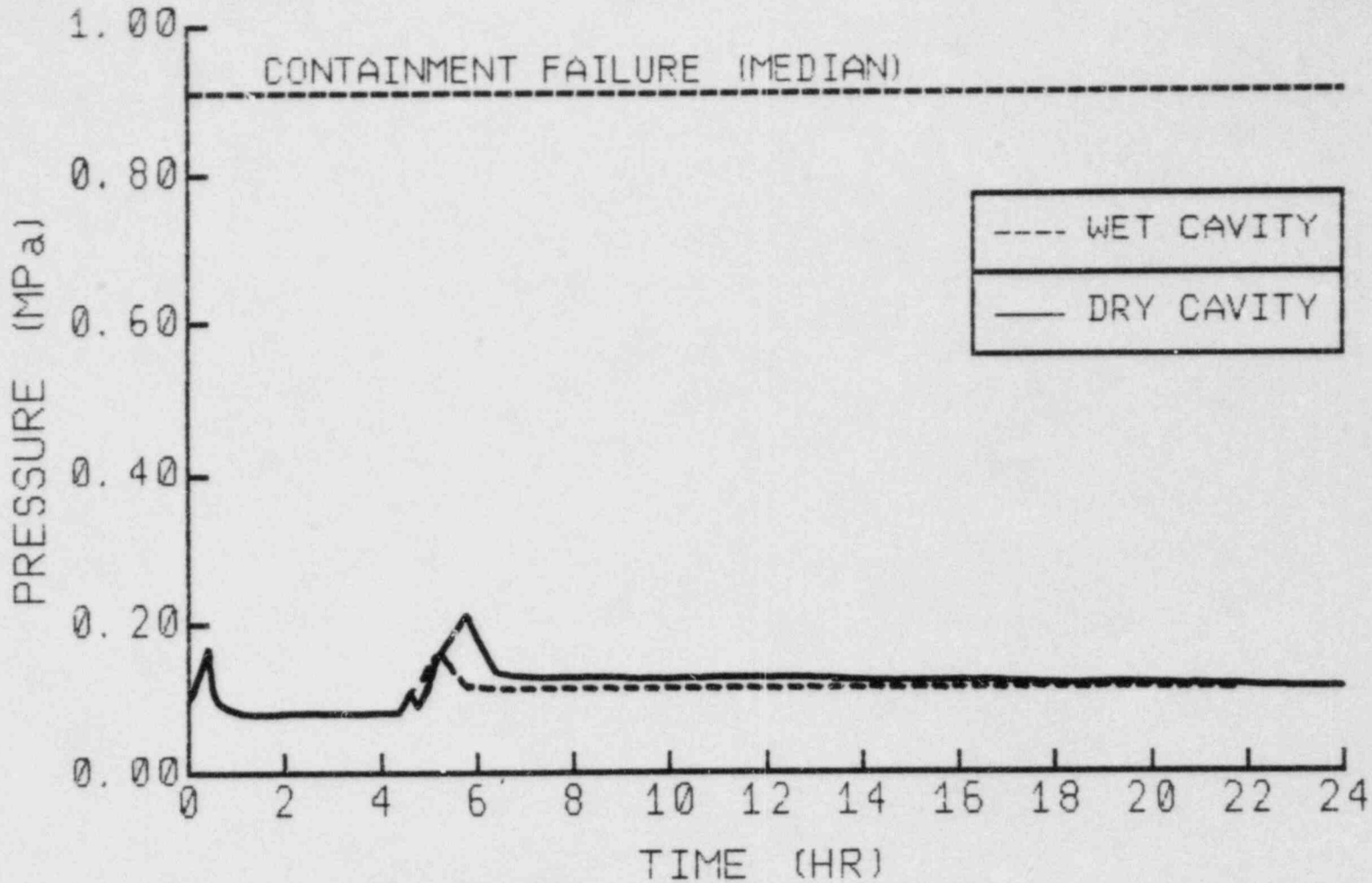

Figure 6. Containment Pressure During a SLC Sequence

ON THE UNCERTAINTIES ASSOCIATED WITH CONTAINMENT ANALYSIS

Lowell Greimann and Fouad Fanous
Ames Laboratory, Iowa State University
Ames, IA

ABSTRACT

The containment structure is designed to prevent leakage for a variety of environment and accident loading conditions. However, loadings more severe than the design loading can be postulated. Approaches to predicting the containment resistance to internal pressure are summarized herein. Uncertainties associated with these approaches are also discussed. Results for individual containments are tabulated.

Containment failure criteria are not well established. Although most investigators agree that the containment has failed when leakage occurs, several criteria have been employed to express containment failure. Among these are: the formation of a limit mechanism, strain or deformation limits and buckling. For concrete containments, additional criteria such as radial shear stresses, liner plate strain and reinforcement steel strain are often used as an indication of failure.

Almost all containment analyses, to date, have been based upon an axisymmetric structural model of the containment shell. For this model, many nonsymmetric features must be neglected or accounted for in an approximate way. The degree of sophistication of the analysis techniques range from hand calculations to finite element methods.

Another source of uncertainty in the prediction of containment strength is the material model. Uncertainties often exist in the data. The analytical description of reinforced concrete is one of the larger uncertainties in the analysis of concrete vessels. Aspects of the steel/concrete interface, i.e., bond, anchorage, are difficult to describe analytically. The cracking, bar yielding and aggregate interlocking problem remain yet unsolved. Soil and pressure modeling are another source of uncertainty.

INTRODUCTION

The purpose of the containment in a nuclear power plant is to prevent the release of radioactivity which may be present as the result of a severe accident. The containment has failed to perform its intended function when leakage of the radioactive material occurs. During the Three Mile Island accident an increase in internal pressure was recorded within the containment. Although this increase was well within design limits for that plant, efforts have since been initiated to investigate the response of several containment configurations to similar pressure increases. Additionally, other severe accidents have been postulated with various consequences which include containment failure as an important consideration. This paper reviews the state-of-the-art for the

analysis of LWR nuclear containments with uniform internal pressure. This includes a review of calculated static failure pressures of various containments, different failure criteria used for predicting containment failure, and comments on possible uncertainties associated with the analysis techniques. This work is in support of an ongoing program at Sandia National Laboratories entitled the Severe Accident Risk Reduction program (SARRP) (1).

Containments subjected to static, internal pressure can fail (leak) in one of a number of different modes and locations. Even though the structural criteria for failure in each of these modes is not necessarily well-established, it is appropriate to identify some of these modes as in Fig. 1.

SUMMARY OF CONTAINMENT ANALYSIS RESULTS

Table 1 represents a summary of the results of various containment analyses by several investigators. The containment name. investigator, and predicted internal static pressure at failure are listed. The failure criteria, and the failure location are briefly identified.

A not-too-close examination of Table 1 may be disturbing to a person being first exposed to containment structural analysis. There is a noticeably wide range in the predicted ultimate strengths for containments within a given type. For example, the predicted failure pressures for PWR ice condensor containments differ by a factor of almost 2.5. However, this difference is easily explained by the difference in the actual containment configuration, i.e., the cylindrical shell of one containment is 3 times as thick. Material properties and stiffener geometries also differ from containment to containment.

More interesting, however, is the difference in the predicted pressure resistance of the same containment by two investigators. Again, closer examination of the two investigations explains the discrepancies. Almost always, the primary difference is in the definition of the failure criteria. All agree that leakage represents failure but few agree what structural definition of leakage is appropriate. Smaller differences can be attributed to differences in material properties (estimated versus actual) and analysis technique (finite element versus hand calculations). Each of these differences is more fully discussed in the following section.

DISCUSSION OF ANALYSIS METHODS

A summary of the analysis methods for containments and the associated uncertainties is presented in this section. The information presented here is, in many cases the result of the authors' opinion which is based upon their mutual experience and a review of the literature in this field.

Geometric Containment Model

Almost all containment analyses, to date, have been based upon an axisymmetric structural model of the containment shell. For this model many nonsymmetric features must be neglected or

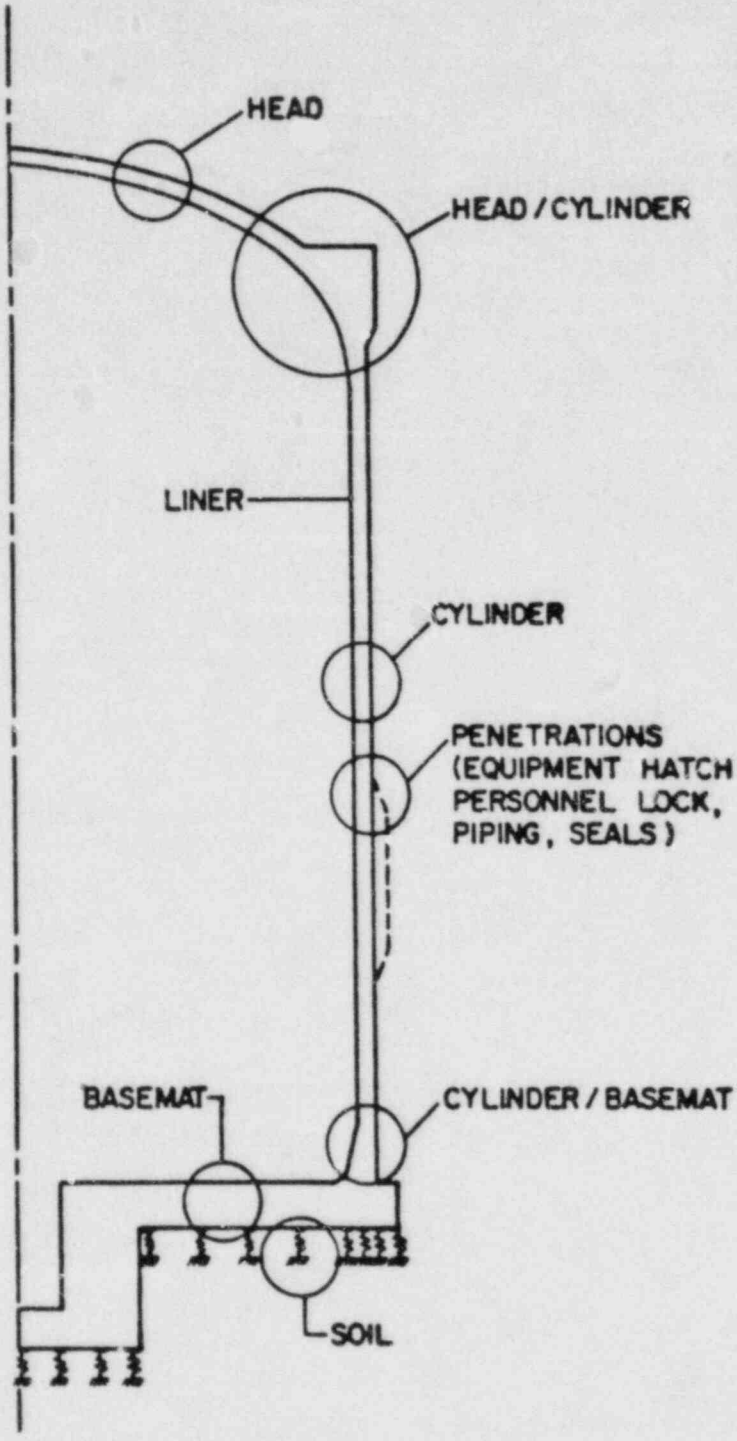

Figure 1 Containment Potential Modes of Failure

Table 1 Predicted ultimate pressure strength of various containments.

Containment, Unit Number	Predicted Ultimate Pressure (psig)	Reference	Failure Criteria and Location
PWR - ice condenser containments			
Sequoyah, 1	60	(2)	deformation twice yield in cylinder
Sequoyah, 1	57	(3)	beyond yield in cylinder
McGuire, 1	84	(2)	deformation twice yield in cylinder
McGuire, 1	*	(4)	beyond yield in cylinder
Watts Bar, 1	98	(5)	twice yield strain in sphere
Watts Bar, 1	120 140	(6)	general yielding in cylinder and equipment hatch buckling
PWR - dry containments			
St. Lucie, 1	95	(7)	twice yield strain in dome
Cherokee, 1	116	(7)	twice yield strain in sphere
Indian Point, 2, 3	110	(8)	yielding of rebars and liner in cylinder
Indian Point, 3	118	(9)	numerical nonconvergence near side wall/basemat junction
Indian Point, 2, 3	126	(10)	yielding of rebars in cylinder near springline
Main Yankee	96 119	(6)	yielding of hoop steel and numerical instability in cylinder/base
Zion, 2	120	(11)	hoop tendons strain reaches 1% in cylinder
Zion, 2	125	(9)	numerical nonconvergence near cylinder/basemat junction
Belefonte	130 139	(6)	general yielding in dome tendons and cylinder tendons
Mark III containments			
Perry, 1	100	(7)	buckling at the head knuckle
Grand Gulf, 1	55	(12)	liner strain and rebar yield in cylinder
Mark III "standard"	80	(13)	general yielding in personnel airlock
Mark III "standard"	59	(14)	ASME, level C at knuckle
Mark III	67	(15)	general yielding in cylinder
Mark II containments			
WPPSS, 2	133	(7)	twice yield strain in cylinder
Limerick	140	(16)	general yielding in cylinder
Mark II "standard"	150	(13)	general yielding in personnel airlock
Mark I containments			
Browns Ferry, 1	117	(7)	twice yield strain at cylinder/sphere intersection
Peach Bottom, 1	175	(17)	stress midway between yield and ultimate in torodial suppression pool

*Pressure-displacement relationship is given.

accounted for in an approximate way. All of these approximations introduce a degree of uncertainty.

Longitudinal stringers are typically smeared in the circumferential direction to obtain an "average" equivalently stiff axisymmetric shell. This is acceptable for certain ranges in stiffener configurations, but cannot be generalized to all cases. (2, 4, 5. 7, 18)

Circumferential variations in thicknesses, ring and stringer sizes, amount of reinforcing steel and shell imperfections can not be incorporated into an axisymmetric model. The usual, and probably conservative approach is to select the worst case, i.e., smallest size or largest imperfection, and assume this case is constant around the circumference. (2, 5, 7)

Penetrations and other reinforced openings introduce nonsymmetric features into the containment which must be ignored in axisymmetric models. Typically, the argument is made that these "local" features are sufficiently small and appropriately reinforced, e.g., thickened steel plates (ASME area replacement rule) or extra concrete reinforcement, so that the strength of the penetrated shell is greater than or equal to that of the unpenetrated shell. Several investigators have looked at isolated penetrations to verify this assumption and found that, in the case of uniform internal pressure, i.e., without buckling, this approximation is acceptable. The reinforcement and welds in the vicinity must be sufficiently ductile to allow redistribution of forces as the limit strength of the shell system is approached. (2, 5, 6, 7, 8, 9, 10, 11, 12, 16, 19)

Prestressed concrete containments have additional features - prestressing tendons and anchorage buttresses - which are not axisymmetric and must be "smoothed" into an axisymmetric model. Prestressing of both the cylindrical and doubly curved portions of the containment present such problems. The effect of these nonsymmetries are generally neglected based upon some heuristic argument. The discrete nature of the tendons is seldom included, but the effects are usually smeared. (6, 9, 11, 20) One investigator (21) has studied the discrete nature of the reinforcing and post-tensioning steel with a three-dimensional analysis. The prestressing ring for the dome was included but cylindrical prestressing buttresses were not. The study suggests that the unsymmetrical anchorage effects can not be represented by an axisymmetric model

Several pieces of equipment or other structures are often attached to the containment. e.g., ice storage areas, walkways, floor systems, cranes, plumbing, seismic anchors. The effect of these "smaller" nonsymmetries has not been studied.

A limited number of three dimensional analyses have been performed on isolated features, e.g., equipment and personnel assemblies. These analyses are usually performed as if the feature were isolated from all other features. (2, 9, 11) Neither interaction between nonsymmetrical parts nor the effect of their behavior on the remote "smooth" shell have been studied.

Interference with adjacent equipment or buildings is usually not considered Thus, interaction with a shield building is often mentioned, e.g " limiting displacements. but not included in the model. (2, 6, 7, 9, 11) The restraint of attached equipment which

is anchored inside or outside containment is not included in the structural model

Base boundary conditions are often highly idealized. For steel containments, the base is usually assumed to be fixed where it intersects the thick basemat. (2, 5, 6, 7) The base is frequently included in the model of concrete containments. Sometimes the base is not allowed to move vertically (no uplift); sometimes uplift is permitted. If the base is included, it and the supporting soil are assumed to be axisymmetric and flat. (6, 8, 9, 10, 11) Geometric imperfections are not modeled directly.

The liner in concrete containments is taken to be intimately attached to the shell wall. Local buckling of the liner due to temperature rises is mentioned by several, but analyzed by few. The structural effectiveness of the liner is debatable - some investigators publish two results: one with and one without the liner participation. (6, 8, 9, 10, 11, 12, 13, 17, 21)

Material Model

Steel The ductility of steel is used in almost all analyses - very few have restricted maximum stresses to the proportional limit.

The uniaxial stress-strain curve is usually approximated by a piece wise linear curve, often elastic-perfectly plastic. (2, 4, 5, 7, 19, 22, 23) The effect of residual stresses and a reduced proportional limit are not included. Their effect is unknown, but probably small in this application.

The Prandtl-Reuss flow rule and the von Mises yield surface are always used in the nonlinear material description This has long been accepted as an adequate description for metal behavior, though questions still arise with regard to deformation versus incremental plasticity theory for buckling applications. (2, 4, 5, 6, 7, 9, 12, 14, 19)

The effect of temperature on steel properties is neglected on the premise that accident temperatures are sufficiently low.

Actual material properties are used if they are available. These properties are usually averages of mill test reports taken from each component plate. Uncertainty often exists in these data due to strain rate differences, specimen location and orientation within the plate, limited sample size and censoring of test data. Material properties vary from plate to plate and, even, from point to point. Thickness also affects yield strength and ductility.

Weld and heat affected zone properties are taken to be the same as the base metal. Good weld quality is assumed. (11)

Reinforced Concrete A "standard" model for concrete under biaxial stress is still evolving. The uncertainty associated with an analytical description of a reinforced concrete segment under biaxial stress is one of the larger uncertainties in the analysis of concrete containments.

The uniaxial compression behavior of concrete is the best described aspect. Actual compressive properties are used, if available. However, the same uncertainties are associated with the collection of this information as are mentioned in the steel

description, e.g., testing techniques, specimen representativeness and sample size.

The uniaxial tensile strength of concrete has wide variations. Some use $6\sqrt{f'_c}$, some use the split cylinder strength. A representative test specimen has not been agreed upon (11, 24, 25)

The introduction of reinforcement into the concrete significantly complicates its description. Aspects at the steel/concrete interface, e.g., bond, anchorage, are difficult to describe analytically, let alone incorporate into a complete analytical model of the containment. The cracking (crushing)/ bar yielding/bond/aggregate interlock problem is still with us.

The biaxial stress-strain behavior is even less universally agreed upon. Various investigators have used the Chen and Chen, von Mises, Tresca and/or Drucker-Prager model. A good description of the tension cracking and post-cracking behavior is particularly missing. Arbitrary cracking criteria and reductions in shear and tension stiffness (50 and 0.01 percent, respectively) are usually used. Crack pattern (size, spacing, orientation and location) predictions are unreliable and semi-empirical at best. (6, 8, 9, 12, 15, 16, 21, 24, 26, 27, 28)

The effect of cracks on other properties is not usually incorporated into the analysis. Hence, radial shear strength and reinforcement bond are apparently related to the biaxial stress state and the extent of cracking, but the effect is not well-described analytically. In other words, a description of the behavior of reinforced concrete under all pertinent stress states up through complete cracking and/or crushing needs work. (9, 12, 15, 16, 21, 26, 28, 29)

Perfect concrete quality is assumed. Possible imperfections, e.g., concrete placement in areas of congested reinforcement, are not considered. Variation in concrete strength with location and time are not included. (17)

Temperature effects on concrete strength are usually rationalized away because of the "low" accident temperatures. (16, 17, 25, 26)

Soil If the soil is included with the base model, it is usually approximated as an axisymmetric Winkler foundation with compression - only springs. Analytical modeling of soil behavior has its own set of uncertainties, princpally having to do with the flow rule, yield surface and material constants. Most likely, this is not a major uncertainty for this application, although it becomes a predominate problem if seismic effects are important. (6, 8, 9, 10, 11)

Load Model

To limit the scope of this review, the load has been restricted to uniform internal pressure.

There is little uncertainty involved in the description of a uniform, static internal pressure for structural analysis purposes. (Whether the pressure is actually uniform and static is not addressed here. Dynamic effects become significant if the pressure

changes rapidly, relative to the containment response time. Locally high pressures cause locally high stresses.)

Temperature effects are often mentioned, but seldom included. Since temperature stresses are self-limiting, the argument goes, they have little effect on the ultimate strength of the containment. (10)

Pre-existing stresses, e.g., concrete shrinkage, steel residual stresses, erection stresses, settlement stresses are not included. These are also self-limiting. (26)

Weight forces are often combined with the pressure forces. Some account is usually taken of attached pieces, but the effect is usually distributed axisymmetrically. (6, 8, 9, 11, 12, 28)

Prestressing forces are included in at least two different ways --external forces (pressures) are applied which are equivalent to the prestress force, or equivalent temperature changes are introduced into the prestress tendons to produce a prestress condition Sometimes concrete creep is included to account for some of the prestress loss. Other prestress losses may or may not be important. (6, 9, 21, 27, 28)

Analysis Methods

Hand Calculations Hand calculation methods are based on equilibrium of an assumed limit mechanism. Limit mechanism solutions are available for uniform reinforced concrete cylinders and spheres, stiffened and unstiffened steel cylinders and cones. collapse and buckling of ellipsoidal and torispherical heads. anchorage bolts, cylinder/cylinder penetrations and cylinder/sphere penetrations. (A less sophistocated hand calculation is to multiply the containment design pressure by the design factor of safety to arrive at the ultimate strength. Fortunately, this approach isn't used much anymore.)

A very basic assumption in limit analysis is that the materials have the ductility to permit the formation of a limit mechanism. If the materials are brittle and/or locally high strains exist, local failure may occur before the complete mechanism forms (2, 7, 8, 11, 17)

Sometimes, e.g., penetrations, the critical mechanism is not clear and several must be examined. Whether the least upper bound mechanism has been found can be uncertain. (17, 30, 31)

By their nature, limit analyses can be applied to quite a specialized and small number of cases Interaction of adjacent mechanisms and complex geometries, e.g., curved knuckles, changing thicknesses, are not easily analyzed. Local details are usually not included. (7)

Large displacement effects are typically omitted. The (usually) strengthening effect of membrane tension is often neglected. (7)

Many of the limit analysis techniques have not been extensively calibrated with experiment. For example, the limit mechanism for a concrete cylinder under internal pressure is reasonably simple, but several questions can be raised regarding the crack size, radial shear strength, bond characteristics, reinforcement participation and the linear behavior over the cracks at the strains associated with the mechanism.

Finite Element or Finite Difference Solutions Finite element or finite difference solutions are relatively powerful in that local geometric and material details can be incorporated into the model. Complete descriptions of the stress-strain state throughout the model are obtained. Complex nonlinear material constitutive relationships and geometric nonlinearities are usually included. However, such an analysis has its own uncertainties.

Characteristics of the basic finite element vary from case to case. Solid elements and shell type elements incorporate different features First and second order elements require different discretizations. Accuracy is affected by element size. aspect ratio, orientation and gradation, in addition to the assumptions involved in the element formulation. (2, 5, 7, 19)

Nonlinear problems always involve some sort of iterative procedure, e.g., Newton-Raphson, modified Newton-Raphson. The convergence properties of the procedure significantly affect the accuracy (and cost) of the solution. Convergence tolerance tightness and convergence criteria, e.g., plastic strains, displacements, must be carefully understood and specified. Numerical stability problems have almost always been encountered in the analysis of concrete containments. This problem is usually associated with the tension cracking and post- cracking behavior of the concrete material model. Large changes in stiffness occur when cracks occur and this causes numerical problems. Often this is also the physical situation, i.e., cracking causes big "jumps" in the physical structure. Whether the numerical instabilities encountered in containment analyses represent corresponding physical instabilities is uncertain. (2, 5, 6, 7, 9, 21)

Several aspects of finite element modeling are unclear. A common model of bar cutoffs (the bond/anchorage problem) is not available. Some investigators taper the bar areas to represent the development of the bars. (24) Rings/stringer/shell attachments are often modeled by rigid constraints, though this represents an approximation. (6)

Reinforcing layers are often represented with orthotropic elements which effectively "smear" the discrete nature of the reinforcing. (6, 8, 9, 11, 12) Bond is assumed to be perfect. (6, 8, 9, 11, 12, 21)

The liner is usually modeled by a shell type element, rigidly attached to the inner concrete surface. (6, 8, 9, 11, 12, 13, 21)

Three-dimensional analyses of, for example, penetrations, have been done in a few cases. Typically, a portion of the structure is isolated from the remaining containment (for practical reasons) and analyzed by, say, two-dimensional shell type elements. Force and displacement boundary conditions at the limit of this isolated region are obtained from an analysis of a larger portion. Uncertainty is associated with this process. Often, the reinforcement detail in the vicinity of a penetration is geometrically complex and is difficult to represent accurately, even with finite element methods. (2, 9, 11)

As with all analysis methods, theoretical and experimental results never exactly agree - even if all the above uncertainties do not exist. Hence, there will always exist some aspects of the physical model which cannot be incorporated into the analytical

model. The scatter in this difference can be reduced, but must always remain a random variable. (2, 5, 7, 8, 9, 32, 33)

Failure Criteria

Failure criteria are one of the two or three major unresolved problems in containment ultimate strength analysis. Most investigators agree that the containments should be considered to have failed when leakage occurs, since it can no longer perform its intended function. However, few would agree as to what this means as related to the current state of structural knowledge, or how to define leakage in structural terms.

The formation of a limit mechanism is often taken to coincide with failure - especially in hand calculation analyses. In many cases, it is not clear that sufficient ductility exists for a formation of a mechanism. On the other hand, the structure may be very ductile and the pressures may increase beyond a limit pressure because of strain-hardening and tension-membrane effects. (2, 5, 10, 16)

Some (few, fortunately) find the ultimate pressure to be that associated with the ultimate tensile strength of the steel (from a smooth tensile specimen). There is little reason to expect that the as-built containment will have the ductility to reach this state. Welds, imperfections, heat-affected zones, local strain concentrations (penetrations, attachments, holes, etc.) will not permit this. Recognizing this, some investigators have used the average of the yield and ultimate tensile strengths. There is little reason for this except that it is not as unconservative as the former approach. (14, 17)

Several investigators have used a strain criteria to predict leakage - the idea being that the material strain is one of the better indicators of material distress and potential separation. This criteria is often applied to the membrane component of the shell strain or the reinforcement strain. Strain concentrations (penetrations and other nonsymmetric geometric discontinuities) are not directly included, but may be considered when the strain limits are set. Hence, strain limits for failure have been defined, by different investi-gators, between two and fifteen times the yield strain. Some have analyzed containments up to fifteen percent strain. (5, 6, 7, 11, 12)

Deformation limits have been established in some cases to define failure. This criteria makes sense if it is recognized that more than just the containment shell is involved here. Attached piping, penetrations, etc. will themselves begin to leak if they are forced to deform too much. Seals and gaskets and sealed electrical penetration assemblies cannot withstand indefinite deformation of the surrounding material. The values for the deformation limits are uncertain at this time. Some have selected strain limits for tendons of one percent based on deformation considerations. (2, 4, 6, 8, 11, 12, 19, 34, 28)

Buckling may be used as a failure criteria, even though the instantaneous bifurcation buckling itself, most likely, does not induce leakage. Only if the post-buckling strains (or displacements) become sufficiently large, as discussed above, is it

reasonable to expect failure. This applies, in this situation, particularly to ellipsoidal and torispherical heads. On the other hand, buckling of an equipment hatch may induce deformations which could cause the seal to leak. (4, 5, 6, 7, 19, 23, 35, 36)

In some cases, numerical instabilty has been interpreted as structural failure. As discussed, this may or may not be true. (6, 9, 21, 37)

In concrete containments, failure is defined by limiting reinforcement, liner and/or concrete compression strain. (6, 8, 11, 12, 13, 15, 17, 26, 27)

Usually concrete tensile cracking is not considered as a failure condition but only as an intermediate stage on the way to ultimate. However, some have predicted that the liner will tear when the concrete cracks become too large. Failure prediction then amounts to selecting the crack size which the liner can tolerate and predicting when this limiting crack size is attained. (12, 17, 27, 38) Another has predicted that the tendon anchorages will fail because of excessive concrete cracking (20)

Radial shear stress is often used as the failure criteria to check peripheral shear around penetrations and the basemat/ cylinder junction for concrete containments. Work on this idea has some way to go and significant uncertainty still exists. For example, the influences of extensive local cracking around the penetration or of hoop reinforce- ment adjacent to the basemat are still being investigated. (6, 9, 11, 17, 26, 29, 39)

If failure criteria are uncertain, failure size is a wild guess. Few investigators have gone beyond predicting that the failure will be small (local) or large (global). These predictions typically rest upon the judgment and experience of the engineers making them. The more experienced engineer may not make this guess.

Additional Uncertainties

One uncertainty that continues to come to mind during a containment analysis is: How close is the actual in-place containment to the fabrication drawings and specifications? Hence, answers to questions about, for example, concrete placement in critical areas, weld quality, tolerance acceptance, and mill test or concrete cylinder representativeness always have an associated uncertainty.

Finally, uncertainty exists in the uncertainty. That is, we are often uncertain whether we have considered all the uncertainties. For example, failure could occur in a location and by a mode the analyst has not thought to investigate.

Uncertainty Assessments

A relatively small number of investigators have attempted to quantify some of the above uncertainties into a reliability analysis of specific containments. (2, 5, 7, 11, 14, 17, 40) Their results are often presented in the form of fragility curves or probability of failure distributions conditional on a prescribed static pressure level. The material properties and geometric configuration are taken to be random quantities which are described

by a mean, standard deviation and distribution type. Analysis uncertainties are quantified by comparing experimental and analytical results. More subjective uncertainties, such as the definition of the failure criteria, actual in-place containment versus the containment described in drawings and other errors, have not yet been introduced into uncertainty assessments.

It is not the purpose of this work to review the state-of-the art in the reliability analysis of structures. Briefly, the uncertainty assessments to-date must be considered preliminary and the results interpreted only as notional probabilities. The results can become meaningful only after these methods have been calibrated with real-world failure experience. However, reliability assessments are very useful tools to focus attention on important uncertain quantities. Thus, for example, sensitivity studies point to the basic structural parameters which are significantly random. More study and data collection should be devoted to these quantities (see the following section).

Summary and Conclusions

A state-of-the-art containment analysis is a finite element solution of an axisymmetric model. Material and geometric nonlinearities are included. Nonsymmetric features may be analyzed on an individual basis but are omitted in the axisymmetric model. State-of-the-art models of the material constitutive relationships are used. Deformation predictions are generally regarded as reliable, assuming the containment configuration is accurately described, e.g., known geometry, material and loads. Predictions of leakage are much more uncertain. There is no general agreement on when and where leakage will occur.

The analysis of steel and concrete containments involves many uncertainties in the containment geometry, the containment material, the containment loads, the analysis techniques, and the failure criteria. Many of these have been summarized above. Each uncertainty represents a potential difference of opinion between two investigators. Hence, two independent investigators will often predict noticeably different results for the same containment. Of the uncertainties presented above, the following uncertainties are, in the opinion of the authors, most often the cause for discrepancies in results:

- In-place versus as-designed containment: How close is the actual containment to the containment specified in the engineering drawings, e.g., welds, reinforcement details, geometric tolerances, material properties?

- Behavior of reinforced concrete under biaxial stress condition: What are appropriate constitutive equations for a steel/ concrete system, particularly at and beyond cracking and/or crushing?

- Failure criteria: What is an appropriate structural definition for failure (leakage)?

- Failure modes: Have all realistically possible failure modes been analyzed, e.g., does an axisymmetric model miss important effects?

Uncertainty can be decreased only if these problems are addressed by further study.

ACKNOWLEDGMENT

The authors would like to express their appreciation for Mr. Joseph Jung from the Sandia National Laboratories for providing some of the information needed to complete this work. This work was conducted at Ames Laboratory, Iowa State University, for Sandia National Laboratories under Sandia Purchase Order Number 47-4020.

REFERENCES

(1) Greimann, L., Fanous, F. and Bluhm, D., "Containment Analysis Techniques, A State-of-the-Art Summary," Final Report submitted to Sandia National Laboratory, IS-4843, October 1983.

(2) Greimann, L., et al., "Reliability Analysis of Containment Strength," Report to U.S. NRC, NUREG/CR 1891, IS-4753, August 1982.

(3) Orr, R., Oral presentation at ACRS Meeting, September 1980, Slides reprinted in NUREG/CR-1891.

(4) Tsai, J.C. and Orr, R.S., "Probabilistic Failure Modes and Locations in Containments Subjected to Internal Pressurization," Proceedings of the Workshop on Containment Integrity, Vol. II of II, NUREG/CR-0033, SAND82-1659, 201-226, October 1982.

(5) Greimann, L., et al., "Probabilistic Seismic Resistance of Steel Containments," Report to U.S. NRC, NUREG/CR-3127, 1983.

(6) Jung, J., "Response of the Watts Bar, Maine Yankee and Bellefonte Containments to Static Internal Pressurization," Proceedings of the ANS/ENS International Meeting on Light Water Reactor Severe Accident Evaluation, August 28 - Sept. 1, 1983, Cambridge, MA.

(7) Greimann, L., et al., "Reliability Analysis of Steel Containment Strength," Report to U.S. NRC, NUREG/CR-2442, June 1982.

(8) Murfin, W.B., "Report of the Zion/Indian Point Study: Volume 1," Report to the U.S. NRC, NUREG/CR-1410, SAND80-0617/1, August 1980.

(9) Butler, T.A. and Fugelso, L.E., "Response of the Zion and Indian Point Containment Buildings to Severe Accident Pressure," Report to the U.S. NRC, NUREG/CR-2569, LA-9301-MS, May 1982.

(10) "Containment Capability of Indian Point Power Plant Unit Nos. 2 and 3 for Internal Pressure Load," A study prepared for the Power Authority of the State of New York and Consolidated Edison by United Engineer and Constructors, Inc.

(11) Walser, A., "Primary Containment Ultimate Capacity of Zion Nuclear Power Plant for Internal Pressure Load," Proceedings of the Workshop on Containment Integrity, Vol. II of II, Prepared for the U.S. NRC, NUREG/CP-0033, SAND-82-1659, 263-318, October 1982.

(12) Sharma, S., et al., "Failure Evaluation of a Reinforced Concrete Mark III Containment Structure Under Uniform Pressure, "Report to the U.S. NRC, NUREG/CR-1967, BNL-NUREG-51543, AN.DR., September 1982, and Transaction of SMIRT 7, Paper No. J 2/8, Chicago, IL, USA, August 1983.

(13) Krishnaswamy, C.N., Namperumal, R. and Al-Dabbagh, A., "Ultimate Internal Pressure Capacity of Concrete Containment Structures," Transactions of SMIRT 7, Paper No. J3/6, Chicago, IL, August 1983.

(14) Gou, P.F. and Love, J.E., "Pressure Carrying Capacity of the Containment Structural System of the Mark III Standard Plant," Proceedings of the Workshop on Containment Integrity, Vol. II of II, Prepared for the U.S. NRC, NUREG/CP-0033, SAND-82-1659, 263-318, October 1982, and Transactions of SMIRT 7, Paper No. J2/6, Chicago, IL, USA, August 1983.

(15) McGaughy, J.P., Lin, F.T. and Sen, S.K., "Ultimate Internal Pressure Capacity of a Reinforced Concrete Mark III Containment," Transactions of SMIRT 7, Paper No. J3/9, Chicago, IL, USA, August 1983.

(16) "Ultimate Pressure Capacity of Limerick Primary Containment," Study in support of Risk Assessment of Limerick Generating Station, conducted by General Electric/Science Application, Inc., Final Report, October 1981.

(17) "Reactor Safety Study: An Assessment of Accident Risks in the U.S. Commercial Nuclear Power Plants," WASH-1400, U.S. Atomic Energy Commission, Appendix E, August 1974.

(18) Zudans, Z., Letter report to Dr. E. Saujo, NRC, August 1980, Reprinted in NUREG/CR-1891.

(19) Blejwas, T.E., et al., "Containment Integrity Program FY82 Annual Report," Report to the U.S. NRC, NUREG/CR-3131/1, SAND83-0417, March 1983.

(20) Atchison, R.J., Asmis, G.J.K. and Campbell, F.R., "Behavior of Concrete Containment Under Over-Pressure Conditions," Transactions of SMIRT 5, Paper No. J3/2, Berlin, Germany, August 1979.

(21) Dooley, W.T., Macek, R.W. and Sadik, S., "Ultimate Pressure Capacity Analysis of a Post-tensioned Reinforced Concrete Nuclear Reactor Containment Building," Work supported by U.S. DOE Contract No. DE-AC07-76ID01570 at EG&G Idaho, Inc., Idaho Falls, Idaho.

(22) Blejwas, T.E. and Horschel, D.S., "Analysis of Steel Containment Models," Proceedings of the Workshop on Containment Integrity, Vol. II of II, NUREG/CR-0033, SAND82-1659, 201-226, October 1982.

(23) Horschel, D.S. and Blejwas, T.E., "An Analytical Investigation of the Response of Steel Containment Models to Internal Pressurization," Transaction of SMIRT 7, Paper No. J6/4, Chicago, IL, August 1983.

(24) Murray, D.W., Chitnuyanondh, L. and Wong, C., "Modeling and Predicting Behavior of Prestressed Concrete Secondary Containment Structures Using BOSOR5," Transactions of SMIRT 5, Paper No. J3/5, Berlin, Germany, August 1979.

(25) Aoyagi, Y., et al., "Behavior of Reinforced Concrete Containment Models Under Thermal Gradient and Internal Pressure," Transactions of SMIRT 6, Paper No. J4/5, Berlin, Germany, August 1979.

(26) Aoyagi, Y., Okada, K. and Tanka, N., "An Experimental and Analytical Study on Radial Shear of Reinforced Concrete Containment Under Pressure and Thermal Effects," Transactions of SMIRT 6, Paper No. J4/12, Paris, France, August 1981.

(27) Carmichal, G.D.T., Rajaraman, A. and Balakrishnan, S., "Nonlinear Analysis of Prestressed Concrete Containments," Transactions of SMIRT 6, Paper No. J3/3, Paris, France, August 1981.

(28) Brochard, J., et al., "Study of the Behavior of Containment Buildings of PWR-Type Reactor, Until Complete Failure in Case of LOCA," Transactions of SMIRT 6, Paper No. J3/1, Paris, France, August 1981.

(29) Aoyagi, Y., Isobata, O. and Tanka, N., "Design Method of Shell Wall End of Reinforced Concrete Containment Vessel (RCCV) Against Radial Shear," Transactions of SMIRT 6, Paper No. J4/6, Berlin, Germany, 1979.

(30) Gill, S.S., "The Limit Pressure for a Flush Cylindrical Nozzle in a Spherical Pressure Vessel," International Journal of Mechanical Science, Vol. 6, 105-115, 1964.

(31) Dinno, K.S. and Gill, S.S., "Limit Pressure for a Protruding Cylindrical Nozzle in a Spherical Pressure Vessel," Journal of Mechanical Engineering Science, 7 (3), 259-270, 1965.

(32) Rizkalla, S., Simmonds, S.H. and Macgregor, J.G., "A Test of a Model of a Thin-Walled Prestressed Concrete Secondary Containment Structure," Transactions of SMIRT 5, Paper No. J4/2, Berlin. Germany, August 1979.

(33) Donten, K., et al., "Results of Strength Test on a 1:10 Model of Reactor Containment," Transactions of SMIRT 5, Paper No. J4/8, Berlin, Germany, August 1979.

(34) Sebrell, W., "The Potential for Containment Leak Paths Through Electrical Penetration Assemblies Under Severe Accident Conditions," NUREG/CR-3234, July 1983.

(35) Fly, G., Bennet, J.G., Baker, W.E. and Babcock, C.D., "Experiments Designed to Assess the Margin-to-Failure of Steel Containment Susceptible to "Knuckle" Buckling," Transactions of SMIRT 7, Paper No. J3/5, Chicago, IL, August 1983.

(36) Meller, E. and Bushnell, D., "Buckling of Steel Containment Shells, Task 1a: Dynamic Response and Buckling of Offshore Power Systems' Floating Nuclear Plant Containment Vessel," NUREG/CR-2836, Vol. 1, Part 1, December 1982.

(37) Butler, T.A., "Failure Modes for Concrete Nuclear Containment Buildings," Advances in Containment Design and Analysis, ASME/ANS Joint Conference, July 26-28, 1982, Portland, Oregon.

(38) Macgregor, J.G., Simmonds, S.H. and Rizkalla, S.H., "Cracking of Prestressed Concrete Containment Due to Internal Pressure," Transactions of SMIRT 6, Paper No. J4/10, Paris, France, August 1981.

(39) White, R.N. and Gergely, P., "Punching and Radial Shear Problems in Reinforced Concrete Containments," Proceedings of the Workshop on Containment Integrity, NUREG/CR-0033, SAND82-1659, 109-122, October 1982.

(40) Fanous, F. and Greimann, L., "Probabilistic Seismic Resistance of a Mark III Steel Containment," Symposium on Advances in Probabilistic Structural Mechanics, ASME, San Antonio, Texas, June 1984.

SESSION D

LEAKAGE OF CONTAINMENTS DURING SEVERE ACCIDENTS

FAILURE/LEAKAGE PREDICTIONS OF CONCRETE STRUCTURES CONTAINING CRACKS*

Y. C. Pan, A. H. Marchertas, and J. M. Kennedy
Reactor Analysis and Safety Division
Argonne National Laboratory
9700 South Cass Avenue
Argonne, IL 60439

ABSTRACT

An approach is presented for studying the cracking and radioactive release of a reactor containment during severe accidents and extreme environments. The cracking of concrete is modeled as the blunt crack. The initiation and propagation of a crack are determined by using the maximum strength and the J-integral criteria. Furthermore, the extent of cracking is related to the leakage calculation by using a model developed by Rizkalla, Lau and Simmonds. Numerical examples are given for a three point bending problem and a hypothetical case of a concrete containment structure subjected to high internal pressure during an accident.

INTRODUCTION

Physical integrity and radioactive release are two major concerns in the assessment of the performance of the reactor containment during severe accidents and extreme environments. The behavior of the containment would be greatly affected by the presence of cracks which not only reduce the load carrying capacity of the containment structure, but also have the potential of increasing the leakage rate of the radioactive materials. The problem is further complicated if the cracks propagate during the accident which will further increase the leakage rate.

At the present time, Argonne National Laboratory is engaged in the development of analytical tools for predicting the behavior of concrete structures under severe loading conditions [1]. One important aspect of the effort is the modeling of cracking. Two distinct models have been incorporated into the computer code to simulate cracking; namely, the conventional sharp crack model and the blunt crack model. The blunt crack model considers the crack to be uniformly distributed throughout the area of the element. In the sharp crack model, the crack surface is treated as the boundary of the finite element mesh. Despite the modeling difference, the results of these two approaches are quite comparable to each other [2,3]. The blunt crack model is found to be particularly suited for large concrete structures due to its ease of implementation and the fact that concrete cracking generally does not have well defined crack surfaces like those of a sharp crack. Four crack propagation criteria, the J-integral, the

*Work performed under the auspices of the U.S. Department of Energy.

energy release rate, the effective strength and the failure surface criterion, have been considered [4]. In this paper the maximum strength and the J-integral criteria are used to determine the extent of cracking. The formulation developed in Ref. 5 is then used to relate the extent of cracking to the leakage rate of pressurized gases through the concrete containment structure. Several numerical examples are given in this paper to demonstrate the capability of the computer code in predicting failure and leakage rate of a concrete structure containing cracks.

Modeling of Concrete Cracks

The initiation of a crack in a finite element analysis is assumed whenever the principal tensile stress in an element reaches the tensile strength of the concrete. The crack is assumed to be smeared over the entire area of the element in the blunt crack model. Hence, the element is assumed to lose its load carrying capacity in the direction of the tensile stress which is perpendicular to the direction of the crack. The propagation of a crack can be determined in a similar manner. However, it is found that the approach utilizing the J-integral criterion would yield more accurate results which are less mesh dependent.

If a crack of length a is assumed to advance in the x-direction, the rate of energy change can be related to the well known J-integral whether the crack is modeled as a sharp crack or a blunt crack [2,3]

$$J = \int \left(W dy - T \cdot \frac{\partial u}{\partial x}\, d\ell\right) , \tag{1}$$

where x and y are Cartesian coordinates with y perpendicular to the crack surface; W is the strain energy; T is the surface traction; u is the displacement; $d\ell$ is a line segment in an arbitrary integration loop surrounding the crack tip. In the J-integral evaluation, it is noted that the surface traction vanishes on the blunt crack surface just as on the sharp crack surface. Therefore, the numerical integration for the blunt crack model is similar to that for the sharp crack model.

The J-integral is not path independent if extensive plasticity exists. In that case, a modified concept called J* integral was introduced by Blackburn [6].

$$\begin{aligned} J^* &= \lim_{\rho \to 0} \int_{\Gamma_1} \left\{\frac{1}{2}\, \sigma_{ij}\, \frac{\partial u_i}{\partial x_j}\, dx_2 - T_i\, \frac{\partial u_i}{\partial x_1}\, d\ell\right\} \\ &= \int_{\Gamma_3} \left\{\frac{1}{2}\, \sigma_{ij}\, \frac{\partial u_i}{\partial x_j}\, dx_2 - T_i\, \frac{\partial u_i}{\partial x_1}\, d\ell\right\} \\ &+ \lim_{\rho \to 0} \iint \left\{\frac{1}{2}\, \sigma_{ij}\, \frac{\partial^2 u_i}{\partial x_1\, \partial x_j} - \frac{1}{2}\, \frac{\partial \sigma_{ij}}{\partial x_1}\, \frac{\partial u_i}{\partial x_j}\right\} dS , \end{aligned} \tag{2}$$

where Γ_1 is a circle of radius ρ around the crack tip, Γ_3 is another contour beyond Γ_1 also surrounding the crack tip and S is the area enclosed by Γ_1 and Γ_3. The Cartesian coordinates are denoted by x_1 and x_2. The tensor notation is used in Eq. (2).

The J* integral is equal to the J integral for an elastic case. Hence the amount of difference between the J and J* integral values is also an indication of the degree of nonlinear deformation of the structures. The J-integral criterion states that the crack will propagate if the J (or J*) integral reaches a critical value which is a material property to be determined by experiments.

Leakage Model

Once the extent of cracking is determined by using the aforementioned fracture criteria, the amount of leakage can be found by the following equation developed for computing leakage through concrete cracks [5].

$$\frac{P_i^2 - P_e^2}{L} = \left(\frac{k^n}{2}\right) \left(\frac{\mu}{2}\right)^n (RT)^{n-1} \left|\frac{P_e Q}{B}\right|^{2-n} \frac{1}{W^3} \qquad (3)$$

where

P_i = internal pressure (lb/sq ft)
P_e = external pressure (lb/sq ft)
L = thickness of concrete structure (ft)
k = surface roughness of the crack
μ = dynamic viscosity of the radioactive gas (lb.sec/sq ft)
R = gas constant (1716 ft^2/sec^2-°R)
T = absolute temperature of the gas (°R)
n = flow coefficient
Q = total flow rate through the concrete wall (cu ft/sec)
B = length of the crack along the wall (ft)
W = average opening displacement of the crack (ft).

In this model, the opening displacement is assumed to be uniform through the thickness of the concrete wall which is valid for cracks generated by pure membrane stress. The surface roughness and flow coefficient have been found to be

$$k = 2.907 \times 10^7 \, (w^3)^{0.428}$$

$$n = \frac{0.133}{(w^3)^{0.081}}$$

Numerical Results

To examine the performance of the blunt crack approach, a three-point bend problem reported in a calculational round robin in elastic-plastic fracture mechanics participated by 17 organi-

zations [7] is chosen for numerical study. The three-point bend specimen is 2.54 cm wide, 10.16 cm high and 2.54 cm thick with a 1.27 cm long center crack. The calculated crack mouth opening displacement and the J and J* values are plotted in Figs. 1 and 2, respectively. Also shown in the figures are the values reported by the organizations participating in the calculational round robin. It is noted that the current J and J*-integrals calculations yield very reasonable results as compared with those obtained in the round robin. Hence it is concluded that the J and J*-integrals approach with both the blunt crack model and the sharp crack model can be used for elastic-plastic fracture mechanics problems.

The second problem studied is a hypothetical case of a concrete containment structure subjected to 150 psi (1 MPa) gas pressure and 750°F (399°C) gas temperature during an accident. A sketch of the containment structure is shown in Fig. 3. The concrete containment is a domed cylindrical structure 70 ft (21.3 m) in radius, 214 ft (65.3 m) high and 3.5 ft (10.7 m) thick. The containment structure usually has many penetrations such as the equipment hatch, the emergency air lock and various piping penetrations. Selected for this study is a piping penetration which is 5 ft (1.5 m) in diameter. Because of the stress concentration at a hole, the area surrounding the piping penetration is the critical part of the structure. The thickness of the containment wall and the radius of the penetration are much smaller than the radius of the containment structure. Therefore, the problem is reduced to a two dimensional plane stress problem shown in Fig. 4 where x is the circumferential direction and y is in the axial direction. Only a quarter of the mesh is set up due to symmetry conditions. Usually, a nuclear containment structure is reinforced. A 2% steel reinforcement would carry about 90% of the load. However, the current model does not include the effect of the reinforcement. Hence, only 10% of the pressure loading is applied to the model which leads to circumferential and axial stresses.

$$\sigma_c = 2\sigma_a = 300 \text{ psi } (2 \text{ MPa}) .$$

The material properties used in this study are

$$E = 2.5 \times 10^{11} \text{ dyne/cm}^2,$$
$$\nu = 0.18,$$
$$\rho = 2.326 \text{ g/cm}^3,$$
$$f_t = 2.41 \text{ MPa},$$

where E is the Young's modulus, ν is the Poisson's ration, ρ is the density, and f_t is the tensile strength of concrete.

Due to its poor thermal conductivity, a concrete structure responds much quicker to a pressure load than to a thermal load. Therefore, the computer run attempted includes only the pressure loading on the structure. The effect of the temperature is only reflected in gas properties. The result is shown in Fig. 5 where the straight line in an element indicates the direction of the crack. Cracks initiate at the 6 and 12 o'clock position of the

circular penetration when the circumferential stresses reach the tensile strength of the concrete and propagate through the model in less than 20 ms. In a reinforced concrete structure, the crack may be stopped by the reinforcing bars. However, that effect is not included in the present model.

To demonstrate the leakage calculation for a more reasonable case, we chose the crack length to 6 in (15.2 cm) in the next computer model and calculated the J and J* values. In order to study the sensitivity of the finite element mesh, the model shown in Fig. 4 is further refined as shown in Figs. 6 and 7. The same loadings are applied. The calculated J and J* values are 382 N/m and 390 N/m respectively. Compared to a critical J value of 32 N/m, this indicates that the crack will propagate. The average opening displacement of the crack is calculated to be 0.007 cm. From Eq. (3), the radioactive leakage rate is calculated to be 0.00012 cu ft/sec. (3.4×10^{-6} m^3/sec) which is less than the acceptable leakage rate of 1% of containment volume per day (0.01 m^3/sec).

SUMMARY AND DISCUSSIONS

1. This paper presents an approach to assess the physical integrity and leakage rate of a concrete containment structure subjected to high pressure and temperature during an accident.
2. In an accident condition, the concrete structure responds quickly to the pressure loading. Cracks initiate as soon as the tensile strength of the concrete is exceeded and propagate under certain conditions through the structure in the order of less than 1 sec which is several orders of magnitude faster than the change in thermal gradient.
3. J (or J*) integral criterion appear to be very reasonable for crack propagation simulations.
4. The leakage rate can be related to the extent of cracking, although more experimental data is needed to cover a wider range of crack configurations such as cracks caused by bending stress rather than by membrane stress.
5. The effect of reinforcement needs to be studied further since it is not included in this study.

REFERENCES

[1] A. H. Marchertas and R. F. Kulak, "A Coupled Heat Conduction and Thermal Stress Formulation Using Explicity Integration", Argonne National LaboratoryReport ANL-82-42 (June 1982).

[2] Y. C. Pan, A. H. Marchertas and J. M. Kennedy, "Finite Element Blunt Crack Propagation - A Modified J-Integral Approach," Paper No. H 5/3, Transactions of the 7th International Conference on Structural Mechanics in Reactor Technology, Chicago, Illinois, Aug. 22-26, 1983.

[3] Y. C. Pan and J. M. Kennedy, "A Comparison of Finite Element J-Integral Evaluations for the Blunt Crack Model and the Sharp Crack Model," Proceedings, Fourth ASCE/EMD Specialty Conference, Purdue University, Indiana, May 23-25, 1983.

[4] Y. C. Pan, A. H. Marchertas, P. A. Pfeiffer and J. M. Kennedy, "Concrete Cracking Simulations for Nuclear Applications," submitted to Journal of Fracture Technology.

[5] S. H. Rizkalla, B. L. Lau and S. H. Simmonds, "Leakage of Pressurized Gases Through Unlined Concrete Containment Structures," Paper No. J 1/5, Transactions of the 7th International Conference on Structural Mechanics in Reactor Technology, Chicago, Illinois, Aug. 22-26, 1983.

[6] Blackburn, W. S., "Path Independent Integrals to Predict Onset of Crack Instability in an Elastic-Plastic Material," Int. J. Fract. Mech 8, pp. 343-346 (1972) and Correction 9, p. 122 (1973).

[7] Larsson, L. H., "A Calculational Round Robin in Elastic-Plastic Fracture Mechanics," Int. J. Pres. Ves. & Piping, 11, 1983, pp. 207-228.

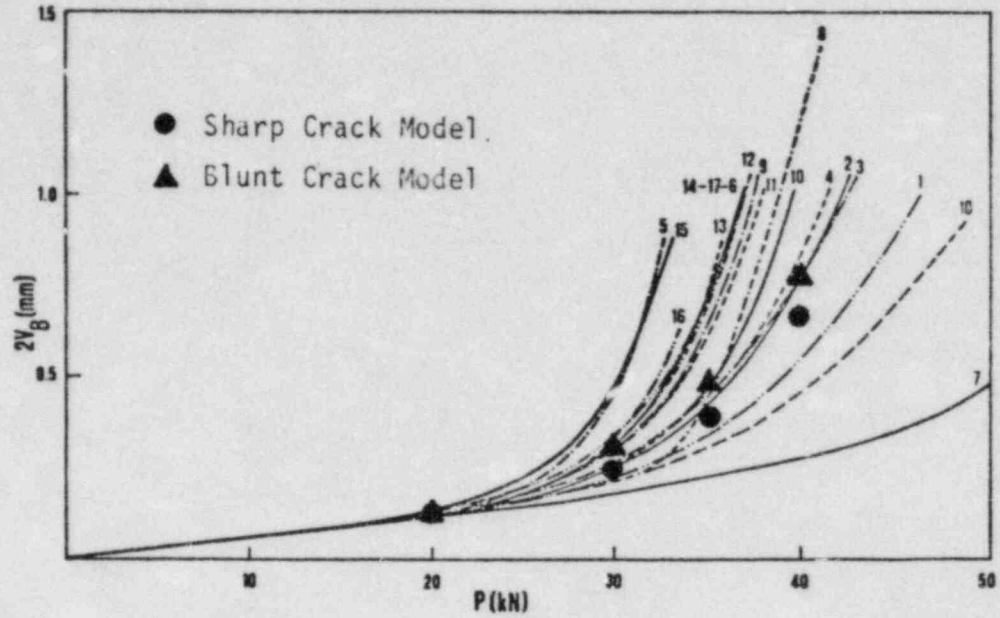

Fig. 1. Crack Mouth Opening Versus Load (Curves are from Ref. 6)

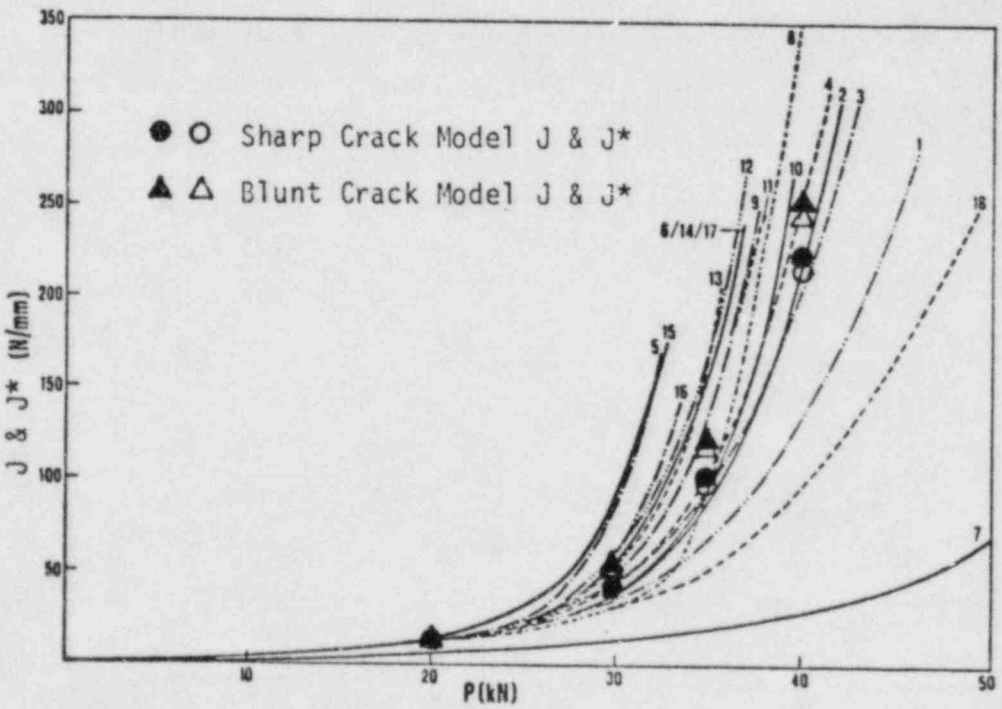

Fig. 2. J and J* Integrals Versus Load (Curves are from Ref. 6)

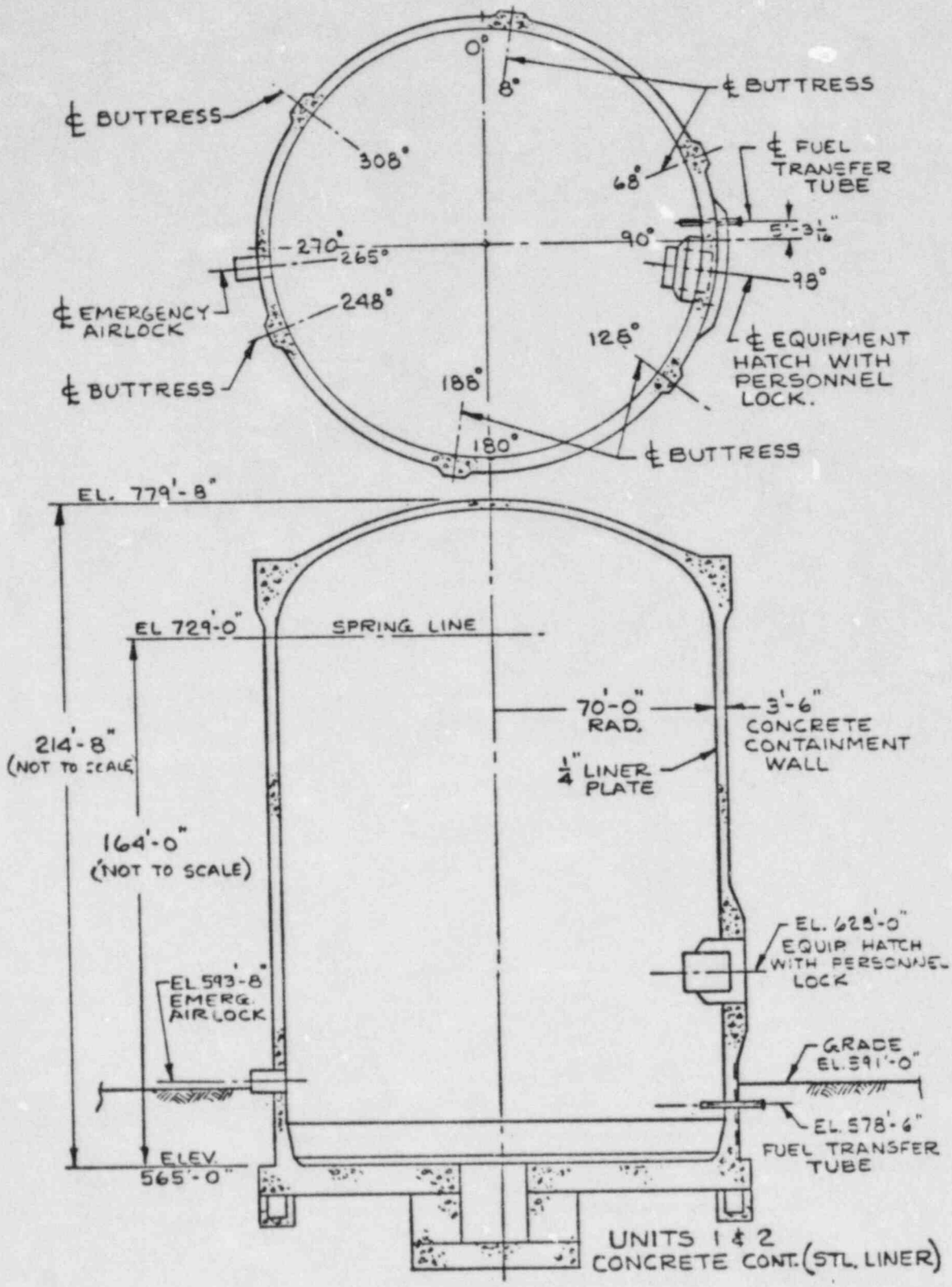

Fig. 3. A Typical Concrete Containment Structure

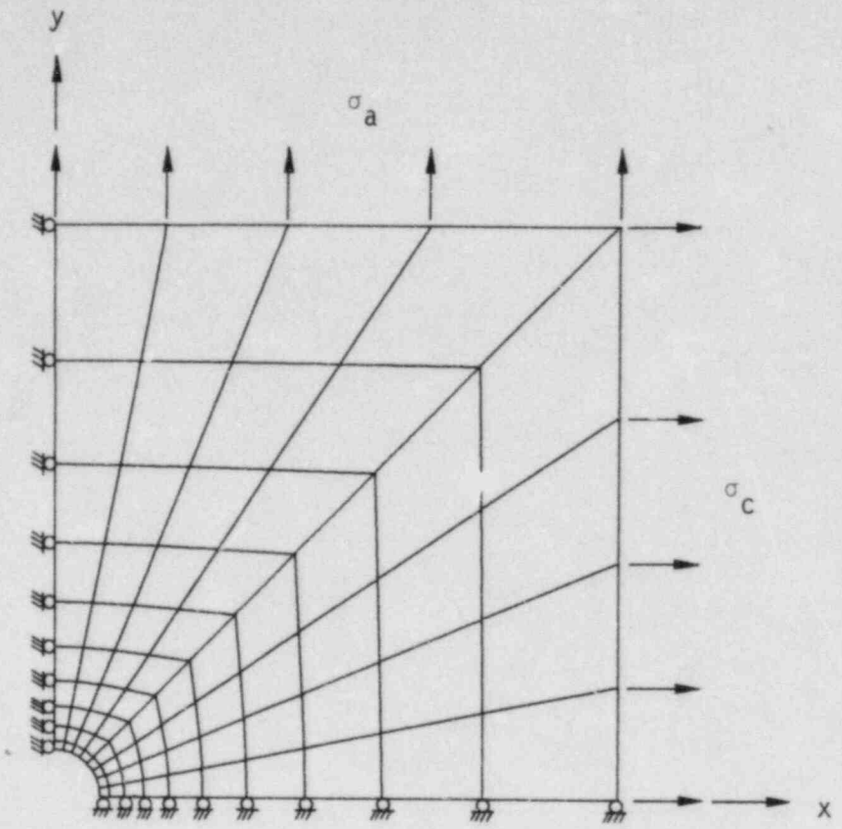

Fig. 4. Finite element model representing a piping penetration in a containment structure

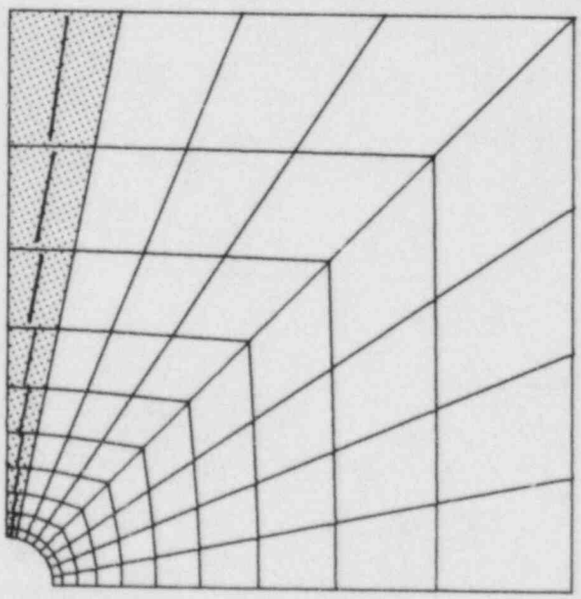

Fig. 5. Cracking pattern for the finite element model shown in Fig. 3

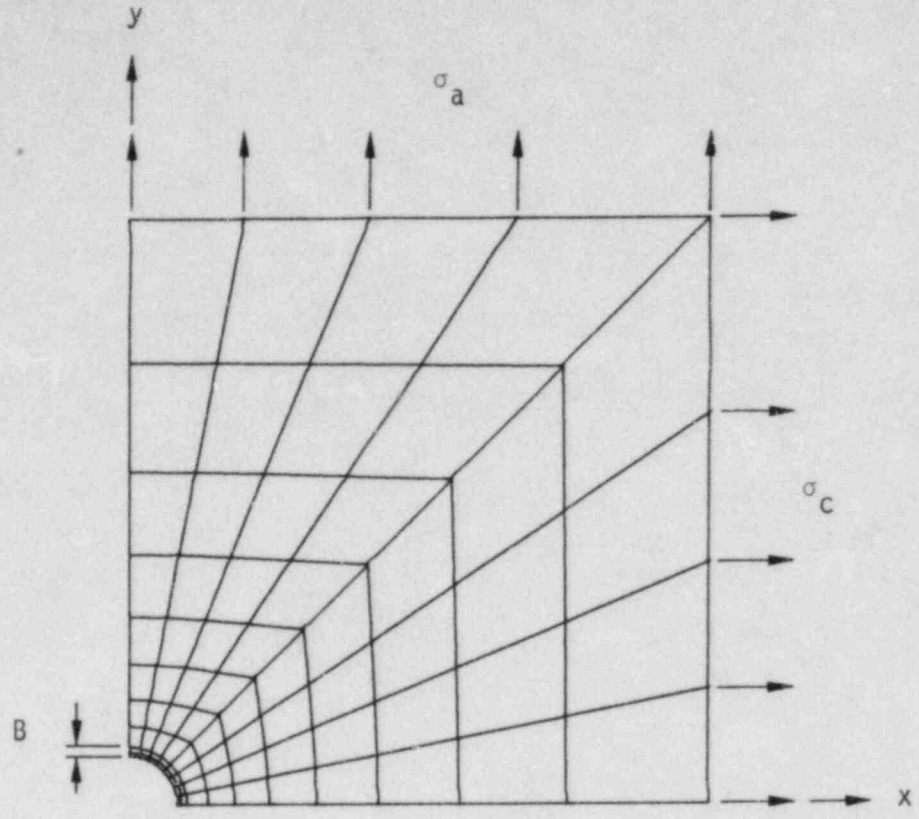

Fig. 6. Finite element model representing a 6" (15.2 cm) crack extending from a piping penetration in a containment structure

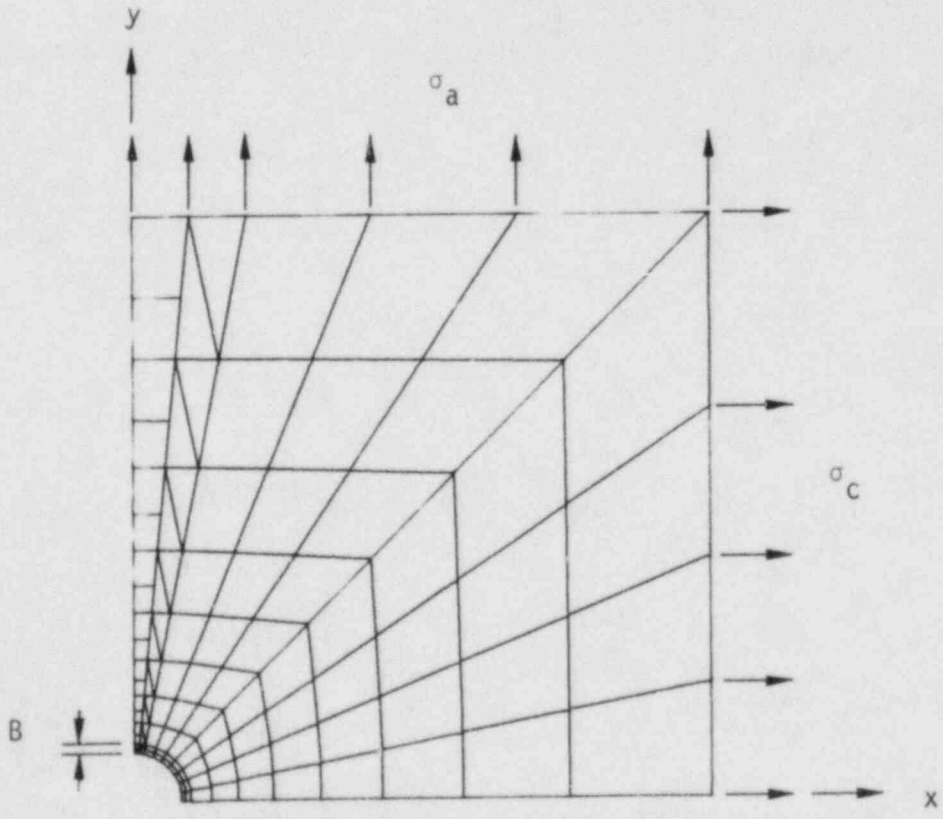

Fig. 7. Refined finite element model representing a 6" (15.2 cm) crack extending from a piping penetration in a containment structure

AEROSOLS AND LEAKING CONCRETE CONTAINMENT WALLS

J. F. van de Vate
Netherlands Energy Research Foundation ECN
P. O. Box 1, 1755 AZ Petten, The Netherlands

ABSTRACT

Two aspects of leaking concrete containments are investigated: leak rates and particulate fission product penetration.

Air-flow rates are measured through cracked and undamaged concrete cylinders. From the results on undamaged concrete, it follows that the normalized leak rate of a standard concrete containment building amounts to 10^{-3}-5 x 10^{-3} vol. %.d^{-1}.$mbar^{-1}$. The standard containment is defined as a spherical concrete building of $10^4 m^3$ volume having 1 m wall thickness. Normalized leak rates due to cracks in a standard containment are roughly 8 x 10^{-3} vol. %.d^{-1}.$mbar^{-1}$ for a crack of 1 m length; this could be more for larger crack widths ($\geq$ 0.1 mm).

Experimental results are presented on aerosol penetration through artificial cracks simulating leaks in concrete walls of safety containments, and through model leaks of glass bead columns. The results on aerosol removal from a leak flow through leak paths can be explained assuming turbulent inertial deposition in a high flow rate regime and sedimentation in a low flow rate regime. Other aerosol removal mechanisms are dealt with too. Special attention is given to the role of diffusiophoresis in removal of particulate fission product matter in leaking cracks in concrete walls and also to the importance of particle growth in particle removal in the leaking flow due to cooling in the leak. For the application of the results of this study to a nuclear safety analysis important knowledge on leaks through containment walls and on aerosol particle size under severe accident conditions is lacking.

1. INTRODUCTION

Containment buildings of nuclear reactors enclose the nuclear installations inside, and have the purpose of preventing important release of radioactive material (gases and aerosols) to the environment. Leak tightness is the primary property of such containments. Radioactive aerosols present in the LWR-containment under post-accident conditions are assumed to have leak rates similar to inert gases which, however, is an unreal and conservative assumption in view of the possibility of deposition of particulate material inside the leak paths. The penetration of particles through leak paths is a function of leak path dimensions, leak rate and particle size. Leak path dimensions and leak rate are

dependent variables. Though uncertainty exists concerning the particle size under post-meltdown conditions (also of major importance as will appear later on) the leak characteristics under these conditions have much larger uncertainty. The large variety of leak paths possible under real accident conditions for various containment types makes application of aerosol knowledge very difficult. Therefore, the recent attention given to containment failure (mainly due to overpressure or internal missiles) can be of great help in the near future for decreasing the complexity of the field of leak paths. This paper serves to indicate the kind of information needed to apply aerosol science to fission product deposition in leak paths.

Leak tightness can be achieved by steel containments, by steel linings inside concrete buildings or by prestressed concrete buildings. This study deals with leak rates of intact and cracked concrete, and with aerosol penetration through cracked concrete. Cracks in concrete containment walls probably don't determine leak rates of steel-lined containments; however, leak rates through cracks in concrete are relevant to concrete containment buildings. Aerosol penetration through cracks in concrete is highly relevant to both concrete and steel-lined concrete containments because of the relatively long residence time (ratio of leak path volume to flow rate) and of the relatively large surface area of leak paths in concrete walls. The importance of both leak path aspects becomes evident below.

As a spin-off of research on the particle size dependent penetration of aerosols through leak paths, indications can be obtained concerning particle size of penetrating aerosols which is of great value for exposure assessment of the reactor surroundings [1].

2. GAS LEAKAGE

2.1. Intact concrete

Leak rates through undamaged concrete test specimens were investigated by analysis of pressure decay curves of a vessel connected airtightly to the test specimen. These specimens were concrete discs (15 cm diameter) of various heights (30 cm and 60 cm), freshly cut from cylinders which were taken from a mother block. This block was prepared according to the specifications for the German SNR-300 containment. The cylinders were cut from the mother block at various dates after its preparation (Table I). The decay curves appeared to be exponential and leak rates were inversely proportional to disc height. This allowed calculation of normalized leak rates Δ defined as the vol.% leaking out of a standard concrete containment (spherical; 10^4 m^3 volume; 1 m wall thickness) at an overpressure of 1 mbar relative to the surroundings. The obtained Δ-values are given in Table I. These results are in reasonable agreement with the results obtained in the early sixties by Atomics International [2] from which Δ-values of 1.5×10^{-3}-10^{-2} vol. %.$d.^{-1}.m^{-1}.mbar^{-1}$ can be

calculated. Some concrete chemistry taking place (hydrate crystal formation) during the first months results in an initial decrease of leak rate.

TABLE 1

Normalized leak rates Δ through test specimens cut from a concrete mother block at various dates after its preparation.

Number of specimens	date of cutting after preparation	cylinder height (mm)	Δ (vol.%.d^{-1}.m^{-1}.$mbar^{-1}$)
2	1 month	31 ; 65	$5.19(\pm 0.02)\times10^{-3}$
3	1 year	63 - 65	$1.03(\pm 0.07)\times10^{-3}$
2	2½ years	31 ; 65	$0.94(\pm 0.05)\times10^{-3}$

Leak tests on concrete specimens with a steel pipe penetration (10cm x 10cm) revealed leakage only slightly larger than without the penetration, even after several days of heating at 70°C. Heating of the penetration at 150°C, however, resulted within a few hours in important crack formation around the steel pipe due to the combined effects of drying and thermal expansion. This could be of importance for the leak tightness of concrete containments under post-meltdown conditions (containment atmosphere with temperatures up to 150°C) where the penetrations through the containment walls are heat-leaks during long periods.

2.2. Cracked concrete

Experimental investigations were performed on artificially cracked concrete cylinders as well as on well-defined model leaks. Concrete test specimens were made by putting together the halves of a split concrete cylinder (fig. 1). Usually, measurement of the flow rate was done simultaneously with that of aerosol penetration, by recording pressure decay in the aerosol vessel (1 m^3) connected to the test specimen (fig. 2).

Leak rate characteristics (flow rate q as a function of pressure drop Δp) were measured of some artificial cracks in concrete cylinders (CCC), and of model leaks of glass bead columns (GBC) assembled to have similar flow charateristics. Fig. 3 shows the results. Obviously, the GBC's have flow properties comparable to those of the CCCs. One exception, CCC #8, is displayed in order to exemplify a crack that behaved abnormally, most likely due to irremediable clogging of the crack. This clogging occurred with most of the test specimens presumedly due to crystalline material released by the air stream from the crack walls to narrow passages in the crack. Firm knocking on the specimens could remove this clogging though not in case of CCC #8. From the linearity of the log-log plots with a slope between 30° and 45° (q is roughly proportional to $\Delta p^{0.8}$) one may deduce that

the flow through the cracks is of a mixed turbulent/laminar type. Assuming linear dependence of flow rate on crack length and on crack depth our flow rate data are roughly half those which can be calculated from the Atomics International investigations |2|. This is an acceptable difference in view of the different experimental crack treatment by AI, viz. cleaning of the crack surfaces prior to assembling.

The similar flow characteristics of GBC's and CCC's implied that similar particle behaviour in these specimens could be expected, thereby aiding in interpreting the observed relations between aerosol penetration, flow characteristics and spatial dimensions of the leak paths.

Our investigations on cracked concrete lead to standardized leak rates ($10^4 m^3$ spherical containment, see above) of about 40 vol %.d^{-1} for a crack length of 1 m and assuming linear extrapolation allowable to the high 5 bar range of containment overpressure under post-meltdown conditions. One single crack with a characteristic length of the containment (25 m) results therefore in an effective half-life of containment pressure loss of 100 minutes.

3. AEROSOL PENETRATION

3.1. General

Aerosol processes during entrance into and penetration of particles through leak paths are similar to those during sampling for aerosol analysis: biases during aspiration and due to sampling line losses. Entrance bias has its analogy in blunt probe sampling |3|; however, significant leak path entrance losses (aspiration coefficients < 0.5) of hypermicron particles occur only for Stokes numbers ≥ 0.1 which relate to linear flow velocities of several $m.s^{-1}$ prior to entering; this is unreal. Reduction of aerosol penetration can be due to several mechanisms dependent on particle size, leak path dimensions and leak rate. Relevant information on sampling line losses can be found in literature |4,5,6,7|.

3.2. Theoretical

Aerosol penetration P (defined as the ratio of the number concentration leaving to that entering the leak path) is given by |4|

$$- \ln P = v \frac{S}{q} \qquad (1)$$

where v = aerosol deposition velocity
S = surface area available for deposition
q = flow rate through the leak

In (1) it is assumed that flow is turbulent which is reasonable for leaking cracks in concrete as shown above.

A number of deposition mechanisms in leaks has to be considered, each with its typical deposition velocity. Table II summarizes the relations for v and P.

TABLE II

Aerosol Deposition Processes in Leaks [a]

deposition mechanism	deposition velocity	penetration exponent (- lnP)	Eq.
diffusion	$v_d = \frac{D}{\delta_d}$	$\frac{D}{\delta_d}\frac{S}{q}$	(2)
thermophoresis	$v_{th} = \alpha \frac{\Delta T}{\delta_{th}}$	$\frac{\alpha}{\lambda_g}\frac{Q}{q}$	(3)
electrophoresis	$v_e = \frac{\mu_e q_e}{2\varepsilon S_e}$	$\frac{\mu_e q_e}{2\varepsilon S_e}\frac{S}{q}$	(4)
diffusiophoresis	$v_{dp} = \frac{D_2}{p_1}\nabla p_2$	$\frac{D_2}{p_1}\nabla p_2\frac{S}{q}$	(5)
gravitational settling	$v_s = \frac{\rho_p g}{18\eta} d^2 F(d)$	$v_s\frac{S_f}{q} = \frac{v_s}{u}\frac{l}{w}$ [b]	(6)
inertial deposition		$A_1\{q^2 d^2 F(d)\}^{B_o}$	(7) [c]

(a) Symbols not explained in text:

$\frac{\Delta T}{\delta_{th}}$ = temperature gradient

λ_g = thermal conductivity

μ_e = electrical mobility

q_e = electrical charge

ε = absolute dielectric constant

S_e = electrically charged surface area

g = gravitational acceleration

η = gas viscosity

(b) For a slit-like path: l = length and w = width.

(c) See text for further explanation and applicability: Eq.(11).

Very small particles ($\lesssim$ 0.1 µm) and vapour molecules are transported to the leak walls by *diffusion*. The boundary layer thickness δ_d at the walls of the leak path depends on Re-number and on the particle's diffusion coefficient D in a complicated way. Recent work shows progress in describing diffusive deposition in a mechanistic way |8|. Usually, diffusive deposition is of minor importance because it is only efficient for very small particles which carry negligible mass.

Thermophoretic deposition due to an aerosol warmer than the walls of the leak can be related to the heat power Q transferred to the cold walls of the leak (Eq.(3); for derivation cf |9|). It can be shown |10| that $\alpha.\lambda_g^{-1} = 0.3\ cm^3.J^{-1}$ for air, independent of temperature and particle size (for d $\gtrsim$ 0.5 µm). Rough calculations indicate that thermophoresis is relatively unimportant in removal of particles in leak paths.

Aerosol particles can be deposited by *electrophoresis* in electrical fields arising due to charges at the particles or at the walls (or both) |10|.
Due to the relatively high radiation fields under post-accident conditions the particles will be at Boltzmann charge equilibrium and only low charging of walls is to be expected.

Gravitational settling removes particles to all upward facing walls (S_f = surface area of the horizontal projection of these walls) and becomes increasingly important for larger particle diameter (d) and for lower flow rates q. Eq. (6) (cf Table II) describes the penetration through a leak of an aerosol undergoing gravitational settling. For a leak (a horizontal crack) of length ℓ = 1 m, width w = 0.1 mm and average flow velocity $\bar{u} = 1\ m.s^{-1}$ one obtains P-values of 0.7, 0.3, and 4×10^{-4} for particle diameters of 1 µm, 2 µm and 5 µm, resp. Another typical feature of gravitational removal is the increase of P with q. Consequently, knowledge of q and d of the leaking aerosol is of great importance for introduction of gravitational settling in leaks. Assuming particle size to be governed by water-vapour condensation in the post-meltdown LWR containment (after 4 hours about 350 kg of water will be present in the containment |11|) particle sizes of about 5 µm result which leads to several orders of magnitude retention in leak paths.

Diffusiophoretic deposition in leaks is particle removal due to water vapour condensing onto cold leak path surfaces. Diffusiophoresis depends (Eq.(5)) on the diffusion coefficient of water-vapour D_2, on total vapour pressure of the aerosol system, and on the vapour gradient ∇p_2. The underlying theory of Stetter is dealt with in |10|. Deposition fluxes due to diffusiophoresis in cracks are roughly 10 x larger than those due to gravitational settling of 5 µm particles ($D_2 = 0.1\ cm^2.s^{-1}$; $p_1 = 100$ kPa; $\nabla p_2 = 1\ MPa.cm^{-1}$), which means an extremely small chance of penetration ($\ln P_{dp} \approx 20 \ln P_s$).

Inertial deposition is likely to be the most important removal process of aerosols in leak paths. The main problems of a good description of this process arise from the coupling between its deposition velocity and the gas velocities inside leaks. Theoretical treatment is also limited |7,12,13|. Agarwal's experimental results |7|, however, are useful.

According to Agarwal we define the parameters V_+ (dimensionless deposition velocity) and τ_+ (dimensionless relaxation time) as follows

$$V_+ = \frac{v}{u_*} \tag{8}$$

where u_* = friction velocity, and

$$\tau_+ = \frac{\tau \rho_g u_*^2}{\eta} \tag{9}$$

where τ = particle relaxation time

ρ_g = gas density

η = gas viscosity

Agarwal [7] has observed that there are two regions (cf fig. 4):

- for $\tau_+ \lesssim 10$, V_+ depends on τ_+ and wall roughness, though for roughnesses with elements > 100 μm this dependence on roughness vanishes (line marked "rough" in fig. 4). The latter condition may be assumed to be met in case of concrete cracks. We assume a power function relation (analogously with smooth channels).

$$V_+ = A_o (\tau_+)^{B_o} \tag{10}$$

Then the penetration under conditions of inertial deposition is governed by

$$-\ln P = A_1 \{q^2 d^2 F(d)\}^{B_o} \tag{11}$$

F(d), the Stokes-Cunningham correction factor, is virtually unity for $d \gtrsim 1$ μm.

- for the high τ_+ region ($\tau_+ \gtrsim 20$), $V_+ = 0.1$. Hence, one may easily derive

$$-\ln P = A_2 \tag{12}$$

In this high τ_+-region P values are exceptionally low. As a rule, however, τ_+ values in leak paths are smaller than 0.1; hence, (11) should be valid there.

3.3. Results and discussions

Penetration measurements were performed on CCCs and GBCs (1 mm bead diameter) in a test rig as shown schematically in fig. 2. Test aerosols consisted of monodisperse polystyrene spheres of various diameters in air. Concentrations of the 4 different particle sizes used were measured by means of an optical particle counter.

Table III represents typical results of particle penetration through a crack test specimen (No.4).

TABLE III

Aerosol penetration P as a function of particle diameter d for various flow rates q and pressure differences Δp across an artificial crack in concrete test specimen No. 4.

Δp (mbar)	d (μm)	q $cm^3 s^-$	P	$\frac{-\log P}{F^2 d^4}$
30	0.48	145	0.80	1.0
30	0.82	145	0.80	0.15
30	1.1	145	0.5	0.15
30	2.0	145	0.11	0.05
60	0.48	250	0.75	1.3
60	0.82	250	0.6	0.34
60	1.1	250	0.2	0.35
60	2.0	250	0.008	0.11
90	0.48	350	0.65	2.0
90	0.82	350	0.45	0.53
90	1.1	350	0.07	0.58
90	2.0	350	0.005	0.12

Generally, penetration is observed to decrease with larger flow rates and with larger particle sizes which is an indication that inertial deposition is the domination process. Therefore, the measuring data were interpreted using Eq.(11). The last column of Table III shows that penetration P of 0.82 μm and 1.1 μm spheres follows Eq.(11) closely. Fine particles (0.48 μm) penetrate less than predicted which could be due to an additional deposition process (probably diffusion deposition, see below). The higher P-values of 2.0 μm spheres could be a measuring artefact or deviations from Agarwal's model in the range of large particle relaxation times.

Another series of measurements has been carried out on a crack with variable width ("0" mm - 0.25 mm). Fig. 5 shows the penetrations P of monodisperse particles for various crack width settings. Analyzing the dependence of P on particle size d, one finds lnP proportional to $d^4F^2(d)$ which is displayed by fig. 6 (also for the previously mentioned specimen No.4). The same relation has been observed by Schwendiman and Postma [4] for a surface-roughened pipe, their exponent to d being 4.26. This means also that $B_o = 2$ in (11). Consequently, lnP should be proportional to q^4. This, however, was not observed; assuming lnP proportional to $d^4F^2(d)$, the exponent to q ranges from 1.8 to 2.6. We conclude that Agarwal's results, being the underlying basis for our analysis, are not uniquely related to q (or in fact u_*) which is also reflected in the scatter in Agarwal's data. For a certain CCC the d- and q-dependence of P is given by

$$-\ln P = 2.8(\pm 1.7) \times 10^{-3} q^{1.8\pm0.07} d^4 F^2(d) \qquad (13)$$

Penetration of spherical particles through a crack-simulating glass bead column (GBC) showed a similar proportionality to $d^4F^2(d)$. However, lnP appeared to be proportional to $q^{2.9}$ which again violates Eq.(11) and indicates the ambiguity of Agarwal's inertial deposition data once again.

The above-given analysis of the oservations concerns the regime of higher flow rates. In the low flow rate regime ($< 10\ cm^3.s^{-1}$) both GBC and CCC have penetration lower than extrapolated from the high flow rate regime giving evidence of a removal mechanism additional to inertial deposition. In some cases, penetration even shows a maximum (fig. 7) which means that this additional process removes particles with a deposition velocity independent or only slightly dependent on flow rate (cf. Eq.(1)). This is essentially different from inertial deposition. The data in this region were evaluated in view of a possible role of sedimentation using Eq. (6) in table II. The data could be explained fairly well when deposition surface areas S_{dep} were assumed to be 200 cm^2 and 1700 cm^2 for CCC and GBC, resp. In case of the GBC this compares fairly well with a calculated horizontally projected surface area of 2500 cm^2. The CCC with dimensions of 45 mm x 290 mm (131 cm^2) has been investigated in a vertical position. Consequently the orientation of a crack in concrete does not influence the sedimentation surface area significantly. This is not an unreasonable observation. Deposition surface areas for smaller particles of 0.5 µm appeared to be factors larger which could indicate an additional removal by diffusion.

4. CONCLUDING REMARKS

1. Inertial deposition in the high flow rate regime and sedimentation in the low flow rate regime explain the experimental observations on aerosol penetration through an artificial crack in concrete:
2. The sedimentation surface area of a crack in concrete is roughly equal to the smoothened surface area independent of its orientation.
3. The presence of large amounts of water vapour in the LWR-containment after a core-meltdown could result in important removal by diffusiophoretic deposition in leaking cracks in concrete containment walls.
4. Fission product particles grown to several µm sizes due to water vapour condensation can hardly penetrate through cracks in concrete due the highly efficient removal process of inertial deposition.
5. The importance of high humidity and slight condensational particle growth mentioned above, has to be proven experimentally by a separate effects test.
6. There is urgent need of definition of leaks as they will be present in containment walls under accident conditions. Basic requirements for further progress in the field of aerosol leakage are estimates of:
   - leak dimensions: width, breadth and roughness,
   - linear velocity in the leak.

   It would be useful when concrete panels failed in realistic mechanical load tests could be made available for aerosol penetration experiments.

REFERENCES

1. S. Nair, The Influence of Source Term Characteristics on Off-site Consequences, and Priorities for Future Research (OECD/NEA-CSNI document, February 1984) SINDOC (83)93.

2. R.L. Koontz, et al, Conventional Buildings for Reactor Containment, NAA-SR-10100 (1965).

3. D.B. Ingham, J. Aerosol Sci. 12 (1981), 541.

4. L.C. Schwendiman and A.K. Postma, Proc. AEC Sixth Air Cleaning Conf. TID-7627, (October 1981), 127.

5. B.Y.H. Liu and T.A. Ilori, Envir. Sci. Technol. 8, 351 (1974).

6. S.K. Friedlander and H.F. Johnstone, Ind. Eng. Chem. 49, 1151 (1957).

7. J.K. Agarwal, Aerosol Sampling and Transport, Thesis Univ. Minneapolis, Minn., USA (1975), Particle Technology Laboratory Publication No. 265.

8. K.W. Lee and J.A. Gieseke, Atm. Envir. 14 (1980), 1080.

9. J.F. van de Vate, in Fast Reactor Programme Annual Progress Report 1980 (Compil. J.C. Plakman), ECN-115 (1982).

10. J.F. van de Vate, Investigations into the dynamics of aerosols in enclosures as used for air pollution studies, Thesis of the Agricultural University of Wageningen, 1980, also published as ECN-86.

11. J.E. Speelman (ECN), private communication (1983).

12. M.S. El-Shoboksky and I.A. Ismail, Atm. Envir. 14 297 (1980).

13. L.W.B. Browne, Atm. Envir. 8, 801 (1974).

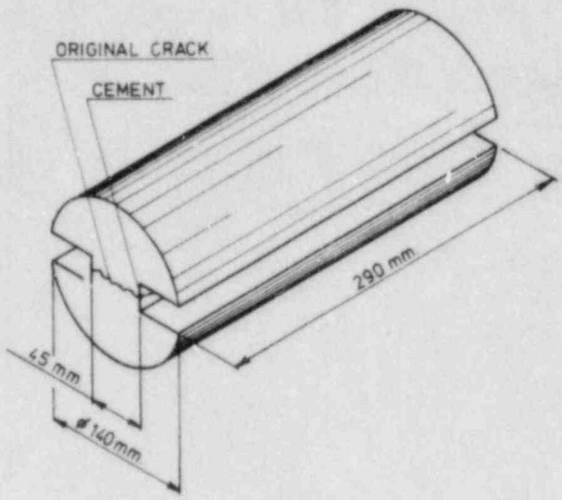

Figure 1. Schematic Drawing of an Artificially Introduced Crack in a Concrete Cylinder

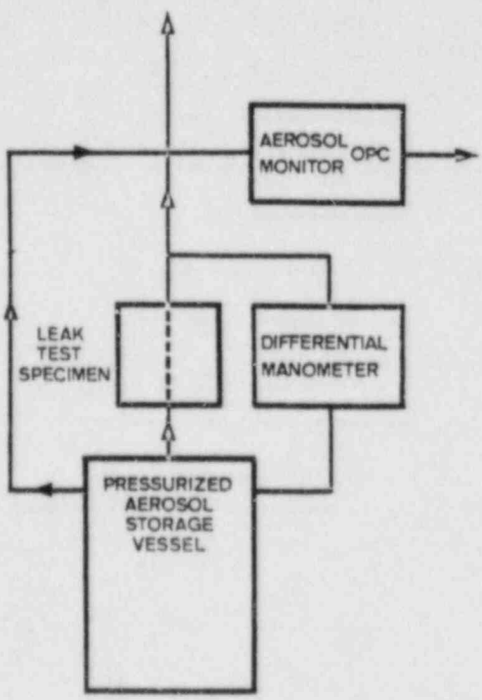

Figure 2. Experimental Rig for Measurement of Leak Flow Rate and Aerosol Penetration Through Concrete Test Specimens

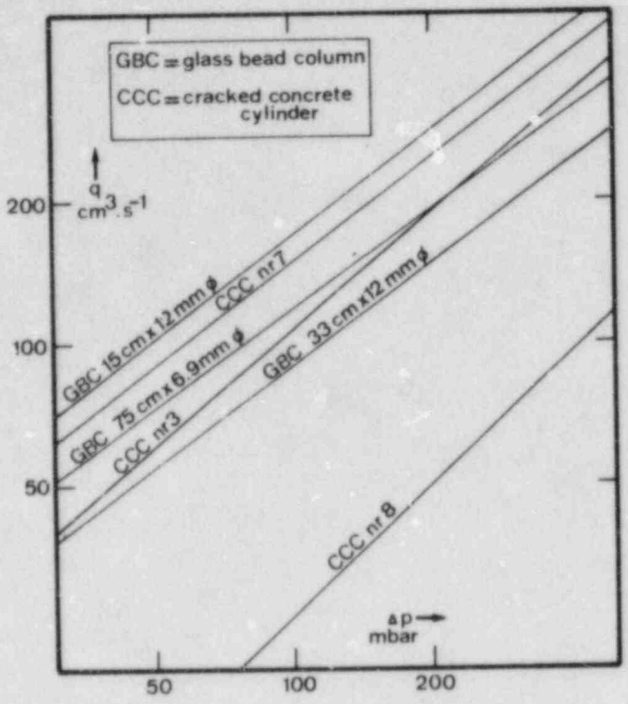

Figure 3. Flow Rates q Through Various Leak Test Specimens as a Function of Pressure Drop Δp

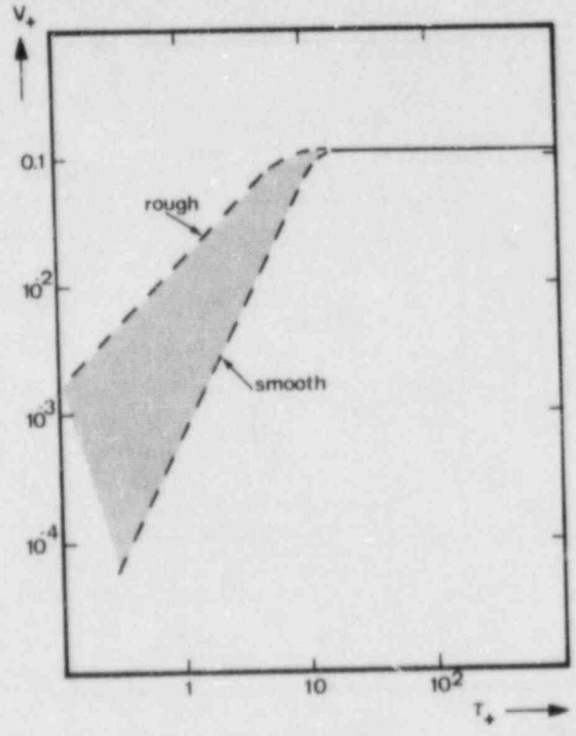

Figure 4. Dimensionless Particle Deposition Rate (V_+) in Tubes with Inner-Walls of Various Roughness. The line "rough" indicates upper V_+-values for roughness > 200 μm. τ_+ is the dimensionless particle relaxation time.

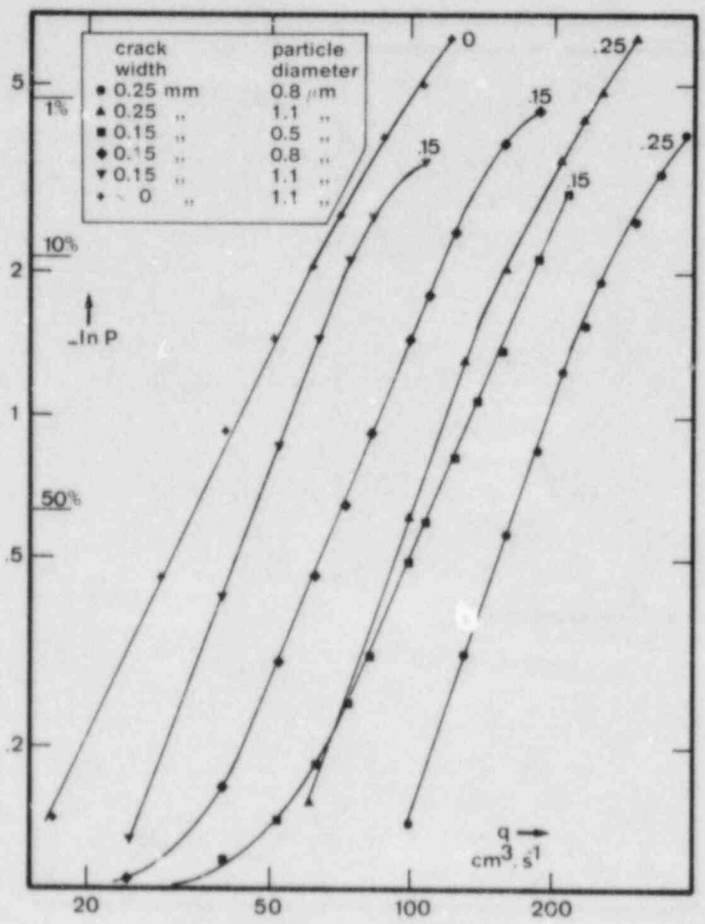

Figure 5. Penetration P as a Function of Flow Rate q of Monodisperse Polystyrene Spheres Through an Artificial Crack in Concrete Cylinder. Crack width variable between "0" mm and 0.25 mm.

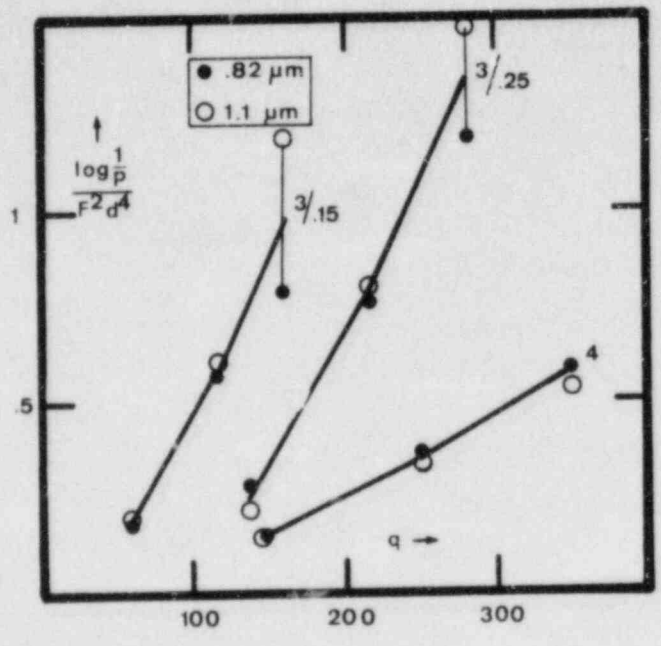

Figure 6. Penetration P as a Function of Flow Rate q ($cm^3\ s^{-1}$) of Polystyrene Spheres (0.82 μm and 1.1 μm) Through Three Different Concrete Specimens with a Crack

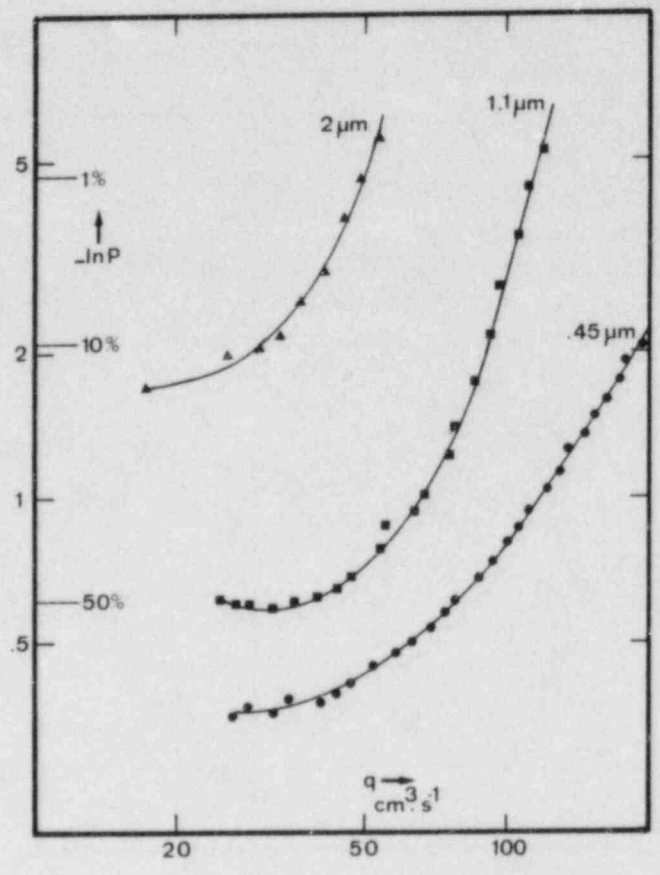

Figure 7. Penetration P of Monodisperse Spheres Through a Glass Bead Column (35 cm x 12 mm ϕ; 1 mm ϕ beads) as a Function of Flow Rate q

STRUCTURAL ASPECTS OF LEAKAGE IN REINFORCED CONCRETE CONTAINMENTS--EXPERIMENTAL APPROACH

Piotr D. Moncarz and John D. Osteraas
Failure Analysis Associates
2225 East Bayshore Road
Palo Alto, CA

ABSTRACT

Containment leakage is largely a function of concrete cracking and liner rupturing, phenomena difficult to predict analytically. Experimental studies are under way that address the various aspects of containment integrity. This paper proposes a methodology for accumulating experimental results for development of analytical techniques to predict leakage through cracked concrete walls. Emphasis is on the need to closely coordinate experimental structural research with the goal of developing techniques to analytically predict flow intensity through containment walls. A parameter set describing aspects of a single crack related to leakage is presented. The relationship between crack parameters and leakage rates is discussed. Extrapolation of scale-model results to prototype domain requires adequate experimental data upon which to calibrate model results. An experimental approach utilizing parametric studies of full-size and scale-model subassemblies in addition to current studies is proposed. A suitable experimental data base utilizing results from current independent research activities would allow the development of empirical or theoretical leakage prediction models.

INTRODUCTION

The main purpose of a containment structure in a nuclear power plant is to protect the environment from an uncontrolled release of radioactive material during an accidental internal build-up of pressure and temperature. This requires that the structural integrity of the containment be preserved and the rate of leakage minimized, even under major accident conditions. The safety margin of a containment structure can be defined only by evaluating these two performance criteria simultaneously. The containment integrity study by the U.S. Nuclear Regulatory Commission (NRC), carried out mainly at Sandia National Laboratories, Albuquerque, and a research program sponsored by the Electric Power Research Institute (EPRI) provide milestones in the integrated assessment of containment integrity.

The authors participated in the Sandia study, developing guidelines for experimental modeling of a reinforced concrete containment structure with a steel liner [1]. In that study it was recognized that leak-tightness of a containment structure subjected to high post-elastic stress levels is poorly

understood. Any development of acceptable theoretical approaches to the problem is impeded by the lack of experimental data providing physical understanding of leakage development in reinforced concrete structures with steel liners.

Two basic conditions are needed to allow through-wall leakage from the containment to the outside environment: rupture of the containment liner and sufficient permeability due to cracking of the concrete wall in the vicinity of the liner crack. Therefore, to assess the leak integrity of a containment structure one must determine both the extent of liner and concrete cracking and the amount of leakage through the damaged wall. Once these determinations have been fully integrated, structural leakage rates can be assessed at different pressure levels. This paper emphasizes methodology for accumulating information necessary to develop the means for determining leakage through damaged concrete walls.

An integrated process of stress analysis and leakage analysis is presented schematically in Figure 1. The stress analysis can utilize any available technique, such as closed form solutions by the classical shell theory or the finite element method. The results provide information on stresses and displacements (line A in Figure 1) and, with nonlinear analysis, on crack extent in the concrete. In an advanced level of analysis, probabilistic strength of materials can be used to determine the crack distribution and extent of cracking (line B). This is particularly true when rupture of the liner is to be determined, as localized flaws will affect the location and the stress level at which the cracking will start. The crack probability model and the analytical prediction of concrete and liner cracking are closely tied to the available experimental results (lines C and D). As a result of this evaluation, concrete crack parameters become available (line E). In order to determine the extent of leakage, relation between crack parameters and leakage intensity must be understood. The data for development of such information could be obtained from ongoing research and from proposed parametric research studies (line F). The crack parameter-leakage relationship (line G), combined with concrete crack parameters (line E), will allow the prediction of leakage (line H).

Some of the needed experimental data can be obtained from full-scale subassembly tests; however, due to technical and economical restrictions, the majority of studies have to be performed on scale models. Correlation between the results obtained from studies with prototype-size specimens and model-size specimens has to be developed to allow the full comparison of data obtained from specimens of different scales. Figure 2 presents this process schematically. The need for coordination and exchange between full-scale studies and model-scale studies is clearly shown in this figure.

CRACKING OF CONCRETE

To predict leakage through structural cracks in concrete, a quantitative description of the crack that develops under imposed stresses is required. A refined understanding of crack development in reinforced concrete allows containment strength assessment and description of crack parameters necessary to predict leakage.

There is significant interaction between the steel liner and the containment wall, for both strength and leakage. However, this discussion addresses conditions in which the flow rate is controlled by the wall crack and not by the liner crack. Development of cracks in concrete precedes rupture of the liner; thus, for a given concrete crack pattern, a localized liner rupture may be superimposed on the crack pattern to predict integrated leakage.

Crack Parameters

The basic geometric characteristics of a through-wall crack are presented in Figure 3. The crack geometry is described by wall thickness, by crack length and width on both sides of the wall, and by surface characteristics of the crack wall surfaces, defined here as roughness. The dimensions of the crack are determined by the stress field causing the cracking. The roughness of the crack will depend mainly on the hardness and brittleness of the cement paste and the aggregate. The reinforcement crossing the crack can significantly decrease the area available to flow and cause major localized flow disturbances.

These crack parameters are controlled by the following quantifiable factors:

- Stress Field. The direction of cracking is controlled by the overall stress field and will vary with the components of tension, compression, bending, and shear present in the stress field. In addition, interaction with the liner will generate local stresses in both the concrete and the liner that vary with liner stiffness and anchorage details. In a typical containment, different force components predominate at various locations--biaxial tension in the cylindrical wall, tension and bending at the spring line, and bending and shear at the base. The relative thickness of the concrete elements results in a triaxial stress state throughout the structure.

- Concrete Strength. For a given stress field, crack size and spacing are a function of concrete strength parameters, including compressive and tensile strengths. A component of concrete strength--aggregate type and strength--affects the roughness of the crack surface.

- Reinforcement. Relationship between crack size and reinforcing parameters depends on concrete cover, bar size, bar

spacing, material stress-strain behavior, and bond. The influence of these factors on crack development is well documented for beams, and cracking behavior of beams may be predicted rationally. Available empirical methods are applicable only for a limited range of concrete and reinforcement properties and do not extrapolate, without correction, to scale model conditions.

Scale Effects

The necessity of conducting experimental studies with reduced scale models introduces additional variables to the test. Modeling experience has shown that, even when the utmost effort is made to follow similitude laws, reduced-scale reinforced concrete models tend to have fewer (and for fixed displacement, presumably wider) cracks than the prototype structure. Thus, as shown in Figure 2, crack parameters and leakage data developed from scale models must be calibrated to full-scale response. Although limited work has been done, the relationship between a model and full-scale crack parameters is not yet available.

Limited data is available for the relationship between crack spacing (or number of cracks) and model scale [2]. The data of five different researchers, all modeling the same prototype structure but at different scales, are presented in Figure 4 to indicate the relationship between the number of cracks and model scale. These data reflect the cracking of a boundary element in a shear wall subjected to bending and shear. The data are based on a single structural configuration and loading. As such, the data are useful as a trend indicator but inadequate for calibration purposes.

Virtually no data are available on the relationship between crack opening and scale. Assuming a similitude in displacement scaling, fewer cracks in the model dictate that they will be proportionately wider than in the prototype.

Experimental Crack Investigation

Scale effects on containment cracking may be quantified experimentally through a series of subassembly tests at full and reduced scales. At a minimum, the test program should include subassembly tests at the scale of the Sandia model (utilizing similar construction techniques) and full-scale components. Testing of additional subassemblies at other scales would yield more reliable results with more general applicability.

The scale modeling program at Sandia and the subassembly test program sponsored by EPRI offer great potential for generating complementary data. Integration of results, however, requires development of a calibration test program that will establish the correspondence between full- and reduced-scale results.

Experimental data collection should include provisions for the systematic monitoring of crack type, location, length, and width. Most past studies have mapped the location of surface cracks but failed to provide useful data on other crack parameters. Past model studies have largely been concerned with structural strength and displacement response. Various studies have shown that, while the crack response may differ significantly, strength and displacement responses generally correlate well with full-scale response. Thus, the cracking patterns have been used almost exclusively for qualitative evaluation of stress distribution and structural response. Development of new techniques for measuring and recording crack parameters in the course of testing would greatly facilitate systematic data collection.

LEAKAGE THROUGH CRACKED CONCRETE

The knowledge of crack field and crack parameters is essential to the prediction of leak rate through the crack network. However, lack of readily available relationships between the crack, the fluid parameters, and the leak rate creates a major barrier in determining the leak-tightness (integrity) of the structure. The development of such relationships is dependent upon a better understanding of dynamic flow through thick wall cracks, and of the influence of other crack characteristics on the flow. Such data can be obtained from ongoing experimental research projects and from a proposed series of independent scale studies on subassemblies.

Flow Through Cracks

First-order estimates show that, for feasible structural cracks, the leakage flow through the crack can be described by continuous flow. When the containment pressure is greater than about 30 psi (2 Atm), a choked flow condition occurs at the minimum cross sectional area of the crack. Any further rise in the containment pressure will not alter the flow rate if the crack geometry stays fixed. Flow through smooth cracks of less than 0.004 in (0.1 mm) in width can be laminar and, hence, exhibit a strong dependence on the Reynolds number which depends on the crack width. Cracks in the containment wall have to be substantially large to result in linear rupture. Thus, flow through cracks in the containment wall will be turbulent, and the Reynolds member dependence would be weak. This observation, together with the sonic flow condition at the crack throat section, enables accurate calculation of the leakage flow rate for idealized fluid and cracks.

The above discussion assumes a noncondensing gas as the fluid. If condensing fluids such as steam are considered, the flow through the crack will result in condensation and evaporation which can significantly influence the flow rate. Flow through a thick-wall, complex crack geometry can practically be determined only experimentally. Comparison of test results obtained at different specimen scales and with various gases

requires a parametric study which would provide basic understanding of flow phenomena under these conditions.

Characterization of Leakage Through Crack

The correlation of crack patterns in different samples is impractical. Therefore, this paper proposes study on a single crack for which all the necessary parameters can be identified. In the calibration of results obtained at different scales, the assumption will have to be made that only the geometric parameters of the crack will be influenced by the specimen scale.

To provide a meaningful coordination between various experimental efforts, the most significant parameters characterizing the flow should be identified. Subsequently, dimensional analysis could be used to establish a functional relationship between the leak rate, crack, and fluid characteristics. The attempt is to provide a set of independent dimensionless products (π-factors) characterizing the problem. The number of such products equals the total number of physical quantities involved in the problem minus the number of fundamental quantities needed to describe the dimensions of all physical quantities. The number of physical quantities considered in a study determines the extent of physical measurements required during the test. Thus, only the most significant quantities should be considered in order to minimize the experimental effort. As the π-factors are dimensionless, theoretically they should remain independent of scale factors and thus allow comparison of experimental results obtained at different specimen scales.

The rate of flow q through the crack shown in Figure 3 can be characterized by the following set of parameters:

$$q = f(p, \gamma, d, R, \rho; a_i, a_o, t_i, t_o) \qquad (1)$$

where

q = leak rate measured as mass of fluid flow per unit of time

p = internal pressure

γ = fluid density at the given internal pressure

d = wall thickness

R = crack roughness coefficient; a constant characteristic to a particular stress condition (shear or tensile) and the properties of the concrete mix ((f'_c/f'_t) ratio, aggregate strength)

ρ = reinforcement ratio for reinforcement crossing the crack; this parameter defines the degree of obstruction the reinforcement bars can provide to the flow through the crack.

a_i, a_o = inside and outside crack length

t_i, t_o = inside and outside crack width

It could be convenient to represent the two last parameter couples by different parameters, namely

$$A = \frac{a_i}{a_o} \qquad B = \frac{t_i}{t_o} \tag{2}$$

To define the dimensionless π-factors, a dimensional matrix can be written using mass (M), length (L), and time (T) as basic units [3,4].

	q	p,	γ,	d,	R,	ρ;	a_i,	t_i,	A,	B
M	1	1	1	0	0	0	0	0	0	0
L	1	1	-3	1	0	0	1	0	0	0
T	-3	-2	0	0	0	0	0	1	0	0

(3)

The rank of the matrix equals 3, and thus 10-3 = 7 independent dimensionless products can be assembled. One possible set of products is presented below.

$$q\sqrt{\frac{\gamma}{p^3}}\,d^2 = F\left(R,\ \rho,\ \frac{t_i}{d},\ \frac{a_i}{d},\ A,\ B\right) \tag{4}$$

Numerous simplifications could be introduced to this functional relationship by determining a priori some of the terms having insignificant influence on the test results. Such could, for instance, be the case with roughness coefficient R for sufficiently wide cracks. The tests could assume cracks of constant length and constant width through the wall, thereby eliminating A and B, and replacing t_i and a_i by constant crack width t and constant crack length a.

Experimental Study of Leakage Through Cracks

The nondimensional functional relationship of Eq. 4 provides basic information necessary to plan a parametric study of leakage through cracked walls. Figure 5 shows how such a study, performed on simple precracked specimens, can provide information on crack parameter and pressure vs. leakage rate.

Variation in the crack parameters can be achieved by controlled specimen cracking, as shown schematically in Figure 6a. Methods of specimen precracking used in shear studies can be found in Ref. [5] to [7]. Under this setup, the same specimens could be used to investigate the effect of progressively widening cracks. The effect of the ratio of crack length to the thickness (a/d) can be studied by testing specimens of different width a. Monitoring of the flow rate and pressure in the chamber provides, together with the crack parameters, a complete set of terms presented by Equation 4.

CONCLUSIONS

Substantial improvement of analytical models for predicting crack development under internal pressure will result from ongoing scale model and prototype experimental studies. The model response distortion introduced by scale effects can be determined comparing prototype-size subassemblies results with results obtained from their scale models. The scale factors obtained from such a comparison could be then applied to all the other scale model results.

To assess the leak integrity of the structure, leak rate through an individual crack could be predicted as a function of given crack parameters. Such a prediction relationship can be developed by utilizing results from ongoing studies and accumulating results from proposed parametric studies relating crack geometric characteristics to leak rate. This empirical data will lead to development of crack parameter-prediction relationships. These relationships can be utilized to assess the leakage rate from the containment by integrating the leakage over the entire crack field provided by the strength analysis.

ACKNOWLEDGMENTS

The research which led to many of the ideas reported herein is part of the project on Safety Margin of Containments carried out by Sandia National Laboratories under the sponsorship of the Nuclear Regulatory Commission (NRC). The authors are grateful for the financial support of the NRC and Sandia National Laboratories that made this project possible. the continuous cooperation and encouragement of Dr. T. Blejwas and Dr. R. Reese of Sandia National Laboratories is especially acknowledged.

REFERENCES

1. Moncarz, Piotr D., Osteraas, John D., and Curzon, Anne M., "Experimental Modeling Techniques for Reinforced Concrete Containment Structures," Failure Analysis Associates Report No. FaAA-83-11-11, prepared for Sandia National Laboratories, Albuquerque, New Mexico, March 1984.

2. Proceedings of the Fourth Joint Technical Coordinating Committee, U.S.-Japan Cooperative Research Program Utilizing Large Scale Testing Facilities, Tsukaba, Japan, June 1983.

3. Blejwas, Thomas E., Dennis, Albert W., Woodfin, Ronald L., and Von Riesemann, Walter A., "Background Study and Preliminary Plans for a Program on the Safety Margins of Containments," Sandia National Laboratories, Report NUREG/CR-2549, SANMD82-0324, Albuquerque, New Mexico, May 1982.

4. Moncarz, Piotr D. and Krawinkler, Helmut, "Theory and Application of Experimental Model Analysis in Earthquake Engineering," Report No. 50, The John A. Blume Earthquake Engineering Center, Stanford University, Stanford, California, June 1981.

5. Mattock, A. H., Hofbeck, J. F., and Ibrahim, I. O., "Shear Transfer in Reinforced Concrete," ACI Journal, Proceedings, Vol. 66, No. 2, Feb. 1969.

6. Jimenez-Perez, Rafael, Gergely, Peter, and White, Richard N., "Shear Transfer Across Cracks in Reinforced Concrete," Report 78-4, Department of Structural Engineering, Cornell University, Ithaca, New York, Aug. 1978.

7. White, Richard N., Holley, Myle J., "Experimental Studies of Membrane Shear Transfer," Journal of the Structural Division, Proceedings, ASCE, Aug. 1972.

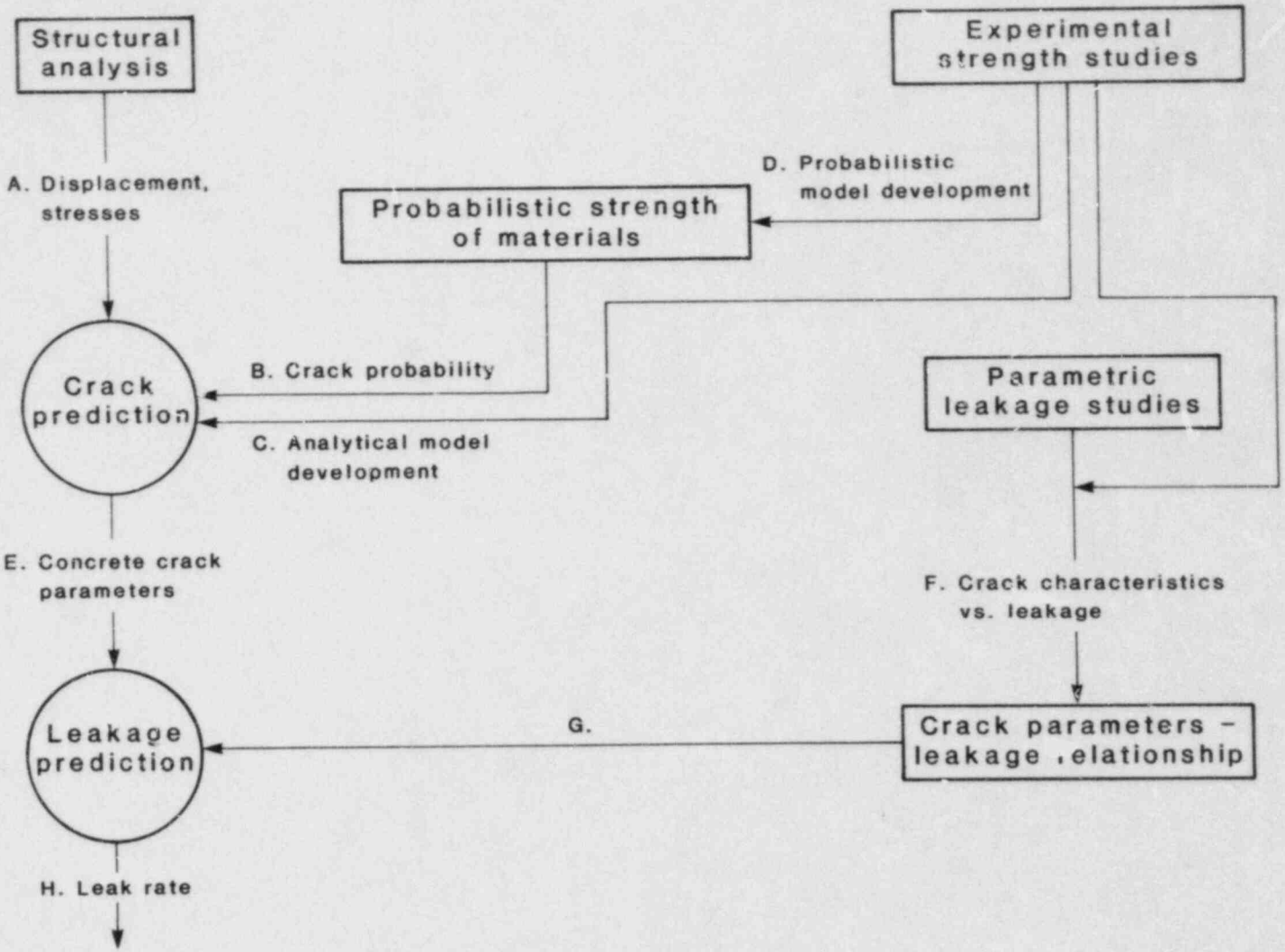

Figure 1. Leakage Rate Prediction Process

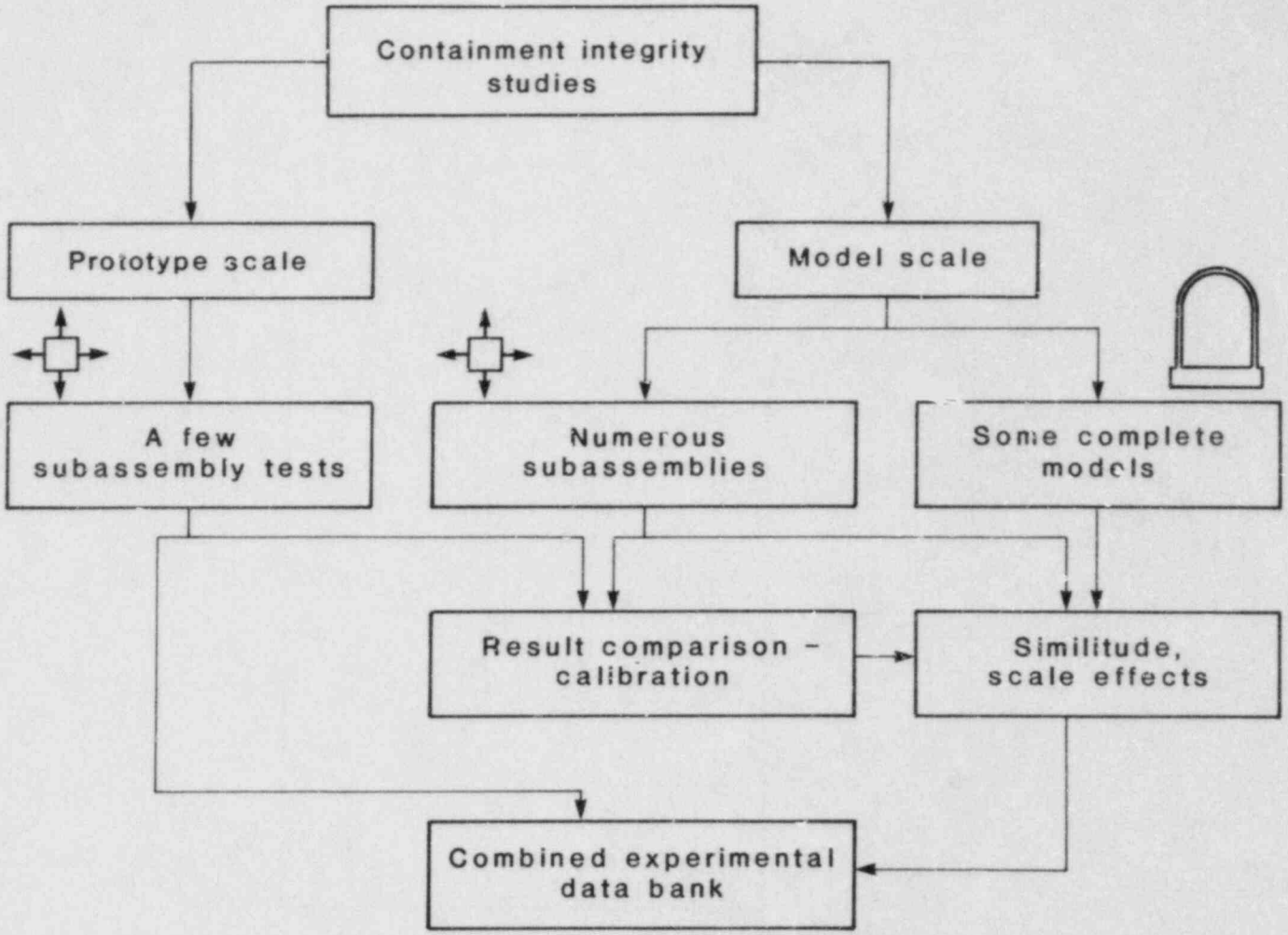

Figure 2. Interaction Between Model Scale and Prototype Scale Experimental Studies

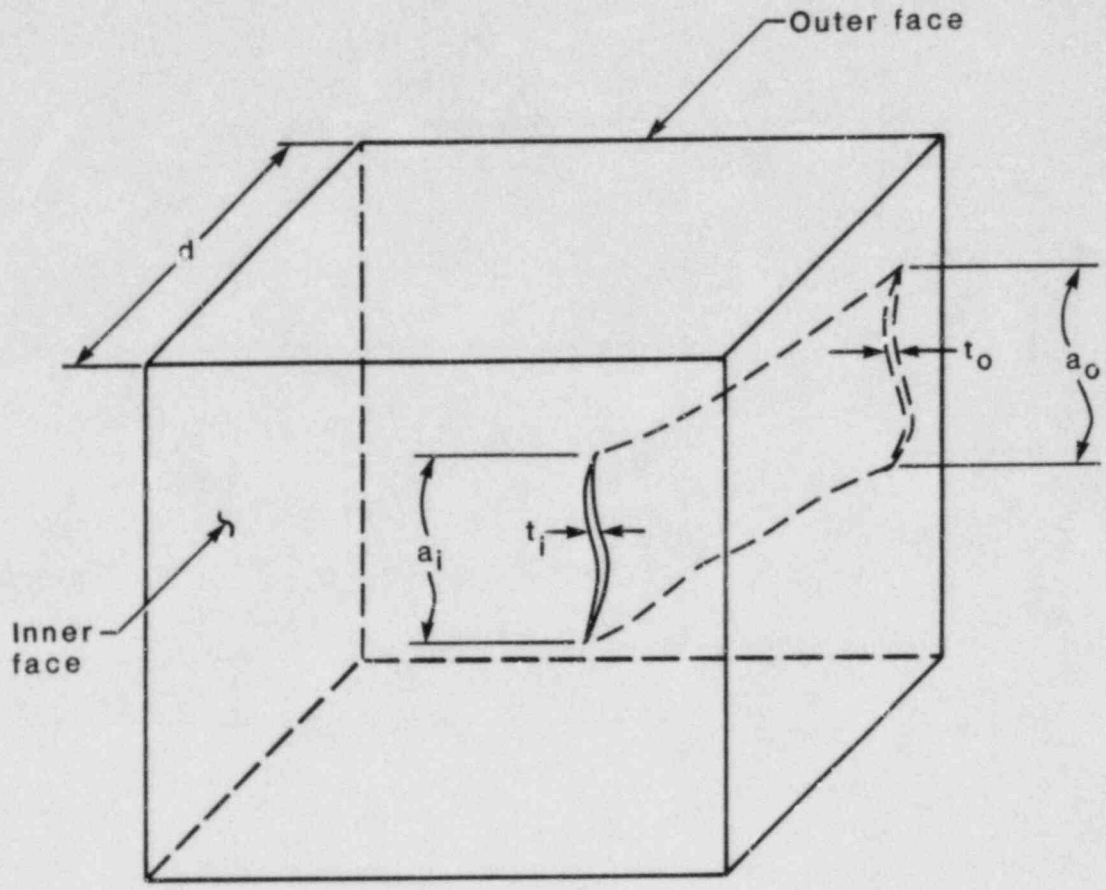

Figure 3. Crack Geometry

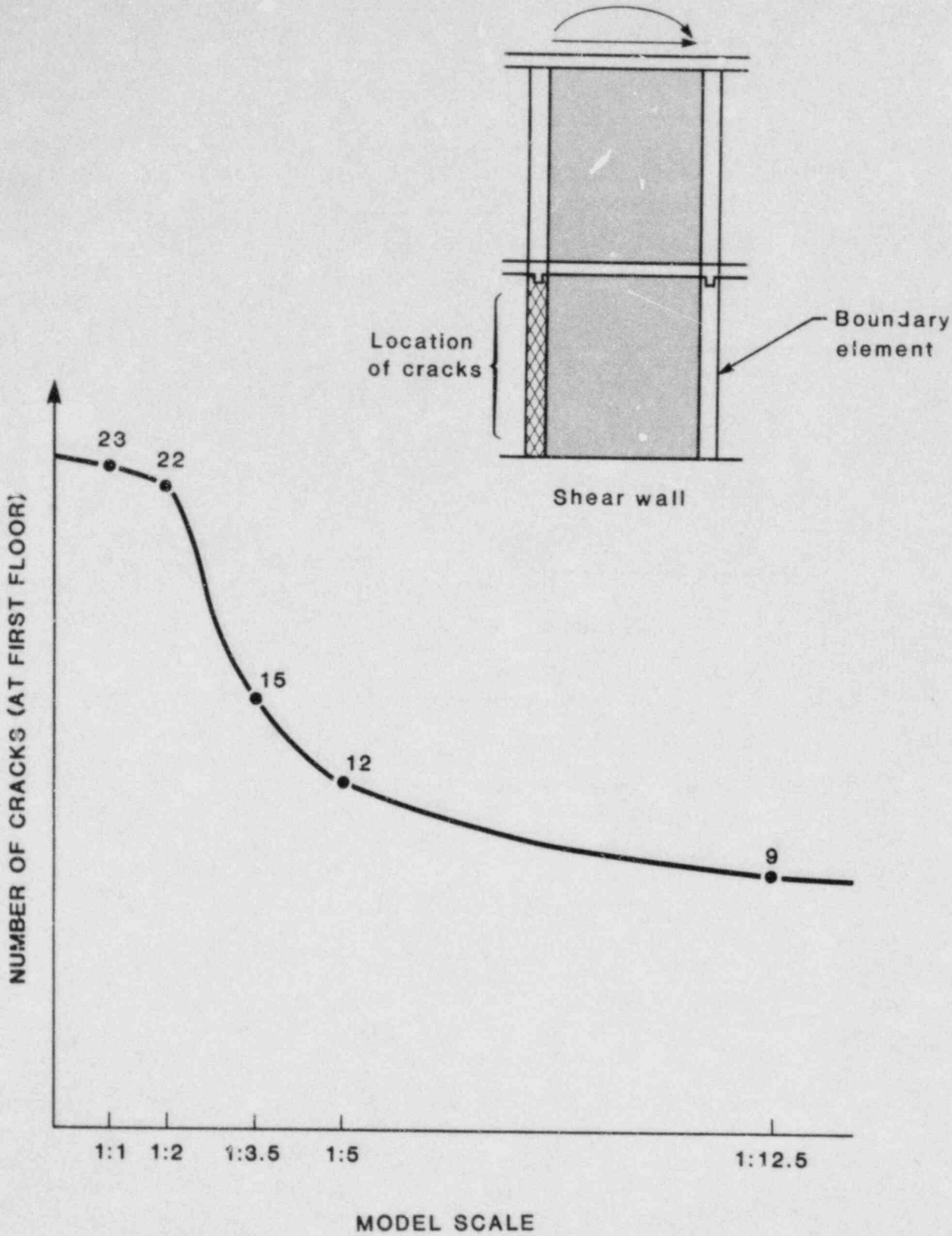

Figure 4. Number of Cracks as a Function of Model Scale

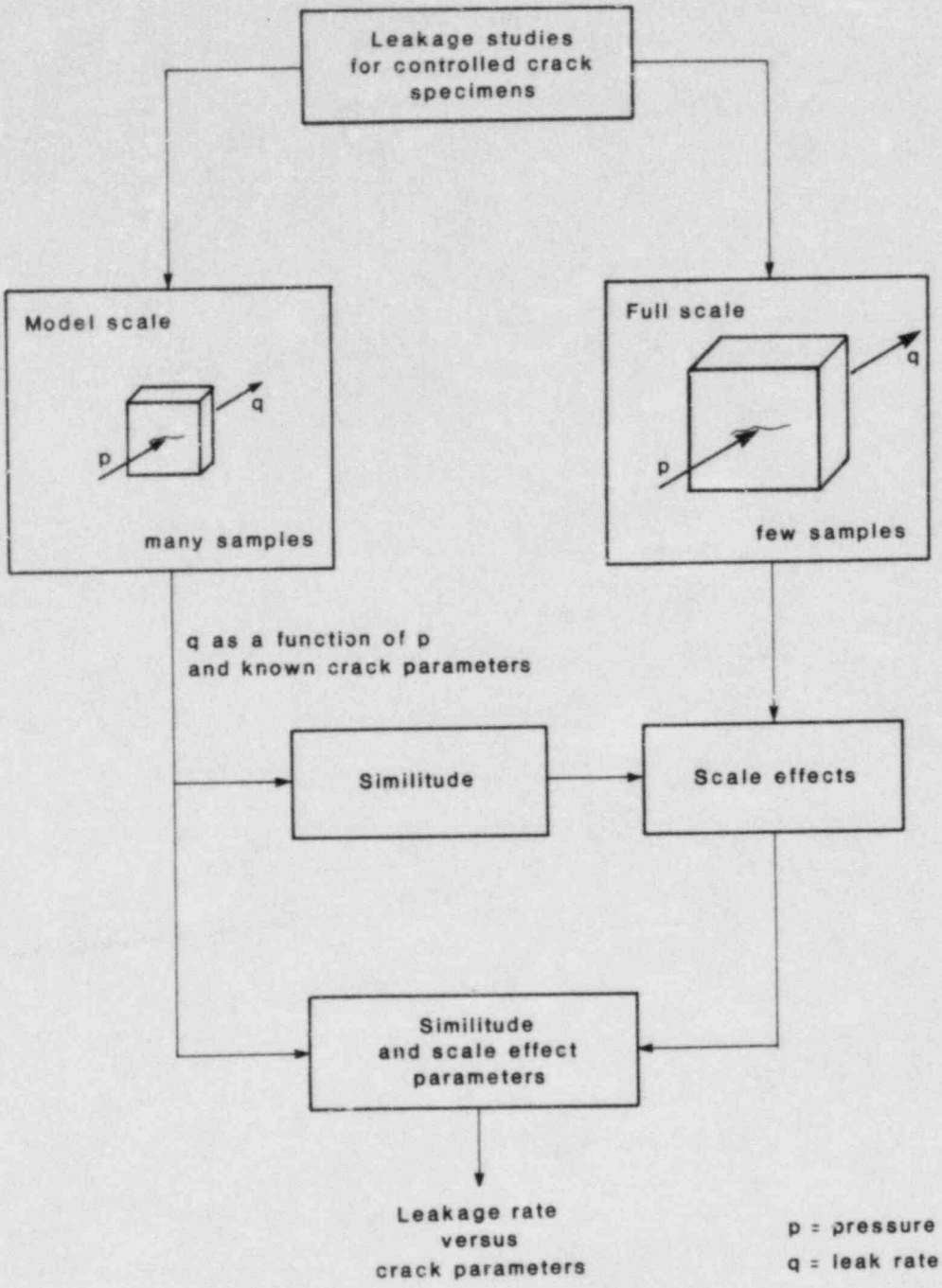

Figure 5. Schematic of Study of Crack Parameter Dependence on Leakage Rate

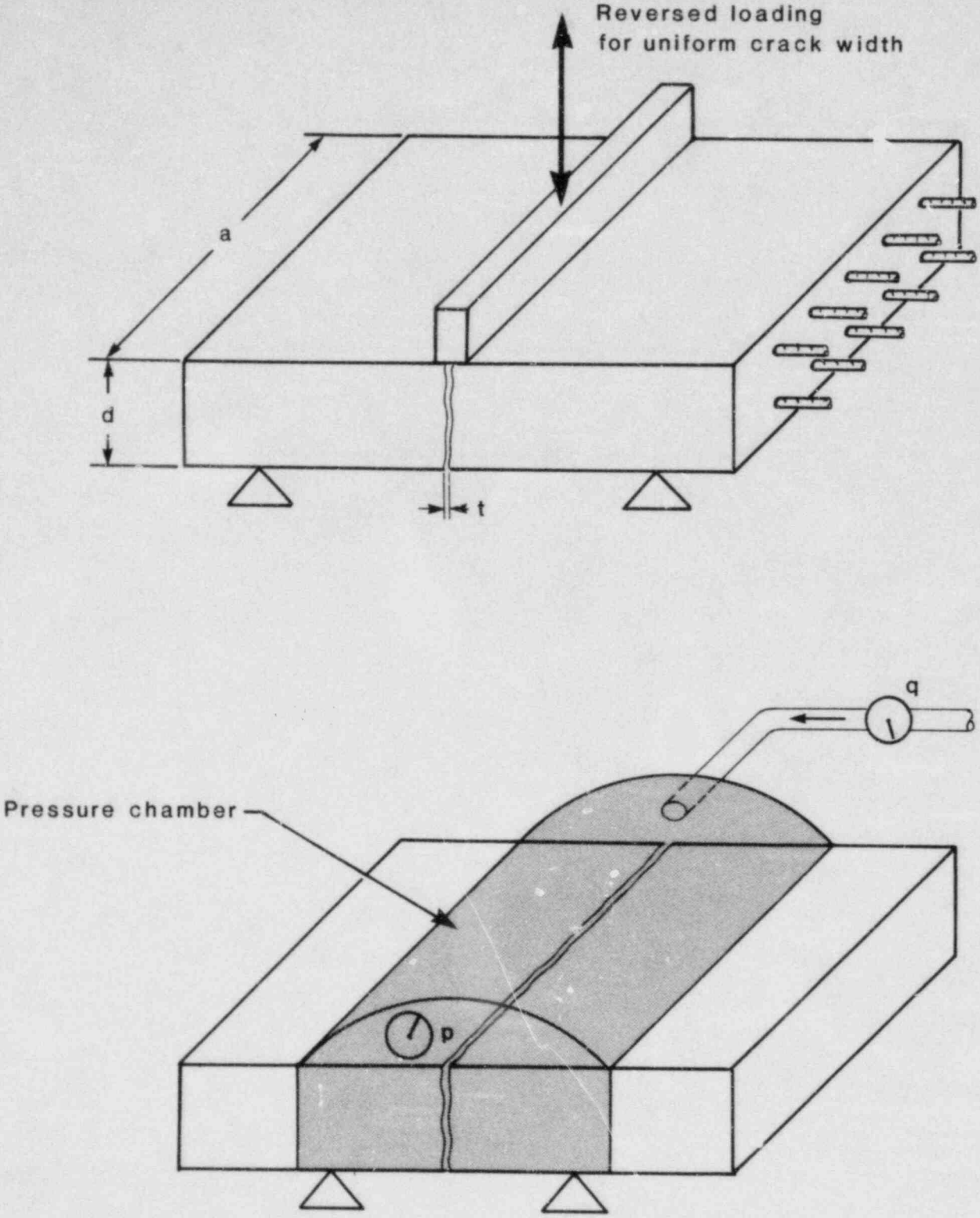

Figure 6. Specimen Precracking and Leakage Measurements
(a) Schematic Representation of Controlled Cracking
(b) Known Crack Versus Leakage Rate

LIMIT LOAD ANALYSIS OF ACTUAL SPHERICAL CONTAINMENTS SUBJECTED TO STATIC INTERNAL PRESSURE AND TEMPERATURE

J. Jeschke
Kraftwerk Union AG - W. Germany
Darmstadt

ABSTRACT

The following report describes potential sources of leakage for a DWR 1300 spherical metal containment (PCV). The critical internal pressure and temperature are given depending on certain influence parameters. Mainly because of the high-ductile material used "leakage-before-failure" seems to be likely.

Introduction

In general containment analysis is based upon linear-elastic behavior, so that the ultimate structural capacity cannot be predicted appropriately. Studying the containment behavior due to increasing internal pressure and temperature we had the following purposes in mind:

- to find the pressure and temperature level (above design) for functional failure.
- to ensure that leakage prior to total failure is likely to happen.
- to obtain the potential sources of leakage and their individual failure mode.
- to determine leakage as a function of internal pressure and temperature, as good as possible.

Because of

- geometrical and physical nonlinearity
- the biaxial stress-strain-condition
- the excessive large deformations

analysis must appropriately be accompanied by experiments

The statistical uncertainties of the various influence parameters due to load variation, fabrication, structural resistance and analysis model are considered as far as known for the performance and interpretation of the results only.

DRW 1300 - Pressure Containment Vessel (PCV)

The steel containment is given a complete spherical shape of 56 metres in diameter surrounded (secondary) concrete containment which is designed to withstand even aircraft crashes (Fig. 1). More than a hundred penetrations for pipes, the thickened plates for the cable penetration assemblies, the equipment hatch, the personnel and the two emergency airlocks form disturbed areas.

The pipe-penetrations are normally compensated against deformations of the PCV by expansion joints.

The locks and the PCV itself are in close contact to the concrete structure at several points, which assure free deformation for design conditions only.

The spherical shape of the containment is obviously well suited to withstand internal pressure.

Material Properties

For the PCV a low-strength pressure vessel steel of extreme high ductility is used; the yield and tensile strengths are similar to that of the A 516, grade A steel (Fig. 2). In contrary to the ordinary stress analysis, one should use the actual or expected strength values--usually 10% over the guaranteed minimum values. Consequently high deformations might be expected without brittle fracture or crack sensibility. The weld seams do not seem to be critical, which allows a welded joint factor of 1.0.

Stress-Strain-Curves

Due to the loading of steady-state gradually increasing pressure and temperature, the uniaxial tensile tests used as a basis for the material law should be performed under similar time-depending conditions, that is for very slowly increasing load, to give time enough for creeping and recovering effects, for room temperature as well as for higher temperatures as 300°F (150°C).

Assumptions

- The loading is limited to static internal pressurization and temperature, neglecting any dynamic or pushing effects, for example sudden change of constraint forces due to large deformations of the PCV and the locks.

- The biaxial stress-condition is described from the uniaxial tensile test data using the MISES yield criterion, which seems to be reasonably confirmed by tests.

Sources of Leakage

Reaching the temperature dependent-yield point (Fig. 3), the strains and hence the PCV-deformations will increase rapidly up to 1% or about 10 inches, respectively.

There are some points of the PCV which are believed to be possible sources of leakage (Fig. 4) for pressures more than 9 barü because of expected strain concentrations or high constraint forces.

The equipment hatch (Fig. 5) with a prestressed bolted connection is not only of interest because of the stress amplification due to the reduced panel cross-section in the bolted area. Beyond the yield strength, the large deformations additionally bring up extreme high constraint forces between the equipment hatch and the concrete structure.

Some rough estimations had been done (Fig. 6). The analysis has to be confirmed and supplemented by tests being in preparation at the **Kernforschungszentrum Karlsruhe.** They should give more information about the strain concentration in the bolted area and the leakage throughout the bolt hole which is 1 mm in diameter larger than the bolt itself (the bolts are believed to reduce or even to leave their normal prestress due to the wall thickness reduction going ahead with severe plastic deformations).

Stress and strain concentrations are expected for all penetration reinforcements (Fig. 7).

Rather difficult to analyze are the points which prevent the PCV from free deformation (Fig. 8) producing severe constraint forces, mainly the concrete platforms outside the PCV, the locks and a steel construction--inside the equipment lock--which is bound to the concrete (by compensated penetrations).

Though the steel is to a high extent flexible--which is demonstrated by the picture (Fig. 9) for a similar material--the constraint forces can reach great amounts.

Unfortunately these constraint forces accumulate in and around the equipment hatch and give an additional contribution to the complex strain-condition at the bolts (the wall of the hole is plastically deformed at the bolts due to the bolt shear forces).

The electrical penetration assemblies as well as seals seem to be less critical.

The pipe penetrations are affected by excessive PCV deformations, but their expansion joints are in general able to withstand (Fig. 10) even large deformations due to designing against fatigue failure under operating conditions and due to the high-ductile austenitic steel. The inner elongated expansion joint is subjected to external pressure while the outer one is compressed and laterally moved simultaneously. The welds at the expansion joint ends might be the critical point. Appropriate tests are necessary.

Obviously for double-compensated penetrations expansion joint failure on only one side of the PCV is not sufficient for leakage. This holds for the equipment lock too with the doors locked both--the inner and the outer one--under operating conditions, whereas the inner door of the personnel and the two emergency locks remain open (for security purposes).

The airlock barrels do not use any connecting flanges and the doors closed are pressed against the end flanges with increasing pressure.

Different Containment Types

This report is concerned with the Primary Containment Vessel of a special plant DWR 1300 (KKP II) being finished now. The PCV is quite similar to standard plants just planned and erected (KONVOI-Reactors), whereas big differences appear compared to former plants. The differences are due to:

- the material used (higher yield strength).
- local stiffness (less or even nonthickened plates around penetrations).
- penetration compensation (with or without).
- some details, concerning the bolted area of the equipment hatch, for example.

Conclusion

A comprehensive presentation of the results is given in the picture (Fig. 11), in which the pressure of severe leakage is plotted against the believed potential leakage sources.

Failure is expected locally. Severe leakage will not happen before the overall plastic condition of the PCV is reached (the yield point decreases with increasing temperature).

Due to variation of influence parameters (material strength and law, fabrication, welding, analysis model), the critical pressure will vary (punctuated fields).

Obviously the expected critical pressures of the various leakage sources do not differ much which is a consequence of the flattened material stress-strain-curve once the yield strength is passed (a change in pressure from 10 to 11 bar will enlarge the radial displacement by 30% (or 4 inches) at 300°F temperature).

The report presented should give you an overview of what might go on in an on-site spherical DWR 1300--containment if the internal pressure and the temperature are increased. To be sure that the prediction is realistic, special tests are recommended.

References

/1/ Containment Integrity Program by Sandia National Laboratories.

/2/ Dynamic Response, Impact and Materials Test Studies for Los Alamos Scientific Laboratory

/3/ Overview of Activities of Containment Performance Working Group 4/1984
C.H. H O F M A Y E R Brookhaven National Laboratory

/4/ The Potential for Containment Leak Paths through Electrical Penetration Assemblies
NUREG/CR-3234

/5/ KfKA-Report Nr. 3589, Karlsruhe
Investigation Program on PWR-Steel-Containment Behavior under Accident Conditions

/6/ KWU-Report R 321/83/117
Ultimate Load Analysis for the KKP II - Pressure Containment Vessel / Part I

/7/ KWU-Report R 321/84/22
Ultimate Load Analysis for the KKP II - PCV/Part II

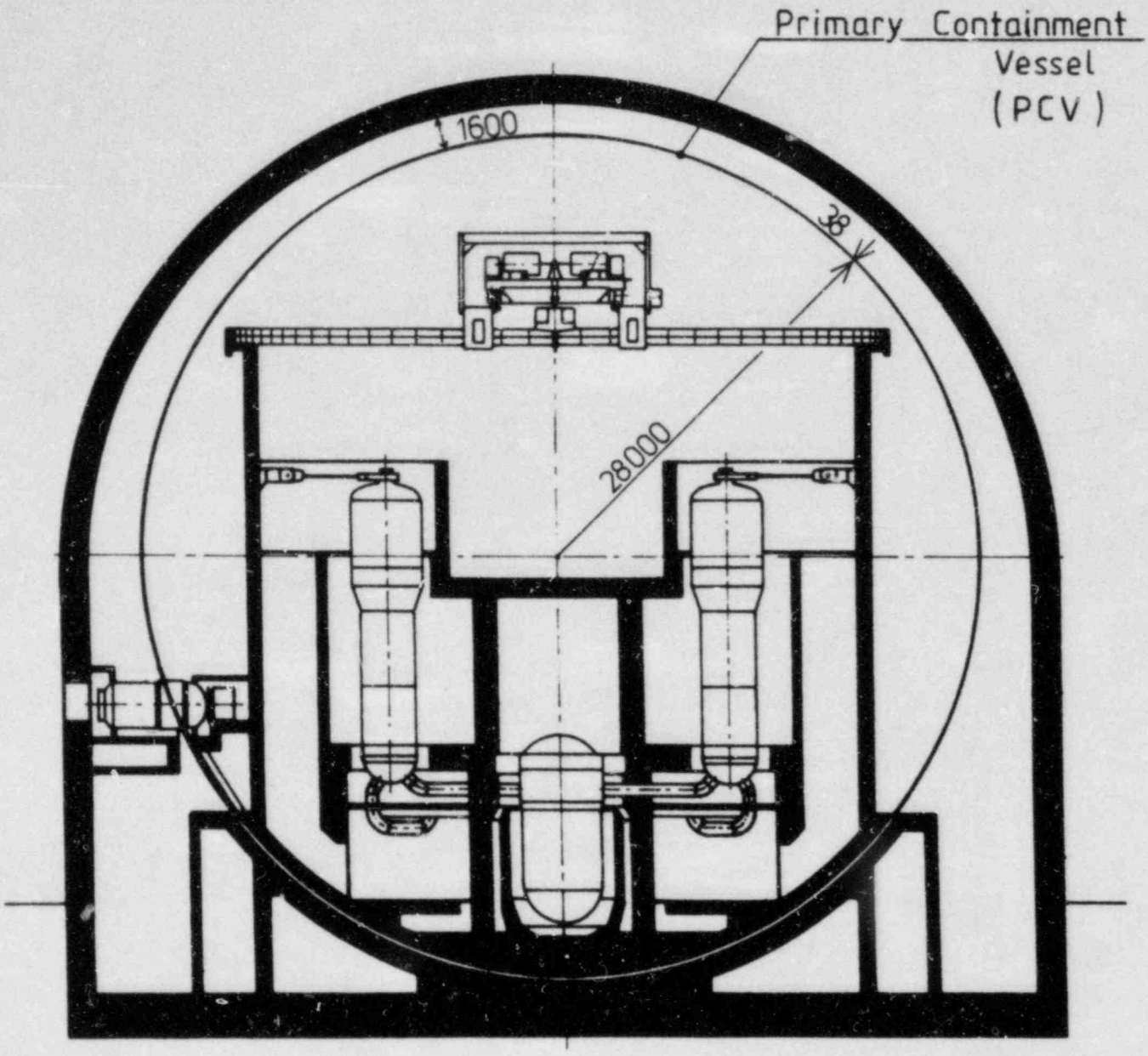

KWU DWR 1300 MWe Power Plant

Basic Dimensions [mm]

Figure 1. Baseline Configuration of PCV DWR 1300

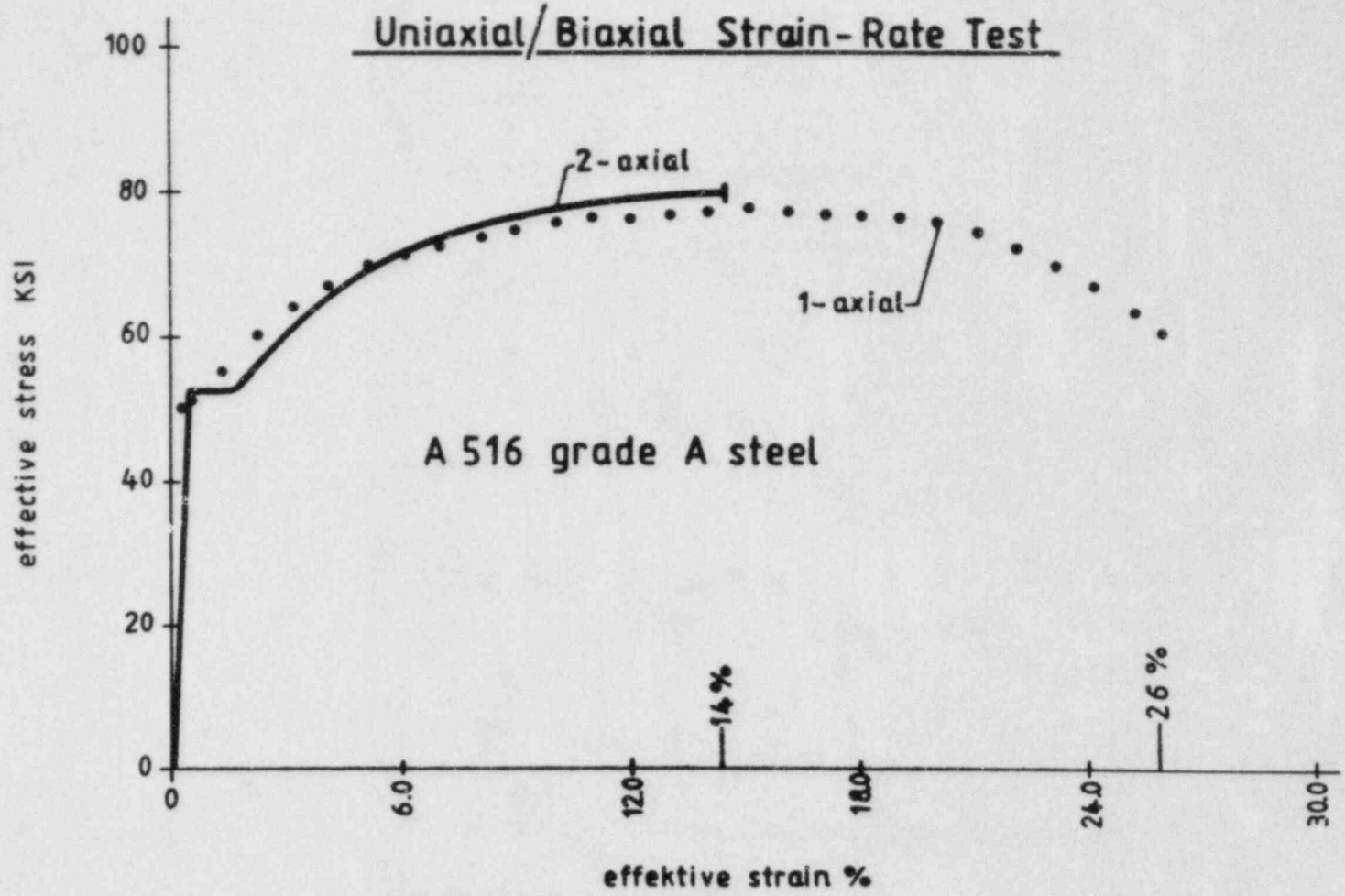

Figure 2. PCV-Material/Uniaxial/Biaxial Strain-Rate Test

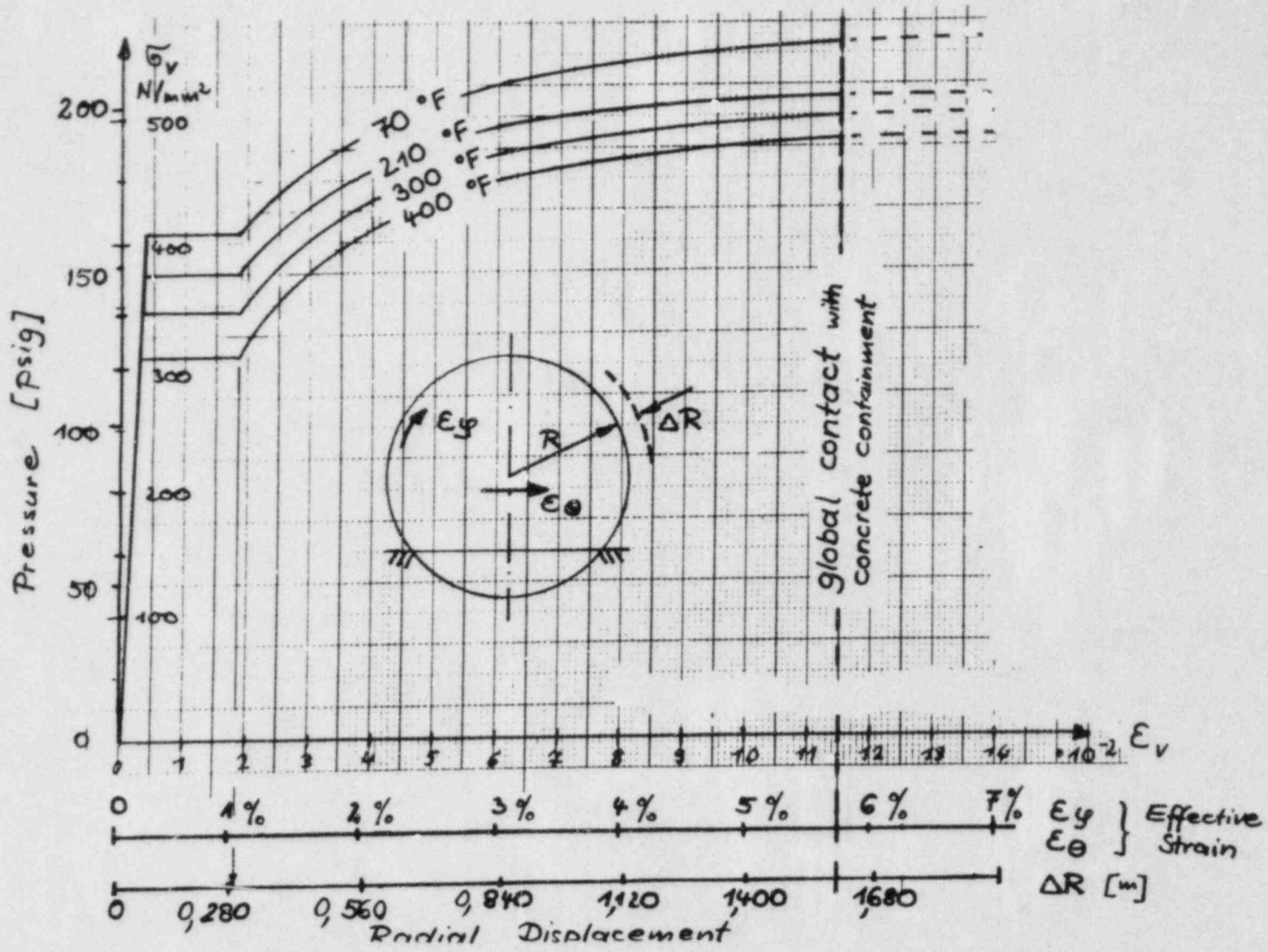

Figure 3. Pressure vs Radial Discplacement at Midheight

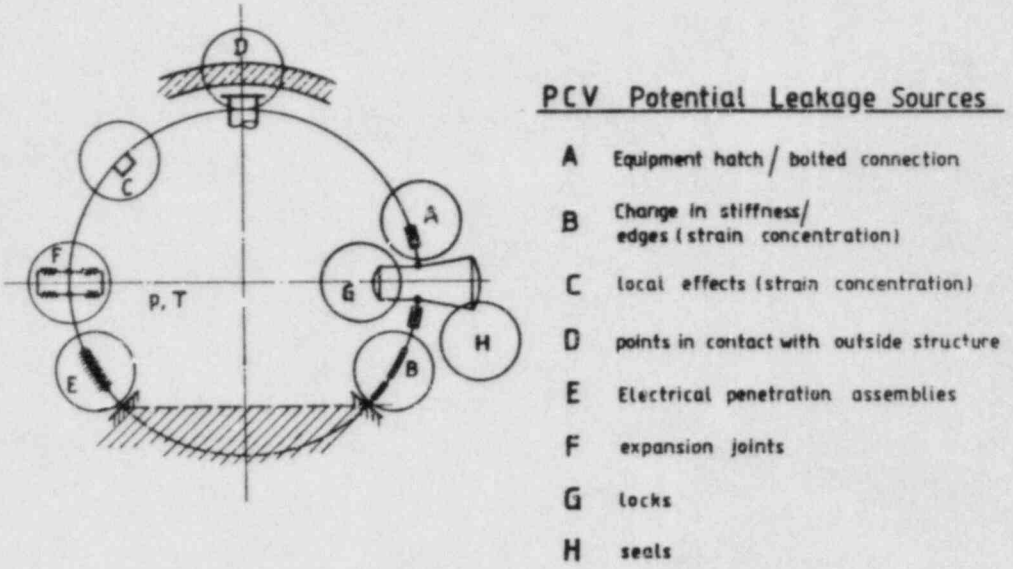

PCV Potential Leakage Sources

- **A** Equipment hatch / bolted connection
- **B** Change in stiffness/ edges (strain concentration)
- **C** local effects (strain concentration)
- **D** points in contact with outside structure
- **E** Electrical penetration assemblies
- **F** expansion joints
- **G** locks
- **H** seals

Figure 4. PCV-Potential Leakage Sources

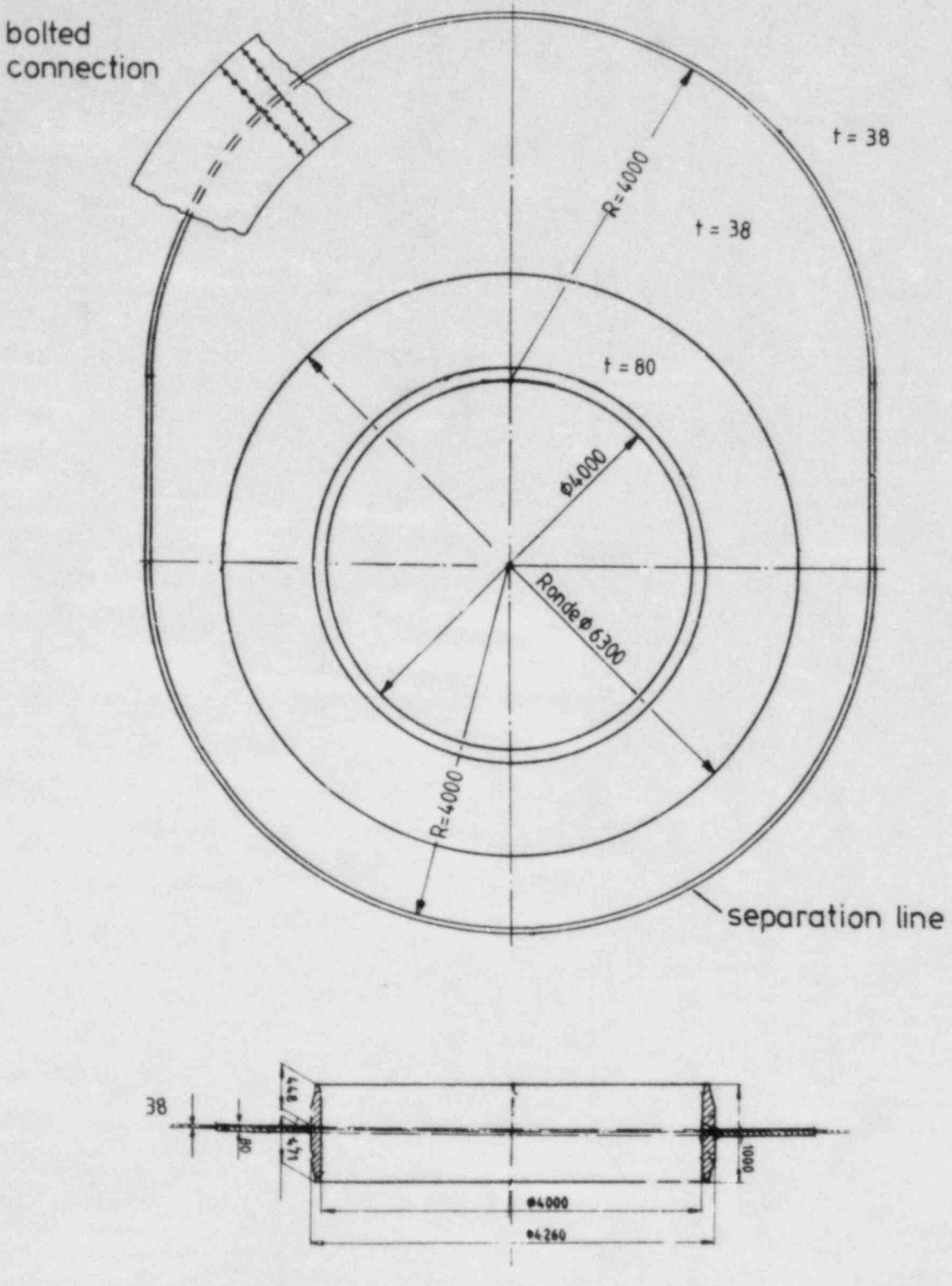

Figure 5. Equipment Hatch/Bolted Connection

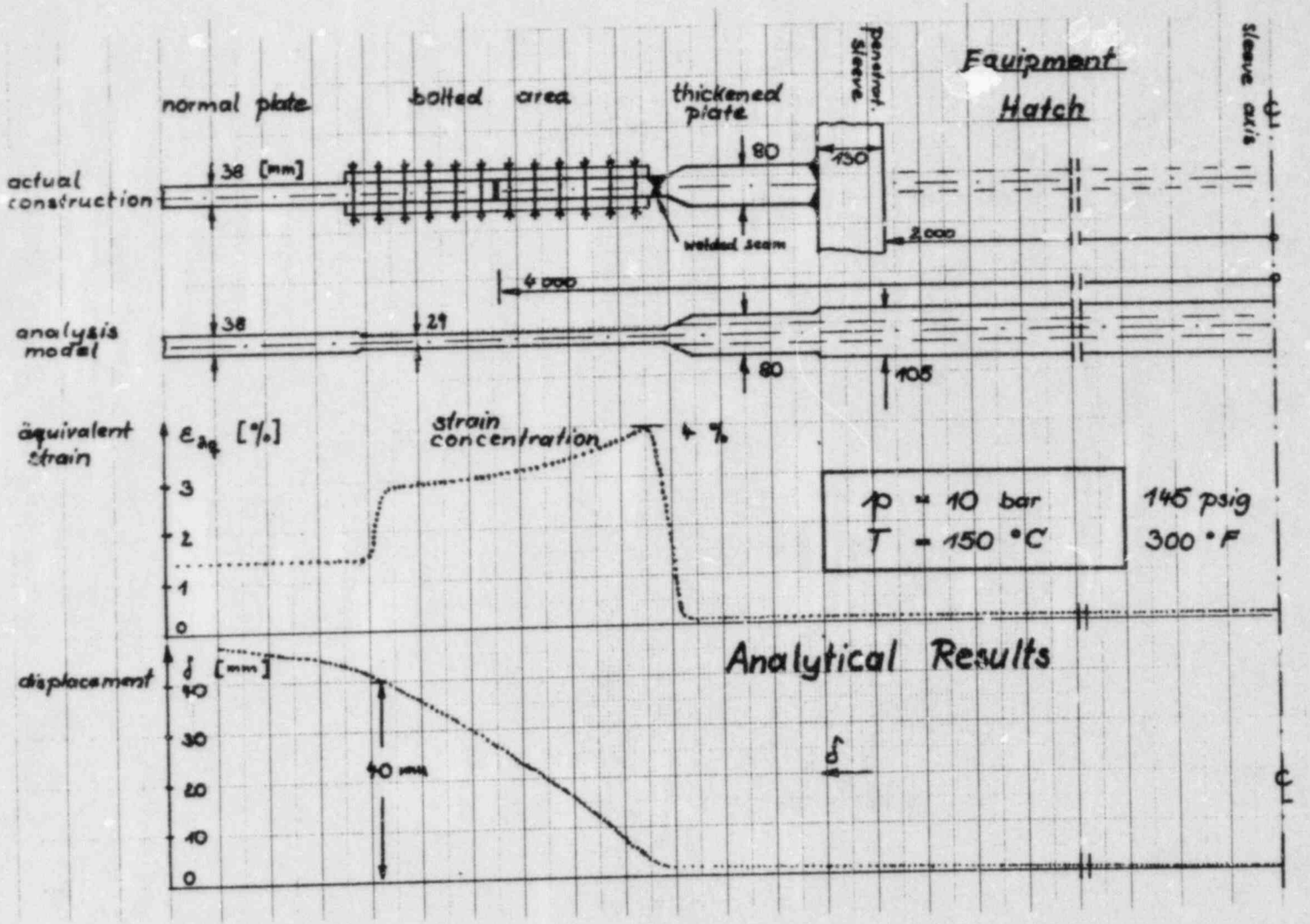

Figure 6. Bolted Connection/Strain Concentration Analysis

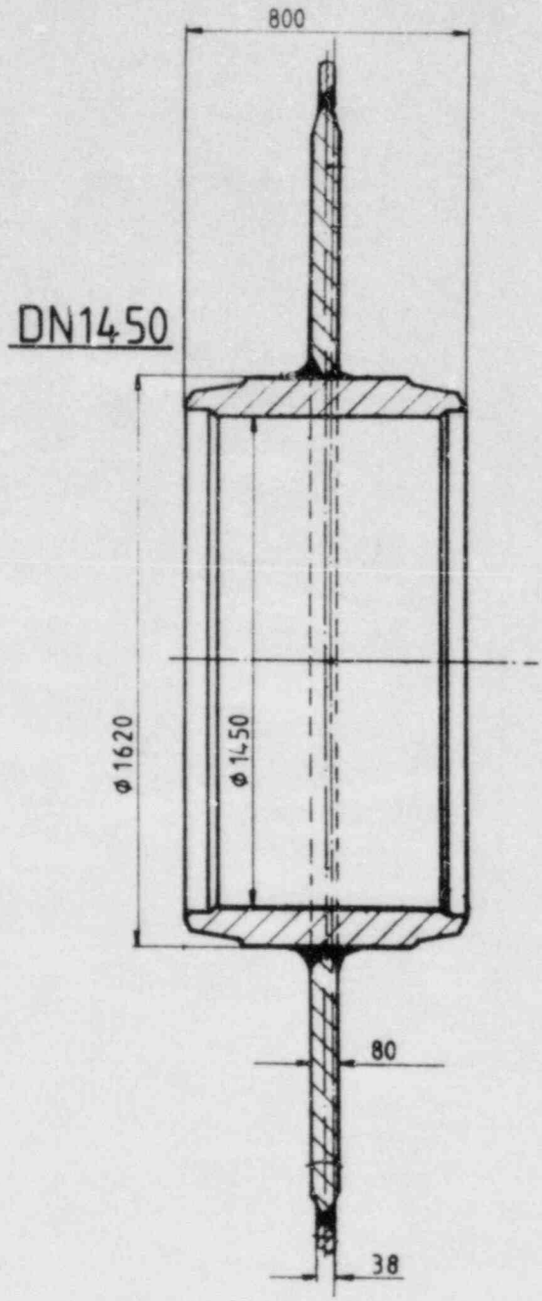

Figure 7. Change in Stiffness/Thickened Penetration Plate

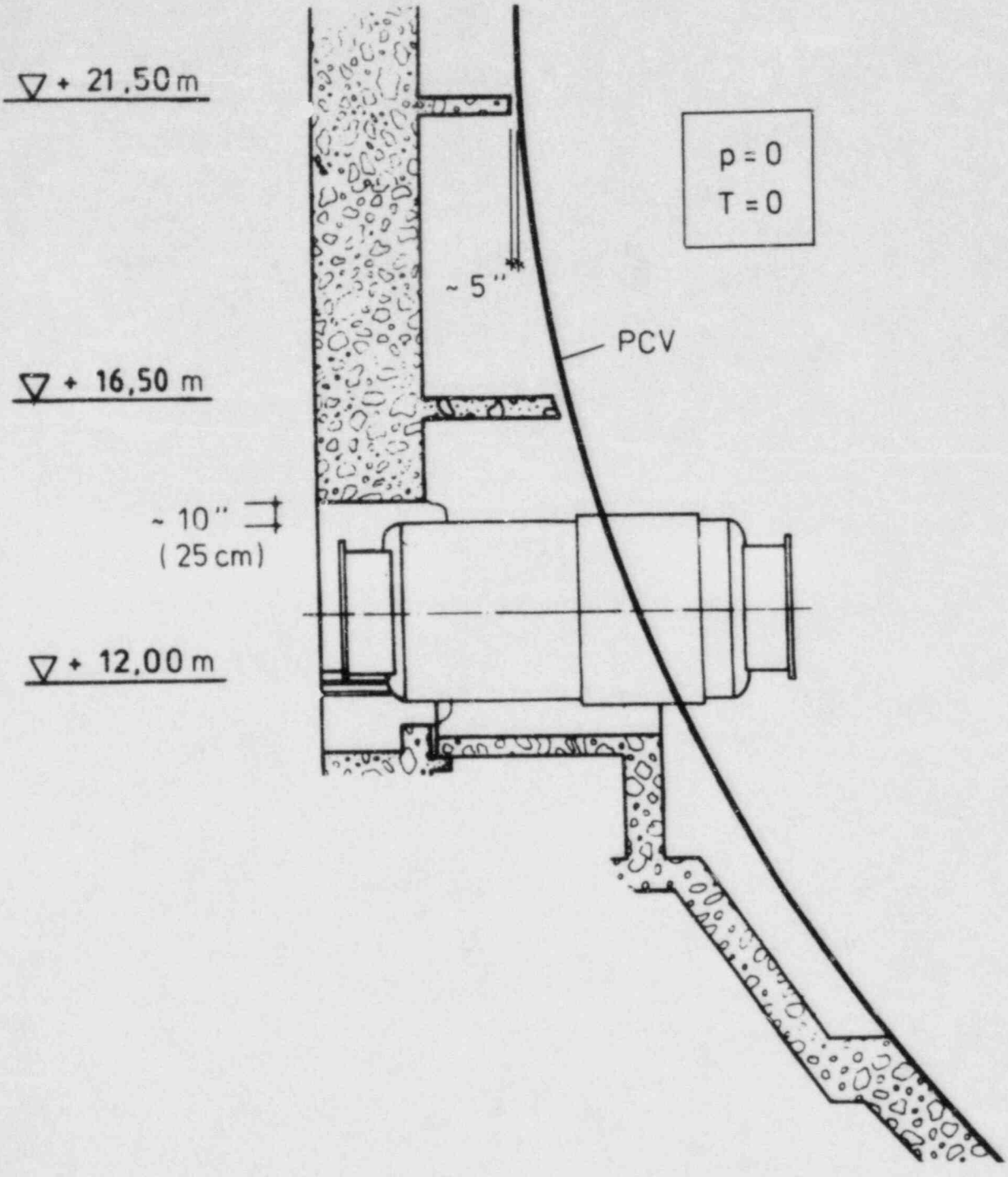

Figure 8. Points of Limited Deformation Possibility/ Airlock and Concrete Platforms

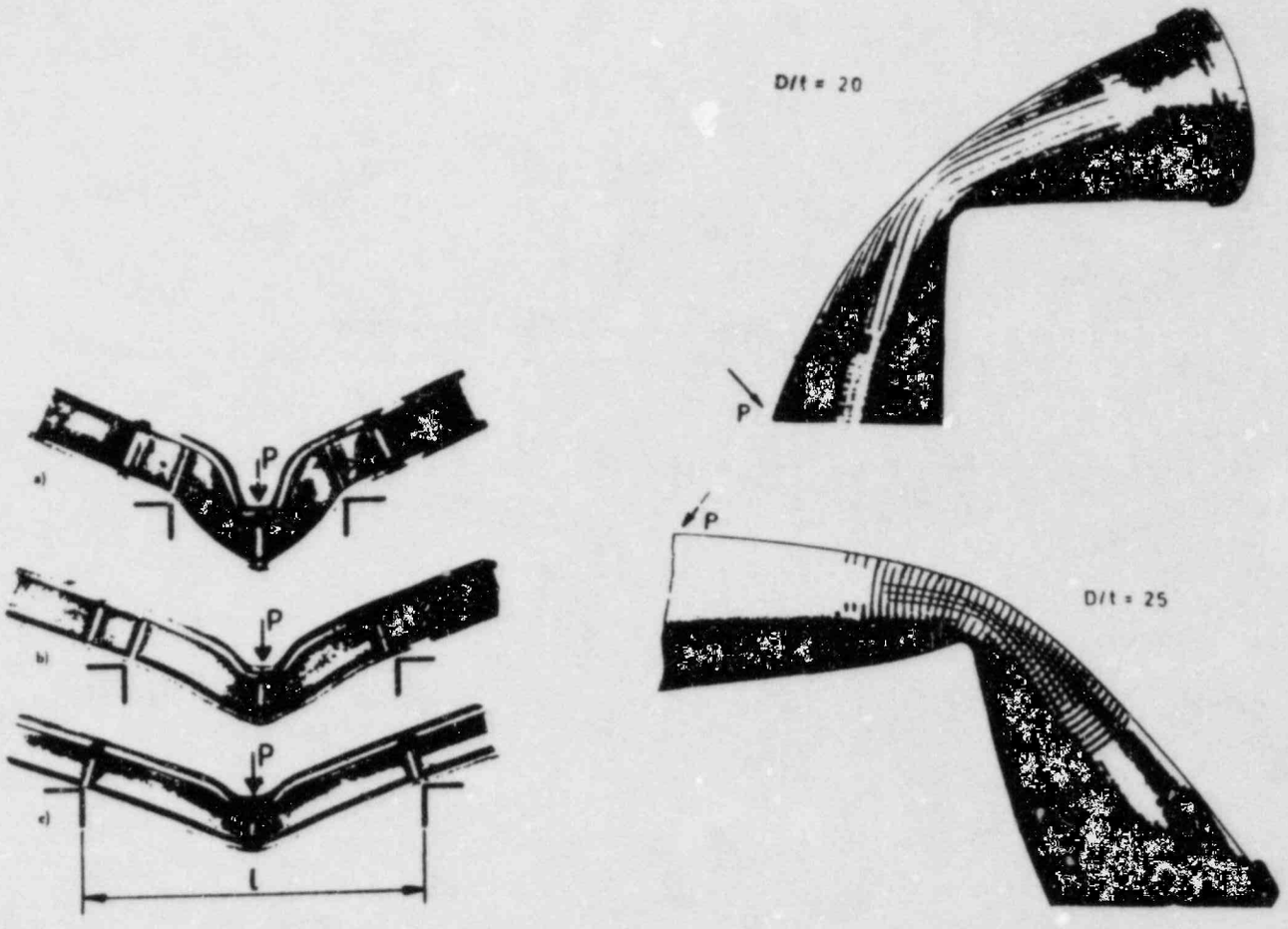

Figure 9. Deformation of Beams and Pipes Due to Single Loads

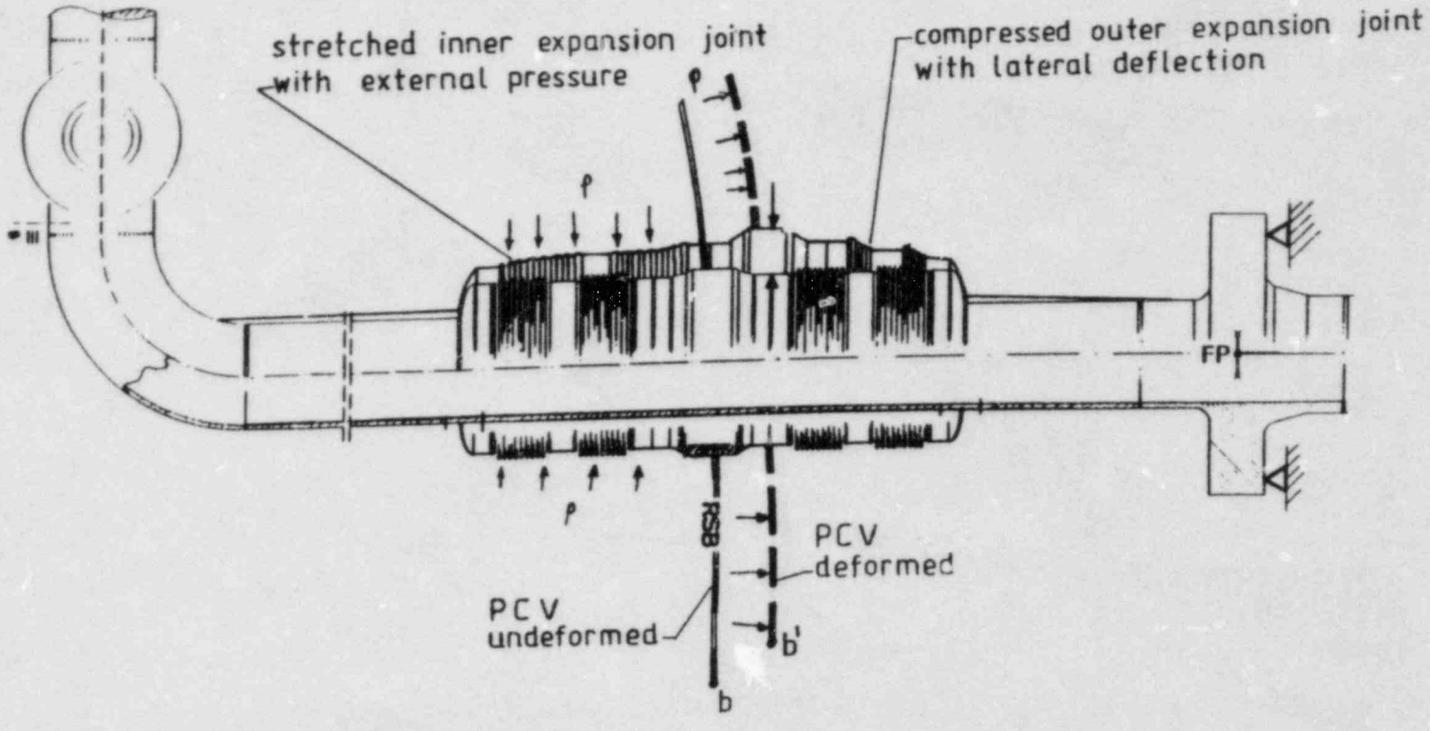

Figure 10. Expansion Joints for Penetrations

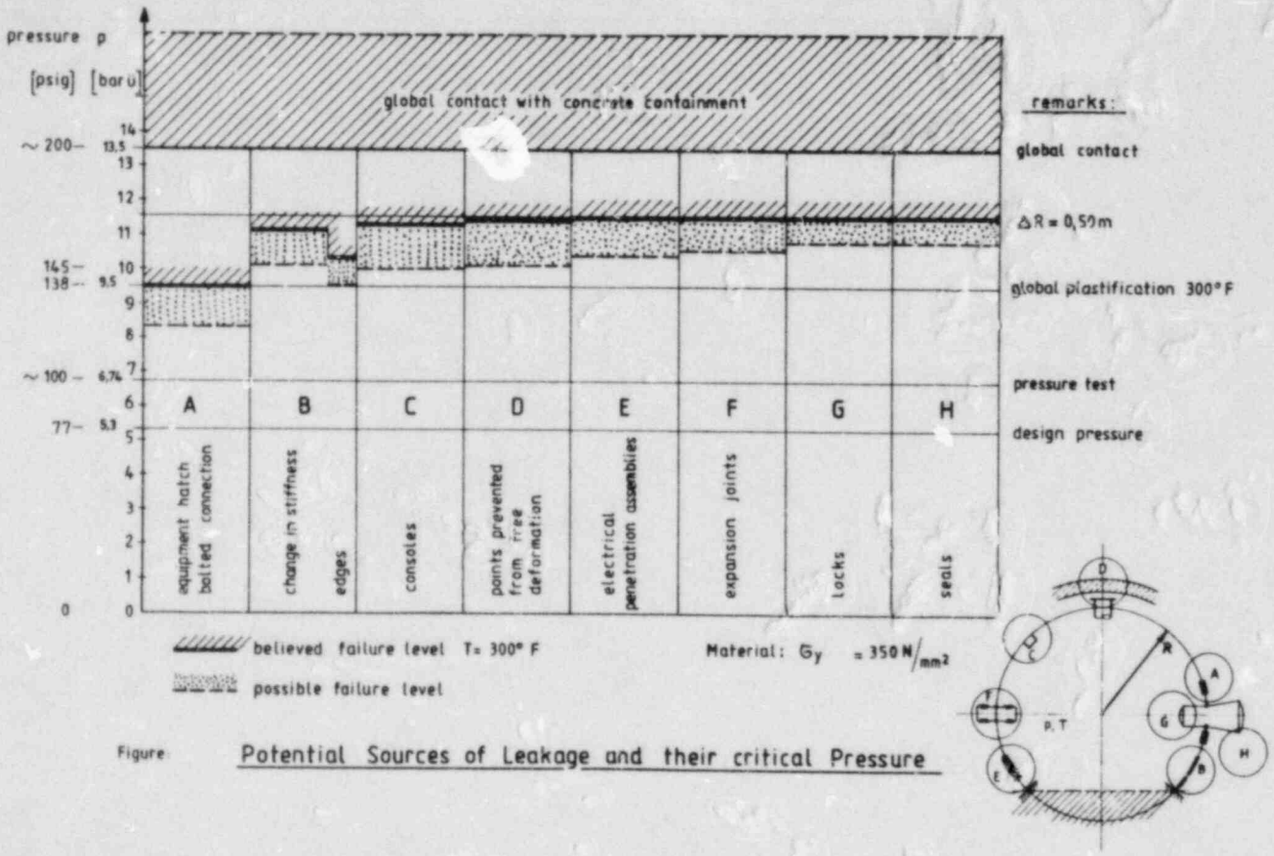

Figure Potential Sources of Leakage and their critical Pressure

Figure 11. Potential Sources of Leakages and Their Critical Pressure

CONTAINMENT LEAKAGE DURING SEVERE ACCIDENT CONDITIONS

C. H. Hofmayer
Brookhaven National Laboratory
Upton, NY 11973

G. Bagchi and V. S. Noonan
U.S. Nuclear Regulatory Commission
Washington, DC 20555

ABSTRACT

An alternate to the "THRESHOLD" model used in most severe accident risk assessments has been investigated. One reference plant for each of six containment types has been studied to determine the magnitude of containment leakage that would result from the pressures and temperatures associated with severe accident conditions. Containment penetrations having the greatest potential for early containment leakage are identified. The studies indicate that containment leakage through penetrations prior to reaching containment threshold pressures (currently reported containment shell failure pressures) should be considered in severe accident risk assessments. Failure of non-metallic seals for containment penetrations can be a significant source of containment leakage under severe accident pressure and temperature conditions. Although studies of containment types are useful in identifying sources of containment leakage, final conclusions may need to be plant specific. Recommendations concerning future studies to better develop the use of continuous leakage models are provided.

INTRODUCTION

Most severe accident risk assessments have utilized a "THRESHOLD" model to characterize loss of containment integrity. If the containment pressure is below a certain threshold pressure it is assumed that the containment does not fail and off-site consequences are quite low. If containment pressure is above the threshold pressure it is assumed that the containment fails and significant fission product inventory is released.

Although this model is useful for risk assessments, it could be misleading since it does not accurately represent the behavior of containments when subjected to the high pressures and temperatures associated with severe accident conditions. Since all containments contain numerous penetrations, the possibility exists that containment leakage will begin to increase as pressures and temperatures increase above the design basis level. For some con-

tainments this leakage may be sufficient to prevent reaching the "threshold" level. For others, the "threshold" level may be reached; however, at this point it is not expected that gross failure of the containment shell will occur. Instead, additional leakage paths are expected to develop as a result of the increased containment deformations corresponding to the high pressure and temperature conditions. Such leakage probably would prevent gross failure of the shell from ever occurring. Only for cases where the pressure rises rapidly (such as loading associated with a hydrogen detonation) and exceeds the "threshold" pressure by a wide margin would one expect the containment to behave in the manner described by a "threshold" model.

OVERVIEW OF PROGRAM

The Nuclear Regulatory Commission (NRC) has been sponsoring studies to determine the magnitude of containment leakage that would result from the pressures and temperatures associated with severe accident conditions. Six containment types have been studied which include large dry, subatmospheric, ice condenser, Mark I, II and III. At present, these studies have concentrated primarily on identifying potential leak paths that may result from pressure and temperature conditions that occur prior to reaching the currently reported containment structural capabilities shown in Table 1.

Table 1

Containment Structural Capabilities

TYPE	REFERENCE PLANT	CAPABILITIY PRESSURE (PSIG)	SOURCE OF INFORMATION
Large Dry	Zion	134	Reference 1
Subatmospheric	Surry	119	Reference 2
Ice Condenser	Sequoyah	50	Reference 1
Mark I	Browns Ferry*	117	Reference 3
Mark II	Limerick	140	Reference 1
Mark III	Grand Gulf	60	Reference 1

*NRC studies utilized Peach Bottom as the reference plant for containment penetration evaluations.

These containment capabilities generally correspond to the point when the containment first reaches an initial general yield state (or 1% tendon strain in a prestressed concrete containment). Consequently, at this time, this study has not investigated potential leak paths that may result from large containment deformations.

The potential sources of containment leakage that were investigated for each containment type included the following containment penetrations:

- o equipment hatch(s)
- o personnel air lock(s)

- o fuel transfer tube
- o piping penetration closures
- o purge and vent valves
- o electrical penetration assemblies
- o drywell head (BWR)
- o suppression pool access hatches (BWR)
- o CRD removal hatch (BWR)
- o other plant unique access hatches

Engineers from Brookhaven National Laboratory, Idaho National Engineering Laboratory, Sandia National Laboratories and Ames Laboratory participated in these investigations.

SIGNIFICANT SOURCES OF LEAKAGE

Based on evaluations of the above penetrations for six reference plants (one for each containment type), the following penetrations were identified as having the greatest potential for early containment leakage (i.e., leakage prior to reaching currently predicted structural capability pressures):

- o pressure unseating hatches
- o BWR drywell heads
- o flat bulkhead doors
- o purge and vent valves

Each of these penetrations is discussed below.

Pressure Unseating Hatches

A typical pressure unseating hatch is illustrated in Detail C of Figure 1. In this design, the internal containment pressure will tend to unseat the flanges and directly challenge the integrity of the seals. In such designs, there are no redundant hatches, thus if containment temperatures are high enough to degrade the seals or if the seals do not have sufficient resilience there will be a direct leakage path to the outside of the containment. This detail was encountered on three of the six reference plants (Surry, Peach Bottom and Limerick). This does not mean that fifty percent of the plants in the United States have such details. In fact, the population of pressure unseating hatches is probably much smaller.

Of these three plants, the maximum flange separation area was calculated to be 8.5 in^2. This area corresponds to the separation area for the two equipment hatches at Limerick at a pressure of 140 psig (Reference 4). It must be emphasized that this area is a separation area and not a leak area. The extent of leakage is very much dependent upon the resilience of the seals and the extent to which the temperatures associated with severe accident conditions may further degrade the seals. However, it does not seem reasonable that one could expect the seals to maintain a leak tight barrier under all potential severe accident conditions. Aging and compression set could be sufficient to result in significant leak-

age under pressure alone. In addition, for BWR containments certain accident sequences could result in containment atmosphere temperatures above 600°F for several hours prior to the containment reaching its structural capability pressure. As illustrated in Figure 2, even silicon rubber which appears to be the most commonly used seal material in equipment hatches, would exceed its design seal life after being exposed to temperatures of 600°F for approximately one hour (Reference 5). It should be noted that the curves in Figure 2 are design curves and therefore probably represent lower bounds on the seal life. Furthermore, the actual temperature of the seal material will be less than the calculated containment atmosphere temperatures. Nevertheless, this example illustrates the point that containment temperatures can influence the leak tight integrity of any seal.

BWR Drywell Heads

The details of the flange assembly for a typical BWR drywell head are shown in Figure 3. Since internal containment pressure will tend to unseat the flanges, the above discussion concerning pressure unseating hatches is appropriate for drywell heads as well. However, the diameters; of these heads are much larger (between 30 to 40 feet in diameter), thus, they have the potential for providing the greatest source of leakage. For the BWR Mark I (Peach Bottom) a separation area of approximately 63 in^2 was calculated at a pressure of 117 psig (Reference 6). For the BWR Mark II (Limerick) a separation area of approximately 33 in^2 was calculated at a pressure of 140 psig (Reference 4). As discussed above a combination of lack of resilience of the seals and degradation due to temperature could result in significant leakage prior to reaching the structural capability pressure. For the BWR Mark I and II containments a leak area of two to three square inches could sufficiently relieve the containment to prevent it from ever reaching the structural capability pressure. Thus, a leak area equivalent to less than 10 percent of the predicted separation area would prevent further increased pressurization. Of course such conclusions are very much dependent upon the pressurization rates associated with the postulated severe accident conditions. In these studies, the drywell head for the Mark III containment was not evaluated since it was judged that the pool of water directly over the Mark III drywell head would provide adequate cooling to the seals and thus prevent the drywell head from being a significant leakage path.

Flat Bulkhead Doors

Many containment personnel air locks consist of two redundant rectangular doors mounted on flat bulkheads at each end of a barrel section. In a number of cases, this barrel section penetrates the equipment hatch as shown in Figure 1. The main concern with these doors is that under increasing pressure the door will begin to separate from its frame and begin to leak.

For Zion, it was predicted that initial yield of the door frame would occur at 105 psig and a maximum separation area of approximately 6 in^2 was estimated at the structural capability pressure of 134 psig (Reference 7). Since these predictions were based on simplifying assumptions relating to the end conditions of the door frame support beams and the behavior beyond yield, more refined analyses are being conducted which will reduce, but probably not eliminate, the predicted separation area. For Peach Bottom, initial yield of the door frame was predicted to occur at 94 psig and a maximum separation area of approximately 1.0 in^2 was estimated at a pressure of 117 psig. For the other air lock doors, the frames were not predicted to yield prior to reaching the structural capability pressure and separation areas did not exceed 0.4 in^2.

As in the case of the drywell head and other pressure unseating hatches, the leakage attributable to air lock doors is very much dependent on the integrity of the seals. An additional factor in this case which would tend to reduce (or at least delay) the effect of any leakage is the presence of two redundant doors. However, the extent to which credit should be given for this redundancy needs to be further assessed since there have been a number of operating experiences associated with the loss of integrity of air lock doors.

Purge and Vent Valves

With regard to containment isolation valves, the valves associated with the purge and vent system are considered to have the greatest potential for containment leakage. These are generally large diameter butterfly valves with non-metallic seals as shown in Figure 4. In most cases the structural integrity of these valves is not a concern (there are some plant specific cases where further evaluations may be required). The main concern is that the non-metallic seals between the valve body and disc will become degraded when subjected to the combination of high pressures and temperatures associated with severe accident conditions. For the reference plants investigated, these valves ranged in size from 20 to 42 inches in diameter, with some smaller by-pass valves. For other plants these valves have even larger diameters. The metal-to-metal clearance between the valve disc and body is normally between 1/16 and 1/8 in (Reference 8). Therefore, for a 42 inch diameter valve the maximum leak area (if the seal totally failed) would be approximately 16 in^2. The potential leak area could be even greater since there normally are at least two containment penetrations containing these valves. On the other hand, each penetration contains two redundant valves which would tend to reduce the potential for any significant leakage.

The majority of the reference plants investigated utilized ethylene propylene as the seal material in their purge and vent valves. As indicated by Figure 2, significant purge valve leakage would not be expected in PWR plants which use this material since the temperatures due to severe accident conditions generally do not exceed 400°F for a long enough time to exceed the seal life of the material. On the other hand, for BWRs, which can see temperatures

in excess of 600°F for extended periods of time, significant seal degradation could occur.

For the Surry plant, the seal material for the purge and vent valves is nitrile. Containment response studies indicate that containment temperatures for certain severe accident conditions could exceed 350°F for more than four hours and are above 400°F for approximately two hours (Reference 9). Again referring to Figure 2, it can be seen that the seal life of the material is exceeded, therefore, the possibility of significant leakage cannot be readily dismissed. As noted above, the redundancy of the valves as well as the use of more refined thermal loads, could provide the basis for demonstrating that significant leakage does not occur.

SUMMARY OF RESULTS

Based on the above discussion it can be seen that the potential for containment leakage prior to reaching the structural capability pressure depends almost entirely on the behavior of non-metallic seals. Additional test data is needed to accurately quantify the leakage that could occur.

The potential for early containment leakage is very plant specific, since each plant has its own unique characteristics. A summary of the findings for the six reference plants currently being studied is presented in Table 2.

Table 2

Summary of Results

TYPE	REFERENCE PLANT	POTENTIAL FOR SUFFICIENT LEAKAGE TO PREVENT OVER-PRESSURIZATION	POSSIBLE SOURCE OF LEAKAGE
Large Dry	Zion	Low	Air lock door
Subatmospheric	Surry	Medium	Purge valves Pressure unseating air lock barrel flange
Ice Condenser	Sequoyah	Low	None identified
Mark I	Peach Bottom	High	Drywell head Purge valves Pressure unseating equipment hatches
Mark II	LimericK	High	Drywell head Pressure unseating equipment hatches
Mark III	Grand Gulf	To be determined	To be determined

The classifications in Table 2 of "low" medium" and "high" are very judgemental and are presented as a means of distinguishing the likelihood of leakage between the different plants. The term "sufficient leakage to prevent overpressurization" is meant to imply that the leakage would be large enough to prevent the containment from reaching the structural capability pressure reported in Table 1. At this point, the radiological consequencies of such leakage have not been assessed.

The Sequoyah plant presents an interesting case since no significant leak sources were identified prior to reaching the structural capability pressure. This plant utilizes a pressure seating equipment hatch and the severe accident temperatures are not high enough to challenge the purge valve seals. This does not imply that the containment will behave like a "threshold" model (except possibly in the case of a very rapid pressurization due to a hydrogen detonation). It is judged that gross failure of the containment shell at or above the capability pressure will not occur, but that the containment deformations at these high pressures will initiate a leakage path sufficient to depressurize the containment. It is anticipated that future studies will identify and quantify this failure mode.

As indicated in Table 2, the Mark III containment is still being evaluated. Early in the accident sequence, the potential exists for developing standing flames in the wetwell above the suppression pool as a result of deliberate ignition of hydrogen. These flames could degrade the seals for the personnel locks in the drywell and wetwell walls and the equipment hatch in the drywell wall. Furthermore, later in the accident sequence the temperatures in the drywell can reach approximately 1000°F for an extended period of time. In both cases, failure of the hatch seals in the drywell couid lead to by-pass of the suppression pool and eventually to direct leakage outside containment as result of the failure of the seals in the wetwell air lock. Preliminary evaluations by the NRC staff indicate that seal degradation due to the presence of the standing flames may not be a problem. However, this matter is being further assessed.

CONCLUSIONS

The containment leakage studies of the six reference plants discussed above have led to the following conclusions:

- The potential for containment leakage through penetrations prior to reaching currently reported containment threshold pressures should be considered in severe accident risk estimates.

- The potential for significant leakage before reaching currently reported containment threshold pressures appears to be greater for BWRs than PWRs.

- Leakage before reaching threshold presssures can also occur with PWRs, but such leakage is much more plant specific.

- It is judged that leakage before gross failure will always occur, however the demonstration of such leakage for some containments will require investigations at pressures above currently reported threshold pressures (large containment deformations).

- Failure of non-metallic seals for containment penetrations (primarily equipment hatches, drywell heads and purge valves) are the most significant sources of containment leakage.

- Although generic studies of containment types are useful in identifying sources of containment leakage, final conclusions may need to be plant specific.

- Current efforts rely on analysis and engineering judgement. Additional test data is needed to better quantify the leak tightness of containment penetrations when subjected to severe accident conditions.

Based on the results to date, both analytical and experimental studies should continue to better quantify containment leakage during severe accident conditions. The use of threshold models should be replaced with continuous leakage models that accurately characterize the behavior of containments throughout the postulated severe accident sequences. Further studies should include:

- Tests to fully assess the behavior of penetration seals.

- The development of accurate analytical models to represent temperature and pressure dependent leakage.

- The identification and quantification of critical leakage paths under large containment strain conditions.

- Sensitivity studies to assess the potential variation of containment leakage within the family of each containment type.

- Sensitivity studies to determine the magnitude and timing of containment leakage which can have a significant effect on radiological consequences.

- An assessment of the potential for plugging of identified leak paths.

- An assessment of the survivability of equipment inside containment during important severe accident sequences.

REFERENCES

1. T.J. Marciniak, E.P. Stroupe, S.H. Fistedis, "Resolution of Containment Structural Response Issues Under Degraded Core Conditions", NUREG/CP-0033, Volume I, October 1982.

2. W.J. Pananos and C.F Reeves, "Containment Integrity at Surry Nuclear Power Station", Stone and Webster Engineering Corporation Report TP-84-13, February 1984.

3. L.G. Greimann, et al., "Reliability Analysis of Steel Containment Strength", NUREG/CR-2442, June 1982.

4. T.L. Bridges, W.T. Dooley, M.J. Russell, "Limerick Generating Station Containment Preliminary Leak Area Estimtes", EGG-EA-6538, February 1984.

5. O-Ring Handbook prepared by Parker Seals Company.

6. T.L. Bridges, W.T. Dooley and M.J. Russell, "Leak Area Estimates for Peach Bottom Power Plant, Preliminary Draft Report", October 1983.

7. T.L. Bridges, C.G. Larsen, M.J. Russell, J.C. Watkins, "Estimates of Leak Area vs. Pressure for Various Types of Containment Designs", EGG-REP-6321, Rev. 1, August 1983.

8. B.E. Miller letter to G. Bagchi, "Evaluation of the Purge and Vent Valves for Surry and Peach Bottom when Exposed to Severe Accident Conditions", October 18, 1983.

9. R.D. Gasser, "Containment Leakage Estimate for the Surry Plant", BNL Letter Report, dated December 1983.

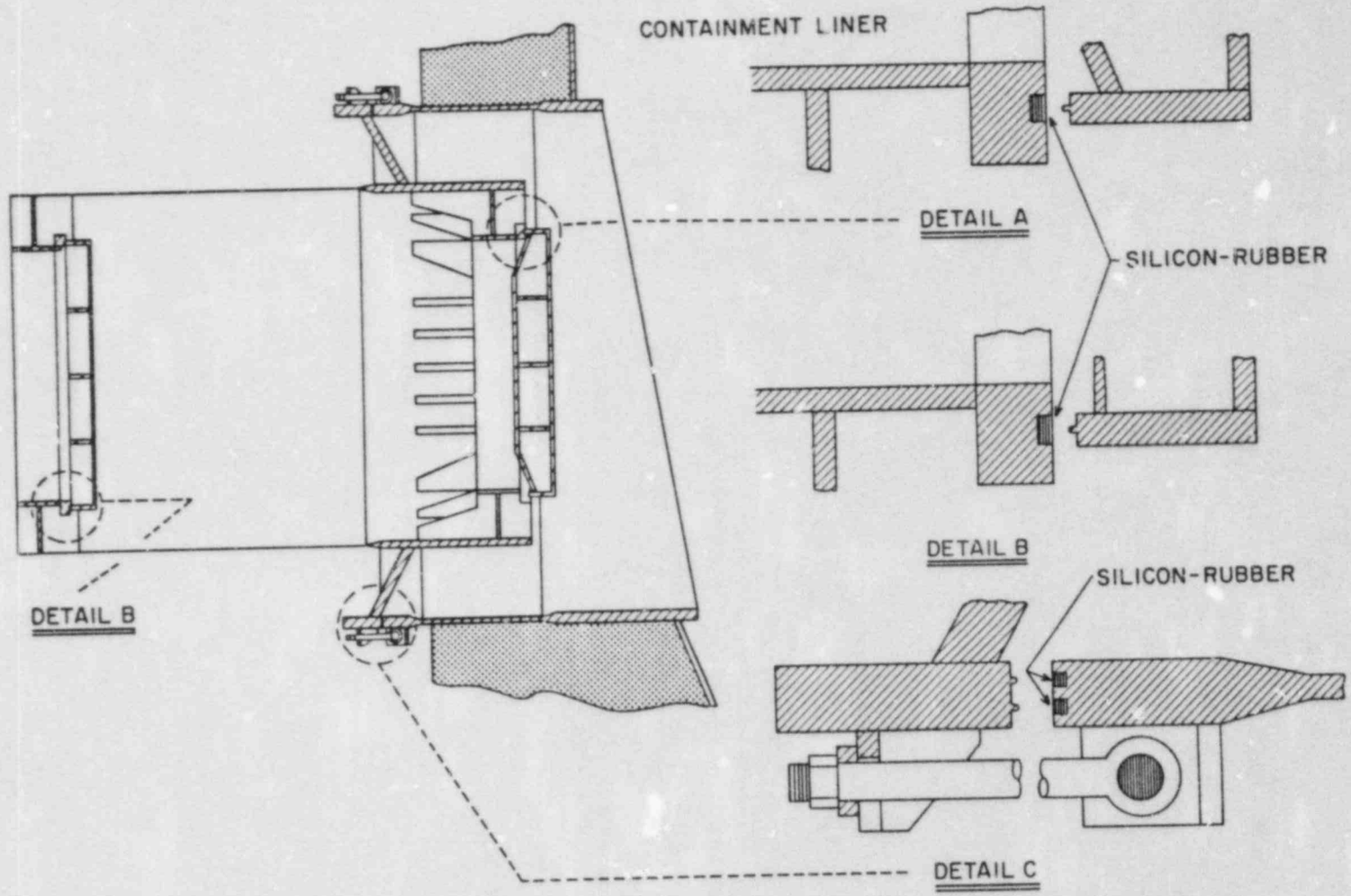

Figure 1. Typical Pressure Unseating Equipment Hatch with Integral Personnel Air Lock

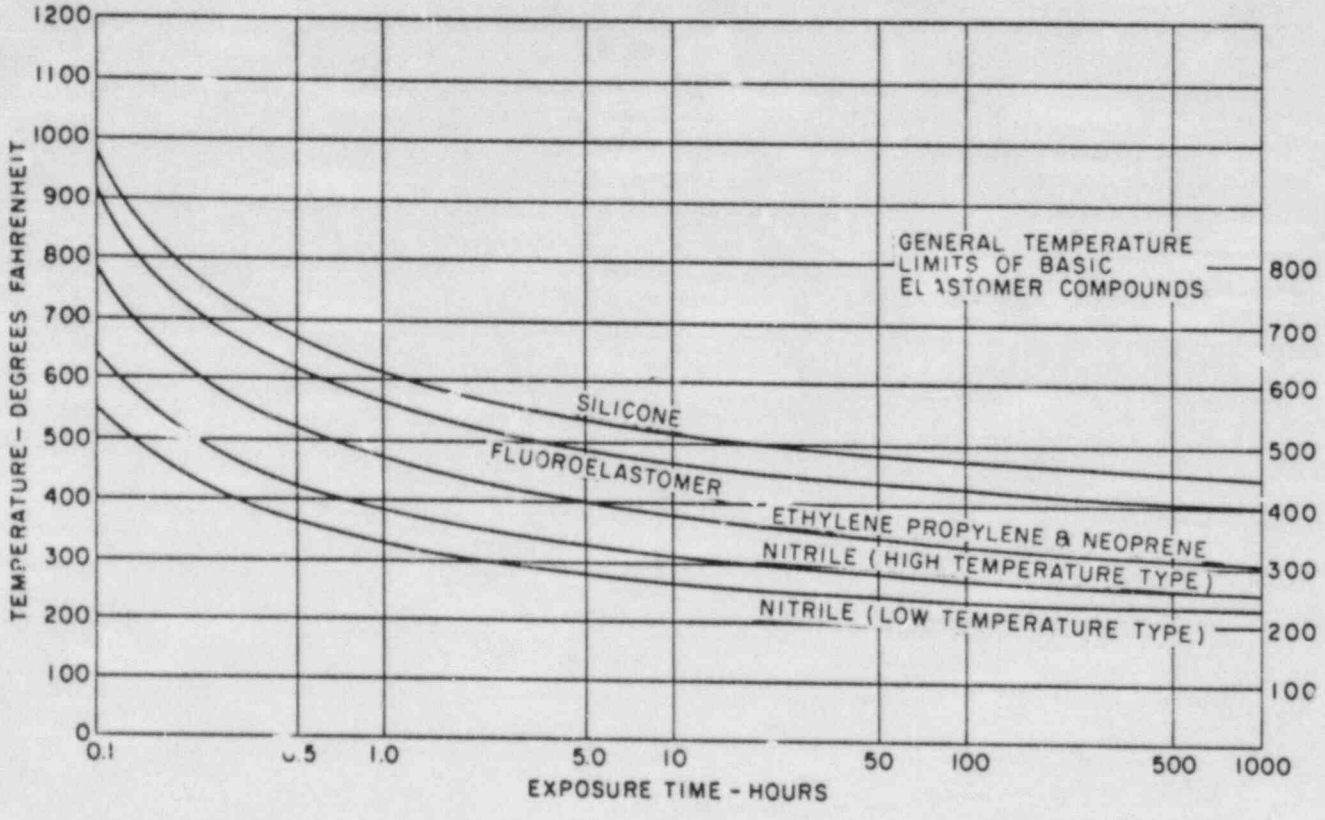

Figure 2. Seal Life as a Function of Time at Temperature
(Ref: Parker Seal O-Ring Handbook)

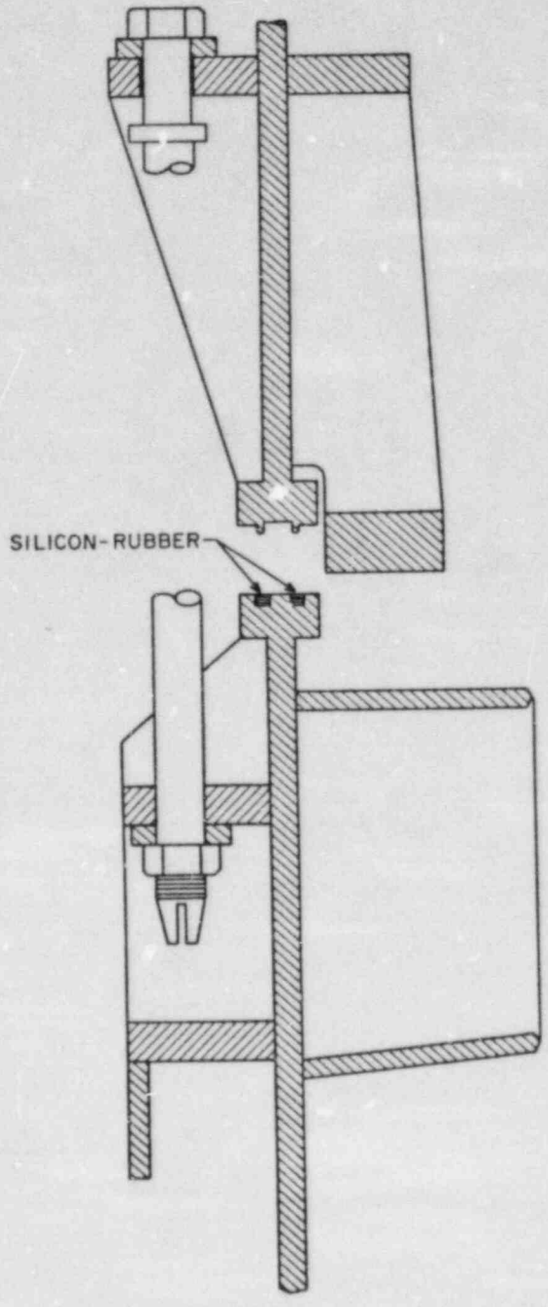

Figure 3. Typical BWR Drywell Head Flange Assembly

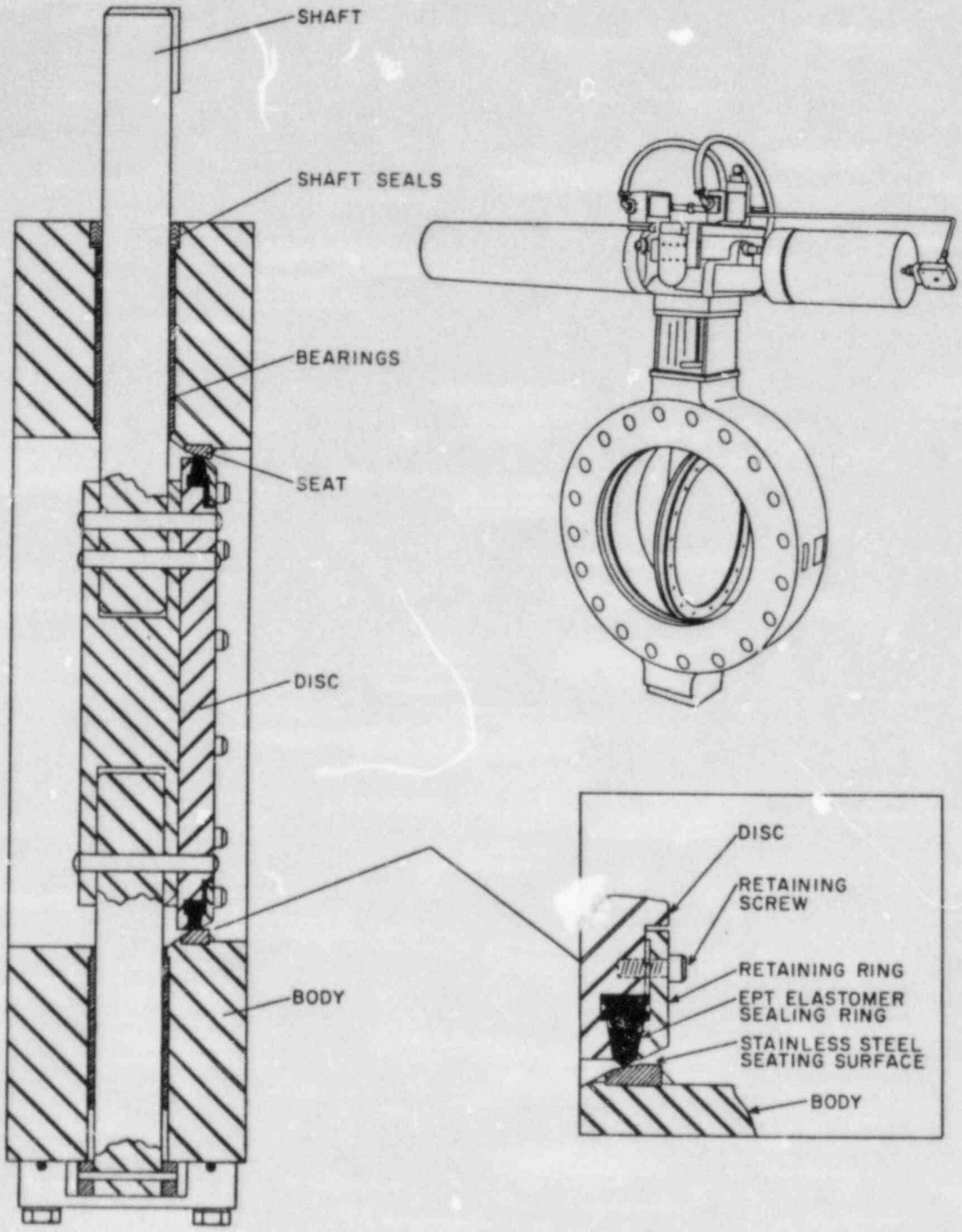

Figure 4. Typical Purge and Vent System Butterfly Valve Manufactured by Pratt

DETERMINATION OF CONTAINMENT LARGE OPENING PENETRATION LEAKAGE DURING SEVERE ACCIDENT CONDITIONS*

T. L. Bridges
EG&G Idaho, Inc.
P.O. Box 1625
Idaho Falls, ID 83415

ABSTRACT

The concept of determining containment behavior during severe accident conditions using a "Leak Before Break" characterization of containments is being investigated. A significant portion of this investigation consists of determining the containment leak area as a function of containment pressure. It has been determined that personnel airlock bulkheads and pressure unseating large opening penetration closures are two of the most likely candidates for significant contribution to containment leakage during severe accident conditions. The aim of this paper is to present the analytical methods used to determine the structural behavior of these items.

PERSONNEL AIRLOCK BULKHEAD ANALYSES

Containment personnel airlocks provide a means for plant personnel to enter and leave containment buildings while maintaining the containment pressure boundary. A majority of the containment personnel airlocks have flat reinforced bulkheads as shown by figure 1 (Limerick's containment personnel airlock). The reinforced bulkheads have different designs. For this particular personnel airlock, the inner bulkhead is stiffened with radial gusset plates between the door frame and barrel section. The outer bulkhead is stiffened with beam members across the top and bottom of the door opening and three horizontal stiffening beams between the door frame sides and barrel section. Some personnel airlocks are designed with both bulkheads similar to this exterior bulkhead. The personnel airlock doors generally consist of a stiffened plate with a framework at the door edges for incorporating the door seals. The door seal designs vary somewhat but generally consist of either double O-rings or a double tongue and groove design with rectangular elastomer seals in the grooves. The doors for personnel airlocks with flat bulkheads are always located on the containment side of the bulkheads so containment pressure will seat the door seals. The doors have a mechanical interlock which will allow only one door to be opened at a time.

*Work supported by the U.S. Nuclear Regulatory Commission, Office of Nuclear Regulatory Research, under Interagency Agreement DOE 40-550-75 with the U.S. Department of Energy.

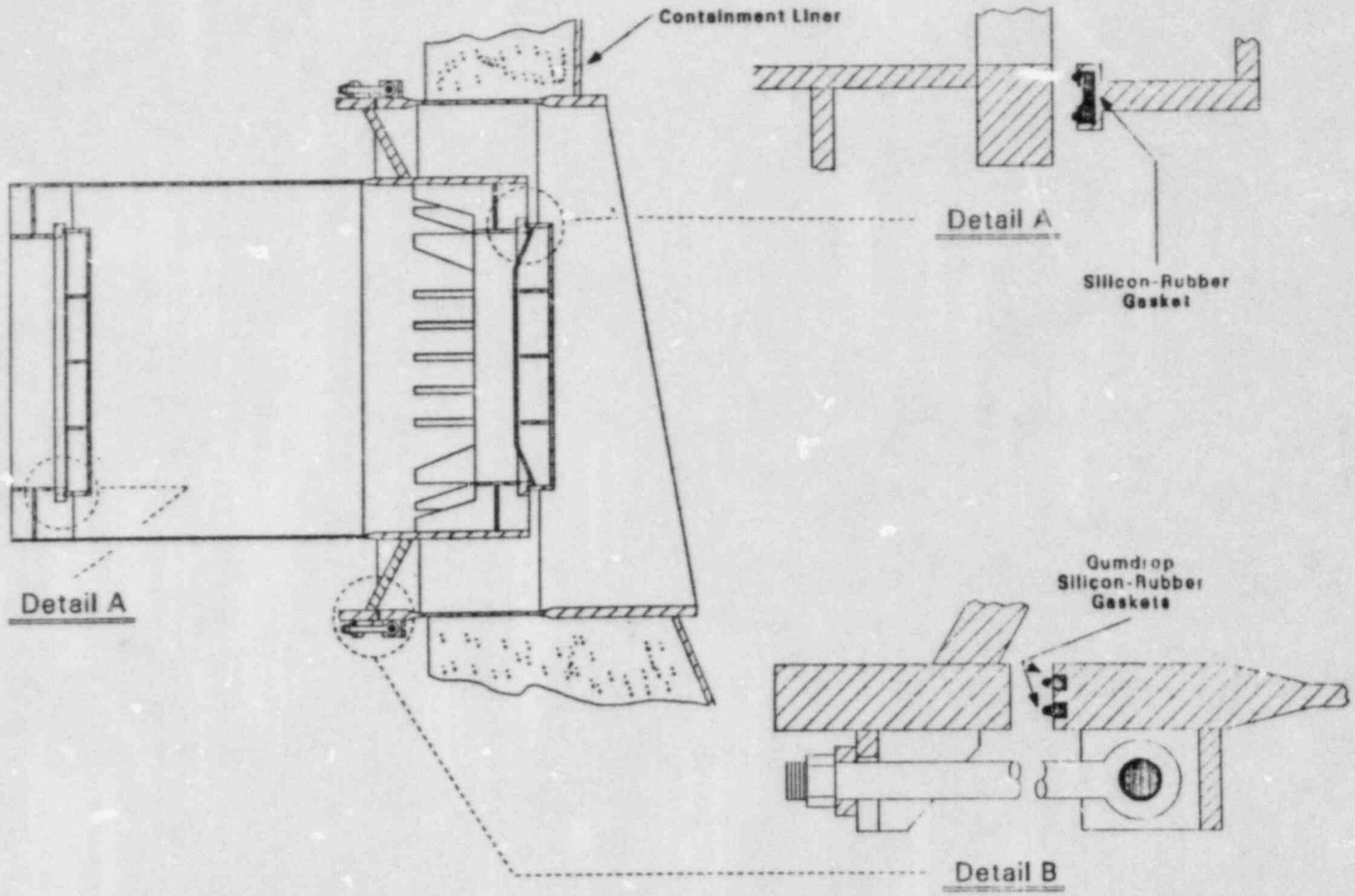

Figure 1. Limerick 12 Ft. Dia. Hatch with Integral Personnel Airlock

Due to the geometry of most flat bulkheads, a circular plate with a rectangular opening, it is quite conceivable that separations may occur between the door and door frame due to pressure loading even though the pressure tends to close the door. Several bulkhead designs have been analyzed to determine the seriousness of this separating effect. Separation was determined to occur to various degrees for all bulkheads analyzed. These analyses were performed neglecting any structural properties of the seals. It is recognized that even though this separation occurs, leakage of the personnel airlocks may still not occur. Other things must be considered, such as the seal material's ability to maintain a seal and the redundancy of the two door designs. These considerations aside, an evaluation of the structural behavior of the doors and bulkheads is the first step required to assess the leak tightness of personnel airlocks.

The analyses performed for the various bulkhead designs were accomplished using linear elastic three-dimensional finite element models of the bulkheads (reference 1). The computer code SAP IV was used to perform these analyses (reference 2). Advantage was taken of symmetry about the bulkhead's horizontal and vertical center line axes, allowing the use of one quadrant models of the bulkheads. The bulkheads were either modeled using plate elements or a combination of plate and beam elements, depending upon the bulkhead design. Figure 2 is an isometric plot of the computer model representation of the Limerick personnel airlock external bulkhead. This bulkhead was modeled using a combination of beam and plate elements. Short, stiff truss elements were placed between the door and door frame. If any of these elements went into tension, indicating separation, they were removed from the model. For this model, separation occurred at the top and bottom of the door only. This analysis was performed for a pressure loading of 140 psig, which is considered the ultimate pressure capacity of Limerick's containment (reference 3). The personnel airlock was designed for a pressure of 62 psi. This is 7 psi above the design pressure of 55 psi for the containment.

The maximum separation between the door and door frame at 140 psig was determined to be only .0003 inch. This maximum separation occurred at the vertical center line of the door, top and bottom. To illustrate the sensitivity of this separation to specific design details, the analysis was redone with the door vertical center line stiffening plate omitted. The maximum separation occurred at the same location and was an order of magnitude larger. Stresses were determined to be below the material yield strength in the Limerick external bulkhead for a pressure loading of 140 psig. This was not the case for all the bulkheads analyzed. Stresses above yield strength were encountered for two similar bulkheads prior to reaching the containment ultimate capacity. This yielding occurred in the main support beams above and below the door opening. Such yield-

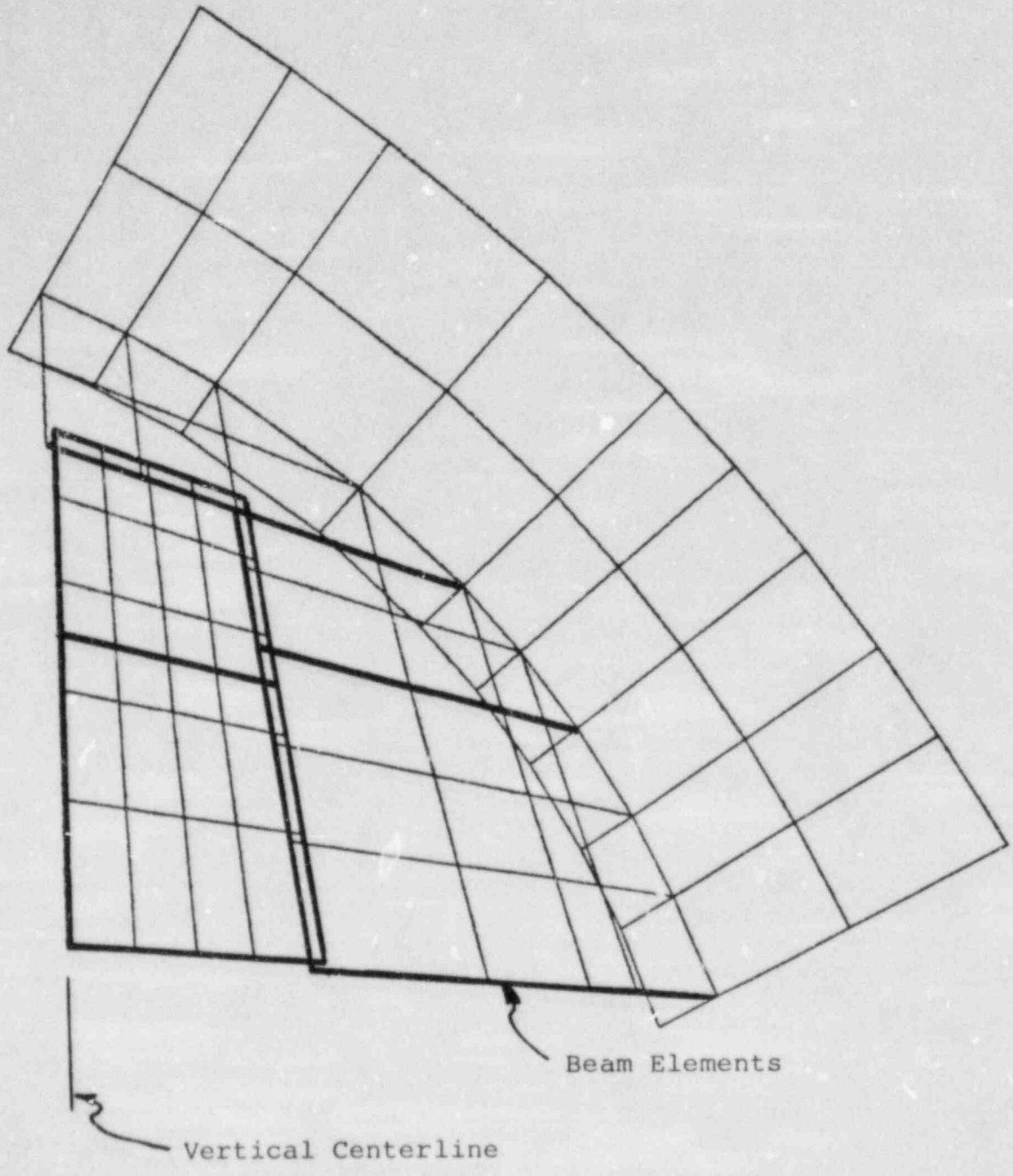

Figure 2. Bulkhead Model

ing will of course result in a greater leak area than is calculated by elastic analysis. This condition is currently being investigated by inelastic methods; however, this task is not complete.

Similar analyses were performed for the bulkheads with the radial stiffening gussets using models with plate elements only. The maximum separation from these analyses was determined to be .007 inch at the containments ultimate pressure capacity. All element stresses were determined to be below the material yield strength for these bulkheads.

PRESSURE UNSEATING CLOSURES ANALYSES

Containment large opening penetrations frequently have closures which are external to the containment, such as the equipment hatch shown by figure 1. These closures are of particular interest, since containment pressure tends to separate the mating flanges. Sufficient separation will result in containment leakage.

Several analyses of this type of closure have been performed using the two spring model depicted in figure 3.

For:

K1 = bolt stiffness
K2 = flange-shell stiffness
F1 = bolt load
F2 = flange load
F = preload
P = applied load.

The solution for the flange load is as follows:

$$F2 = \frac{P\ (K2)}{(K1 + K2)} - F. \qquad \text{(reference 4)}$$

The initiation of flange separation occurs when F2 becomes zero. Setting F2 = 0 in the above equation and solving for the required applied load to cause flange separation (P_S) results in the following equation

$$P_S = \frac{(K1 + K2)}{K2} F.$$

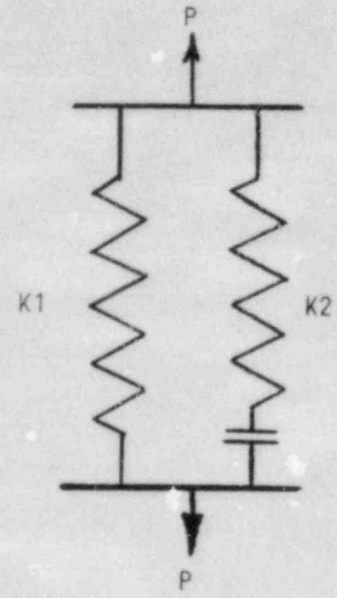

Figure 3. Model for Determination of Flange Separation for Pressure Unseating Closures

The flange separation (Δ) for applied loadings greater than P_S is given by the following equation

$$\Delta = \frac{P - P_S}{K1} S \cdot$$

The analyses performed using this method neglected any structural properties of the seal materials, since the seal materials are very soft relative to the other stiffness values. For situations where the seal design was such as not to allow the mating flanges to make metal to metal contact, the flange separation was determined assuming there was no preload. As can be seen from the equations used to perform these analyses, calculation of the flange separation due to pressure loading is somewhat sensitive to the stiffness values; however, determining the preload is of greater concern. This is particularly true when the preload must be determined from a specified bolt torque value, since the coefficient of friction can take on such a wide range of values depending on the lubrication conditions used.

An analysis of the Limerick containment large opening penetrations required determining the flange separation for several large opening, pressure unseating closures. The results for those closures are tabulated below.

Penetration	Penetration Circumference (in.)	Pressure Required to Initiate Flange Separation (psig)	Separation Due to 140 psig. (in.)
Drywell Head	1425.5	84.5	0.0230
Equipment Hatches	452.4 each 904.8 total	74.5	0.0094
Drywell Head Manhole Hatch	75.4	0.0	0.0011
Control Rod Drive Removal Hatch	113.1	0.0	0.0010
Suppression Chamber Access Hatches	163.4 each 326.7 total	0.0	0.0046

The results contained in Table 1 illustrate quite clearly where the greatest potential for containment leakage lies. The larger openings of the drywell head and equipment hatches not only have the larger circumferential perimeter to allow leaking, but the flange separations for these closures are significantly larger than those of the smaller penetrations.

CONCLUSIONS

Structural analyses of several containment large opening penetrations have been performed to determine their leak areas as a function of containment pressure during severe accidents. Metal to metal separation at sealing surfaces does occur for personnel airlock doors and pressure unseating closures. The leak area for personnel airlock doors is nearly insignificant, provided the bulkhead structural members do not yield. containment leakage of the larger pressure unseating closures may be significant depending upon the seal material's ability to maintain a seal for flange separations up to .023 inch.

REFERENCES

1. Containment Performance Working Group Containment Leak Rate Estimates, NUREG-1037, Fourth Draft, April 4, 1984.

2. Computer Program Manual, "SAP-IV--Structural Analysis Program for Static and Dynamic Response of Linear Systems," University of California, Berkeley, California, June 1973.

3. Containment Structural Capability of Light Water Nuclear Power Plants, IDCOR Technical Report 10.1, Technology for Energy Corporation, July 1983.

4. Mechanical Design Analysis by M. F. Spots.

NUMERICAL STUDIES OF LARGE PENETRATIONS AND CLOSURES FOR CONTAINMENT VESSELS SUBJECTED TO LOADINGS BEYOND THE DESIGN BASIS*

R. F. Kulak, B. J. Hsieh, J. M. Kennedy,
J. E. Ash, and G. A. McLennan
Argonne National Laboratory
9700 South Cass Avenue
Argonne, IL 60439

ABSTRACT

Numerical simulations of the macro-deformations of the sealing surfaces (gasketed junctures) of a PWR steel containment vessel's equipment hatch and a BWR Mk II containment vessel head have been performed. Results for the equipment hatch juncture indicate that the rotations of the hatch cover and penetration sleeve must be accounted for when performing leakage analysis because they can effect the compression of the gasket even though the gasket is in a pressure-seated configuration. Results from a leakage analysis indicated that excessive leakage can occur if the surface roughness is high and/or the compression set is high.

Results for the Mk II head show that both the temperature and pressure loadings must be taken into account to obtain realistic responses. The temperature difference between the flanges and bolts has the important net effect of keeping the gasketed juncture closed, that is in metal-to-metal contact. Due to the high accident temperature, the gasket itself was found to achieve 100 percent compression set and thus could not perform its sealing function within the juncture.

INTRODUCTION

The Reactor Analysis and Safety Division (RAS) and the Components Technology Division (CT) of Argonne National Laboratory (ANL) are performing analytical/numerical simulations of the response of selected large penetrations and closures, which use some type of seal or gasketed joint, for containment vessels subject to pressure and thermal loads that are beyond the design basis (BDB). This work is part of the ANL Penetration Integrity Program (PIP) which is being sponsored by the U.S. Nuclear Regulatory Commission and managed by the Sandia National Laboratories (SNL). This report covers the work performed in Task 2 - Analysis of Fixed and Operating Penetrations. The objectives of this task were to identify the methodology required to simulate the structural response of selected penetrations/closures to BDB loadings and to apply this methodology to representative penetrations/closures.

*Work performed under the auspices of the U.S. Department of Energy.

STRUCTURAL RESPONSE OF AN EQUIPMENT HATCH OF A PWR STEEL CONTAINMENT VESSEL

The major components of a PWR nuclear power plant are installed within a containment vessel. The containment vessel is typically a cylindrical shell with closed ends, the wall of which may be penetrated by certain other pipe-shell structures (e.g., personnel locks, equipment hatches, etc.). During very unlikely but potentially severe accidents the containment vessel may be subjected to pressure and temperature loadings that may be much larger than the design values. Studies on the response of steel containments to internal pressurization were reported by Blejwas and Horschel [1], Derbalian et al. [2], and von Riesemann and Blejwas [3].

Our primary objective here was to determine the sealing surface deformations of a particular containment penetration, known as the equipment hatch, under severe accident conditions. Figure 1 shows the loadings that we were provided with by SNL [4]. A secondary objective was to integrate these quantitative predictions into leakage rate information that will be used to evaluate overpressurization and to quantify leakage of the containment atmosphere.

Equipment Hatch Details

The scope of ANL's work in the Penetration Integrity Program includes (1) the identification and classification of major penetrations in PWR and BWR containments (Task 1), which is reported in Ref. 5, and (2) the analysis of selected penetrations for structural failure or leakage (Task 2). This report covers the analysis aspect. However, since the identification task and this analysis task are concurrent, we did not have final details available to us at the onset of our work. Because of the time schedule, we had to start our analysis work and to use a "best estimate" design for an equipment hatch. The dimensions and layout of our best estimate design were obtained from limited information that was available to us. We used our design judgment to estimate values for the missing dimensions.

Figure 2 is a generic schematic of an equipment hatch for a steel containment vessel. The hatch consists of a penetration sleeve, a cover, a reinforcing ring/plate, and seals (gaskets). Table 1 gives the dimensions of our best estimate design for an equipment hatch for a steel containment vessel.

Numerical Studies of Equipment Hatch Cover, Penetration Sleeve, and Sealing Surfaces

The structural response under hypothetical pressure loads of an equipment hatch penetration has been analyzed with the STRAW [6] finite-element structural analysis code. Our approach to this problem was to perform a decoupled analysis of the hatch cover and the penetration sleeve, that is, independent models were developed for the cover and the penetration sleeve. If our results would indicate that a coupled analysis was necessary, we

would reanalyze the problem using a coupled approach. Analysis of the structural response of the penetration has been performed for the following two models:

(1) a computational model for the dome and ring assembly inboard of the seal junction acted upon by the pressure loading alone, and

(2) a computational model involving the essential features of the penetration sleeve acted upon by the combined loading of the direct pressure forces, the forces exerted by the global expansion of the containment shell, and an equivalent load from the cover.

Response of Hatch Cover

The purpose of first series of computations was to determine the deformations of the sealing surface of the cover ring and the collapse load of the cover door. The computational model is shown in Fig. 3. The pressure loading was applied incrementally up to 250 psi. The relative effects of the cover-plate and the ring were illustrated by increasing the ring-thickness from 3 in. to 4 in., and the cover-plate from 1-1/8 in. to 1-1/2 in. The effects of dome thickness and ring thickness upon the ring distortions at the seal joint are shown in Fig. 4. For the "best estimate design" (i.e., 1-1/8 in. thick cover plate, 3 in. thick ring, and 30 ksi yield stress) the response is essentially elastic up to a pressure of about 175 psi. Increasing the ring thickness is beneficial for reducing the distortion in the vicinity of the seal and increases the effective elastic range to a pressure of 250 psi. We found that this cover goes plastic at about 250 psi.

Response of Penetration Sleeve and Sealing Surface

Our second series of computations was performed to determine the deformations of the sealing surface of the penetration sleeve. To accurately determine the displacements of the sealing surface we constructed a model that included the penetration sleeve, reinforcing plate, and a portion of the containment vessel wall. Since we had restricted our initial analysis to axisymmetric geometry, we cannot exactly model the cylindrical containment vessel. The reason for this is that our axis of symmetry for the model was choosen to be along the axial direction of the peretration sleeve. This choice provides the proper geometric representation for the penetration sleeve and seal surface, which are of primary interest. However, this choice also forces the cylindrical containment vessel to be treated as a spherical containment vessel.

For this initial study, we used a 45 deg. sector of the sphere with a 1350 in. radius to capture representative interactions between the sleeve and vessel. Our model for the penetration is shown in Fig. 5. Three thicknesses were considered for the purpose of evaluating the plates' effect on seal surface deformation. The 4.5 in. plate thickness conforms with the area replacement rule for openings in cylinders; the 3.0 in. and 6.0

in. plates were purposely chosen to be smaller and larger, respectively, but otherwise arbitrary.

The deformed shape of the penetration sleeve is shown in Fig. 6 for the vessel with a 4.5 in. ring at an internal containment pressure of 86 psig. We see that the reinforcing ring has pulled the penetration sleeve into a crimped shape in the region of the penetration sleeve-reinforcing ring juncture. This primarily causes the seal surface to undergo large translational and rotational displacements that can lead to leakage. The radial displacement of the sealing surface provides a shearing action to the seals. The seal surface rotation tends to decrease the compression of the seal. The relation of these deformations to leakage from the containment is evaluated in the next subsection.

Table 2 summarizes the displacement results for several thicknesses of the reinforcing plate. It is seen that the reinforcing plate has a significant effect on the seal surface deformation. We can view the effect of these deformations in the region of the gaskets in Fig. 7 for the case of a 3.0 in. reinforcing ring. The undeformed shape of the gumdrop type gasket has been superimposed to give a feel of gasket compressibility or lack of compressibility.

Leakage Analysis

A preliminary analysis has been performed to estimate the leakage rate from the seals (gaskets) of an equipment hatch cover during an overpressurization. The seal geometry was taken from Fig. 2. The displacement of the seal faces was taken from very preliminary estimates of the ring rotations, which are not reported here. The seal leakage rate was modeled using results from an analytical/experimental study reported in Ref. 7 which includes a rather detailed study of leakage past O-rings, where the significant parameters are the final seal compression (initial compression and compression sets) and the machined surface roughness. Figure 8 shows the leakage rate for these O-rings (DuPont E60C polymer) for a variety of surface finishes as a function of actual seal compression. Reference 7 contains an expression for the final compression, C_F, as a function of the initial compression C_i, and the compression set, C_s, as a function of O-ring diameter, d, and flange separation, X. This final compression can be written as

$$C_F = \frac{C_i(1 - C_s) - \frac{X}{d}}{1 - (C_i C_s)} \qquad (1)$$

Reference 7 also includes a thermal transient compression set C_{st} which may be significant, but has been ignored for the analysis.

The flange separation X was taken to be at the center of the outer gasket shown in Fig. 2 and due only to the ring rotation. The presence of the inner gasket was ignored, because the separation there is much higher.

Leakage past the seal was approximated from Fig. 8 using the worst cases (curves C and D) and a less pessimistic case (curve A), approximating these curves by a linear fit

$$\text{Log } (L) = B - A \cdot C_F \qquad (2)$$

with the values B = 6.2 and A = 49.6 approximated from curves C and D, and B = -1 and A = 42.4 for curve A. The leakage obtained from Eq. (2) is standard cc per atmosphere pressure and per cm of circumference of the seal (which is 615-3/4 in. = 1564 cm for this gasket). For this study (as in Ref. 7), the compressions were initially taken to be C_i = 25% (common practice) and C_s = 20% (lack of actual data). The compression set C_s could be as large as 100% (no recovery if unbolted) so C_s was treated as a parameter, ranging from 0.2 to 0.8.

Figure 9 shows the calculated leakages as functions of pressure for various C_s for the worst case. As can be seen, for low pressure, the leakage rate is "small" but can get rather high. For comparison purposes, estimating the containment volume to be about 2×10^6 ft^3, then 1% leakage per day would be approximately 6500 cc/sec. This value would be exceeded at about 105 psi on Fig. 9 for C_s = 0.2, and much sooner for higher compression sets. For $C_s > 0.2$, some of the curves stop before 150 psi because the final compression C_F goes to zero, in which case the leakage model is no longer applicable.

The less pessimistic case does not get to 1% leakage per day, for any C_s before the gasket compression goes to zero. Thus, if the seals and machined surfaces had this quality, leakage may not become excessive (> 1% vol/day) for this <u>one</u> penetration using this leakage model, but the gap would open during flange rotation.

Concluding Remarks

Our finite element model for the cover exhibited elastoplastic buckling at about 250 psig. The maximum specified pressure inside the containment was 155 psig, and therefore we do not expect this cover to buckle.

A finite element analysis of the penetration sleeve revealed that its sealing surface can undergo large rotations which can lead to leakage. A value of 7° at a bursting pressure of 86 psig was computed for the "best estimate" design. We found that the thickness of the reinforcing plate had a significant effect on the amount of rotation. Thus, both numerical simulations and scale model experiments must take into account the reinforcing plate in order to obtain meaningful results for seal surface deformations, which are subsequently used in a leakage model.

We must remember that we have performed an axisymmetric analysis of a three-dimensional structure, which eliminates some of the deformation modes. In particular, we cannot capture the oval shape that the penetration will deform into. Thus, in reality, we expect that the sealing surface rotations will vary along the circumference and that our predicted values will neither be maximum nor minimum values. A three-dimensional anal-

ysis is highly recommended in order to obtain these variations as well as to provide additional insight into the behavior of this structure.

A preliminary analysis to estimate the leakage rate from the seals has been performed using the finite element predicted deformed configurations. The simple leakage model indicated that excessive leakage can occur if the surface roughness is high and/or the compression set is high.

STRUCTURAL RESPONSE OF A MK II CONTAINMENT VESSEL HEAD

The approach developed to assess the structural integrity of a BWR Mk II containment vessel head, which contains non-pressure seated gaskets, to mechanical and thermal loadings that are beyond the design basis is described here. Our concern focused on the macro-deformations of the sealing surfaces between the removable head and the conical shell. This juncture contains two continuous gumdrop gaskets in a configuration classified as non-pressure seating. During BDB loading the sealing surfaces were expected to separate and unseat the gasket and, thus, provide a potential leak path for the containment atmosphere.

Containment Vessel Head Description

The top head is an elliptical shell that is bolted to a conical skirt. As shown in Fig. 10 the conical skirt is connected to the reinforcing-steel support ring and the steel vessel liner plate. The reinforcing steel support ring is held securely against the containment wall by the reinforcements. The specific design for which we performed a finite element analysis had a 1-3/8 in. thick elliptical shell that was welded to a 4 in. thick upper flange. The 1-1/2 in. thick conical skirt was welded to a 4 in. thick lower flange at its uppermost elevation and to a 2-1/2 in. thick reinforcing-steel support ring at its lower elevation. Sixty 2 in. thick stiffeners are welded to the conical skirt and reinforcing-steel support ring. The surface of the lower flange contains two grooves each of which houses a 3/4 in. x 1/2 in. continuous gasket. The upper flange surface has two nubbins that mate with the gaskets in the lower flange to form a seal. A pretensioned bolting system is used to maintain leak tightness during internal pressurization of the containment. Each pretensioning bolt is mounted between 1-1/2 in. thick upper and lower bolt mounting rings. These rings are welded to their respective flanges and reinforced by 3/4 in. thick gusset plates located on each side of the bolt. Each bolt is 3 in. in diameter and approximately 36 in. long. There are a total of 60 bolts equally spaced around the periphery of the head. Each bolt is tightened to an initial bolt load of 290,000 lb. SNL [4] has provided us with anticipated drywell pressure and temperature histories (Fig. 11) that are based on information which they had obtained for incorporation into their Electrical Penetration Assembly (EPA) test plan.

Numerical Studies of the Vessel Head

In order to obtain reasonable predictions of the response of the drywell flange seal junction for leakage analysis it was necessary to perform a finite element analysis. Because we feel that the thermal loading will play a significant role in determining the leak tightness of the juncture, it must be taken into account. An examination of the rate of mechanical loading and the maximum applied temperature indicate that the structural analysis and the thermal analysis can be decoupled. Thus, the thermal analysis can be performed first to determine the temperature field histories, and then the structural analysis can be completed using the pressure and temperature histories as input. This is the approach that we have taken.

The main results from our thermal analysis, which is not discussed here because of space limitations, are that (1) there is about a 5.6 minute time lag between the inside wall temperature and the mid-thickness temperature, which implies that the membrane temperature loading should be delayed by the 5.6 minutes from the pressure loading in the structural analysis, and (2) the average temperature of the bolts would be about 312° F, in the steady state, less than the average temperature of the flanges due to convective heat losses.

Structural Analysis

The drywell head is seen to be primarily an axisymmetric structure. The elliptical shell, flanges, conical skirt, bolt mounting rings and gaskets are all continuously axisymmetric. The bolts, gussets, and stiffeners are discretely axisymmetric. That is, they occur at discrete locations every 6 deg. around the periphery of the head. Therefore, for a first analysis of this problem, an axisymmetric model should provide reasonable insight into the major response and identify the important parameters.

Finite element model and loads

Figure 12 shows the axisymmetric finite element model that was used in our numerical simulations. Thin shell elements are used to represent the elliptical shell, upper flange, and upper bolt mounting ring of the head cover as well as the lower flange, conical skirt, tendon support ring, and lower bolt mounting ring. The gusset plates and stiffeners are modelled using plane stress continuum elements. A rod element is used to simulate the structural behavior of the bolts. An ad hoc gap-contact element with friction was implemented into the STRAW code to simulate the mechanics at the juncture of the upper and lower flanges.

The model was loaded in two stages. During the first stage the bolts are preloaded to an initial tension value of 290,000 lb each, which corresponds to a bolt stress of about 41,000 psi. This preloaded the bolts in tension and the upper and lower flanges in compression. During the second stage the internal pressure and temperature loadings were applied to the model.

Figure 13 shows the variation of bolt stress during the loading history. The preload brings the bolt stress to its design value of 41,000 psi. The stress rises slightly as the internal pressure builds up (Points A-B). At point B the membrane thermal load is applied and the bolt stress rises rapidly to its yield value of 100,000 psi (Point C). Thereafter it increases slightly.

A set of computer runs was performed to determine the effect that bolt preload has upon the leak tightness of the juncture using both pressure and thermal loading. The preload was reduced from 290,000 lb/bolt to 198,000 lb/bolt and finally to 84,000 lb/bolt. The results for the juncture stress are shown in Fig. 14 for the two cases. For the preload level of 198,000 lb/bolt, the basic history of the juncture stress follows the same pattern as that for the design value preload with the stress levels, as expected, being reduced. Here the juncture also remained closed throughout pressure and thermal loading cycles. In contrast, a bolt preload level of 84,000 lb/bolt produces a leakage path at the juncture when the internal pressure reaches 35 psig.

The gasket of the head is subjected to a thermal transient during an accident. The temperature history experienced by the gasket is assumed to be the same as that of the inside of the reactor containment shell. The compression set, C_s, due to a thermal transient was computed using the methodology of Ref. [6] and the results indicate that all the compression is lost 17 min. after the gasket reached 750° F.

Concluding Remarks

A study of the structural response of a Mk II containment head subjected to BDB pressurization and thermal load with emphasis on the macro-deformations of the gasketed juncture was performed. An examination of the pressure and temperature histories indicated that the thermal analysis and structural analysis can be decoupled, and this was the approach taken.

Our analytical thermal analysis indicated that the thermal strain response of the flanges would lag the pressure loading by about 5.6 min. It was also found that, in the steady state, the average temperature of the bolts would be about 312° F less than the average temperature of the flanges due to convective heat losses. This has the important net effect of keeping the gasketed juncture closed.

REFERENCES

[1] Blejwas, T. E. and Horschel, D. S., "Analysis of Steel Containment Models," Proceedings of the Workshop on Containment Integrity, NUREG/CP-0033, SAND 82-1659, pp. 201-226 (1982).

[2] Derbalian, G., Fowler, G., and Thomas, J., "Three-Dimensional Finite Element Analysis of a Scale Model Nuclear Containment Vessel," Failure Analysis Associates report, FaAA-83-4-5, ME 08 (1983).

[3] Von Riesemann, W. A. and Blejwas, T. E., "The NRC Containment Integrity Programs," presented at Seminar No. 7, Issues in Containment Analysis and Design (CONFABRE-4), SMiRT-7, Chicago, IL (August 1983).

[4] Letter, Subramanian, C. V., SNL, to Bump, T., ANL, dated November 8, 1983.

[5] Bump, T. R., Seidensticker, R. W., Shackelford, M. H., Gambhir, V. K., and McLennan, G. A., "Characterization of Nuclear Reactor Containment Penetrations," NUREG XXX, SAND XX, ANL-84-83 (1984).

[6] Kennedy, J. M., "Nonlinear Dynamic Response of Reactor-Case Subassemblies," ANL-8065 (January 1974).

[7] Chivers, T. C., George, A. F., and Hunt, R. P., "High Integrity Static Elastomer 'O' Ring Seals and Their Performance Through Thermal Transients," Ninth International Conference on Fluid Sealing, pp. 37-54 (1981).

Table 1. Equipment Hatch Dimensions

Reinforcing Plate		Cover Dome	
Thickness, t_{RP}	3 in.	Radius R_{CD}	16 ft SPH
Width, W_{RP}	33 in.	Thickness, t_{CD}	1-1/8 in.
Penetration Sleeve		Cover Ring	
Radius, R_{ps}	8 ft.	Height, H_{CR}	1 ft 3 in.
Inboard Thickness, T_{psi}	3 in.	Thickness, t_{CR}	3 in.
Inboard Length, L_{psi}	1 ft 3 in.		

Table 2. Variation in Rotation with Reinforcing Plate Thickness

Thickness (in.)	Rotation (Deg.)
3	17
4.5	6.8
6	4.9

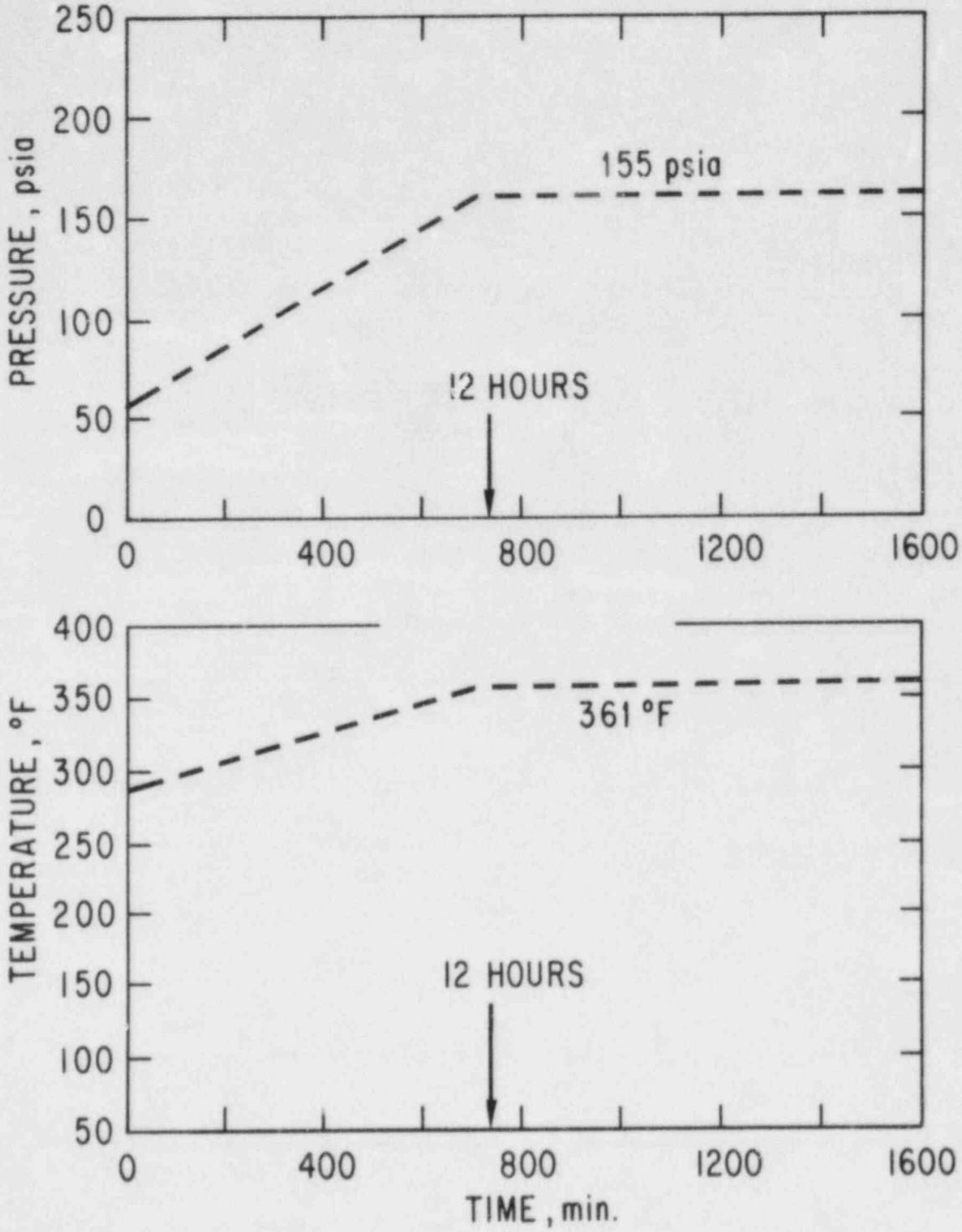

Figure 1. PWR Pressure and Temperature Histories

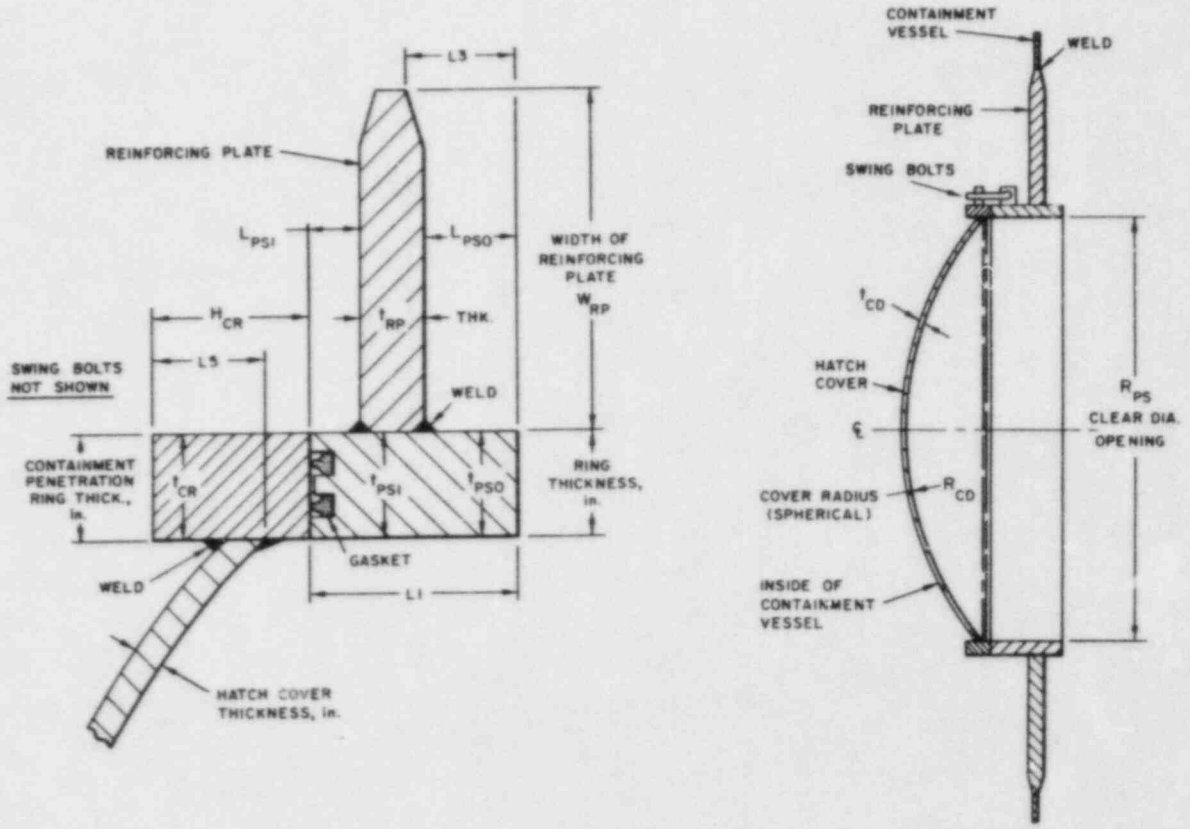

Figure 2. Generic Schematic of an Equipment Hatch for a Steel Containment Vessel

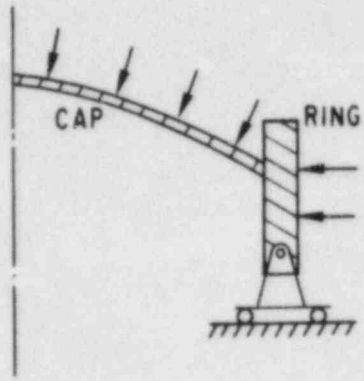

Figure 3. Computational Model for Equipment Hatch Cover

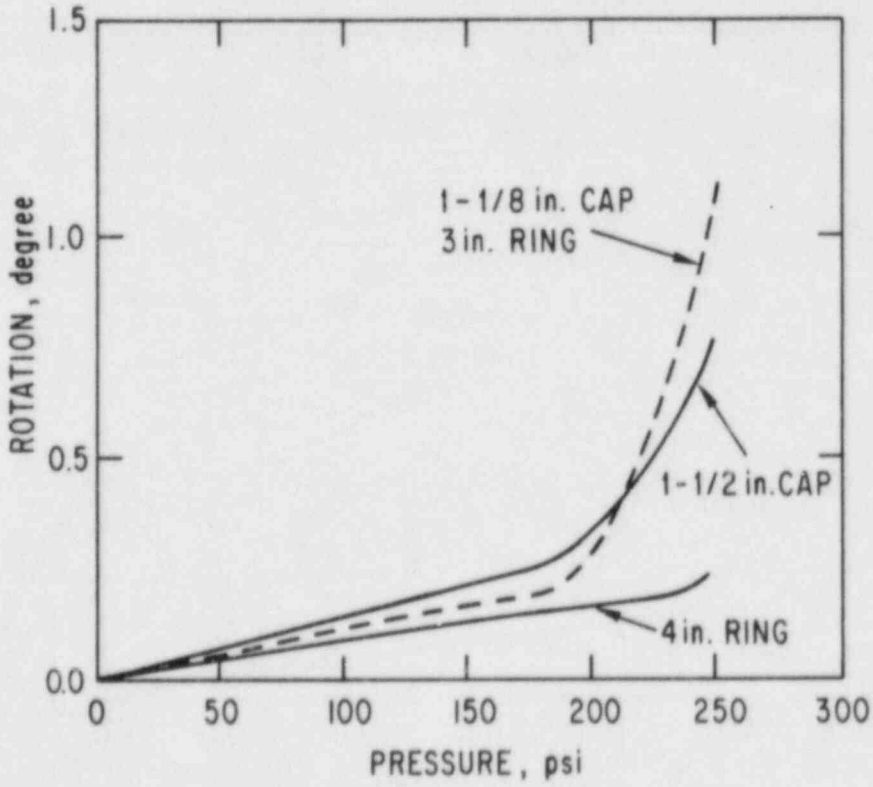

Figure 4. Rotational Displacement of the Sealing Surface of the Hatch Cover

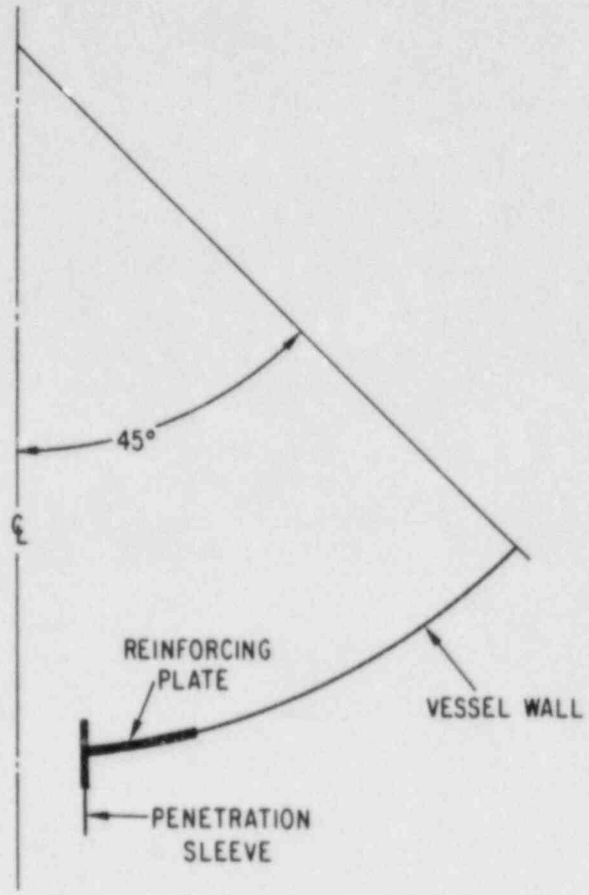

Figure 5. Penetration Model

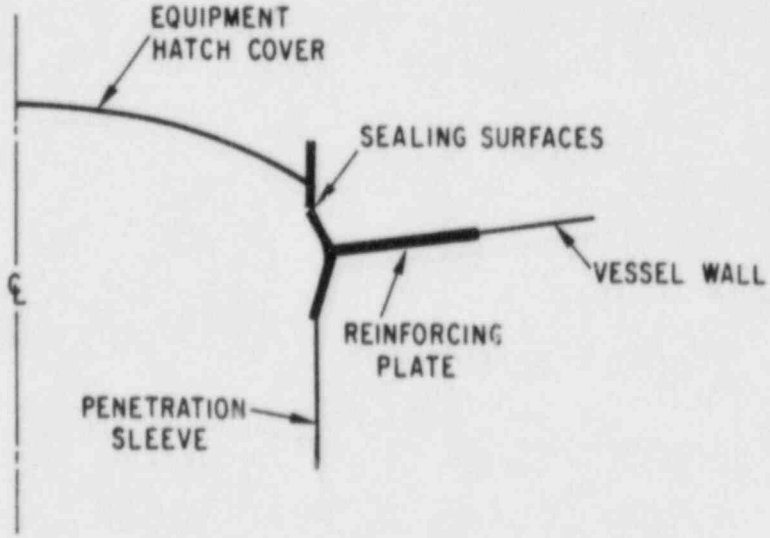

Figure 6. Deformed Shape of the Penetration Sleeve

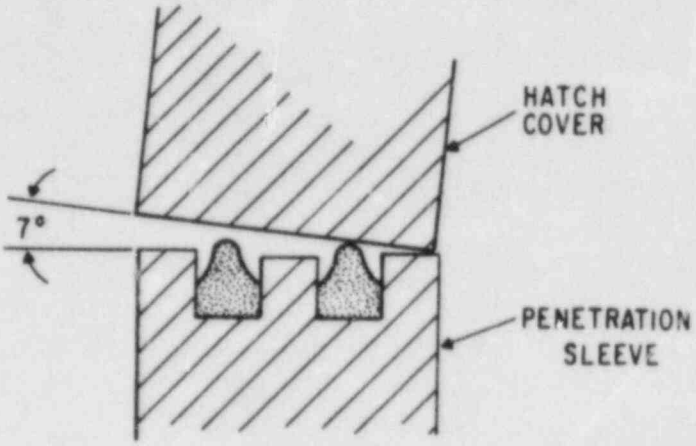

Figure 7. Deformed Profile of Sealing Surfaces

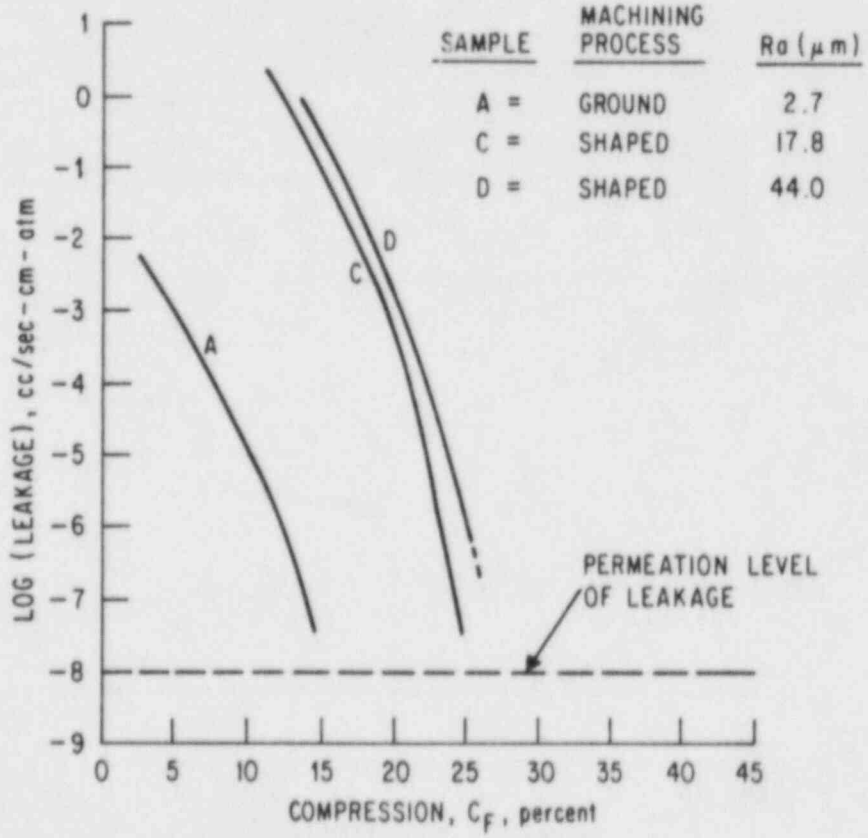

Figure 8. Variation of Leakage with Seal Compression

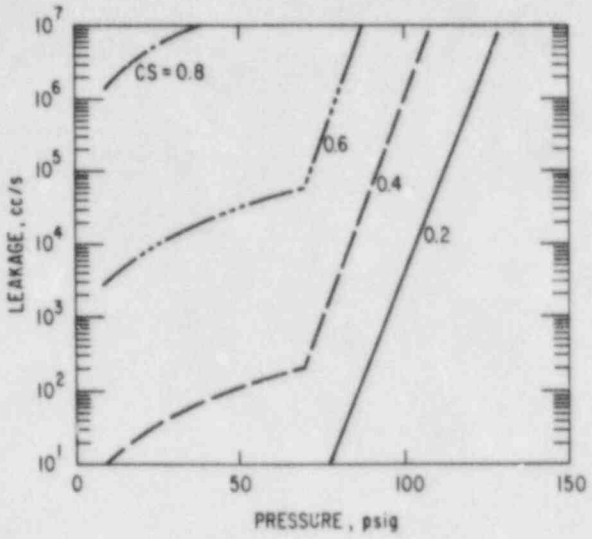

Figure 9. Calculated Leakages for Worst Case

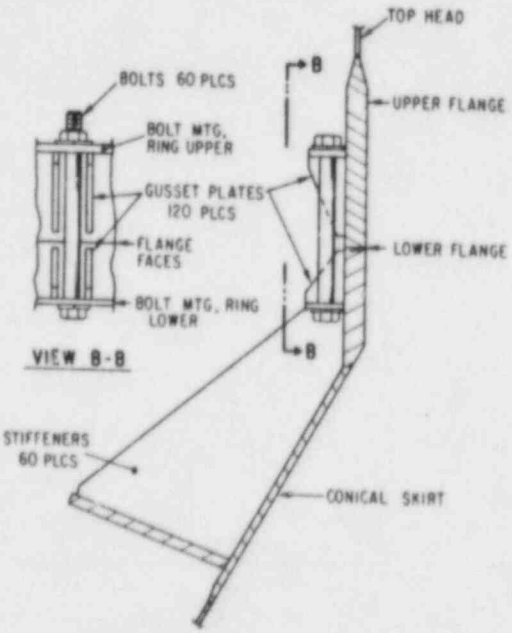

Figure 10. Top Head Juncture

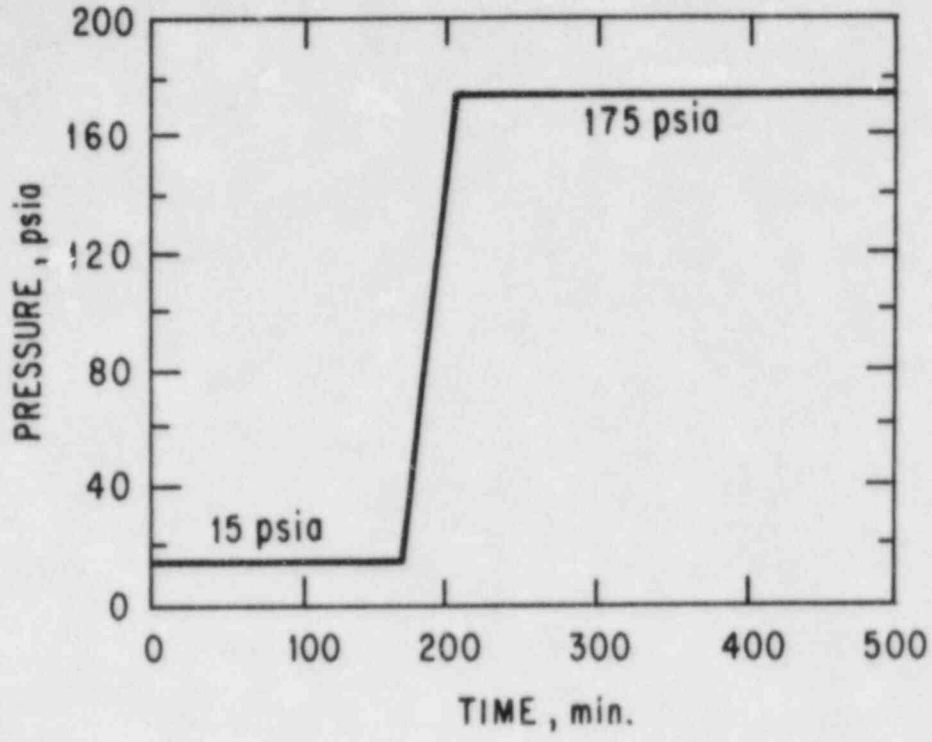

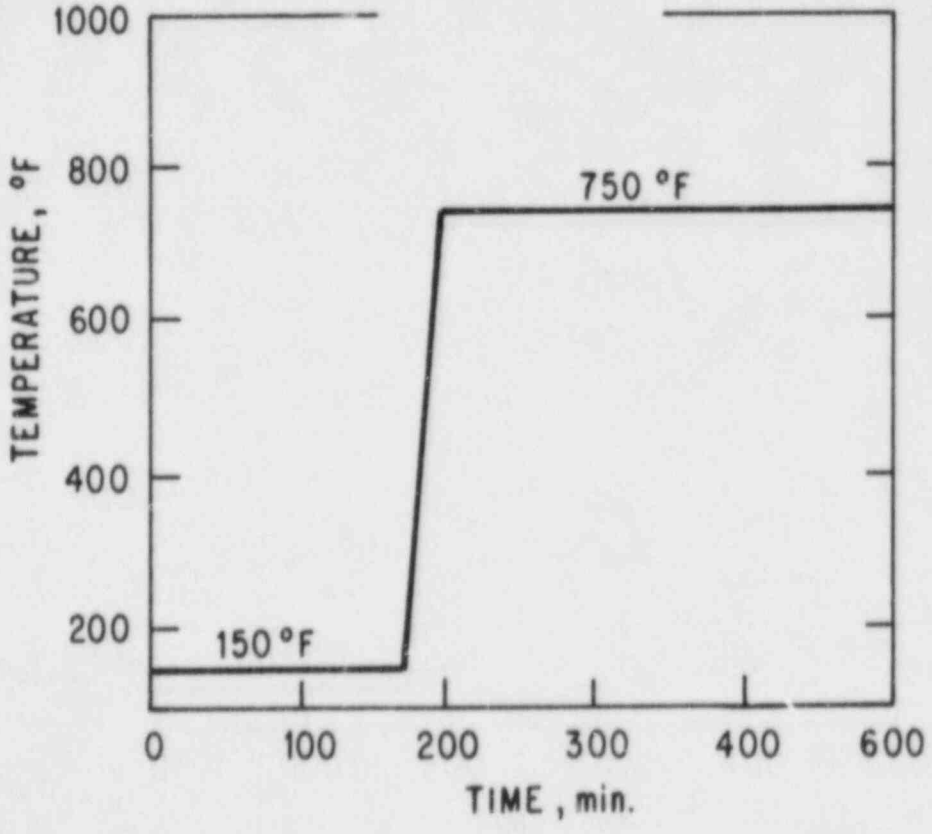

Figure 11. Drywell Pressure and Wall Surface Temperature Histories

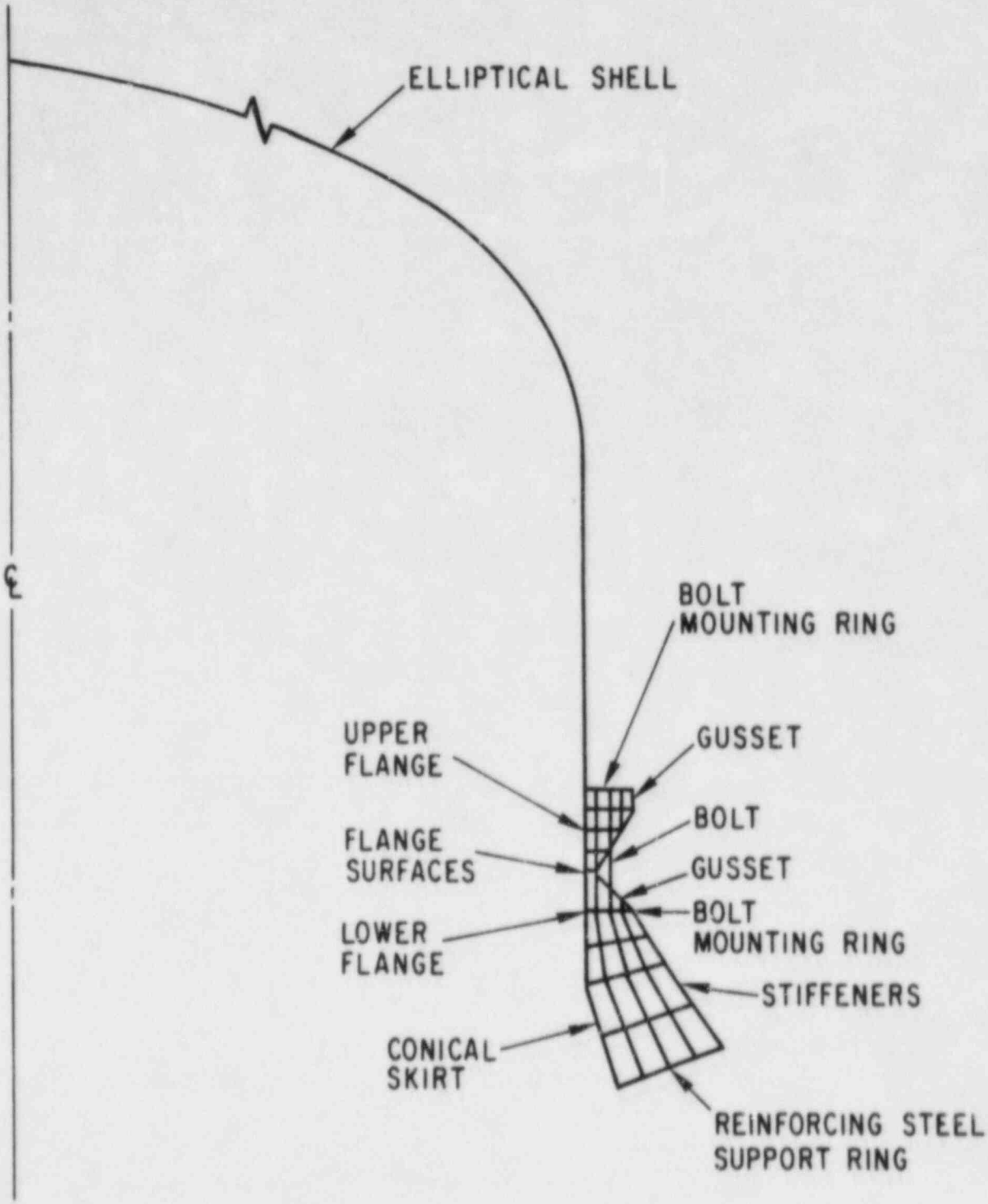

Figure 12. Finite Element Model of Containment Vessel Head

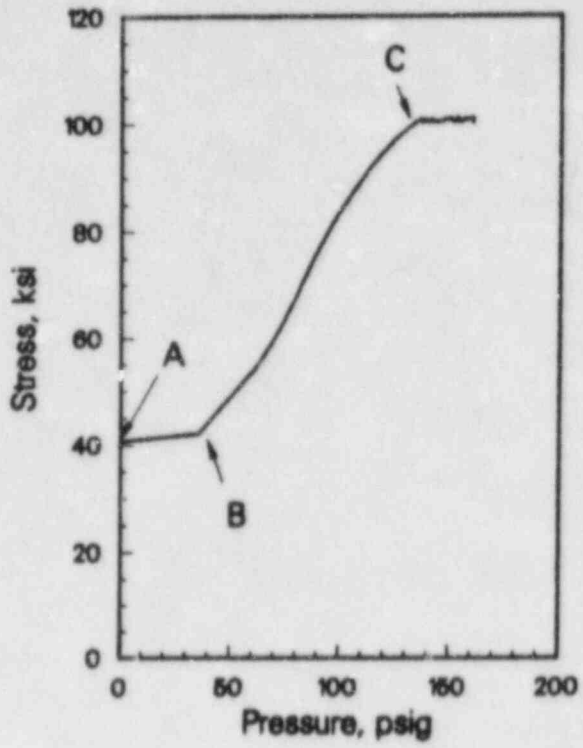

Figure 13. Variation of Bolt Stress for the Case with Pressure and Thermal Loadings

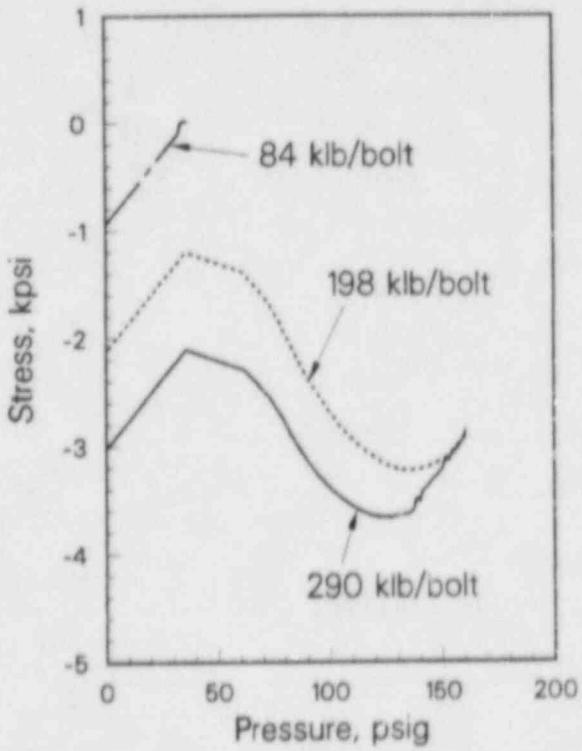

Figure 14. Effect of Level of Bolt Preload on Juncture Compression

CONTAINMENT PENETRATION ELASTOMER SEAL TEST*

B. L. Barnes
EG&G Idaho, Inc.
P.O. Box 1625
Idaho Falls, ID 83401

ABSTRACT

Under the predicted extremes of nuclear reactor containment pressure associated with severe accidents, the mating metal surfaces of some "pressure unseating" penetrations will separate, thereby partially removing the static precompression on the elastomer seals between these surfaces. Two seal designs similar to those employed by containment penetrations on the Surry and Peach Bottom nuclear power plants were leak tested as functions of flange separation and at containment pressures and temperatures approximating severe accident conditions. Both seal designs were found to be very leak resistant for the short time periods tested at all but the most extreme conditions of flange separation and operational temperatures. Flange separations required to produce incipient leakage at ambient temperatures greatly exceeded worst case severe accident predictions.

PROBLEM DESCRIPTION

For nuclear reactor containment pressures less than the design pressure, separation of the "pressure unseating" bolted flanges is impossible because the combined preload of the flange bolts is greater than the product of the design pressure and the area of the penetration over which this pressure acts. However, given that predicted severe accident pressures exceed design pressures by a factor of about 2.5, some "pressure unseating" penetrations employing bolted flanges have been shown to separate on the order of 0.010 to 0.030 in.

The average amount of flange separation is very easy to calculate given the principle dimensions of the penetration, number and size of flange bolts, and a peak severe accident pressure. With considerably more effort, one can even accurately calculate the separation of the flanges at any point around the perimeter of the sealing surfaces. For symetrical penetrations, the separation being in general less near the flange bolts and greatest equidistant between the flange bolts. If the penetration is assumed to be without an elastomer seal, it is even possible to make a

* work supported by the U.S. Nuclear Regulatory Commission, Office of Nuclear Regulatory Research under DOE Contract No. DE-AC07-76ID01570.

reasonably accurate prediction of gas leakage by analytically modeling the flange separations as one or more convergent/ divergent nozzles in series releasing gas to the atmosphere.

The great difficulty appears when an attempt is made to calculate gas leakage with the presence of an elastomer seal between the flanges which fully or partially blocks the flow path. To even calculate with certainty whether or not a seal leaks at all is very difficult. Because such calculations are very difficult, and the results would most certainly be controversial, the problem appears to best lend itself to experimental methods which are not without controversy, but which can if done correctly, provide credible results.

Because the cost of testing full sized penetrations was prohibitive, it was decided to test two seal designs with full size cross-sectional dimensions, but of reduced circumference or length. The idea being that if the cross-sectional dimension of the test model were full size and the circumference reduced, the leakage per inch of circumference would be essentially the same as on a larger diameter full size penetration. Flange separation was incrementally increased using shims between the mating flanges. Equivalence of results between full size and reduced circumference incrementally separated models is compromised in the areas shown below:

1. Unlike the full sized penetration, the reduced circumference model employs flat relatively rigid metal surfaces which make the flange separations very nearly uniform around the sealed perimeters. The full size penetration, on the other hand, is relatively flexible so separation near the flange bolts is less than the separation at positions equidistant between bolts. This translates to constant leak areas versus variable leak areas for model and full size penetrations, respectively. Predicted rotation of full size flanges for "pressure seating" designs is similarly compromised by models not duplicating rotation.

2. Given model and full size double concentric elastomer seal designs, the ratio of inner seal circumference to outer seal circumference in both cases approaches unity, but they are not equal. The smaller the models circumference, the greater the departure from unity.

3. The incremental separation of the flanges used in these tests differs from the actual separation on full size penetrations which is a linear function of pressure above the limiting pressure where flange bolt preload is exceeded by pressure times penetration area forces.

Considering the above compromises, it was decided to perform a scoping test using a pair of 18 in.-900 lb ANSI reducing flanges

(32 in. O.D. x 4 in. thick with 20 bolts 1-7/8 in. diameter) to test two different seal designs each employing a different elastomer seal material. The plan was to first machine the flanges to retain double concentric neoprene, type W O-Rings of 19.74 in. I.D. x 0.50 in. diameter and 22.74 in. I.D. x .50 in. diameter in trapezoidal O-Ring grooves as schematically shown in Figure 1. This configuration is used for the Surry PWR personnel air lock hatch, fuel transfer tubes, CRD hatches, and equipment hatches.

After completing the first test series on the O-Rings, the flanges were remachined, this time to duplicate the tongue-in-groove configuration typical of the Peach Bottom equipment hatch and drywell head seals. Figure 2 schematically depicts the double rectangular tongue-in-groove Garlock Silicone compound #8364 seals. These seals were retained in 19.5 in. I.D. and 22.5 in. I.D. grooves and were, before compressed installation, nominally 0.765 in. wide x 0.523 in. deep. All flange and seal dimensions were made to the approximate middle of the dimensional tolerance range specified on the engineering drawings of the full size commercial containment penetrations. This was intentionally done because the results obtained here were known to be sensitive to dimensional variations involving the seal size and the mating metal surfaces.

TEST APPARATUS

Figure 3 schematically shows the apparatus used to perform these tests. The fully instrumented 18-in.-900 lb flanges (item 1-Figure 3) were heated electrically and pressurized by nitrogen from a pressure controlling valve (item 11) which in turn was supplied by a large nitrogen bottle trailer (item 16). Three sizes of turbine flow meters (item 13) operating in parallel and individually throttled by manual valves (item 12) allowed for measuring a broad range of steady gas flows which would leak from between flanges whose separation was maintained and controlled by six circumferentially placed matched shim stacks. Thermal insulation placed around the flanges sped heatup time and minimized thermal gradients within the approximately 1800 lb of flange material. All essential test data was simultaneously recorded on four dual channel 10 in. wide strip chart recorders. A visual flow indicator, not shown in Figure 3, consisted of 1 in. wide x .002 in. thick plastic strips hung from a round hoop around the outside of the insulated flange pair. Though not providing a quantitative measurement of gas leakage from between the flanges, the plastic strips were capable of detecting flange leakage far below the ranges measurable with the smallest of the three turbine flow meters.

TEST PROCEDURE SUMMARY

The test plan used is briefly summarized below. In general, the plan followed NRC approved model data sheets, each consisting of graphical plots (a family of curves) of estimated leakage versus vessel pressure as a function of flange separations of 0.000,

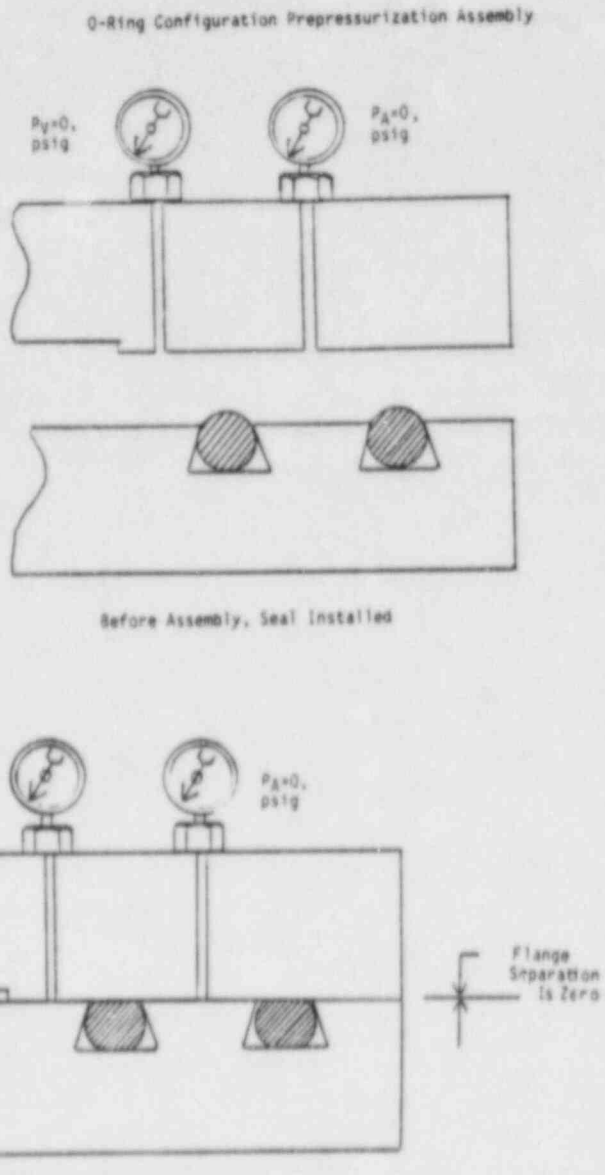

Figure 1. O-Ring configuration prepressurization assembly.

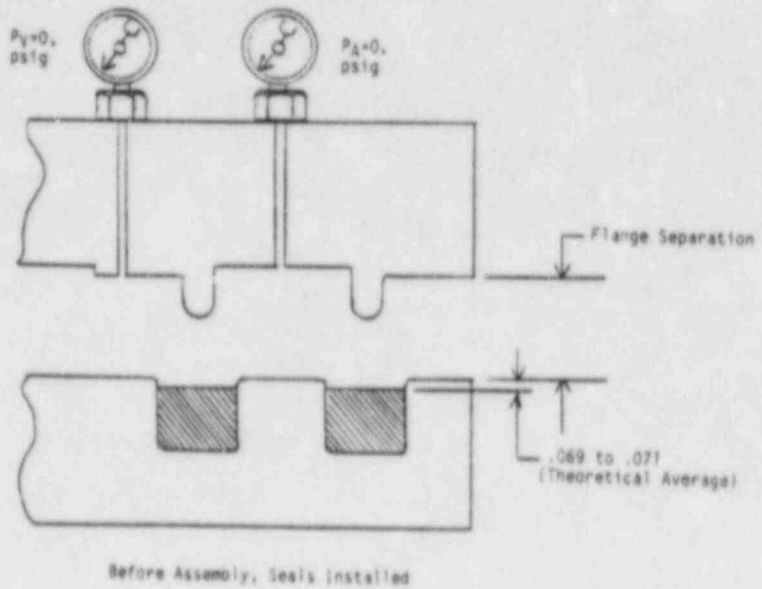

Figure 2. Tongue-in-groove prepressurization assembly.

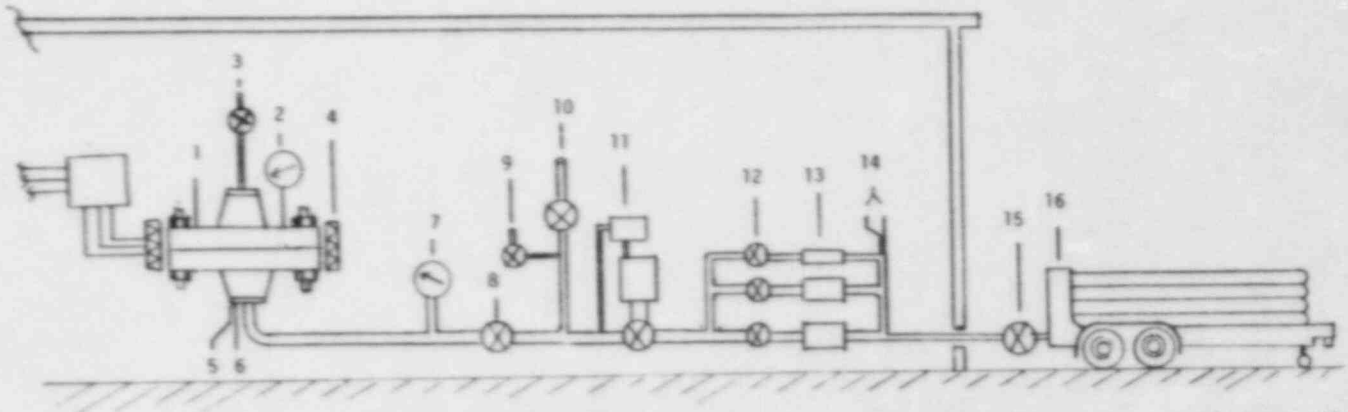

1 18"x6"-900 lb ANSI weld neck reducing flange pair with faces machined to retain 0.50 inch O-Ring seals in double trapezoidal grooves. These flanges were remachined to accept rectangular silicone tongue-in-groove seals after the O-Ring seal tests were complete. As built dimensions for both seal configurations are shown elsewhere in the text.

2 One of three circumferentially located dial indicator gauges measuring flange separation to within ± .0005 inch. Flange separation was controlled with shims placed between the flanges; the dial indicator gauges were used to check the proper placement and selection of the shims. Integral jack screws (3) were used to separate the flanges for shim insertion and seal inspection.

3 1/4" bleed valve used to depressurize the flanges before adjusting flange separation

4 Electrical resistance heaters which clamp to the flange circumferences. 480 VAC 3Φ power from the schematically depicted temperature controller above and to the left of the flanges was used to control flange temperature via a thermocouple feedback link.

5 Dual pressure taps monitoring vessel pressure and the pressure between the seals (annulus) via bourdon tube gauges and electric pressure transducers tied to two of four dual channel 10" wide strip chart recorders. The calibrated bourden gauges were used only as a quick visual check of system pressure and not as a source of test data.

6 Dual thermocouple taps monitoring vessel central body temperature and annulus temperature. Calibrated thermocouples were electrically tied to two of four 10" wide dual channel strip chart recorders.

7 Redundant bourdon tube gauge placed close to pressure controller (11) for operator convenience.

8 1 1/2" ball block valve-4000 psi rating

9 1/4" manually operated bleed valve to atmosphere

10 Pressure relief valve to prevent overpressurization of flanges

11 1 1/2"-2500 lb ANSI valve with attached pressure controller and air driven positioner.

12 One of three manually operated combination turbine throttling and block valves used to select and control each of three turbine flow meters.

13 One of three turbine flow meters of 1/2", 1", and 1 1/2" sizes.

14 Pressure and temperature transducer taps and transducers for monitoring turbine flow meter inlet pressures and temperatures. Transducers were connected to two of four dual channel 10" wide strip chart recorders for permanent recording of data.

15 2" block valve-integral to nitrogen trailer.

16 Nitrogen bottle semi-truck trailer-2000 psig working pressure with approximately 40 individually valved bottles each about 20 feet long.

Figure 3. Schematic diagram of experimental seal test apparatus.

0.010, 0.020, and 0.030 in. For the neoprene type W seals, there were four such graphical plots to guide the experiment progress for operational temperatures of 61, 248, 370, and 420°F. For the rectangular silicone tongue-in-groove seals, four similar graphical plots were used which called for flanged seal temperatures of 70, 475, 550, and 606°F. Additionally, one test using the tongue-in-groove configuration was run as a base line for leak data with no elastomer seals in place. Because the seals were found to be more resistant to leakage than anticipated, much more data was taken for larger values of flange separation than originally planned. Flange separations for the neoprene, type W O-Rings of up to 0.218 inch were ultimately tested at ambient temperature. Similarly for the silicone seal tongue-in-groove configuration, flange separations of up to 0.301 in. were tested.

Referring to Figure 3, with valve (item 15) open and one or more valves (item 12) open, the heated flanges were pressurized with nitrogen in at least six stepped approximately equal increments of pressure between zero and at least 160 psig. At each pressure step, the visual flow indicators and the smallest turbine flow meter were checked for leakage. If leakage was observed, up to two turbine meters were monitored and recorded at once. By varying the nitrogen supply pressure from the trailer (item 16) as measured at (item 14), rangeability of the turbine flow meters could be adjusted to accurately measure both small and large leak rates. At the conclusion of each test, the electric power to the flange heaters was turned off, and the internal (vessel) pressure of the flanges was reduced to atmospheric pressure by opening bleed valves (item 3) and (item 9) and closing valves (item 8) and (item 12). Because the flanges were very rigid and the test pressures very low, only six of the twenty flange bolts were used. Flange separation was varied by loosening the six flange bolts working through holes in the thermal insulation. Three circumferentially positioned jack screws located radially outside the seal area were then used to separate the flanges so each of the six shim stacks could be changed to vary flange separation. Once the shims were placed, the jack screws were backed off until the upper flange rested atop the six shim stacks. The six flange bolts were then retorqued to a minimum value of 255 ft-lb to ensure that the bolt preload forces exceeded vessel pressure times area forces thereby precluding further flange separation in response to vessel pressure. Observation while testing of the dial indicators (item 2) verified that flange separation did not change because of vessel pressures exceeding 200 psig. Shims were changed at flange temperatures up to 606°F using gloves.

EXPECTED RESULTS

O-Rings

Because the 0.502 in. diameter O-Rings in 0.416 in. deep trapezoidal grooves protruded 0.086 in. above the surface of the lower flange, leakage was anticipated for flange separations in the

neighborhood of 0.086 in., the "theoretical separation point." This geometry can be best understood by examining Figures 1 and 4. Leakage was thought to be certain for flange separations significantly exceeding 0.086 in.

Tongue-in-Groove Seals

Refer to Figures 2 and 4. With the silicone seals initially below the surface of the lower flange by 0.069 to 0.071 in. and the tongues protruding below the flat surface of the upper flange by 0.320 to 0.321 in., a "theoretical flange separation point" of about 0.249 to 0.252 in. would in all probability define the approximate flange separation where incipient leakage would occur.

ACTUAL RESULTS

O-Ring Seals

For ambient temperatures, flange separations were increased in 30 increments of flange separation between 0.000 and 0.188 in. before the first leakage was observed at a separation of 0.188 in. This was the point of incipient leakage; Figure 5 shows maximum leakage was often observed at lower pressures. At higher pressures leakage often dropped off or stopped completely. For incipient leakage to occur at 0.188 in. separation is surprising; this is far in excess of 0.086 in., the "theoretical separation point". Flange separation was next incrementally increased to a value of 0.218 in.; the seals again reseated at high pressure for each of the three separation increments. Leak flow for the 0.218 in. separation was not plotted because the data was erratic and flow was both time and pressure path dependent. These extremes of flange separation were far beyond the range of practical interest relating to severe accidents.

At all stated test temperatures below 420°F, no O-Ring seal leakage was observed for flange separations of 0.000, 0.020, 0.030, 0.040, or 0.060 in.; because there was no leakage, no plots were made for those temperatures. However, at 420°F, the flanges were observed to leak slowly. Leakage was so slow that measurement with a 1/2 in. turbine flow meter was impossible and detection with the plastic visual flow indicators was difficult at all but the highest pressures near 180 psig.

Though these tests were not designed to measure very low levels of leakage (seepage), a rough estimate of the magnitude of these leaks was made by repeated use of the universal gas law as applied to a pressure-time decay curve. Figure 7 was generated based upon calculating the mass m_1 of gas in the known volume V of the system with the known gas temperature T_1 and pressure P_1 by the universal gas law, $P_1V = m_1RT_1$. At a later known time when the pressure had decayed to a level P_2 with associated temperature T_2, the mass m_2 was again calculated using $P_2V = m_2RT_2$. Next, the mass loss of gas during time period Δt was taken as

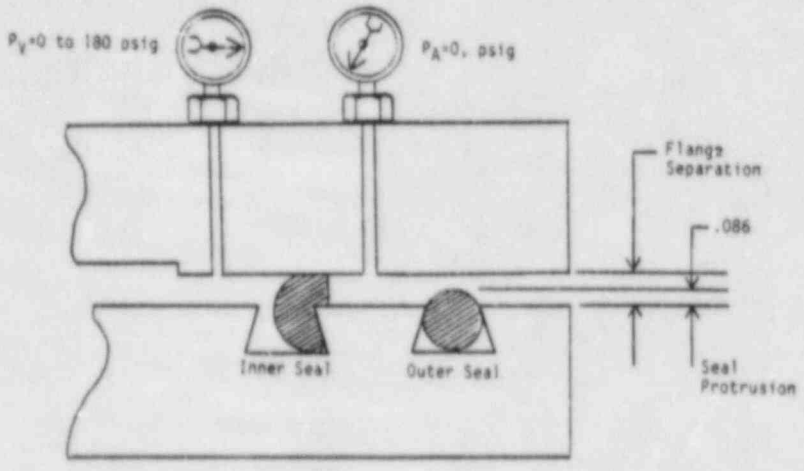

O-Ring Seal Post Pressurization Configuration

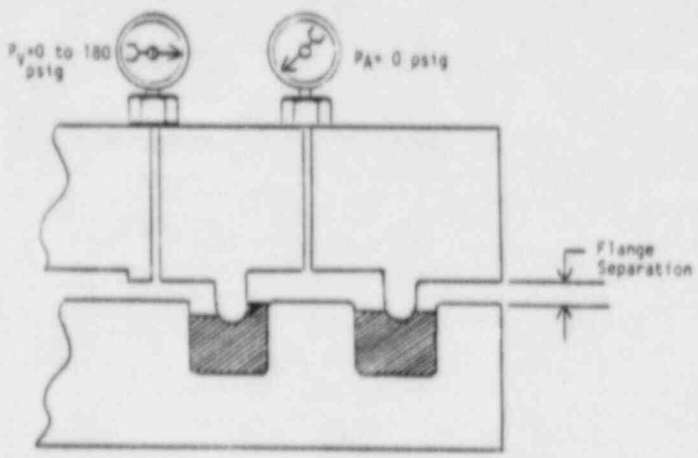

Tongue-in-Groove Post Pressurization Configuration

Figure 4. Post pressurization.

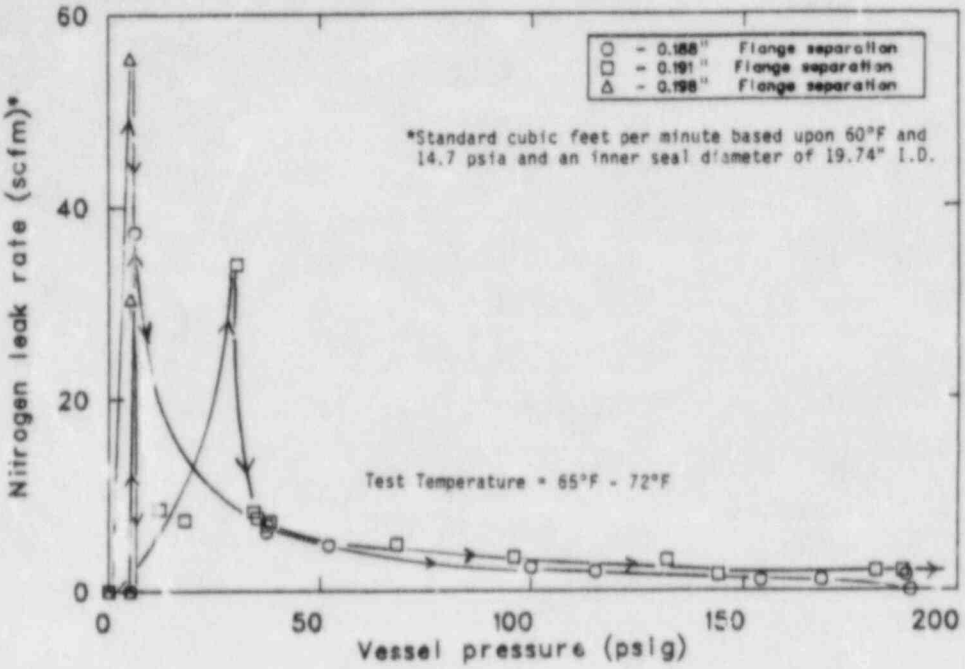

Figure 5. Double O-ring seals in trapezoidal grooves.

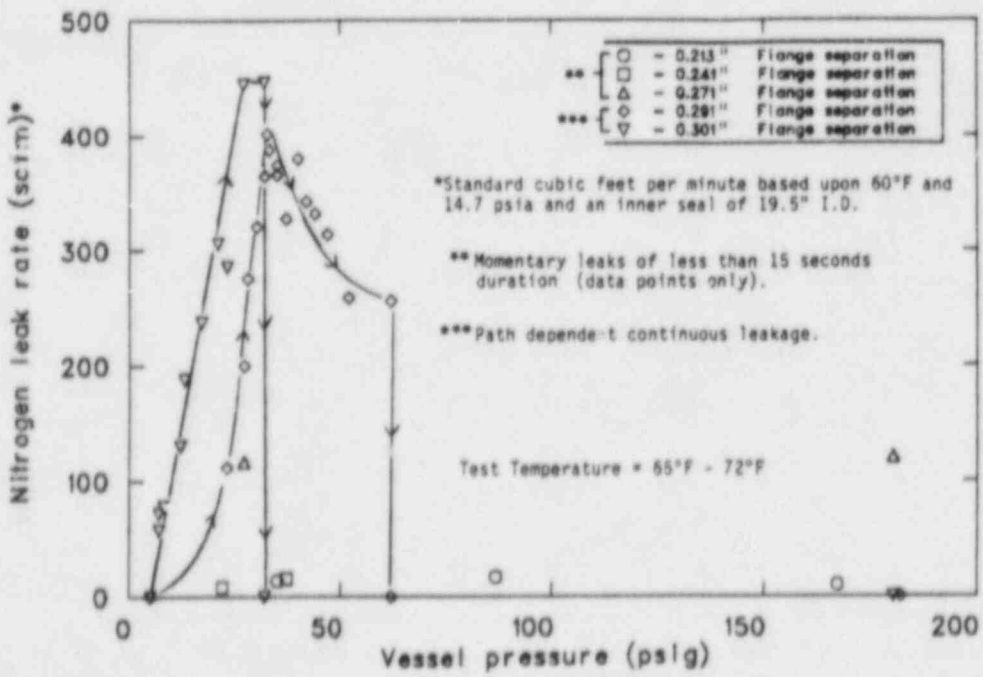

Figure 6. Double rectangular silicone seals in tongue-in-groove configuration.

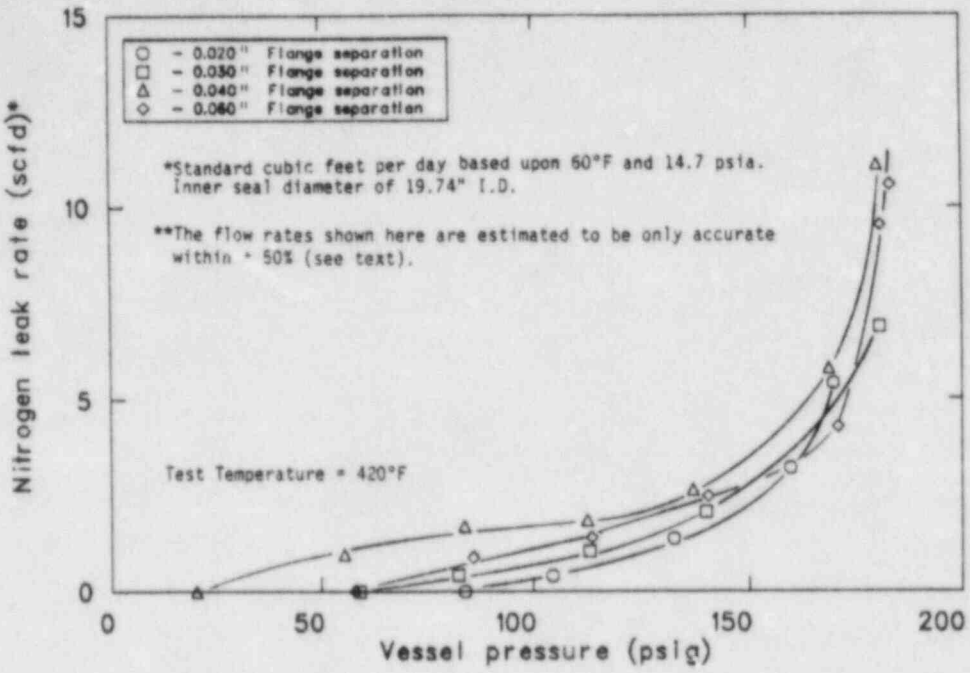

Figure 7. Approximate** seepage for double neoprene, type-W O-ring seals per inch of inner seal circumference.

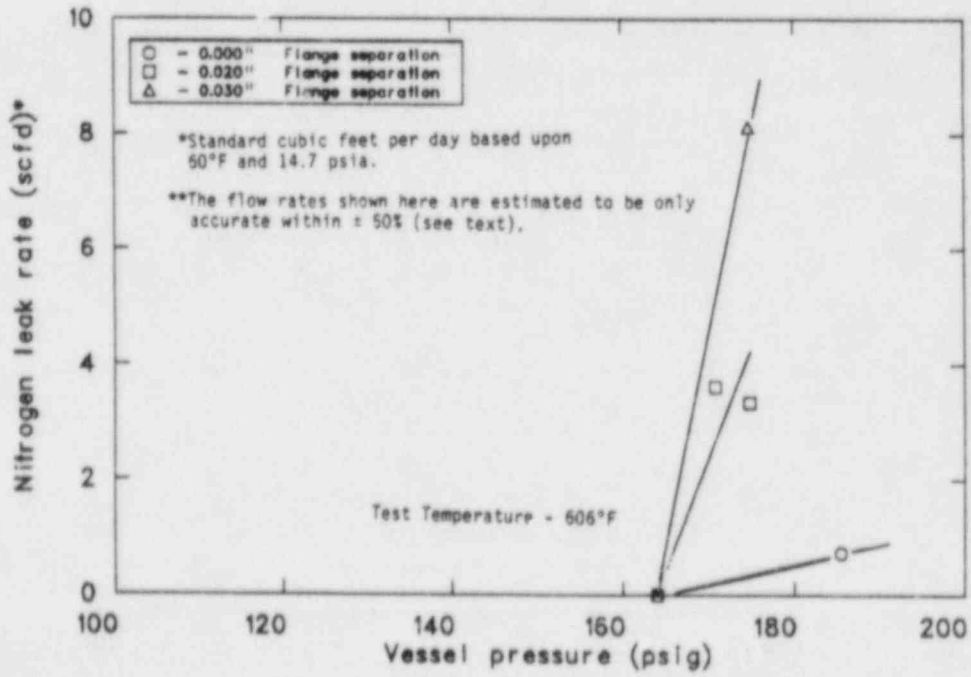

Figure 8. Approximate** seepage for double silicone tongue-in-groove seals per inch of inner seal circumference.

$(m_1 - m_2) = \Delta m$ and the universal gas law was used a third time as shown below to calculate the standard volume V_S that Δm would occupy at 60°F (520°R) and 14.7 psia = P_S. With V_S and Δt now known,

$$P_S V_S = \Delta m R T_S$$

a rough estimate of the average or integrated leak rate occurring during the pressure decay between P_1 and P_2 can be obtained by simply dividing V_S by Δt to get the standard cubic feet per unit time lost due to leakage at the average pressure $(P_1 + P_2)/2$.

The principle weakness of this calculation is with the loss of significant figures of accuracy when one subtracts values of m_1 and m_2 which are nearly equal. A quick sensitivity analysis applied to this data shows that these numbers are in some cases only accurate to within $\pm$50% because of the aforementioned loss of significant figures.

These calculated values of seal seepage were detectable only at 420°F for the neoprene type W seals; hence they are only of significance for this particular material if PWR severe accident temperatures equal or exceed 420°F for sufficient time to bake, crack, and deformation set the seal material as observed here. Though no planned aging was included in this test series, the 420°F test temperature did permanently deform the O-Rings to a cross-sectional shape resembling the capital letter D.

Tongue-in-Groove Seals

Unlike the O-Ring seals which did not leak until flange separations greatly exceeded the "theoretical separation point", the tongue-in-groove seals experienced incipient leakage at low pressures (~35 psig) at a flange separation of 0.213 in. which was less than the 0.249 to 0.252 in. "theoretical separation point." Figure 6 for the tongue-in-groove seals is similar to the O-Ring seals ambient temperature leakage as shown in Figure 5 in that maximum seal leakage most often occurred at lower pressures and in many cases slowed or stopped at higher pressures.

For the silicone seals no leakage was observed for flange separations of 0.000, 0.020, and 0.030 and 0.060 in. at test temperatures of 475°F and 550°F. For this reason no plots of leakage were made for these test temperatures.

At 606°F the silicone seals were observed to leak slowly (seepage) in much the same way the neoprene seals did at 420°F. The seepage was calculated using the same method described earlier. It is significant to note however, that no seepage was observed below 164 psig as shown in Figure 8. The silicone seals did resist leakage very well considering that the two seals melted together and were later removed as one. These pressure tests were of short

duration; for long periods of time, a temperature of 606°F is likely to result in gross leakage of the magnitude described by Figure 9 for the case of tongue-in-groove design without seals in place. Even the smallest of temperature increases above 606°F for silicone seals of this type are likely to result in gross leakage. Again, the significance of this leakage is strongly dependent upon how closely BWR severe accident temperatures approach 606°F and remain at these temperatures long enough to heat the seal material itself to these temperatures. Thermal lag time and steady state thermal gradients are expected to provide both significant and dependable assurance that penetrations employing these designs and materials survive all but the most extreme of severe accidents extending over the longest time periods.

CONCLUSION

For the seal designs and materials tested here, flange separation resulting from extremes of severe accident related pressures is not likely in itself to be the source of significant containment leakage. Extremes of temperature lasting over a sufficiently long period of time are however, a significant factor that may contribute to gross containment leakage. These conclusions may not be applicable to seal materials and designs differing from those tested here.

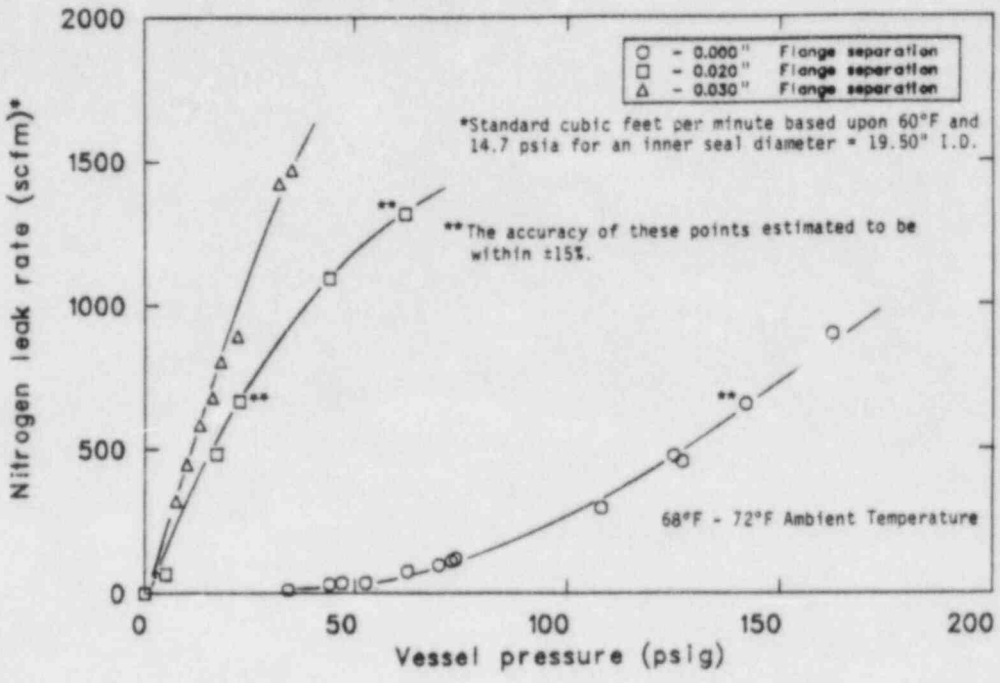

Figure 9. Leakage for double tongue-in-groove design without seals.

SESSION E

PROGRAMS ON CONTAINMENT INTEGRITY

THE KFK/PNS RESEARCH PROGRAM ON PWR STEEL CONTAINMENT BEHAVIOR UNDER ACCIDENT CONDITIONS

W. Gulden
Kerforschungszentrum Karlsruhe GmbH.
Projekt Nukleare Sicherheit
Postfach 3640
D-75 Karlsruhe 1
Federal Republic of Germany

ABSTRACT

The mechanical behavior and possible failure of spherical steel containments for German PWRs will be investigated. The assumed loads could be caused by postulated accidents as a core melt accident, a deflagration of hydrogen, local loadings and severe earthquakes. Appropriate computer programs will be developed and checked by experiments including several bulge tests with circular membranes and oscillation and buckling tests with a high precision spherical shell. Additional experiments will be performed to evaluate the possible failure mechanism of non-homogeneous areas of the containment shell.

1. OBJECTIVES

The containment of a nuclear power plant represents the last barrier for the fission product release under accident conditions. Therefore the behavior and the possible failure mechanisms of the containment play an important role in the evaluation of the radiological consequences to the environment.

The containment research program /1/ of the Project Nuclear Safety (PNS) of the Kernforschungszentrum Karlsruhe (KfK) concentrates on steel containments of the actual type used for German pressurized water reactors. Emphasis is placed on the possible failure mechanisms of the containment shell itself and of the non-homogeneous parts of the containment (penetrations, sealings, bellows, locks, reinforcement plates around nozzles, etc.). The possible failure mechanisms are studied under different loading assumptions resulting from different types of accidents.

The aim of the investigation program is twofold:

- Evaluation of the safety margin for containment integrity under design basis accident conditions.

- Evaluation of failure mechanisms for loadings from beyond design basis accidents.

2. PROGRAM DESCRIPTION

The objectives of the containment behavior program are concentrated on the investigation of the containment response to the following four types of accidents which are beyond the common design and licensing practise.

- Containment behavior under quasi-static pressure increase up to containment failure

- Containment behavior under high transient pressures

- Containment oscillations due to earthquake loadings (consideration of shell imperfections)

- Containment buckling due to earthquake loadings

Both theoretical and experimental work will be performed.

3. CONTAINMENT BEHAVIOR DURING A QUASI STATIC PRESSURE INCREASE UP TO CONTAINMENT FAILURE

During the course of a hypothetical core melt accident, the pressure inside the containment will exceed the design limit. As the pressure increase is expected to occur rather slowly, failure of the containment must be considered after some days /2/.

In earlier investigations, it has always been assumed that, after attainment of a pressure of 8.5 bar in the reactor containment, the airborne radioactivity present at that time in the reactor containment is released directly into the environment. This is equivalent to the concept of a pressure impact destroying large areas of both the steel shell and the concrete shielding.

As a matter of fact, experts in the Federal Republic of Germany unanimously agree today that the limit of failure of the undisturbed steel shell of a German 1300 MWe PWR of standard design will occur above 14 bar and that the "leak-before-break" criterion applies to the reactor containment as well. This leads to a plausible instruction for conducting further analyses:

> It is necessary to determine that point of the reactor containment where with rising pressure, considerable leakages must be expected to occur first. The pressure drop resulting from that leak or - in the most favorable case - the resulting stabilization of pressure precludes failure at other points to take place at even higher pressure levels.

Therefore, investigations of the load carrying capability were performed at different locations of the reactor containment, the goal being to quantify the type of failure for a steadily rising internal pressure and to indicate the associated cross sections of the openings.

From extensive experiments carried out elsewhere and from broad experience gained during ultrasonic screening of many containment shells it is known that weldings do not represent the weak parts. Also the different types of containment nozzles, the containment reinforcement plates around the nozzles and the containment clamping at the bottom are designed such that failure should not occur there. This has been shown by several stress analyses. Even the contact between an extremely deformed containment shell and protrusions of the encasing concrete shell are not likely to initiate containment failure. This has been shown by a large deformation shell analysis with the computer program ROTMEM /3/ developed at KfK.

Finally as rather weak parts of the containment the following regions have been identified:

- Zones of the containment shell in the neighbourhood of reinforced sections.

  Usually these sections contain nozzles, locks, etc. Since the strains in the reinforced sections are rather low, the circumferential strains and stresses around the reinforced sections must be low, too. In order to satisfy equilibrium with the internal pressure, the stresses in the meridional direction must be rather high. That means large plastic strains may be concentrated in the neighbourhood of reinforced sections. A detailed analysis will be given in /4/.

- The bolted connection between the spherical shell and the material lock.

  Here a large number of small holes are drilled in the shell without any reinforcement. That means, considerable local plastic strains may be concentrated around these holes. In addition, before mechanical failure considerable leakages may occur at these holes. The following section contains a more detailed description of the PNS activities in this area.

- Sealings at locks and bellows connecting pipes with containment nozzles.

  Under pressure loadings beyond the design pressure sealings may loose their tightness. For large plastic containment deformations bellows will be overstrained and may fail.

The problems identified here must be investigated in some detail in order to determine both the maximum pressure before failure and the type of failure.

Fig. 1 illustrates first results of theoretical investigations performed at KWU /5/. It shows that failure of the steel shell must be expected to occur first at the material lock door at about 9 bar internal pressure.

At a pressure of 11 bar and a temperature of 170 ^{o}C radial expansions of as much as approx. 40 cm and vertical tangential displacements at the equator of about 30 cm occur in the undisturbed shell zone. Deformations of this size are not tolerated by the surrounding structure; even before attainment of the loading condition indicated before, substantial constrained deformations take place at the disturbed points and hence leakages develop.

4. THE BEHAVIOR OF THE MATERIAL LOCK

As a consequence of being the weakest part of the containment, the material lock has to be investigated in more detail.

The bolted connection between the steel shell and the reactor containment and the required sealing box are represented in Fig. 2. Obviously, the great number of holes to be drilled into the spherical shell constitute weak points of the system.

The behavior of the bolted connection shortly before the time of failure is extremely complex. Some of the forces are transmitted by friction induced connection, some of them by bolt bearing pressure. A comparatively precise description with a computer code does not seem possible.

On the other hand, a precise description is urgently needed. As a matter of fact, if high strains occur in the whole bolted connection, the sealing box will be the first to fail, as represented in Fig. 3. The resulting leakages will then probably impede a further rise in pressure and large area mechanical failure. If, by contrast, the bolted connection behaves like a compact unit, lower mean strains have to be anticipated. In this case the pressure would continue to rise and failure would have to be expected to occur in the outermost row of bolts. Then it would have to be feared that the reactor containment is subjected to large-area rupture.

To be able to decide reliably whether the pressure at failure of the bolted connection is lower than that prevailing at the other weak points and whether the less harmful type of failure mentioned first (fracture of the sealing box) must be anticipated, conduct of an experiment is being discussed the results of which could be transferred directly to real conditions without requiring an expensive computer program. It is planned to subject a section of the bolted connection reduced on a 1:4 scale to a two-axis tensile stress corresponding to real conditions. The planned device has been sketched in Fig. 4. It is intended that in the course of the test the two-axis stress condition (reactor containment internal pressure) will be gradually raised and the increasing leakage flow through the bolted connection measured.

According to the present state of knowledge the leak to be expected can only be limited in size. The leak size ranges between 300 cm^2 and a value which is sufficiently high to

prevent a further continuous pressure rise from occurring in the reactor containment. This value depends exclusively on thermodynamic parameters because just the energy and mass flows generated in the reactor containment at the time of overpressure failure must be removed through the leak. The leak is also strongly influenced by the layout of the containment. For reactor containments of German PWRs of standard design a 20 cm^2 cross section is sufficient to limit to 9 bar the pressure in the reactor containment. In case the more detailed analyses described before validate the observed tendency, this would mean that at the lowest pressure level (in this case in the zone of the material lock at about 9 bar internal pressure) higher pressure values cannot be attained in the reactor containment after substantial leakages have occurred at the first weak point.

5. CONTAINMENT BEHAVIOR UNDER HIGH TRANSIENT PRESSURES

In recent years also transient containment loadings caused by postulated hydrogen explosions received increased attention. Here it should be shown that even strong transient pressures are not able to damage the containment such that it looses its tightness. However, certain plastic deformations should be tolerable.

The investigation of this problem is closely related to the containment under quasi-static pressure increase discussed before. Especially the weak parts of the containment are the same.

However, it should be noted that now the containment loading may have a non-uniform character and that the containment stiffness may be relatively low in this case.

As computational tool, an extended version of the program ROTMEM could probably be used when inertia terms are added. Special experimental investigations are not planned so far. However, it is believed that many of the results obtained

for the quasi-static problem are applicable here. Furthermore, some of the oscillation experiments described in the next paragraph will also give a certain support, as long as the containment deformations do not exceed the elastic region.

6. CONTAINMENT OSCILLATIONS DUE TO EARTHQUAKE LOADINGS

Analysis of containments under different types of dynamic loadings is common licensing practice. The computations are based on simplified models. Deviations from the ideal spherical geometry caused by a number of different nozzles with reinforced sections or due to inevitable manufacturing tolerances are usually not considered.

However, from several experiments with thin cylindrical shells it is known that small deviations from the ideal geometry may have significant influence on the dynamic response. For instance a cylindrical shell under earthquake excitation should oscillate only in modes with first circumferential order. In reality, inevitable small imperfections give rise to oscillations in modes with higher circumferential order. Since the stiffness of thin shells against such modes is rather low, the amplitudes of such modes can reach rather large values /6/.

It is conceivable that this effect can also occur in thin spherical shells. However, no corresponding investigations are known so far. Therefore investigations to this problem will be carried out within this program.

Computational methods for this problem must still be developed. It is believed that modelling of the slightly imperfect geometry by standard methods will not be appropriate, since the geometric deviation might be in the order of computational inaccuracies. Rather special methods, where the influence of imperfections is studied directly (perturbation methods), should be applied.

It is evident that the theoretical investigations should be checked and completed by experimental work. However, manufacturing of an appropriate spherical shell model is very difficult. The large dimensions and the high manufacturing standard of real containments lead to very small relative tolerances. But the model should reveal even smaller tolerances in order to provide first the reference results for an almost ideal geometry. Later on results should be obtained for geometries with well defined disturbances, i.e. for geometries with additional masses or stiffening plates attached to the shell.

Careful consideration have shown that usual manufacturing processes for the model like deep drawing or welding are by far not sufficient to satisfy the above requirements. Finally it turned out that manufacturing the model by turning using a numerical controlled lathe will probably provide the best results. Details of the manufacturing process are mentioned in Fig. 5.

With the largest lathe available, the diameter of the spherical shell model has been determined to about 1400 mm. The wall thickness will be 1 mm. The angular aperture will be 100^{o}. While the accuracy of the shape is expected to be relatively high with deviations of less than 1 % of the sphere diameter, the accuracy of the wall thickness will be relatively small with deviations in the order of 10 % of the thickness. However, the later deviations are expected to have a smooth distribution which can be analytically described, if required. The accuracy of the shape will be determined by a measuring machine. The accuracy of the thickness will be determined using an ultrasonic sensor.

To obtain the eigenfrequencies and the corresponding mode shapes, an experimental modal analysis of the spherical shell model will be carried out. Both undisturbed models (original) and disturbed models (with additional masses and

stiffening plates) will be examined. The spherical shell models will be subjected to transient excitation with an impulse hammer, a snapback-device or a narrow-band random force of short duration. The corresponding response will be simultaneously measured with a set of miniature accelerometers or contactless displacement transducers. To extract the set of eigenfrequencies, mode shapes and critical damping ratios from the simultaneously measured response signals, a modified version of the computer code EVA /7/ will be used. It had been developed and applied to other shell and structural dynamics problems in recent years. The objective of the intended modification is the improvement of the frequency resolution and of the ability to separate multiple modes. This is expected to be necessary because of the extraordinarily dense spectrum of eigenfrequencies of spherical shells obtained in precalculations. The experimental procedure will be tested during preliminary modal measurements performed with a welded forerunner model of the shell having a diameter of only 700 mm(Fig. 6).

In the later stage of experiments, the spherical model will be mounted on a table coupled with an electrodynamic shaker and subjected to harmonic or random excitation. Both the excitation and the response will be measured and mutually correlated. Special attention will be paid to the excitability of modes with higher circumferential orders and to the influence caused by shell imperfections. These experiments are planned to support the theoretical work on the earthquake loadings of containments.

7. CONTAINMENT BUCKLING

The lowest oscillation mode of the containment under earthquake loading is similar to the lowest oscillation mode of a short beam (Fig. 7). During half the oscillation period the meridional membrane stresses in the lower part of the containment shell assume negative values. As a consequence, during this time, local buckling might occur. This effect

should be investigated in more detail.

The computations may possibly be based on known methods where large deformations are considered.

More important are appropriate experiments. They will be done using the high accurate spherical shell manufactured for the oscillation experiments described in the paragraph before. In a first series of tests the earthquake loading will be approximated by a horizontal static force applied at the upper pole of the spherical shell. This force will be monotonically increased close to the point of buckling. However, care must be taken since during these tests buckling should not damage the model. Especially plastic deformations should not occur.

8. TIME SCHEDULE

Table 1 shows the actual time schedule. Starting in 1979 the quasi static investigations will be ended in 1985. Due to the fabrication process of the spherical steel containment model first experimental results for containment oscillation and buckling are expected to be available in 1985.

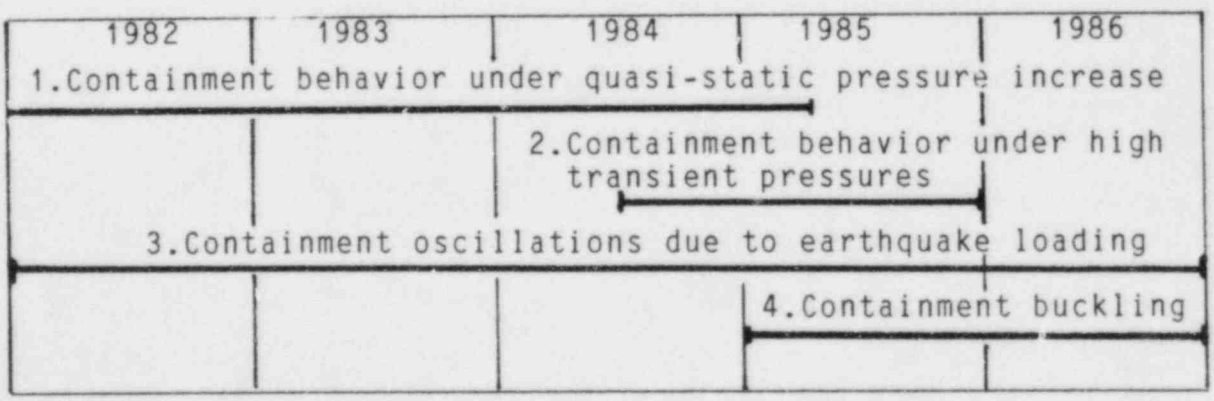

Table 1: Time Schedule PNS/KfK Containment Program

9. LITERATURE

/1 / R. Krieg et al.
Investigation Program on PWR-Steel-Containment Behavior under Accident Conditions,KfK 3589(Okt.83)

/2/ J.P. Hosemann
On the Fission Product Release into the Environment during a PWR Core Meltdown Accident. 1oth Water Reactor Safety Research Inf.Meeting,Gaithersburg, Oct.15(1982)

/3/ B. Göller
Zum Verhalten eines DWR-Containments unter hohem, quasistatischem Innendruck - Grundlagen des Programms ROTMEM. Internal report.

/4/ B. Göller et.al.
Behavior of Spherical PWR-Containments Close to Reinforced Sections under Excessive Internal Pressure. Second Workshop on Containment Integrity, Washington, D.C., June 13-15(1984)

/5/ J. Jeschke
Limit Load Analysis of Actual Spherical Containments Subjected to Static Internal Pressure and Temperature. Second Workshop on Containment Integrity, Washington, D.C., June 13-15(1984)

/6/ R.W. Clough, et.al.
Experimental Seismic Study of Cylindrical Tanks. J. of the Structural Division, Proceedings of the ASCE, Vol. 105, No. ST9(Dec. 1979)

/7/ F. Eberle, J. Kadlec
Extraction of Eigenfrequencies, Mode Shapes and Critical Damping Ratios of HDR Core Barrel Mockup from Step Relaxation Response Signals Measured in the Snapback Test Series V59, KfK 34o8 (Okt. 1982)

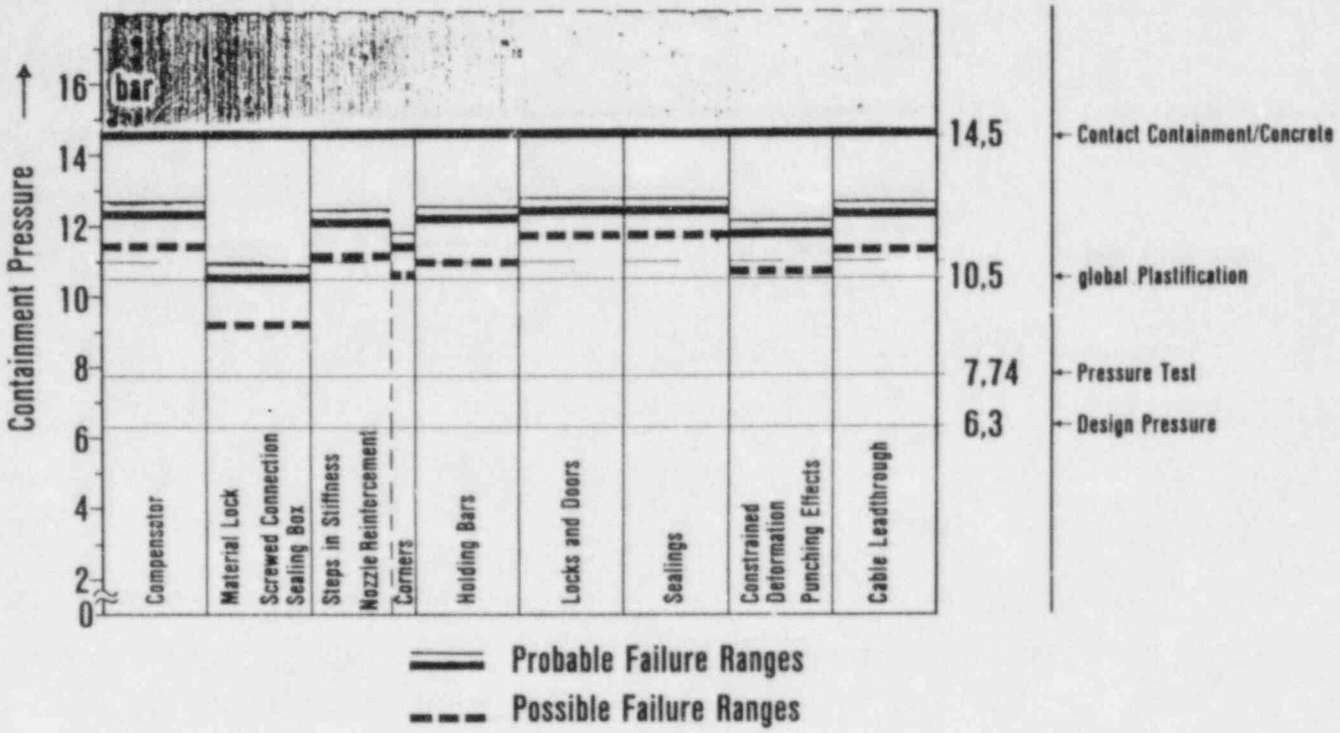

Figure 1. Failure Pressure Variations of Containment

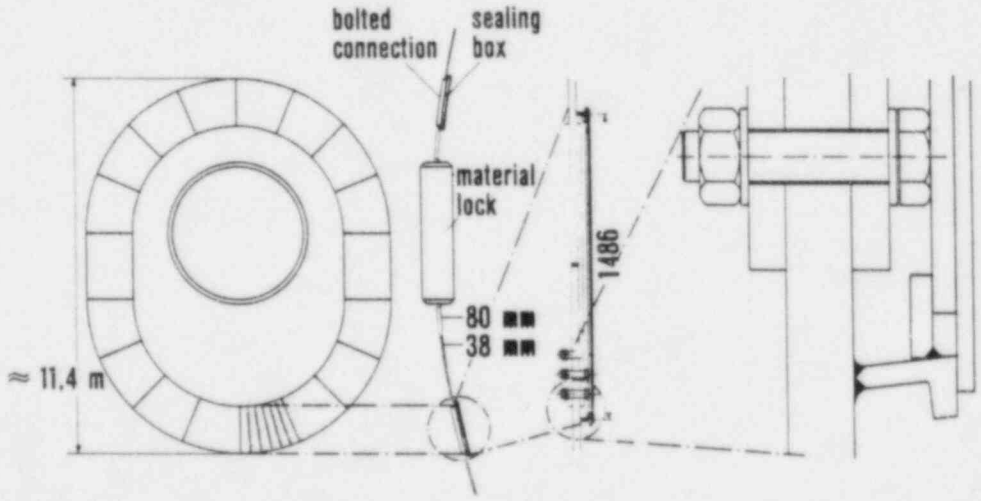

Figure 2. Bolted Connection Between Containment Shell and Material Lock

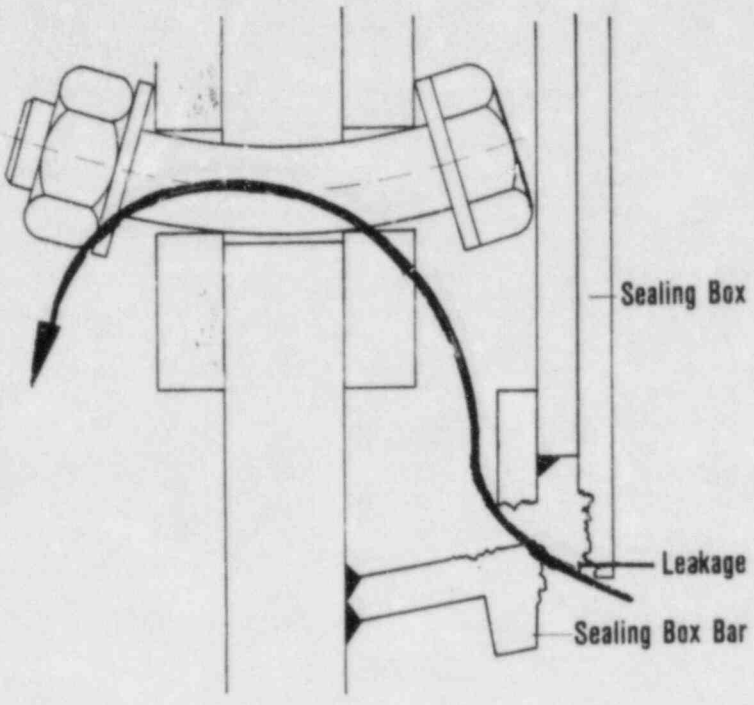

Figure 3. Failure of Sealing Box, Leakage Through the Bolted Connection

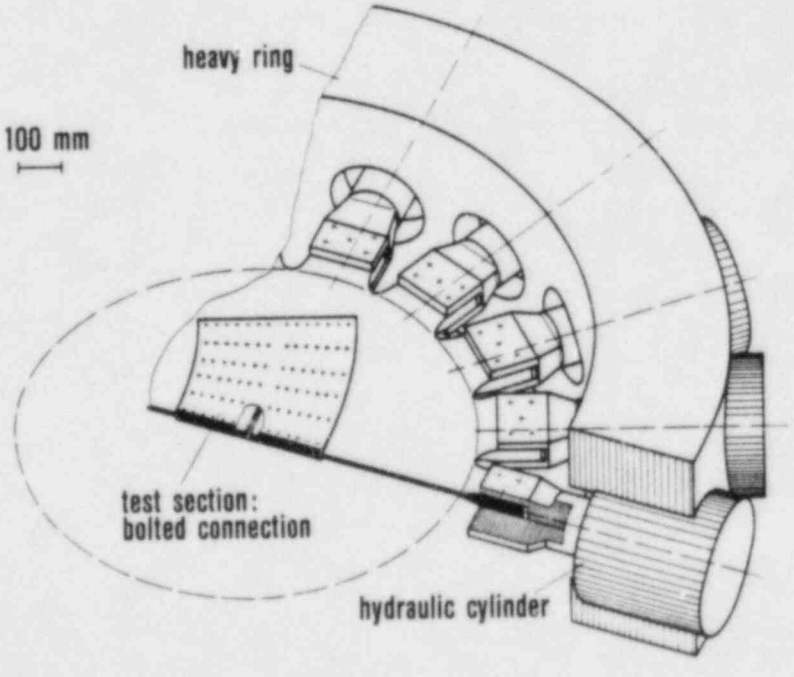

Figure 4. Two-Axial Test of the Bolted Connection Between Containment Shell and Material Lock

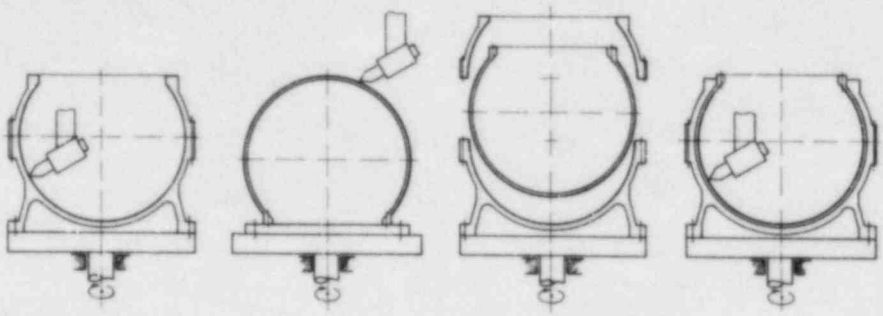

1. Inside cutting of supporting case
2. Outside cutting of the sphere
3. Clamping of sphere within the case
4. Inside cutting of the sphere

Figure 5. Cutting of the Sphere Using a Numerically Controlled Lathe

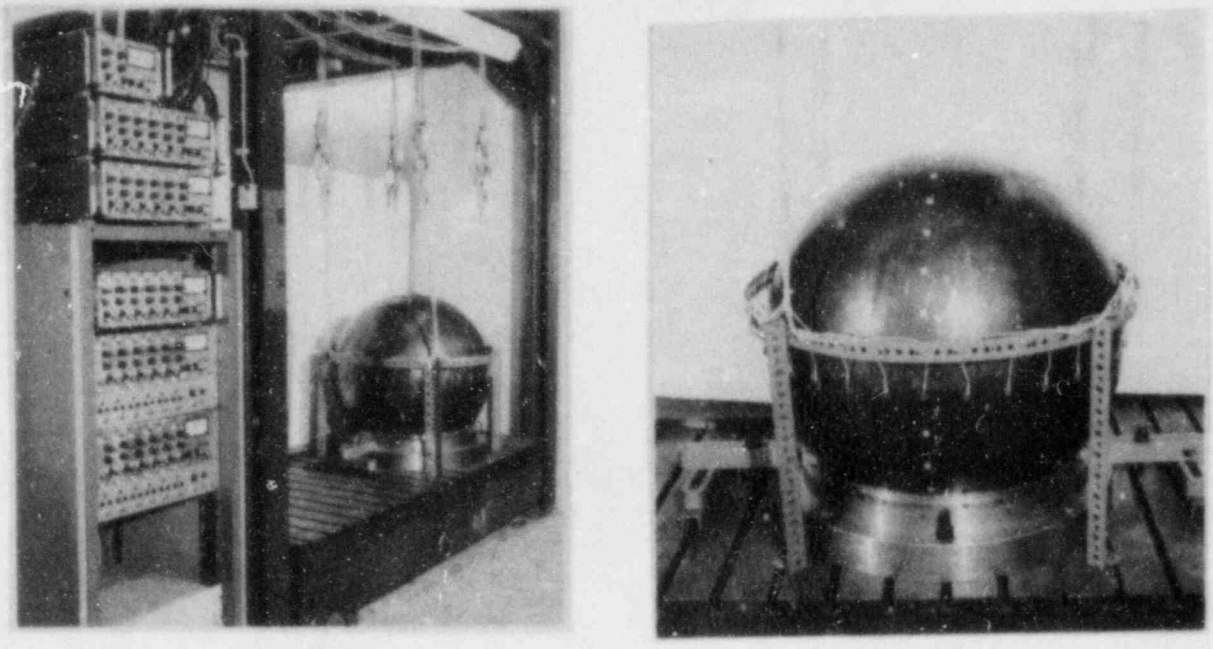

Figure 6. Experimental Setup and Spherical Test Model with Installed Accelerometers for Modal Measurements

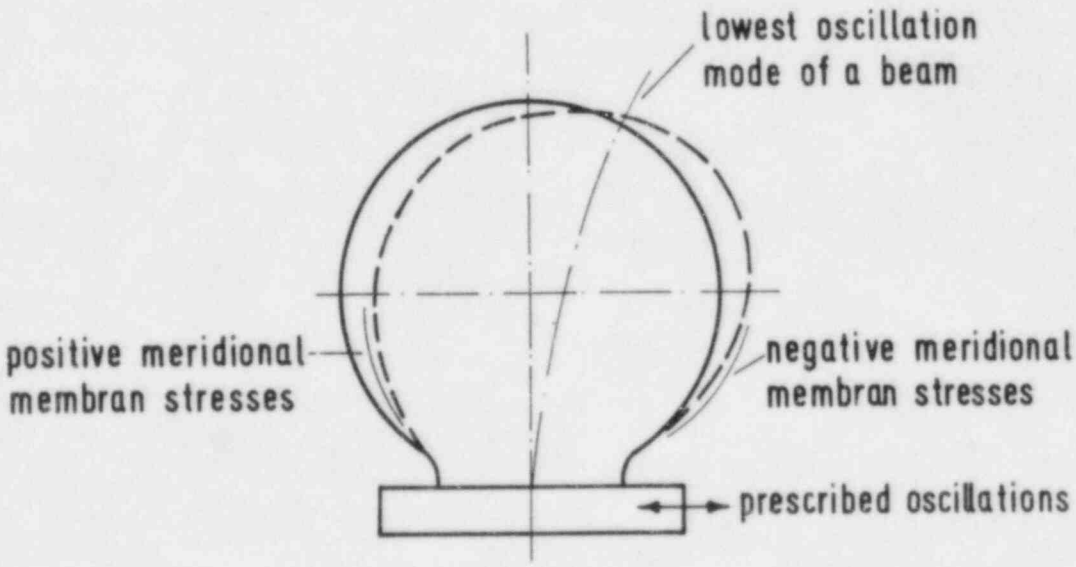

Figure 7. Lowest Oscillation Mode and Resulting Membrane Stresses of the Containment Shell

CONCRETE CONTAINMENT INTEGRITY PROGRAM AT EPRI

R. K. Winkleblack and Y. K. Tang
Electric Power Research Institute
Palo Alto, CA

BACKGROUND

Many of the practitioners in our business believe that the catastrophic failure mode for reactor containment structures is unrealistic. One of the goals of our program is to demonstrate that this is true. The catastrophic failure mode assumes that the structure would contain large overpressures, due to a hypothetical severe LOCA and hydrogen burn, until the liner and rebar reach ultimate stess and the integrity of the containment is totally lost. For this to be the true case, judgment tells us that the steel would have to be straining fairly uniformly, i.e., very little stress concentration existing (particularly in the liner). A close look at the actual designs identifies many probable stress concentration points where the liners possibly could crack and leak. Since the concrete would crack long before rebar or prestressing tendons reach yield, a crack in the liner would initiate a leak that would tend to be peak pressure limiting. (Leaks through penetrations are additional possibilities which are not covered in this program. The Sandia program is addressing these probabilities.) So, it seems likely that the catastrophic conditions would never occur. Actually, the very high internal pressures, relative to the design basis, certainly are low in probability of occurring. However, if a situation were to arise where pressure were increasing significantly above safe loading, it would be best that cracks and leaks occur, limiting the peak pressure before a catastrophic failure could dump the bulk of the inventory of radioactivity from the containment structure into the atmosphere. Less activity would be expected to be released through the leaks that served to limit the peak pressure in the structure. The risk associated with the postulated more realistic mode would be much smaller than the one with catastrophic failure in the probabilistic risk assessment (PRA) context.

OBJECTIVE

The objective of the EPRI program is to provide the utility industry with an experimental data base and a test validated analytical method for realistically evaluating the actual over pressure capability of the concrete containment buildings and to

predict leakage behavior if higher pressures were to occur. The ultimate goal of this R&D is to characterize the containment leakage mode and leak rate as a function of internal pressure and time so that the risk can be realistically assessed for hypothetical severe degraded core conditions.

APPROACH

EPRI's approach is to have tests and analyses conducted in parallel. The experimental work is contracted to the Construction Technology Laboratories (CTL) of the Portland Cement Association. The analytical work is contracted to Anatech International Corp. There is close coordination between CTL, Anatech, and EPRI. Anatech develops mathematical models and does pretest analyses which are discussed in detail with CTL and EPRI. CTL designs their test specimens, instrumentation and test procedures to provide, as directly as possible, experimental verification or correction to the results of the pretest analyses.

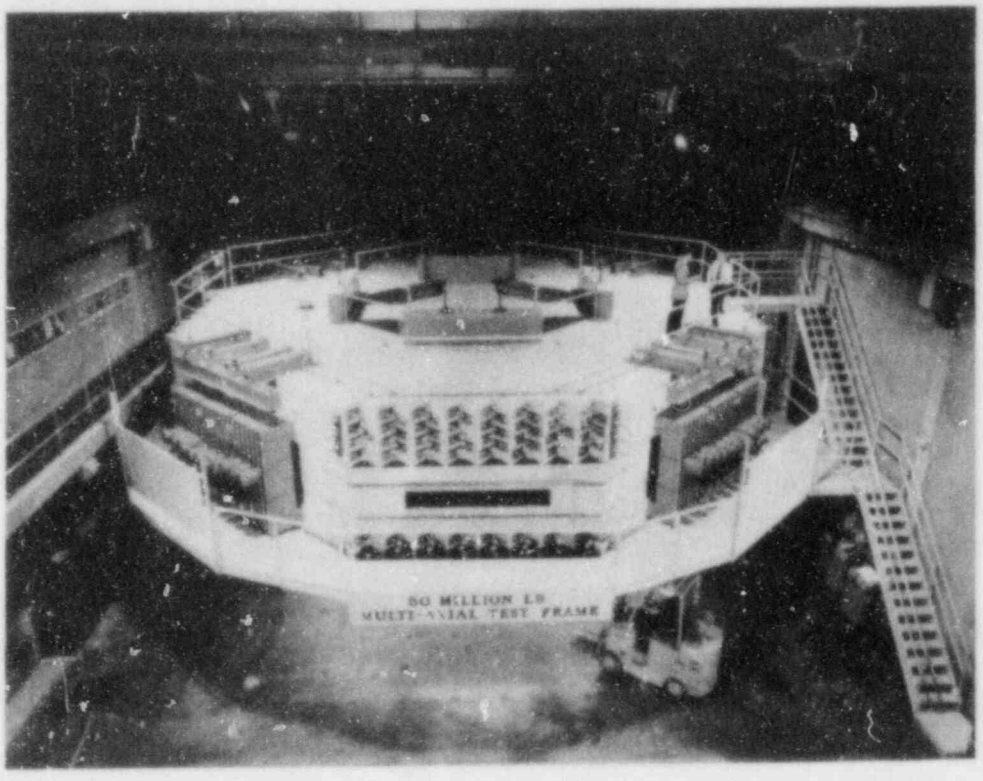

Biaxial Test Frame

CTL has developed a very large test rig in which they do these tests. Don Schultz of CTL will be discussing that facility (that he, Norm Hanson, and their CTL colleagues designed and built) and some of the results of the phase 1 testing that was accomplished on a smaller test rig which was built with NRC funding. Also, he will describe the phase 2 test specimens

that they have designed and are scheduled to test on the large new rig this year.

Joe Rashid and Bob Dunham, Anatech, will be describing their part in the program. They are trying to develop analytical models that recognize the stress concentrations (particularly in the liner plates) that exist at certain types of weld joints, discontinuities, penetration sleeves, intersections between the cylindrical wall and the base mat, and the intersection between the wall and the dome at the spring line. The hope is to develop techniques that can be verified by the CTL tests and then be applied to evaluate the actual containment capabilities assuming hypothetical degraded core situations.

PROGRESS

The current test program is to be carried out in three phases. To avoid the uncertainties associated with small-scale modeling of detailed structural response and leakage rates, the test program focuses on testing of large and full-scale segments of concrete containments starting with simple uniaxial and biaxial tension tests on square structural specimens to define material behavior and then following up with more systematic testing of prototypical containment segments with penetrations and structural discontinuities to produce a data base on leakage through local liner breaches.

The first phase of testing at CTL was aimed at defining material behavior of typical reinforced and prestressed containment wall designs using simple tests on structural elements. Eight uniaxial and biaxial tension tests were conducted on 5 ft square by 2 ft thick, flat concrete slabs representing elements from the walls of containments away from penetrations and discontinuities. The slabs were about half the thickness of typical containment walls, had full-size rebar and aggregate, and were of both reinforced and prestressed design.

With loads applied to reinforcing bars, the tests provided extensive data on elongation, strains, and crack opening as a function of loading well into the inelastic region. In addition, four biaxial tension tests were conducted on 4 ft square liner plate specimens. These tests showed that, even with butt welds or pipe penetrations, the plates can withstand up to six percent or more elongation without rupturing. Data from the first phase tests have been used to benchmark analyses being performed in Anatech's parallel effort and also to develop loading techniques to be used in phase 2 tests.

The analytic effort in this research is to develop and validate the EPRI-sponsored nonlinear finite element code ABAQUS-EPGEN as a qualified method for concrete containment integrity analysis in predicting the concrete cracking pattern as well as local liner fracture under progressively increased internal

pressure. The concrete modeling capability based on Chen-Chen theory of placiticy was incorporated into the ABAQUS-EPGEN code by Hibbitt, Karlsson, & Sorenson (HK&S). The first phase analytic effort has been completed by Anatech and results will be issued in an interim report by EPRI. In this first phase study, the current ABAQUS-EPGEN code capability and limitations have been evaluated by conducting correlation analyses on selected CTL phase 1 test specimens as well as by performing state-of-the-art ultimate strength analysis on typical concrete containment structures. Four CTL specimens were chosen for the correlation analyses, they are specimen UA1, BA2, PC1 and UA2. In general, the measured and the predicted responses, such as concrete and rebar strains and total elongations, compared reasonably well. The Anatech paper will show some typical results. However, the existing code capability (during phase 1) only allowed diffused cracking patterns and crack strains that do not agree well with the discrete cracking observed in the experiments. The ABAQUS-EPGEN analysis of typical concrete containments were performed for both prestressed and reinforced concrete structures. The analyses were conducted in two stages. A global structure analysis subject to internal over-pressurization was performed first and results were used to define the local effects models. In the subsequent analysis, the local effects models were used in selected regions of stress/strain concentration or strong stiffness discontinuities. This analysis was to demonstrate the local effects on the ultimate integrity of the liner. The analysis results demonstrated that significant local liner strain concentration at concrete cracking locations could occur, and could lead to liner rupture before rebar or tendons reach their ultimate capacity. However, to truly validate such local behavior prediction, further local effect experiments are needed as well as code improvements for more realistic constitutive relations and more refined modeling techniques. These efforts are to be carried out in the second phase tasks.

The second phase analytic effort is underway at Anatech. Areas of model improvements, for enhancing local effect prediction, have been identified and the code implementation is being carried out by both Anatech and HK&S. The major areas of code improvements include interface elements modification for a realistic liner-concrete and rebar-concrete bond/slip characterization, orthotropic failure criteria for better prediction of discrete concrete cracking pattern, and rebar shear dowel model for closed simulation of local stiffness effect. Anatech's effort in this phase also includes the analysis and design, jointly with CTL, of the phase 2 test specimens planned for 1984, particularly the dislocation specimen for local liner failure simulation. In addition, pretest analysis and posttest correlation of selected CTL phase 2 tests are planned using the improved ABAQUS-EPGEN code capabilities.

Phase 2 of the testing work is in the detail design and planning stage at CTL. Seven test specimens are planned, which include stress concentration points due to weld details and anchors in liner plates, penetration sleeves where punching shear

will occur, strain discontinuities representing the interface between the wall and base mat, and thermal stress simulation. Some of the specimens are being cast and testing will begin soon. The details of the test specimens and the planned tests are discussed in the CTL paper which follows this afternoon.

FUTURE PLANS

Phase 3 of the program is to be an outgrowth of the results of phase 2. It is anticipated that a few more tests will be needed to firm up the correlations of phases 1 and 2 test results and analytical models with the behavior of the actual containment structures. It probably would be desirable to devise some tests of one or two containment buildings at cancelled plants. This is an ambitious objective and has a number of difficulties to be overcome before such testing could be implemented. A study has to be made to see if some meaningful tests can be conducted on an actual reactor containment building. Other test alternatives may exist. For example, a large scale complete ring segment might be built to test the most likely area (e.g., wall-dome or wall-basemat intersections) for a first significant crack to occur in the liner. When one considers how such a test structure would be loaded, to simulate the behavior of a complete building, the task and cost loom large indeed. Phase 3 planning still presents a very real challenge. Close coordination with the NRC's scaled concrete containment test program will be very important in defining the third phase of the test program.

The third phase analytical effort will emphasize containment leakage quantification in addition to further qualification and benchmarking of reinforced/prestressed concrete and liner interaction model against test results. It is expected that the NRC's 1/6 scale model test results will serve as a good data base for checking out the analytical capability to accurately predict concrete containment behavior under sever IDCORE hypothetical conditions.

PROCEDURES AND OBJECTIVES FOR TESTING A 1/8 SCALE MODEL OF A STEEL CONTAINMENT*

L. N. Koenig
Sandia National Laboratories
Albuquerque, NM

ABSTRACT

A 1/8 scale model of a steel containment building will be tested in late summer of this year by the Containment Integrity Division of Sandia National Laboratories, Albuquerque, NM. The test is part of the NRC-sponsored Containment Safety Margins program that is described in several references [1,2,3,4,5]. Included in the the model are pipe penetrations, personnel locks, and operable equipment hatches.

The 1/8 scale model will be pressurized in steps to well above the design pressure and data taken at each step via a computer controlled data acquisition system. Strain gages, thermocouples, and displacement and pressure transducers have been placed strategically throughout the inside and outside of the model to record data on the model's response to each pressure step. Particular effort has gone into instrumenting the area around and near penetrations although regions away from penetrations are also instrumented for comparison purposes. The equipment hatches are equipped with special instrumentation to record relative movement and separation of the sealing surfaces. Photometrics data from cameras placed at three locations overlooking the model will be used to determine global displacements. In addition, a theodolite system will be used to measure displacements of specific targets placed on the outside of the model.

Instrumentation has also been included to make leak rate calculations. These calculations will be made during hold periods.

The results of this experiment will give a better understanding of the behavior of containment buildings at pressures well beyond the design level. Experimental data will be compared with analytical data obtained from various computer programs to verify their performance in the post yield region.

*This work supported by the United States Nuclear Regulatory Commission and performed at Sandia National Laboratories which is operated for the U.S. Dept. of Energy under contract number DE-AC04-76DP00789.

DESCRIPTION OF THE MODEL

The large steel model is a 1/8 scale model of a steel containment building, Figure 1. A concrete shield building is not included. The model was designed and built by Chicago Bridge and Iron, Co. (CB&I) to the ASME code but has no code stamp since radioactive material will not be contained in the structure.

The model is built of A516 steel to a design pressure of 40 psig. A516 steel was chosen because it is used extensively in steel containments and steel lined reinforced concrete containments. Features incorporated into the model include operable equipment hatches, pipe penetrations, a constrained pipe penetration, personnel lock representations (inoperable), stiffening rings, and thickened sections around penetrations. The personnel locks are inoperable because size constraints limit the detail that is feasible. Full size personnel locks will be tested as part of a separate program.

Details of the equipment hatches are shown in Figure 2. The equipment hatch covers are thicker than scaling would dictate due to the method used to close the cover.

The steel cylinder and dome of the model are most representative of hybrid steel containments that have a reinforced concrete basemat. Instead of the basemat, a stiff bottom head 1 1/2 inches nominal thickness has been substituted. Access to the model is through an equipment hatch in the bottom bulkhead. Also located in the bottom head are pass-throughs for instrumentation wires and nitrogen pressurization lines.

OBJECTIVES

A major goal of the large steel model experiment is to replicate more accurately fabrication techniques, material properties, construction details, and other features in an actual containment building. With this added detail, more meaningful objectives can be designed into the experiment.

The instrumentation used in the large steel model experiment has been selected and positioned to achieve the following objectives:

1. To measure the distortion and possible leakage through the equipment hatches. The detection and location of leakages will be done via a periodic leak test and an acoustic detection system. These will be discussed later.

2. To measure the affects of constrained penetrations on shell behavior. The constrained penetration is an 8 inch pipe running diametrically across the model and is welded to a thickened shell area at each end. The constraint

penetration represents pipe penetrations in an actual containment building that are fixed to an immovable internal or external object. Measurements will be made with displacement transducers and strain gages running horizontally and vertically away from the point of attachment to the shell.

3. To measure local straining around thickened shell sections through which all penetrations are run. Strain gages have been placed to measure the affect of thickened sections on local shell behavior.

4. Measure strain in areas away from penetrations to quantify the behavior of the model and to compare with other strain readings throughout the model.

5. To ultimately qualify methods for predicting the structural capacity of light water reactor (LWR) containments to function under loading caused by severe accidents and extreme environments.

PROCEDURE

The large steel model test program consists of a structural integrity test, an integrated leak rate test (ILRT), and a static pressure test.

A standard structural integrity test will be run at 15% above design (46 psig). This test also serves to verify the instrumentation and data acquisition system.

The integrated leak rate test will ensure that the leakage is below 0.1% mass/day at design pressure. Leak rate will be calculated from pressure and temperature readings taken with the data acquisition system. Both the "total time" method and the "mass plot" methods will be used. Fourteen resistance temperature devices (RTD's) and one quartz manometer will be used to measure the temperature and pressure respectively. The RTD's are located in the model's interior and their readings weighted according to the volume represented by each transducer.

At the conclusion of the ILRT, the model will be depressurized and any necessary repairs made. The sequence will be repeated until a leak rate below 0.1% mass/day at design pressure is achieved. The integrated leak rate test also serves as a test bed for the instrumentation and data acquisition system.

During the static pressure test, the model will be pressurized in steps at a nearly constant temperature. Pressure steps will be initially in 20 psi increments. Smaller increments will be applied as membrane yield is approached and passed. During pressure steps, any two strain gages, displacement transducers, and pressure transducers can be scanned continuously to determine model stability. Once the

model stabilizes at a pressure level, a single scan of all data channels will be made. At selected intervals a hold period (no mass added) will be declared and leak rate measurements made. An acoustic detection system will be used to locate any leaks. A temperature slightly above ambient will be maintained with internal heaters and a temperature controller.

The test will be concluded when a leak of sufficient magnitude develops to exceed the capacity of the pressure control system (on the order of 200% mass/day at 200 psig).

INSTRUMENTATION LAYOUT

A variety of transducers and other techniques will be used during this test to measure strain, displacement, temperature, pressure, and leak rate. Figures 3 and 4 summarize some of the instrumentation on the model's interior and exterior surfaces. Gages near or on penetrations are not shown. All total there will be 14 RTD's, 37 thermocouples, 51 displacement transducers, 5 pressure transducers, and 722 strain gages.

Strains

Strains are being measured with gages that consist of annealed constantan on a high elongation polyimide backing. In general a .250 inch nominal gage length is used except in regions of suspected high strain gradients where a .125 inch nominal gage length is used. In most applications three arm rosettes are used so that principal strain and direction can be determined. Behind the stiffening rings, "T" rosettes are used. In some regions of high bending, strip gages opposite each other on the inside and outside of the model are used.

Displacements

Displacements are determined using three techniques: displacement transducers, photogrammetrics data, and theodolite data.

The displacement transducers are of the variable potentiometer type to minimize electrical and acoustic noise. Displacement transducers are located primarily around the constrained peretration and on the equipment hatches to record relative movement and separation of the sealing surfaces.

Other displacement measurements will be taken from photogrammetric data obtained from cameras positioned at the three theodolite stations around the model.

Finally, additional displacement data will be obtained from theodolite readings of targets on the model's exterior using the principle of triangulation. The three theodolite heads will view about half of the model's circumference.

Temperature

Temperature measurements will be made using both thermocouples and RTD's. Copper constantan (type T) thermocouples are placed on the inside and outside surface of the model to provide temperature compensation for the strain gages.

The RTD's are placed throughout the interior of the model to measure the internal air temperature. RTD readings will be used for temperature control and leak rate calculations.

Pressure

Two types of pressure transducers are being used. Four 0-10 volt pressure transducers are used for pressure control and measurement. A 0-10 volt output was selected for a high signal to noise ratio. A quartz manometer will be used to measure the pressure used in leak rate calculations. The quartz manometer was selected for its high stability and accuracy, thus permitting shorter hold times.

Acoustic

Because access to the model will be limited during testing, an acoustic detection system employing 24 acoustic detectors positioned around the exterior surface of the model will be used to determine the location of leaks.

DATA ACQUISITION SYSTEM

The data acquisition system is composed of Hewlett Packard HP1000 and HP9845 computers, and an Analog Devices Macsym controller.

The HP1000 is used to control data acquisition of all strain, displacement, and thermal channels, and to convert these into engineering units and to perform temperature corrections and other compensation.

The HP9845 is used in conjunction with three theodolite heads to which it is connected via fiber optic cable. The HP9845 calculates displacements from theodolite data. A data link to the HP1000 is provided so that theodolite data can be passed for storage and further reduction.

The Macsym controls the pressure system and temperature. It is responsible for raising, lowering, or holding the model pressure as directed by an operator and to maintain the model's interior temperature within a tolerance band.

SCHEDULE

The test is scheduled for late August or early September of 1984. The structural integrity test and integrated leak rate test will take from one to two weeks. The static pressure test to first failure will also take from one to two weeks. Should the failure mode be leakage, the model may be repaired and used for other tests.

SUMMARY

Data gathered during the test of the large steel model will provide insight into the behavior of a containment subjected to overpressure. In particular, the effects of different penetrations and thickened sections on shell behavior will be measured. The location of leaks and their magnitude as a function of pressure and deformation will be determined. Finally the data collected during the test will be used to qualify different types of analytical methods used to predict containment behavior beyond design based conditions.

REFERENCES

[1] W. A. von Riesemann, T. E. Blejwas, A. W. Dennis, R. L. Woodfin, "NRC Containment Safety Margins Program for Light-Water Reactors," Nucl. Eng. Design 69, pgs. 161-168, (1982).

[2] D. S. Horschel, T. E. Blejwas, "An Analytical Investigation of the Response of Steel Containment Models to Internal Pressurization," Transactions of the 7th International Conference on Structural Mechanics in Reactor Technology, Vol. J6/4, August, 1983.

[3] R. L. Woodfin, A. W. Dennis, "Techniques Used in Static Pneumatic Pressure Experiments on Models of a Generic Steel Containment Building," Transactions of the 7th International Conference on Structural Mechanics in Reactor Technology, Vol. J6/2, August, 1983.

[4] R. L. Woodfin, A. W. Dennis, "Results Obtained from Static Pneumatic Pressure Experiments on Models of a Generic Steel Containment Building," Transactions of the 7th International Conference on Structural Mechanics in Reactor Technology, Vol. J6/3, August, 1983.

[5] T. E. Blejwas, W. A. von Riesemann, J. F. Costello, "The NRC Containment Integrity Program," Transactions of the 7th International Conference on Structural Mechanics in Reactor Technology, Vol. J1/1, August, 1983.

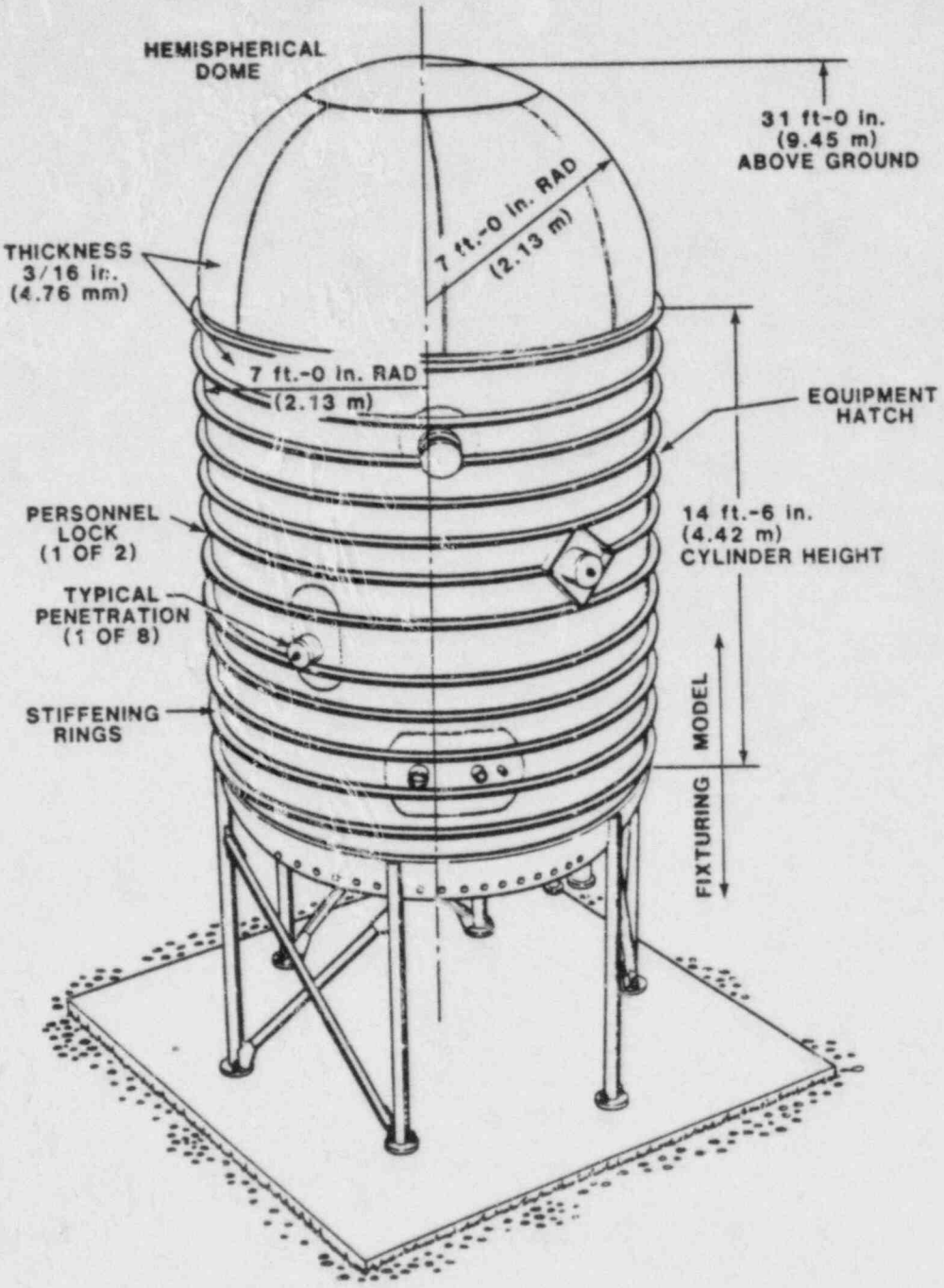

FIGURE 1. LARGE STEEL MODEL

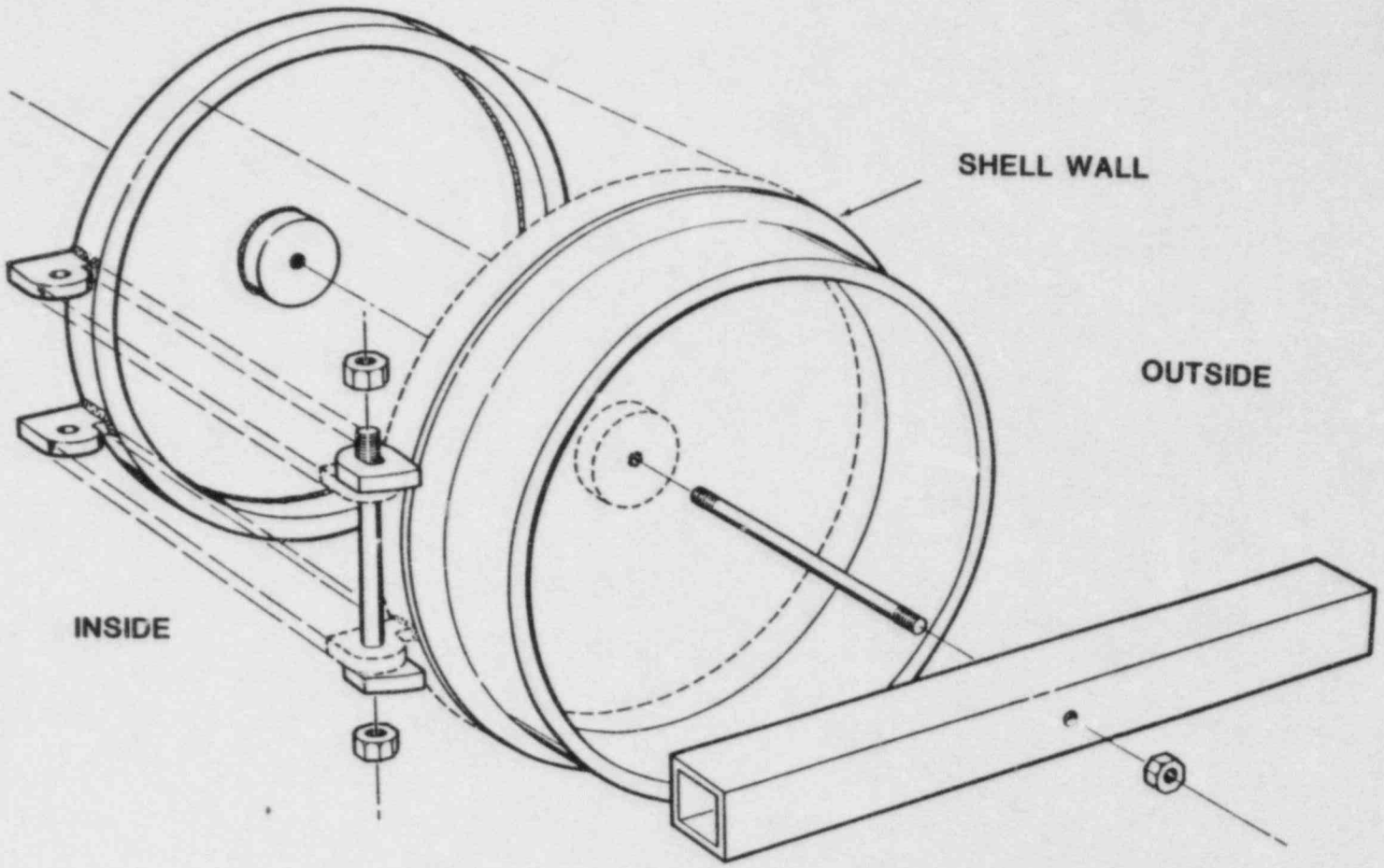

FIGURE 2. EQUIPMENT HATCH

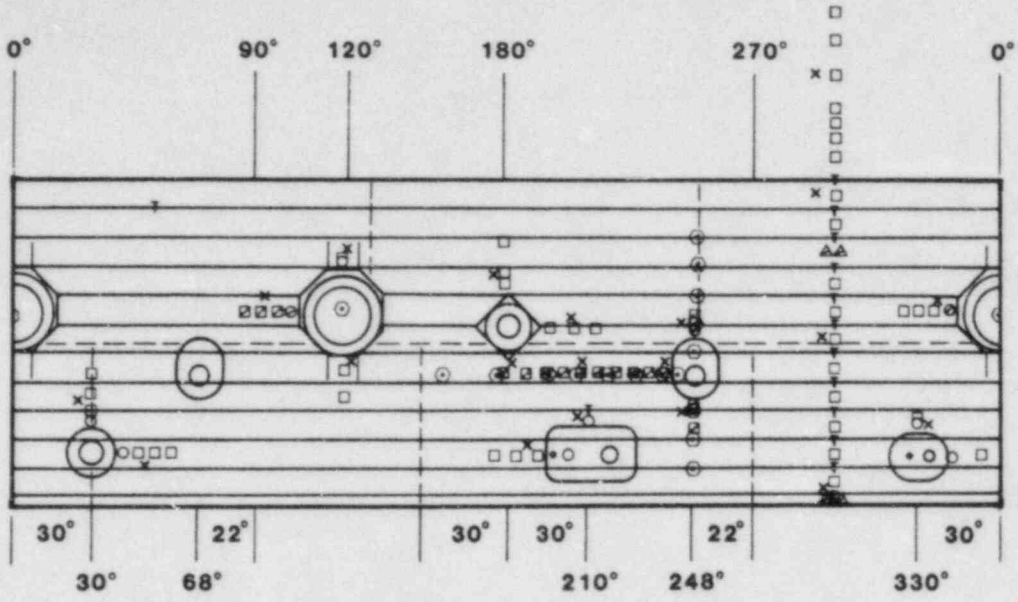

FIGURE 3. INSIDE INSTRUMENTATION

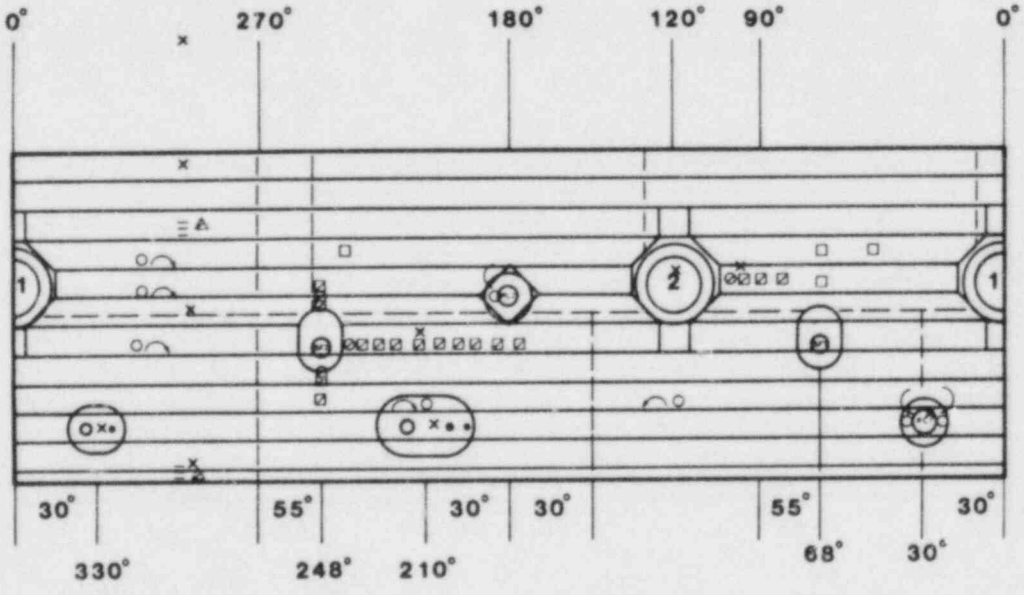

FIGURE 4. OUTSIDE INSTRUMENTATION

PLANS FOR A 1/6TH SCALE REINFORCED CONCRETE CONTAINMENT MODEL[1]

Joseph Jung
Sandia National Laboratories
Albuquerque, NM 87185

ABSTRACT

As part of the U. S. Nuclear Regulatory's (NRC's) Containment Safety Margins Program at Sandia National Laboratories, a 1/6 scale model of a reinforced concrete containment structure will be built and tested to further study the structural and leakage behavior of nuclear containment buildings during severe accidents. The concrete model will be approximately 35 feet high and 24 feet in diameter. The cylindrical wall will be approximately 9 inches thick. The conceptual design calls for #3 reinforcing bars for its main reinforcing and a 1/16 inch thick steel liner. Other features of the model include operating equipment hatches, personnel lock representations, constrained and unconstrained piping penetrations, and thickened liner sections around penetrations. An important part of the project will be the support tests. These tests are designed to confirm that a high quality model can be built and also to provide a data base of the properties of the various materials used in the model. The current plans call for the model to be ready for testing around the middle of CY86.

INTRODUCTION

As part of the NRC's Containment Safety Margins Program being conducted at Sandia National Laboratories, static pressurization

---

1. This work is supported by the United States Nuclear Regulatory Commission and performed at Sandia National Laboratories, which is operated for the U. S. Department of Energy under Contract number DE-AC04-76DP00789.

tests of scale models of nuclear containment buildings are currently in progress. To date, four 1/32 scale steel models have been tested, and a 1/8 scale model of a steel containment will be tested later this year. These tests are performed by statically pressurizing the model with nitrogen gas until the gas leakage is excessive or the structural deformations exceed predetermined large levels. These models have been heavily instrumented to document the structural behavior.

Following the 1/8 scale steel containment test, Sandia will test a 1/6 scale reinforced concrete (R/C) containment model. Testing this model will give important information regarding the leakage behavior of the seals and structural failure modes, such as concrete-liner interaction that may lead to tearing of the liner.

The R/C containment model will be tested in a similar fashion to the steel containment models, i.e., near ambient temperatures and by pressurizing it internally with nitrogen gas.

BACKGROUND

As the first step to designing the model, Sandia contracted Stone & Webster and Failure Analysis Associates to independently study the feasibility of building a R/C model. Both companies were asked to develop conceptual designs, identify potential problems, and propose methods for constructing the model [1,2]. The final conceptual design of the model is a composite of the ideas of Stone & Webster, Failure Analysis Associates, the Containment Safety Margin's Peer Review Committee, the NRC, and Sandia. The concensus of these groups was to build as large a model as economically feasible. A relatively large model would allow commonly available construction materials to be used and the behavior of the model would be more prototypical than that of a small model. For these reasons a 1/6 scale was selected. At this scale, the #18 main reinforcing bars in a prototypical containment scales down to commonly available #3 bars; the liner will be 1/16 inch thick and will probably be thick enough to avoid many of the complications inherent with handling and welding thin metal sheets; and the seals for the equipment hatches will be representative of thoses in actual containments.

MODEL DESCRIPTION

The proposed design pressure for the model is 46 psig. This value represents the average design pressure from a survey of 17 R/C containments [1]. The design details for the model will be representative of those found in actual containments. The seismic reinforcing will be geometrically scaled from that of actual containments.

The major features of the model are listed below.

1. 1/6 scale
2. #3 rebar as the major reinforcement
3. 1/16 inch thick steel liner with stud attachment
4. Two operating equipment hatches with seals
5. Two personnel lock representations
6. Constrained piping penetrations
7. Other piping penetrations
8. Thickened liner sections around penetrations
9. A "flat" basemat
10. A hemispherical dome

At 1/6th scale, the model is approximately 35 feet high and 24 feet in diameter with a 9 inch thick cylindrical wall. The overall model dimensions (as envisioned by Stone & Webster [1]) are shown in Figure 1. The locations of the penetrations have not been finalized.

Figures 2 and 3 show a possible reinforcing plan [1] for the cylindrical wall and basemat of the model. The main hoop reinforcing for the cylinder wall will be #3 bar (preferably made from A615 Gr 60 steel) with a 2 inch typical spacing. Although the seismic reinforcing bars are shown as the outer most layer, their placement has not been finalized. All reinforcing bar splices must satisfy the ASME Section III, Division 2, Subsection CC requirements.

The 1/16 inch thick liner will be preferably made from A516 Gr 60 steel. The total amount of welding for the liner will be minimized, i.e., the liner will be composed of as few plates as possible. Studs will be used to anchor the liner to the concrete. The recommended stud is 0.11 inches in diameter and 0.5 inches long. The stud diameter is approximately 1/6 the prototypical stud diameter, but the stud length is one half of what similitude requires. The shorter stud length was selected to avoid interference between the studs and the main reinforcing during construction. The stud pattern used will have a one to one correspondence with prototypical stud spacings around the major penetrations, spring line, and the base mat-cylinder wall interface. Because a pressure loading does not stress studs highly in other regions, the stud spacing in other areas will be greater than that required for a true replication.

In order to test as many configurations as possible, two equipment hatch penetrations and three hatch covers are planned for the model. On one of the equipment hatch penetrations, there will be a pressure seated hatch cover. On the other penetration there will be a pressure unseated hatch cover on the exterior end of the penetration sleeve and a pressure seated hatch cover on the interior end of the sleeve. The pressure seated cover will be closed if leakage from the pressure unseated cover becomes excessive.

Each equipment hatch cover will have a different type of seal. Seals being considered include double tongue and groove, double dog ear, double O-ring, and gum drop gaskets.

There will be two personnel lock representations in the model. The possibility of having sealing surfaces in the locks is being investigated.

Two pipe penetrations will be partially constrained from radial movement. These penetrations will be scaled from typical main steam line dimensions. The degree of constraint has not been selected yet.

The 28 day target properties for the concrete are listed below.

Compressive Strength	4,000	psi
Spliting Tensile Strength	410	psi
Static Modulus of Elasticity	3,600,000	psi
Poisson's Ratio	0.15-0.18	

No single pour of concrete will be more than three feet high.

SUPPORT TESTS

A series of preconstruction and post construction support tests are planned to help insure that the model can be built and have prototypical behavior. In addition, these tests will provide a data base of the properties of the various materials used in the model. The following preconstruction tests will be conducted.

1. Concrete mix tests
2. Liner tensile tests
3. Liner tests with welds
4. Tensile tests of liner with studs
5. Stud strength tests
6. Liner formability tests
7. Reinforcing bar strength tests
8. Reinforcing bar splicing tests
9. Shear bar assembly tests
10. Liner fabrication tests

The concrete mix tests should verify that the desired properties can be obtained. The liner related tests (tests #2 through 6) are designed to determine the liner and stud strenghs, and the effects of welding the liner and studs. The reinforcing bar tests (tests #7 through 9) are designed to determine the reinforcing bar strengths and the effects of splicing or welding

the bars together. The liner fabrication tests must demonstrate that the liner can be fabricated and erected.

The postconstruction support tests will consist of testing concrete samples taken during the model construction and testing three flat reinforced concrete panels that are representative of the cylinder wall of the model. The flat reinforced panels will be tested by pulling the reinforcing bars and the liner. The results of these panel tests will be compared to the results of the model test and the results of similar panel tests performed by the Electric Power Research Institute (EPRI). These comparisons will provide a critical link between the EPRI and Sandia programs.

EXPECTED SCHEDULE

Although the final schedule for this project depends upon negotiations with the contractor, we hope that the model will be ready for testing in mid CY86.

REFERENCES

1. Martinez, Salvador and John Steere, Jr., Modeling Techniques for Containment Structures, Stone & Webster Engineering Corporation, Report # 14531-S(B)-1, 1983.

2. Moncarz, Piotr D.; Osteraas, John D.; and Curzon, Anne M.; Experimental Modeling Techniques for Reinforced Concrete Containment Structures, Failure Analysis Associates, Report #FaAA-83-11-11, December, 1983.

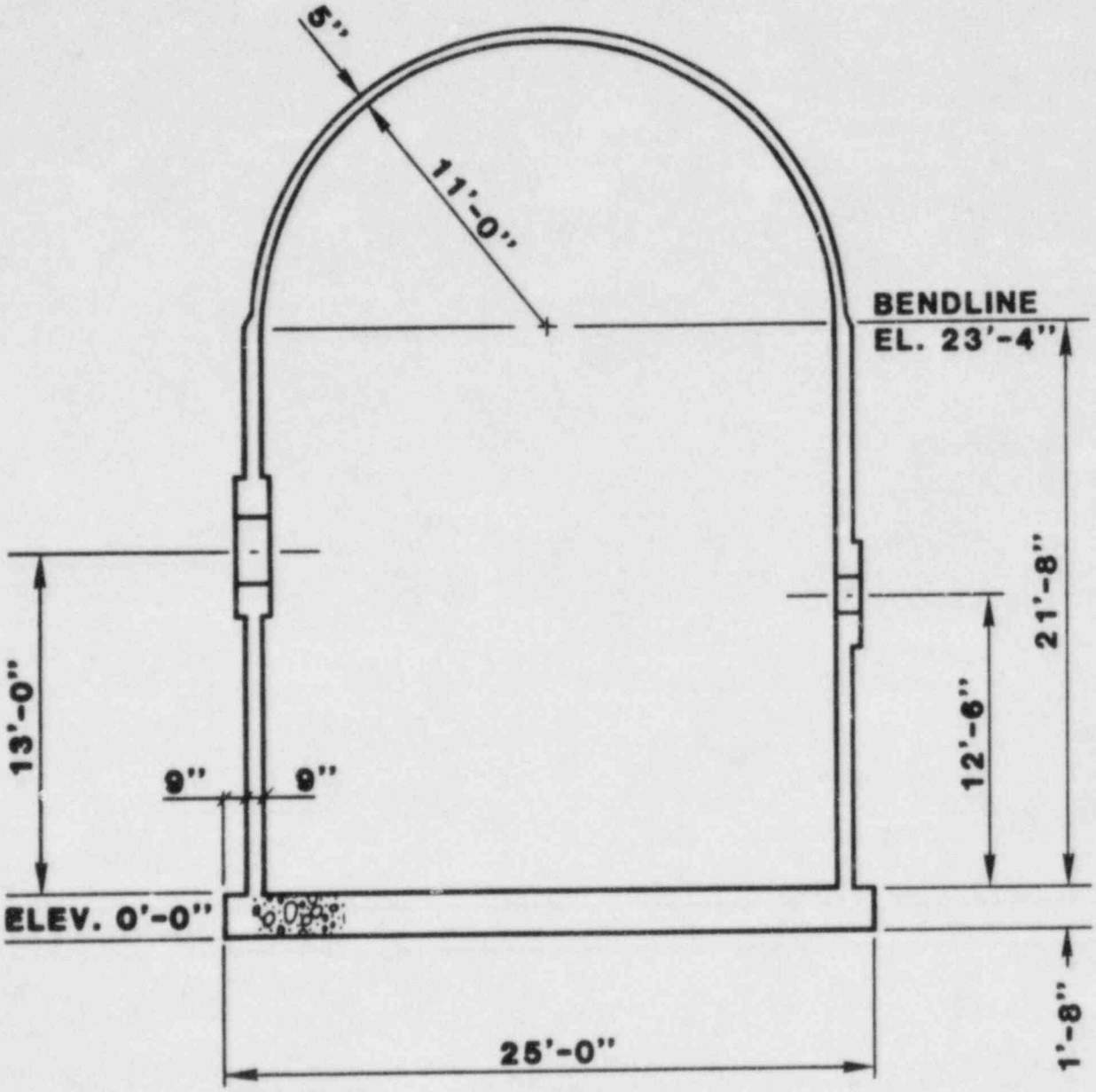

Figure 1. Overall Dimension of the 1/6th Scale R/C Containment Model

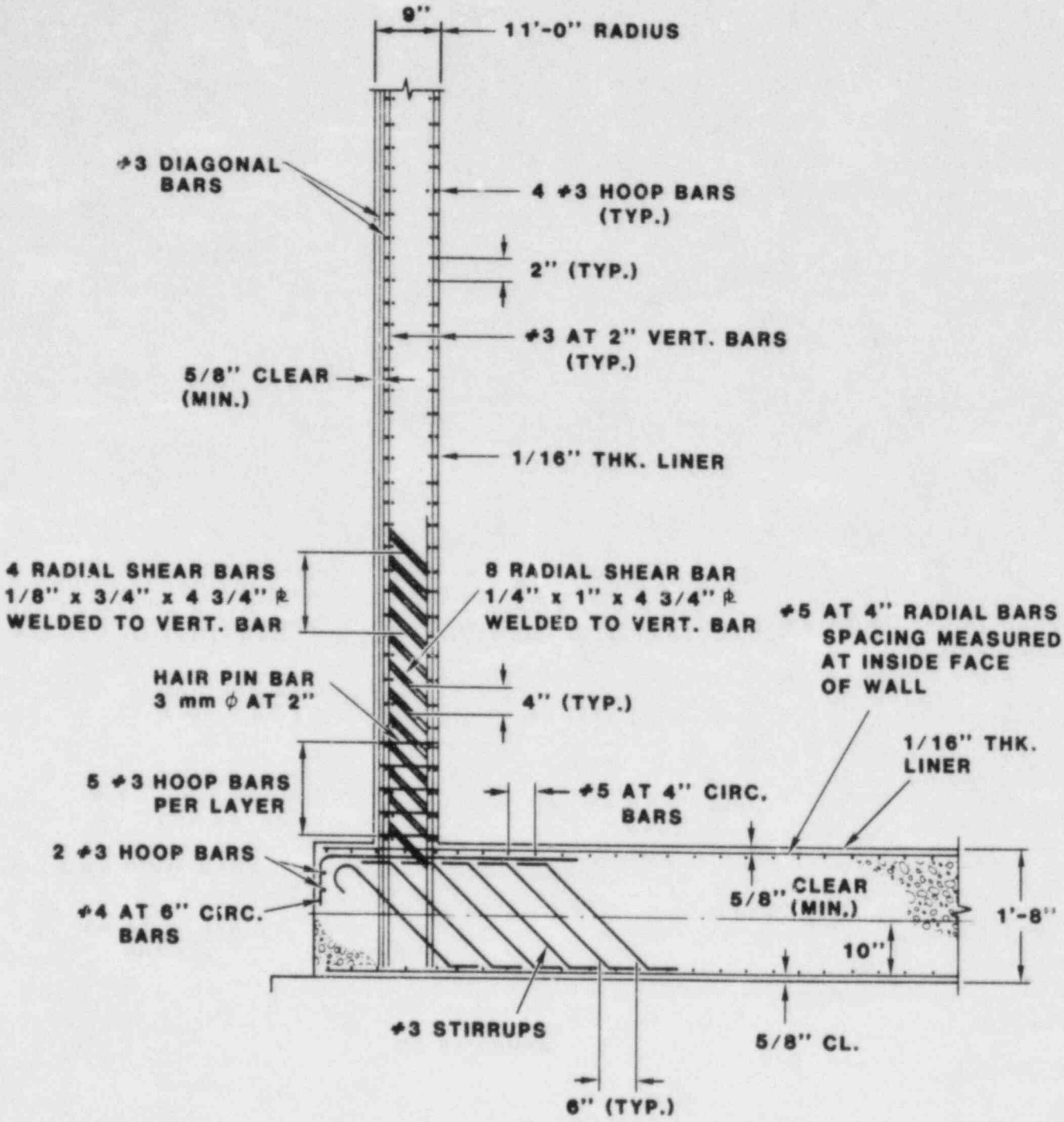

Figure 2. Reinforcement for the Cylinder Wall and Base mat

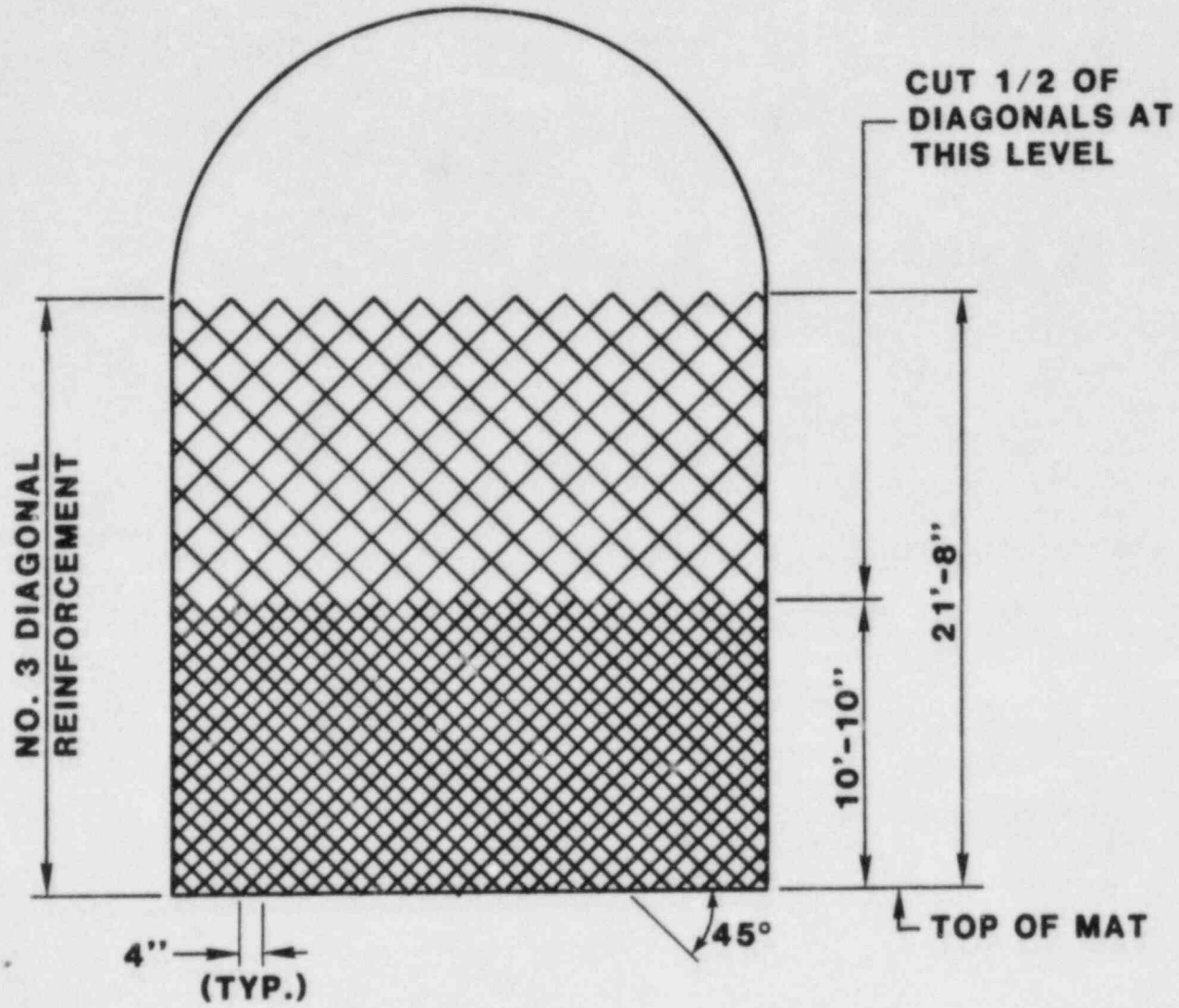

Figure 3. Seismic Rebar Spacing

INTEGRITY OF CONTAINMENT PENETRATIONS UNDER SEVERE ACCIDENT CONDITIONS*

C. V. Subramanian
Sandia National Laboratories
Albuquerque, NM 87185

ABSTRACT

The knowledge of the leakage behavior of containments beyond design conditions is required for the evaluation of severe accident mitigation strategies, risk studies, emergency preparedness planning, and siting. Strategies for managing these severe accidents will be severely hampered unless a methodology for predicting the timing, mode and location of containment failure or leakage is developed.

Since each containment building has a large number of penetrations, these represent a large number of potential leak paths from the containments. Four NRC programs - the Containment Safety Margins program, the Integrity of Containment Penetrations under Severe Accident Conditions program, the Electrical Penetration Assemblies program and the Isolation Valves program are currently in place to evaluate containment integrity and the potential for leakage beyond design conditions.

This paper will summarize the details of two of these programs the Integrity of Containment Penetrations Under Severe Accident Conditions and the Electrical Penetration Assemblies. The test plan, the input loads, the number and types of penetration to be tested under these two programs will be discussed.

BACKGROUND

Since the accident at Three Mile Island, a major effort in safety studies has been directed toward the risk and consequences of severe accidents. As a part of this effort, several studies are currently underway to understand the functional failures of containments. The knowledge of the integrity and the leakage behavior of containments beyond design conditions is required for the evaluation of severe accident mitigation strategies, risk studies, emergency preparedness planning and testing. Strategies for managing these severe accidents will be severely hampered unless a methodology for predicting the mode, timing and location of containment failure or leakage is developed.

Each containment building has a large number of electrical and mechanical penetrations. Typically, there exist anywhere

*This work supported by the U.S. Nuclear Regulatory Commission and performed at Sandia National Laboratories which is operated for the U.S. Department of Energy under Contract Number DE-AC04-76DP00789.

from 60 to 100 electrical penetrations and anywhere from 100 to 300 mechanical penetrations in pressurized water reactors (PWRs)

and boiling water reactors (BWRs). All these penetrations represent a large number of potential leak paths from the containments. Four NRC programs - the Containment Safety Margins Program, the Integrity of Containment Penetrations Under Severe Accident Conditions Program (henceforth called the Containment Penetrations Program), the Electrical Penetration Assemblies (EPAs) Program and the Isolation Valves Program are currently in place to evaluate containment integrity and the potential for leakage beyond design conditions.

The severe accident studies and the data on the performance behavior of penetrations obtained from the various in-plant tests (integrated leak rate tests (ILRT) and the licensing event reports (LER) provided a major impetus to an in-depth investigation into the physical integrity of containment buildings and penetrations. For example, in one such study (Reference 1), a severe accident analysis conducted on a Mark I BWR indicated very high temperatures in the drywell area, which is the location of the majority of the EPAs. Because of the high temperatures, it was postulated in Reference 1 that the sealants would fail and all the EPAs would leak before structural failure would occur. Since other BWR containments have similar EPAs, Reference 1 concluded that all BWR containments would experience the same type of failure. A follow-on study (Reference 2) however, concluded that many of the EPAs have a low potential for leakage, because at least one set of EPA seals is exposed to a lower temperature. These seals are outboard of the containment, which provides a thermal lag during an accident progression. However, other types of penetrations including those with o-ring seals on header plate and those with just inboard seals could have a high potential for leakage if they are sealed with organic materials and are exposed to elevated temperatures and pressures.

Similarly, an examination of LERs through February 1983 indicate that for all types of penetration failures that are reported, the most serious (from the number of incidents and leakage) has been in personnel locks and equipment hatches.

The severe accident conditions which are beyond the design basis conditions (and hence not considered in the design), can result in even higher temperatures and pressures beyond the design basis conditions. A given penetration may develop increased leakage in these severe environments, by either failure of the seal or gasket to retain their original leak tightness, or actual structural failure of some part of the penetration assembly (e.g., a structural crack or tear of a welded joint or in a bellow connection), or by a combination of any of these. Leakages may also increase in gasketed joints as a result of relative movements between mating seal faces, such as opening of the joint gap or by relative rotation of the seal

surfaces caused by interaction with the containment structure displacements. Obviously, leakage behavior will also be a function of whether the gasketed joint tends to be pressure-seating or pressure unseating.

From these, it can be concluded that it is important to understand and predict the structural integrity and the leakage behavior of containment penetrations.

ELECTRICAL PENETRATION ASSEMBLIES (EPA) PROGRAM

EPA Selection

The objective of the EPA program is to evaluate the potential for leakage and failure of EPAs under severe accident conditions. The current state-of-the-art is such that no analysis can be performed which will be accurate enough to predict leak paths and leak rates through the EPAs because of their complex design and behavior and the different types of materials used in their construction. Hence, it will be necessary to perform experiments to locate their leak paths and leak rates under the severe accident environment.

Test specimens for the program were selected based on (i) those with highest potential for leakage (ii) availability and (iii) those types from plants near large population centers. In addition, EPAs were selected to match representative severe environments.

The EPAs with the highest potential for leakage are (i) those with organic seals and gaskets (ii) those with elastomer O-rings on header plates and (iii) those designed for low pressure capability. Regarding the ready availability of the EPAs, of the identified 18 suppliers, only 3 suppliers are active today from whom actual full size EPAs similar to those supplied to the existing nuclear power plants can be obtained. These are D. G. O'Brien, Westinghouse and Conax. The EPAs supplied by these three vendors satisfy the other two requirements. Hence, efforts are underway to procure EPAs from these three manufacturers for testing them under the severe accident conditions.

Severe Accident Environment Test Input Profiles

The EPAs will be tested for the severe accident environments under all characteristics for both PWRs and BWRs to determine their leakage. These severe accident profiles are based on calculations performed under the Severe Accident Sequences Analyses (SASA) program, also funded by the NRC. Where such information is not available, other sources including data from probabilistic risk analysis (PRA) studies of plants were used.

For the PWR environment, the accident cases which produced the maximum containment pressures and temperatures (cases when both the heat removal systems and cooling systems are inoperable) and which had a high frequency of occurrence were selected from data in Reference (2). The envelop of three individual accident scenarios was selected as the test profile for the PWR environment and are shown in Figure 1.

For the BWR environment, the currently available information indicate that the environments for Mark I and Mark II are very similar, with Mark I generally bounding the Mark II and significantly higher than that of Mark III. Hence, it was decided to use Mark I and Mark III environments thereby bounding the Mark II environment. The severe accident case selected for both Mark I and Mark III was one of the dominant accident sequences in almost all BWR-PRA studies. In addition, for Mark I, another accident sequence which is also quite dominant was considered and the envelop of the two sequences was used for the test profile. In these profiles for both Mark I and Mark III, the point where the pressure sharply drops off is the assumed failure point of the containment as used in the SASA studies. The test profiles for Mark I and III which are based on data available in References 3 and 4 are shown in Figures 2 and 3.

Test Sequence

As indicated earlier, the EPAs selected for testing are the Westinghouse, Conax and D. G. O'Brien. The test plan calls for the following test sequence.

1. Radiation age to the end of service life and LOCA accident for a total dose of 200 mrads at a dose rate of less than 1 mrad/hr.
2. Post radiation inspection to IEEE 317/1976.
3. Thermal aging at a temperature of 150°C (302°F) for 168 hours.
4. Post thermal aging to IEEE 317/1976.
5. Test to severe accident environment and measure leak rate during the test.
6. Post accident inspection and functionality measurements including leak rates.

The severe accident environment will be a steam environment with the leak rate measuring instrumentation calibrated to measure from 1 cc/sec. to 10,000 cc/sec.

The Westinghouse penetration will be tested in the BWR - Mark III environment because of the large numbers of them found in these plants. D. G. O'Brien penetrations will be tested in

the PWR environment because of their low pressure capability and the high pressures that are predicted in a PWR severe accident environment. A Conax penetration will be tested in the BWR - Mark I environment because quite a few of them are found in these and General Electric penetrations which are more common in BWR - Mark I, are no longer manufactured and hence not readily available.

Summary - EPA Program

A program is in place to test 4 full size EPAs for the BWR and PWR severe accident environments to evaluate their leakage potential under these severe accident conditions. The test matrix is shown in Table 1. The expected end product of the program is to obtain leakage behavior information and measured leakage data through the EPAs if leakage occurs, measured thermal gradient along the EPAs, and an evaluation of electrical degradation (insulation resistance) with time.

Table 1: EPA TEST MATRIX

EPA	PLANT	SEVERE ACCIDENT ENVIRONMENT
Conax	BWR - Mark I	700°F, 135 psia
Westinghouse	BWR - Mark III	400°F, 75 psia
D. G. O'Brien	PWR	360°F, 155 psia

CONTAINMENT PENETRATIONS PROGRAM

As indicated earlier, a detailed program plan is currently being developed. The objective of this program is to determine the characteristics of containment penetrations that contribute to leakage during severe accident sequences beyond the design basis conditions. The penetrations that will be included in this program are all the fixed and operable mechanical penetrations except valves (which are considered in another program) and the EPAs (which are considered in the program described earlier).

Plant operating experience has shown that major penetrations (operable and fixed) are susceptible to leakage under the design operating environment primarily due to the limited capability of seals and gaskets that are used in them. Under the severe accident conditions the susceptibility of these penetrations to leakage even though unknown due to lack of data, is expected to increase which may further be aggravated as a result of relative movements between mating seal faces, such as the opening of the joint gap or by relative rotation of the seal surfaces, caused by interaction with the containment structure displacements. Currently adequate models for predicting leak rate in severe accident environments for containment penetrations with seals and gaskets does not exist because of their complex structural behavior, uncertain leak paths, the

severe accident environment and the numerous types of penetration designs that exist. Hence, this program was established to determine the leakage behavior of penetrations and to develop a methodology for predicting leak rate through penetrations.

Program Definition

Because of the different types of major penetrations that exist in a nuclear power plant which are susceptible to leakage and because of the large number of designs that exist for a given type of penetration, a comprehensive survey is in progress to determine the different types of designs that exist for all of the major penetrations. The survey which is being performed by Argonne National Laboratory (ANL), Argonne, Illinois, includes all containment types, materials, penetration designs, and types of seals and gaskets. Based on the survey data, a program plan is being developed by ANL (Reference 5) which will identify penetrations which are most susceptible to leakage and recommend a methodology to predict leakage through these penetrations. To better evaluate the relative leakage potential for the different penetrations, a number of figures of merit analyses were made. These figures of merid analyses are based on the structural behavior of the penetration-containment system and on the geometry and material variations of the seals and gaskets that are used in the various penetrations. Utilizing these figures of merit, a comparative analysis is being performed on different types of penetration designs to come up with a list of penetrations which are most susceptible to leakage and hence may need to be tested to determine their leakage behavior. The preliminary list includes BWR drywell top head (bolted type), pressure unseating equipment hatch, bellow connections, personnel air lock with inflatable seals, pressure-seating equipment hatch and personnel air lock with pressure seating seals.

In addition, a test matrix for seals and gaskets based on the gasket material used, sealing surface geometry, aging effects, scaling effects, and fluid/temperature/pressure loading is also being developed. Some of the common geometries that are being considered are: O-ring type, tongue and groove type, double dog-ear type, gum drop type and inflatable seal type. All these geometries are quite commonly used in large mechanical type penetrations (eg. equipment hatch, personnel air lock, etc.). The O-ring type is also commonly used in EPAs. Some of the material which are under consideration are silicone rubber, ethylene-propylene type rubbers (EPR/EPDM) and Viton. Silicone rubber is commonly used in mechanical penetration assemblies and silicone rubber, EPDM and Viton are commonly used in EPAs. The test matrix for the seals and gaskets will evaluate the effects of radiation aging and temperature. Also, the test matrix will include different sizes to determine the effects of scaling.

Seals and Gaskets Experiments

Once the text matrix for the seals and gaskets is completed, they will be tested using the EPA test facility at Sandia National Laboratories to measure leakage through them for the BWR and PWR severe accident environments. As indicated earlier, the expected results of this task is (i) to determine the leakage potential of the various seals and gaskets under the severe accident conditions and (ii) to determine the effects of variations in material, geometry, temperatures, radiation aging, and scaling. The test data from this task can then be used to develop simple analytical models to determine leakage through seals and gaskets which will be useful in developing a methodology for predicting leakage through penetrations under severe accident conditions.

Penetration Assembly Experiments

The tentative list of penetrations to be tested was provided under the program definition subsection. In addition, the scale size for these penetration tests and also the incorporation of the containment structure-penetration interaction effects need to be decided before the test plan is finalized. The scale size of the tests to be performed will primarily depend on the test facilities that are available to perform these tests and obtain the needed leakage data in a BWR or a PWR severe accident steam environment. On the question of whether to include structure-penetration interaction effects or not, analyses work is in progress to determine how significant these effects are in the sealing surface deformation of the various penetrations under consideration. Results from these analyses will be used to determine what the test model for these penetrations would be.

The BWR or the PWR severe accident environment generated for the EPA tests will also be utilized for these large scale tests to determine the leakage potential of the penetrations under consideration.

Penetration Analyses

Under this task, it is planned to perform scoping analyses of all the penetrations to be tested under the severe accident conditions to determine (i) the shell-penetration interaction effects (ii) the sealing surface deformation in order to estimate if there is a potential for leakage and (iii) to determine the significant parameters in the penetration assembly which may affect the leakage potential. In addition, some scoping calculations using simplified assumptions will be made to make a pre-test prediction of leakage for the penetrations to be tested.

It is also proposed to perform analyses on other types of penetrations which are not being tested but can be evaluated by

analyses under the severe accident conditions. Typical examples include those penetrations with no gaskets, seals and bellows, or fixed piping penetrations, etc.

Methodology Development

Currently, adequate models for predicting leak rate through containment penetrations with seals and gaskets do not exist. The reasons for this are (i) the complex behavior of the containment-penetration system (ii) lack of knowledge of the leak paths through the penetrations, (iii) the severe accident environment that are of concern (iv) the different types of penetration designs that exist and (v) the lack of information on the behavior of the seals and gasket materials under extreme environment. Hence, the objective of this task is to identify and evaluate existing methods (if any) which could be used to predict leakage through containment penetration by extending or modifying them or, develop empirical methods by utilizing the bench mark data from the seals and gaskets tests and the large scale penetration tests. This methodology will then be used to predict overall leakage through all the containment penetrations.

Summary - Containment Penetration Program

A program has been established to evaluate the behavior of seals and gaskets and major fixed and operable penetrations under postulated severe accident conditions. The program will also provide a methodology to predict leak rate of containment penetrations under the severe accident conditions. However, it must be noted that there are some potential concerns which may affect the expected output. This includes scaling concerns on leak rate prediction, generic application or extension of test results because of large number of different penetration designs, the limited number of tests that can be performed and the effects of potential presence of aerosols in the containment atmosphere during the severe accident which may affect the results.

Acknowledgements

The preparation of this paper required collecting information from various sources. This includes F. V. Thome of SNLA on the EPA program and R. W. Seidensticker, T. R. Bump, and M. H. Shackelford of Argonne National Laboratory (ANL). The author is grateful to them for their efforts in providing the needed information.

REFERENCES

1. D. H. Cook, et al, "Station Blackout at Browns Ferry Unit One - Accident Sequence Analysis," NUREG/CR-2182, ORNL/NUREG/TM-455/V1, (Oak Ridge, TN: Oak Ridge National Laboratory, November 1981).

2. W. A. Sebrell, "The Potential for Containment Leak Paths Through Electrical Penetration Assemblies Under Severe Accident Conditions," NUREG/CR-3238, SAND83-0538, Sandia National Laboratories, Albuquerque, NM, July 1983.

3. W. T. Pratt, et al, BWR-Mark I and Mark II Standard Problem," Performed for the Containment Load Working Group, Brookhaven National Laboratory draft report, November 16, 1983.

4. Letter Report by Accident Analysis Group," Review and Evaluation of GESSAR-II Probabilistic Risk Assessment - Containment Failure Modes and Fission Product Release, Brookhaven National Laboratory, prepared by U.S. NRC, at July 27, 1983.

5. T. R. Bump, et al, "Characterization of Nuclear Reactor Containment Penetrations," report to be published by Argonne National Laboratory, Argonne, IL.

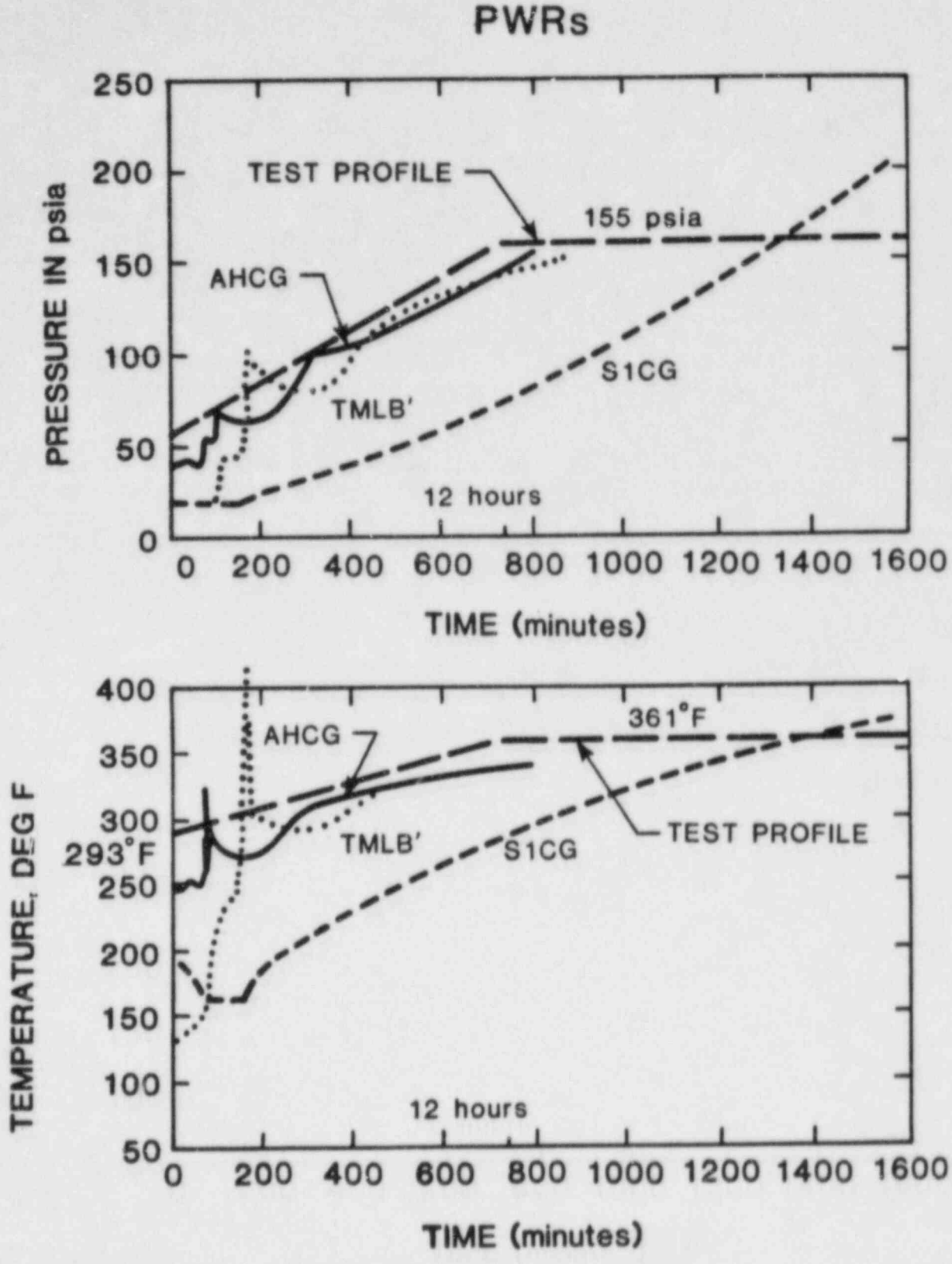

FIG. 1: ACCIDENT PROGRESSION FOR PWRs.
(CONTAINMENT ATMOSPHERE)

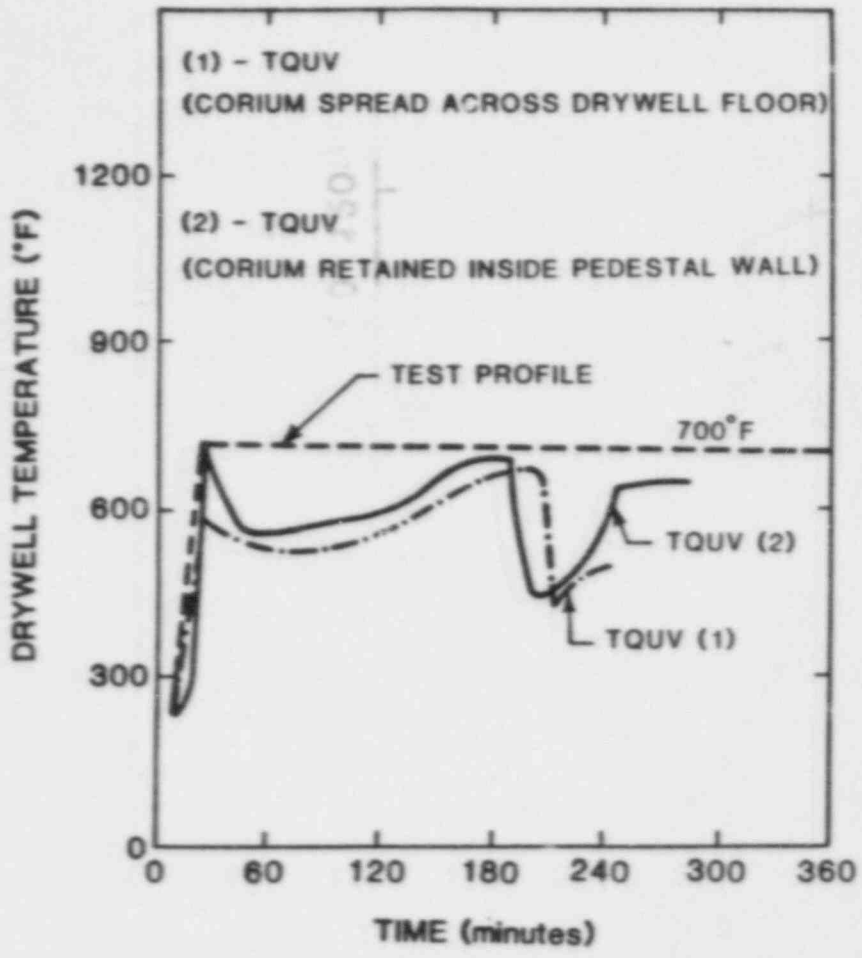

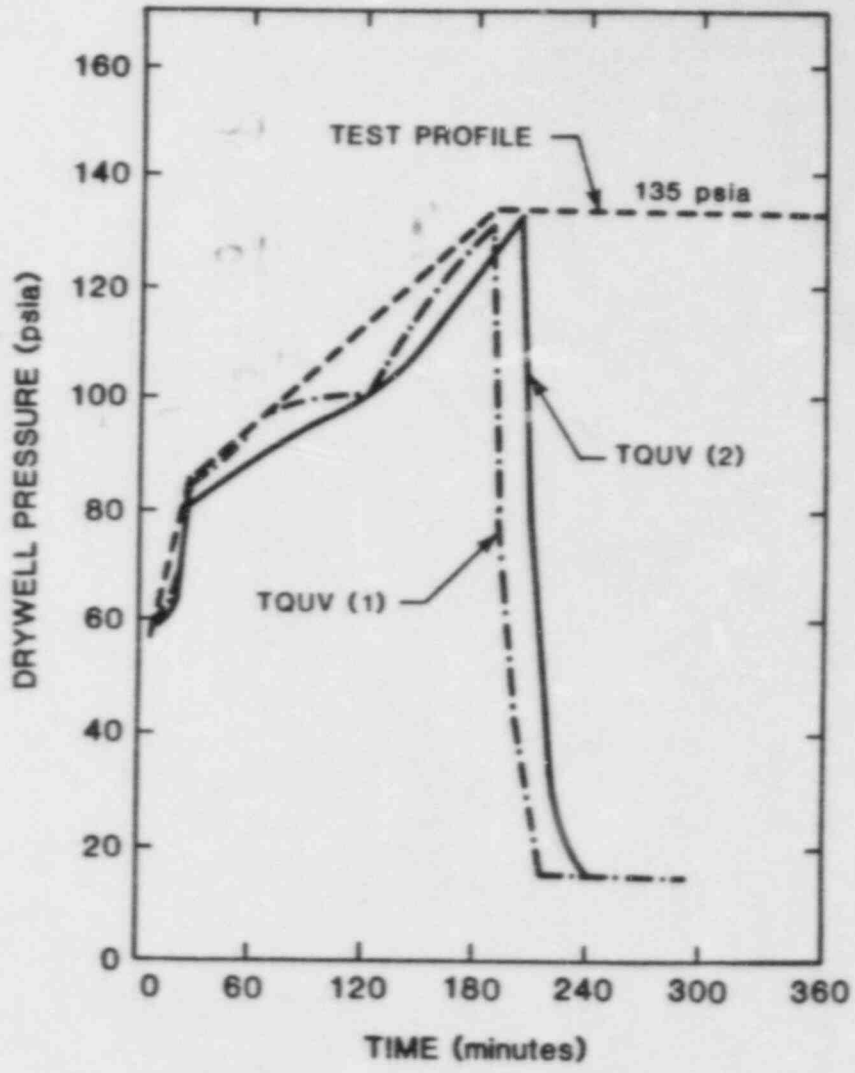

FIG. 2: ACCIDENT PROGRESSION SEQUENCE FOR BWR MARK I
(DRYWELL ATMOSPHERE)

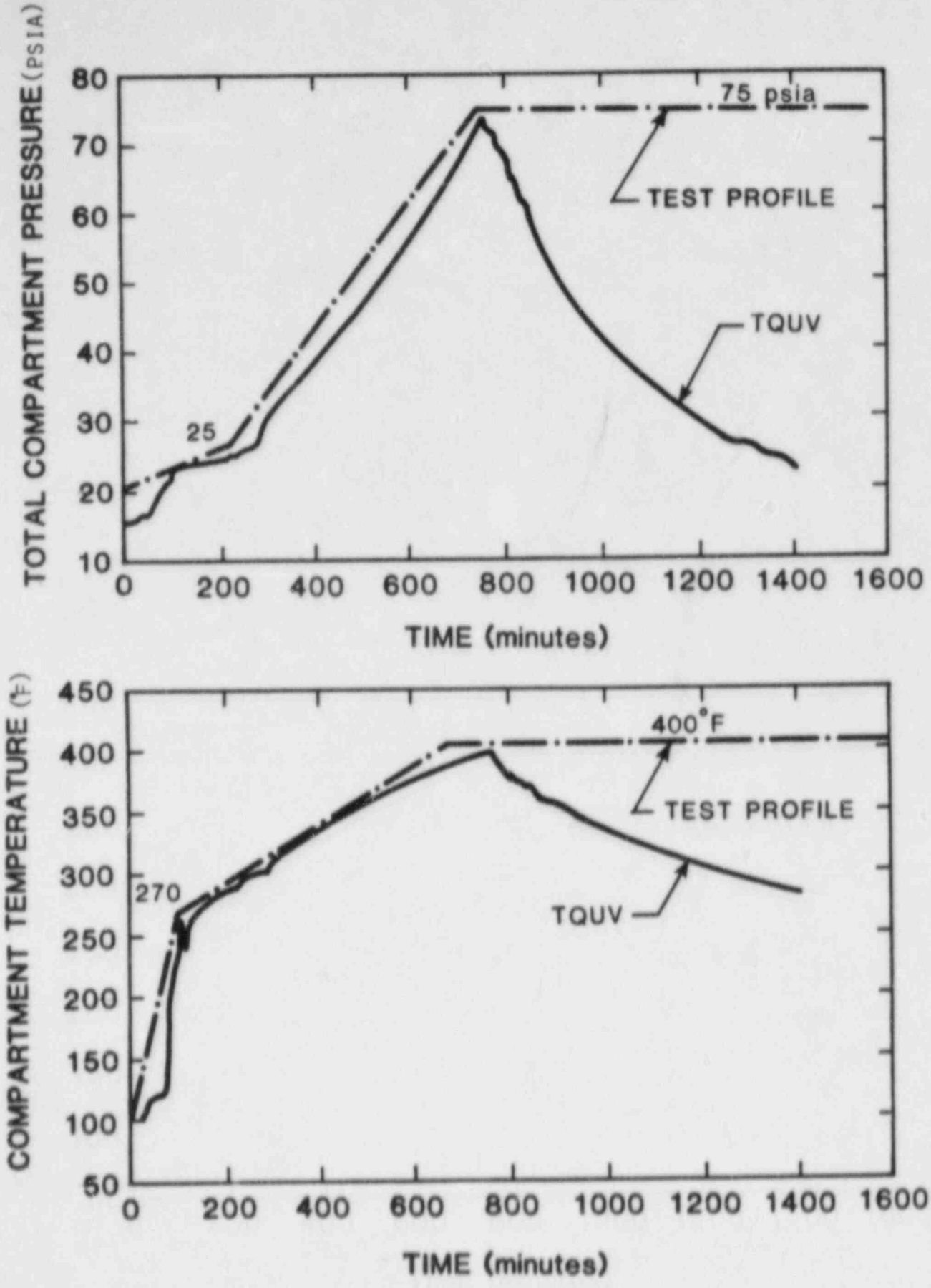

FIG. 3: ACCIDENT PROGRESSION FOR BWR-MARK III
(WETWELL ATMOSPHERE)

ANL SURVEY OF LWR CONTAINMENT PENETRATIONS: A PROGRESS REPORT

T. R. Bump, R. W. Seidensticker, and M. H. Shackelford
Argonne National Laboratory
Argonne, IL 60439

ABSTRACT

Argonne National Laboratory is currently working on specific tasks in a containment penetration integrity program funded by NRC and managed by the Sandia National Laboratories. The first of these tasks is called "Characterization of Existing Penetration Designs". The objective of this task is to identify those penetrations in nuclear reactor containments which, because of historical data or expected behavior under accident loads, are believed to have a relatively high probability of developing leakage when subjected to temperatures and pressures well beyond the containment design basis values. The program focuses on large and operating penetrations -- such as personnel airlocks, equipment hatches, and bellows seals -- and excludes electrical penetration assemblies and valve penetrations. (Sandia is working on electrical penetrations and EG&G is studying valve penetration assemblies.)

This task will determine which penetrations require detailed study to determine leakage characteristics, and will identify which types of penetrations may require specific model and/or large-scale testing to obtain such characteristics.

The survey is concentrating on containments built primarily between 1970 and 1982, and includes a comprehensive sample involving not only all types of containment types and materials, but also includes work performed by a large number of A-E design firms. The survey includes a good sample of containment penetration fabrication vendors. About 20 containments have been completed at this time, and about 20 more will be completed by mid-August 1984.

SCOPE AND PURPOSE OF ANL PROGRAM

Argonne National Laboratory (ANL) is currently performing work on leakage and structural behavior of penetrations in nuclear reactor containment structures, when such structures are subjected to pressure and thermal loads beyond the design basis. This work is being managed by the Sandia National Laboratories, as a part of the overall containment program funded by NRC. Not all penetrations are included in this work; specifically excluded are valves and electrical penetration assemblies. The ANL work concentrates on large major penetrations which generally employ some type of seal or gasketed joint, such as airlocks and equipment hatches. Also included are some bellows sealed joints, and some pipe penetrations.

The ANL program consists of three tasks:

*This work supported by the U.S. Nuclear Regulatory Commission.

Task 1 - Survey of Penetrations in Existing Containment Structures
Task 2 - Structural Analysis of Selected Penetrations (pressure-seating, pressure-unseating, and bellows)
Task 3 - Survey and Evaluation of Existing Test Facilities

This paper describes work performed in Task 1 - Characterization of Existing Penetration Designs, and includes the evaluation of plant-specific data compiled from a detailed survey of 22 nuclear power plants. The current study reported here includes both PWR and BWR plants, and includes steel, reinforced concrete, and prestressed concrete containment structures. An additional 17 plants will be reviewed, characterized, and included in a report to be issued by August 15, 1984. Some of the work performed under Task 2 is reported in Session D of this Workshop (R. F. Kulak, et al.).

The main objectives of Task 1 of the ANL program include an evaluation of the existing penetration designs to determine what tests are required on seals, gaskets, and penetration assemblies to enable NRC, designers, and plant owners to evaluate leakage characteristics of a specific nuclear power plant. In addition, an evaluation is made to determine which penetrations can be adequately characterized on the basis of analysis alone, rather than by test, in order to obtain leakage and/or structural behavior.

To aid the evaluations, figures of merit related to leakage potential were developed, calculated or estimated, and compared. Many of the figures of merit have the basis that relative elastic behavior at containment design pressure is a reasonable indication of relative plastic behavior at fractional overpressure, and practical to use because of its simplicity. This basis is weak when there is no constant ratio between anticipated beyond-design-basis-accident equivalent* pressures and containment design pressures. A proposed method to compensate for this weakness is described. In the later discussion of the figures of merit, some are described in more detail than others. This merely reflects the space limitations for the entire paper and has no bearing on the relative importance of the different figures of merit.

SURVEY PLAN

At this time the survey includes 22 nuclear power plants. Table 1 is a summary of the plants surveyed and includes plant type, type of containment, and combinations of architect-engineers (A/Es) and major penetration suppliers involved in the survey. Each plant was assigned a coded number, such as BWR Mk I, Unit 1. Summary data sheets and penetration design details were then prepared for each of these plants.

Table I. Summary of Types of Containments Surveyed

Architect-Engineer	Equipment Supplier	Plant Type (No. of Plants)	Containment Type Ref. [1]
Bechtel	Southern Boiler Industries (SBI)	PWR(2)	Prestressed Concrete

*Modified by temperature, radiation, etc.

Table I. Summary of Types of Containments Surveyed (Contd.)

Bechtel (Contd.)	Woolley (W), and Chicago Bridge and Iron (CBI)	BWR Mark I(1)	Steel
Ebasco	CBI	PWR(4)	Steel
Fluor-Pioneer	CBI	PWR(3)	Steel
Gibbs and Hill	CBI	PWR(1)	Reinforced Concrete
Sargent and Lundy	CBI	PWR(5)	Prestressed Concrete
		BWR Mark I(2)	Steel
		BWR Mark II(3)	Prestressed Concrete
		BWR Mark III(1)	Reinforced Concrete

The survey was conducted by a study of the plant FSAR (where readily available) followed by a personal visit to the designer of the facility. Written permission to use the plant specific data (in the format described in the preceding paragraph) was obtained from either the plant owner, designer, or both. Detailed discussions were held with the plant and equipment designers to gain insight into design philosophy and detailed design approaches. Copies of pertinent drawings were then obtained and used to generate the detailed data packages. The ANL sketches were sent back to the appropriate designers for review to assure that these sketches accurately depicted their designs. The cooperation of all parties involved was excellent and contributed to the completeness of the information obtained.

One important, and not unexpected, result of the survey is that there is virtually no standardization of penetration designs. There may even be variations in equipment designed by a single supplier reflecting design improvements which have evolved over time. Also, for concrete containments in particular, the structural load paths between the building liner and penetration sleeves vary considerably. The manner in which the penetration sleeve (or barrel) is anchored in the concrete containment wall also varies from design to design. These differences make it difficult to develop generic designs of test articles. However, it is believed that careful selection of test article features can result in meaningful test results to which any given penetration design can be compared to estimate its leakage behavior.

POTENTIAL LEAK BEHAVIOR OF PENETRATIONS

A given penetration may develop increased leakage (at pressures and temperatures beyond the design basis) by failure of the seal or gasket to retain their original leak tightness, by actual structural failure of some part of the penetration assembly (e.g., a structural crack or tear of a welded joint or in a bellows), or by a combination of both of these. Leakages may increase in gasketed joints as a result of relative movements between mating seal faces, such as opening of the joint gap or by relative rotation of the

seal surfaces caused by interaction with the containment structure displacements. Obviously, leakage behavior will also be a function of whether the gasketed joint tends to be pressure-seating or pressure unseating.

It is interesting to note that even for pressure-seating penetrations (e.g., personnel airlock doors, and equipment hatches) increasing pressure beyond the containment design pressure may result in increased leakage. This is because there is usually a growing mismatch between the mating gasketed-seal faces as containment pressure increases. For example, in the case of a personnel airlock the door itself tends to deflect less than the corresponding part of the door frame located in the penetration bulkhead, thus creating an opening in the joint at the midspan of the door edges. Another example was found during the structural analyses of an equipment hatch penetration. In the latter example, it was observed that significant relative rotation and sliding could occur between mating seal faces.

From all of this we see that the potential for increased leakage at any penetration will depend on the gasket design and gasket material, the interaction between the various structural parts of the penetration assembly, and the degree to which the containment structure's behavior is reflected at the sealed joint of the penetrations. The next section presents a figure of merit approach used to evaluate potential leakage of penetrations.

FIGURE OF MERIT ANALYSES

Nomenclature

Symbol	Description	Units
A	Effective area	$in.^2$
A_{sh}	Shear area	$in.^2$
D	Shell ID	ft
d	Sleeve diam.	in.
d'	Reinforcing ring OD	in.
E	Modulus of elasticity	$lb_F/in.^2$
e	Strain	---
F'	Load per unit length	$lb_F/in.$
f	Fraction of steel in area	---
ℓ	Beam length	in.
ℓ_i	Sleeve segment length	in.
n	No. of wave lengths	---
P	Containment design pressure	$lb_F/in.^2$ gage
P_c	Critical pressure	$lb_F/in.^2$ gage
P_{SA}	Severe accident equivalent pressure	$lb_F/in.^2$ gage
R	Effective radius, spherical radius	in.
r_i	Sleeve segment radius (d/2)	in.
t'	Reinforcing ring thickness	ft
t_c	Cover thickness	in.
t_i	Sleeve segment thickness	in.

To better evaluate the relative leakage potential for penetrations, eight figures of merit related to that potential were developed and numerical values

of the figures of merit were calculated or estimated and compared. The first seven figures of merit are based on structural behavior while the eighth relates to gasket and seal geometry and materials. The calculations were performed on a microcomputer using a penetration data base generated for that purpose. It is anticipated that eventually the figures of merit can be developed to a point where they will be able to indicate whether any penetration has higher or lower leakage potential than a penetration that has already been tested, or analyzed in detail, for its leakage characteristics.

Many of the figures of merit have the basis that relative elastic behavior at containment design pressure is a reasonable indication of relative plastic behavior at fractional overpressure, and practical to use because of its simplicity. This basis is weak when there is no constant ratio between anticipated beyond-design-basis-accident equivalent* pressures P_{SA} and containment design pressures P. To compensate for this weakness, as a first approximation it is suggested that the present relevant figures of merit be multiplied by P/P_{SA}, which is essentially the same as using beyond-design-basis-accident equivalent pressures in the figure of merit formulations instead of design pressures.

Descriptions of the figures of merit follow:

Sleeve Wave Lengths. As discussed in Ref. [2], large containment shell deformation can produce enough load on a penetration sleeve welded to the shell to cause sleeve deformation. When a sealing surface is an integral part of the sleeve (as is the case with many equipment hatches), and within the zone of influence of the shell to sleeve weld (within one "wave length" of the radial load), the sleeve deformation could result in sealing surface separation and seal leakage, even in the case of pressure-seated sealing surfaces.

The associated figure of merit is based on the number of wave lengths between shell to sleeve weld and sealing surface (along a sleeve) as compared to the amount of nearby elastic shell strain at design pressure. With regard to shell strain (Ref. [3]), the design load per unit equivalent circumferential length on the reinforcing ring is:

$$F' = 12\ PD/2$$

Nominal hoop strain of the ring is

$$e = F'R/(AE)$$

$$R \sim (d + d')/4$$

$$A \sim 12\ ft'(d' - d)/2$$

where f is 1 for steel containment and currently assumed 0.01 for concrete containments. Eventually, actual f values for each concrete containment will be used. Thus,

*Modified by temperature, radiation, etc.

$$e = PD(d + d')/\{4\, ft'(d' - d)E\}$$

With respect to number of wave lengths, one wave length equals the textbook value $1.83\,(r_i t_i)^{0.5}$; thus

$$n \propto \sum (\ell_i/(r_i t_i)^{0.5})$$

where the summation accounts for sleeve dimension variations between containment shell and sealing surface. The figure of merit is

$$F_1 \propto n/e$$

$$F_1 = (\Sigma(\ell_i/(r_i t_i)^{0.5}))ft'(d'-d)/(PD(d'+d))$$

Even though the amount of shell strain at design pressure may be trivial, it is considered to be a realistic normalization factor for indicating the relative effect of fractional overpressure on shell strain. Also, as stated above, relative elastic behavior is considered to be a reasonable indication of relative plastic behavior.

The F_1 values for steel containment penetrations in general are not comparable with those for concrete containment penetrations, because the reinforcing ring in steel containment is anchored much more securely to the sleeve than in the case of concrete containment. For the relevant steel containment penetrations the Fig. 1 equipment hatch has the highest F_1 value found to date (0.18*) and the Fig. 2 hatch has the lowest value (0.03*). This variation is at least partly because the former hatch has more than 2 ft of sleeve length between shell and sealing surface whereas the latter has less than a third of that distance, at least locally. Thus, the latter is judged to have the greatest leakage potential with respect to sleeve deformation, in the steel containment category.

For the concrete containment penetrations, the Fig. 3 equipment hatch has the highest F_1 value (0.08*) and the Fig. 4 hatch has the lowest (0.01*). Again, this is at least partly because the former has 1-1/2 ft of sleeve length between wall and sealing surface while the latter has less than a third of that distance.

Cover Strength. The critical pressure for buckling of a spherical-segment cover pressure-loaded on the convex side is discussed in Ref. [2]. Buckling, at a minimum, could cause sealing surface rotation and leakage. The associated figure of merit is based on the critical pressure as compared to the containment design pressure:

$$F_2 \propto P_c/P$$

$$F_2 = (t_c/R)^2/P$$

---

*$\times 10^{-6}$

Again, design pressure is considered to be a reasonable normalization factor for indicating the relative effect of fractional overpressure on leakage potential.

For the penetrations with spherical-segment covers, the Fig. 2 equipment hatch has the highest F_2 value (124*) and the Fig. 5 hatch has the lowest value (6*). This variation is primarily because the former's cover is four times thicker than the latter's cover. The latter hatches are judged to have the greatest leakage potential with respect to cover buckling.

Frame Strength. A potential source of leakage results from the inherent greater stiffness of the top and bottom (the short sides) of a rectangular door, as compared to the stiffness of the mating frame members. Under pressure the frame members tend to bend more than the door edges, thus potentially producing seating surface separation and seal leakage, even in the case of pressure-seated sealing surfaces. The maximum elastic deflection of a uniformly loaded beam of uniform cross section at containment design pressure is the basis of the associated figure of merit.

Shear Strength. The amount of steel shear area provided for penetration sleeves anchored in concrete varies widely among penetrations, even when normalized on the basis of sleeve axial load. The associated figure of merit is based on the steel shear area as compared to the sleeve axial load at containment design pressure:

$$F_4 \propto A_{sh}/(\pi d^2 P/4)$$

$$F_4 = A_{sh}/(d^2 P)$$

No credit is given here for the steel shear area associated with the bevel that is found on many sleeves. The bevel tapers are typically shallow; any concrete dilation or separation from the sleeve would allow failure strains to occur in the sleeve-liner connection before concrete support of the bevel surface could occur.

For the relevant concrete containment penetrations the Fig. 4 equipment hatch has the highest F_4 value (21**) and the Fig. 6 hatch has the lowest value (2**). This variation is primarily because the former has a "sealing-surface-sleeve-stub", with an OD that is significantly larger than the concrete opening ID, butted against the reinforcing ring, so that the length of the stub contributes to the steel area. On the other hand, the Fig. 6 hatch has a larger diameter sleeve, without the stub feature, a thinner reinforcing ring, and its anchor straps are not equivalent to the Fig. 4 hatch anchor rings. The latter hatch is believed to have the greatest leakage potential with respect to sleeve-anchor shear.

Ring Strength. The height or protrusion extent of anchor rings that are sometimes provided for penetration sleeves anchored in concrete varies widely among penetrations, even when normalized on the basis of potential concrete dilation away from the sleeve. Low ring heights mean that should concrete dilation occur, the shear plane area (in the concrete now unsupported by the

*$\times 10^{-7}$; **$\times 10^{-4}$

sleeve) is smaller than with high ring heights, increasing the concrete shear stresses. The associated figure of merit is based on ring height as compared to radial concrete dilation at design pressure.

Unseating Strength. In the case of pressure-unseating gaskets and seals, the strength of the fasteners is of course important with respect to leakage potential. The associated figure of merit is based on the fastener cross sectional area as compared to unseating load at design pressure. At present it is assumed that the preload stress in all fasteners is the same. The actual preload stress in the field will always be uncertain to some extent, due to variables in such factors as thread lubrication.

Plate Strength. In the case of penetration closures that resemble flat plates, bending of the plates could foster sealing surface deformation and consequent seal leakage. The associated figure of merit is based on, and proportional to, the reciprocal of the maximum deflection of a uniformly loaded circular flat plate at design pressure.

Gaskets and Seals. Figures of merit in this category were selected by first ranking both geometries (double dog ear, double O-ring, etc.) and gasket materials individually. The figure of merit for a gasket and seal design is taken to be the sum of its geometry and material values. The geometry ranking was based on discussions with vendors and A/Es, and the material ranking was based on a gasket vendor's curves of life vs. temperature.

Closing Remarks. This section is not expected to constitute the final word on suitable figures of merit for penetration leakage potential evaluation. In the categories considered there are probably other expressions that other analysts would prefer, and of course there are many other categories for which suitable expressions can be developed. Nevertheless, it is believed that the figures of merit given here are adequate to show relative strengths and weaknesses of many important penetration features, and they emphasize the wide variations that exist in the field.

Finally, the wide scatter in figure-of-merit values here deserves some discussion. First, we are taking it for granted that all the penetrations, including those that have low figures of merit, met all code and regulatory requirements at the time of construction. The situation that some penetrations have larger figures of merit can be attributed to regulatory requirements being different at the times the different plants were built, to design evolution, and to other miscellaneous factors.

PENETRATIONS WHICH MAY BE QUALIFIED BY DETAILED ANALYSIS ONLY

At present, if any penetration should commence leaking due to severe accident conditions, the leakage rate probably could not be calculated with defensible precision. Nevertheless, much can be done at once by analysis only to reduce testing requirements, and, by pursuing the right mix of testing and analysis, the capabilities of analyses to reduce further testing can probably be increased greatly.

To start, relatively simple calculations (elastic and, if necessary, inelastic) on an individual containment's penetrations, can show that some of its penetrations are highly probable to leak much more than others for any

beyond-design-basis situations. In fact, the calculations can show that the former penetrations are acceptably probable to Leak Enough, either to (a) violate environmental limitations or (b) prevent higher containment pressures and temperatures, that the leakage behavior of the latter penetrations is Irrelevant. (In subsequent discussions, these are called Class LE and Class IR penetrations.) The Class IR penetrations are those which can be predicted, by relatively simple analysis alone, to have no potential to leak. (Regarding violation of environmental limitations, specifically on radioactivity releases under beyond-design-basis conditions, the specification of such limitations is, by necessity, expected to proceed at a pace compatible with that of the analyses described here.)

Typical Class IR penetrations are those that have no gaskets, seals, bellows or, in the case of piping penetrations, close-coupled piping restraints. Another example of a Class IR penetration is a BWR Mark I control rod drive removal hatch, which is enormously stronger than the plant's suppression chamber access hatch. Typical Class LE penetrations are those that have been recommended for test.

Note that enough similarity exists among plants and penetrations that many of the simple elastic calculations would not have to be repeated for other plants. Consideration of the figures of merit approach in comparing penetrations should also be beneficial in reducing the amount of work necessary to separate Class LE and Class IR penetrations in a plant. Also, both experimental and analytical work in the near term on gaskets and seals should make it possible in the simple calculations to be more definite about the influence of gaskets on leakage rate after sealing surface separation is calculated to occur.

In the case of a plant's Class LE penetrations, the proposed plan is to test some typical types of them that have average figures of merit. Those other similar penetrations that have all higher figures of merit should have lower leakage rates than the tested unit, and those having all lower figures of merit should have higher leakage rates. This information should be adequate to qualify (or "disqualify") at least some of the Class LE penetrations, in which case it would be due to analysis only.

To elaborate, if a test should show that a penetration has low resistance to beyond-design-basis conditions, then all similar penetrations having all lower figures of merit would be expected to have even less resistance. All similar penetrations having all similar figures of merit would be expected to have similar resistance. The main difficulty is that, although those similar penetrations having all higher figures of merit would be expected to have higher resistance, it would not be straightforward to prove exactly how much higher. Conversely, if a test should show that a penetration has high resistance to beyond-design-basis conditions, the main difficulty is that although those similar penetrations having all lower figures of merit would be expected to have lower resistance, it would be difficult to prove exactly how much lower. To handle these difficult units analytically, the following procedure is suggested:

For the tests being performed, make pre-test predictions, using "first principles," of the leakage behavior to be measured. First, calculate the width, length, and height of the leakage path, as with finite element meth-

ods. Using these leakage path dimensions, calculate the leakage rate, with standard fluid mechanics equations available for that purpose. Compare the calculated (predicted) leakage rate with the measured leakage rate. If the two rates agree within an "expected error band," then confidence is gained that first-principles calculations can be used to qualify a plant's Class LE penetrations that resemble the penetrations tested. The expected error band can be "large": leakage rate is very sensitive to (a) particles in the leaking fluid (Ref. [4]); (b) variations in sealing-surface roughness, gasket compression set, and gasket thermal transient compression set (Ref. [5]); and (c) leakage path minimum transverse dimension (the height, Darcy pressure-drop equation). These sensitivities are of course a problem for experimentally determined leakage rates as well as for analytically predicted rates.

In first principles leakage rate calculations, macro-analyses are used to determine sealing surface deformations and gross-gasket stresses. Then micro-analyses that consider both sealing surface and fluid forces (the latter both static and dynamic) on the gasket, at the surface roughness level, are used to refine the calculation of the leakage path dimensions. The pressures exerted by the gasket on the sealing surfaces are continually compared with the containment pressure. When the latter is higher, the containment pressure determines the gasket shape and leakage path dimension rather than the sealing surfaces. Furthermore, the pressure drop of a leaking fluid can influence local gasket shape and leakage path dimensions.

To summarize, many penetrations can be qualified by detailed, and even not so detailed, analysis only. Relatively simple calculations, bolstered by figure of merit considerations and by forthcoming new gasket and seal data, can separate individual plant's penetrations into Class LE and Class IR categories. The former leak enough that the latter are irrelevant; therefore, the latter are qualified without testing.

Typical Class LE penetrations, proposed to have average figures of merit, will be tested. Other similar penetrations that have all higher figures of merit would be expected to have lower leakage rates than the test units, and vice versa. This information should be sufficient to allow releasing some additional Class LE-type penetrations from the need for testing.

Finally, if proposed pre-test analytical (first principle) predictions, of leakage rates to be measured in future penetration and gasket and seal tests, are accurate within an expected error band which can be "large," then it can be concluded that from that point the determination of a penetration's leakage behavior can be done as accurately by analysis as by test. Certainly, the first principles analysis approach offers a more economic path to attaching precision indices (e.g., standard deviation) to leakage rates than does testing of complete penetrations.

PROPOSED TESTS FOR MAJOR PENETRATIONS

The ultimate objective of this task of the ANL program is to develop a suggested matrix for large-scale tests of major penetrations. In arriving at a rational test program for predicting penetration leakage and structural behavior, several factors must be considered. The following list represents some of these factors believed important in influencing leakage behavior of any given penetration:

a. The size of the potential leakage path.

b. The sensitivity of the gasket-seal leaktightness to containment shell deformations.

c. The sensitivity of the gasket-seal leaktightness to deformations of the penetration assembly itself.

d. The specific gasket/seal joint design used -- e.g., whether single or double seal, inflatable seals versus solid compressible seals, and other features.

e. Whether the penetration is pressure-seating or pressure-unseating.

f. The extent to which the penetration seal is "opened" and "closed" during its design life.

g. The existence of historical problems with actual penetrations during leak rate tests made at design pressure.

It is suggested that the main testing medium be steam to better simulate actual containment atmospheres. Where gaskets are used, tests should be run using both new gaskets and aged gaskets (obtained from existing service in a nuclear containment or by equivalent simulated service). External loadings, such as seismic, tornadoes, etc. are excluded. The proposed test program will address only those operative-type of penetrations using gaskets and seals, and penetrations in which very large structural deformations might be expected, such as bellows seals.

The figures of merit described earlier in this paper may be used to obtain an initial list of penetrations to be tested and the relative priority of the penetrations. In addition, the figures of merit may be used as a basis for specific design features of the test articles.

In selecting figure of merit values to be sought in test articles, several things should be kept in mind. On the one hand, if a test article should have low figures of merit, all penetrations having higher figures of merit could be said to have much better leakage behavior than the test article, although it would be difficult to quantify these lower leakages. Conversely, a test article having high figures of merit could exhibit such favorable leakage behavior that it might make it difficult to assess leakage behavior of penetrations having much lower figures of merit.

Accordingly, we believe it is advisable to recommend "average" figures of merit to be sought in test articles. A side benefit of this is that it will facilitate making extrapolations of test and analysis results to the extremes of the figure-of-merit range.

The results of the proposed tests would be used to:

a. Establish a basis of leakage behavior useful in estimating leakage in similar type penetrations in specific plants.

b. Confirm leakage estimates made based on reduced-scale gasket/seal

tests and results of model tests, or leakage estimates based on analysis.

c. Increase the confidence level in predicting overall leakage of a given plant for loading conditions beyond the design basis.

ACKNOWLEDGMENTS

The authors wish to express their appreciation to the architect-engineering firms and major penetration equipment suppliers for the fine cooperation extended to us in collecting and interpreting all the information. We are also indebted to the following utilities for their excellent cooperation in providing access to relevant information on their nuclear power plants:

Cincinnati Gas and Electric, OH
Commonwealth Edison, IL
Consumers Power, MI
Florida Power and Light, FL
Illinois Power, IL
Iowa Electric Light and Power, IA
Iowa-Illinois Gas and Electric, IL
Louisiana Power and Light, LA
Northern States Power, MN
Public Service, IN
Texas Utilities, TX
Washington Public Power, WA
Wisconsin Public Service, WI

The authors are grateful to Vinod Gambhir, George McLennan, Leonard Frost, and Paul Basnar of ANL for their tireless efforts in collecting data and preparing the large number of sketches needed to characterize all the plants. We are also pleased to acknowledge the skillful typing efforts of Joanne E. Harmon, Diane M. Myers, Celeste B. Kinsella, Audrey Salzbrunn, and Kathleen M. Mowrey, all of ANL. Gerald Rosenberg and Stanley Fistedis, ANL, made helpful comments during this study. Finally, the guidance and support provided by the Sandia Project Officer for this work, C. V. Subramanian, Walter von Riesemann, Supervisor, Containment Integrity Division of Sandia, and the NRC Program Manager, Hans Ashar, are sincerely appreciated.

REFERENCES

1. T. E. Blejwas, et al., "Background Study and Preliminary Plans for a Program on the Safety Margins of Containments," NUREG/CR-2549 (May 1982).

2. R. F. Kulak, ed., "Structural Response of Large Penetrations and Closures for Containment Vessels Subjected to Loadings Beyond the Design Basis," NUREG (TBD), SAND(TBD), ANL-84-41 (draft, May 1984).

3. P. E. Mast, P. E. Mast Consulting Engineering, Chicago, IL, Personal Communication (Sept. 1982).

4. H. A. Morewitz, "Leakage of Aerosols from Containment Buildings," Health Physics, 42:2, 195 (1982).

5. T. C. Chivers, et al., "High Integrity Static Elastomer 'O' Ring Seals and Their Performance Through Thermal Transients," 9th Intl. Conf. Fluid Sealing, Netherlands (April 1981).

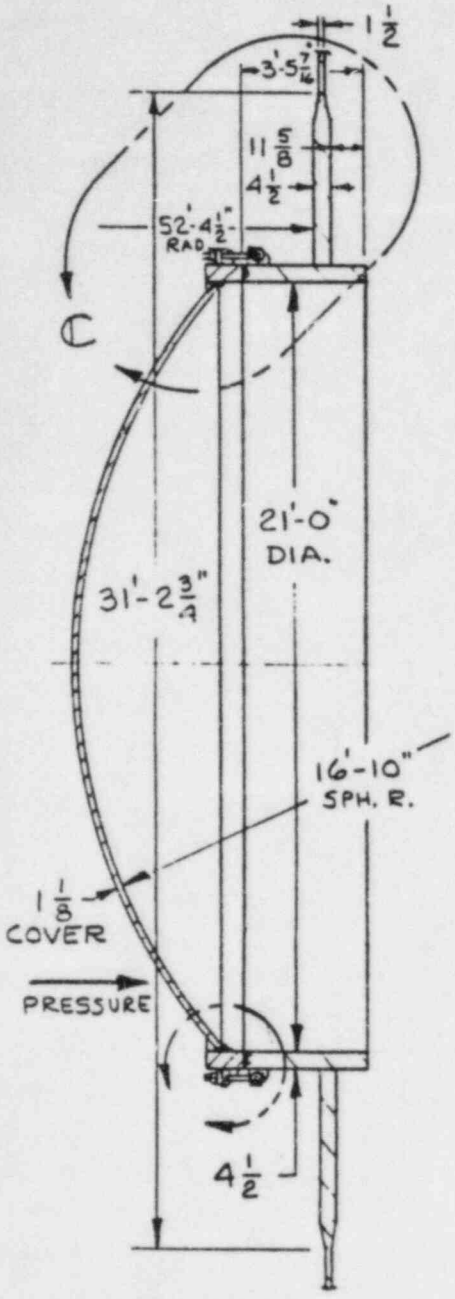

ELEVATION VIEW

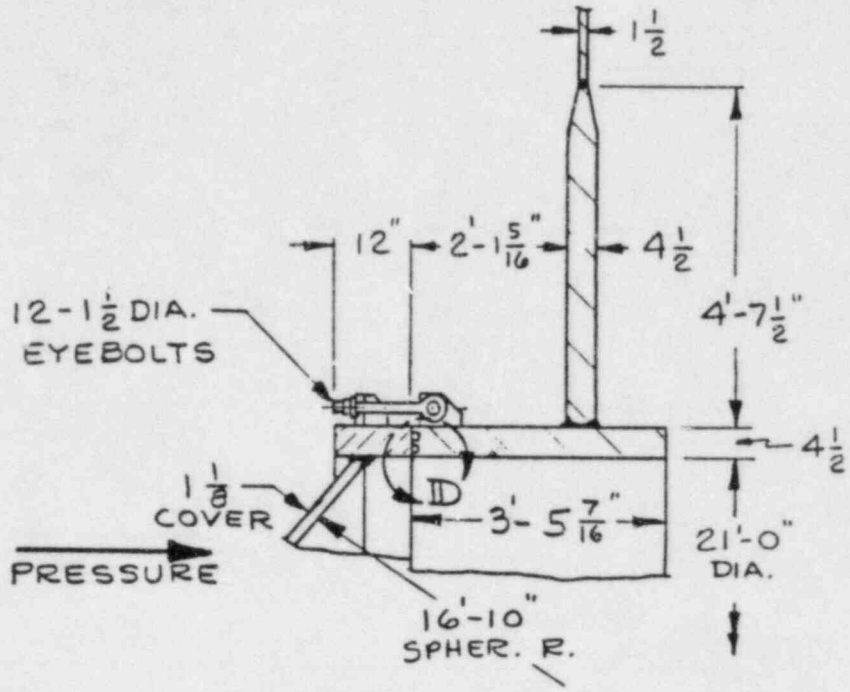

DETAIL C

Figure 1. Steel containment equipment hatch (highest F_1)

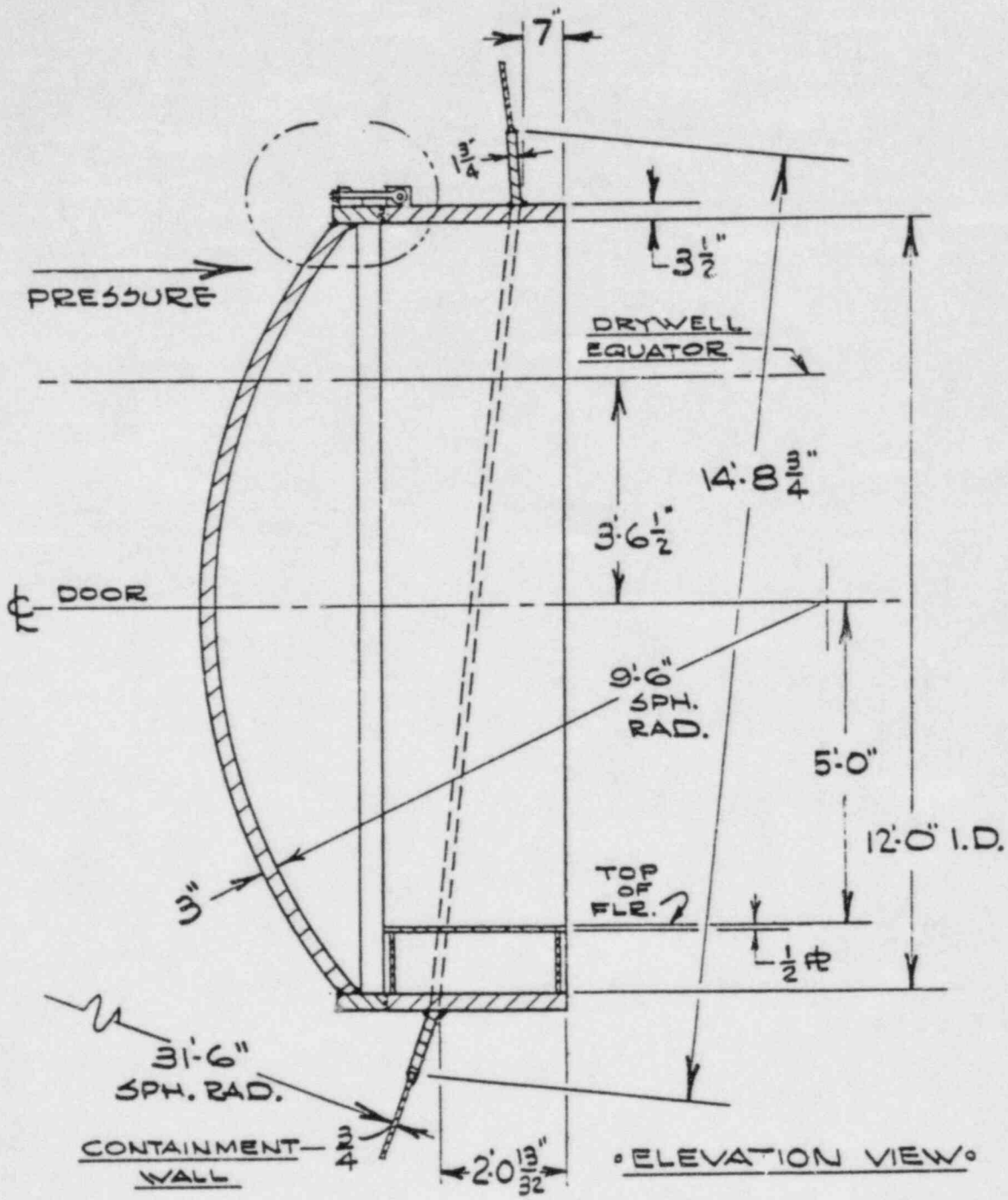

Figure 2. Steel containment equipment hatch (lowest F_1 and highest F_2)

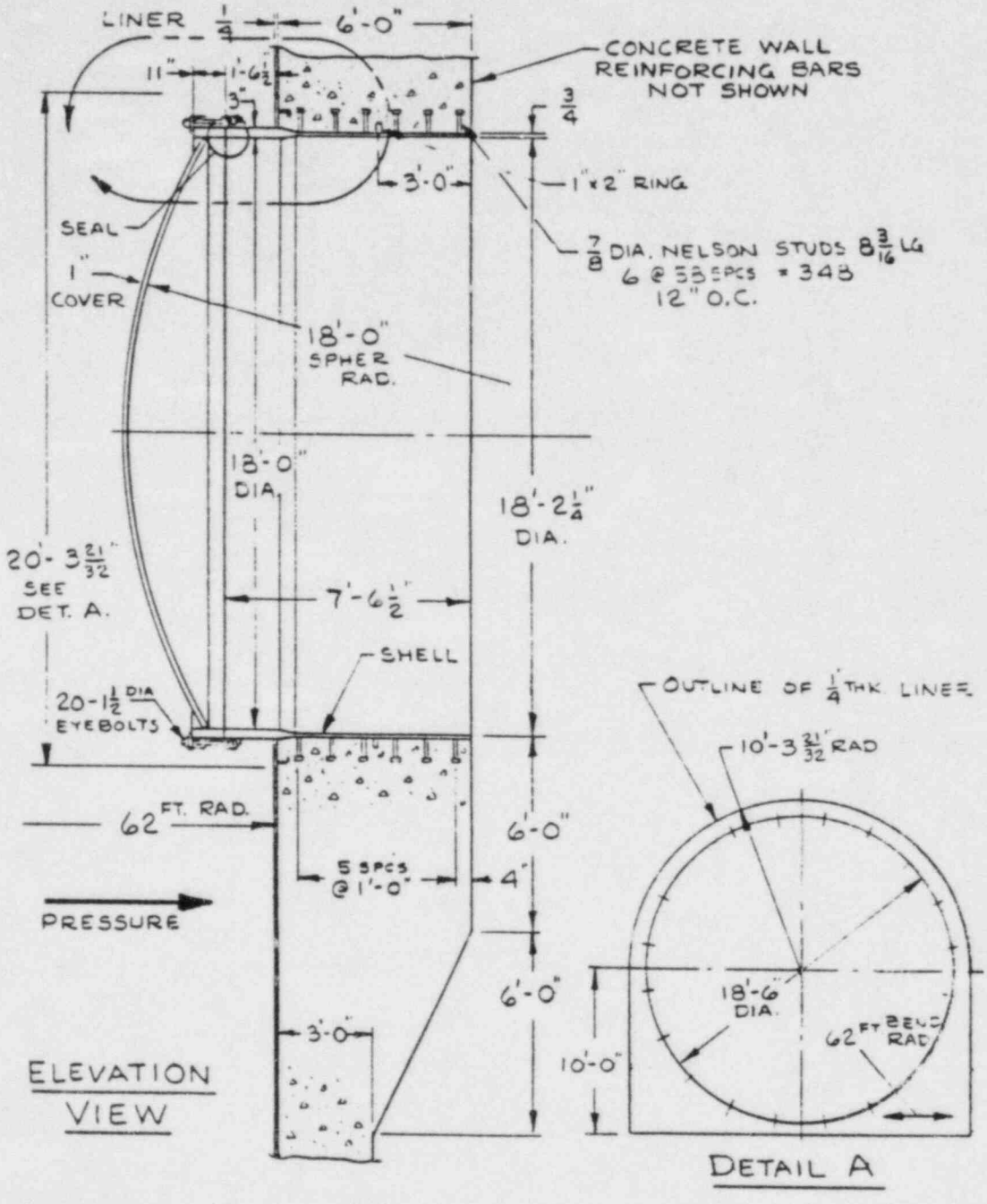

Figure 3. Concrete containment equipment hatch (highest F_1)

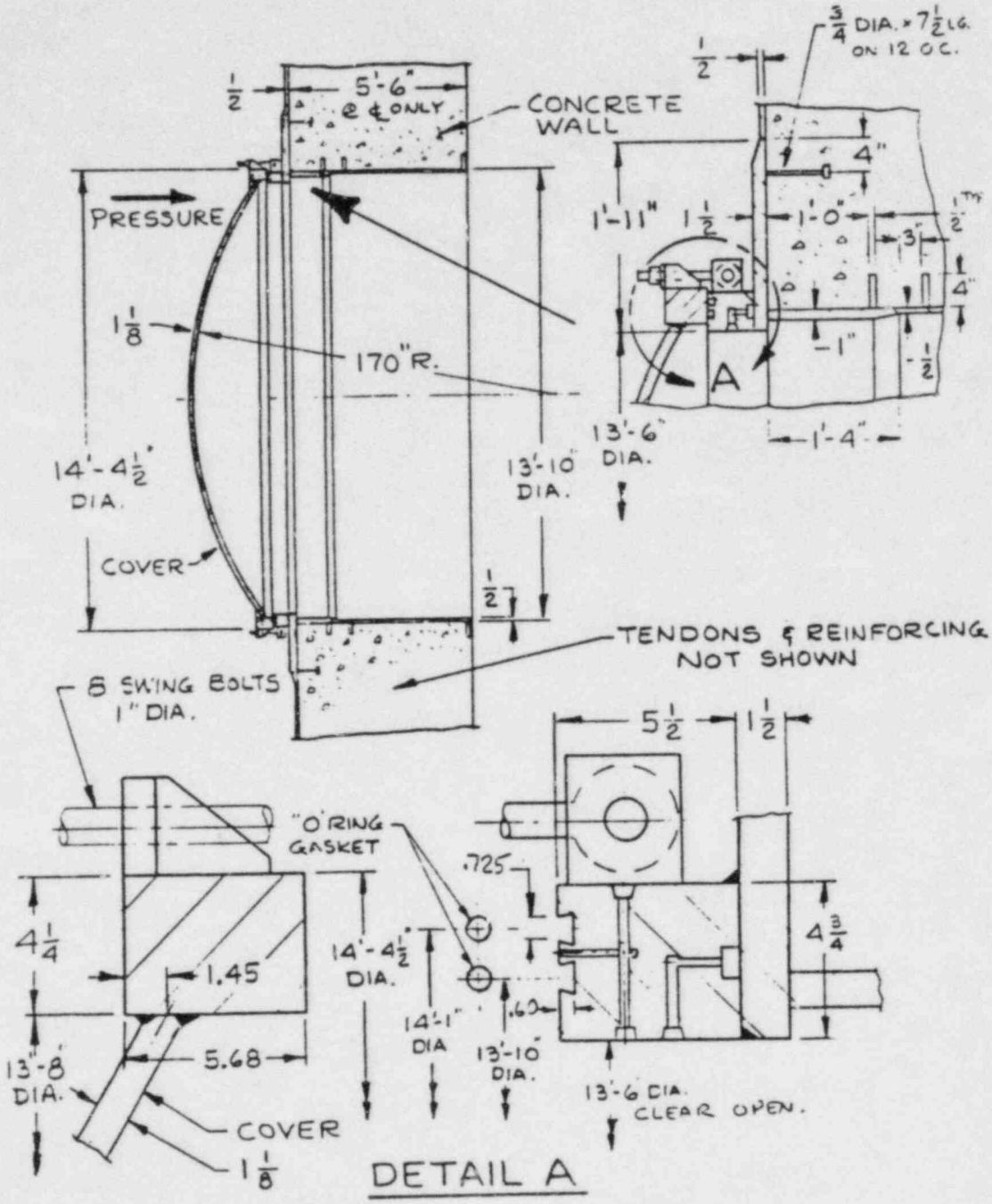

Figure 4. Concrete containment equipment hatch (lowest F_1 and highest F_4)

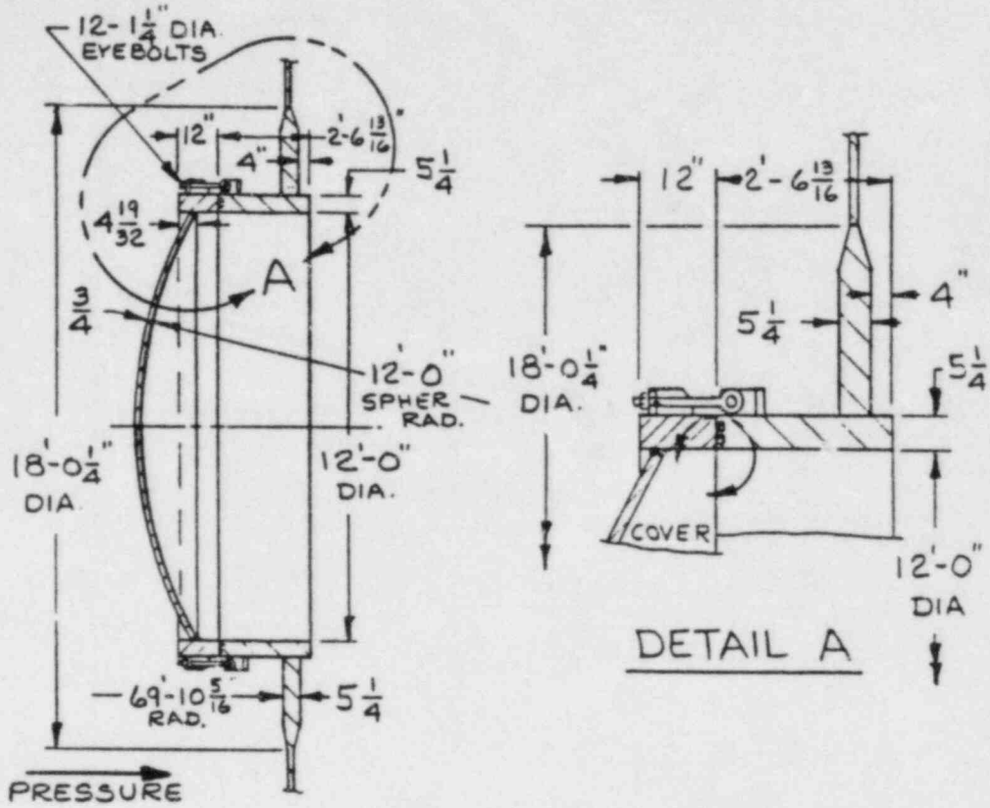

Figure 5. Equipment hatch (lowest F_2)

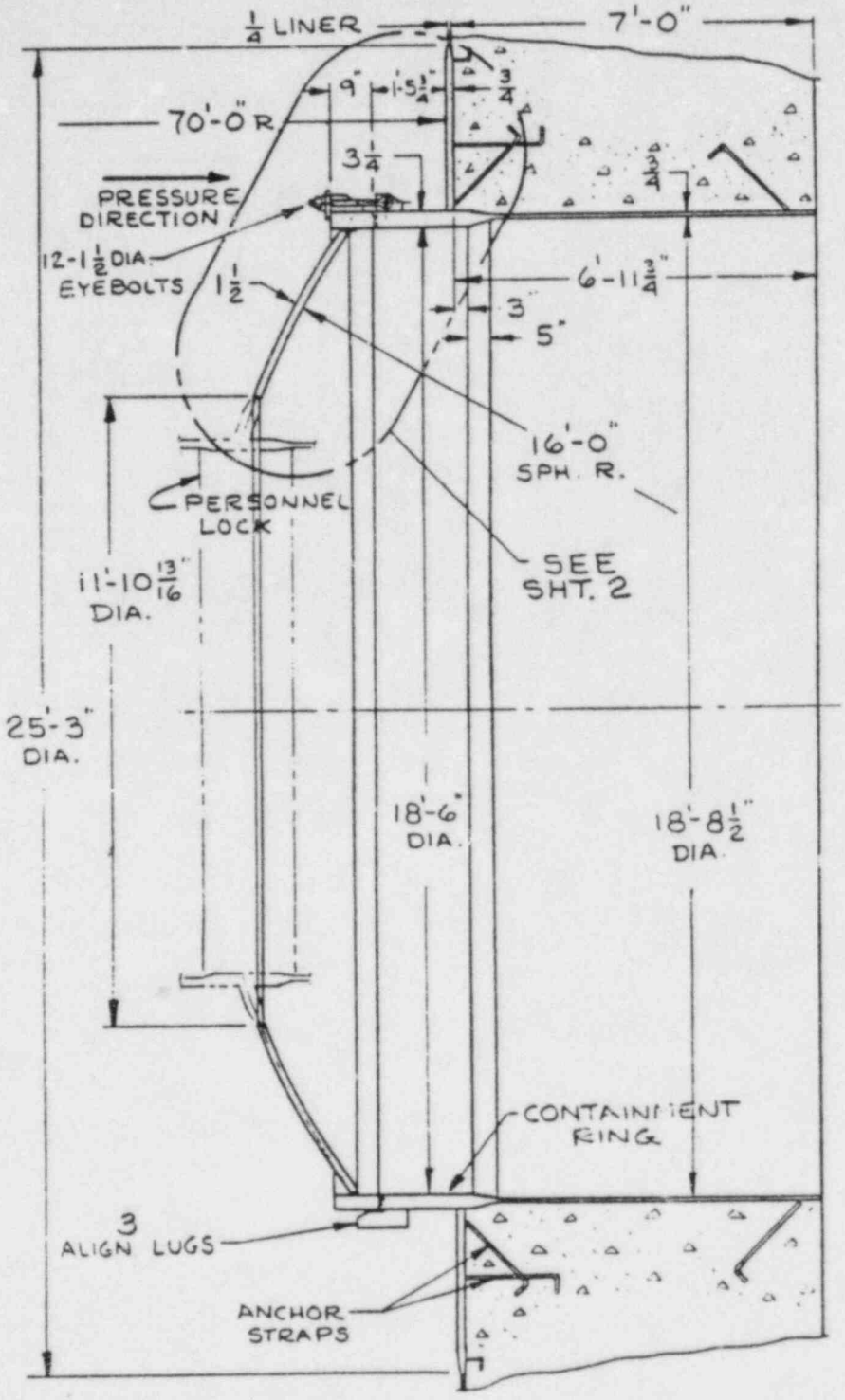

Figure 6. Equipment hatch (lowest F_4)

SESSION F

TESTING/ANALYSIS OF CONTAINMENT STRUCTURES

COMPUTER MODELLING OF THE SEALING BEHAVIOR OF GASKETS IN FLANGED JOINTS

B. S. Nau
BHRA, The Fluid Engineering Centre
Cranfield, Bedford. MK43 OAJ
England

Paper for presentation at

2nd Workshop on Containment Integrity
Washington D.C.
13-15 June, 1984

Abstract

A computer program is described which is designed to predict the gasket stress distribution in flanged joints. The program incorporates finite element modules for calculation of flange deflections in response to loads applied by bolts, gasket and fluid. Account is taken of non-linear gasket load--compresssion curves and hysteresis, thermal deflections, etc..

1. INTRODUCTION

This paper is concerned with the sealing of flanged joints, rather than with stress levels in the metal components of the joint. It is a modified and extended version of that in Ref. 8.

The design of the gasketed flanged joints has been codified for many years, in the UK by BS5500 and in the USA by the ASME Pressure Vessel Code. The former is derived from the latter. These codes are intended to ensure that the stresses in the metal members are within safe limits and that the gasket is adequately compressed to ensure effective sealing. However, it has been known for some years that these codes do not always ensure effective sealing.

In an attempt to ensure effective sealing, these codes use two factors: the "seating stress", y, and the "gasket factor", m. Currently, single values are tabulated for these for each of a number of gasket types. These values are currently under review by the Pressure Vessel Research Committee in the USA, since it is now known that y and m are not the simple constants for each gasket type that was once thought to be the case. In fact, it is now known that m depends on y and the choice of values depends on the degree of effectiveness of sealing required. A joint is not simply "sealed" or "leaking", there are degrees of leakage depending on the refinement of the measuring technique. The codes also fail to take account of the effects on sealing of the flexure of the flange, under the combined effects of: bolt loads; gasket reaction; fluid pressure; and thermal loads. Flange flexure causes the gasket sealing stress to deviate from the uniform stress assumed by the codes. For large flanges these effects become increasingly significant and it is required both to know what the true stress distribution is, and to know how this will affect leakage.

The computer program "JOINT" described in this paper provides a tool to attack the problems of flange flexure by providing a means of predicting gasket stress distribution.

2. PROGRAM CONCEPT

The purpose of the program is to predict the gasket stress distribution over the gasket/flange interface. The gasket stresses are the main factor affecting sealing performance of the joint. At present, there is a lack of experimental data enabling gasket stress distribution to be related to leakage values. This is an area requiring quantification if joints are to be designed on a rational basis. The gasket stresses are affected by a number of factors which can be grouped under these headings:-

i) Load changes - as the sealed fluid is pressurised the resulting end load changes the closing load on the gasket interface. The closing load on the gasket may also change due to thermal transients. In particular, if the bolt temperature

lags the flange temperature, an increase in load can result.

ii) Flange distortion - distortion modes affecting the gasket include radial coning of the flange and circumferential bending between bolts. These are responses to loadings which include those due to the bolts, fluid pressure and thermal effects. Interactions between the flanges and the vessel wall have also to be considered.

ii) Gasket properties - as the flanges displace or distort, the gasket responds to the variations of compression in a complex fashion: the load-compression curve is usually very non--linear; the curve exhibits hysteresis; the gasket may exhibit time-dependent effects such as creep and/or stress relaxation; the above are all temperature dependent.

To generate a comprehensive computer model is an ambitious undertaking, even if the necessary gasket compression characteristic data were available. The present program was, therefore, conceived as the initial stage in the evolution of a more comprehensive package. At present, three versions have been developed, which include various features from those listed above. Each is a stand-alone program which does not depend on the use of a general-purpose finite element package (e.g. Nastran). This is crucial to maintaining flexibility and ease of use.

The different versions of JOINT all include a finite element distortion analysis of the structural components of the joint (flange, vessel wall and bolts), the gasket stress appears as one of the loadings in the F.E. analysis. The finite element routines are embedded in "user friendly" pre-processing and post-processing routines for ease of use. In fact, the finite element analysis is invisible to the user. In each version too, the program first models a bolt-tightening phase during which flange deflections and corresponding gasket stresses are calculated for zero fluid pressure and constant bolt load. Following this is an operational phase in which the fluid is pressurised and the bolt load is allowed to vary in response to flange displacement at the bolts. In both phases iteration is applied to ensure compatibility of gasket stress distribution and flange deflections.

In its simplest version JOINT incorporates axisymmetric shell elements for the finite element analysis. This model is a steady--state isothermal analysis and is available to handle either plate flanges or taper-hub flanges. The gasket load-compression curve was originally modelled by a piece-wise linear approximation, this has now been refined to allow realistic modelling of non-linear curves with hysteresis. With this version it is possible to simulate curves as measured in the PVRC gasket research programme.

The second version of JOINT is similar to the original program above, but incorporates time-dependence, allowing gasket properties and fluid pressure to vary with time. The same axisymmetric model is used as in the steady-state version.

A third version of JOINT allows a non-axisymmetric analysis of the isothermal steady-state. In this version, a quadrilateral plate element, with bending, shear and in-plane stresses, is used for the finite element analysis. This is particularly suitable for joints having complex geometry, as in heat exchangers or non-circular applications. A non-linear gasket load-compression curve is used.

In each version the user input comprises the flange, bolt and vessel wall dimensions and their physical properties. There may be two similar flanges or one flange and a rigid counterface. The program is pre-set to assign the details of the topography to the finite elements. The program output comprises the normal deflections of the flange-gasket interface and the gasket stress distribution.

3. PROGRAM DETAILS

3.1 Program Structure

The general structure of the program is shown in Table 1. The main complications lie in the fact that the flanges being analysed in the F.E. analysis are not fixed in space axially. The absolute position of the flanges depends upon the degree of gasket compression, which is not known a priori. Because of this indeterminancy, it is necessary to ensure an exact balance between the axial forces acting on the flange in order to avoid arbitrarily large solid body axial displacements due to numerical rounding effects. The axial force balance is also the constraint which determines the absolute axial position of the flange in reality, thus, for a locally linear gasket characteristic:

$$p_{1,1} = \frac{N_n}{A_1}\left[F_B - F_F - \sum_{e=2}^{N_e}(\bar{p}_e A_e)\right] - \sum_{e=2}^{N_e} p_{1,i} \qquad (1)$$

where $p_{e,i}$ is the gasket stress at node i of element e
$\bar{p}_e$ is the average gasket stress in element e
F_B is the total bolt load
F_F is the fluid end load
A_e is the gasket contact area for element e
N_e is the number of elements in the gasket contact zone
N_n is the number of nodes per element

also: $$p_{e,i} = p_{1,1} + \frac{N_f . E_g}{Tg_o}(u_{1,1} - u_{e,i}) \qquad (2)$$

hence:
$$\bar{p}_e + p_{1,1} + \frac{N_f \cdot E_g}{N_n \cdot T_{go}} \sum_{i=1}^{N_n} (u_{1,1} - u_{e,i}) \qquad (3)$$

where N_f (= 1 or 2) is the number of flanges deflecting
E_g is the effective local modulus of the gasket
T_{go} is the uncompressed thickness of the gasket

If the gasket stresses at the nodes are calculated from equations (1), (2) and (3) with $u_{e,i}$ in an arbitrary frame of reference, then the absolute gasket thickness at any node can be derived from the characteristic curve of the gasket and hence the absolute co-ordinates of the displaced flange are determined. An alternative implementation of this procedure is to employ an iterative method working in terms of stress and compression only. This is used when non-linear gasket load-compression curves are to be used.

The force balancing procedure is applied in both the bolt tightening and the pressurised fluid routines of Table 1. Each of these two routines is iterative in order to ensure compatibility of flange deflections with the gasket and bolt loads. These iterative loops are potentially unstable and require damping to obtain stable convergence.

3.2 The Finite Elements

3.2.1 Axisymmetric shell element

The axisymmetric shell element used takes account of membrane and bending effects. The notation is shown in Fig. 1. The strain vector is written as:-

$$\begin{pmatrix} \varepsilon_s \\ \varepsilon_\vartheta \\ \chi_s \\ \chi_\vartheta \end{pmatrix} = \begin{pmatrix} \frac{du}{ds} \\ (w\cos\varphi + u\sin\varphi)/r \\ -\frac{d^2w}{ds^2} \\ -\frac{\sin\varphi}{r}\frac{dw}{ds} \end{pmatrix} \qquad (4)$$

and the stress-strain equation is:

$$\begin{Bmatrix} N_s \\ N_\vartheta \\ M_s \\ M_\vartheta \end{Bmatrix} = [D]\{\varepsilon\} \qquad (5)$$

with:

$$|D| = \frac{Et}{(1-\nu^2)} \begin{bmatrix} 1 & \nu & 0 & 0 \\ \nu & 1 & 0 & 0 \\ 0 & 0 & t^2/12 & \nu t^2/12 \\ 0 & 0 & \nu t^2/12 & t^2/12 \end{bmatrix} \qquad (6)$$

The interpolation functions are:

$$\begin{aligned} u &= a_1 + a_2 s \\ w &= b_1 + b_2 s + c_3 s^2 + c_3 s^3 \end{aligned} \qquad (7)$$

From equations (4) to (7) a stiffness matrix is formed in the usual way to allow discretisation of the element.

A disadvantage of the shell model concerns the moment applied to the radial part of the flange by the axial part. A pure radial expansion of the latter applies a radial force which does not actually pass through the centroid of the former, this represents a moment which is not reproduced in the shell model.

3.2.2 Plate element

The requirements for this element were that it should be suitable for modelling both a plane annular flange configuration and a general cylinder, and should take account of both bending and shear, as well as membrane effects. The notation is shown in Fig. 2.

A strain energy formulation is used, the energy U being the sum of the components due to the three effects:

$$U(u,v,w,\vartheta_x,\vartheta_y) = \frac{E}{24(1-\nu)} \{I_B + I_S + {}_M I\} \qquad (8)$$

where: $$I_B = \iint_A t^3 \left[\left(\frac{\delta \vartheta_x}{\delta x} \right)^2 + 2 \frac{\delta \vartheta_x}{\delta x} \frac{\delta \vartheta_z}{\delta y} + \left(\frac{\delta \vartheta_y}{\delta y} \right)^2 + \frac{1-\nu}{2} \left(\frac{\delta \vartheta_x}{\delta x} + \frac{\delta \vartheta_y}{\delta y} \right)^2 \right] dxdy \quad (9a)$$

$$I_S = 6K(1-\nu) \iint_A t \left[\left(\frac{\delta w}{\delta x} - \vartheta_y \right)^2 + \left(\frac{\delta w}{\delta y} - \vartheta_x \right)^2 \right] dxdy \quad (9b)$$

$$I_M = \left(\frac{12}{1+\nu} \right) \iint_A t \left[\left(\frac{\delta u}{\delta x} \right)^2 + 2\nu \frac{\delta u}{\delta x} \frac{\delta v}{\delta y} + \left(\frac{\delta w}{\delta y} \right)^2 \right] dxdy \quad (9c)$$

An isoparametric formulation is employed, the shape function being:

$$[N] = \tfrac{1}{4}[(1-x)(1-y),\ (1+x)(1-y),\ (1+x)(1+y),\ (1-x)(1+y)] \quad (10)$$

So that displacements at points within the element are given by:

$$u = [N]\ \{u\}\ \text{nodes} \quad (11)$$

and element thickness by:

$$t + [N]\ \{t\}\ \text{nodes} \quad (12)$$

Combining equations (8) to (12) and minimising the integral terms with respect to nodal displacements completes the discretisation process.

Further details are given in Nau and Smith (1982 c).

3.2.3 Distribution of elements

The user input is interfaced to the finite element routines by a routine which assigns the element distribution in a predetermined manner. Thus, the topology is fixed, but the dimensions and physical properties can be varied by the user. An example of the topology for an axisymmetric tapered-hub flange is given in Fig. 3.

Further details are given in Nau and Smith (1982 b).

3.3 Gasket Properties

The main problem hitherto with regard to gasket properties has

been the lack of reliable data. At its simplest, a load-compression curve is required, but from PVRC data (Refs. 1 and 2) this is now known to be not only non-linear, but also to exhibit hysteresis. Some creep and stress-relaxation data is also now available (Ref. 3), but there is still a lack of data at elevated temperature.

The gasket characteristic in the JOINT program has taken various forms at different times. In one the program is written in terms of effective gasket modulus and effective initial gasket thickness based on a locally linear approximation. In another, the gasket characteristic curve is fitted by approximate analytical expressions relating gasket stress and compression, with program logic handling different branches of the characteristic. The second method is preferable where a wide range of stress levels is possible and is also used where gasket "hysteresis" is to be modelled, as in Fig. 5.

4. RESULTS

4.1 Axisymmetric Analysis of an ANSI B16.5 Class 600 Joint

A joint analysed comprised a pair of 4.0 inch (100 mm) nominal pipe size taper hub flanges (Fig. 4), with a stainless steel, spiral-wound gasket having asbestos filler. There were eight bolts. For this analysis the gasket characteristic was approximated by a linear segmentation model.

The input data is set out in Table 2, illustrating the simplicity of use of the program, and a sample output in Table 3. The output shows gasket stress and joint deflections: (a) after tightening to the specified bolt-load; and (b) when the working pressure is applied to the sealed fluid.

Additional results are illustrated graphically in Figs. 6 and 7. The former shows the radial variation of gasket stress at two initial bolt-loads, each for three levels of fluid pressure. The flanges are very stiff and are seen to rotate in a solid ring mode giving a linear gasket stress variation. Fig. 7 illustrates the change in bolt-load as fluid pressure chananges, for four initial bolt-load levels. The measurements were made by Raut (1979) as part of the PVRC experimental study of gasket properties.

Further details are given in Nau and Smith (1982 b).

4.2 Non-axisymmetric Analysis of a Large Diameter Flange

As an illustration of the use of the plate element version, Fig. 8 shows the stress contours calculated for an annular flange, of which a sector only is illustrated. The sector shown includes two bolts and it can be seen that the stress distribution for this joint is saddle-shaped with a minimum mid-way between the bolt centres.

5. FURTHER DEVELOPMENT

In keeping with the concept of an evolving program, additional facilities are currently being incorporated. An important extension was incorporation of thermal deflection effects. This is illustrated by Fig. 9. In support of this, a time-dependent temperature analysis has been written and tested and attention is now being given to the modelling of thermal lag in the bolts.

6. CONCLUSIONS

The use of an integrated gasket stress prediction program is a powerful tool for gaining insight into the interactions of flange deflections and gasket. By the use of appropriate finite element modules, written specifically for this purpose and buffered from the user by easy-to-use input and output routines, it is possible to produce a very cost effective tool. This is in respect both of data preparation, which is minimal, and run-time overheads. Such a program is seen as essential for the realistic design of critical joints where leakage levels are important.

7. ACKNOWLEDGEMENTS

The author wishes to acknowledge the valuable contributions made to the program by Mrs. K. Smith and Mr. T. Banks. Program development was supported by the Department of Industry's Mechanical Engineering and Machine Tools Requirements Board and analysis of the ANSI joint by the Pressure Vessel Research Committee of the US Welding Research Council.

8. REFERENCES

1) Bazergui, A., Leon, G.F. & Payne, J.R. "Observations and status of PVRC gasket test program" 9th Intl. Conf. on Fluid Sealing, Paper B2, BHRA, 1981.

2) Bazergui, A. & Payne, J.R. "Progress in gasket testing - milestone results" ASME Pre-print, 83-PVP-45, 1983.

3) Bazergui, A. (in press) "Short term creep and relaxation behaviour of gaskets"

4) Raut, H. "PVRC exploratory gasket tests surface finish sequence" Report to PVRC Sub-committee on Bolted Flanged Connectors, Welding Research Council, USA, 1979.

5) Nau, B.S. & Smith, K.A. "Effects of flange distortion on the gasket contact pressures of a spiral-wound gasket in an ANSI B16.5 Class 600 flanged joint" BHRA report RR1811, February 1982 a.

6) Nau, B.S. & Smith, K.A. "The "JOINT" computer program for analysis of gasket sealing stresses in flanged joints" BHRA report RR1845, May 1982 b.

7) Nau, B.S. & Smith, K.A. "The "PLATE" finite element program" BHRA report RR1863, June 1982 c.

8) Nau, B.S. "Computer modelling of sealing in gasketed joints" Proc. 10th Intl. Conf. on Fluid Sealing, Paper B3, BHRA, 1984.

9) Bazergui, A. & Marchand, L. "PVRC milestone gasket tests - first results" Welding Research Council Bulletin 292, February 1984.

Table 1. General Structure of JOINT-Series Programs

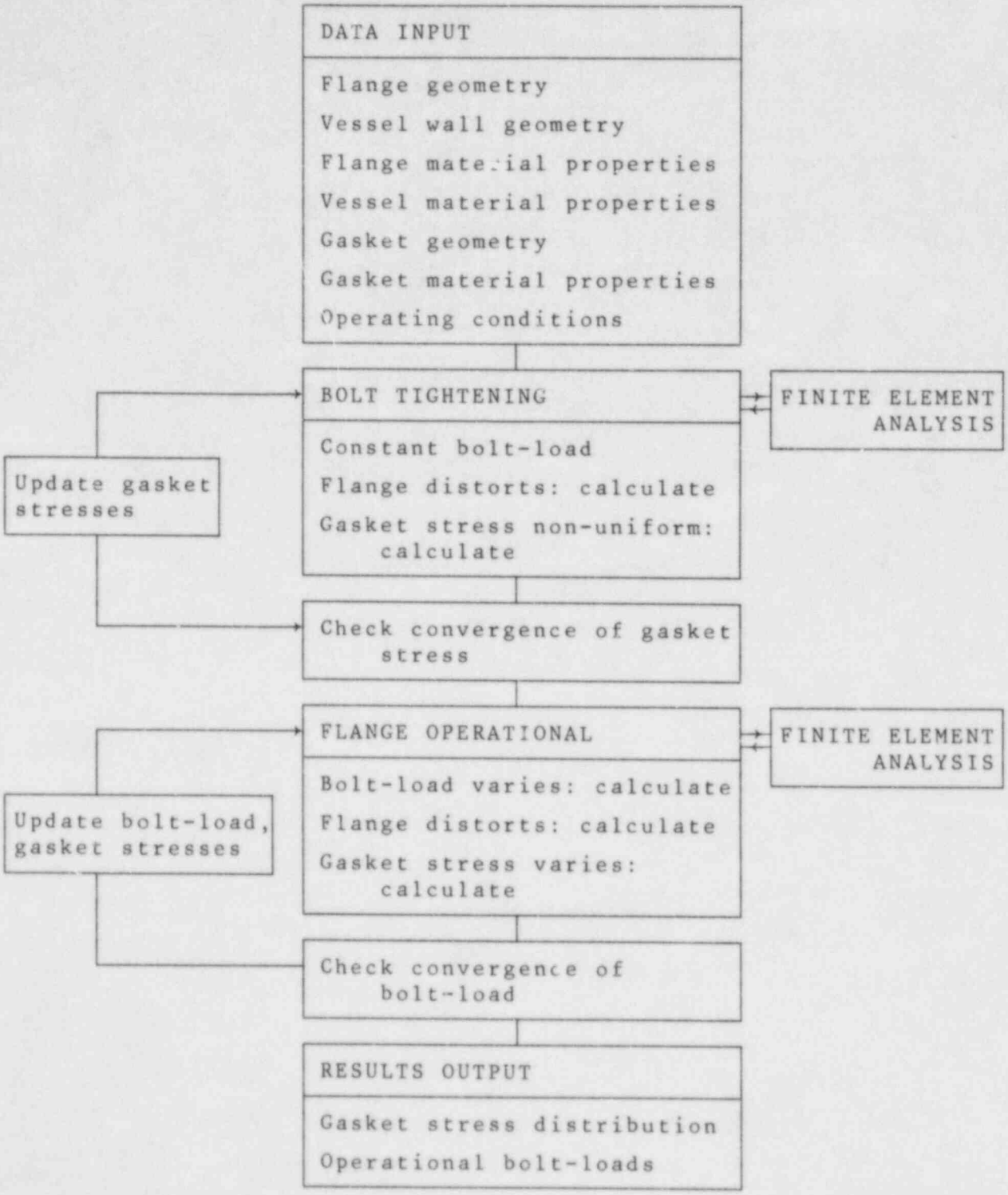

Table 2. Sample Input Data for the JOINT Program (Axisymmetric Version) Corresponding to Figure 4

```
                    RUN  1
                    -------

          PVRC RAUT DEC 79 DATA(C-1 PAGE 17) GASKET: 304 S/S SWG WITH ASBESTOS FILLER
          RAUT PRESSURE VESSEL/FLANGES(FIG 2-2 PAGE 6) UNITS IN,LBF,SEC


                    BOLT DATA
                    ---------

NUMBER OF BOLTS,NB.................       8
INITIAL BOLT LOAD PER BOLT,BO..... 0.20620E+04
LENGTH OF BOLT,BL................. 0.43750E+01
DIAMETER OF BOLT PITCH CIRCLE,DFB.. 0.85000E+01
DIAMETER OF BOLT,DB............... 0.87500E+00
ELASTIC MODULUS OF BOLT,EB........ 0.30000E+08


                    FLANGE DATA
                    -----------

NUMBER OF FLANGES(1 OR 2),NF.............. 2
OUTSIDE DIAMETER OF FLANGE,DFO............ 0.10750E+02
THICKNESS AT OUTER PART OF FLANGE,TFO..... 0.12500E+01
FLANGE THICKNESS AT GASKET,TFG............ 0.12500E+01
INSIDE DIAMETER OF FLANGE,DFI............. 0.40000E+01
THICKNESS AT INNER PART OF FLANGE,TFI..... 0.12500E+01
ELASTIC MODULUS OF FLANGE AND CYLINDER,EF.. 0.30000E+08


                    GASKET DATA
                    ------------

OUTSIDE DIAMETER OF GASKET,DGO......... 0.57500E+01
INSIDE DIAMETER OF GASKET,DGI.......... 0.47500E+01
INITIAL THICKNESS OF GASKET,TGO........ 0.18750E+00
INITIAL ELASTIC MODULUS OF GASKET,EGO.. 0.26560E+04


                    HUB DATA
                    --------

THICKNESS OF HUB,G1.... 0.11250E+01
LENGTH OF HUB,H........ 0.18750E+01


                    CYLINDER DATA
                    -------------

LENGTH OF CYLINDER WALL,CL....... 0.35000E+01
THICKNESS OF CYLINDER WALL,G0.... 0.50000E+00
THICKNESS OF CYLINDER CAP,TCAP... 0.50000E+00


                    PRESSURE DATA
                    -------------

NUMBER OF PRESSURE VALUES,NPR....  3

  NUMBER          VALUE

     1        0.10040E+03
     2        0.20050E+03
     3        0.40020E+03
```

Table 3. Sample Output from the JOINT Program (Axisymmetric Version) Corresponding to the Input Data for Table 2

CONDITIONS WHEN BOLTS HAVE BEEN TIGHTENED TO GIVE THE REQUIRED LOAD

OUTPUT TABLE 1.. BOLT CONDITIONS

INITIAL BOLT STRESS,BSTRSS	0.34291E+04
INITIAL BOLT STRETCH,BDLIN	0.50008E-03
PRESENT BOLT STRETCH,BDL	0.50008E-03
INITIAL BOLT FORCES(SUM OF BOLTS),BOLTIN	0.16496E+05
PRESENT BOLT FORCES(SUM OF BOLTS),BOLT	0.16496E+05

OUTPUT TABLE 2.. GASKET CONDITIONS

ELASTIC MODULUS OF GASKET,EG		0.555E+05
APPARENT INITIAL GASKET THICKNESS		0.152E+00
NODAL THICKNESSES OF GASKET	(1)	0.1465E+00
	(2)	0.1468E+00
	(3)	0.1469E+00
NODAL PRESSURES AT GASKET	(1)	0.206E+04
	(2)	0.200E+04
	(3)	0.194E+04

OUTPUT TABLE 3.. NODAL DISPLACEMENTS

	NODE	AX.-DISP.(X)	RAD.-DISP.(Y)	ROTATION
FLANGE:	1	-0.0220	-0.000	0.0004
	2	-0.0218	-0.000	0.0004
BOLT	3	-0.0216	-0.000	0.0004
GASKET	4	-0.0211	-0.000	0.0004
GASKET	5	-0.0210	-0.000	0.0003
GASKET	6	-0.0209	-0.000	0.0003
	7	-0.0209	-0.000	0.0002
CYLINDER WALL:	8	-0.0208	-0.000	0.0002
	9	-0.0208	0.000	0.0001
	10	-0.0208	0.000	0.0000
	11	-0.0208	0.000	-0.0000
	12	-0.0208	0.000	-0.0000

RESULTS AT PRESSURE VALUE 1 WITH FLUID PRESSURE = 100.40

OUTPUT TABLE 1.. BOLT CONDITIONS

INITIAL BOLT STRESS,BSTRSS	0.34291E+04
INITIAL BOLT STRETCH,BDLIN	0.50008E-03
PRESENT BOLT STRETCH,BDL	0.54134E-03
INITIAL BOLT FORCES(SUM OF BOLTS),BOLTIN	0.16496E+05
PRESENT BOLT FORCES(SUM OF BOLTS),BOLT	0.17857E+05

OUTPUT TABLE 2.. GASKET CONDITIONS

ELASTIC MODULUS OF GASKET,EG		0.555E+05
APPARENT INITIAL GASKET THICKNESS		0.152E+00
NODAL THICKNESSES OF GASKET	(1)	0.1454E+00
	(2)	0.1457E+00
	(3)	0.1459E+00
NODAL PRESSURES AT GASKET	(1)	0.201E+04
	(2)	0.195E+04
	(3)	0.188E+04

OUTPUT TABLE 3.. NODAL DISPLACEMENTS

	NODE	AX.-DISP.(X)	RAD.-DISP.(Y)	ROTATION
FLANGE:	1	-0.0221	-0.000	0.0004
	2	-0.0219	-0.000	0.0004
BOLT	3	-0.0216	-0.000	0.0004
GASKET	4	-0.0210	-0.000	0.0004
GASKET	5	-0.0209	-0.000	0.0004
GASKET	6	-0.0208	-0.000	0.0003
	7	-0.0208	-0.000	0.0003
CYLINDER WALL:	8	-0.0207	-0.000	0.0002
	9	-0.0207	0.000	0.0001
	10	-0.0207	0.000	0.0000
	11	-0.0207	0.000	-0.0000
	12	-0.0207	0.000	-0.0000

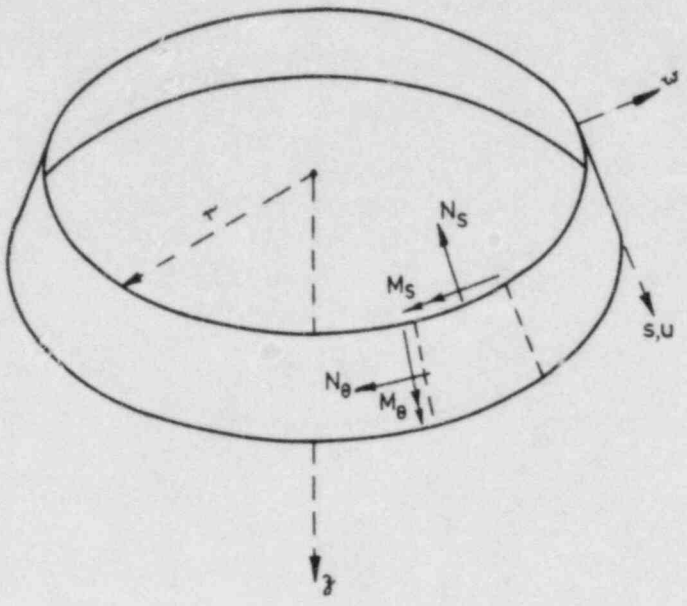

Figure 1. Notation for Axisymmetric Shell Element

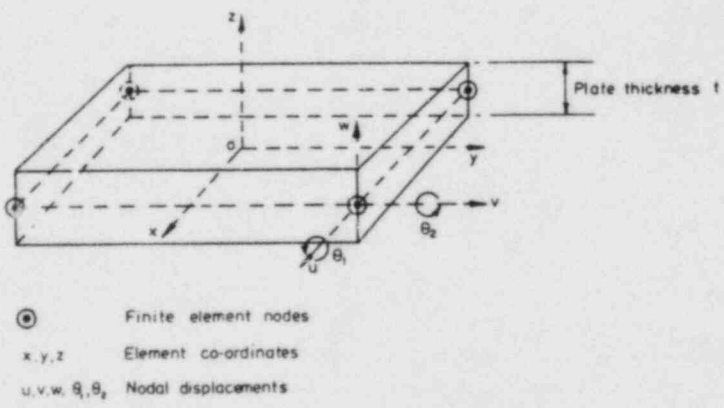

Figure 2. Notation for Plate Element

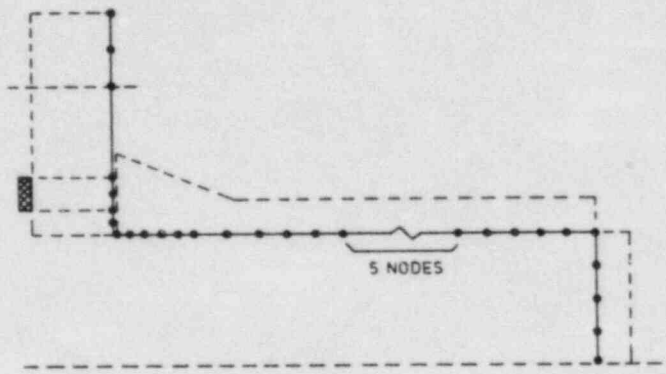

Figure 3. Distribution of Elements in an Axisymmetric Tapered Hub Flange

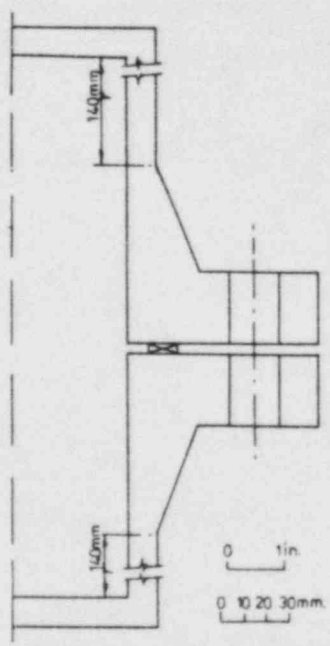

Figure 4. Cross Section of ANSI B16.5 Class 600 Joint Analyzed (Axisymmetric Version of JOINT)

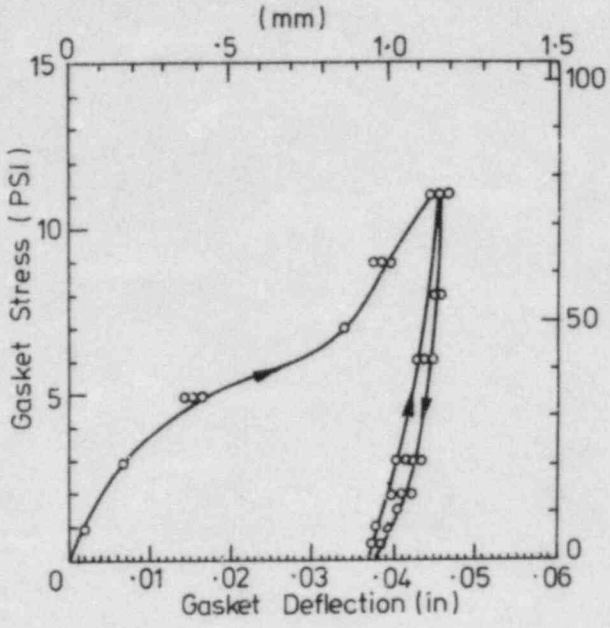

Figure 5. Stress vs. Deflection for a Spiral-Wound Gasket (Ref. 9)

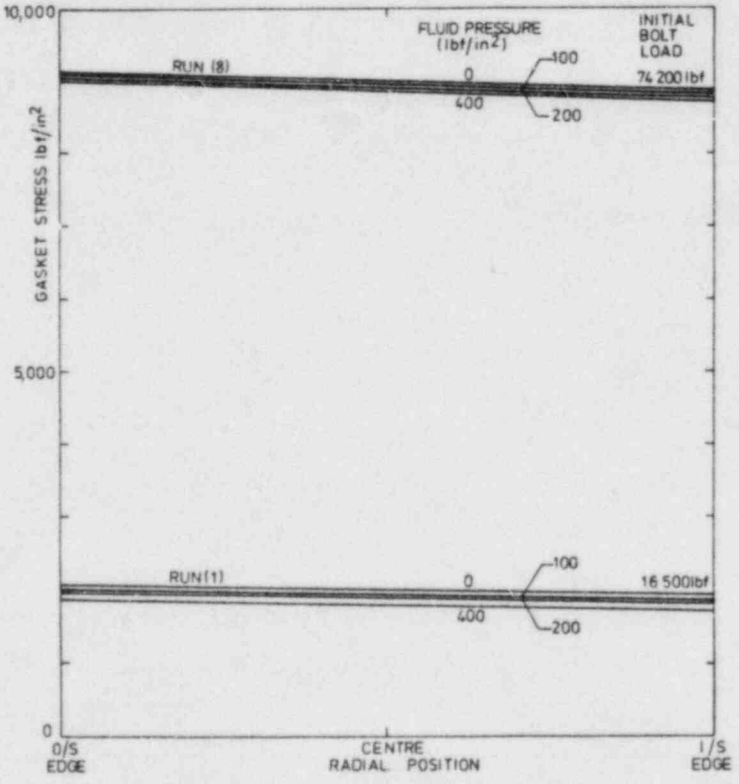

Figure 6. Computed Radial Variation of Gasket Stress with Fluid Pressure and Bolt-Load for NASI Flange Test Problem

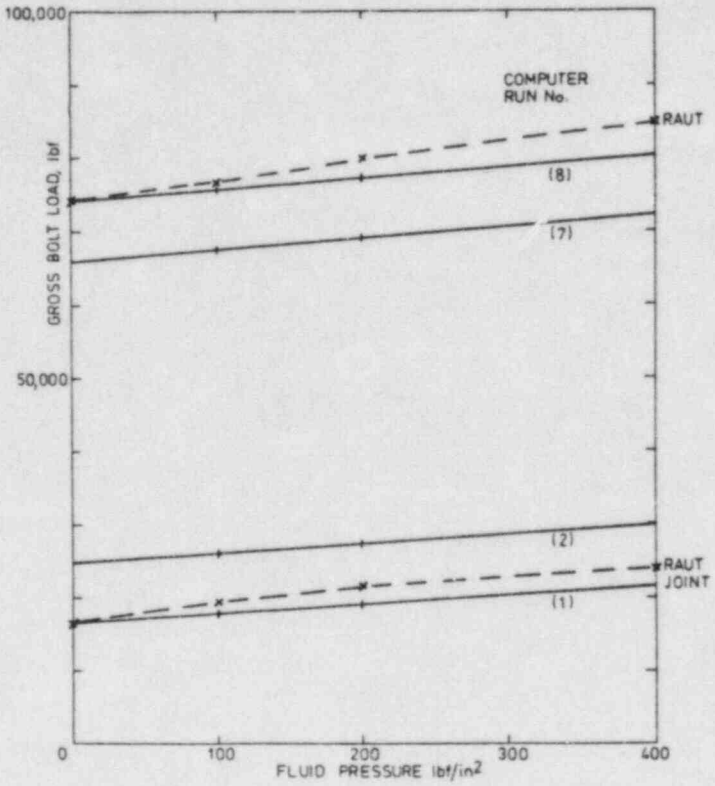

Figure 7. Computed Variation of Bolt-Load with Fluid Pressure for Various Initial Bolt-Loads, Experimental Data (Raut 1979) Shown as Broken Lines

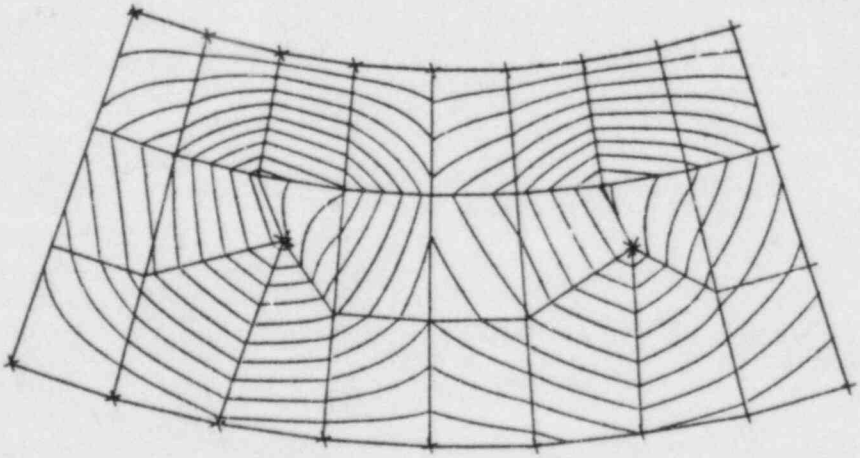

Figure 8. Calculated Gasket Stress Contours Over a Sector of a Circular Flange Including Two Bolts (Indicated by '*') (Gasket CAF, Flange 1400 x 1000 mm ϕ, 50 mm Thick, 20 Bolts of 50 mm dia.)

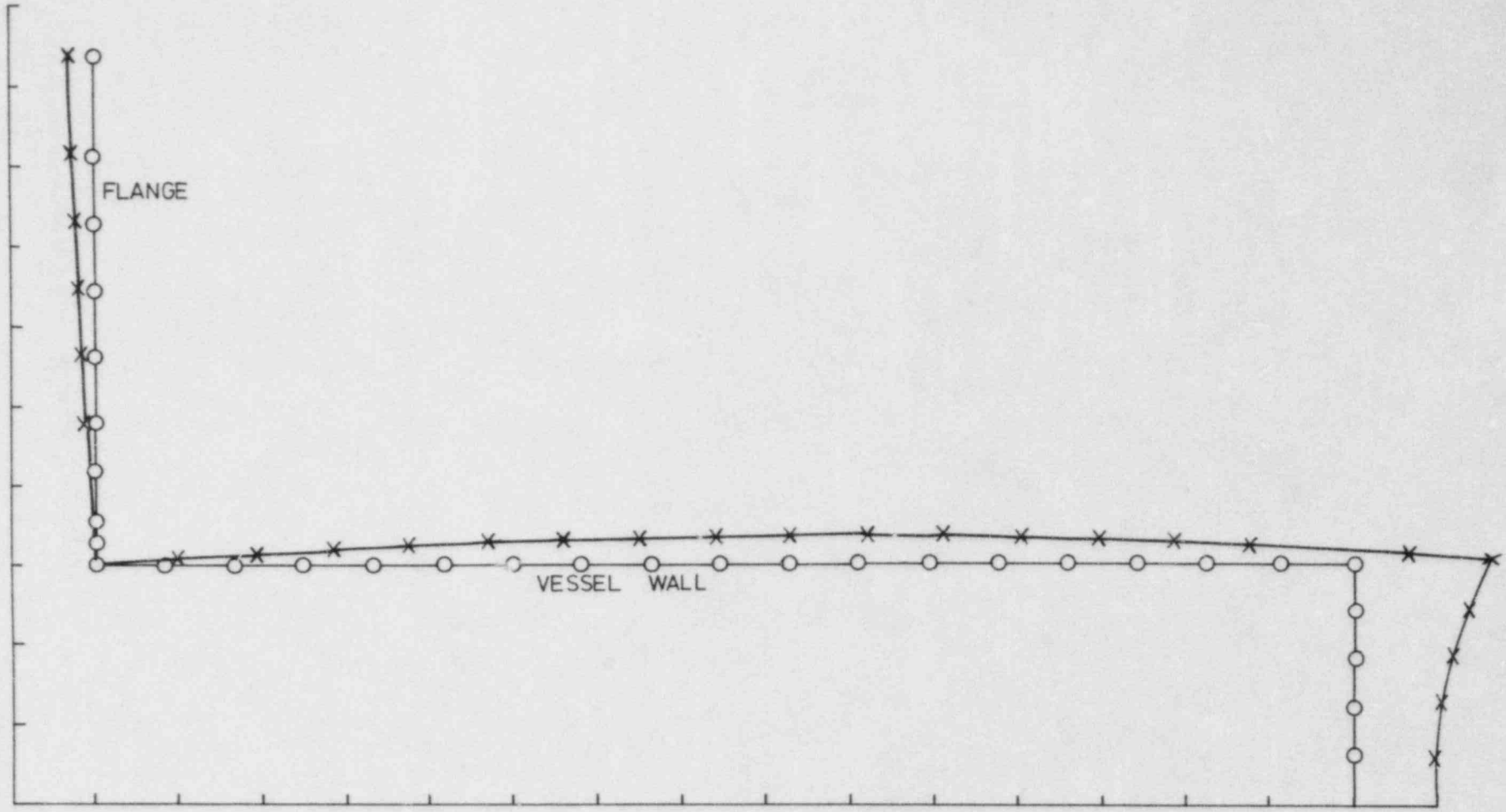

Figure 9. Example of Thermal Rotation of Flange Due to Temperature Lag of Flange Relative to Vessel. (Deflections magnified: x 1000).

NONLINEAR ANALYSIS OF CONCRETE CONTAINMENTS UNDER STATIC PRESSURIZATION EVALUATION OF THE RISK OF LEAKAGE

A. Combescure, A. Hoffmann, P. Jamet, and A. Millard
CEA-IRDI/DEDR.DEMT, CEN, SACLAY

R. Avet-Flancard, B. Barbe
CEN-IPSN/DAS, CEN, FONTENEY-aux-ROSES

ABSTRACT

Concrete containments for french 900 MW and 1300 MW PWR plants are designed according to a conventional reference accident (Sudden loss of coolant). However, from a safety point of view, it is necessary to characterize the behaviour of such structures, when subjected to loading conditions exceeding the nominal case. In particular, leakage and local, or overall failure, of the structures should be accurately predicted.

In order to solve this problem, a study was undertaken by C.E.A. The purpose of this paper is to describe the main stages of the work and to suggest necessary improvements of the present analytical tools:

- development of a concrete model and implementation within the CEASEMT finite element system.
- Finite element analysis of the 900 MW and 1300 MW containments.
- Validation of the analysis on a simple structure.
- Future improvements.

1 - INTRODUCTION

Concrete containments for french 900 and 1300 MW PWR plants are designed on the basis of the reference loss of coolant accident. However, from a safety point of view, it is

necessary to characterize the behaviour of such structures, when subjected to loading conditions exceeding the nominal case. In particular, leakage and local, or overall failure, of the structures should be accurately predicted, in order to estimate the safety coefficient associated to the actual design. Within this frame, the case of a simultaneous increase of pressure and temperature, above the nominal conditions was considered. Slow rates were assumed: 0.03 MPa per hour, from 0.4 MPa for pressure and 2°C per hour from 140°C for temperature.

The overall study consisted in three stages:

- development of a concrete model and implementation within the CEASEMT finite element system.
- Finite element analysis of the french 900 MW and 1300 MW containments.
- Test on a simple structure in order to obtain preliminary informations concerning the relation between mechanical damage and leakage.

2 - CONCRETE MODEL

2.1 - Position of the Problem

In order to perform accurate analysis of containment structures up to overall failure, plasticity of steel, as well as non-linear behaviour of concrete have to be taken into account. Two different damage modes can lead to non-linear behaviour of concrete:

- tensile failure which for example occurs, because of the hoop stresses due to internal pressure.
- Shear failure under compressive stresses at discontinuities.

Tensile failure of concrete is a relatively well-known phenomenon, and it can be considered that sufficient data exists in the literature, in order to formulate a reasonable model. On the other hand, failure of concrete under compressive stresses has been extensively studied [1] [9]. However, most of the tests were run by means of experimental devices which did not allow to observe strain softening, after the maximum load bearing capacity of the specimen was reached. A series of triaxial experiments was therefore performed, in order to characterize the post-peak behaviour of concrete.

2.2 - Triaxial Testing of a Micro-Concrete

For convenience, the triaxial tests were performed on a micro-concrete [9]. It was assumed that, at least qualitatively, the obtained data would be representative of the behaviour of actual concrete. The specimens were cylinders, (diameter 110 mm, height 220 mm). Before the tests, they were

jacketed in rubber sleeves, which has been studied to avoid any leakage, even after fracturation. The triaxial cell was a classical one. The axial load was applied by means of a servo-hydraulic testing machine. The specimens were first loaded hydrostatically, up to the chosen confining pressure. They were then strained axially under a constant displacement rate of 0.11 mm/s. Three independent tests were performed, for each of the following pressures: 0 MPa, 3 MPa, 10 MPa, 25 MPa. Figure 1 presents the mean curves obtained for each confining pressure. For 0 MPa confining pressure, a drastic strain softening behaviour is observed, while the residual stress of the material becomes negligible after 2.5% axial strain. When the confining pressure increases, the descending branches of the stress-strain curves become less and less steep; for very large strains the behaviour of the material tends to become perfectly plastic. For 25 MPa confining pressure, strain softening almost vanishes.

After the tests at 0 MPa confining pressure, well individualized sub-axial fractures could be observed in the specimens. For 3 MPa and 10 MPa confining pressures, the fractures had the same general aspect, but their inclination with respect to the axial axis of the specimens was about 25 degrees. For 25 MPa confining pressure, the fractures were less open, more numerous and smaller in length. Their inclination was about 30 degrees.

The experimental results show that any realistic concrete model should take strain-softening into account, as well as the dependence of this phenomenon upon confining pressure. On the other hand, the observed fracture patterns are strongly non isotropic and depend upon the stress state; these facts should also be taken when establishing any relation between mechanical damage an permeability of the material.

2.3 - Concrete Modeling

2.3.1 - General Principles for the Model

Extensive work has already been carried out in the field of concrete modeling [10] [11] [12]. Endochronic and plastic fracturing models are probably the most appealing ones, since their representation of internal changes within the material allow them to apply to many different types of loadings (cyclic for example). On the other hand, they use a very important set of parameters which have to be numerically fitted, in order to obtain the necessary constants for application to a specific case. Considering overall behaviour of concrete containments, a simpler model is probably sufficient to account for the main phenomena occuring within the structure.

Such a model was formulated. It uses an elastic plastic formulation with a multi criterion loading surface. The classical plastic constitutive equations were adjusted in order to eventually take strain-softening into account. Two types of damages are described: tensile and shear.

2.3.2 - Tensile Failure

The behaviour of the material was assumed to be elastic brittle. Tensile failure occurs when one of the principal stresses acting on the material reaches its tensile strength. The corresponding stress is then set to zero, and the strain energy released by the fracture is returned to the structure. The directions in which failure occured are kept in memory, preventing the material from sustaining any further tensile or shear stresses along a fracture plane. In the axisymmetric case, two cracking modes can then be described:

- radial cracking,
- cracking in the diametral plane with two possible orthogonal directions.

2.3.3 - Shear Failure

In order to simplify the model, the complete stress-strain curves obtained through triaxial testing were first linearized as shown by figure 2: the material is first elastic, it then undergoes strain softening, its ultimate behaviour is perfectly plastic. In order to represent the strain softening and perfectly plastic behaviours, two independent Drücker Prager criteria were used (13). Their traces in the $\sigma_1, \sigma_2 = \sigma_3$ plane are represented by figure 3. The outer criterion corresponds to strain-softening: it undergoes isotropic "shrinking" as the material is strained. The inner criterion is fixed, it is associated to the assumed ultimate perfectly plastic behaviour of concrete. Strain energy is actually consumed through the process of shear failure. The normality principle is assumed for plastic flow.

In the principal stresses space, the two plasticity criteria correspond to two cones, the outer one moving inwards, towards the inner fixed one.

This shear model, as well as the tensile failure one, have been implemented into the code INCA of the CEASEMT finite element system [14].

3 - FINITE ELEMENT ANALYSIS OF 900 MW ET 1300 MW CONTAINMENTS

900 MW and 1300 MW containments are considered as axisymmetrical structures, without defects or penetrations, and a complete thermal/mechanical calculation is performed for both containments up to the collapse point, with due allowance for concrete and rebar steel non-linear behavioural laws.

These calculations were preceded by a "test case" study: calculations by four different computer codes conducted by different design offices relating to a limited area of the containment and aiming to provide knowledge of the accuracy to be expected from such non-linear calculations when applied to prestressed concrete.

3.1 - "Test Case" Study

This analysis, which related to a limited containment area (barrel to base mat junction zone) made it possible to determine the state of the art for concrete structure elastic/plastic calculations and to highlight the inadequacies of some of the concrete models, in order to specify result uncertainties (four codes were used). These calculations, which included modelling of all the containment load-bearing elements (finite element modelling with non-linear behavioural laws) showed:

- good agreement on final collapse (between 1.15 and 1.3 MPa gage). The latter is related to the rupture of the barrel horizontal prestress cables and the final mechanism is simple.

- however, there is wider scatter affecting the intermediate concrete cracking mechanisms. The influence of the concrete models is direct and accuracy is lower (for example transverse barrel cracks appear between 0.6 and 1K1 MPa gage).

3.2 - Mechanical Strength of 900 MW PWR Containments

After a critical examination of the above test calculations, a complete study of this metal-lined containment was conducted and led to the following conclusions:

- final collapse is due to rupture of the barrel horizontal prestress cables and (almost simultaneously) of the dome prestress cables for an internal pressure of about 1.2 MPa.

- Metal liner deformation is still moderate just before collapse (less than a few %). This suggests that the risks of liner tearing in the zones free of discontinuities are low. Therefore, if no tear appears in the area of the penetrations and if the liner exhibits no initial defects, these containments would remain leaktight right up to the end. Intermediate concrete cracking mechanisms are less important and do not have a direct effect on collapse.

3.3 - Mechanical Strength of 1300 MW PWR Containments

French 1300 MW PWR containments have dual concrete walls instead of metal liners. When cracks spread across the concrete of the inner containment wall, the wall starts to leak and its mechanical strength is dependent on this leak, which tends to reduce internal pressure.

Finite element analysis of such a containment was performed. The obtained results suggest the following interpretation, concerning the risk of leaking:

- during the first hours after the Design Basis Accident,

leaktightness is provided by a concrete layer (highly compressed because of heat shock) on the inner face of the inner containment wall.

- However, transverse concrete cracks appear over a large area of the dome at internal gage pressures of about 0.6 MPa and 0.75 MPa in the barrel zone free of discontinuities. This results in leakage through the crack lattice, which tends to offset the steam production in the containment due to the accident. A straightforward mechanical study is inadequate in this case and it is necessary to analyse the possible distribution of the cracks, their opening and related leakage, the recovery of this leakage in the inter-wall space or the possible rise of containment pressure... Containment mechanical strength and the entire accident scenario depend on leakage rate.

3.4 - Conclusion

Pending final conclusions; it can be stated that the behaviour of the 900 MW PWR metal-lined containments is very different from that of 1300 MW PWR containments with dual concrete walls and cannot be covered by the same type of study. 900 MW PWR containments exhibit purely mechanical behaviour in that they probably remain leaktight right up to the end, whereas the behaviour of the 1300 MW PWR containments is much more complex and is largely dependent on concrete cracking and associated leakage.

A containment depressurization system is currently being studied in France, which would cover both cases. The study will determine the pressure above which the system should enter into service in each possible scenario.

4 - STUDY ON A SIMPLE STRUCTURE

4.1 - Test on a Circular Slab

Finite element analysis of the french containments have shown that one of the most critical parts of these structures are the gussets between their shafts and their floors. A test was therefore performed on a simple slab where the geometrical singularity of the real structures as well as the stresses acting on them, were reproduced as accurately as possible. The main motivation for the test were the following:

- check the validity of the non-linear mechanical analysis.

- Obtain preliminary informations concerning the relation between mechanical damage and risk of leaking.

The slab was circular, its diameter is 1.50 metre. Its thickness varied between 9 and 16 centimetres. It was made of the same micro-concrete as the one used for triaxial testing. Figure 4 shows its reinforcement. It was simply supported

around its outer radius. The load was applied at its center by means of a circular ring of 40 cm outer diameter and 2.5 cm thickness. The displacements were monitored, at various points, as shown by figure 5.

A waterproof ring was placed on the top surface of the slab, opposite the support. Water was placed inside the ring, directly in contact with the concrete, before the beginning of the test. The bottom face of the slab was continuously under visual observation, so that the onset of major leaking could be detected. Figure 6 shows the force deflection curve corresponding to the center of the slab.

In a first step, radial cracks appeared at the bottom face of the structure, followed by circumferential cracks in the center part, and at the junction between the conical part and the region with smaller uniform thickness. When the slab reached its ultimate state, a compressive failure could be observed on the top face of the slab, opposite the junction between its conical part and the region with smaller thickness. Leaking could only be observed at the end of the test, as shown by the arrow on figure 6. This test shows that major connection of cracks only occurs after the structure has reached its ultimate mechanical state.

4.2 - Finite Element Analysis

Finite element analysis of the slab was performed using the mesh represented by figure 7. The reinforcing steels were represented by cable and shell elements. Full compatibility was assumed between steel and concrete displacements.

Figure 6 presents the numerically computed force-deflection curve, the comparison between numerical and experimental results leads to the following conclusions:

- the initial elastic compliance is accurately computed.
- The ultimate load bearing capacity of the structure is well predicted.
- The crack patterns predicted by the model (radial and circumferential) agree well with experimental results.
- The displacements at failure are strongly under-estimated by the analysis; work is currently performed in order to solve this problem.

5 - FUTURE IMPROVEMENTS

From a purely mechanical point of view, several improvements are considered for the present model:

- better representation of steel-concrete interaction: instead of assuming a purely brittle behaviour for concrete in traction, tensile stiffening could be incorporated, by use of a descending branch in the stress-strain curve. Dowel action

could also represented by means of a residual shear strength along fractures planes.

- If the model is to be applied to accidental situations in fast breeders reactors, the effect of temperature on the characteristics of steel and concrete should also be incorporated.

- The model should also be generalized to three dimensional situations in order to investigate penetrations or defects problems. To avoid excessive numerical complications, the shear model should probably be simplified. However, it seems possible to leave the traction failure model unchanged.

Concerning the relation between mechanical damage and risk of leakage, two different points of view can be suggested:

- if the only concern is the risk of major leak and if an estimation of the leak rate is not needed, non-linear mechanical analysis is probably sufficient. Major leak can then be assumed to happen when a series of adjacent elements have failed in tension or shear, in such a way that a path is created through the containment. In case of bending, major leak probably happens for loads corresponding to the maximum bearing capacity of the structure. However, this conclusion might not apply to the case of hoop stresses, because through cracks can appear while the reinforcements still behave elastically.

- If a leak rate has to be estimated, a formal coupling has to be established, between mechanical damage and permeability. Tests on simple structures have already been performed or planed, in order to give informations about this problem, in case of tensile fracturing of concrete [15] [16]. Expressions have been proposed, in order to determine the leak rate, as a function of the mean opening of cracks. However, in order to apply such expressions in conjunction with mechanical analysis, the number of cracks has to be estimated. This problem is not solved in the general case, and more work is needed to overcome this difficulty. On the other hand, the contribution of shear failure to permeability has not been quantified. This problem is even more complicated, since shear cracks do not coincide with the principal stress direction, as shown by triaxial testing. New tests should be performed where permeability could be monitored, simultaneously with stresses and strains. Such data could constitute a basis for a model formulation, where induced anisotropic permeability could be expressed, as a function of mechanical damage.

6 - CONCLUSION

A non-linear concrete model applicable to mechanical analysis of concrete containment has been presented. The application to the case of the french 900 MW and 1300 MW containments allowed to obtain first estimation of the margins associated with their actual design. Comparison between experimental and numerical results obtained in the case of a simple

slab representative one of the most critical part of the real structure, gave good results concerning crack orientations and ultimate load. It was also shown that major leak of structure only appeared after its maximum load bearing capacity had been reached.

It is suggested that mechanical analysis is probably sufficient to predict the onset of a major leak. In order to evaluate leak rates, more work is however needed. In particular, the average spacing of cracks has to be accurately estimated, in the general case of tensile loading. In the case of shear failure under compressive loading, more laboratory tests could be performed, in order to correlate unduced anisotropic permeability with mechanical damage.

REFERENCES

[1] J.J. Gardner, "Triaxial behaviour of concrete". ACI Journal Tittle n°66-15, Feb. 69, pp. 136-146.

[2] Green S.J. and Swanson S.R., "Static constitutive relations for concrete". Technical Report n°AFWC-72-2. Terra Tek Inc., Salt Lake City, Utah, Apr.73.

[3] Kupfer H.G., Hilsdorf H.K. and Rüsch H., "Behaviour of concrete under triaxial stresses". American Concrete Institute Journal, vol. 66, Aug. 69, pp. 656-666.

[4] Launay P. and Gachon H., "Strain and ultimate strength of concrete under triaxial stress". First International Conference on Structure Mechanics in Reactor Technology, Berlin, Germany, Paper H 1/5, Sept. 71.

[5] Masure P., "Cisaillement des mortiers de ciment et comparaison avec l'essai triaxial". Revue des Matériaux de Construction n°659-660. Sept. 70, pp. 229-241.

[6] Mills L.L. and Zimmerman R.M., "Compressive strength of plain concrete under multiaxial loading conditions". Proceedings, American Concrete Institute, vol. 57, n°10, Oct. 70, pp. 802-807.

[7] Palaniswawy R. and Shah S.P., "Fracture and Stress-strain relationship of concrete under triaxial compression", Journal of Structural Division, ASCE, n°ST 5, Proc. Paper 10547, May 74, pp. 901-916.

[8] Richart F.E., Brandzaeg A. and Brown R.L., "A study of the failure of concrete under combined compressive stresses", Engineering Experiment Station, University of Illinois, Bulletin n°185, 1928.

[9] Jamet Ph., Millard A. and Nahas G., "Triaxial behaviour of a micro-concrete, complete stress-strain curves for confining pressures ranging from 0 to 100 MPa", RILEM symposium on triaxial behaviour of concrete, Toulouse, 1984 (to be published).

[10] Bazant Z.P., "Inelastic and failure of concrete: A survey of recent progress". Analisi delle strutture in cemento armato mediante il metodo degli elementi finite. Politecnico di Milano, 1978, pp. 5-59.

[11] Bazant Z.P., "Advances in deformation and failure models for concrete". Introductory report - IABSE Colloquium, Delft, 1981, pp. 9-39.

[12] Ting E.C., Marchertas A.M., "Modelling and code development for concrete structures: an over view", SMIRT n°7, Paper H 4/1, Chicago, Aug. 1983.

[13] Drücker D.C. and Prager N., "Soil mechanics and plastic analysis of limit design". Quaterly of applied mathematics, vol. 10, pp. 157-165, 1952.

[14] Jeanpierre F. et al., CEASEMT, "System of finite element computer programs". IAEA/IWGFR specialists meeting on high temperature structural design technology of CMRBRs. Champion, Pa, 1976.

[15] Rizkalla S.H., Lau B.L., "Leakage of pressurized gases through unlined concrete containment structures". SMIRT n°7, Paper J 1/5, Chicago, Aug. 1983.

[16] Julien J.T., Schultz D.M., "Tension tests of concrete containment wall elements", SMIRT n°7, Paper J 5/1, Chicago, Aug. 1983.

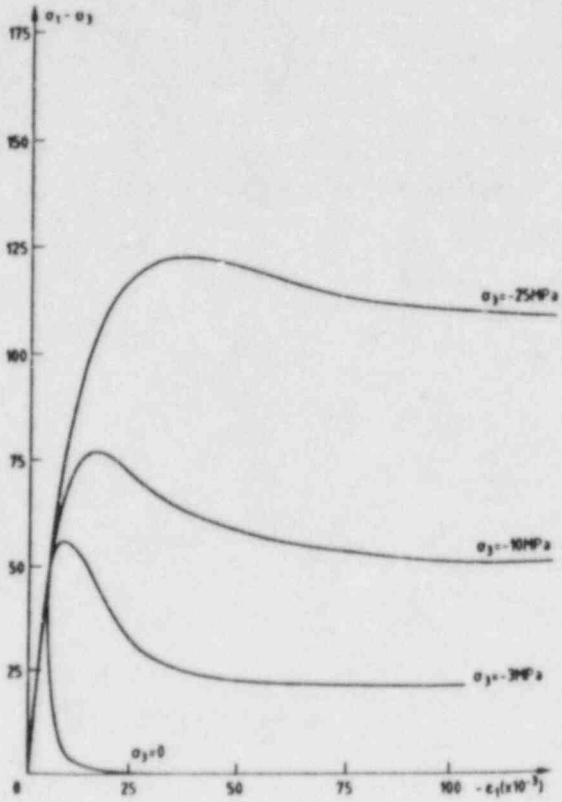

Figure 1 - Complete stress strain curve for micro-concrete.

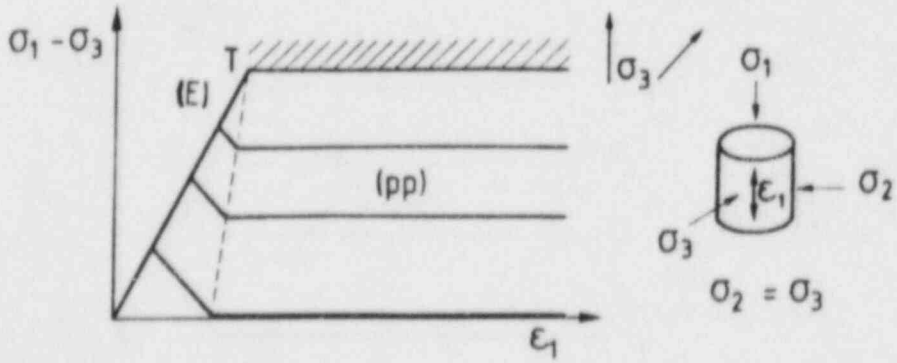

Figure 2 - Linearization of experimental stress-strain curves.

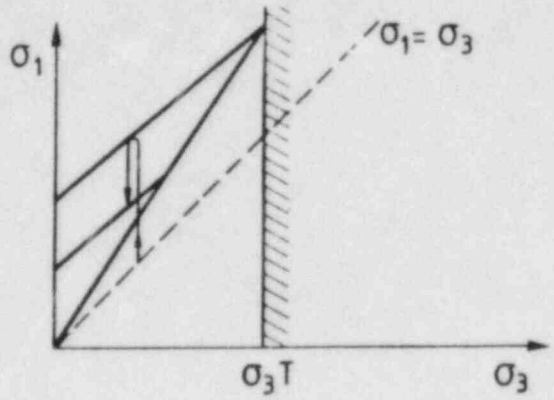

Figure 3 - Shear plasticity criteria in the σ_1, $\sigma_2 = \sigma_3$ plane.

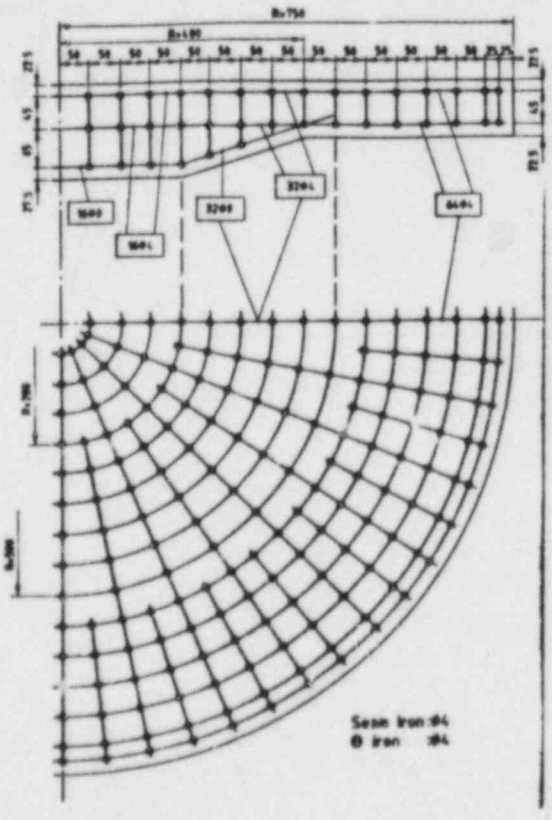

Figure 4 - Slab reinforcement.

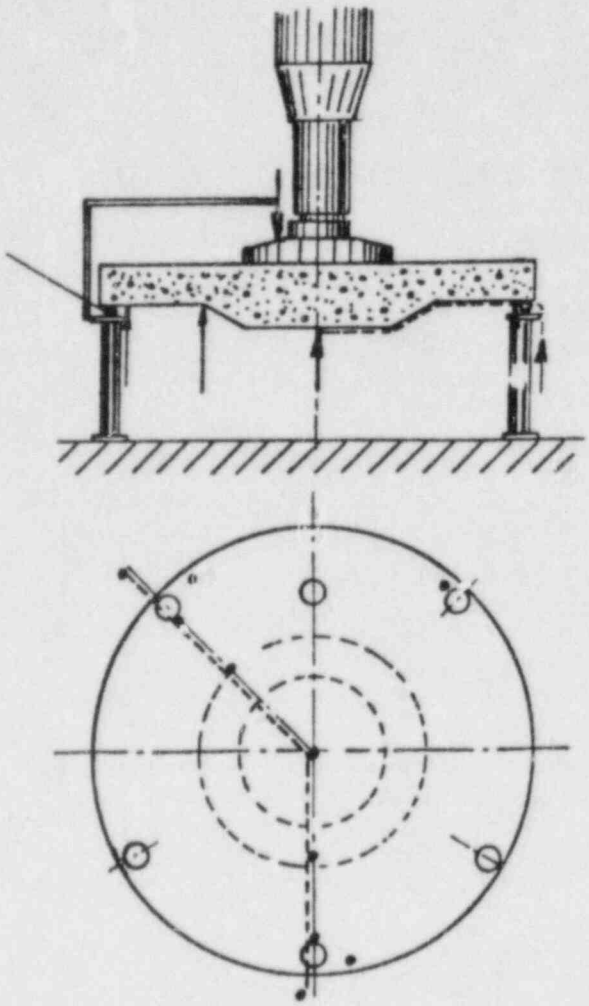

Figure 5 - Experimental set up for the test on the circular slab.

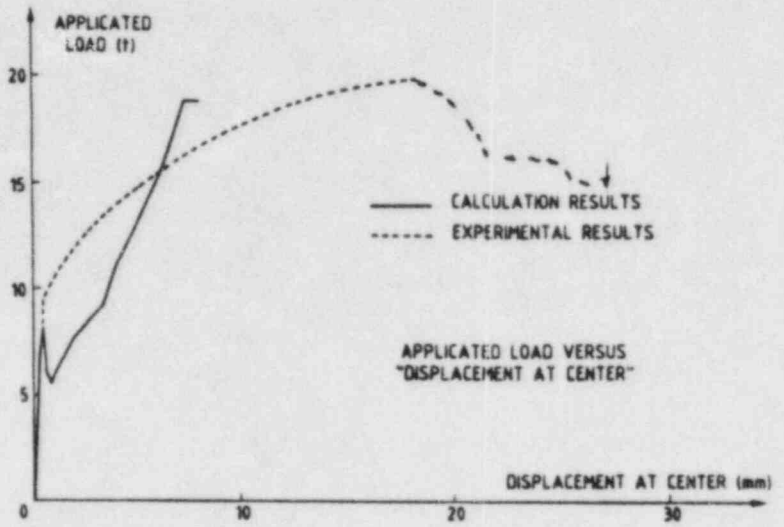

Figure 6 - Experimental and numerical force deflection curves for the circular slab.

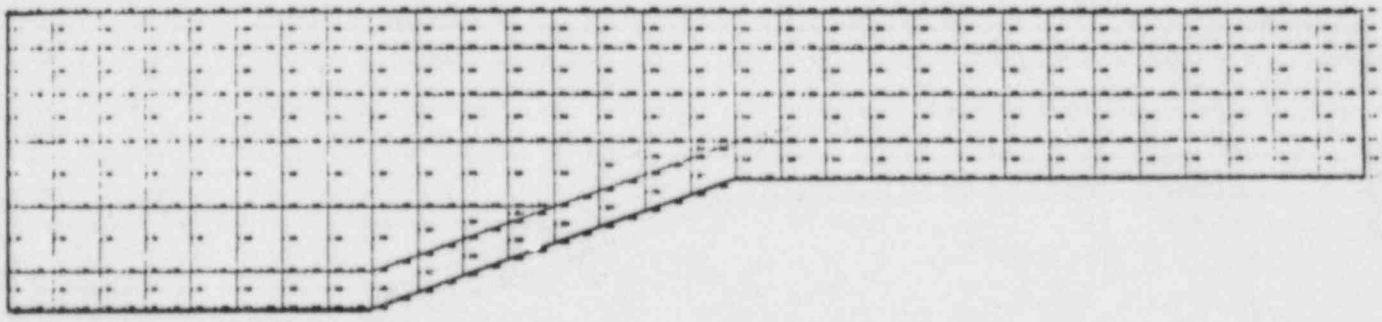

Figure 7 - Mesh used for finite element analysis of the slab.

FULL-SCALE LEAK-RATE TESTS OF CONCRETE CONTAINMENT WALL ELEMENTS

D. M. Schultz and N. W. Hanson
Construction Technology Laboratories
A Division of the Portland Cement Association
5420 Old Orchard Road
Skokie, IL 60077

ABSTRACT

The tests described in this report are part of an Electric Power Research Institute (EPRI) program to provide a test-verified analytical method for estimating capacities of concrete reactor containment buildings. The three-phase testing program being performed at Construction Technology Laboratories (CTL) will determine strength, deformation characteristics, and air leak-rates of specimens representing half-thickness and full scale elements from the walls of reinforced and prestressed concrete reactor containment buildings. Applied loads are representative of those occurring during an extreme overpressurization beyond a design basis accident. Results from this testing program are being used to confirm analytical models for predicting strength and deformation of containment walls. This analytical modeling is being conducted by others in a separate parallel investigation sponsored by EPRI.

INTRODUCTION

To investigate the structural behavior of reactor containment buildings subjected to overpressurization, the Electric Power Research Institute (EPRI) has undertaken a three-phase research program at Construction Technology Laboratories (CTL). The three phases are identified by the following broad categories.

Phase 1 - Half-Thickness Concrete Wall Element Tests and Full Thickness Liner Plate Tests
Phase 2 - Concrete Wall Element Tests with Penetration Sleeves and Other Perturbations
Phase 3 - Tests of Containment Building Segments with Structural Discontinuities

The objective of the EPRI testing program is to provide a test-verified analytical method for estimating capacities of concrete reactor containment buildings under internal overpressurization from postulated degraded core accidents. These estimates are needed to perform plant-specific probabilistic risk assessments. Results from this testing program are being used to confirm analytical models for predicting strength and deformations of containment walls. This analytical modeling is

being conducted by others in a separate parallel investigation sponsored by EPRI (1).

PHASE 1 - HALF-THICKNESS CONCRETE WALL ELEMENT TESTS

The objective of testing the half-thickness concrete elements was to determine strength and deformation characteristics of specimens representing wall elements of reinforced and prestressed concrete reactor containment buildings (RCB) for nuclear power plants. Forces applied to the wall elements in this test program represent those caused primarily by internal pressure within the containment, as illustrated in Fig. 1. Each specimen was approximately 60 in. (1525 mm) square and 24 in. (610 mm) thick and had full-size reinforcing bars. Table 1 lists specimen design variables.

TABLE 1 - PHASE 1 SPECIMEN REINFORCEMENT AND DESIGN VARIABLES

Specimen Reinforcement and Design Variables	Specimen Name							
	UA1	UA2	UA3	BA1	BA2	BA3	PC1	LP1
Hoop Reinf. (No. 18) (Loaded) A_s/A_g = 0.022*	X	X	X	X	X	X		
Meridional Reinf. (No. 14) (Unloaded) A_s/A_g = 0.013			X					
Meridional Reinf. (No. 14) (Loaded) A_s/A_g = 0.013				X	X	X		
Diagonal Reinf. (No. 10) (Unloaded)			X		X			
Diagonal Reinf. (No. 10) (Loaded)						X		
Preformed Cracks		X						
Minimum Rein., Both Ways (No. 7) A_s/A_g = 0.0042							X	
Liner Plate, Each Side								X

*A_s/A_g = Ratio of area of reinforcement to gross cross-sectional area of concrete.

Six specimens were representative of typical reinforced concrete containment designs. Hoop reinforcement of typical size and spacing was the only common feature for the first six specimens. Although in the full thickness wall element, usually two mats of reinforcement are placed in each face, only one mat was used in each face in the half-thickness test specimens. Features of the specimen designs were varied systematically to provide comprehensive data on how these features influence structural behavior. Reinforcement details for Specimens UA3, BA1, BA2, and BA3 are shown in Fig. 2.

Two specimens represented typical prestressed containment designs. Tendon ducts were simulated using thin-walled tubing. One specimen contained minimum reinforcement used in prestressed containments to control stress due to drying shrinkage and temperature differentials in the concrete wall. Minimum orthogonal reinforcement was located in both faces of this test specimen. The second prestressed containment test specimen had liner plates anchored to both faces of the concrete. Liner anchorage consisted of angles welded to both liner plates. Orthogonal reinforcement was not provided. Prestress due to post-tensioned unbonded tendons was not provided.

In a prestressed RCB, typical post-tensioning precompression ratio is 2:1 (hoop:meridional). During an overpressurization, the precompression of the containment in each direction would nominally reach zero at about the same pressure. From that point on, the containment does not know it was precompressed. It behaves as a normal under-reinforced concrete section even though there is additional stress in the tendons within the ducts. Therefore, the testing of PC1 and LP1 began at the point where there were no prestressing forces on the section. Since tendons are unbonded in the duct in a containment, there is no strain compatibility or any other mechanical interaction between concrete and the prestressing strand during internal pressurization. In addition, no strand was placed within the ducts. Consequently, the deformations observed in these tests should be viewed as those that would take place subsequent to relief of precompression in a pressurized RCB.

Specimen loading included uniaxial loads, biaxial loads, and biaxial loads combined with diagonal loads. The biaxial and biaxial plus diagonal loading systems are shown in Fig. 3. All specimens were loaded statically beyond yield stress of reinforcement or liner plate. This was accomplished by pulling on the reinforcement with hydraulic rams reacting against a concrete reaction frame. The reaction frame was constructed by CTL for the U.S. Nuclear Regulatory Commission in a previous program where membrane shear behavior during simulated earthquake loading was investigated.

Different reinforcement configurations and loading arrangements resulted in data that permit a comparison of the effect of controlled variables on cracking and subsequent interaction between concrete and reinforcement. The consistent introduction of variables from specimen to specimen allowed isolation of effects of each variable on both cracking and overall performance of the specimen. Certain specimens such as BA1, BA3, and PC1 were detailed and loaded nearly identically to that of an element from a typical concrete containment building. Conditions at the cylinder wall midheight and near the basemat were modeled in Specimens BA1 and BA3, respectively. To more fully represent the extreme condition, Specimen BA1 had no diagonal reinforcement. The remaining specimens were detailed and loaded to isolate certain effects. These latter specimens were planned

to develop a data base against which the analytical model developed by others could be compared. Certain specimens such as UA2 with crack formers, and UA3 and BA2 with unloaded diagonal bars were included within the test series as rigorous exercises for the analytical modeling. Unloaded diagonal bars in Specimens UA3 and BA2 were also used to determine whether nominal amounts of diagonal reinforcement could alter overall specimen response.

Specimen behavior was measured using external and internal instrumentation. Loads, deformations, crack widths, and steel strains were measured.

The following comments are based on test results from Specimens UA1 through BA3. Where extrapolations are made to a typical RCB, the RCB has a 150-ft (45.7-m) diameter and a 4-ft (1.22-m) wall thickness.

1. Applied hoop loads at specimen yield in the hoop direction were equivalent to an RCB pressurization of approximately 80 psi (0.55 MPa). Overall specimen hoop strain at yield load was approximately 0.3%. This strain is equivalent to an RCB diameter increase of approximately 0.42 ft (0.13 m).

2. Maximum applied hoop loads were equivalent to an RCB pressurization of over 100 psi (0.69 MPa). Overall specimen hoop strain at maximum load was on the order of 2%. This strain is equivalent to an RCB diameter increase of over 3 ft (0.91 m).

3. For uniaxially reinforced Specimens UA1 and UA2, under hoop loading, only through-wall cracks transverse to the main reinforcement occurred. Spacing of cracks in Specimens UA1 and UA2 due to hoop load was approximately 18 in. (455 mm). The crack former in Specimen UA2 delayed subsequent cracking in the remainder of the specimen as compared to the occurrence of first cracking in Specimen UA1.

4. For orthogonally reinforced Specimens BA1 and BA3, under biaxial loading, cracking due to hoop loading was generally independent of meridional reinforcement locations. Spacing of through-thickness cracks ranged from 18 to 24 in. (457 to 610 mm). It is concluded that in these specimens, meridional reinforcement did not function as crack formers.

5. For orthogonally reinforced Specimens BA1 and BA3, under biaxial loading, cracking due to meridional loading was dependent on hoop reinforcement locations. Spacing of through-thickness cracks was equal to the spacing of hoop reinforcement, 12 in. (305 mm). It is concluded that in these specimens, hoop reinforcement functioned as crack formers.

6. Extrapolating the results of (4) and (5) above to a typical reinforced concrete RCB, it could be concluded that horizontal cracks in the containment building wall may be regularly spaced and may occur at hoop reinforcement location. Vertical cracks, in the containment wall, however, may occur irregularly and at greater spacings, since they are not dependent on meridional reinforcement locations.

7. The presence of unloaded diagonal reinforcement in Specimens UA3 (uniaxially loaded) and BA2 (biaxially loaded) was a major influence on the behavior. Spacing and orientation of through-thickness cracks were significantly different or compared to specimens without diagonal reinforcement or with loaded diagonal reinforcement. These results indicated that small amounts of diagonal reinforcement as compared to orthogonal reinforcement can alter overall behavior of the specimen if boundary conditions are not properly modeled, that is, if the diagonals are not loaded as they would be in a containment.

The percentage of reinforcement used in Specimen PC1 was typical of that used in prestressed concrete reactor containment buildings. Although the percentage was low, the nominal hoop and meridional reinforcement in Specimen PC1 transferred sufficient load to the concrete to crack the section at three separate locations. However, since the section was underreinforced, first cracking due to hoop load occurred suddenly. It appeared that the tendon duct had little influence on the cracking pattern of the specimen.

In Specimen LP1, the concrete section developed through-cracks at angle anchorages. The cracks propagated from the angle anchorages of the liner plate on each side of the specimen and joined in the center of the concrete section. It appeared that the tendon duct had little influence on the cracking pattern of the specimen. Propagation of cracking from the angle anchorages in this test can be compared with predictions of crack propagations by the analytical model.

Consistent variation in data from specimen to specimen has indicated a relatively low "error bar" in the test program. The data should be useful for benchmarking analytical methods that require modeling of material behavior including concrete cracking and reinforcement/concrete interaction.

General background material is presented in References 2 and 3.

PHASE 1 - FULL THICKNESS LINER PLATE TESTS

The objective of the liner plate tests was to determine strength and deformation characteristics of isolated liner plate

specimens representing the inner liner of wall elements of a prestressed concrete RCB.* Tests were conducted using combinations of forces simulating those that could occur in the liner of walls of an RCB.

Each specimen was 48 in. (1220 mm) square and 1/4 in. (6.4 mm) thick. Table 2 lists specimen design variables. Specimen ILP1 was a solid liner plate with no special details. Specimen ILP2 included meridional angles welded to the liner plate. Specimen ILP3 contained a T-weld representing the junction of three plates in a liner. Specimen ILP4 contained a 10-in. (254-mm) diameter penetration. Details of Specimen ILP4 are given in Figure 4.

TABLE 2 - PHASE 1 SPECIMEN DESIGN VARIABLES

Specimen Design Detail	Specimen Name			
	ILP1	ILP2	ILP3	ILP4
48-in. (1220-mm) square liner plate 1/4 in. (6 mm) thick	X	X	X	X
Meridional Angles		X		
T-weld			X	
10-in. (25.4-mm) Penetration				X
Hoop to Meridional Load Ratio = 2:1	X	X		
Strain Control Loading			X	X

All specimens were loaded in biaxial tension. Load was applied through an edge bar welded to the perimeter of each plate specimen. Details of the loading hardware are given in Figs. 5 and 6. All specimens were loaded statically beyond yield stress. Two tests were conducted using approximately 2:1 ratio of hoop to meridional load. Two tests were conducted with strain control following relationships calculated considering the liner plate as part of a prestressed concrete containment building subject to increasing internal pressure. Different configurations and loading arrangements resulted in data that permit a comparison of the effect of controlled variables on strain capability of liner plates.

Specimen behavior was measured using external instrumentation. Loads, deformations, and steel strains were measured.

*A secondary objective was to establish a biaxial loading procedure which could be used in the full scale Phase 2 specimens.

Tests were ended when limits of the loading hardware were reached rather than at maximum specimen strength or strain. The following comments are based on test results from Specimens ILP1 through ILP4. Where extrapolations are made to a typical prestressed RCB, the building has a 150-ft (45.7-m) diameter and a 4-ft (1.22-m) wall thickness.

1. Applied hoop loads at specimen yield were equivalent to a prestressed concrete RCB pressurization of approximately 115 psi (0.79 MPa). Overall specimen hoop strain at yield load was approximately 0.15%. This strain is equivalent to a prestressed concrete RCB diameter increase of approximately 0.21 ft (46 mm).

2. Maximum applied hoop loads were equivalent to a prestressed concrete RCB pressurization of over 144 psi (0.99 MPa). Overall specimen hoop strain at maximum load was on the order of 5%. This strain is equivalent to a prestressed concrete RCB diameter increase of over 7.5 ft (2.29 m).

3. None of the details of the four biaxial liner plate test specimens precipitated cracking. Hoop direction strain up to 5.7% was imposed without local distress.

General background material is presented in Reference 4.

PHASE 2 - FULL SIZE CONCRETE WALL ELEMENT TESTS WITH PENETRATIONS AND OTHER PERTURBATIONS

The objectives of this second phase are (1) to determine strength, deformation, and air leak-rate characteristics of full scale concrete wall elements and (2) to determine thermal response of liner plate anchored to concrete. Details for individual specimens are outlined in Table 3. Four square specimens (1 through 4) loaded in biaxial tension represent elements located in the containment cylinder wall. One rectangular specimen (5) loaded biaxially represents the junction region between wall and basemat. Two specimens (6 and 7) represent typical liner to wall anchorage for thermal studies.

Certain details of Specimen 1 parallel those of the specimens from the Phase 1 test program. Data from testing of Specimen 1 will be used to correlate results of Phase 1 with results of Phase 2. Specimens 2 through 7 are detailed based on the design practice which was employed in existing prestressed concrete RCB's. These specimens are full scale and completely representative of existing construction.

Square specimens range from 2 ft (0.6 m) to 3.5 ft (1.1 m) thick and from 5 ft (1.5 m) to 11 ft (3.4 m) square. Selected typical details employed in existing containment structures are used in the specimens. Details include liner plate welds,

TABLE 3 - PHASE 2 SPECIMEN DESIGN VARIABLES

Specimen Design Requirements	Specimen No.						
	1	2	3	4	5	6	7
Prestressed Concrete Design	X	X	X	X	X	X	
Reinforced Concrete Design							X
Biaxial Load	X	X	X	X	X		
Thermal Buckling						X	X
Leak-Rate Test		X	X	X	X		
5 ft (1525 mm) Square	X						
7 ft (2135 mm) Square		X	X			X	X
11 ft (3355 mm) Square				X			
7 ft x20 ft (2.1 m x 6.1 m)					X		
2.0 ft (610 mm) Thick	X						
2.7 ft (823 mm) Thick						X	X
3.5 ft (1065 mm) Thick		X	X	X	X		
36-in. (915-mm) Diameter Penetration Sleeve with Shear Studs				X			
Controlled Leak		X					
Wall-Base Discontinuity					X		
Discontinuous Angles for Anchorage			X		X		
Continuous Angles for Anchorage	X	X		X		X	
Studs for Anchorage							X

interrupted angle anchorages, and a large pipe penetration. Biaxial loads on each specimen are applied to ensure uniform strain across each face of the specimen as would occur on a hoop or meridional plane in a containment. This is accomplished by varying the ratio of reinforcement load to liner load during the test to simulate the load ratio that would be induced by their structural response as part of a containment wall. The test specimen with the penetration is also subjected to punching (peripheral) shear loads applied to the penetrations. Details of Specimen 4 are given in Fig. 7. Air leak-rate characteristics are determined while applying external loads, as well as a range of surface pressures.

Specimen 5 is rectangular and represents the basemat-junction region. This specimen is subjected to radial loading in addition to biaxial tension and surface air pressure. Specimens 6 and 7 are tested to represent conditions at and behavior of the liner plate during a sudden temperature increase in the containment. Surface heating and surface pressure are applied to the liner plate to observe any buckling modes. Leak rate is not measured in Specimens 5 through 7.

The biaxial test frame required for Phase 2 testing is shown in Fig. 8. The frame is a large prestressed concrete structure specially designed for the EPRI program at CTL. It provides the reactions for biaxial tension loads applied to the test specimens. The frame has the capacity to test a specimen up to 11 ft (3.4 m) square and 4 ft (1.1 m) thick. The total triaxial loading capacity is 50 million lb (222 MN).

The air leak-rate test fixture consists of two reaction slabs, O-rings, and a pressure chamber. The test specimen is positioned between the reaction slabs and the entire assembly is placed within the large biaxial test frame. The air leak-rate test fixture and reaction frame arrangement are shown in Fig. 9.

The thermal heating fixture required for testing Specimens 6 and 7 provides surface heating and air pressure. The fixture has the capacity to test a 7-ft (2.1-m) square specimen.

Results of the test program for Phase 2 should be available in 1985.

PHASE 3 - TESTS OF CONTAINMENT BUILDING SEGMENTS WITH STRUCTURAL DISCONTINUITIES

The objective of the third phase is to determine strength, deformation, and air leak-rate characteristics of concrete test specimens representative of structural discontinuities in containment vessels. Examples of such discontinuities include connection of wall and roof to ring beam and the intersection of the cylinder wall and basemat. Although specific test details have not yet been defined, pneumatic pressurization of large-scale, full 360° segments of a containment building are envisioned.

ACKNOWLEDGMENT

This work is supported by the Electric Power Research Institute, Palo Alto, California, as a part of Structural Integrity Research in the Nuclear Power Division's Risk Assessment Program. Mr. R. K. Winkleblack is the manager of this program for EPRI.

REFERENCES

1. Dunham, R.S., Rashid, Y.R., Yuan, K.A., Lu, Y.M., "Methods for Ultimate Load Analysis of Concrete Containments," Interim Technical Draft Report to the Electric Power Research Institute, Inc., Anatech International Corporation, December, 1983.

2. Julien, J.T., Weinmann, T.L., and Schultz, D.M., Concrete Containment Structural Element Tests Phase 1 - Final Report, "Volume I - Half-Thickness Element Tests: Descriptions and Results," report to Electric Power Research Institute, Inc., Palo Alto, California, submitted by Construction Technology Laboratories, a Division of the Portland Cement Association, March, 1984.

3. Julien, J.T., Weinmann, T.L., and Schultz, D.M., Concrete Containment Structural Element Tests Phase 1 - Final Report, "Volume II - Half-Thickness Element Tests: Detailed Test Data," report to Electric Power Research Institute, Inc., Palo Alto, California, submitted by Construction Technology Laboratories, a Division of the Portland Cement Association, March, 1984.

4. Hanson, N.W., Julien, J.T., Schultz, D.M., and Weinmann, T.L., Concrete Containment Structural Element Tests Phase 1 - Final Report, "Volume III - Liner Plate Tests," report to Electric Power Research Institute, Inc., Palo Alto, California, submitted by Construction Technology Laboratories, a Division of the Portland Cement Association, March, 1984.

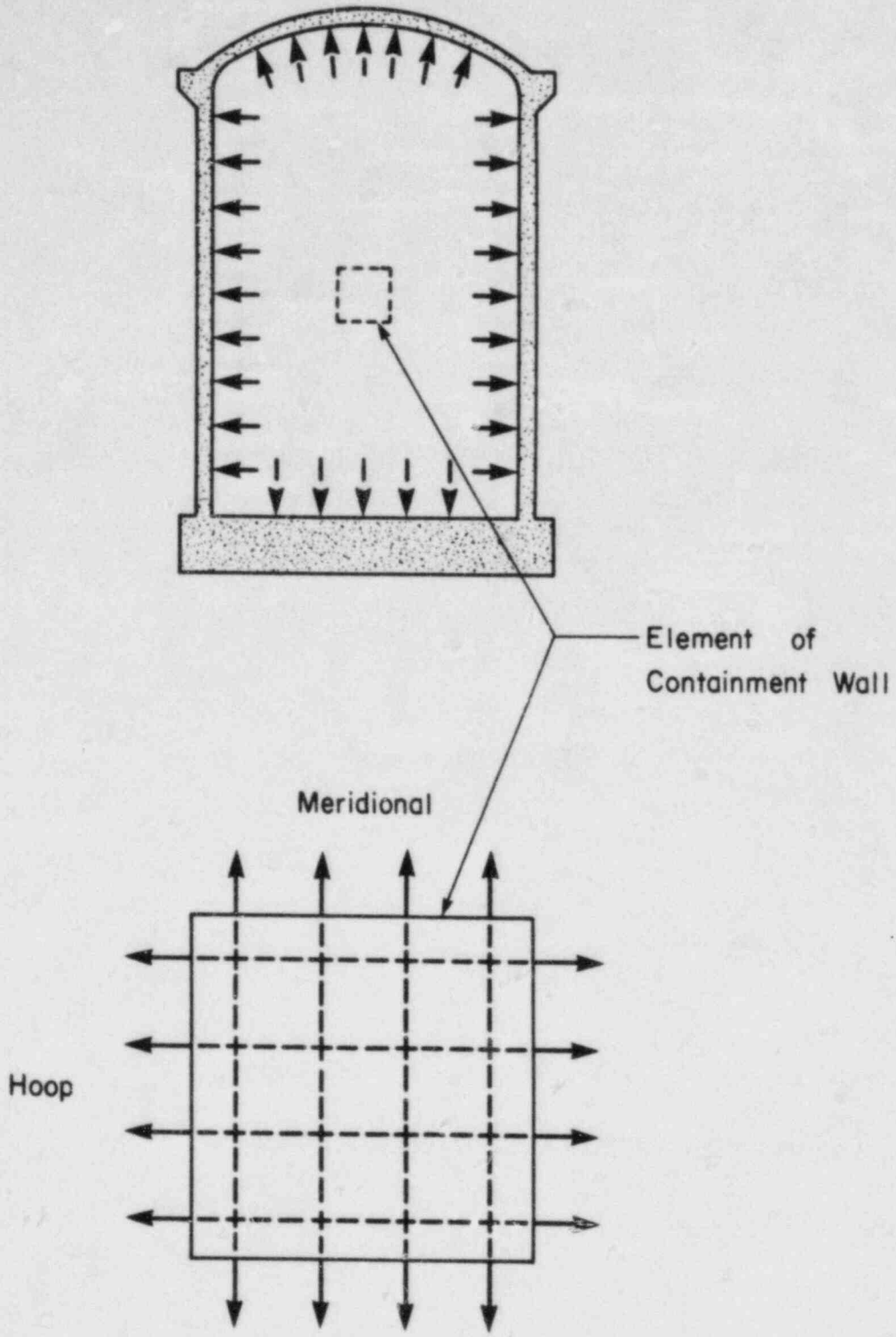

Figure 1. Biaxial Tension Due To Internal Pressurization

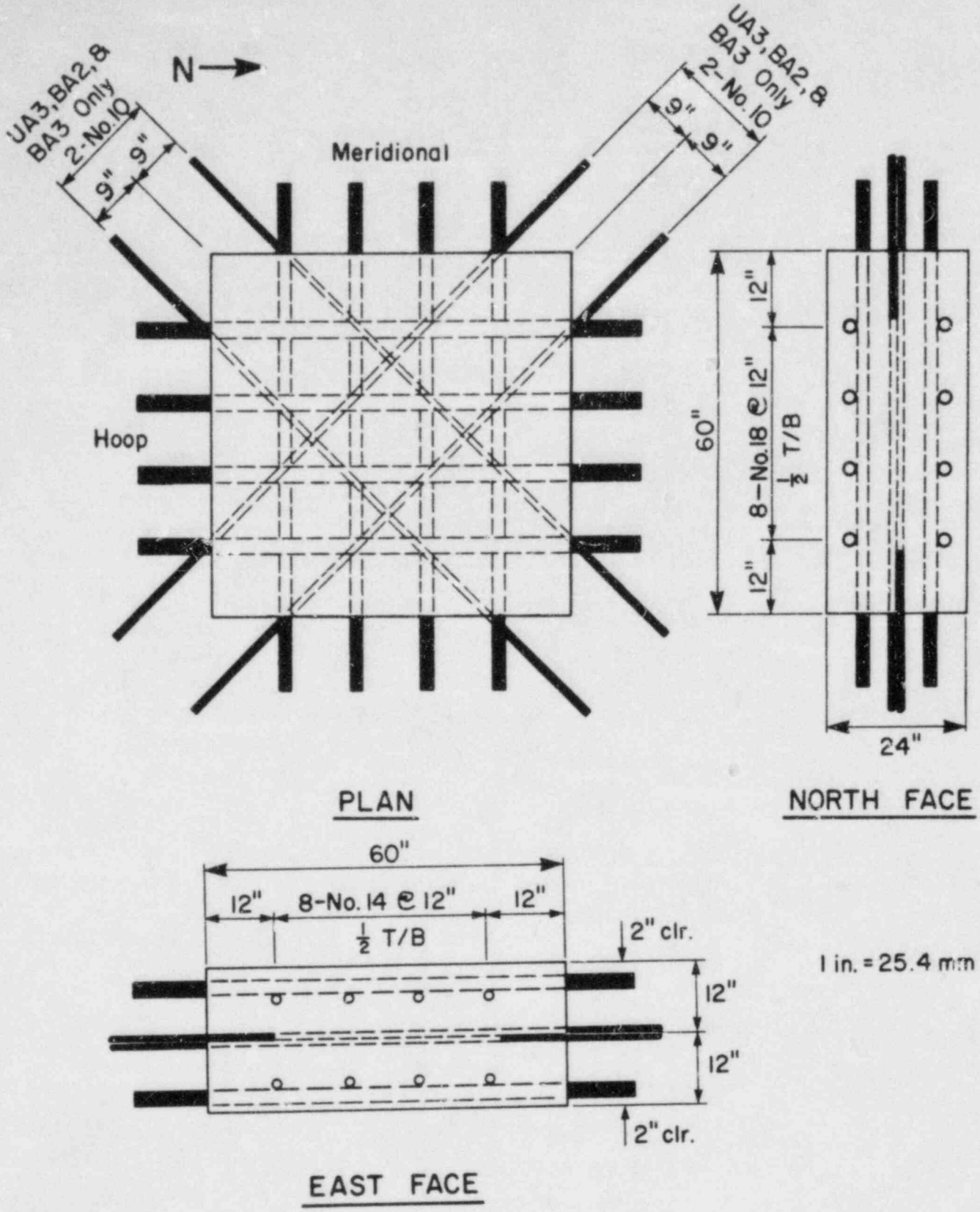

Figure 2. Reinforcement Details For Specimens UA3, BA1, BA2, and BA3

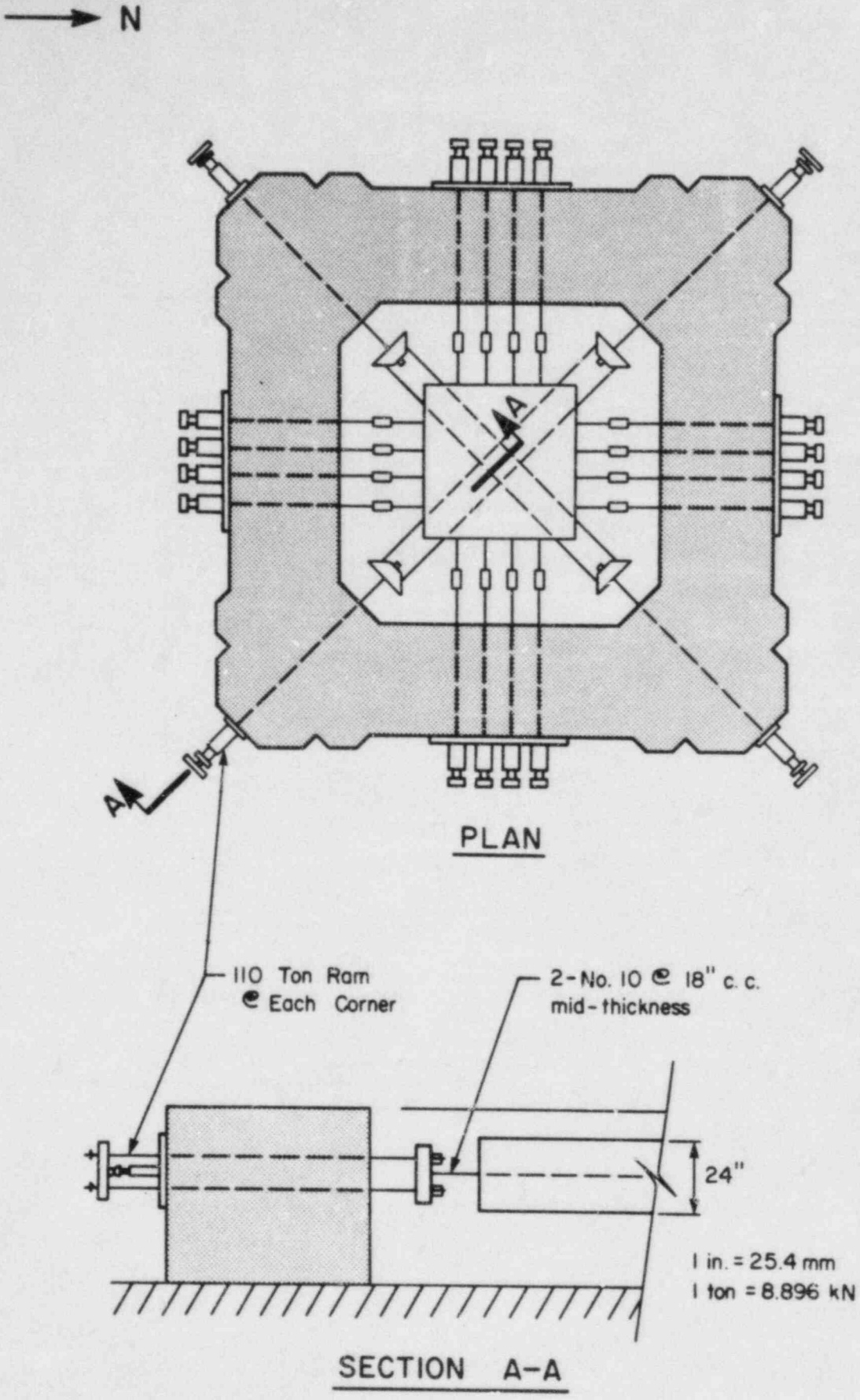

Figure 3. Biaxial and Biaxial Plus Diagonal Loading Systems for Half-Thickness Concrete Wall Specimens

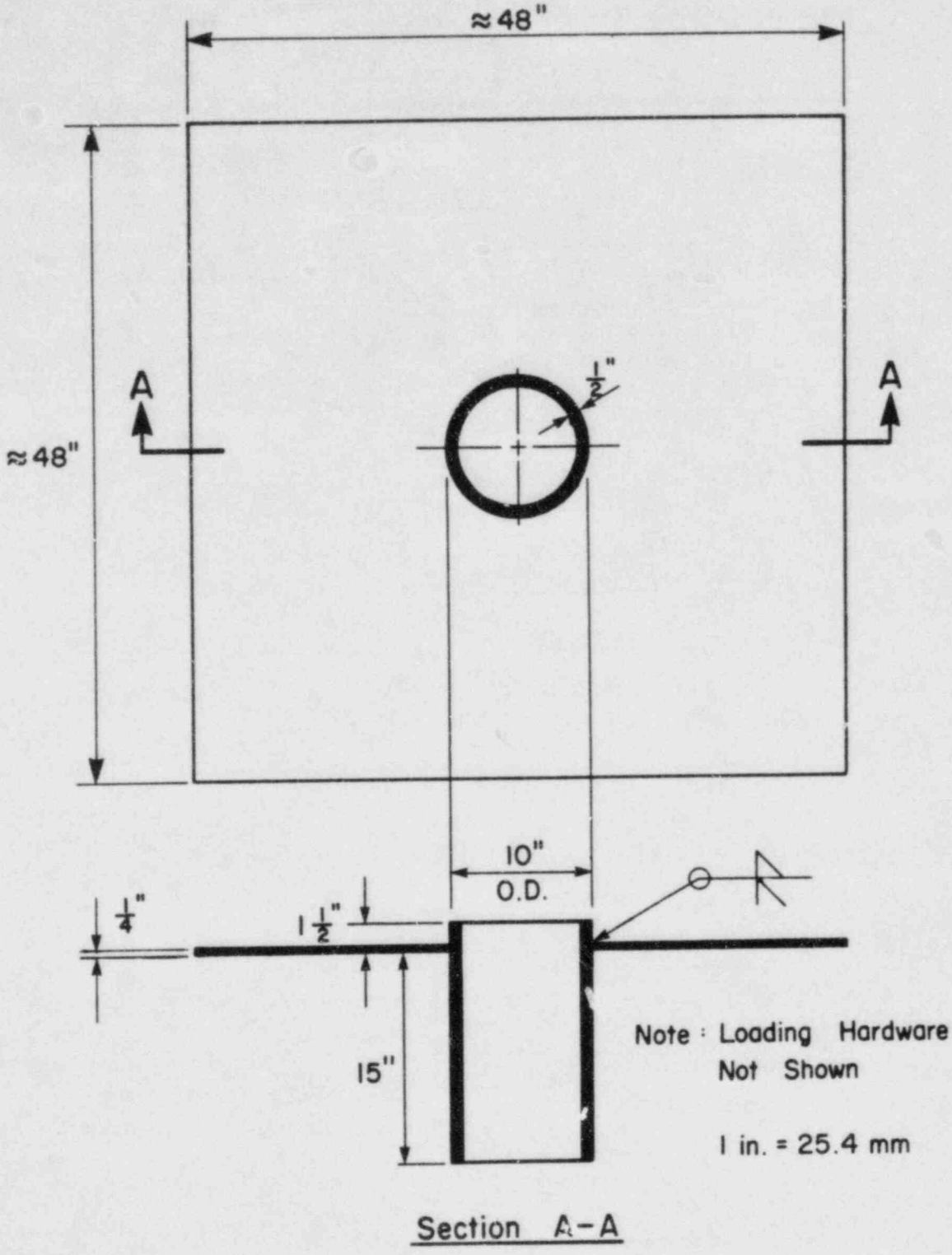

Figure 4. Details of Phase 1 Specimen ILP4

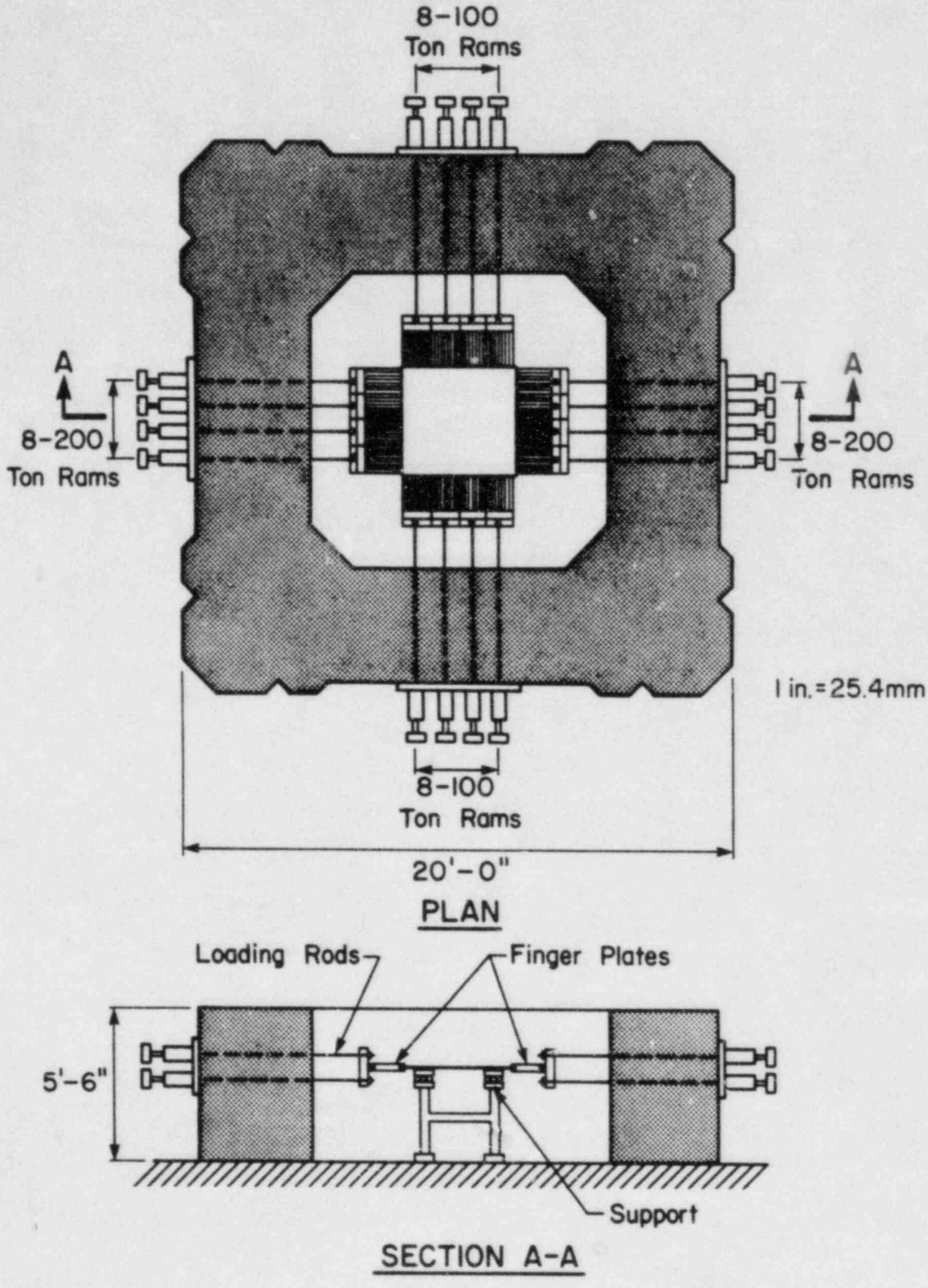

Figure 5. Biaxial Loading System For Phase 1 Liner Plate Specimens

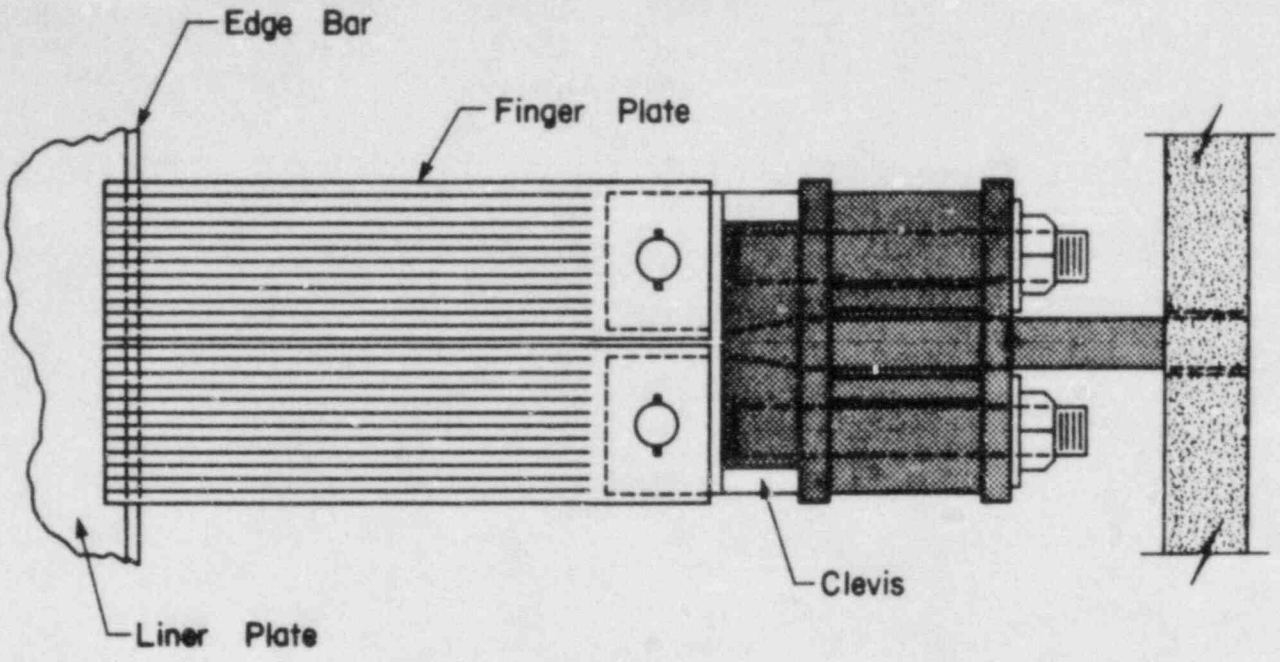

PLAN

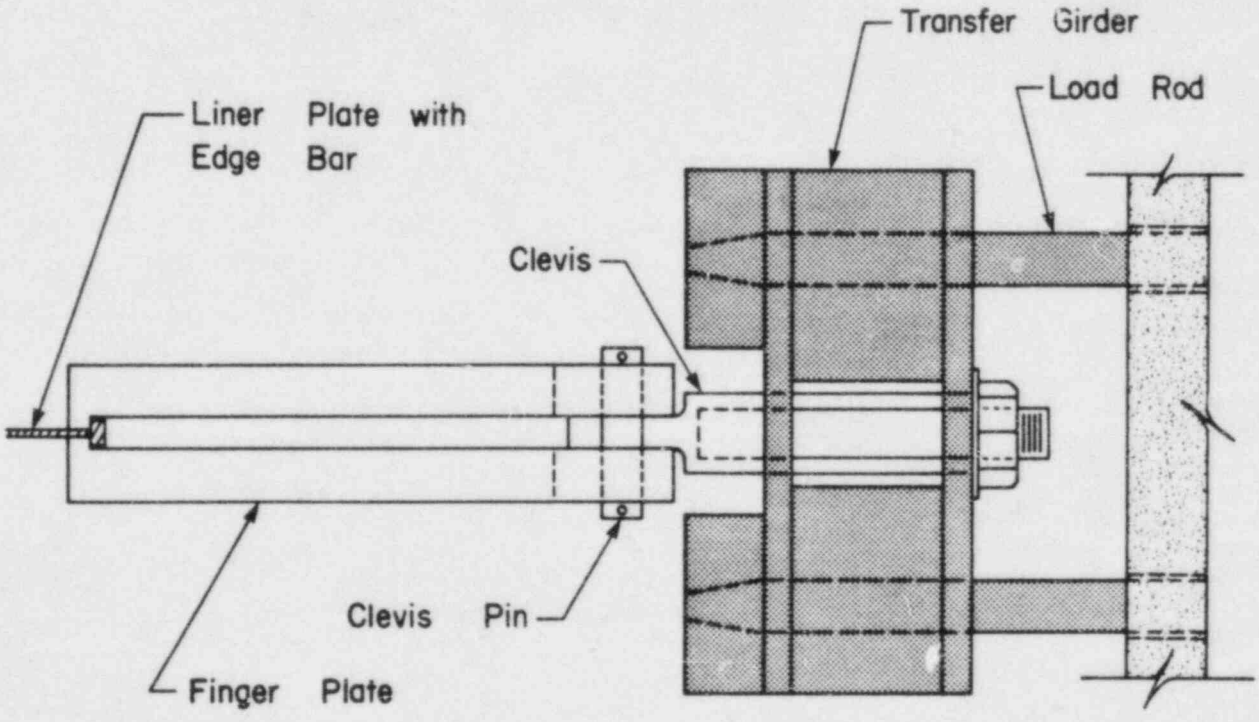

ELEVATION

Figure 6. Finger Plate Loading Hardware Details For Phase 1 Liner Plate Specimens

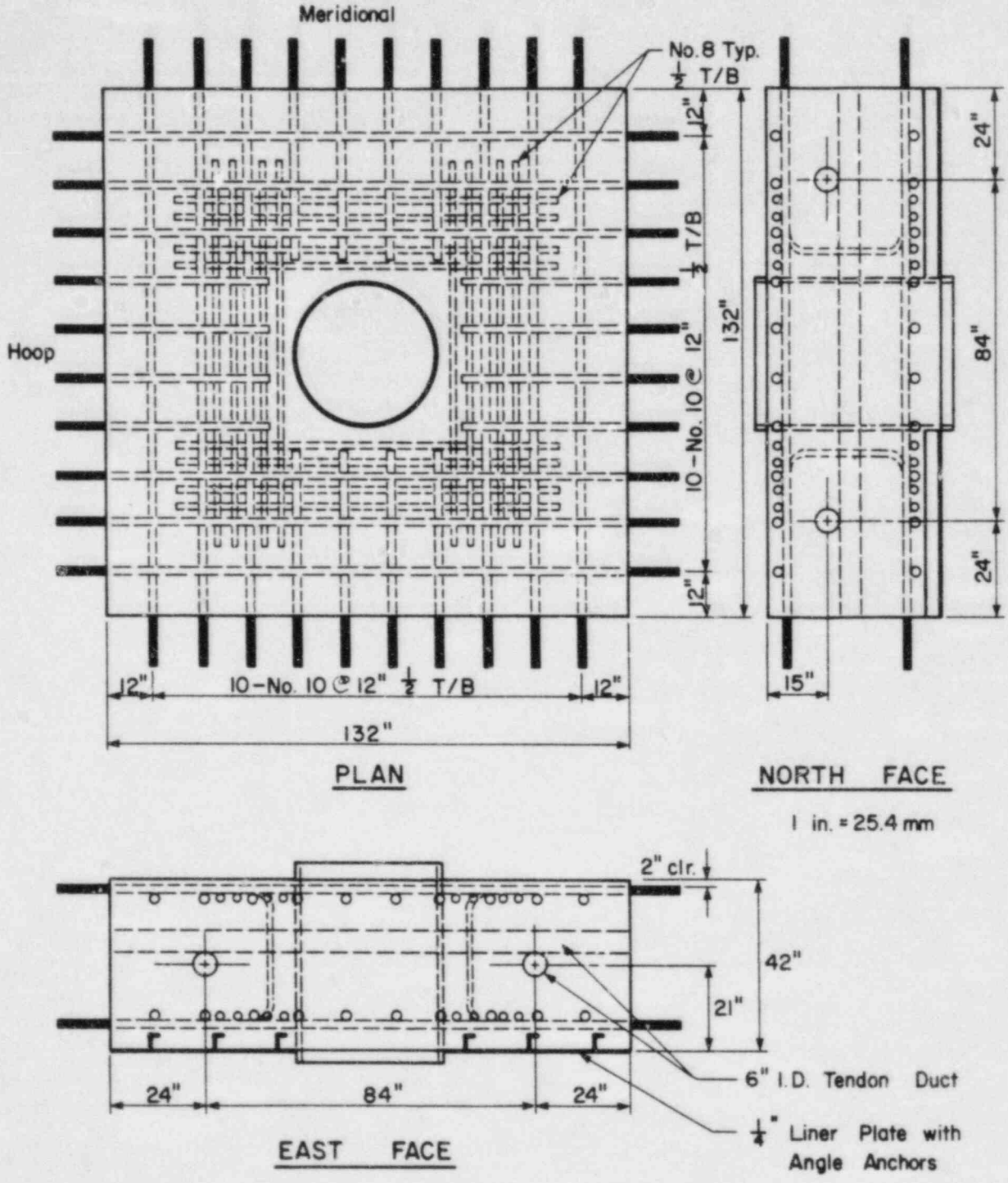

Figure 7. Reinforcement Details For Phase 2 Specimen 4

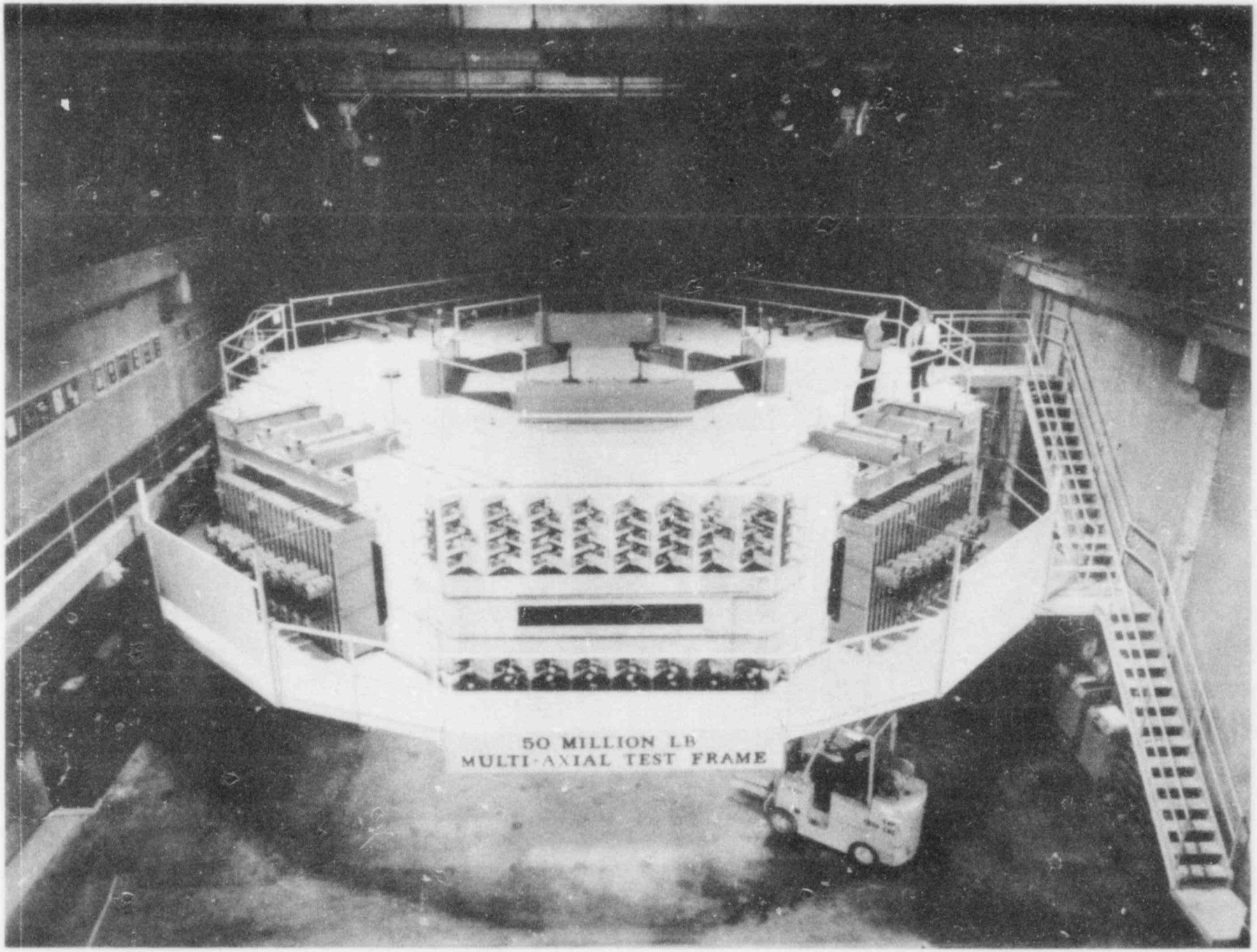

Figure 8. Biaxial Test Frame

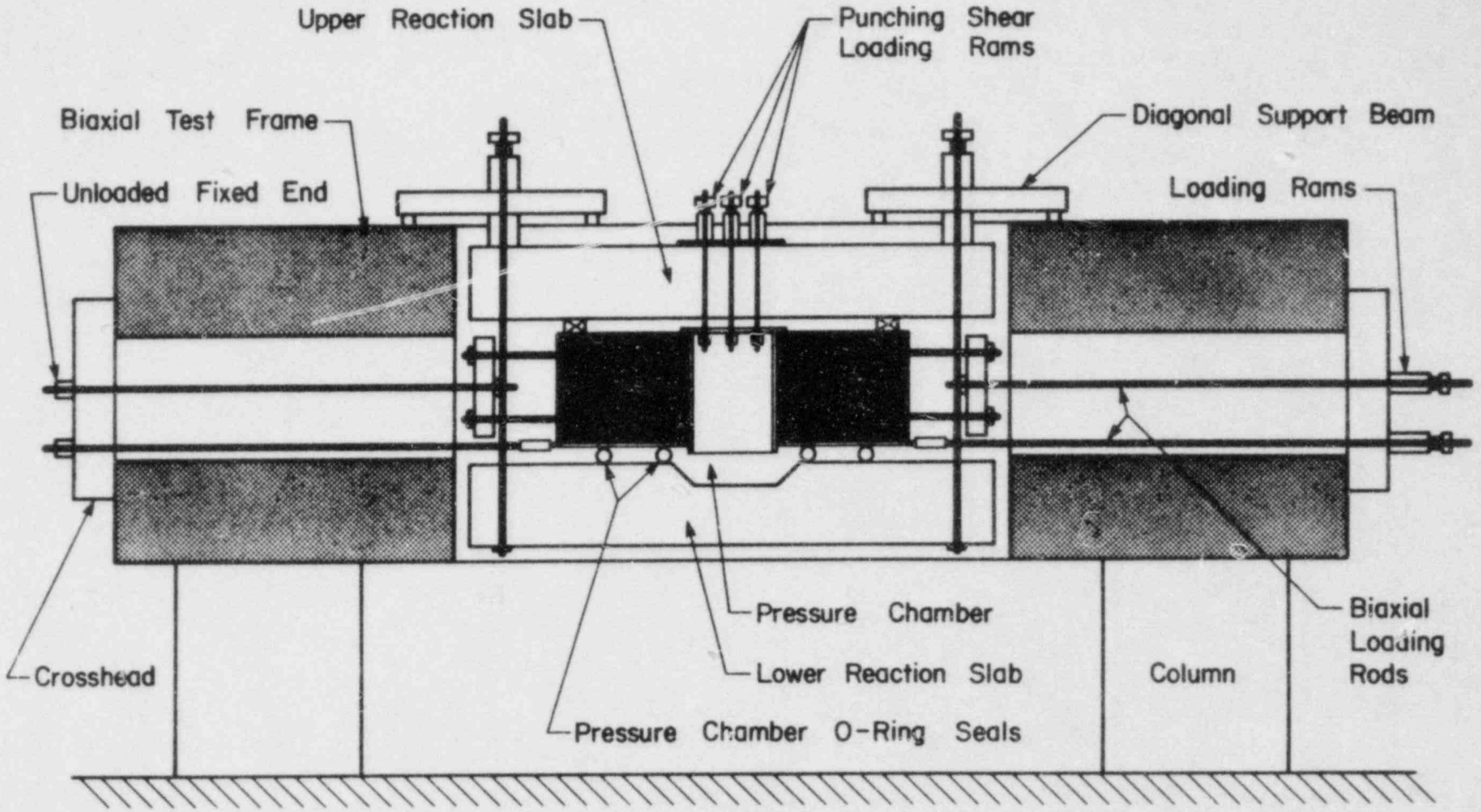

Figure 9. Cross-Section Of Air Leak-Rate Test Fixture and Biaxial Test Frame

LINER INTEGRITY IN OVERPRESSURIZED POST-TENSIONED CONCRETE CONTAINMENTS

C. N. Krishnaswamy and R. Namperumal
Sargent & Lundy
55 East Monroe
Chicago, IL 60603

ABSTRACT

This paper discusses the ultimate internal pressure capacity and the corresponding liner strains of typical post-tensioned PWR and BWR Mark II containments and concludes that the leaktight integrity of the liner plate will not be impaired at the computed ultimate capacity of the pressure boundary.

The probable modes of failure of the pressure boundary and conservative failure criteria for defining ultimate pressure capacity are described. Simple equations based on force equilibrium considerations are presented to manually compute the ultimate capacity and the nonlinear response of the critical membrane section in the concrete pressure boundary. Results of nonlinear finite element analyses and field data on containment wall displacement response measured during overpressure testing of these containments are used to corroborate the equations presented. Nonlinear response plots of internal pressure versus containment wall displacement and versus strains in the liner, reinforcing bars, and post-tensioned tendons at the most stressed section in the containments are presented.

It is shown that the maximum liner strain at the computed ultimate pressure is well within the values allowed in the ASME Code to ensure leaktightness of the containment liner. The effect of strains imposed on the liner by creep and shrinkage of concrete and by restrained thermal expansion of the liner are discussed. It is also shown that the strain level in the weld seams in the liner plate is not critical and is always less than its yield.

1. INTRODUCTION

The lesson learned from the accident at the Three Mile Island (TMI) nuclear plant has necessitated the determination of the ultimate internal pressure capacity of the containment structure as a licensing requirement in the U. S. Analytical studies and scale model tests of containment structures confirm that the containment pressure boundary is structurally capable of withstanding several times the magnitude of the design accident pressure. Recently, however, increased attention has been given the structural capacity being limited by excessive leakage resulting from rupture of the containment liner.

This paper reports on the determination of the ultimate internal pressure capacity and the corresponding liner strains of two typical post-tensioned concrete containments shown in Figures 1 and 2. The design accident internal pressure for the BWR Mark II containment shown in Figure 1 is 45 psig and that for the PWR containment shown in Figure 2 is 47 psig. The principal dimensions of the containments are shown in the figures. Both containments are lined on the inside with a 1/4-inch thick steel plate to ensure leaktightness. Each containment is provided with an equipment hatch, personnel lock, and necessary electrical and piping penetrations through the wall.

The probable modes of failure and the critical containment sections are described in Section 2. Conservative criteria for determining structural failure and ultimate capacity are defined in Section 3. Equilibrium equations to manually compute the ultimate capacity and nonlinear response at membrane sections of the concrete shell are presented in Section 4. A nonlinear axisymmetric finite element analysis performed to obtain the response of the entire shell including nonmembrane sections and to verify the manually computed results is described in Section 5. Results of the analysis and field data on containment response measured during overpressure tests, leaktightness of liner, and thermal effects are discussed in Section 6.

2. POSSIBLE FAILURE MODES AND CRITICAL SECTIONS

As the internal pressure builds up beyond the design value due to a more severe postulated accident, failure of the containment pressure boundary can result from one or more of the following causes:

a. failure of concrete in secondary compression

b. failure in flexural shear at discontinuities

c. failure in peripheral shear around penetrations

d. failure of steel pressure retaining components by buckling or by rupture

e. failure of containment liner by rupture

f. rupture of post-tensioning tendons

g. separation of the steel drywell head (BWR Mark II) from the containment wall

The potential critical sections associated with the failure modes of the pressure boundary backed by concrete are shown in Figures 1 and 2.

3. FAILURE CRITERIA FOR ULTIMATE CAPACITY

Though the ultimate failure of the containment may occur well past general yielding of the critical section with attendant large displacements, the capacity of the containment is conservatively defined here as the attainment of any one of the following limits:

a. tensile yielding of post-tensioning tendons (corresponding to a strain of 0.01 in./in.) resulting in a state of general yielding of any section

b. shear capacity of the containment in flexural shear or peripheral shear

c. buckling or yielding of steel pressure retaining components

d. rupture of containment liner

These limits are conservative. There is some reserve capacity beyond the limits defined above.

4. EQUATIONS OF EQUILIBRIUM

In general, a containment structure is designed to be essentially elastic under the design pressure. However, as the postulated internal overpressure is assumed to build up and reach the ultimate, the containment response will turn nonlinear as it sequentially passes through cracking of concrete, yielding of liner plate, yielding of reinforcing steel, and yielding of tendons. For these critical response stages, the internal pressure capacity at a membrane hoop section can be predicted by means of the following equations based on equilibrium considerations.

The internal force P per foot width of the shell at a membrane section can be computed as:

Force/ft at the start of pressurization,

$$P_o = \text{dead load} + \text{prestress} \qquad (1)$$

Force/ft at concrete cracking,

$$P_{cr} = A_c E_c \varepsilon_{cr} + (n-1)(A_l + A_s + A_t) E_c \varepsilon_{cr} + P_o \qquad (2)$$

Force/ft just after concrete cracking,

$$P_{cr} = E_s \varepsilon'_{cr} (A_l + A_s + A_t) + P_o \qquad (3)$$

Force/ft at liner yielding,

$$P_{yl} = E_s (\varepsilon_{yl} - \varepsilon'_{cr})(A_l + A_s + A_t) + P_{cr} \qquad (4)$$

Force/ft at rebar yielding,

$$P_{ys} = E_s (\varepsilon_{ys} - \varepsilon_{yl}) (A_s + A_t) + P_{yl} \quad (5)$$

Force/ft at tendon yielding,

$$P_{yt} = E_s (\varepsilon_{yt} - \varepsilon_{ys}) A_t + P_{ys} \quad (6)$$

where:

A_c = Gross area of concrete per foot of shell

A_l, A_s, A_t = Area of liner, rebar, and tendon, respectively per foot of shell

ε_{cr} = Cracking strain in concrete

ε'_{cr} = Strain just after concrete cracking

$\varepsilon_{yl,ys,yt}$ = Yield strain in liner, rebar, and tendon, respectively

E_c = Modulus of elasticity for concrete

E_s = Modulus of elasticity for steel (liner, rebar, and tendon)

n = Modular ratio

The internal pressure corresponding to any of the response stages is then obtained as

$$p = P/R \quad (7)$$

where:

P = Force per foot of shell

R = Radius of the containment at the section considered

Also, the radial displacement, $\Delta = R.\varepsilon$ (8)

Equations (2) through (6) include the liner as a strength element. If the liner acts as a nonstrength element, A_l should be set equal to zero in these equations.

Using the above equations and the properties listed in Figures 1 and 2, the response and pressure capacity of the example containments were computed at the most stressed section under design pressure, which is the membrane section near midheight of the containment cylinder.

5. FINITE ELEMENT ANALYSIS

A nonlinear axisymmetric finite element analysis of these containment shells under incremental internal pressure was performed to verify the manually computed results and to determine the nonlinear behavior of the entire shell including nonmembrane sections. The analysis model consisted of laminated shell finite elements to represent the liner, concrete, reinforcing steel layers and post-tensioning tendons. Nonlinear stress-strain property of each material was considered. Only material nonlinearity was considered; geometric nonlinearity was ignored because of small displacements for concrete shell structures.

Since membrane tension controls the response under overpressure, concrete was idealized as a linearly elastic and perfectly plastic material in compression and linearly elastic up to $6\sqrt{f'_c}$ in tension. Failure criterion for concrete under biaxial stresses is shown in Figure 3.

Material strengths obtained from uniaxial test specimens were used. The dead load of the structure, the hydrostatic load on the suppression pool boundary (BWR Mark II), post-tension loads, and the incremental internal pressure were applied simultaneously. Incremental internal pressure was applied as the structure passed through the critical response stages of concrete cracking, liner yielding, rebar yielding, and tendon yielding.

The computer program, DYNAX, used for the shell analysis is based on Reference 1. The mechanics of nonlinear analysis of laminated shells is described in References 2 and 3. The internal pressure due to the postulated accident was treated as quasi-static based on the investigation reported in Reference 4.

6. DISCUSSION OF RESULTS

6.1 Containment Response and Pressure Capacity

Results of the nonlinear finite element analysis confirmed that the most stressed section under design pressure, namely the membrane hoop section near midheight of the cylinder, remained the most stressed section all the way up to failure. This was true for both the BWR and PWR containments. This behavior was anticipated since: (1) the meridional flexural critical section at the containment wall-basemat junction is typically designed for discontinuity

bending moments based on elastic analyses, which is conservative, and (2) unlike membrane tension, the discontinuity moment and shear do not increase linearly with internal pressure since the wall stiffness decreases more than linearly with pressure.

The structural response and pressure capacity obtained from the nonlinear finite element analysis and from equilibrium equations presented in Section 4 were almost identical.

The response of the concrete pressure boundary of the BWR containment as it passes through critical stages of concrete cracking, liner yielding, rebar yielding and tendon yielding is shown in Figure 4. The ultimate capacity is 228 psig, which is about 5 times the design pressure of 45 psig and corresponds to incipient yielding of the hoop tendons in the membrane section near midheight of the cylinder. The pressure magnitudes and the corresponding wall displacements and strains in the containment liner, reinforcing bars, and post-tensioning tendons at the most stressed section are presented in Table 1.

Table 1

BWR CONTAINMENT RESPONSE TO INTERNAL PRESSURE*

	Containment Response Stage	Internal Pressure (psig)	Radial Displacement (inch)	Liner Strain (in./in.)
1.	Zero internal pressure	0	-0.12	-0.0002
2.	Concrete cracking	144	0.06	0.0001
3.	Personnel airlock bulkhead yielding**	150	0.56	0.0010
4.	Liner yielding	162	0.74	0.0014
5.	Rebar yielding	192	1.25	0.0023
6.	Tendon yielding	228	3.00	0.0054

*At the most stressed (hoop) section near midheight of suppression pool cylinder.

**Pressure boundary not backed by concrete.

The response of the concrete pressure boundary of the PWR containment is shown in Figure 5. The ultimate capacity is 134 psig, which is 2.85 times the design pressure of 47 psig. This corresponds to incipient yielding of the hoop tendon in the membrane section near midheight of the cylinder wall. The pressure magnitudes, the corresponding wall displacements and strains are presented in Table 2.

Table 2

PWR CONTAINMENT RESPONSE TO INTERNAL PRESSURE*

	Containment Response Stage	Internal Pressure (psig)	Radial Displacement (inch)	Liner Strain (in./in.)
1.	Zero internal pressure	0	-0.20	-0.0002
2.	Concrete cracking	86	0.09	0.0001
3.	Liner yielding	105	1.44	0.0017
4.	Rebar yielding	117	2.00	0.0023
5.	Equipment hatch flange gusset and liner yielding	130	3.80	0.0044
6.	Tendon yielding	134	4.43	0.0052

* At the most stressed (hoop) section near midheight of suppression pool cylinder.

A separate linear elastic analysis was performed to determine the ultimate capacity of the pressure boundary not backed by concrete such as the equipment hatch, personnel locks, electrical penetrations, steel drywell head, etc. Details of the analysis are outside the intended scope of this paper and therefore only the results are used for this discussion. The personnel airlock in the example BWR containment has a capacity of about 150 psig and the equipment hatch in the example PWR containment has a capacity of about 130 psig. Typically, the steel pressure boundary components of the equipment hatch or personnel lock may govern the ultimate pressure capacity of concrete containments.

Results of the finite element analysis and field data on the containment wall radial displacement measured during overpressure testing of the BWR Mark II containment are presented in Table 3. During the overpressure testing, the containment was incrementally pressurized to 1.15 times the design pressure. The radial displacements were measured at six points equally spaced along the circumference of the containment wall. The maximum of all six measurements and their average at each pressure level are listed in the table. The measured responses are also plotted in the containment response curve shown in Figure 4. The measured responses are in excellent agreement with the predicted responses demonstrating adequacy of the analysis procedures.

The ultimate capacities reported previously for concrete pressure boundaries are lower bound values because of the conservative nature of the failure criteria defined in Section 3. Nonlinear analysis to realize the reserve capacity beyond the lower bound may be worthwhile only if the attendant large displacements can be functionally tolerated, and if the pressure boundary not backed by concrete has higher capacity.

Table 3

BWR CONTAINMENT OVERPRESSURE PROOF TEST RESPONSE*

Measured and Predicted Radial Displacements

Internal Pressure (psig)	Measured Maximum (inch)	Measured Average (inch)	Predicted Average (inch)
0.0	0.000	0.000	0.000
13.9	0.024	0.015	0.017
23.0	0.033	0.024	0.029
33.0	0.043	0.033	0.041
43.0	0.052	0.042	0.054
52.4**	0.061	0.052	0.066

* At the most stressed (hoop) section near midheight of suppression pool cylinder.

** Peak test pressure = 1.15 x design pressure.

6.2 Liner Leaktightness

The strains imposed on the liner by concrete prestress and incremental internal pressure are traced in Figure 4 for the BWR containment and in Figure 5 for the PWR containment. Until the concrete starts cracking the strains in the liner are controlled by concrete. The liner strains are linear in this range. This is also verified by the field data obtained from the overpressure testing of the BWR containment and plotted on the containment response curve shown in Figure 4.

Once concrete starts cracking, the strains in the liner as well as the rebar and the post-tensioned tendon increase more rapidly under increasing pressure. This is indicated by progressive flattening of the curve beyond the pressures corresponding to concrete cracking, liner yielding, and rebar yielding. This nonlinear liner strain response was also evidenced by scaled model testing of a High-Temperature Gas Cooled Reactor (HTGR) pressure vessel [5].

The magnitudes of liner strains at critical stages of containment response are listed in Table 1 for the BWR containment. The liner strain at 228 psig, the ultimate capacity of the concrete pressure boundary, is 0.0054 in./in. At 150 psig, the ultimate capacity of the steel pressure boundary, the liner strain is below its yield limit.

Liner strains in the PWR containment are listed in Table 2. The maximum tensile strain in the liner at 134 psig, the ultimate capacity of the concrete pressure boundary, is 0.0052 in./in. At 130 psig, the ultimate capacity of the steel pressure boundary, the liner strain is 0.0044 in./in.

The actual tensile strain level in the liner will be lower than the values discussed if compressive strains due to restrained thermal expansion, creep, and shrinkage discussed in Section 6.5 are also included. The ASME Code, Section III, Division 2 on the design of concrete containment liner defines the allowable strains in the liner to ensure leaktightness of the liner plate. With reference to these allowables, maximum strains in the liner corresponding to the computed ultimate capacities did not indicate a potential for degradation of leaktight integrity of the liner. It should also be noted that these strain levels exist only at the most stressed section and are lower at all other points. Therefore, greater overall leaktightness is inherent.

6.3 Strain Concentration Effects Around Penetrations

6.3.1 Large Penetrations

The actual strains in the containment liner locally around penetrations may be greater than the overall liner strain because of possible strain concentration. The equipment hatch opening of a typical (PWR) containment with a thickened boss around the opening is shown in Figure 6. During the overpressure integrity testing of the containment, liner strain around the hatch opening was obtained at 12 locations as shown in the figure. The values obtained at the peak test pressure are listed in Table 4. Also, the strains measured on the wall liner at points farther away from the equipment hatch are listed in Table 5. The measured strain values indicate that there is no strain concentration effect around the embossed hatch opening.

Table 4

PEAK STRAINS NEAR EQUIPMENT HATCH IN A PWR CONTAINMENT

Measured at 52 psig During Overpressure Proof Test

Strain Gage Location	Hoop Strain (Micro in./in.)	Vertical Strain (Micro in./in.)
1	-53	10
2	153	-17
3	0	7
4	40	40
5	-183	-57
6	93	-40
7	-197	-130
8	30	-133
9	357	223
10	173	253
11	427	233
12	330	147

6.3.2 Small Penetrations

Tests conducted on a specimen containing four unreinforced penetration openings [6] measured local strain concentrations up to 0.018 in./in. in the liner, which was almost five times the overall strains in the specimen. No signs of failure in the liner plate or in the welds joining the liner plate and penetration liner were found even though the maximum strain was increased eventually to 0.048 in./in.

Table 5

PEAK LINER STRAINS IN PWR CONTAINMENT WALL

Measured at 52 psig During Overpressure Proof Test*

Strain Gage Location (Azimuth)	Hoop Strain (Micro in./in.)	Vertical Strain (Micro in./in.)
1°	433	113
61°	313	120
241°	283	140
301°	393	83

*At the same elevation as that of strain gage 12 of Table 4.

6.4 Seam-Weld Integrity

The weld at liner seams has a substantially higher yield strength than the liner plate. Force equilibrium at the liner seam will require that the stress at the seam does not exceed the yield stress of the liner. Consequently, the strain level in the liner weld is not critical and is always less than its yield value.

6.5 Thermal, Shrinkage, and Creep Effects

Constraint to liner thermal expansion under accident temperature imposes compression in the liner and tension in the restraining containment wall. The combined restrained strain in the liner due to accident temperature, creep, and shrinkage varies from 0.002 in./in. to 0.003 in./in. This restraining compression is offset by the tension induced by pressure. Therefore, buckling of the liner under tension is not likely when the high internal pressure tends to brace the liner against concrete. Also, the pressure-induced tensile strain in the liner is partly compensated by compressive strain induced by creep, shrinkage, and restrained thermal expansion. The net strain level in the liner is within the values allowed by the ASME code to ensure leaktightness of the liner.

When general yielding of the post-tensioned steel occurs, loads due to restrained thermal expansion of the liner are fully relieved. Therefore, this is not a factor affecting the ultimate pressure capacity of the concrete pressure boundary.

7. CONCLUSIONS

Based on the foregoing discussion, the following conclusions are in order:

a. At membrane sections of the concrete pressure boundary, the nonlinear response and ultimate capacity can be manually computed using simple equilibrium equations.

b. The hoop membrane section near midheight of the cylinder, which was the most stressed section under design pressure, remained critical all the way up to the ultimate pressure.

c. Computed liner strains indicate that the leaktightness of the liner will not be impaired at the computed ultimate pressure.

d. There is no strain concentration effect around embossed large penetration openings.

e. Liner rupture is not likely to occur around small penetrations at the computed ultimate pressure.

f. Restrained deformation loads due to thermal expansion, creep, and shrinkage are relieved at ultimate and do not affect the true ultimate capacity.

REFERENCES

[1] S. Ghosh and E.I. Wilson, "Dynamic Stress Analysis of Axisymmetric Structures Under Arbitrary Loading," EERC Report 69-10, College of Engineering, University of California, Berkeley, April 1969.

[2] T.P. Khatua, et al., "Application of the Finite Element Method to the Nonlinear Analysis of RC Structures," ASME Convention and Exposition, Chicago, October 16-20, 1978, Preprint 3427.

[3] C.S. Lin and A.C. Scordelis, "Nonlinear Analysis of RC Shells of General Form," Journal of the ASCE, Structural Division, Vol. 101, No. ST3, Proceedings Paper 11164, March 1975, pp. 523-538.

[4] R. Kamil, et al., "Investigation of the Behavior of TMI-2 Containment Structure for Hydrogen Burn Accidents," Paper J5/8, SMiRT 6, Paris 1981.

[5] "Prestressed Concrete Reactor Vessel Model 1, AEC Research and Development Report GA-7097, General Atomics, October 25, 1966.

[6] A.G. Young and L.A. Tate, "Design of Liners for Reactor Vessels," Conference on Prestressed Concrete Pressure Vessels, Institution of Civil Engineers, London 1967.

Figure 1--BWR Mark II Post-Tensioned Concrete Containment

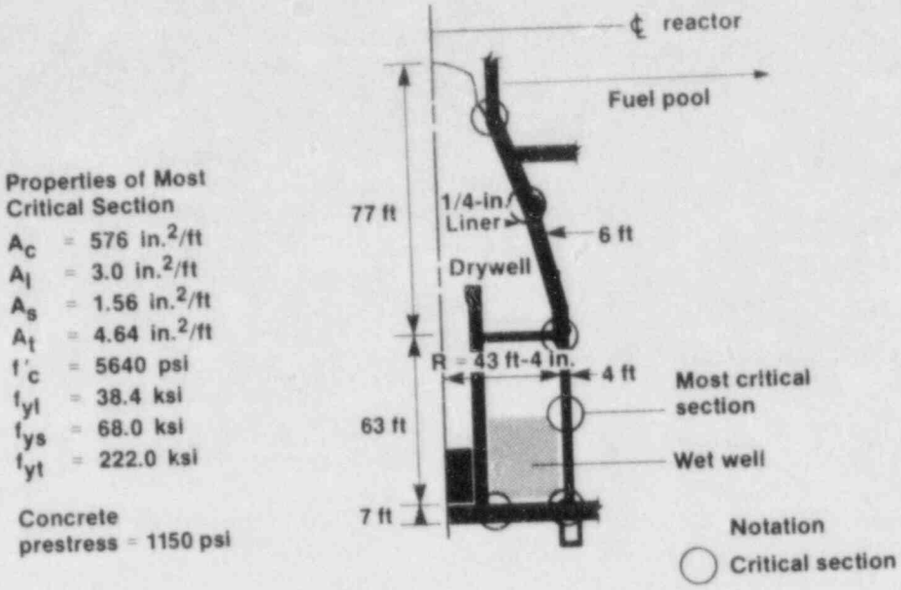

Figure 2—PWR Post-Tensioned Concrete Containment

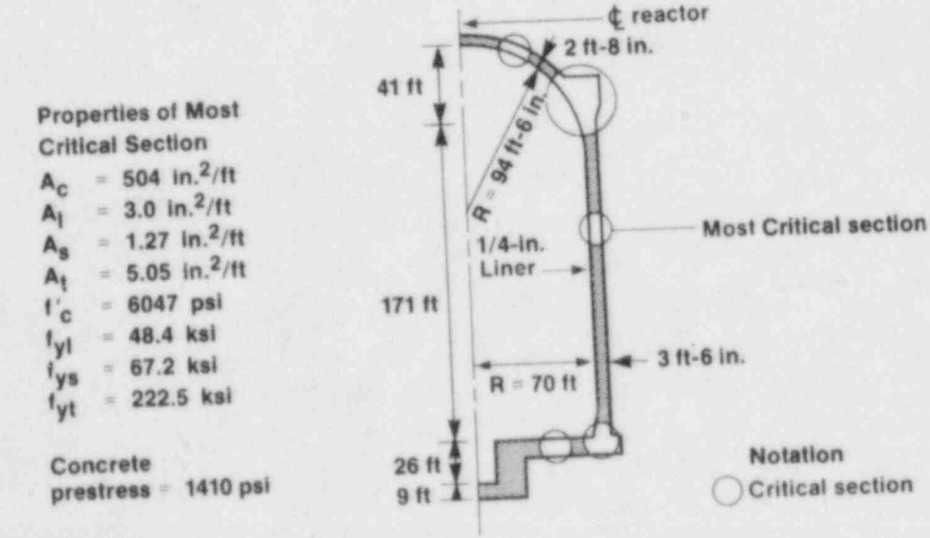

Figure 3—Failure Criterion for Concrete Under Biaxial Stress

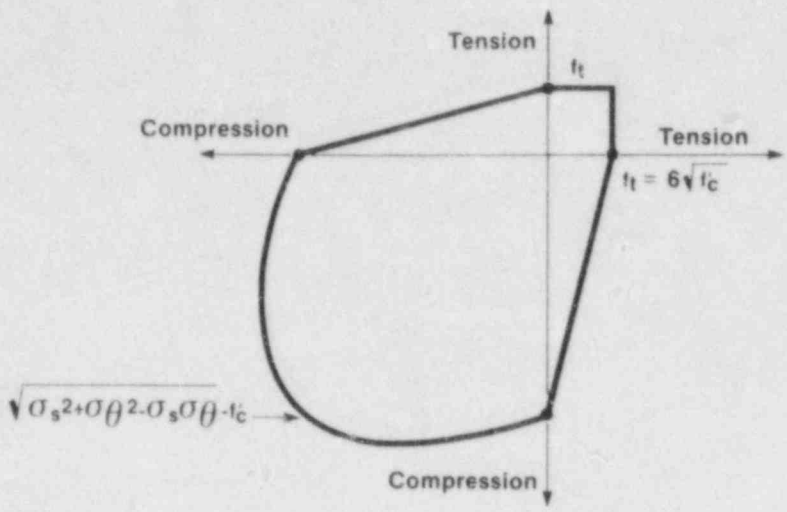

Figure 4—Response of BWR Mark II Post-Tensioned Concrete Containment at the Most Stressed Section

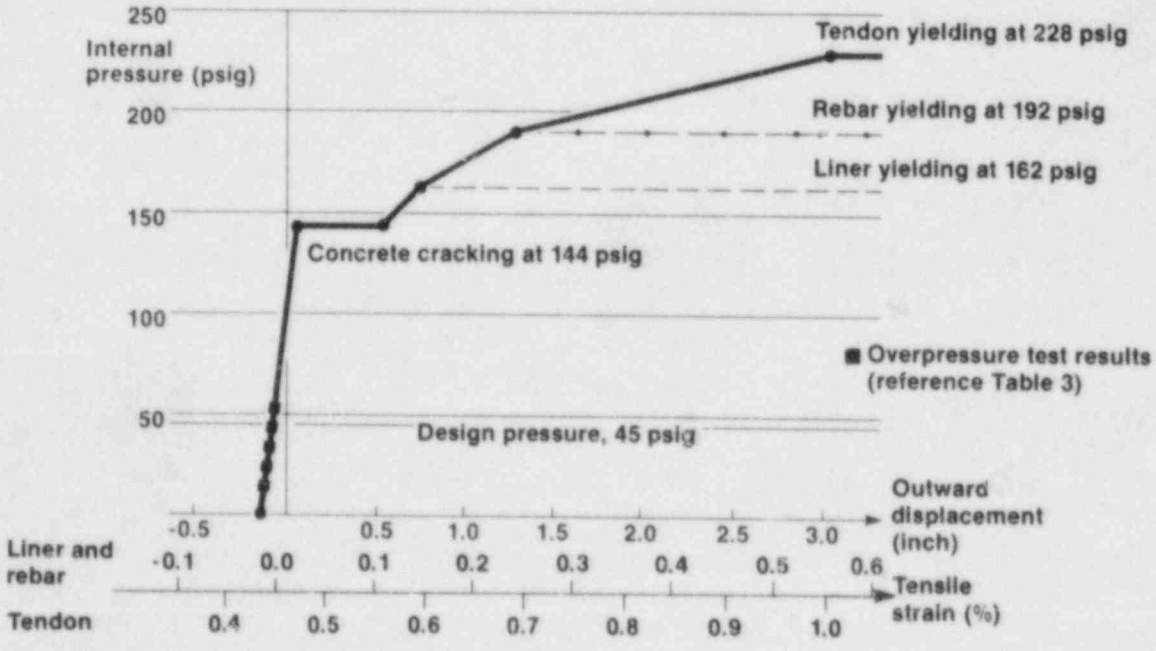

Figure 5—Response of PWR Post-Tensioned Concrete Containment at the Most Stressed Section

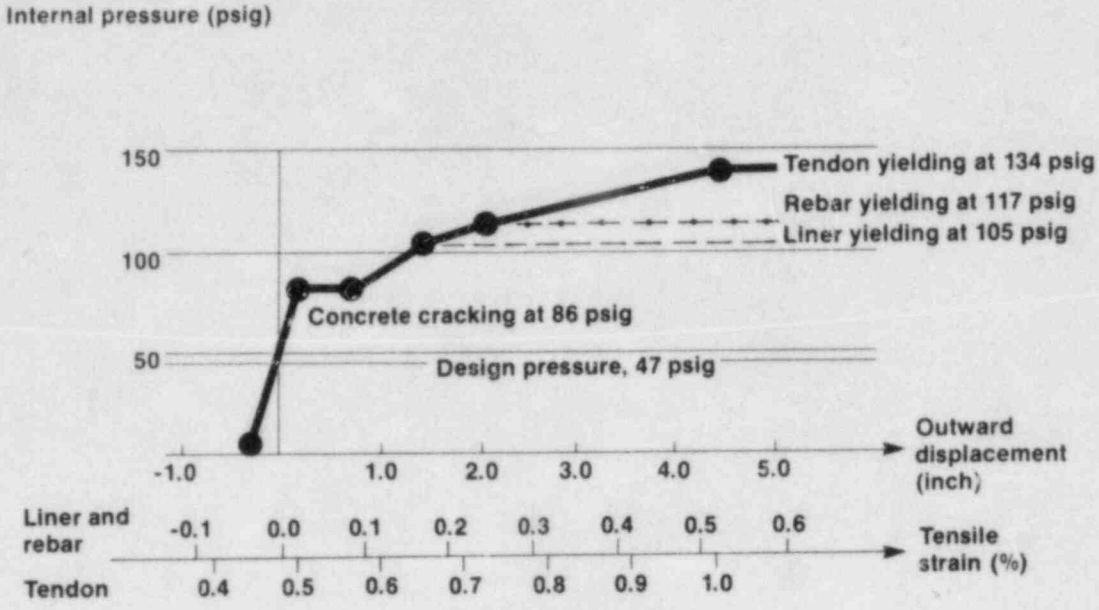

Figure 6—Strain Instrumentation for PWR Containment Around Equipment Hatch

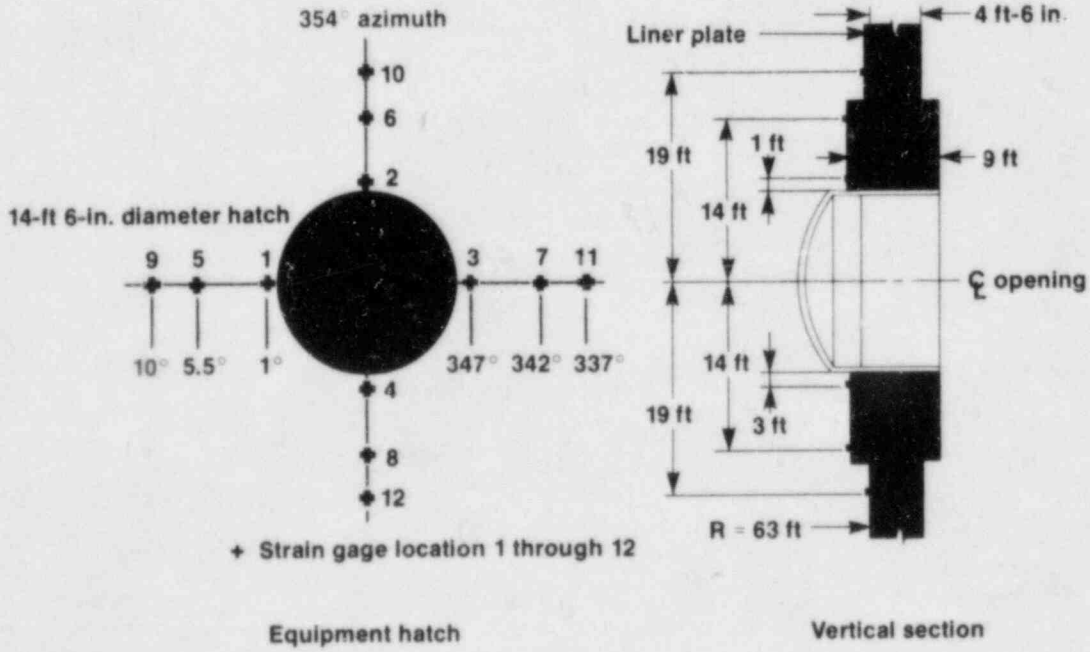

STRUCTURAL BEHAVIOR OF PENETRATIONS IN REINFORCED CONCRETE SECONDARY CONTAINMENT VESSELS

Richard N. White and Woo Kim
Department of Structural Engineering
Cornell University
Ithaca, NY 14853

ABSTRACT

The structural behavior of steel penetrations through reinforced concrete slabs was studied by conducting 22 experiments on small scale model slab/penetration combinations. In all cases the penetrations were anchored to the concrete with model shear studs. Three loading cases on the penetrations were used: torsion alone (12 tests), punching alone (2 tests), and combined torsion and punching (8 tests). Four values of concrete strength were used for the torsional loading cases. The results show that: (a) torsional shearing strength of the concrete is considerably higher than predicted by commonly used expressions, (b) failure in torsion shows substantial ductility, and (c) interaction between torsional shear and punching shear is very weak because the failure modes assocated with each action are nearly independent.

INTRODUCTION

Punching action on penetrations through the walls of reinforced and prestressed concrete nuclear containment structures is a common design loading. Current ASME Code provisions treat this problem on an elastic principal stress calculation basis that has been shown to be extremely conservative for situations involving simultaneous in-plane tension forces (Ref. 1), and proposed changes to the Code to reflect actual behavior are currently in the review and approval processs. Torsional shearing forces may also be applied to penetrations in nuclear structures. Again, design approaches are based strictly on elastic stress calculations with no confirming experimental evidence to justify this approach. "Allowable" values of torsional shearing stress acting in the concrete do not reflect the in-plane confinement effects that are inherent to this situation. Finally, some penetrations may be subjected to combined punching shear and torsional shear. To date, there has been no rational manner for combining these effects, nor any fundamental understanding of how the two effects may interact.

The research reported here was directed at studying the strength and deformation characteristics of small-scale concrete slabs with penetrations loaded in torsion alone, in punching alone, and in various combinations of punching and torsion. Steel penetrations with two different ratios of diameter to slab thickness (1.0 and 0.5) were anchored to 1 inch thick model concrete slabs with small-scale shear studs. For the torsion shear tests, four strengths of concrete were utilized to better assess the potential for shear distress in the concrete. The effects of in-plane confinement were also studied.

DESIGN OF SPECIMENS

A small-scale model approach was selected because it permits maximum investigation of this complex problem with a minimal budget. A flat specimen was chosen for simplicity, and reinforcing ratios for the slab steel were selected to be representative of those in containment walls. The specimen was not intended to be a model of a section of a particular nuclear structure, but rather to have the essential characteristics of some general section. While the numerical values of strength and deformation measured are certainly of substantial interest, there may be some size effects present that preclude direct application of the results to containment design. However, the greatly improved understanding of how torsional failures may occur, and how penetration regions respond to combined torsional loads and punching loads, should be of considerable benefit in assessing full-scale prototype behavior. The influence of in-plane tension has not been considered in this experimental study.

Slab Geometry: Twenty of the 22 slabs were 1 in. thick by 8 in. square, simply supported at the edges and restrained against torsional movement. They were reinforced with 0.11 in. diameter deformed model reinforcing bars in both faces in both directions, with steel ratios of 0.0222 and 0.0194 in the two directions. Reinforcement yield stress was 32 ksi. The model concrete had f'_c values ranging from 1700 to 4400 psi; only a few tests were done with the lower strength concretes. Average split cylinder strength for the model concrete was $6.7\sqrt{f'_c}$.

The other two slabs had a reduced central region width (5 in.) in one direction and also had lower steel ratios (0.0055 and 0.0166) to reduce the in-plane strength and confinement capability of the slab.

Penetrations: Penetrations were either 1 in. or 0.5 in. outside diameter. Those used for the combined loading series had a flange on the punching load side of the slab, extending 1/4 in. beyond the surface of the penetration, as shown in Fig. 1(b).

Shear Studs: Model shear studs are shown in Figs. 1 and 2. Commercially available nails (finishing nails), 0.048 in. diameter by 1.0 in. length, were used in all specimens. Yield strength was 110 ksi and the shear strength was 150 lbs per nail in direct shear. A prototype stud-anchored penetration is shown in Fig. 3, and a comparison of model and prototype stud geometries is given in Table 1.

	Stud Diameter	Stud Length	Sleeve Diameter	Slab Thickness	Steel Ratio at Interface
Prototype	5/8"	8 3/16"	84"	78"	0.002
1:80 Scaled Down Dimension	0.008"	0.102"	1.05"	0.975"	0.002
Model Specimen	0.048"	0.25"	1.0"	1.0"	0.04

Table 1 - Comparison of Dimensions Between Prototype and Model

It is seen that stud length, stud diameter, and stud steel percentage at the interface are all distorted, and all in the direction of providing more shear capacity. This was done deliberately in order to be able to stress the concrete as highly as possible. The stud percentage used in the models was abut 20 times that of the prototype shown in Fig. 3.

One design detail for the studs needs explanation here -- the spacing arrangement. The 1 in. penetration had 4 horizontal rows of 16 studs each, terminating in the central hollow region of the penetration. The 1/2 in. penetration had a staggered spacing utilizing 13 nails that ran completely through the penetration, giving 26 shearing areas, as shown in the right side of Fig. 2. This unsymmetrical arrangement in the smaller penetration affected the failure mode, as will be explained subsequently.

Details of stud installation are given in Refs. 2 and 3. These references also describe the special loading device built to apply simultaneous torsional shear and punching shear.

TEST RESULTS -- TORSION ALONE

Typical load-slip curves for the 1 in. penetration specimen and 0.5 in. penetration specimen which were subjected to one cycle of loading applied after maximum load was reached is shown in Figure 4. From the beginning of loading the curves show nonlinear behavior. The slip increased rapidly around the maximum load point. After the maximum load was reached, the slip increases along with a very slow decrease of load. Considerable ductility was observed in all specimens.

Failure was initiated by splitting cracks occurring at the studs closest to the free surfaces of the slab, as shown in Figs. 5(a) and 5(b). The splitting crack defined a nearly circular path on the slab surface with the 1 in. penetrations because there were 16 stud forces equidistant from the surface of the slab, but the crack path was quite unsymmetrical for the 1/2 in. penetration because only 2 studs were close to the surface.

Concrete Strength Effects:

The influence of decreasing concrete strength is shown in Fig. 6 for 1 in. penetrations and is summarized in Table 2 for both penetration sizes (in the table, A = 1/2 in. diameter and B = 1 in. diameter penetrations).

The load-slip curves show that the slopes of the curves at every loading stage are almost proportional to the corresponding concrete strengths. They also show that maximum load is reached in each case at a slip of about 0.02 in., and that the first visible crack was observed at or near the peak of the load-slip curve. The decreasing post-peak slope of the load-slip relationship for Specimen 1TB is steeper than for the other specimens because the higher strength concrete was strong enough to load some of the central shear studs to failure; in fact, in this specimen, after it had been deformed to a total twist angle of more than 10°, all 32 studs in the middle two rows were sheared off. The average load per stud at peak load was 113 lbs in this specimen -- when the outer studs began to carry less shear as splitting cracks progressed, higher loads were transferred to the inner studs, and eventually sufficient redistribution

Specimen	Concrete compressive strength, f'_c	Maximum torsional load, T_u (in-lbs)	Ultimate shear stress at interface, v_{tu} (psi)	$\frac{v_{tu}}{f'_c}$	$\frac{v_{tu}}{f'_{sp}}$	$\frac{v_{tu}}{\sqrt{f'_c}}$	Each stud resistance (lbs/stud)
1TA	4488	935	2380	0.53	5.3	35	144
1TB	4488	3602	2294	0.51	5.1	35	113
2TA	3766	781	1990	0.53	4.9	32	120
2TB	3766	3212	2043	0.54	5.0	32	102
3TA	2640	715	1820	0.69	5.3	35	110
3TB	2640	2623	1670	0.63	4.9	33	83
4TA	1878	522	1330	0.71	4.6	31	80
4TB	1625	1512	963	0.59	3.6	24	48
5TA	4545	847	2157	0.48	4.8	32	130
5TB	4545	2475	1576	0.35	3.5	23	77

Table 2 - Torsion Test Results

occurred to fail all interior studs. Specimen 1TA showed similar behavior, with 23 of the 26 studs eventually failing. This did not happen with the weaker concretes, except in specimen 2TA.

In-Plane Confinement Effects:

Specimens 5TA and 5TB had a reduced width of 5 inches in the middle third of the slab in one direction, and substantially reduced reinforcement. In Specimen 5TB, with a 1 inch diameter penetration, failure was initiated by extensive in-plane cracks that ran completely through the weakened section of the slab at a load of 77 lbs per stud (68% of the strength of the full-width slab 1TB). The reinforcement across these body cracks yielded, and eventually the splitting cracks common to the other specimens also developed. Behavior is summarized in Table 2.

The "bursting stresses" generated from the torsional load on the larger penetration were critical in the behavior of Specimen 5TB. In the smaller penetration specimen, 5TA, the much smaller total torsional forces were carried successfully by the slab, and it behaved very much like the full-width, more heavily reinforced Specimen 1TA.

Effects of Flange on One Side of Slab:

Two specimens, 6CA and 6CB, had a flange on one side of the slab, as shown in Fig. 1(b). These specimens are classed as part of the combined test series because they were to serve as the base values for constructing the interaction curves for combined torsional and punching shear loadings. The presence of a flange on one side had a major influence, however, and these effects will be presented here before the combined test series is described.

Failure of flanged specimens is shown in Fig. 7. The presence of the flange on the top side of the slab provided sufficient confinement to prevent the development of a splitting crack, and failure was initiated by splitting cracks that developed only on the bottom side of the slab. Load-slip curves were similar to the unflanged specimens except that the peak of the load-slip curve was reached at a higher value of slip and at a load level some 20% higher than in the companion specimens 1TA and 1TB (no flanges). After applying a large torsional rotation to the penetrations, stud failure occurred in the three top layers of studs, with only the "unloaded" studs at the lower splitting crack surviving.

Strength Summary:

Three non-dimensional values of shear stress computed at the interface between the concrete and the penetration are given in Table 2. In each case the shear stress is defined as

$$v_{tu} = \frac{T_u}{2\pi r^2 t}$$

where v_{tu} is the in-plane shear stress normal to a radius from the center of the penetration, T_u is the applied peak value of in-plane torsional load, r is the radius of the penetration, and t is the slab thickness. The three concrete strength parameters are the uniaxial compressive strength f'_c, the split cylinder strength f'_{sp}, and the square root of the compressive strength, $\sqrt{f'_c}$. The ratio of v_{tu} to f'_{sp} provides the most consistent non-dimensional relationship for torsional strength, which is not surprising seeing as how the initiation of failure was governed by tensile splitting cracks at the outer rows of studs.

A conservative estimate of torsional shear strength for these specimens is $v_{tu} = 5f'_{sp}$. Note that the strength expressed in terms of the square root of f'_c is considerably higher than given in the ASME Code.

Behavior Model for Pure Torsion:

The behavior of torsionally loaded penetrations anchored with shear studs is shown in Fig. 8. The torsion induces reactive forces in the concrete that may be idealized as compressive struts that are anchored at one end by the shear studs and at the other end by the surrounding concrete in the slab, at a radius defined approximately at the free ends of the studs. The "bursting effect" on the slab is a potential failure mode (as in Specimen 5TB), but the predominant mode seen here was splitting from the dowel force action on the studs closest to the slab surface, as shown in Fig. 5. After these cracks develop, redistribution of stud forces occurs and final failure is by stud shear, or potentially by distress in the concrete struts. Very little evidence of the latter failure mode was observed in these tests, however, and it can be concluded that the concrete behaved extremely well in this semi-confined state of stress. Confinement in the third direction by a flange on the penetration improved strength even further.

Additional details on the behavior model are given in Ref. 2.

TEST RESULTS -- COMBINED TORSION AND PUNCHING LOADS

Twelve specimens with a nominal concrete strength of 4400 psi were utilized in this series -- two in pure torsion (T), two in pure punching (P), and eight in combined torsion and punching (T+P). All specimens had a flange of the side of the slab loaded in punching shear. For each load combination, one 1.0 in. penetration and one 0.5 in. penetration were tested. Load sequence effects were studied by varying the P-T load histories. Results are summarized in Table 3.

The two torsion tests, 6CA and 6CB, were described in the previous section.

The two punching tests, 1CA and 1CB, showed the usual brittle punching failure mode, with typical flat conical-shaped failure surfaces. Failure stresses calculated at d/2 from the face of the loaded flange were $10\sqrt{f'_c}$ and $9\sqrt{f'_c}$ for the two specimens. These values are higher than would be measured on slabs of prototype thickness, most likely because of the expected size effect that exists in punching strength of slabs.

A detailed discussion of results is beyond the scope of this paper, and only the main aspects of behavior will be presented here.

Behavior - Combined Load Specimens

The tests reveal the fact that there is very little interaction between torsion and punching, with the two failure modes being completely different in both location and behavior -- brittle in punching and relatively ductile in torsion.

Figure 9 shows the traces of the punching failure modes for the three 1 in. diameter penetration specimens 1CB, 2CB, and 3CB. These specimens carried the following combinations of P and T: 1CB -- P = 3447 lbs, T = 0; 2CB -- P = 3047 lbs, T = 2426 in-lb; and 3CB -- P = 2819 lbs, T = 3751 in-lb. The two types of load were increased simultaneously in small increments.

The cone angle for punching becomes steeper with increasing torsion, but the punching strength decreases only about 20% with T at nearly $0.95T_o$ (T_o = strength under pure torsion). Load-deflection curves for the three specimens are given in Fig. 10. Behavior up to a punching load of nearly $0.5\ P_o$ was essentially identical for all three specimens. Radial cracks from the punching load occurred earlier as the torsion level was increased, which in turn decreased the slab stiffness at higher punching loads.

Specimens 4CA and 4CB were loaded to failure in torsion with a punching load of $0.3P_o$ applied first and then torsion applied incrementally. Failure occurred in both specimens at very close to $1.0\ T_o$ by splitting action at the bottom cover, as in the earlier tests on pure torsion. The lower crack path in Fig. 11 shows this failure. The only apparent effect of the $0.3P_o$ punching load level was to increase the torsional stiffness, most likely because of the additional restraint afforded to the concrete by the compressive punching stess under the flange area.

Specimen	Combined Load State at Failure		Combined Stress State at Failure			Normalized Failure Stress		Failure Mode
	Punching P (lbs)	Torsion T (in-lbs)	at d/2 face v_p (ksi)	at d/2 face v_{t1} (ksi)	at interface v_{t2} (ksi)	at d/2 face $\frac{v_p}{\sqrt{f'_c}}$	at interf. $\frac{v_{t2}}{f'_c}$	
1CA	2985	0	671	0		10.05	0	punching
1CB	3447	0	606	0		9.09	0	
2CA	2368	605	533	120	1541	7.92	0.34	punching
2CB	3047	2426	536	294	1545	7.97	0.34	
3CA	2394	1106	539	220	2815	8.03	0.62	punching
3CB	2829	3751	498	455	2387	7.42	0.53	
4CA	897	1040	198	206	2640	2.99	0.60	torsion
4CB	1097	3944	190	479	2512	2.88	0.58	
5CA	2640	452	583	90	1152	9.04	0.27	punching
5CB	3254	2144	573	260	1366	8.71	0.32	
6CA	0	1037	0		2640	0	0.64	torsion
6CB	0	4053	0		2580	0	0.62	

Table 3 - Results of Combined Torsion and Punching Tests

In Specimen 4CA, with T held constant at $1.0T_o$, the punching load was then increased from $0.3P_o$ to a peak value of $0.8P_o$, at which time the punching failure shown by the upper crack in Fig. 11 occurred. The near independence of the two actions was clearly shown in this specimen.

Specimens 5CA and 5CB had an initial increment of $0.6T_o$ applied, with P then increased gradually to failure. Load-deflection behavior and strength results were the same as with specimens 2CA and 2CB, where both loads were incremented together from zero.

Strength and Interaction

Punching shear stresses were computed on a section located d/2 from the face of the loaded flange, by conventional ACI approaches, and torsional stresses were computed at two locations -- d/2 from the flange face to give stress v_{t1}, and at the interface, as for pure torsion, to give stress v_{t2}. All values are provided in Table 3.

P/P_o is plotted versus T/T_o in Fig. 12, where it is seen that punching strength decreases by about 20% when the applied torsion is at $1.0T_o$. Some interaction exists, but it is weak.

CONCLUSIONS

It is emphasized that the conclusions stated here are based on experiments conducted on small scale model structures with one type of shear connection between a steel penetration through a reinforced concrete slab.

1. The most probable mode of initiation of failure for torsionally-loaded, stud-anchored penetrations is by loss of concrete cover from dowel splitting effects on the studs. This action is followed by redistribution of stud shear forces and eventually, after large rotations have taken place, by shear failure of the studs.

2. Ultimate torsional shear stress capacity, calculated at the face of the penetration, is larger than $0.5f'_c$. A conservative lower bound is best represented by $v_{tu} = 5f'_{sp}$, where f'_{sp} is the concrete split cylinder tensile strength. This measured shear strength is considerably higher than values commonly used in design of nuclear structures.

3. The addition of a flange on one side of the slab prevented a splitting failure on that side and increased the torsional capacity by 20%.

4. The torsional test specimens showed considerable ductility.

5. In specimens subjected to combined punching shear and torsional shear, the mode of failure associated with punching has little relation to the mode of failure associated with torsion. There is relatively little interaction between the two types of loading, and the interaction diagram is nearly square.

6. As the torsional force level was increased in the combined loading specimens, the punching load needed to produce radial cracking was reduced, the deflection at punching failure became smaller, and the conical-shaped failure surface tended to have a steeper slope.

8. Current design provisions for penetrations loaded in torsion, and in combined torsion and punching, are undoubtedly highly conservative. Additional experiments on thicker slabs are needed to arrive at improved, realistic design methods.

ACKNOWLEDGEMENTS

This research was conducted in the Structural Models Laboratory at Cornell University. The second author received financial support from the Education Ministry of the Government of Korea.

REFERENCES

1. Jau, W-C., White, R.N., and Gergely, P., "Peripheral Shear Strength of Biaxially Tensioned Reinforced Concrete Wall Elements", Nuclear Engineering and Design, Vol. 69, 1982, No. 2, May (I). Also published as NUREG/CR-2920, September 1982.

2. Kim, W., Combined Punching Shear and Torsional Shear in Reinforced Concrete Slabs, M.S. Thesis, Department of Structural Engineering, Cornell University, Ithaca, NY, August 1984.

3. Kim, W., and White, R.N., "Modeling Punching and Torsional Shear in Penetrations in Reinforced Concrete Slabs", Proceedings of Design of Concrete Structures -- The Use of Model Analysis, November 1984, London.

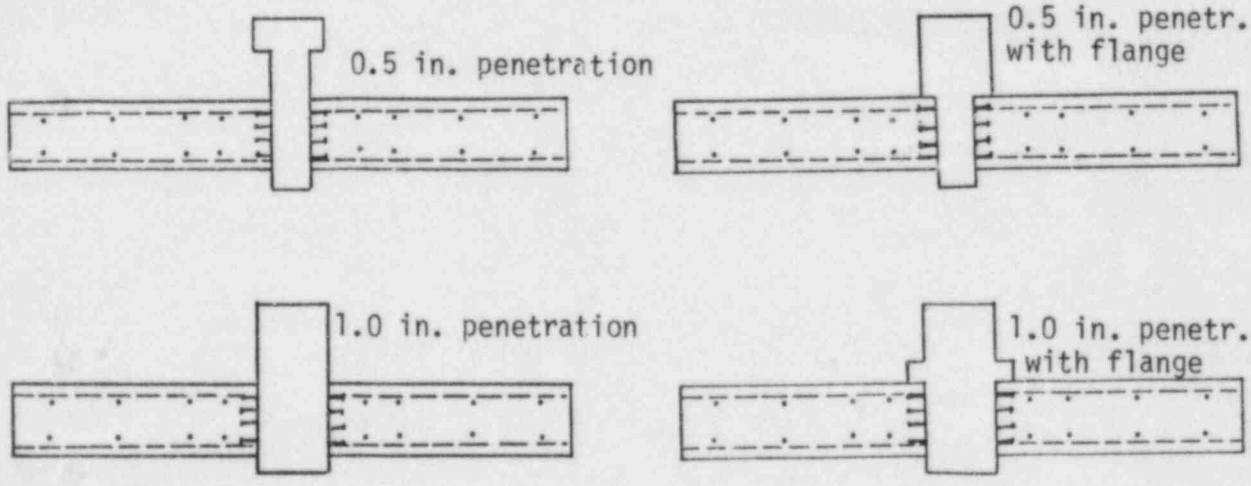

(a) Torsional test series

(b) Combined test series

Fig. 1 Sectional Views of Test Specimens

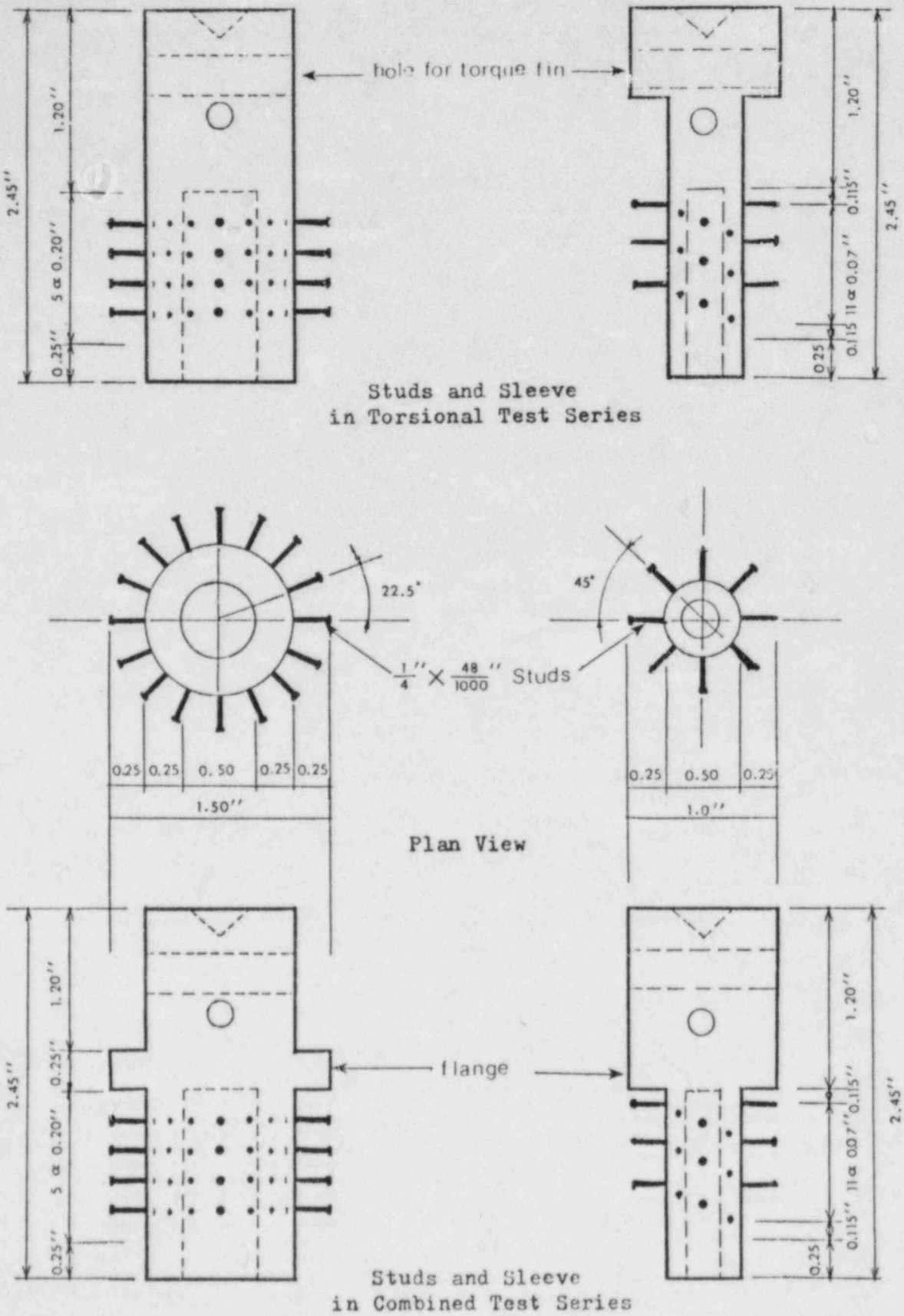

Fig. 2 Penetration Details

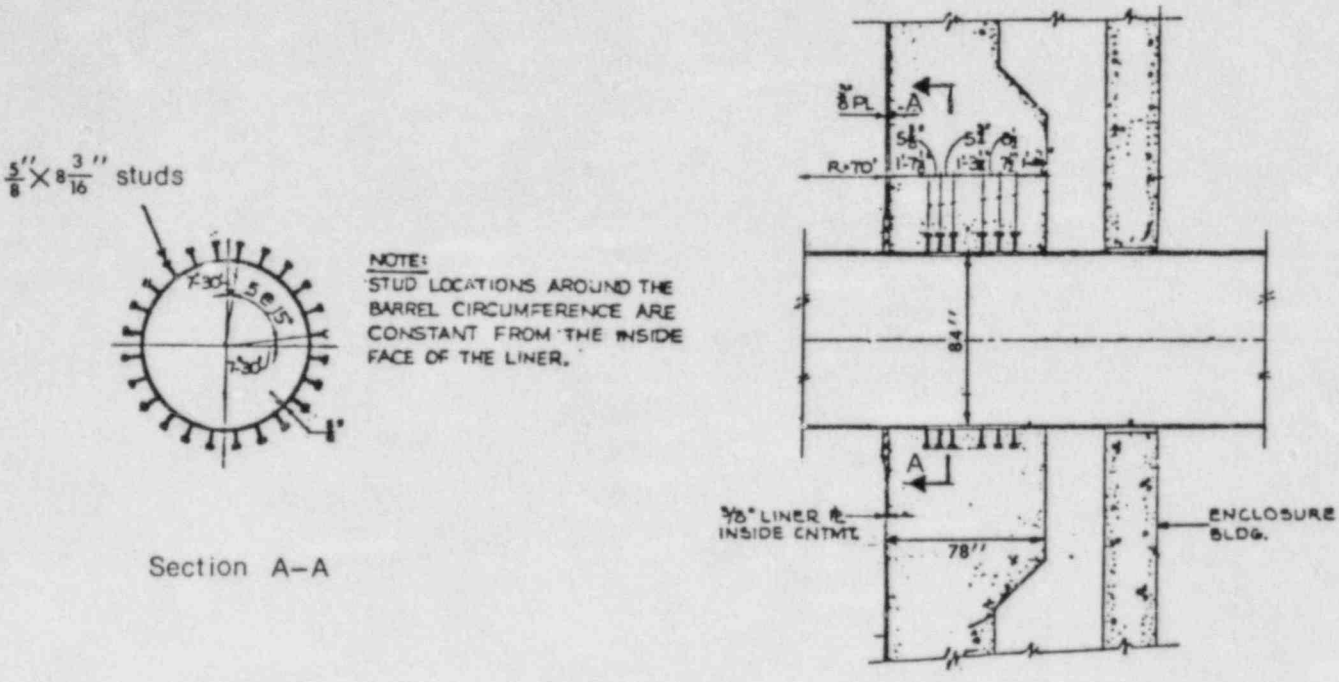

(a) A Typical Stud Anchored Penetration in a Nuclear Reactor Containment

Comparison of Dimensions Between Prototype and Model

	Stud Diameter	Stud Length	Sleeve Diameter	Slab Thickness	Steel Ratio at Interface
Prototype	$5/8$"	$8\ 3/16$"	84"	78"	0.002
1:80 Scaled Down Dimension	0.008"	0.102"	1.05"	0.975"	0.002
Model Specimen	0.048"	0.25"	1.0"	1.0"	0.04

(b) Comparison of Dimensions Between Prototype and Model

Fig. 3 Prototype Structure and Comparison with Model

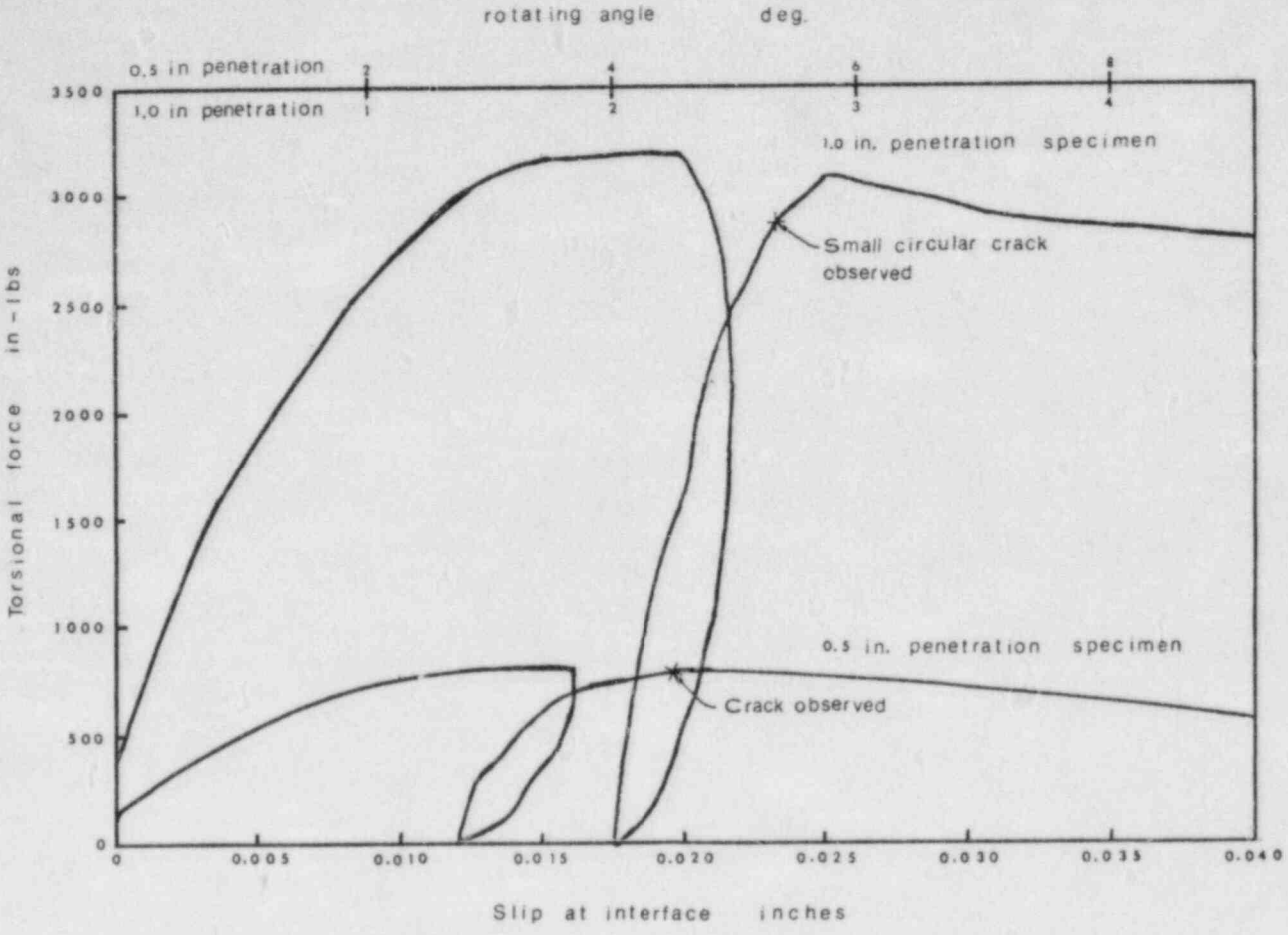

Fig. 4 Typical Load-Slip Curves for Both Size Penetrations

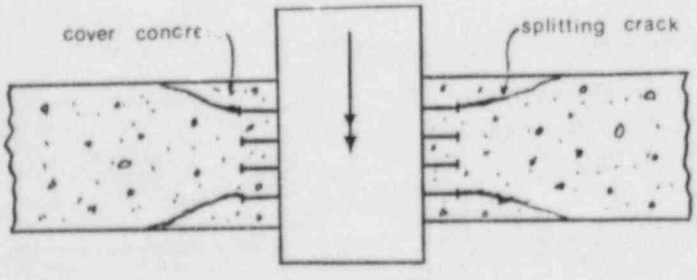

(a) Typical Crack Pattern for Torsioral Shear Failure

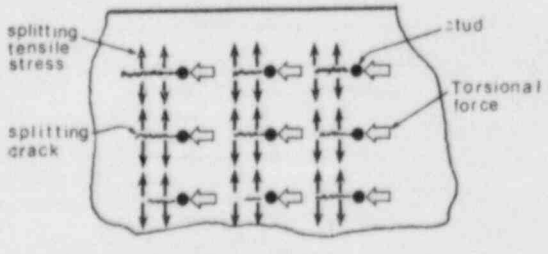

(b) Concrete Splitting Mechanism Under In-Plane Torsional Loadins

Fig. 5 Failure Mechanism for Torsional Shear

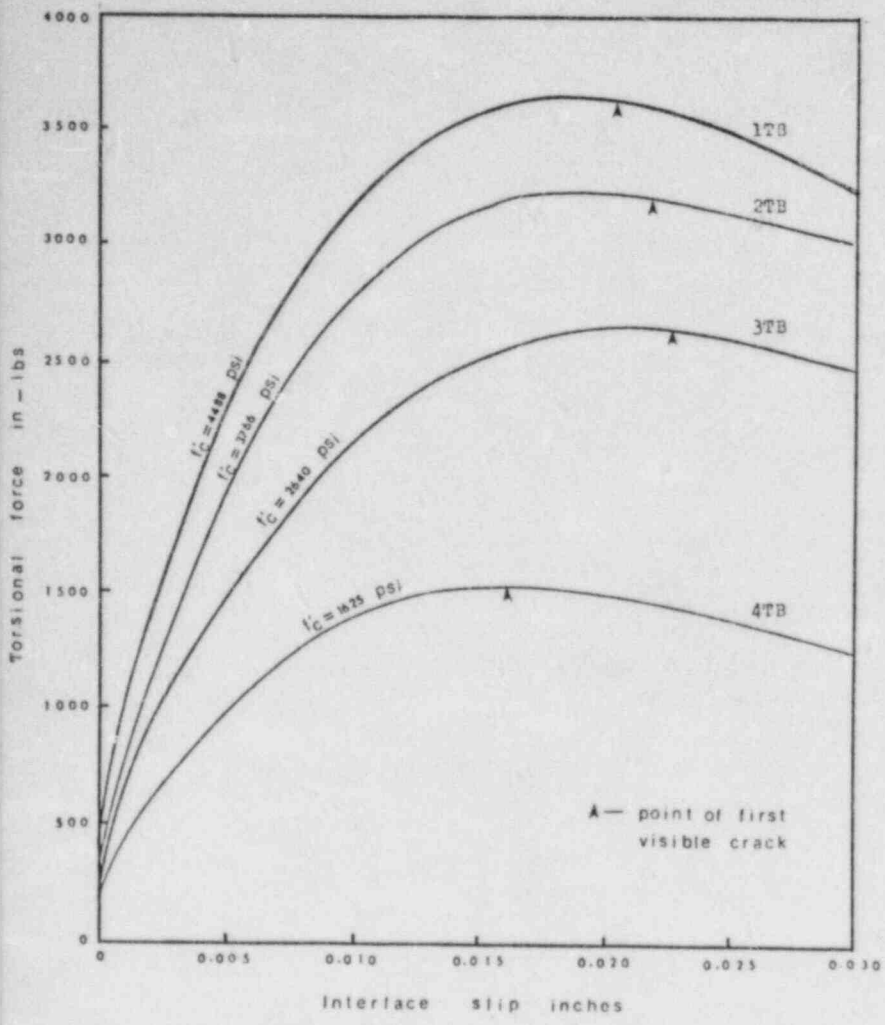

Fig. 6 Influence of Concrete Strength on Load-Slip Behavior, Pure Torsion

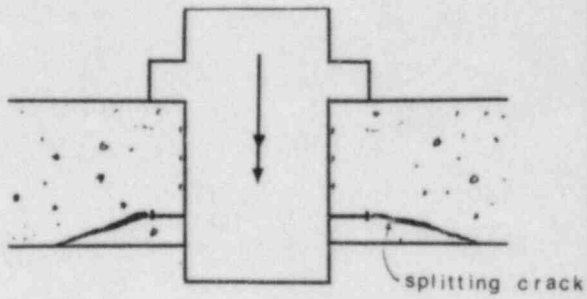

Fig. 7 Influence of Flange on One Side of Slab

v_t = in-plane shear stress

σ_r = radial compressive stress [expension force]

σ_t = tangential tensile stress [hoop tension] induced by expension force

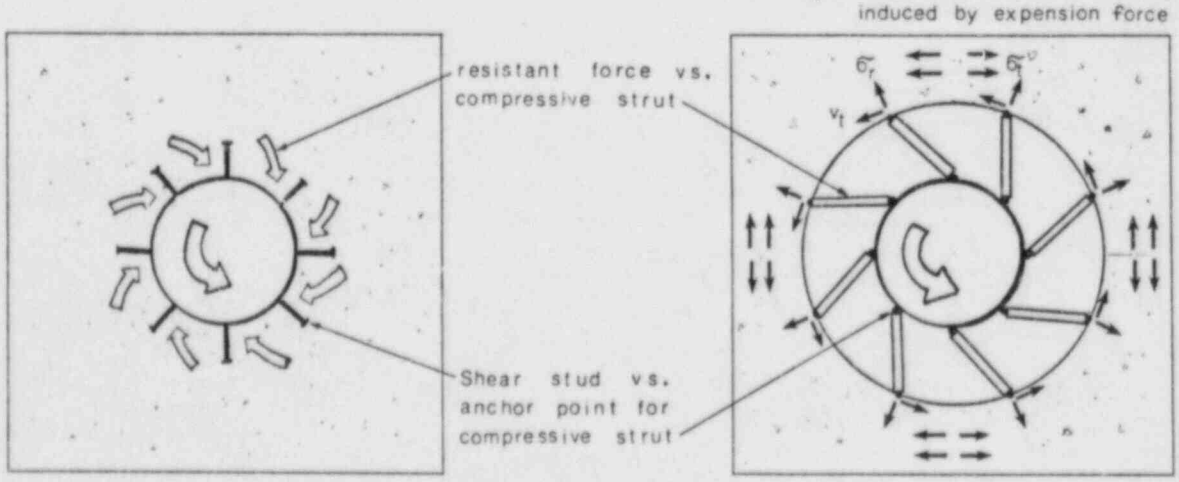

(a) Real Behavior

(b) Idealized behavior

Fig. 8 Behavior Model for In-Plane Torsional Loading

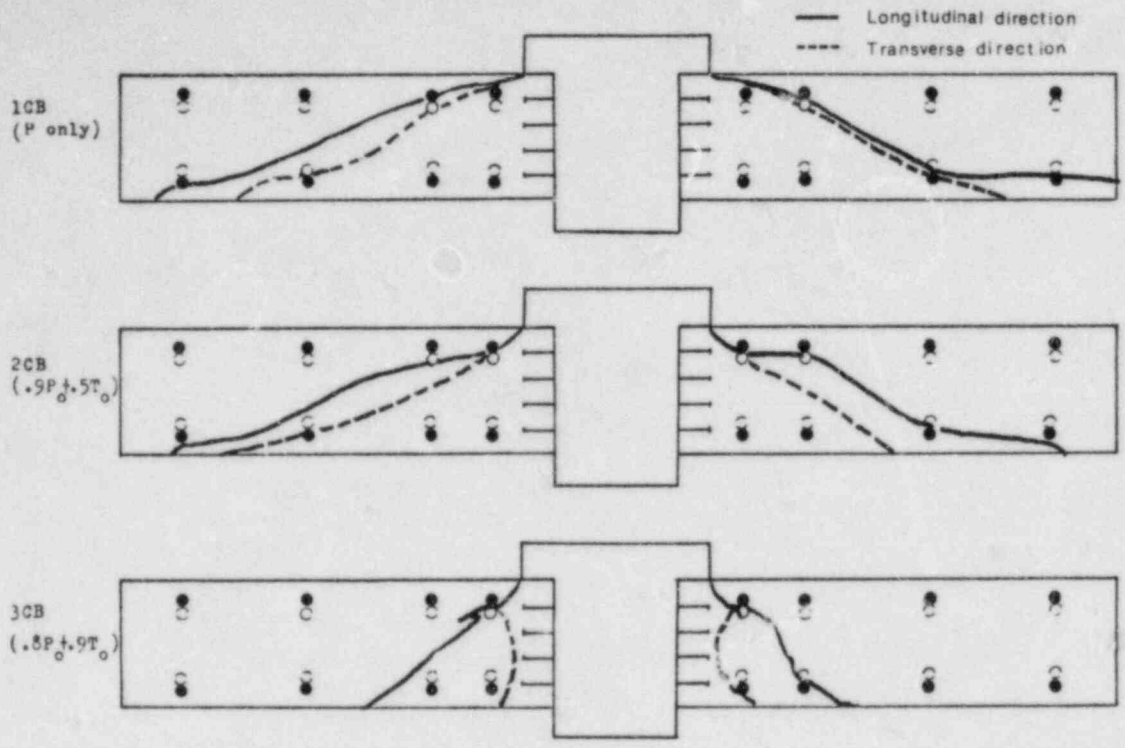

Fig. 9 Failure Surfaces for 1.0 in. Penetration Specimens Under Varying P + T

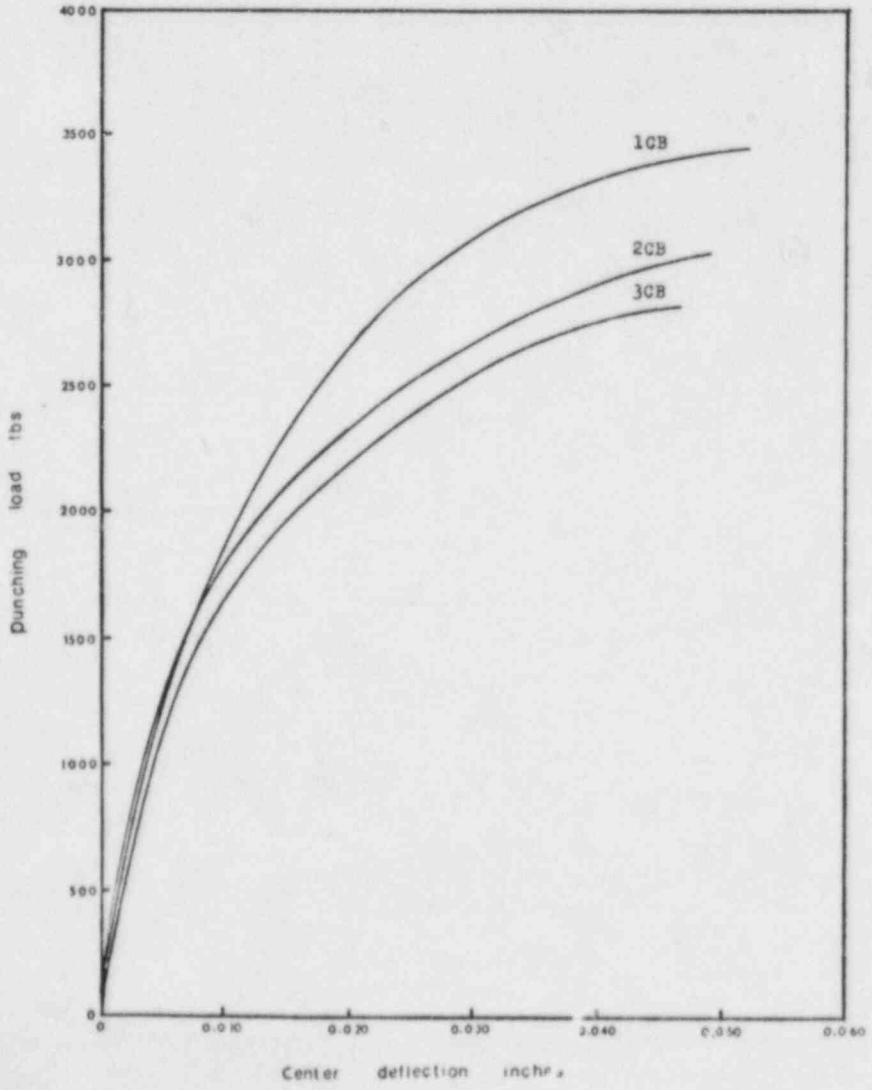

Fig. 10 Load-Deflection Curves for Specimens with Combined P + T

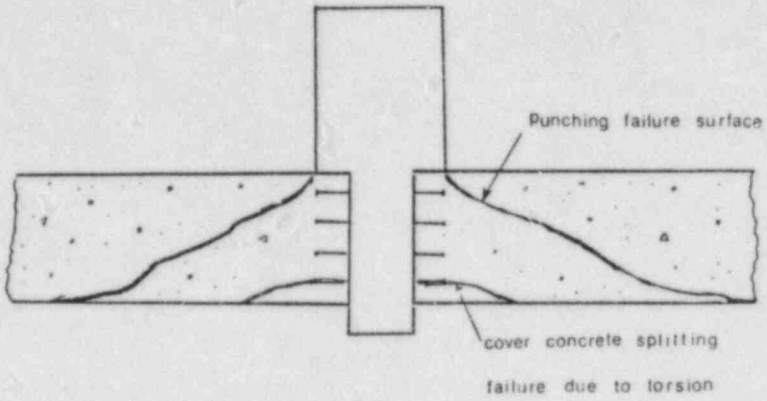

Fig. 11 Failure Surfaces for Specimen 4CA

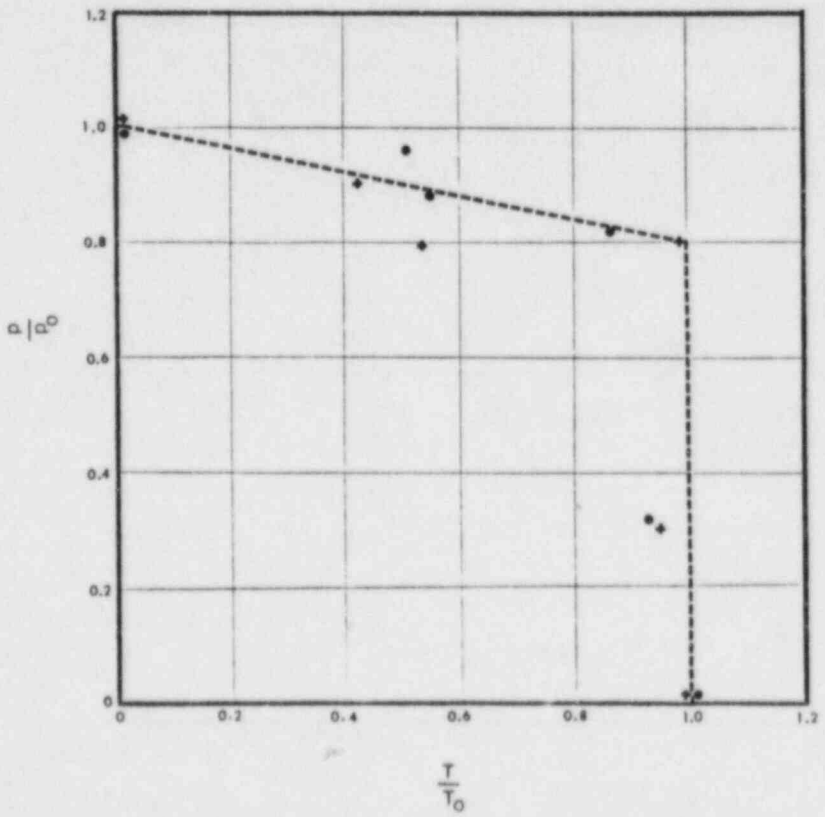

Fig. 12 Interaction Diagram for Combined Punching and Torsional Shear

NONLINEAR FAILURE ANALYSIS OF A REINFORCED CONCRETE CONTAINMENT UNDER INTERNAL PRESSURE

S. Sharma, Y. K. Wang, and M. Reich
Brookhaven National Laboratory
Structural Analysis Division
Upton, NY 11973

ABSTRACT

A detailed nonlinear finite element model is used to investigate the failure response of the Indian Point containment building under severe accident pressures. Refined material models are used to describe the complex stress-strain behavior of the liner and rebar steels, the plain concrete and the reinforced concrete. Structural geometry of the containment is idealized by eight layers of axisymmetric finite elements through the wall thickness in order to closely model the actual placement of the rebars. Soil stiffness under the containment base mat is modeled by a series of nonlinear spring elements. Numerical results presented in the paper describe cracking and plastic deformation (in compression) of the concrete, yielding of the liner and rebar steels and eventual loss of the load carrying capacity of the containment. The results are compared with available data from the previous studies for this containment.

1. INTRODUCTION

Structural integrity of nuclear containments under severe accidental pressures due to hydrogen burn following a postulated loss of coolant accident has received considerable attention in recent years. For reinforced concrete containments several detailed analysis results have appeared in the literature. A comparison of the results, however, shows that different failure mechanisms and failure pressures have often been predicted for the same containment. Essentially, the structural failure is either due to shear failure of the concrete at the cylinder-basemat junction, or from the failure of the hoop reinforcement, located below the dome-cylinder junction. The predicted pressure for shear failure is considerably lower than the pressure calculated for hoop reinforcement failure.

The different answers can be attributed due to differences in structural models, especially, in the non-linear models used for the concrete. In order to correctly predict shear failure in concrete, it is necessary to employ a reliable material model that can represent siginficant plasticity in compression, fracture in both compression and tension, and the complex interactions that occur between the cracked concrete and the rebars. In this paper the failure mechanism of a typical reinforced concrete containment i.e., the containment for the Indian Point Unit 3 Reactor, is evaluated using a detailed finite element model in which the material modeling aspect is emphasized. Comparisons with results in the literature are made.

2. CONTAINMENT STRUCTURE

The Indian Point, Unit 3, containment building (Fig. 1) is a conventionally reinforced concrete structure consisting of three basic parts: (1) a base mat, (2) a circular cylinder, and (3) a hemispherical dome. The base mat is a 9 ft. thick circular slab with a sump at the center. The outer

diameter of the slab is 145.8 ft. The 4.5 ft. thick cylindrical wall has an internal diameter of 135 ft. and a height of 148 ft. as measured from the top of the base mat to the dome-cylinder junction (springline). Above this junction the containment is capped by the hemispherical dome which has the same internal diameter (135 ft.) as the cylinder, but a reduced wall which is equal to 3.5 ft.

The interior surface of the containment is lined with a ductile steel (ASTM A442 Grade 60) liner of varying thickness. Its thickness is 0.25 in. in the dome section and at the bottom 30 ft. section of the cylinder. The thickness the remaining sections of the cylinder is 0.38 in.

Reinforcing bars (nominal yield stress of 60 ksi) of various sizes, mainly #18, #14 and #11, are placed in different patterns and spacings to reinforce the containment building. The primary membrane reinforcement in the cylindrical wall and dome is divided into two equal groups placed near the inside and outside faces of the containment wall. Each group consists of two layers of hoop bars and one layer of meridional bars as depicted in Fig. 2. In addition, a layer of helical bars at +45° and -45° with the vertical axis is placed near the outside face to resist in-plane shear forces. These bars extend from the top of the base mat to the bottom third of the dome. Further details pertaining to the reinforcing bar sizes and spacings can be found in Ref. [1].

3. MATERIAL MODELS

As mentioned previously, in order to predict the containment failure mechanism and failure response, nonlinear materials models that can accurately describe the complex stress-strain behavior of the concrete and steels must be used. The material models used in the present finite element analysis are discussed in this section.

3.1 Steels

A von Mises plasticity model with an isotropic strain hardening rule was adopted to represent the nonlinear response of the liner and reinforcement steels. Since this is a well-known material model, only the major equations are briefly outlined.

Under the influence of current stresses σ_i, i = 1, 2, ... 6, the state of deformation a steel element is defined by a loading function f_s of the form

$$f_s = \frac{1}{2} S_i^T S_i - \kappa^2 = 0 \qquad (1)$$

where S_i and S_i^T denote the stress deviator and its transpose, respectively, and κ is a function of plastic work, W_p:

$$\kappa = \kappa (W_p) \qquad (2)$$

and

$$W_p = \int \sigma_i \, d\varepsilon_i^p \qquad (3)$$

where ε_i^p are the plastic strain components.

The incremental plastic strain components are given by the following flow rule

$$d\varepsilon_i^P = d\lambda \quad \frac{\partial f}{\partial \sigma_i} \tag{4}$$

where $d\lambda$ is a plastic parameter. Following the standard procedure used in plasticity theory, an incremental stress-strain relation in matrix form can be derived from Eqs. (1) to (4) as

$$\{d\sigma\} = \left[C_{EP}^1\right] \{d\varepsilon\} \tag{5}$$

where $\left[C_{EP}^1\right]$ is an elastic-plastic matrix of the steel element.

3.2 Plain Concrete

The nonlinear material behavior of plain concrete is characterized by two main features: i) some plastic deformation before crushing under high compressive stresses, and ii) cracking under relatively low tensile stresses. These features can be represented by an elastic-plastic model combined with a fracture criterion for crushing and cracking.

Elastic-plastic Model - An elastic-plastic model origniated by Chen and Chen [2] was used for the present analysis. It predicts the nonlinear concrete behavior with sufficient accuracy, and is formulated in a manner that allows for implementation in finite element programs. This model defines two different but similar loading functions to describe the yielding of concrete in different stress regions.

Compression-compression stress state:

$$f_c = \frac{J_2 + (\beta/3)\ I_1}{1 - (\alpha/3)\ I_1} = \tau^2 \tag{6}$$

Tension-compression or tension-tension stress state:

$$f_c = \frac{J_2 - \frac{1}{6}\ I_1^2 + (\beta/3)\ I_1}{1 - (\alpha/3)\ I_1} = \tau^2 \tag{7}$$

where α and β are material constants and τ is a strength parameter [2]. J_2 is the second invariant of stress deviator, and I_1 is the first invariant of stress components. Initial and subsequent loading surfaces defined by Eqs. (6) and (7) are shown in Fig. 3. With these loading functions and the flow rule given by Eq. (4), an incremental stress-strain relationship for the concrete can be derived as

$$\{d\sigma\} = \left[C_{EP}^2\right] \{d\varepsilon\} \tag{8}$$

where $\left[C_{EP}^2\right]$ is an elastic-plastic material matrix for the concrete [2].

Fracture of Concrete - A dual fracture criterion in terms of both stresses and strains is used. The stress-based criterion is obtained simply

$$g(\varepsilon_i) = J_2(\varepsilon) + \frac{A_u}{3}\frac{\varepsilon_u}{f'_c} I_1(\varepsilon) = (\tau_u)^2 \left(\frac{\varepsilon_u}{f'_c}\right)^2 \quad (9)$$

or

$$\varepsilon_{max} = \varepsilon_t \quad (10)$$

where $J_2(\varepsilon)$ is the second invariant of strain deviator; I_1, the first invariant of strain components; f'_c, uniaxial compressive strength of concrete; A_u, a material constant; ε_u, ultimate compressive strain; ε_t, ultimate tensile strain and ε_{max}, maximum principal strain obtained from the analysis. The fracture surface in a biaxial strain plane is shown in Fig. 4.

When the concrete fractures in a compressive stress state (crushing), its stiffness and stresses in all directions are set to zero. In the case of tensile fracture (cracking), however, only those stiffness and stress terms that are associated with the normal to the cracked plane are gradually reduced to specified minimum values. The gradual reduction of these terms as a function of the strain normal to the cracked plane is carried out in the present analysis in order to represent such effects as tension-stiffening and loss of shear strength in the cracked concrete.

3.3 Reinforced Concrete

Reinforcing bars in the concrete can be modeled either discretely as truss or beam elements, or in a distributed sense in which the reinforced concrete is treated as a composite material. The latter approach is computationally more efficient and in addition can model the concrete steel interaction effects more accurately. In the present analysis, a consistent smearing procedure [3,4] has been used to idealize the reinforced concrete as an equivalent nonlinear composite material. Essentially, the smearing procedure assumes that specified components of strains and stresses are uniform in both the concrete and steel. The incremental constitutive matrix for the reinforced concrete can then be derived as a function of stress, strain and constitutive matrices for both of its constituents, concrete and steel. Similarly, once the overall deformation of the smeared reinforced concrete is obtained, a de-smearing procedure (an inverse process to the smearing procedure) can be used to calculate stresses and strains in the concrete and steel. The stresses and strains are then used to assess the yielding of steel or fracture of concrete. A detailed description of the smearing approach for elastic-plastic composites with a derivation of relevant equations is given in Ref. [4].

4. FINITE ELEMENT MODEL

The containment building is assumed to be axisymmetric for the finite element idealization. The effect of containment penetrations, which are non-axisymmetric, is ignored in this analysis since it is mainly aimed at determining the global response of the containment. This simplification with

respect to the penetrations is justified since the penetrations are small when compared to the containment size. Furthermore, areas around the penetrations are provided additional reinforcement to prevent any localized failure. All steel reinforcements, including vertical and diagonal rebars, are assumed to be axisymmetric in a distributed sense. This is also a valid approximation in view of the smearing and de-smearing procedures used for modeling the reinforced concrete.

The finite element model of the containment, shown in Figure 5, was constructed using a nonlinear finite element code, NFAP, developed at the Brookhaven National Laboratory. The model consists of 407 eight-noded axisymmetric elements resulting in a total of 1399 nodes. In addition, a set of nonlinear spring elements (high stiffness in compression and zero stiffness in tension) were used under the base mat in order to model the soil restraint and to allow uplifting of the base mat. As shown in the figure, the model has 8 layers of axisymmetric elements in both the cylindrical wall and the hemispherical dome, and 6 layers in most of the base mat. The element layers are chosen to represent separately the liner, the plain concrete, and the reinforced concrete with different reinforcing bars. The spacings and sizes of the layers are selected to model the actual placement of the reinforcements. For the liner and reinforcing steels, Young's modulus of elasticity and Poisson's ratio were taken to be 29,000 ksi and 0.3, respectively. As-built values for the mean yield strength, 48.4 ksi for the liner and 69.7 - 71.0 ksi for various rebars, were used. A bi-linear stress-strain idealization with a plastic tangent modulus of 100 ksi was used for all steels. Material parameters for the plain concrete as required by the Chen and Chen [2] model are given below:

Young's modulus = 3,700 ksi
Poisson's ratio = 0.19 ksi
Yield strength in uniaxial tension = 0.216 ksi
Yield strength in uniaxial compression = 1.8 ksi
Yield strength in biaxial compression = 2.160 ksi
Fracture strength in uniaxial tension = 0.4 ksi
Fracture strength in uniaxial compression = 4.0 ksi
Fracture strain in tension = 0.000125
Fractuare strain in compression = 0.003

5. ANALYSIS RESULTS

The loads considered in the analysis were the dead weight or gravity loads and internal pressure. The entire gravity loads were applied to the containment in the first load step at the beginning of the analysis. The internal pressure was, however, incrementally applied. The pressure increments were 1 psig following the onset of nonlinear response. In the nonlinear range, a Newton-Raphson procedure with stiffness reformation for each equilibrium iteration was used to obtain convergent solutions.

5.1 Deformation Response

Undeformed and deformed (before failure) shapes of the containment are depicted in Fig. 6. For clarity, the displacements for the deformed shape are multiplied by a factor of 50. The figure shows large bending deformations at

the cylinder - base mat junction, and comparatively large radial displacements in the middle of the cylindrical wall. The deformations of the base mat indicate that up-lifting occurs below the cylindrical wall at the junction.

The growth of the deformation field is illustrated in Fig. 7 where radial displacements at mid-cylinder and vertical displacements at the top of the dome are plotted versus internal pressure. As can be seen, the displacements are small until tension cracks develop in the concrete at, internal pressure between 25-33 psig (see below). The displacements then grow more rapidly as the concrete loses its load carrying capacity. The rates at which these displacements increase are then controlled by the stiffnesses of the steel members and by the tension-stiffening effect of the cracked concrete.

5.2 Cracking and Shear Failure of Concrete

Vertical cracks due to hoop stresses first appear in the middle of the cylindrical wall at 25 psig. The cracks spread quickly with increasing pressure covering almost the entire length of the cylinder at 26 psig. Only a small section above the cylinder - mat intersection remain uncracked. The hoop strains are very low in this region due to the radial constraints provided by the base mat. As the pressure increases to 29 psig, perpendicular cracks due to both hoop and meridional stresses are initiated in the entire section of the dome.

The next set of cracks appear at the cylinder - mat intersection when the pressure reaches 33 psig. These cracks are due to high tensile meridional stresses and shear stresses in the elements at the inside of cylinder wall which arise as a result of large bending deformations at the intersection. The cracks are formed at some small angles from the horizontal plane because of the combined effect of tensile and shear stresses. The cracking progresses through the intersection with increasing pressure reaching the middle of the intersection (i.e., the cylindrical wall thickness) at 48 psig. At this pressure, horizontal cracks due to meridional stresses also in the entire cylindrical wall except in the outside of the wall near the intersection. The concrete in the region is under compression because of the bending deformations. As the internal pressure is increased further from 48 to 77 psig, the cracked regions expand slowly but essentially with the same crack configurations. Above 77 psig, high shear stresses at the cylinder - mat intersection introduce another set of cracks perpendicular (approximately) to the original cracks in this region. When this occurs, the concrete is assumed to fail in shear and its shear stiffness is greatly reduced. In the present analysis, ten percent of the uncracked shear stiffness is retained in order to approximately represent the cumulative effect of interface shear transfer, dowel mechanism and the stiffness contributions from the reinforcement ties and stirrups.

Shear failure of the concrete progresses through the wall with increasing pressure. At 110 psig, 50 percent of the intersection has failed in shear. The extensive cracking relieves some of the bending moment and shear force in this region. The depth of shear failure, however, keeps increasing, reaching the outside face meridional bars (72 percent of the wall thickness) at 125 psig. Above this pressure (i.e., at 126 psig), a convergent numerical solution could not be obtained. This indicates that the cylinder - mat intersection cannot carry any further increase in the load.

Plasticity of concrete in compression is initiated at 110 psig in some elements at the cylinder base on the outer surface. The plastic zone spreads to neighboring elements with increasing pressure. However, the effective stress in all these elements remains considerably below the fracture strength of the concrete in compression (4 ksi) even at the peak pressure of 125 psig.

5.3 Liner and Rebar Stresses at Cylinder-Mat Intersection

Meridional stresses in both the liner and inside vertical rebars at the cylinder-mat intersection are depicted in Fig. 8. These stresses grow linearly at a slow rate until the concrete begins to crack at 29 psig. The stresses then grow rapidly with pressure to 84 psig as the cracks progress through the wall and the concrete meridional loads are transferred to the steel members. At 84 psig, 7 psig above the pressure at which a second set of cracks develop at the intersection (77 psig), the liner become fully plastic. Additional meridional stresses above 84 psig presssure are carried mainly by the inside vertical rebars, and to some extent by the small section of intact concrete. As shown in the figure, the rebar stresses grow at an even higher rate after the liner has become plastic. Finally, the rebars become plastic at 120 psig. This is soon followed by the shear failure at the intersection at 126 psig as discussed previously.

5.4 Liner and Rebar Stresses at Cylinder Mid-Height

Hoop stresses in the containment are greatest at the cylinder mid-height, at an elevation of 114 ft. For a section at this elevation, hoop stress versus internal pressure curves for the liner, hoop rebars and diagonal rebars are plotted in Fig. 9. The stresses in all the steel members are low until the onset of cracks due to hoop stresses at 25 psig. Above this pressure and up to 104 psig, the stresses grow almost linearly with increasing pressure. Note that the hoop stress in the liner, because of the multi-axial stress state, is higher than that in the hoop rebars in this pressure range. Also, the hoop stress in the diagonal rebars is much lower (approximately 25 percent) since they are inclined 45° to the horizontal axis.

The liner becomes plastic at 104 psig under combined hoop and meridional stresses. Additional hoop stresses are then transferred to the hoop and diagonal rebars as shown in the figure by the higher growth rates of hoop stress versus pressure. Both the hoop and diagonal rebars, however, remain elastic up to 125 psig internal pressure. Analysis results could not be obtained above this pressure because of the shear failure at the cylinder-mat intersection.

5.5 Comparison with Results in the Literature

Finite element analysis results for the failure of Indian Point containment building have been presented previously by Von Riseseman, et al [5], Fardis, et al [6], and Butler and Fugelso [7]. In the first two studies, the containment failure is predicted to result from the yielding of steel members due to large hoop stresses near the cylinder mid-height. References [5] and [6] do not provide any details for the cracking and post-cracking behavior of the concrete. Also, the results presented do not discuss any shear failure of the concrete at the cylinder-mat junction. This may be due to the reason that very simple materials models are used in [5] and [6] to

represent the nonlinear stress-strain response of the concrete. These models may not, therefore, be able to adequately describe the complex plasticity and cracking behavior at the intersection.

Numerical results in [7] were obtained with a computer code ADINA [8] which has a more realistic concrete model. This nonlinear model allows for cracking in tension, crushing in compression and strain-softening. The overall containment failure response described in [7] is in reasonably good agreement with the results described in this paper. The shear failure at the cylinder-mat intersection is predicted at 118 psig as compared with 126 psig in the present analysis. There are, however, two notable differences in the two analyses: (1) only large plastic deformations of concrete on the outside of the wall near the cylinder base are obtained in this study in contrast with significant compression crushing (and corresponding stress increase in rebars) predicted in [7], and (2) the calculated base mat uplift from the present analysis is 1.8 in. at 118 psig which is considerably less than 4.4 in obtained in [7].

6. CONCLUSIONS

Analysis results based on a detailed nonlinear finite element model have been presented in the paper for the failure behavior of the Indian Point containment building. The results show that the cracking of concrete begins in the cylindrical wall due to hoop stresses, and at the cylinder-mat junction due to meridional and shear stresses at 25 and 33 psig, respectively. Secondary cracks on the inside of the intersection develops at 77 psig initiating a loss of concrete shear strength. The transfer of concrete stresses to the steel members in this region leads to the yielding of the liner at 84 psig, and subsequently that of the inside vertical rebars at 120 psig. Further increase in the internal pressure to 125 psig propagates the shear failure at the intersection up to the outside reinforcement bars (72 percent of the wall thickness). The intersection is then unable to carry any further increase in the loads. At the cylinder mid-height, the liner yields at 104 psig, but both the hoop and diagonal rebars remain elastic even at the peak pressure of 125 psig.

REFERENCES

1. "Indian Point Nuclear Power Plant, Unit 3, Final Safety Analysis Report", Docket 50286.

2. Chen, A.C.T. and Chen, W.F., "Constitutive Relations for Concrete", Journal of the Engineering Mechanics Division, ASCE, 101(1975), pp. 465-481.

3. R. Hill, "Theory of Mechanical Properties of Fibre-Strengthened Materials: I. Elastic Behavior," Journal of Mechanics and Physics of Solids, 12(1964).

4. Chang, T.Y. and Aoki, H., "A Constitutive Model for Structural Analysis of Fusion Magnets", Nuclear Engineering and Design, 58(1980), pp. 237-245.

5. Von Riesemann, W.A., Huerta, M., Chen, E-P. and Swenson, D.V., "Structural Response of the Indian Point 2 and Indian Point 3 Containment Buildings", Section 3.2, Report of the Zion/Indian Point Study: Vol. 1, Prepared by W.B. Murfin, Sandia National Laboratory, Albuquerque, NM, Report No. NUREG/CR-1410, SAND80-0617/1, August 1980.

6. Fardis, M.N., Nacar, A. and Delichatsios, M.A., "Reinforced Concrete Containment Safety Under Hydrogen Explosion Loading", Report No. NUREG/CR-2898, U.S. Nuclear Regulatory Commission, Washington, DC, September 1982.

7. Butler, T.A. and Fugelso, L.E., "Response of the Zion and Indian Point Containment Buildings to Severe Accident Pressure", Report No. NUREG/CR 2569, U.S. Nuclear Regulatory Commission, Washington, DC, May 1982.

8. Bathe, K.J., "ADINA: A Finite Element Program for Automatic Dynamic Incremental Nonlinear Analysis", Report 82448-1, Acoustics and Vibration Laboratory, Dept. of Mechanical Engineering, Massachusetts Institute of Technology, Cambridge, MA, 1978.

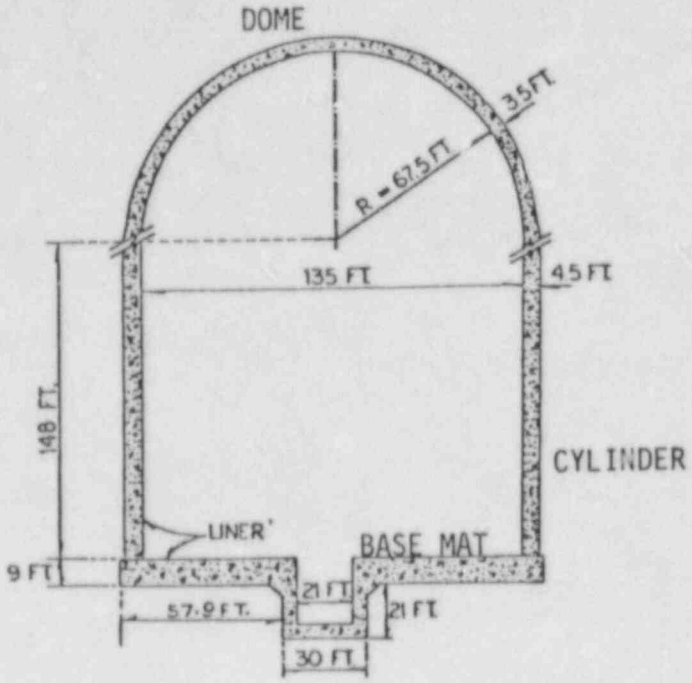

Figure 1. Indian Point Containment Building

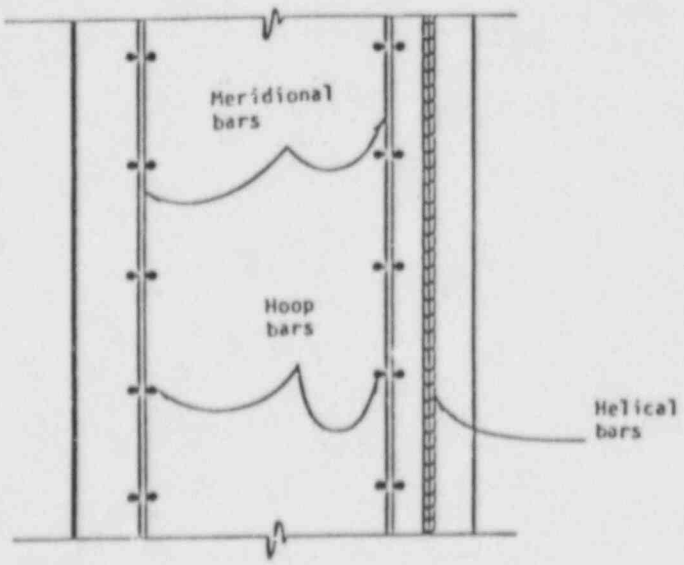

Figure 2. Reinforcement Bars in Cylindrical Wall

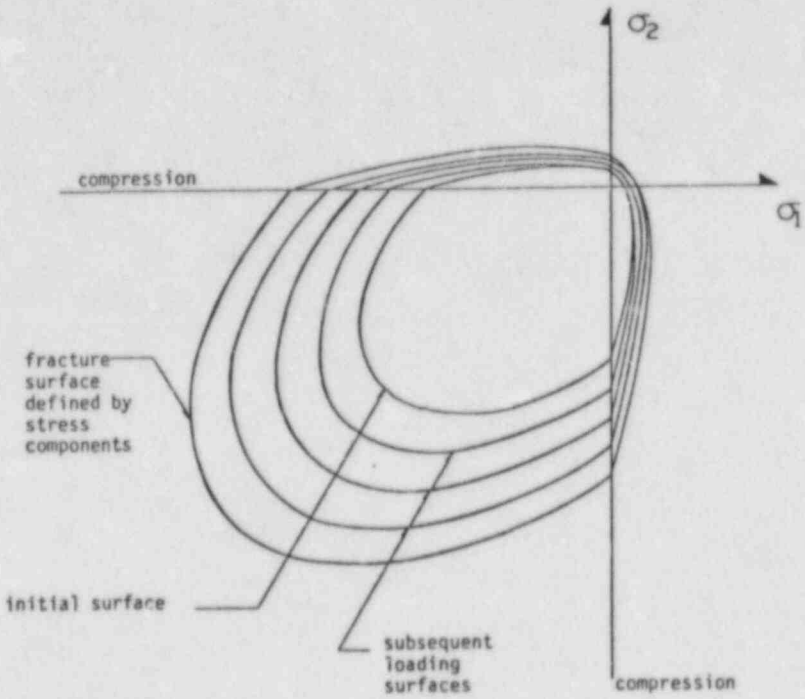

Figure 3. Loading and Fracture Surfaces of Concrete in Biaxial Stress Plane

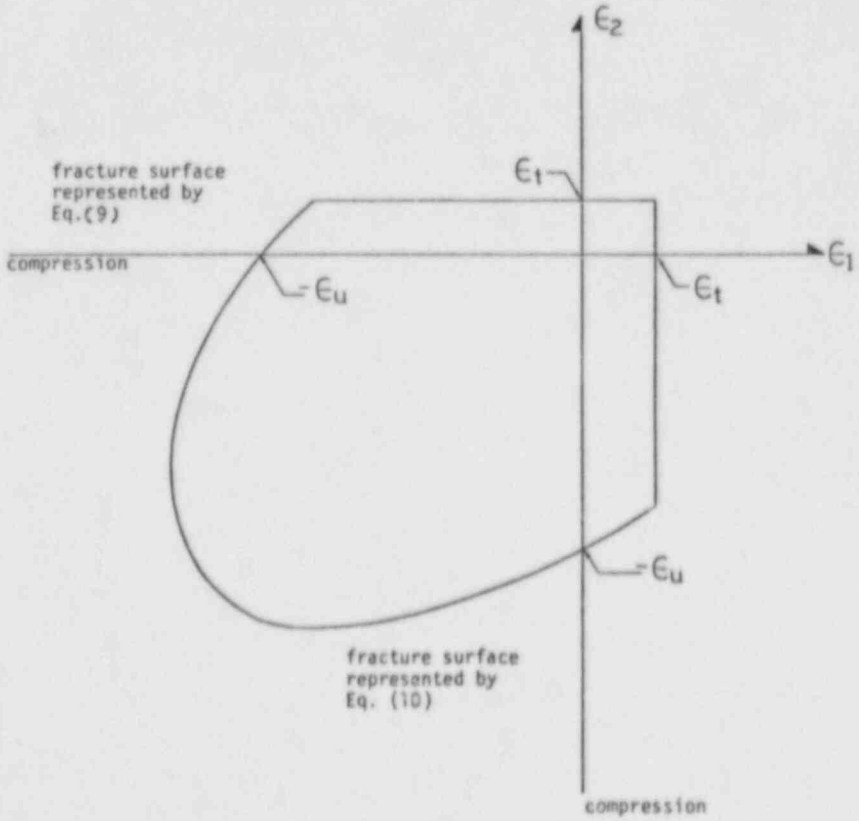

Figure 4. Fracture Surface of Concrete in Biaxial Strain Plane

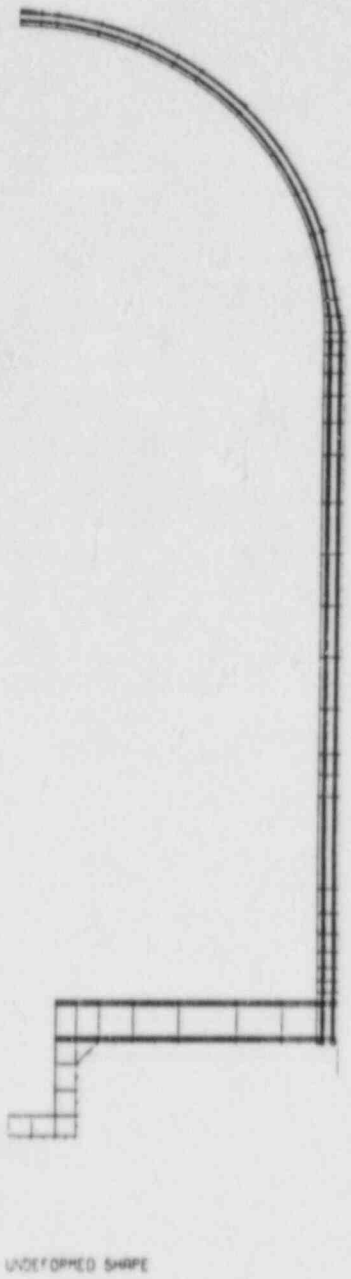

Figure 5. Finite Element Idealization of the Indian Point Containment Building

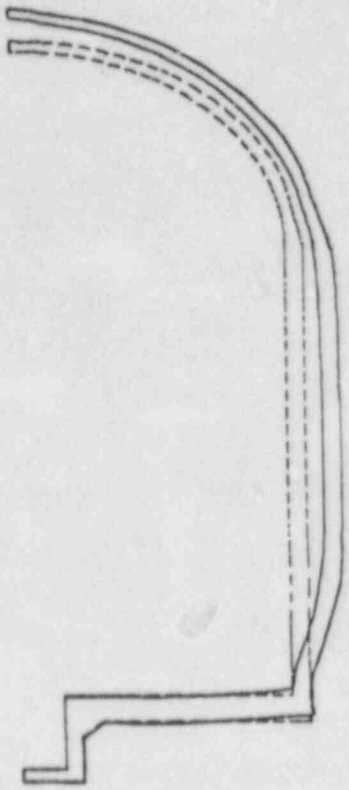

Figure 6. Undeformed and Deformed Shapes of the Indian Point Containment Building

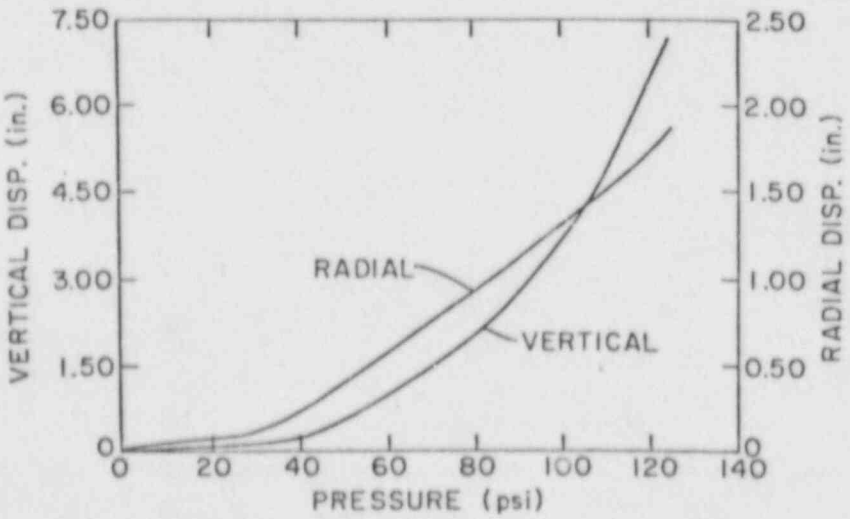

Figure 7. Radial Displacement at Cylinder Midheight and Vertical Displacement at Dome Apex Vs. Pressure

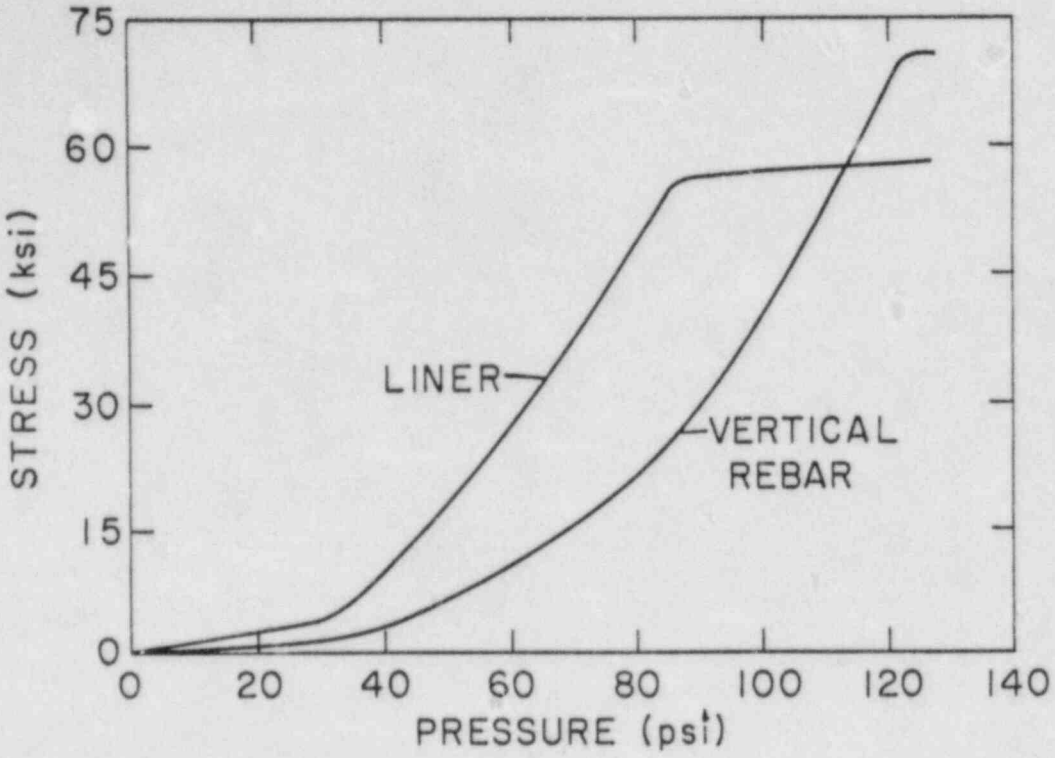

Figure 8. Meridional Stresses in the Liner and Inside Vertical Rebars Vs Pressure

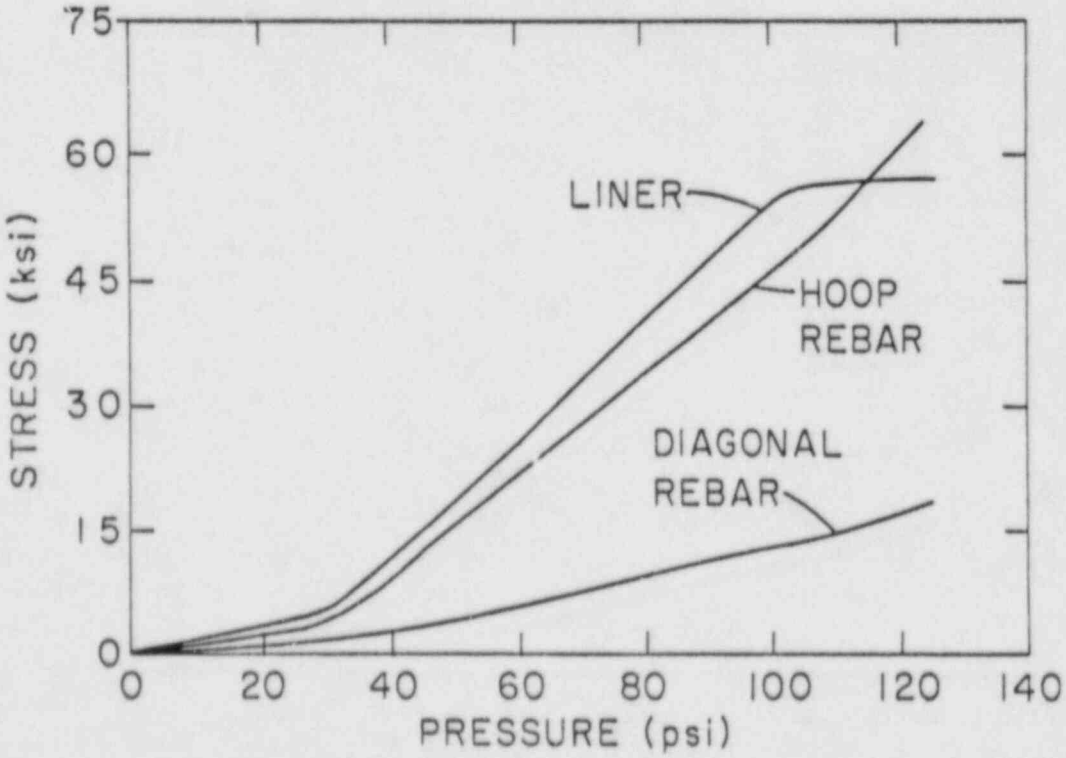

Figure 9. Hoop Stresses in the Liner, Hoop Rebars, and Diagonal Rebars Vs. Pressure

RECENT RESULTS ON THE EVALUATION OF THE OVERPRESSURE RESPONSE OF CONCRETE AND STEEL CONTAINMENTS

R. S. Dunham and Y. R. Rashid
ANATECH International Corporation
3344 N. Torrey Pines Court, Suite 320
La Jolla, CA 92037

Y. K. Tang
Electric Power Research Institute
3412 Hillview Avenue
Palo Alto, CA 94304

ABSTRACT

Several analytical studies have been carried out over the past two years as part of EPRI's program for the development of a verified methodology for the ultimate load analysis of concrete containment structures. In addition, analyses of steel containment models have been completed for EPRI in support of the NRC/Sandia program to validate computer codes for the analysis of steel containment structures. This paper reports on some of the results of these analyses, dealing first with the global ultimate load behavior of typical prestressed and reinforced concrete containment structures. The results of these analyses are described with particular attention given to the definition of local effects and failure mechanisms of concrete containment structures. On the basis of the global analysis results, local effects analyses were carried out. These clearly demonstrate large liner strain concentrations. The utility of the ABAQUS-EPGEN code is also tested for Sandia's three pressurized steel containment models: a thin cylindrical clean shell clamped at the base with a hemispherical dome; the same geometry stiffened with rectangular ring stiffeners in the cylinder; and a cylindrical shell geometry with penetrations, but without ring stiffeners. The results of these calculations are presented.

1. INTRODUCTION

The purpose of this paper is to provide additional analytical information on the ultimate load behavior of concrete containment structures and the overpressure response of steel containment models. The development of a realistic constitutive model for concrete and its implementation in the ABAQUS-EPGEN code were presented in a recent paper [1]. Calculational results using this code were compared to measurements on near-full-sized reinforced concrete structural specimens, designed and tested by the Construction Technology Laboratory of PCA, which simulate the behavior of a cylindrical wall section of a containment structure. Reasonably good agreement between measurements and calculations were obtained, which demonstrates that the concrete

constitutive model and the code can be used for the prediction of the ultimate pressure capacity of concrete containment structures. It should be stated, however, that the model's constitutive and numerical representation of concrete cracking and rebar-concrete bond, both of which follow the standard literature, lead to a structural response characteristic of smeared cracking and smooth deformations which are at variance with the discrete cracking and dislocation behavior of concrete structures. Consequently, the ultimate pressure capacity predicted using such a global model is generally higher than the anticipated leakage pressure. This is borne out by a number of experiments on prestressed concrete pressure vessel models [2] where it was consistently found that the experimental leakage pressure is significantly smaller (almost by a factor of two in some cases) than the global ultimate as determined by analysis [3]. Although containment structures differ in many respects from pressure vessels (for example, pressure vessels are thick structures and designed for much higher pressures), both types of structures exhibit similar local failure mechanisms induced by the liner-concrete interaction at major crack locations. Whether the wide separation between the leakage failure mode and the burst failure mode observed in prestressed concrete pressure vessels exists also in concrete containment structures is one of the important objectives of the EPRI containment programs currently underway. It might be of interest to point out, in this regard, that the evolution of the local effects which lead to liner rupture is a strong function of the global stiffness of the structure and, as such, are more likely to appear earlier in the much stiffer pressure vessel structures than in containment structures because of the larger capacity of the latter to develop uniform deformations. From an analytical point of view, however, the prediction of the local failure mode remains elusive to general purpose computer codes with standard concrete/reinforcement models currently known in the literature. Such models are suited to global analyses and are, therefore, capable of predicting global (burst) failure modes only.

In an attempt to circumvent the present limitations in the analytical capabilities, the concrete containment analyses reported upon in this paper follow a two-step process. The first step is to calculate the global response of typical reinforced and prestressed concrete containment structures subjected to internal pressure until failure. The primary value of the global analyses, in addition to defining the burst pressure, is to identify the local effects regions with strain/stress concentrations such as the cylinder wall/dome and wall/base mat junctures and the mid-wall of the cylinder. The second step in the analysis process deals with local effects calculations. Two local effects models are analyzed to assess the potential for liner rupture as a result of cracking and combined cracking and stiffness discontinuity. The first model deals with a radial crack to demonstrate the significance of local strain concentrations in the liner as a result of the breathing mode. However, this would not be the lowest failure mode and would probably occur at or

near the pressure to cause rebar yield. A potentially earlier failure mode is treated in the second model, which deals with a meridional-crack/dislocation that results from stiffness discontinuity. In this model, the liner sustains higher localized biaxial strains, which further enhance liner rupture because of reduced liner ductility under biaxial tension. These analyses are presented in Section 3 of the paper.

The calculations performed for Sandia's three pressurized steel containment structural models use the new large-strain thin shell element capability of the ABAQUS-EPGEN code. The behavior of the shells will be evaluated through the pressure/hoop strain response. These results are presented in Section 4 of the paper.

2. GLOBAL ANALYSIS OF CONCRETE CONTAINMENT STRUCTURES

Space limitation prevents a detailed presentation in this paper of the geometric details and complete analysis results. For these, the reader is referred to Reference [4]. Only selective results relevant to the present discussion are included here.

2.1 Prestressed Concrete Structure

The geometry and finite element grid are shown in Figure 1. The primary steel consists of a three-way tendon system in the dome amounting to 1.3% steel/concrete area ratio, and meridional and hoop tendons amounting to 0.5% and 0.75% steel/concrete area ratio, respectively. The hoop reinforcement in the cylinder consists of two layers of #8 bars at 40" spacing on the inside and #11 bars at 10" spacing on the outside. The meridional reinforcement in the wall and the hoop reinforcement in the dome consist of two layers of #11 bars at 10" spacing. The base mat contains #18 bars placed in two layers at 8" spacing in both radial and hoop direction. The skirt and transition section between the base mat and the wall contain #18 and #11 bars at 10" spacing. The liner thickness is 0.375 inches. The prestress load is based on 175 ksi tendon stress which is about 70% of the tendon's ultimate stress of 250 ksi.

The wall and dome are constructed from concrete having a minimum compressive strength of 5000 psi at 28 days. The 28-day minimum compressive strength of the base mat concrete is 3000 psi. Liner material conforms to ASME SA516, Grade 55. Reinforcement bars conform to ASTM A615, Grade 60. Prestressing tendon strands conform to ASTM A416, Grade 270.

The concrete is modeled with 4-node axisymmetric continuum elements integrated at the 2 x 2 Gauss points. The liner is modeled with 2-node thin axisymmetric shell elements integrated at two points along the length and three points through the thickness. Rebars and hoop tendons are modeled with the *REBAR sub-element modeling capability of ABAQUS-EPGEN. Meridional tendons and stirrups are modeled with 2-node axisymmetric truss

elements. Four layers of concrete elements are used through the thickness of the containment except as shown in the haunch region. The 2 ft. thick base slab is modeled with one layer of concrete elements. The anchors for the meridional tendons are modeled with 4-node axisymmetric continuum elements using steel material properties. A total of 657 elements and 591 nodes are used. The model assumes full symmetry boundary conditions along the centerline of the containment and vertical displacement constraints across the base mat where it is in contact with the bedrock. There are no constraints under the tendon gallery. The liner is assumed to be bonded to the concrete containment inner surface.

The loading of the containment consists of a single load step of two load increments to apply the prestress to the tendons followed by a series of load steps and load increments to apply the internal pressure. The prestress is applied as a negative thermal strain for only the tendon elements.

2.1.1 Analysis Results

The uniform hoop strain history at wall midheight and the deformed shape at the highest pressure achieved are shown in Figure 2. The plot is for the strain at a typical concrete element integration point; however, since the hoop strain distribution is nearly constant across the wall, the strains in the liner and rebar are virtually the same. The hoop strain is initially compressive due to the prestress load and becomes tensile at about 120 psi. As shown on Figure 2, the containment loses the concrete stiffness at approximately 130 psi following extensive cracking. The liner has yielded but the hoop rebars and hoop tendons have not. At 150 psi the wall steel is fully plastic and cannot resist further pressurization.

Prior to the onset of extensive cracking at 130 psi, there was only nominal cracking in the haunch and skirt regions. These local cracks are associated with the stiffness discontinuity which is clearly illustrated in the deformed shape of Figure 2. These displacements have been magnified by a factor of 10 so as to better illustrate the behavior. Note the near total loss of stiffness in the midheight region while the haunch and skirt regions remain almost rigid. The crown region shows a downward displacement, apparently caused by the prestress.

As can be deduced from Figure 2, the three local effects regions are the lower skirt, the wall-dome juncture and the belt line. The hoop strains are highest for the latter; however, the meridional strains are highest for the other two locations. These are illustrated in Figures 3 and 4. These figures show the final cracking patterns and strain contours in the skirt and wall-dome regions, respectively, for cracks whose normal lies in the r-z plane. In the figures, a "P" indicates an integration point that is in a state of tension yield but has not reached

failure. The crosses indicate points which have cracked in two orthogonal directions.

Of primary importance to the local effect modeling is the distribution of strain and strain concentration in the skirt and haunch regions as shown in the strain contour plots; these contour lines exclude strains below the cracking strain. The radial cracks caused by the hoop strains do not extend much below the knee or above the haunch, the result of which is large stiffness discontinuities between the cylindrical wall and the base mat and dome.

Figure 5 shows profile plots of the liner strains at pressures of 130 and 150 psi.The solid lines are meridional strains and the dashed lines are hoop strains. The origin of the plots (x = 0) is at the cylinder/base mat intersection. The springline between the cylinder and dome is at 1884" (157 ft), and the top of the dome (crown) is at approximately 2800". As can be seen in this figure, the liner strains are largest in the dome prior to 130 psi pressure and largest in the cylindrical midwall after concrete cracking and liner yield. It is important to note also that there are substantial strain concentrations in the dome near the springline.

2.2 Reinforced Concrete Structure

The geometry and finite element grid are shown in Figure 6. The main wall reinforcement includes an inner and outer layer, each of which consists of #18 meridional rebars at a 12" spacing sandwiched by two layers of #18 hoop rebars at a 14" spacing. In the mid-plane of the wall there is a layer of #18 diagonal rebars oriented at ±45° with respect to the hoop rebars. The spacing of the diagonal bars is 21" for the lower half of the wall and 42" for the upper half. The dome also has inner and outer layers of reinforcement. Each layer consists of #18 meridional and hoop rebars, each at a 12" spacing. The reinforcement ratio for the wall is 2.1% in the hoop direction and 1.2% in the meridional direction. Stirrups and reinforcing steel in the base mat is similar to the prestressed containment model.

The modeling of concrete and reinforcement is similar to the prestressed structure except for the fact that only two layers of concrete elements were used to model the wall through the thickness. This was done in the interest of economy. A total of 106 elements and 112 nodes were used. The purpose of this rather coarse model is to confirm the general characteristics of the global behavior exhibited in the more accurate model of the prestressed structure.

2.2.1 Analysis Results

Concrete strains vs. pressure are shown in Figure 7. Figure 7a shows the calculated concrete hoop strain history for a typical point in the cylindrical mid-wall region. Again, this

figure represents the strain in the steel as well. Concrete hoop cracking began at about 30 psi. The liner reached yield at about 60 psi. Neither of these events are evident in Figure 7a which does not indicate inelastic behavior until first hoop rebar yield is reached at about 105 psi. Final rebar yield is reached at about 115 psi after which all structural stiffness is virtually lost. The calculation was continued to 125 psi where the mid-wall hoop strain exceeded 6%. Figures 7b and 7c show the concrete maximum principal (solid lines) and hoop (dashed lines) strains in the wall-dome and wall-base mat regions, respectively. As in the case of prestressed structure, the three regions of local effects are the wall-base mat juncture, the springline and the belt line. Detailed contour plots for these regions repeat the previous plots and, therefore, are not included here.

3. LOCAL EFFECTS ANALYSES

The global analyses of containment structures presented above help to identify potential local failure locations. These are: the midwall under large hoop strain, and the wall-base mat and wall-dome junctures under large meridional strains. The first can be represented as a radial crack in a segment of the mid-wall of the cylinder; the latter two can be represented as a meridional crack in the wall/dome juncture region. Because of the stiffness discontinuity, the latter is expected to produce more severe local effects. The hoop crack was selected because hoop cracks can be expected to occur at low pressure and over extensive portions of typical reinforced containments. Both local effects models were chosen from the reinforced containment geometry for convenience and to avoid complications in handling the prestressing tendons.

3.1 Radial Crack Model

The geometry and finite element grid of the radial crack model are shown in Figure 8. The width of the model of 18" is based on experimental observations. The concrete is assumed to have a 0.2" through-the-thickness crack in the center of the section. The 0.2" crack width corresponds to approximately the maximum crack opening displacement measured by PCA [5]. It should be noted, however, that the 0.2" crack width represents the final deformation state rather than the initial as assumed here. The evolution of the liner's local strain is the result of a concrete crack opening due to the rebar partial debonding. Therefore, an accurate local effects analysis requires a bond slip model which is not presently available. As a substitute, parametric analyses for several crack widths can be conducted from which the liner local strains can be inferred. The analysis described here represents one case corresponding to one crack width.

The grid consists of 8-node bi-quadratic quadrilateral elements, 30 for the concrete and 16 for the liner, and 14 3-node quadratic truss elements for the hoop rebar. A total of 60

elements and 173 nodes were used. The liner elements were integrated using the 3 x 3 Gauss rule, whereas the concrete elements were integrated using the 2 x 2 Gauss rule.

One of the important features of this local geometry is the load transfer mechanism between the liner and the concrete. Accurate modeling of this interface requires a bond-slip model, as discussed above, which is not presently available. Since the main contribution of the concrete is to provide the load transfer mechanism from the liner to the rebar, the concrete and concrete/liner interface was modeled as an elastic orthotropic concrete with the hoop modulus reduced to 1% of the normal value and the radial and shear moduli were held at their usual elastic values. Poisson's ratio was taken as zero.

3.1.1 Analysis Results

Figure 9a shows the liner hoop strain as function of pressure for the outer integration points near the center (solid lines) and crack edges (dashed lines). Figure 9b shows the history of the rebar strain for the inner (solid lines) and outer (dashed lines) rebar layers. It can be seen from these figures that the maximum liner hoop strain was approximately 3% when the inner rebar reached yield. After the outer rebar layer yielded, the liner strain increased rapidly. The analysis was terminated at 110 psi with a maximum computed liner hoop strain of approximately 9%.

The global analysis at 110 psi shows that the liner (and concrete) hoop strain is approximately 0.4% (see Figure 7); whereas, in the local model the maximum liner hoop strain is 9%, which represents a substantial strain concentration. It is interesting to note, however, that the global and local models show loss of resistance at about the same pressure (110 to 115 psi), which verifies the significant fact that the burst pressure capacity of the structure is not affected by local concentrations and vice versa.

3.2 Meridional Crack Model

The second local effects model chosen for detailed analysis is an axisymmetric section taken at the cylinder wall-dome juncture. It is not possible to use symmetry boundary conditions at the edges of the local model; therefore, the local model was included in a coarse grid of the entire containment as shown in Figure 10.

As before, the concrete was modeled as an elastic orthotropic material. Again, the orthotropic properties were chosen to reflect the extensive hoop cracking in the global model. The hoop modulus was reduced to 1% of the normal value and the radial, meridional and shear moduli were kept at their usual elastic values. The properties of the liner and rebar are the same as for the radial crack local effects model.

3.2.1 Analysis Results

Figure 11a shows the liner effective strain and rebar strain histories. The liner strains are shown for the three integration points near the outer surface. Figure 11b shows the meridional rebar strain history for the inner (solid lines) and outer (dashed lines) rebar layers. As noted earlier, this model reflects more severe conditions than the previous radial crack model because of the stiffness discontinuity. As seen in the figure the liner effective strain, prior to rebar yield, is 5% (compared to 3% for the radial crack model) at a pressure of 100 psi.

4. STEEL CONTAINMENT MODELS

Calculations were performed for three pressurized steel containment structural models: a clean shell (radius-to-thickness ratio: R/t = 486) clamped at the base with a hemispherical dome; the same geometry stiffened with rectangular ring stiffeners in the cylinder; and the same geometry with penetrations, but without ring stiffeners. The axisymmetric geometries of the stiffened shell and the penetration are shown in Figure 12. Due to lack of space, selected material only is presented here. The reader is referred to Reference [6] for geometric and modeling details and more complete analysis results.

4.1 Finite Element Models

The ABAQUS-EPGEN code has two axisymmetric thin shell elements that can be used to model these shell structures, namely, the SAX1 and SAX2 elements [7]. As described in the theory manual, these elements are formulated using the reduced-integration penalty method [7,8]. This method permits the development of efficient low-order shell elements by replacing pointwise compatibility with the classical thin shell approximations with reduced integration and penalty functions. The SAX1 element uses linear interpolation (straight) and has 2 corner nodes; the SAX2 element uses quadratic interpolation and has 3 nodes, 2 corner and 1 mid-side. The SAX2 element was used to model the dome and cylindrical sections because it is curved and gives a better representation of the dome geometry and because its quadratic interpolation gives more accurate results.

4.1.1 Clean Shell

A total of 31 axisymmetric 3-node (quadratic) shell elements (SAX2) and 63 nodal points are used. There are 13 elements in the dome, 10 spaced at 8.1° from the crown and 3 spaced at 3° near the springline. There are 18 elements in the cylinder. The thickness of the dome varies from the crown as follows: 2 elements at 0.0705"; 4 at 0.0645"; 4 at 0.0544"; and 3 at 0.0426" at the springline. Symmetry boundary conditions are used at the crown, and the base is clamped. Three Gauss points are used through the thickness, and the stiffness matrix for the SAX2

element is integrated using 2 Gauss points along its length; whereas, the consistent nodal point force integration for pressure is done with 3 Gauss points. These integration formulas give an accurate representation of the stiffness and nodal point forces. There are 184 active degrees-of-freedom for the clean shell model.

4.1.2 Stiffened Shell

The finite element model used for the stiffened shell is similar to the clean shell. Starting at the crown of the dome, there are 10 3-node SAX2 elements spaced at 8°, 2 at a thickness of 0.0705", 4 at 0.0645" and 4 at 0.0544"; near the springline there are 2 elements spaced at 5° with a thickness of 0.0426". (This is virtually the same as the clean shell.) In the cylinder there are 21 elements, one between the springline and the closest stiffener, and two between each pair of stiffeners. Thus, there are 33 elements and 67 nodes in the shell. Five integration points are used through the thickness. The stiffeners are modeled with SAX1 elements, thus adding 10 nodes and elements. The SAX1 linear interpolation elements are used because the stiffeners are expected to provide only hoop membrane resistance. For the entire stiffened shell, there are 77 nodes and 226 degrees-of-freedom.

The stiffeners are 0.260" wide by 0.125" thick; however, double-sided brazing adds considerable material to the stiffeners [9] estimated at 50%. This is accounted for by increasing the thickness of the stiffener elements by 50% to 0.1875" in the finite element model.

4.1.3 Shell with Penetrations

A complete model of the shell with penetrations requires a general doubly-curved three-dimensional shell element. The cost of such a three-dimensional model would be large. Furthermore, at the time this work was done, ABAQUS-EPGEN did not have large strain capability for a general shell element. Therefore, an axisymmetric model of the larger penetration was selected for detailed study. A similar model was used by Sandia [10].

The penetration model consists of 11 SAX2 elements in the spherical cap, 4 SAX2 elements in the sleeve and 5 SAX2 elements in the cylinder. A total of 20 SAX2 elements and 59 nodes are used. Symmetry conditions are imposed on the axis and at the edge of the grid in the cylinder, approximately 5" from the sleeve. In order to correctly model the cylindrical hoop stress in a spherical geometry, the radius of the "cylinder" is doubled to 43.172" in the model.

4.2 Material Properties

All the material properties used in the analyses are based on tensile coupon specimen data measured by Sandia [10,9]. For all

steels, Young's modulus is 30.5 x 10^6 psi and Poisson's ratio is 0.32. The following table gives the piece-wise linear plastic properties for the three steels: the stress at zero equivalent plastic strain (ε_p) is the yield stress.

PIECE-WISE LINEAR REPRESENTATION OF
STRESS VS. EQUIVALENT PLASTIC STRAIN FOR ALL STEELS

Cylinder Steel		Dome Steel		Stiffener & Sleeve Steel	
σ(ksi)	ε_p	σ(ksi)	ε_p	σ(ksi)	ε_p
40.0	0.0	45.0	0.0	40.0	0.0
41.3	.01	50.0	.01	46.0	.02
45.6	.03	61.5	.21	55.0	.06
50.6	.06	61.5	∞	60.0	.10
55.7	.12			65.0	.16
65.4	.27			65.0	∞
65.4	∞				

Isotropic hardening is assumed for all steels. Since one of the objectives of this effort is to predict extreme overpressure behavior, the maximum elongation, especially for the cylinder steel, is an important property. The uniaxial ductility for the cylinder steel varies from 29% to 33% equivalent plastic strain. The ductility of the stiffener steel is considerably less and varies from 17% to 21%. The ductility of the dome steel is not a significant factor.

4.3 Analysis Results

The clean shell strain histories are presented in Figure 13. This figure shows the meridional (solid line) and hoop (dashed line) strain histories for the most highly strained element which is located near the mid-height of the cylinder. At 128 psig the largest hoop strain is 23% and the meridional strain at this point is 3%. As the hoop strain continued to increase, the pressure that the cylinder could support fell because of thinning of the cylinder. At 128 psig. the shell thinning is approximately 26%. In the final configuration, which is beyond the ductility limit (<30%) of the cylinder steel. the shell supported approximately 122 psig at 34% strain.

The strain histories for the stiffened shell are shown in Figure 14. The general behavior is similar to that of the clean shell except for the increased pressure capacity (147 psig vs. 128 psig) due to the stiffeners. The analysis was discontinued at a strain of 30%. In this final configuration the shell supported 134 psig and the wall thinning is approximately 25%. The deformed shapes at maximum pressures are shown for the two shells, for easy comparison, in Figure 15. The displacements in these plots are unmagnified.

Similar comparison in Figure 16 shows profile plots of the averaged meridional (solid line) and hoop (dashed line) strains

at the maximum pressures for the two shells. The zero position is at the apex, the springline is at 34", and the base is at 77".

The results for the spherical cap are shown in Figure 17. The spherical cap experienced a snap-through type instability at approximately 78 psig, which is well below the pressure to yield the cylinder. Figure 17a shows the vertical displacement of the apex as a function of the pressure. Following the initiation of the snap-through instability, the pressure drops to approximately 15 psig after the apex displaces about 0.6". Beyond this point the loading path becomes stable again. Figure 17b shows the unmagnified displaced configuration of the entire axisymmetric penetration model at the end of the computation. Considerable bending has occurred in the knuckle region of the cap. Figure 17c shows the history of meridional strain on the outside surface near the knuckle region.

4.4 Conclusions

In the absence of experimental data comparisons, the analyses of the steel containment models provide a qualitative validation of the computational models in ABAQUS-EPGEN code; the computational results are consistent with expected behavior. The following failure pressures are estimated for the various models.

CLEAN SHELL: Based on the assumption that the biaxial effective strain ductility limit is 25% less than the measured uniaxial ductility and that the minimum thickness in the mid-cylinder region is 0.0435", we anticipate the clean shell to fail at 122 psig and 17% hoop strain.

STIFFENED SHELL: Based on a ductility limit of 17% for the stiffeners (which is the same as the hoop strain ductility for the clean shell) and a minimum thickness of 0.0435", we anticipate the stiffened shell to fail at 142 psig and 17% hoop strain.

SHELL WITH PENETRATIONS: The large reverse-curvature spherical cap penetration is predicted to experience a severe snap-through instability at 78 psig. This instability could cause failure in the knuckle or weld and result in a blowout.

REFERENCES

1. Nuclear Engineering and Design, Special EPRI Edition, Vol. 75 (1983) No. 1, October 1983. R. S. Dunham, et al., "Evaluation of Calculational and Material Models for Concrrete Containment Structures" and J. T. Julien, et al., "Tension Tests of Concrete Containment Wall Elements."

2. Conference on Prestressed Concrete Pressure Vessels at Church House, Westminster, S.W.I., March 13-17, 1967, The Institution of Civil Engineers, London, 1968.

3. Y. R. Rashid, "Ultimate Strength Analysis of Prestressed Concrete Pressure Vessel," Nuclear Engineering and Design, Vol. 7, 1968.

4. R. S. Dunham, et al., "Methods for Ultimate Load Analysis of Concrete Containments," ANATECH, ANA-83-013, Final Report to EPRI, RP2172-1, December 1983.

5. J. T. Julien, et al., "Concrete Containment Structural Element Tests - Phase 1," Construction Technology Laboratories, Final Report to EPRI, RP2172-2, April 1983.

6. R. S. Dunham, et al., "Evaluation of Overpressure Response of Steel Containment Structures," ANATECH, ANA-83-014, Final Report to EPRI, TPS82-661-2, February 1984.

7. H. D. Hibbitt, et al., "ABAQUS-EPGEN Version 4-4 Volume 1 User's Manual and Volume II Theoretical Manual," EPRI Report NT-2709-CCM, October 1982.

8. T. J. R. Hughes, et al., "A Simple and Efficient Element for Plate Bending," Int. J. Num. Meth. Eng., 11, No. 10., 1977, pp. 1529-1543.

9. D. S. Horschel and T. E. Blejwas, "Analytical Investigation of the Responses of Steel Containment Models to Internal Pressurization," Trans. SMiRT 7 Paper J 6/4, Chicago, August 1983.

10. T. E. Blejwas, et al., "Containment Integrity Program FY82 Annual Report," NUREG/CR-3131/1 and SAND83-0417, March 1983.

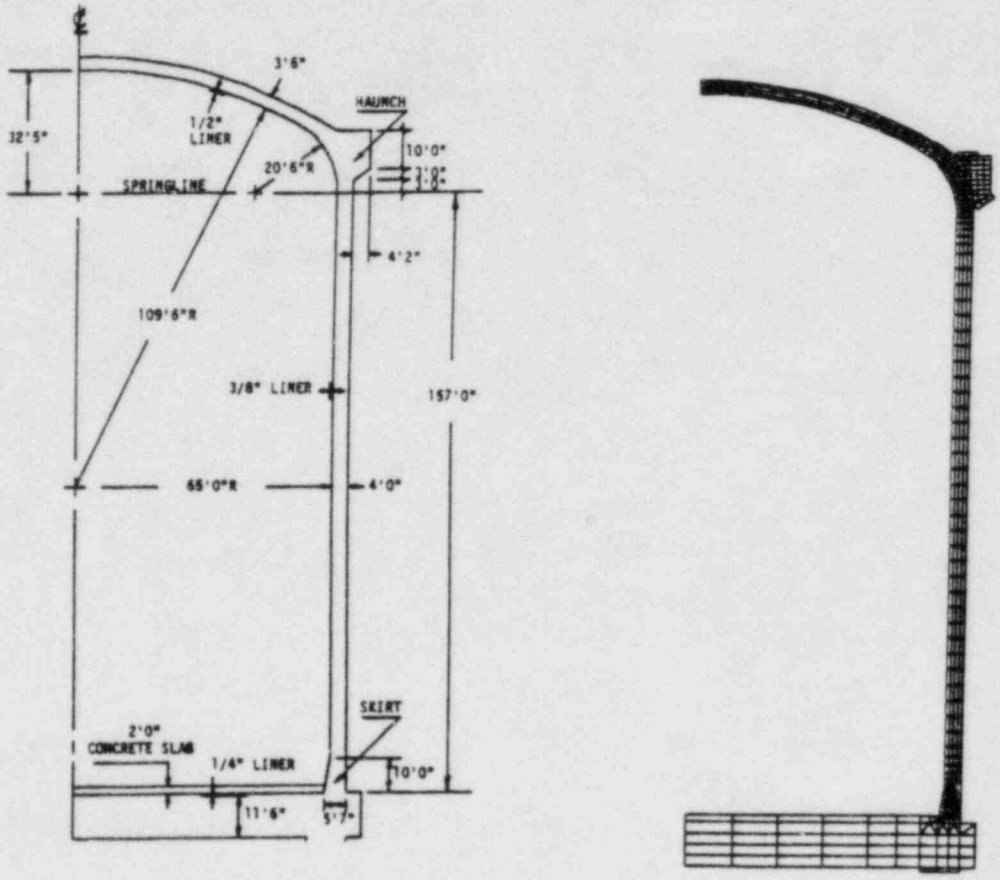

Figure 1. Geometry and Finite Element Grid of Prestressed Containment

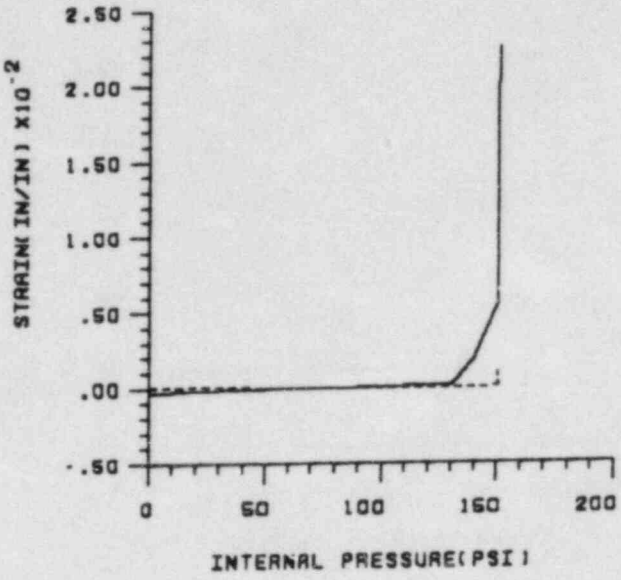

(a) MID-WALL CONCRETE STRAIN

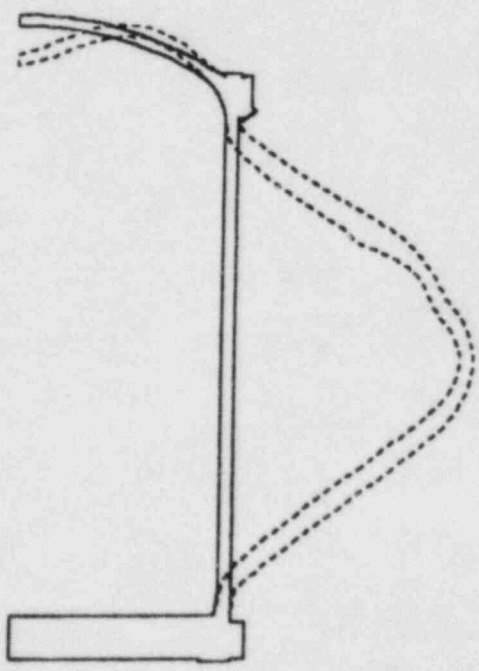

(b) DEFORMED SHAPE AT 151 PSI

Figure 2. Strain and Deformed Shape for Prestressed Containment

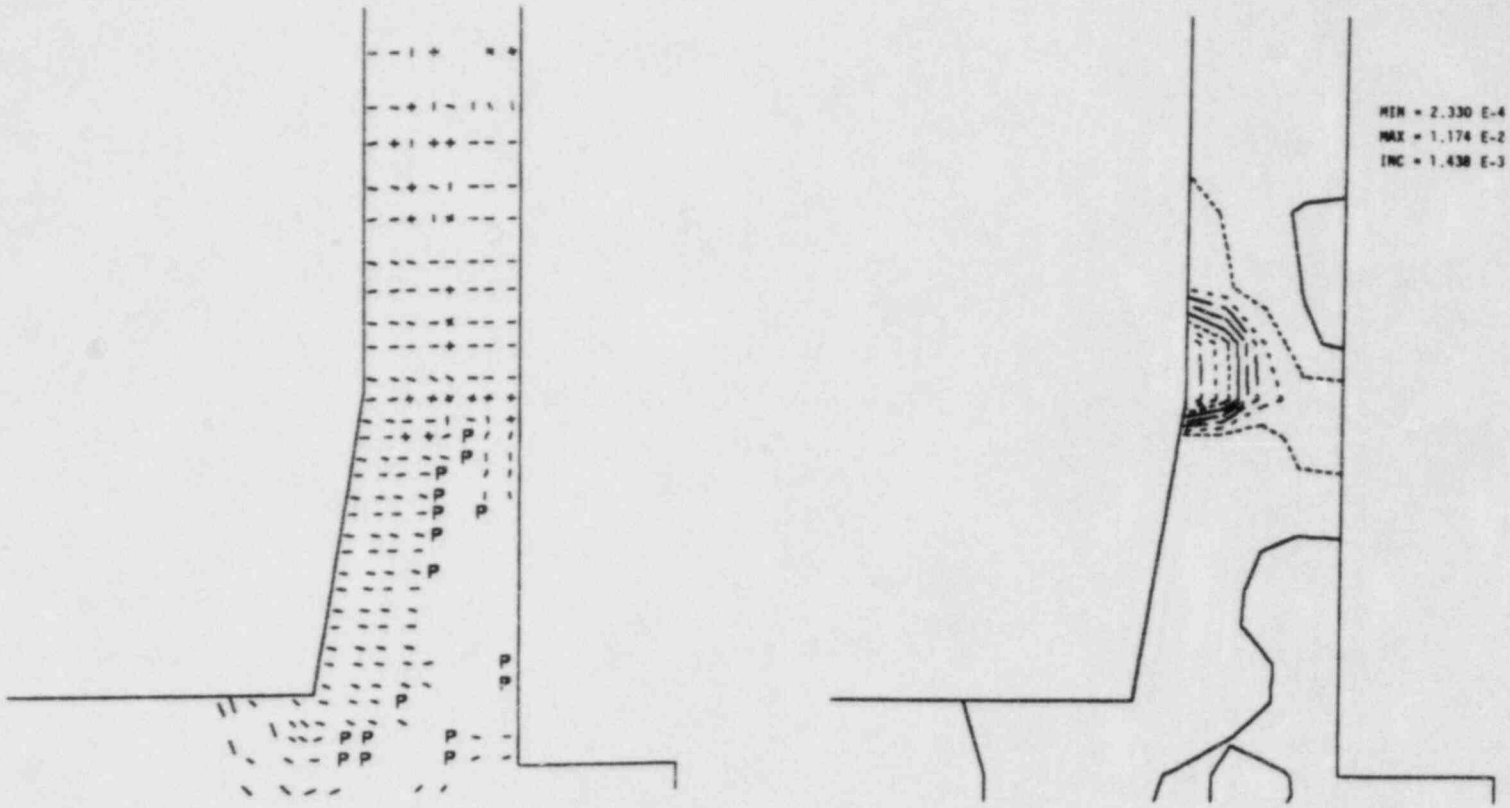

Figure 3. In-Plane Cracking Patterns and Maximum Strain Contours Near Skirt for Prestressed Containment

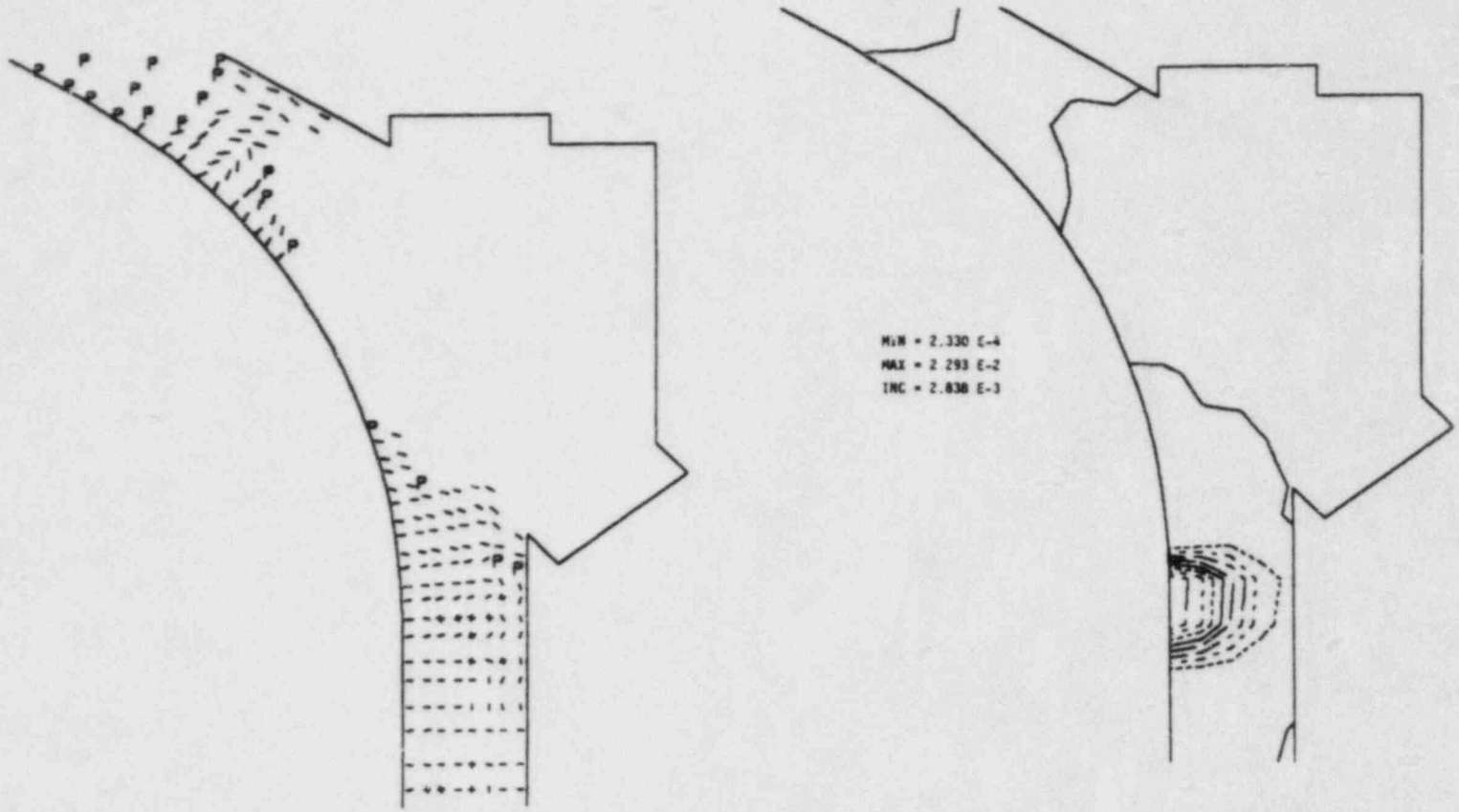

Figure 4. In-Plane Cracking Patterns and Maximum Strain Contours Near Haunch for Prestressed Containment

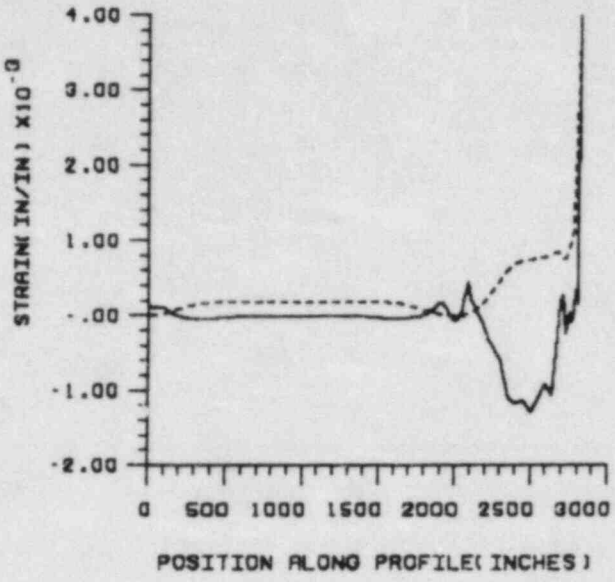

(a) 130 PSI PRESSURE

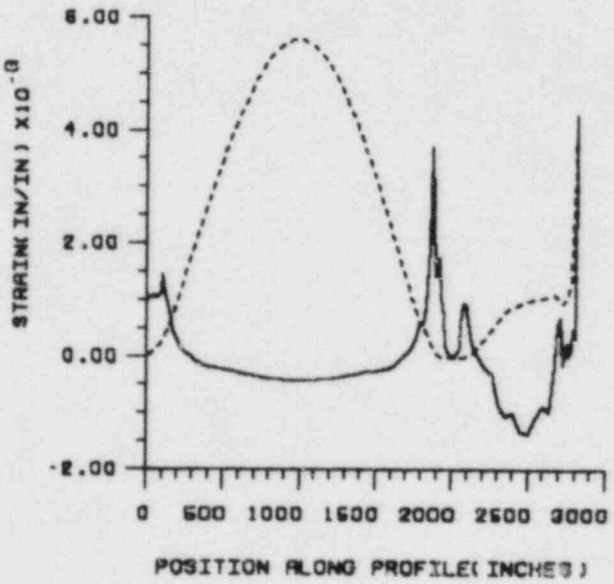

(b) 150 PSI PRESSURE

Figure 5. Liner Strain Profiles for Prestressed Containment

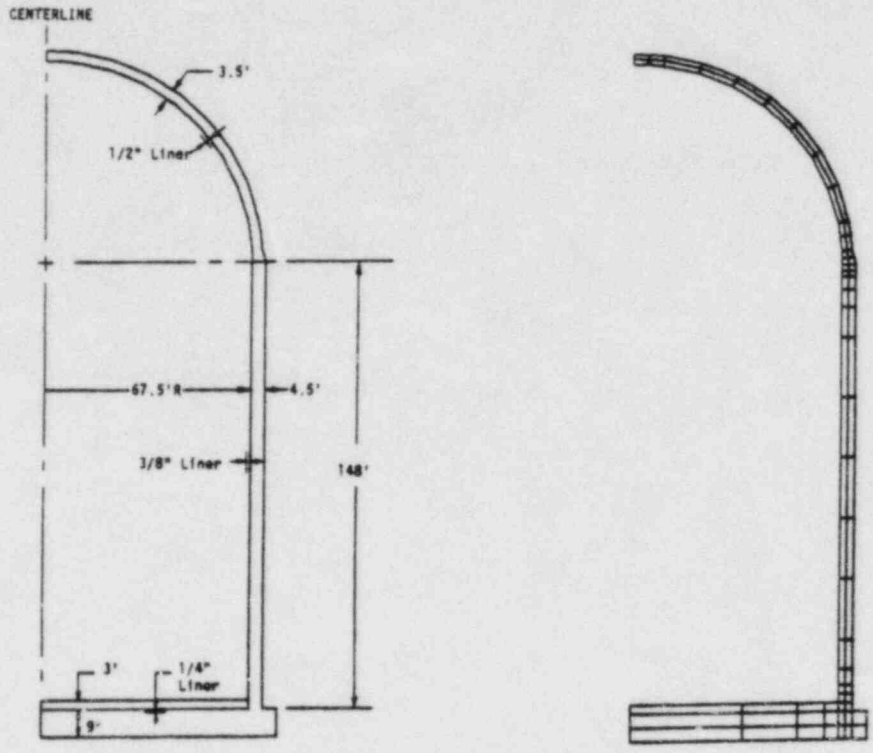

Figure 6. Geometry and Finite Element Grid for Reinforced Containment

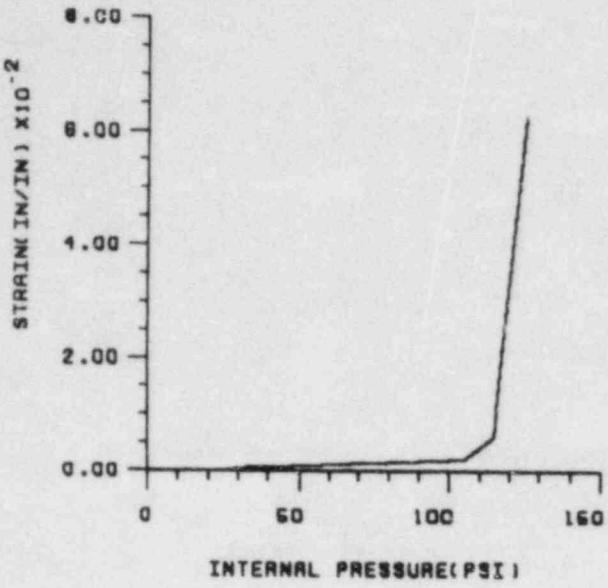

(a) MIDWALL

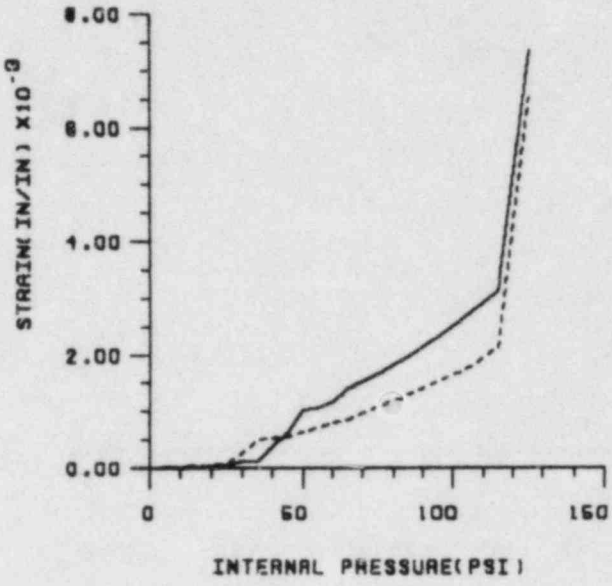

(b) WALL-DOME JUNCTURE

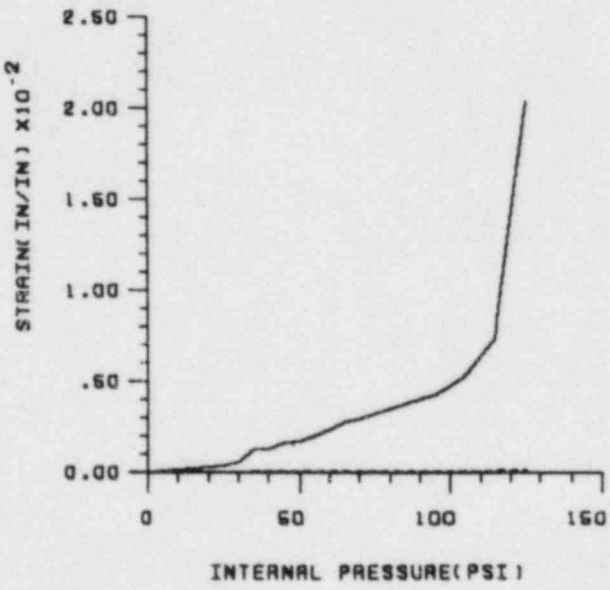

(c) WALL-BASE MAT JUNCTURE

Figure 7. Concrete Strains in Reinforced Containment

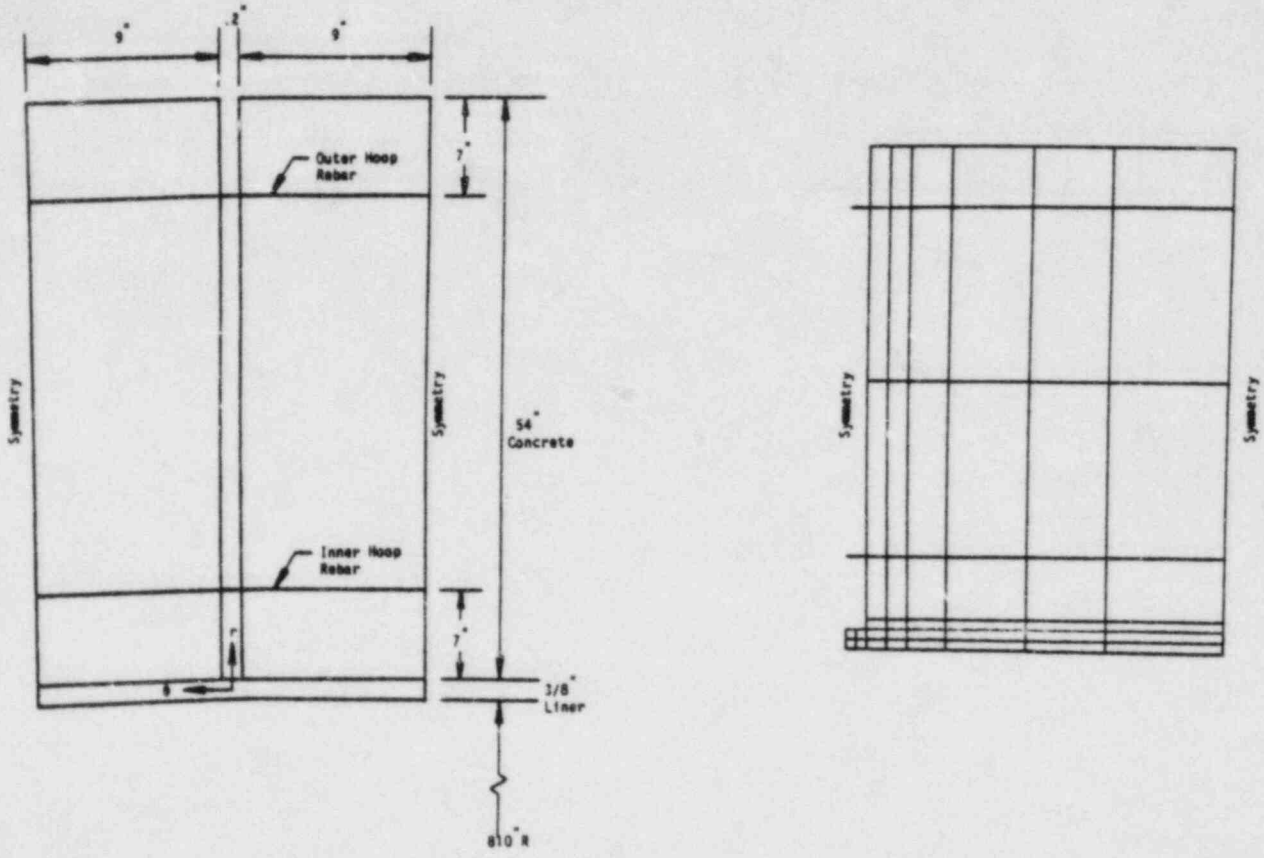

Figure 8. Radial Crack Local Effects Geometry and Finite Element Grid

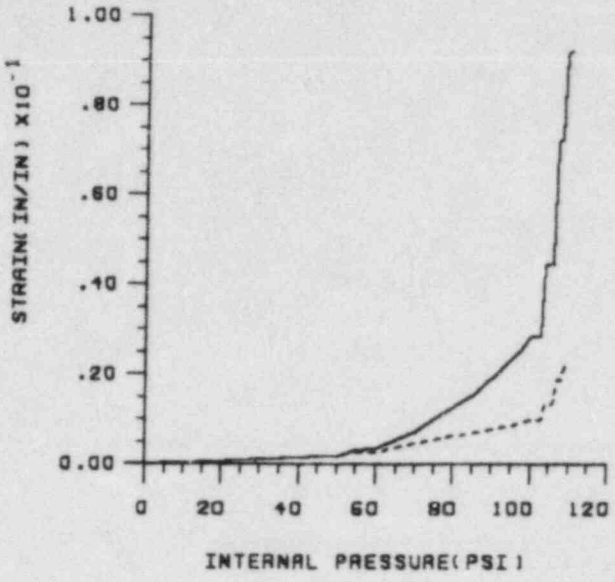

(a) LINER STRAIN

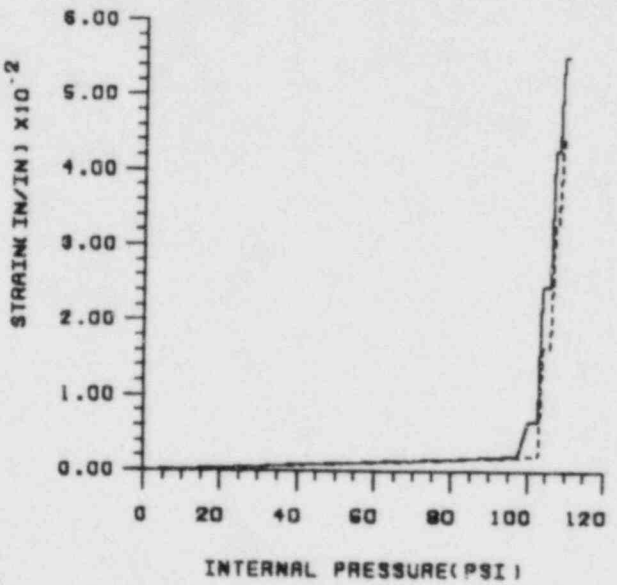

(b) REBAR STRAIN

Figure 9. Radial Crack Local Strins

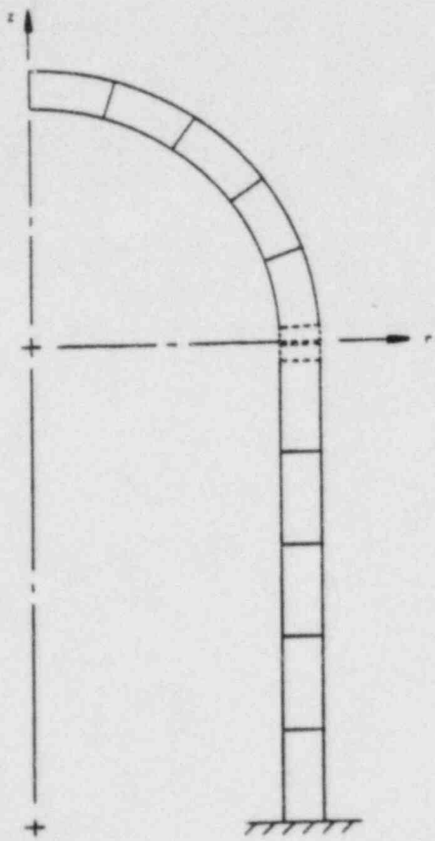

(a) COARSE GRID

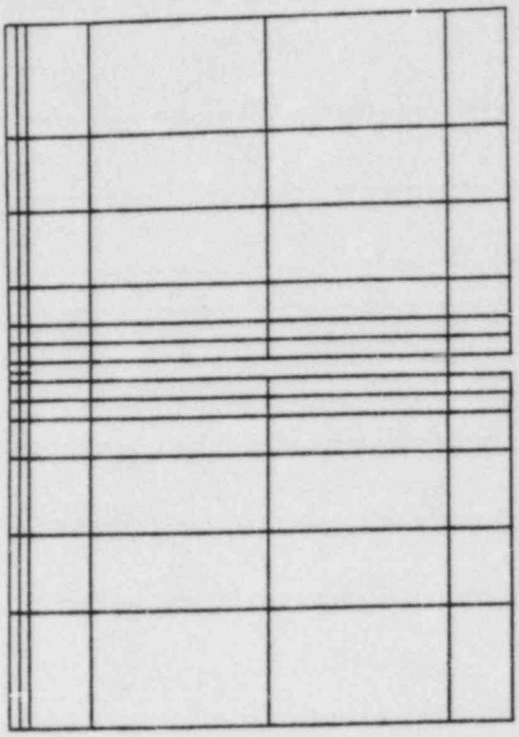

(b) FINE GRID REGION

Figure 10. Meridional Crack Local Effects Model

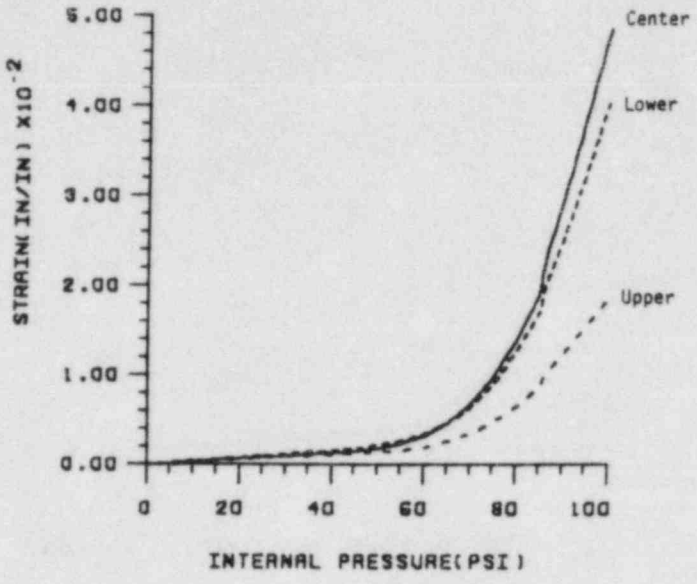

(a) EFFECTIVE STRAIN IN LINER

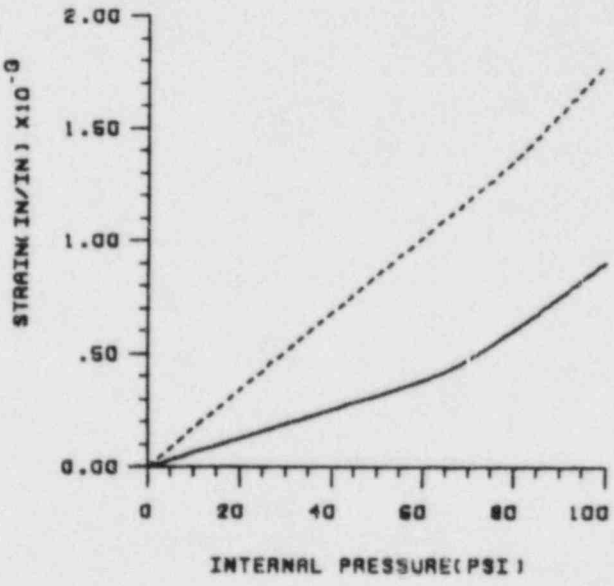

(b) REBAR STRAINS

Figure 11. Meridional Crack Local Strains

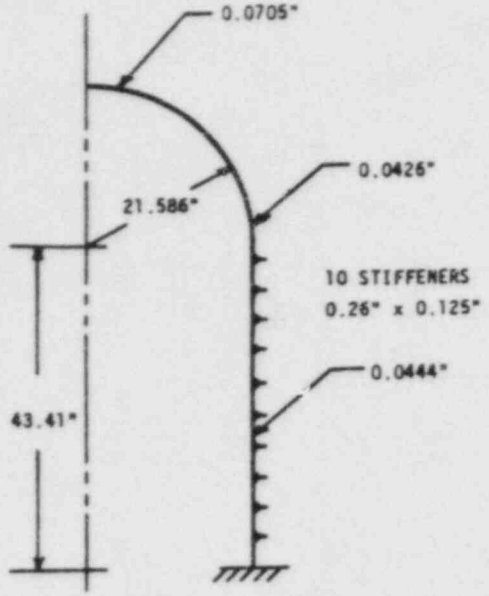

(a) STIFFENED SHELL

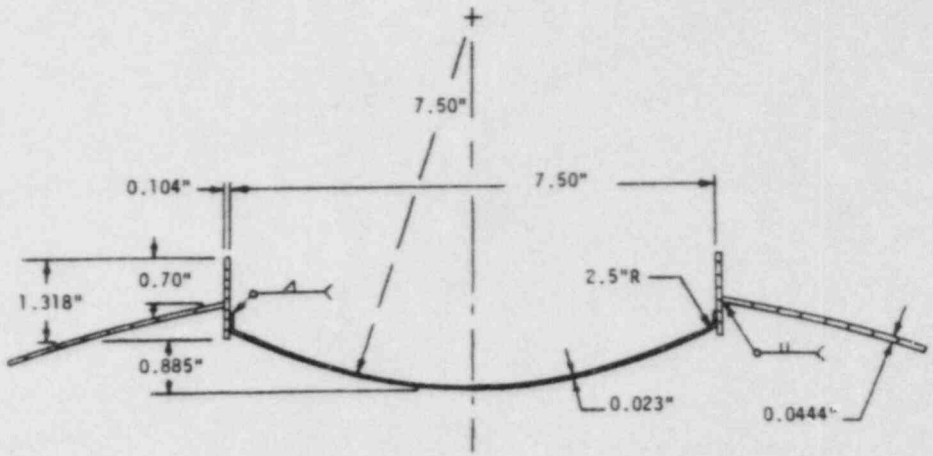

(b) DETAILS OF THE LARGE PENETRATION

Figure 12. Axisymmetric Shell Geometry

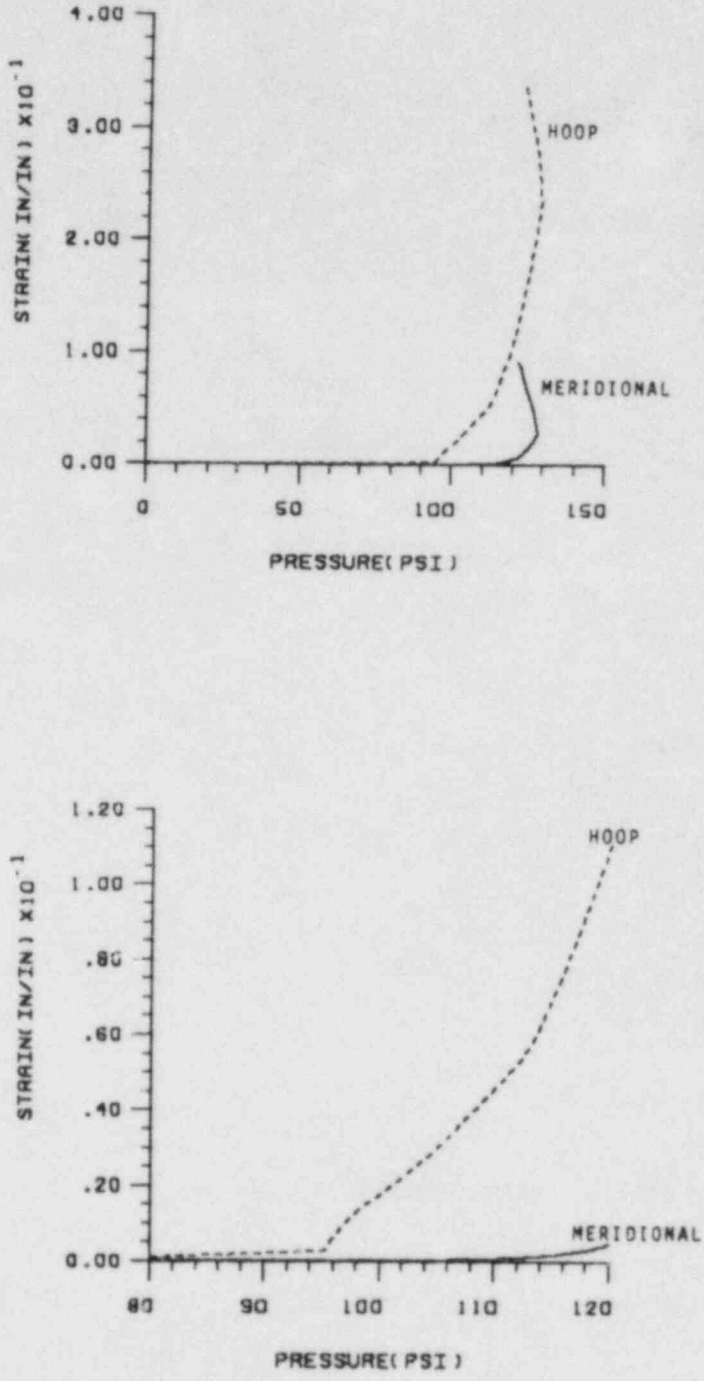

Figure 13. Clean Shell Mid-Cylinder Strain Histories

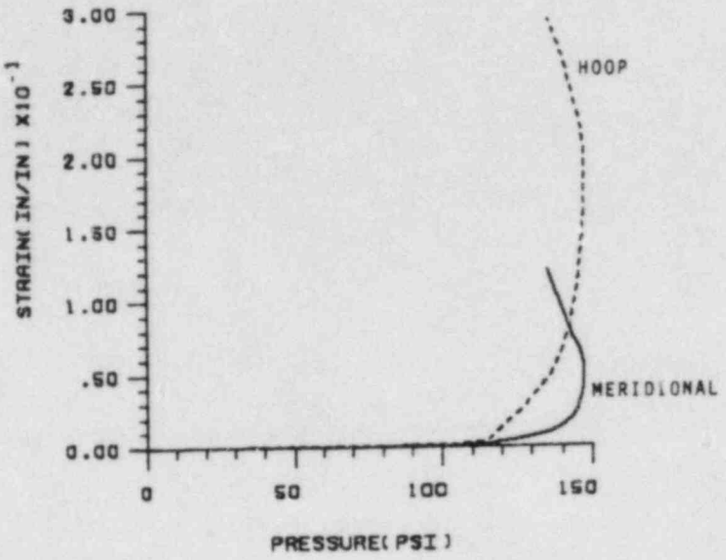

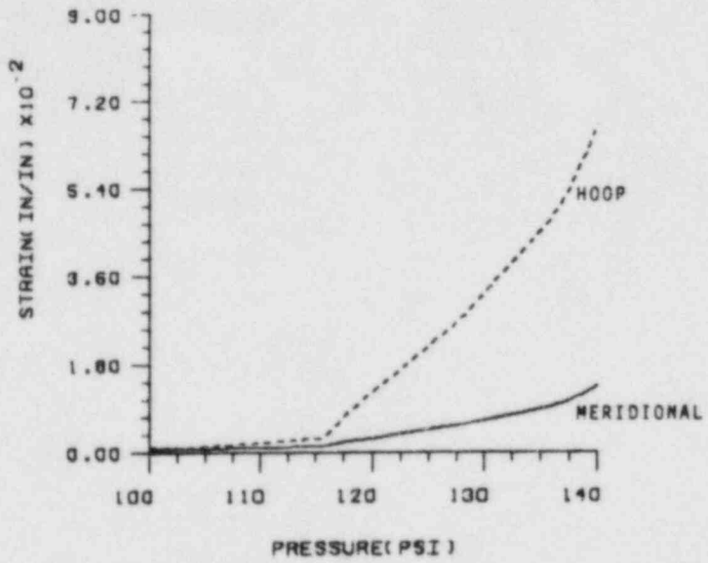

EXPANDED SCALE

Figure 14. Stiffened Shell Mid-Cylinder Strain Histories

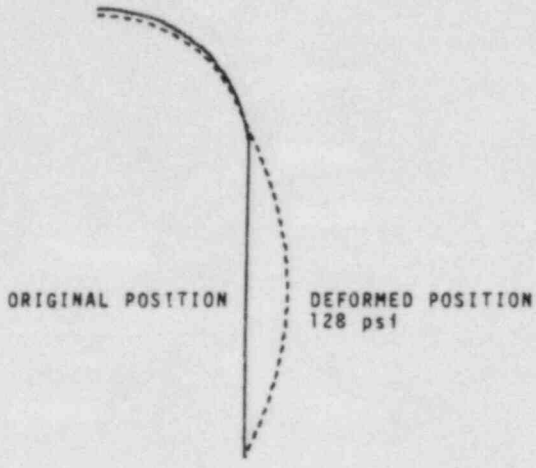

(a) CLEAN SHELL DEFORMATION AT 128 PSI

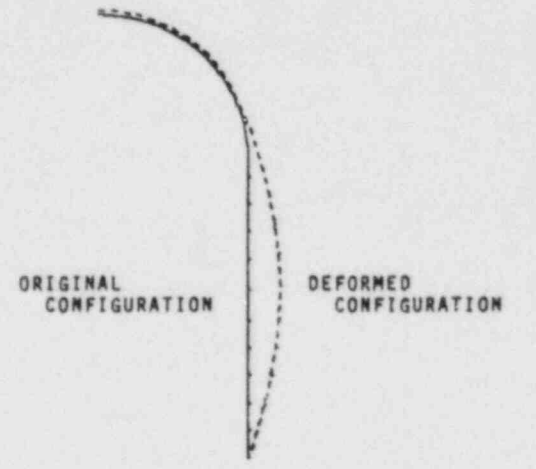

(b) STIFFENED SHELL DEFORMATION AT 147 PSI

Figure 15. Deformed Shapes of Steel Containment Models

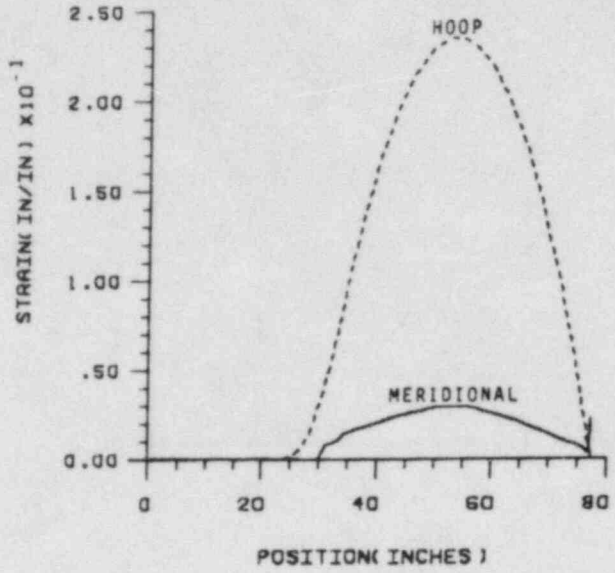

(a) CLEAN SHELL STRAIN PROFILE AT 128 PSIG

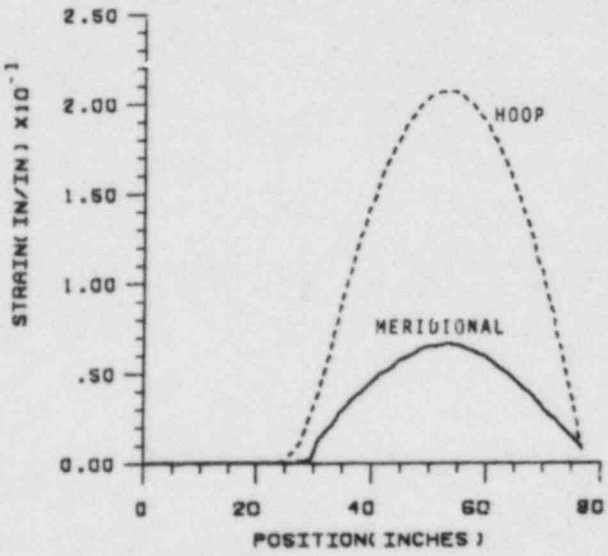

(b) STIFFENED SHELL STRAIN PROFILE AT 147 PSIG

Figure 16. Strain Profiles for Steel Containment Models

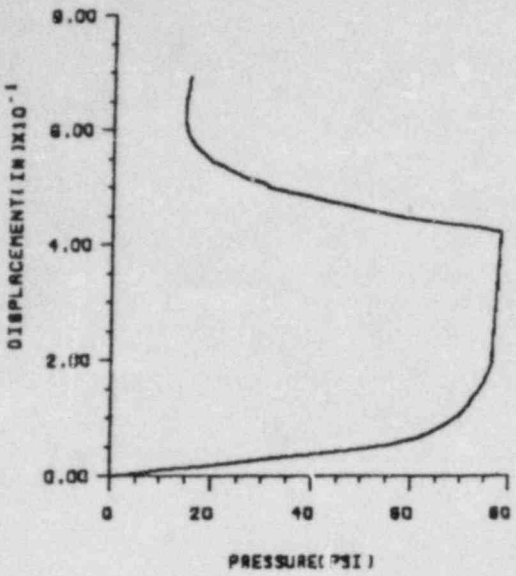

(a) SPHERICAL CAP APEX DISPLACEMENT

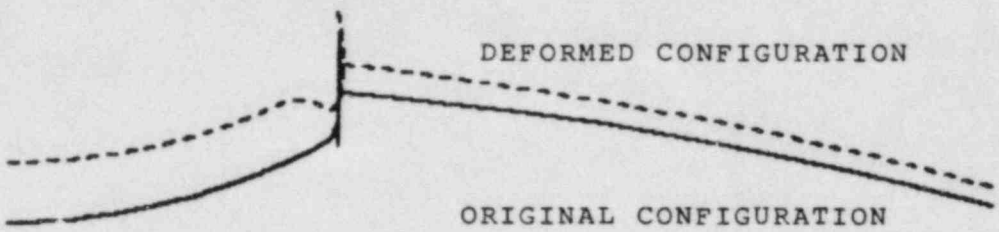

(b) FINAL DEFORMED SHAPE AT 15 PSIG

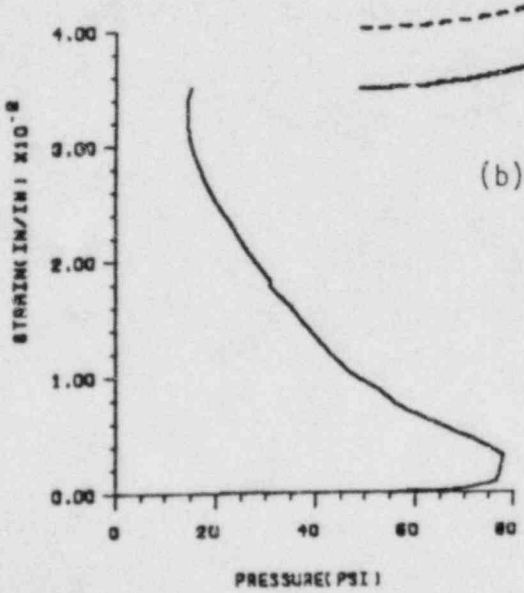

(c) OUTSIDE SURFACE MERIDIONAL STRAIN NEAR KNUCKLE

Figure 17. Strains and Deformations in Steel Containment Model Penetration

THERMAL STRESSES IN PWR-CONTAINMENTS UNDER LOSS OF COOLANT ACCIDENTS

B. Göller, G. Hailfinger, R. Krieg
Kernforschungszentrum Karlsruhe GmbH
Institut für Reaktorentwicklung
Projekt Nukleare Sicherheit
Postfach 3640
D-7500 Karlsruhe, FRG

ABSTRACT

A local circular temperature increase is assumed in a slice, a cylindrical shell and a spherical shell and the resulting stresses are calculated. For the slice and the cylindrical shell the maximum membrane stresses are relatively high, but for the spherical shell the membrane stresses are small. The reason for this difference is discussed in some detail and the conclusion is made, that investigations of thermal stresses in cylindrical shells can hardly be extrapolated to spherical PWR-containments.

1. Description of the Problem

Considerable temperature variations over PWR-containment shells are expected during a loss of coolant accident. They may cause high thermal stresses in the containment shell as measured during some HDR-experiments /1/. However, these stresses are self-equilibrated and thus the resulting strains remain in the order of the thermal expansion which is far away from the ultimate strain of the material. Moreover a loss of coolant accident will occur not more than once during the life time of a reactor. Therefore the thermal stresses have almost no influence on the structural integrity of the containment shell.

Nevertheless in the German design rules /2/, limits are given for the thermal stresses in containment shells in case of a loss of coolant accident. Therefore thermal stresses caused by a local temperature increase, which is expected for a loss of coolant accident, are investigated here.

Two different spatial temperature distributions are assumed, a discontinous-type and a cosinus-type. They are shown in Fig. 1. The heated region has the radius a. The maximum temperature increase is $T = 100\ ^{o}C$. The coefficient of the thermal expansion is $\alpha = 1.2 \cdot 10^{-5}\ 1/^{o}C$.

In order to study the influence of different geometries, thermal stresses are calculated for a slice, a cylindrical shell and a spherical shell. The material is assumed to be linear elastic with a Youngs Modulus of $E = 2.1 \cdot 10^{11}\ N/m^2$. The boundaries

of the slice and shells are free to move. Mechanical lo ds are not applied.

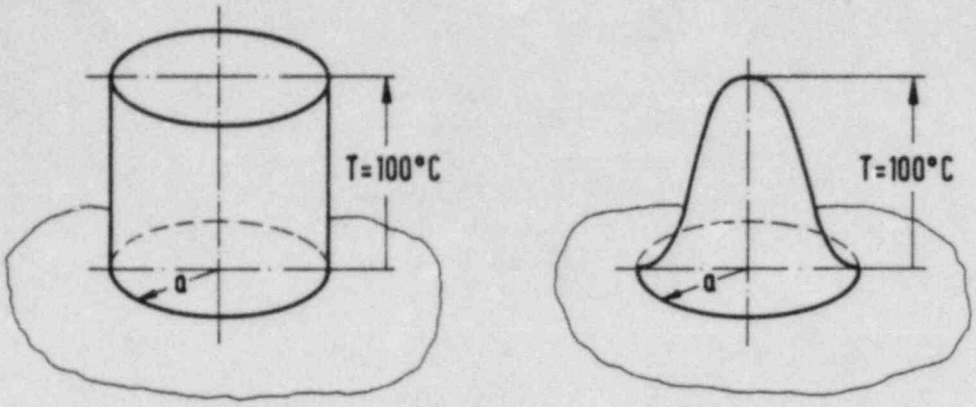

discontinous-type temperature distribution

cosinus-type temperature distribution

Fig. 1: Types of local temperature increase

2. Thermal Stresses in a Slice

The thermal stresses in an infinite slice can easily be calculated using Airy's stress function /3/.

Discontinous-type-temperature distribution

At a distance r from the center of the temperature increase the radial stress σ_r and the tangential stresses σ_t are

$$\left.\begin{aligned}\sigma_r &= -\frac{E\alpha T}{2}\frac{a^2}{r^2}\\ \sigma_t &= \frac{E\,T}{2}\frac{a^2}{r^2}\end{aligned}\right\} \quad r > a \qquad \left.\begin{aligned}\sigma_r &= \\ \\ \sigma_t &=\end{aligned}\right\} -\frac{E\alpha T}{2} \quad \Bigg\} \quad r < a$$

With the quantities given above the resulting stresses are shown in Fig. 2. The maximum stress is $|\sigma|_{max} = 1/2\ E\alpha T = 125\ N/mm^2$.

Cosinus-type-temperature-distribution

In this case the shapes of the stress distributions are more difficult to describe. They can be approximated by superposition of stress distributions for discontinous-type-temperature distributions. The maximum stress occurs at the center of the temperature increase and assumes the same value as before, namely $|\sigma|_{max} = 1/2\ E\alpha T = 125\ N/mm^2$.

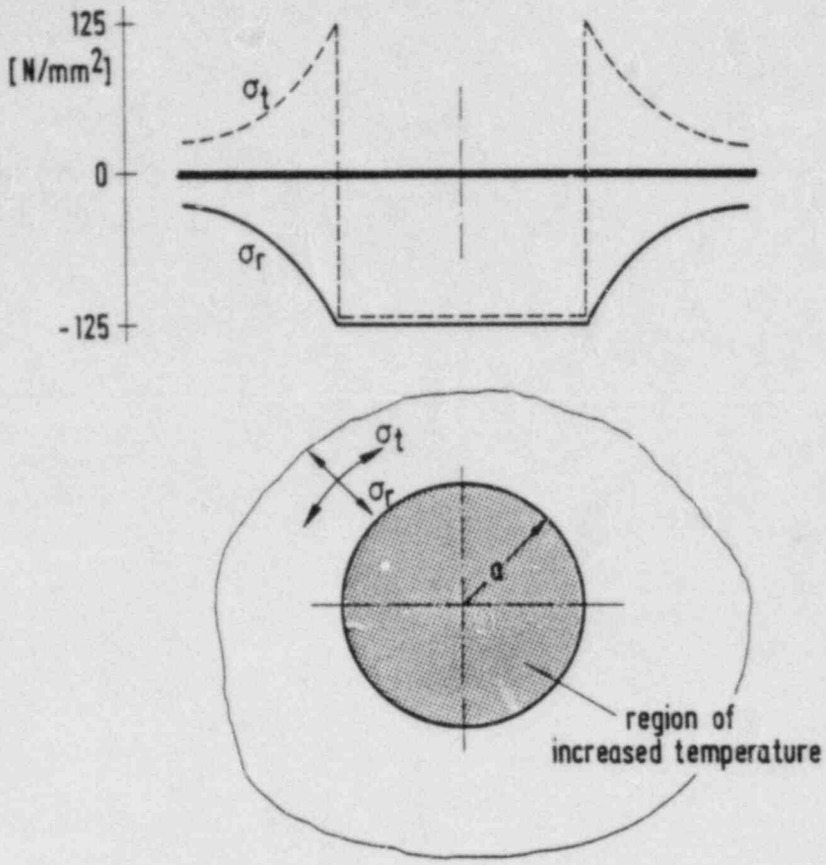

Fig. 2: Stress distribution in an infinite slice with a discontinuous type of temperature distribution

3. Thermal Stresses in a Cylindrical Shell

If bending stresses are neglected, the membrane stresses in tangential direction are proportional to the pressure loading acting in normal direction. However, for the thermal stress problem investigated here, the pressure loading vanishes. Consequently, if shell bending stresses are neglected, the membrane stresses in tangential direction vanish, too.

If furthermore the shell deformations are assumed to be small, also the membrane stresses in axial direction and the shear stresses can easily be determined from the conditions of equilibrium /4/. Again, for the thermal stress problem without external loading, the membrane stresses in axial direction and the shear stresses vanish.

On the other hand, from simple considerations it is evident that in cylindrical shells without external loading but with nonuniform temperature distributions, membrane stresses may occur. Consider, for instance, a cylindrical shell, where a small axial strip is heated. Therefore it can be concluded that the

neglect of bending and at the same time the assumption of small shell deformations may be not acceptable.

Thus, in order to solve the thermal stress problem, bending is included. The calculations are carried out by the finite element program STRUDL /5/. The model used is shown in Fig. 3.

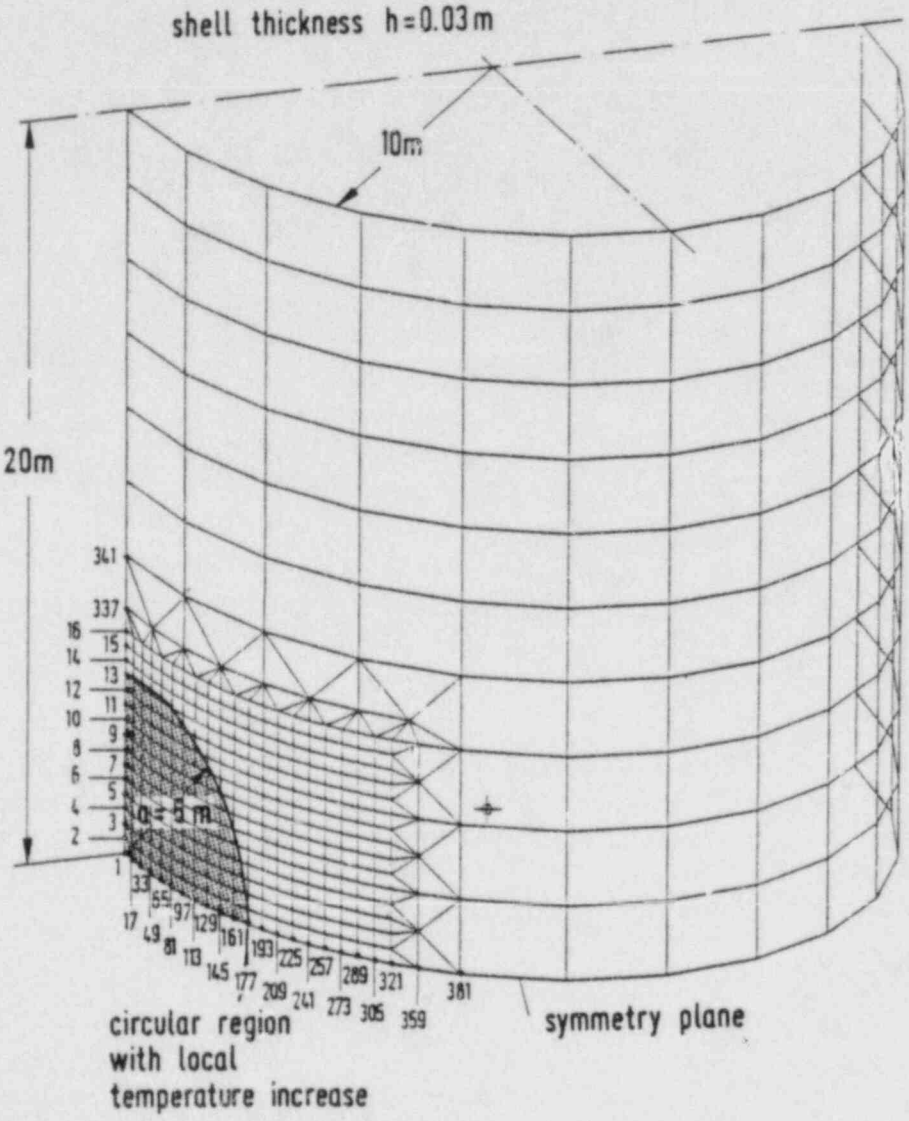

Fig. 3: Finite element model of the cylindrical shell

In order to check the adequateness of the finite element discretization, besides the model in Fig. 3, two additional models with different element sizes have been used. Comparison of the results showed that in the region of the increased temper-

ature and in the close neighbourhood the element size should not exceed the decay length of $s = 0.778\sqrt{R \cdot h}$. For the cylinder radius $r = 10$ m and the shell thickness $h = 0.03$ m the decay length is $s = 0.42$ m. The model in Fig. 3 meets this requirement.

Discontinous-type-temperature distribution

Fig. 4 shows the resulting displacements 50-times enlarged. Fig. 5a and b confirms that the membrane stresses in circumferential direction vanish as predicted in the previous paragraph. Only in the transition region, where the temperature step occurs, the membrane stresses in the circumferential direction have narrow peaks. In contrast to this Fig. 5c and d show that the membrane stresses in axial direction do not vanish. Their maximum value is 125 N/mm^2, which is the same number as obtained for the slice.

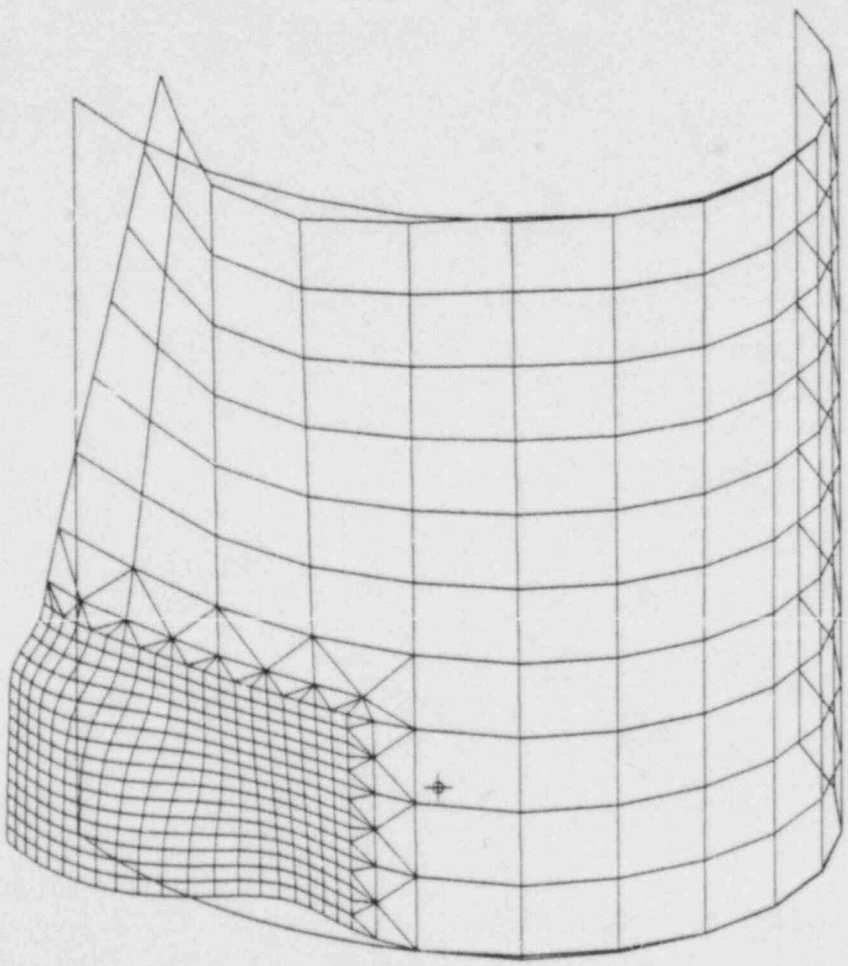

Fig. 4: Displacements (enlarged scale)
Discontinous type of temperature distribution

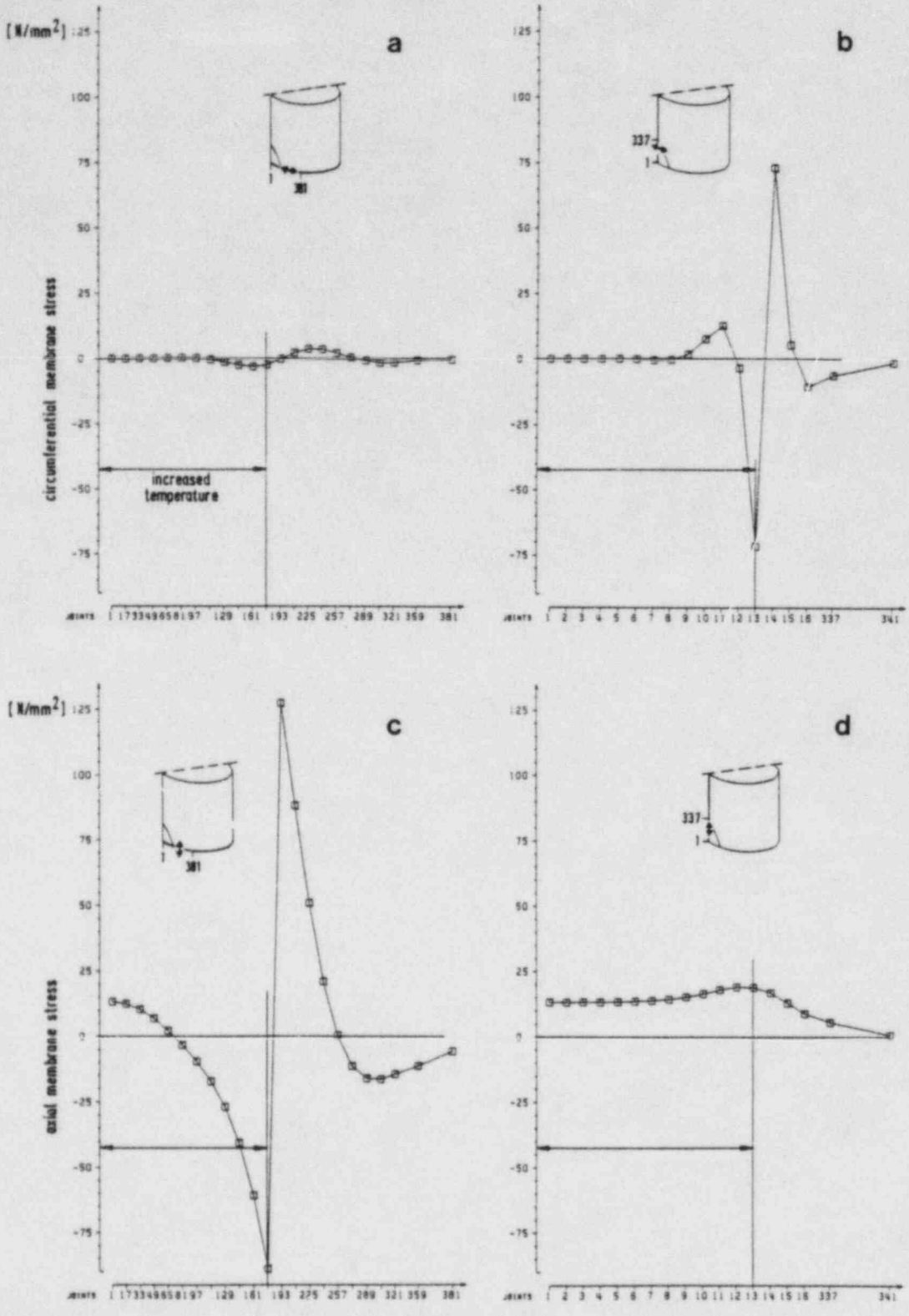

Fig. 5: Membrane stresses in circumferential and axial direction along the cylinder circumference and along the cylinder generator. Discontinous-type temperature distribution.

Cosinus-type-temperature distribution

Fig. 6 shows the resulting displacements again 50-time enlarged. Now the gradients are much smaller than those obtained for the discontinous-type-temperature distribution. Fig. 7a and b confirm very clearly that the membrane stresses in circumferential direction vanish, while the membrane stresses in axial direction assume a maximum value of 21 N/mm^2. (Please note the different scales in Figs. 5 and 7.)

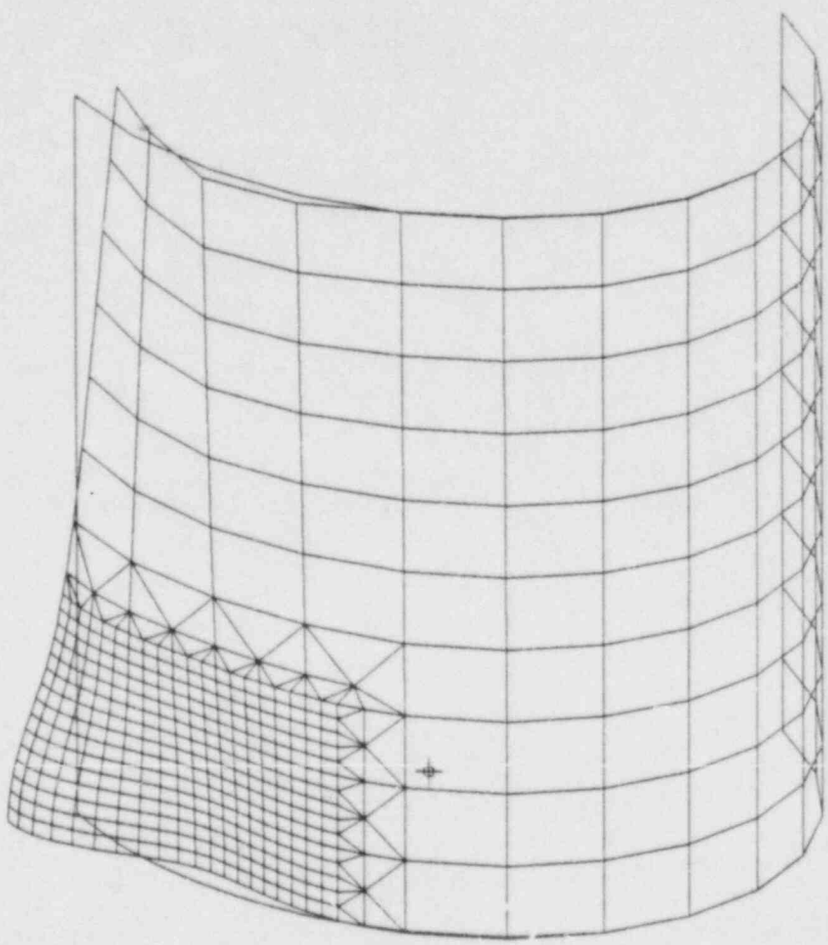

Fig. 6: Displacements (enlarged scale)
Cosinus-type-temperature distribution

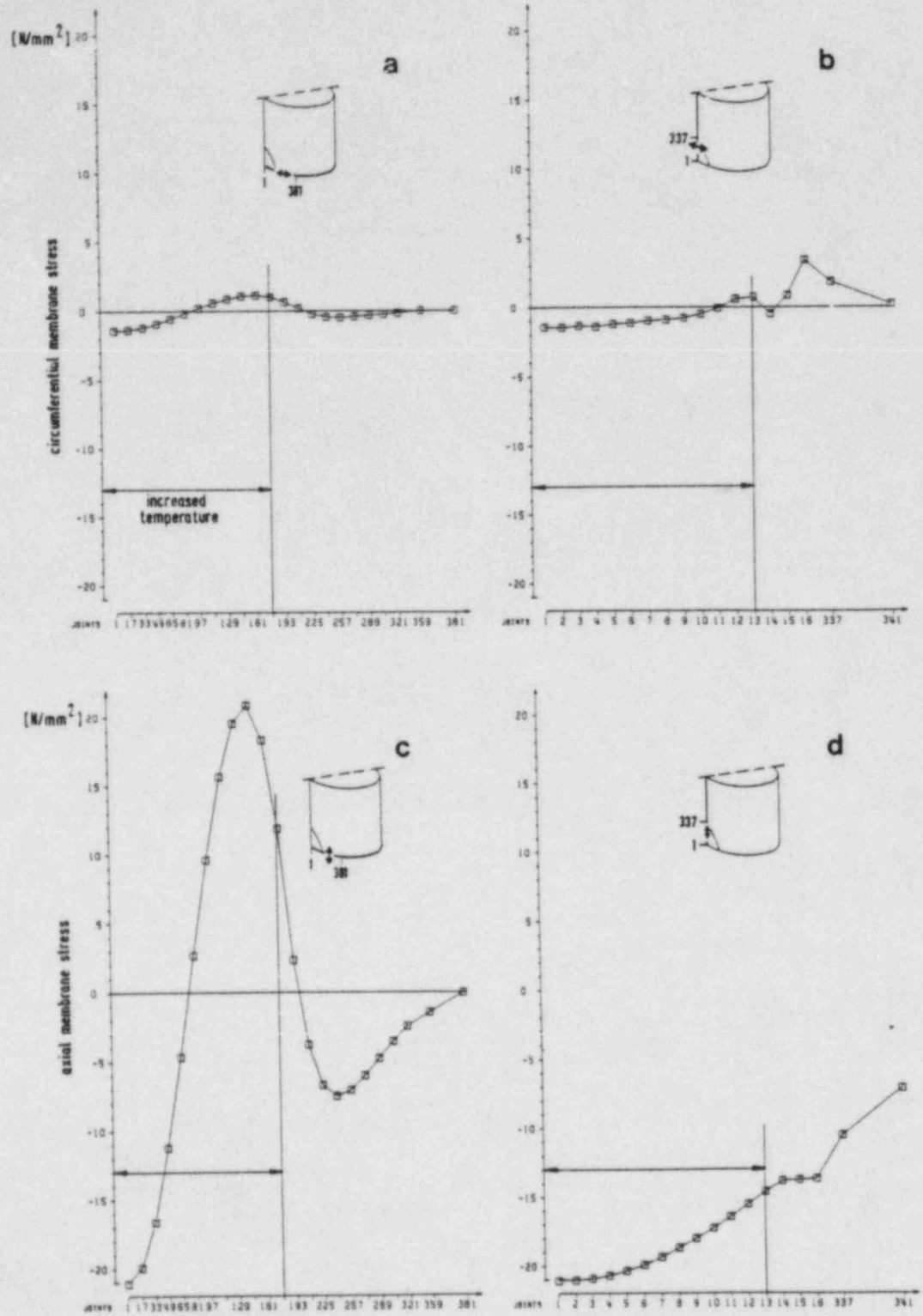

Fig. 7: Membrane stresses in circumferential and axial direction along the cylinder circumference and along the cylinder generator. Cosinus-type-temperature distribution.

4. Thermal Stresses in a Spherical Shell

If shell bending stresses are neglected and the shell deformations are assumed to be small, local temperature increases do not cause membrane stresses.

This can be seen using the following model: Assume that in a ring region of a sphere, shown in Fig. 8a, the temperature has been increased by ΔT. If stresses are omitted, the width b and the diameter d of the ring will be increased to $b\cdot(1+\alpha\Delta T)$ and $d\cdot(1+\alpha\Delta T)$, respectively. This is equivalent with the statement that the radius R will be increased to $R\cdot(1+\alpha\Delta T)$, while the angle δ remains constant. Now, any circular temperature distribution on a spherical shell can be approximated by concentric rings shown in Fig. 8b. The resulting deformations can be approximated by increased ring radii R_i. Since the angels δ_i remain unchanged, the rings fit together without additional strains and stresses. The compatibility conditions are fulfilled automatically. If the deformations are assumed to be small, the transition from one ring to the other does only cause bending stresses, but no membrane stresses. If the restriction of small deformations is no longer applied, the transition from one ring to the other (inclination of the ring surfaces) also causes certain membrane stresses which, however, are small in comparison to the stresses discussed in chapter 2 and 3. This means, the above restrictions of no bending stresses and small deformations are realistic.

For the cylindrical shell the statement of vanishing membrane stresses was the same. However, both together, the neglect of the bending stresses and the assumption of small shell deformations was not allowed.

For the spherical shell the statement of vanishing or small membrane stresses has been confirmed by calculations with the program ROTMEM /7/. The radius of the sphere was 28 m, the wall thickness 0.038 m and the radius of the circular region with the increased temperature was again a = 5 m. Neglecting shell bending stresses (which is certainly reasonable for this very thin shell), but allowing for large shell deformations, the cosinus-type-temperature distribution yielded a maximum membrane stress of 2+4 N/mm^2. The unsharpness of this result is caused by the fact, that for large deformations a superimposed inside pressure does not only add an additional type of stress, but also does influence the thermal stresses.

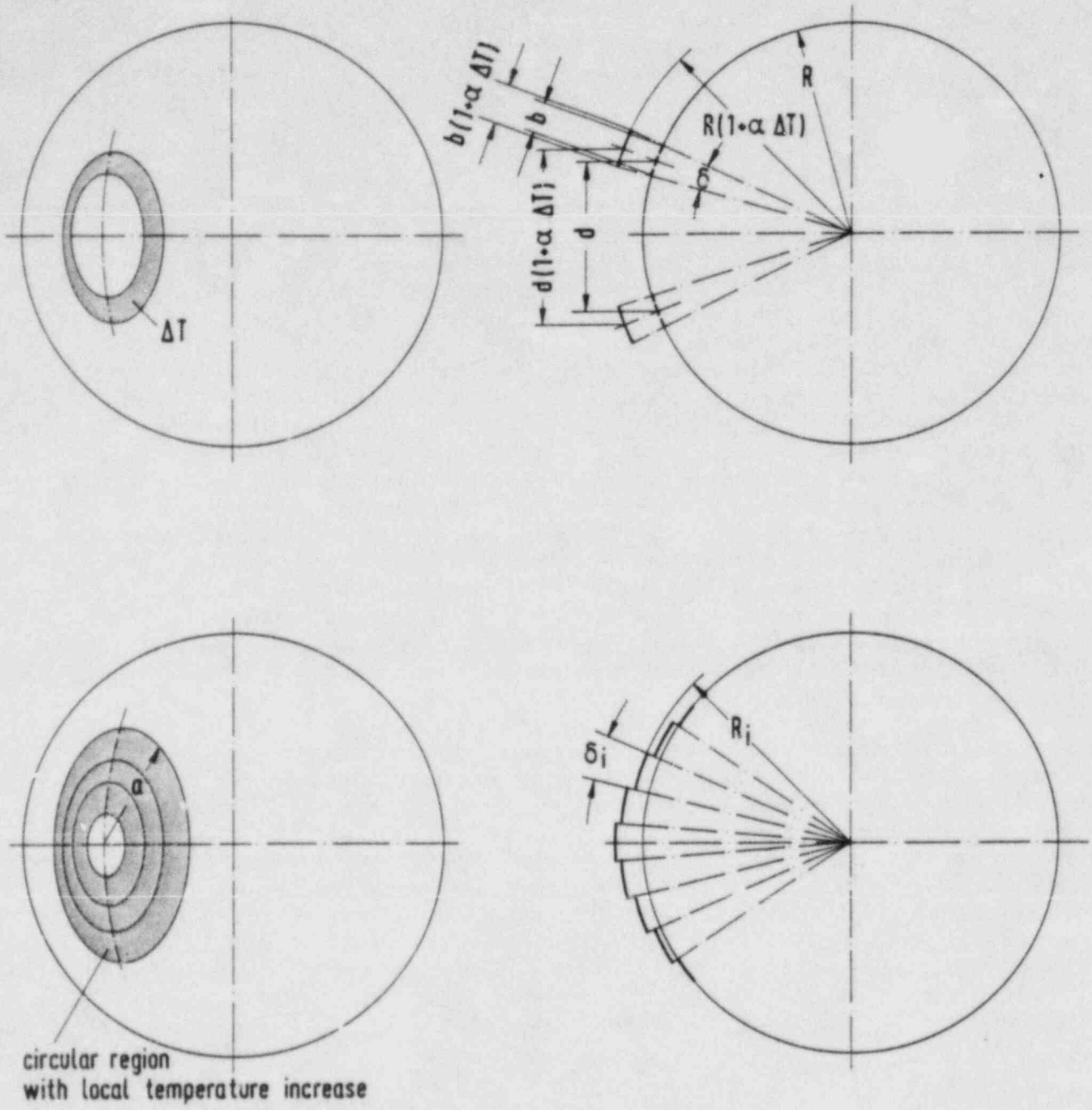

Fig. 8: Spherical shell
Circular region with local temperature increase approximated by concentric rings

5. Conclusions

The main results are shown in Fig. 9. It says, that a local temperature in a slice causes large membrane stresses, in a cylindrical shell it may cause smaller membrane stresses (depending on the spatial temperature gradients) and in a spherical shell it causes almost no membrane stresses. This means, thermal stress investigations carried out for a cylindrical shell may hardly be used to draw conclusions for thermal stresses in spherical PWR containments.

Furthermore, it has been found, that care must be taken for calculation of thermal stresses in cylindrical shells. The neglect of bending stresses and at the same time the assumption of small shell deformations is not allowed. This is due to the fact, that in axial direction the behavior of a cylindrical shell is similar to that of a slice, where the compatibility conditions cause high thermal stresses, but in circumferential direction it is similar to that of a curved shell (spherical shell), where compatibility is obtained almost automatically.

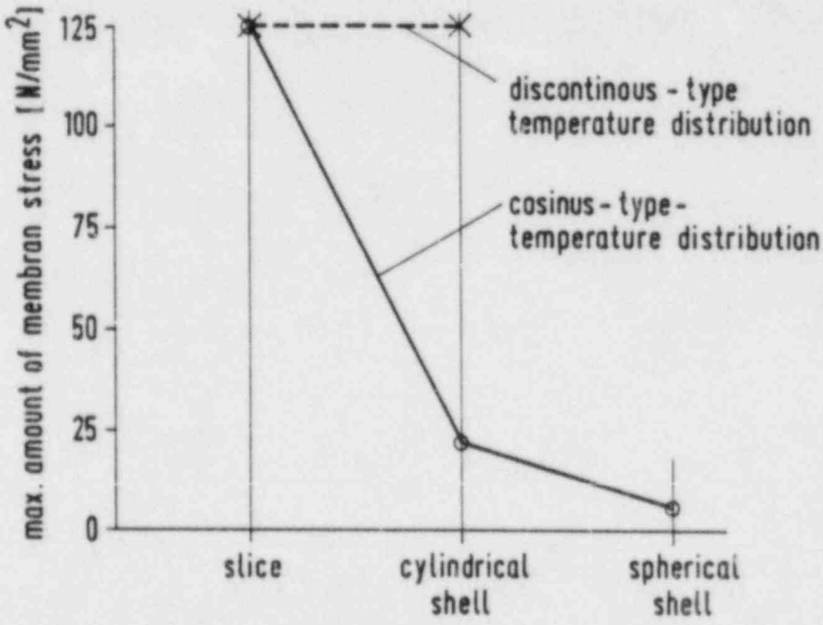

Fig. 9: Comparison of membrane stresses caused by local temperature increase in a slice, a cylindrical shell and a spherical shell

6. References

/1/ J. Jansky, Ch. Doltsinis, G. Katzenmeier: Stress of Containment Steel Shell under Blowdown Loading; 7th Int. Conf. on Structural Mechanics in Reactor Technology, 1983, paper J6/7

/2/ Sicherheitstechnische Regel des KTA, 3401.2, Reaktorsicherheitsbehälter aus Stahl, Auslegung, Konstruktion und Berechnung; Carl Heymanns Verlag KG, Gereonstr. 18-32, 5000 Köln

/3/ I. Szabb: Höhere Technische Mechanik; Springer-Verlag Berlin/Göttingen/Heidelberg

/4/ W. Flügge: Statik und Dynamik der Schalen; Springer-Verlag Berlin/Göttingen/Heidelberg

/5/ MAN-MBB-Handbuch für ICES-STRUDL, Band 1+2, MAN Nürnberg, 1981

/6/ B. Göller: Schalendynamisches Verhalten des kugelförmigen Containments eines Siedewasserreaktors bei Dampfkondensation im Druckabbausystem; KfK 2778, Mai 1979

/7/ B. Göller: Zum Verhalten eines DWR-Containments unter hohem, quasistatischem Innendruck - Grundlagen des Programmes ROTMEM; Internal report

BEHAVIOR OF SPHERICAL PWR-CONTAINMENTS CLOSE TO REINFORCED SECTIONS UNDER EXCESSIVE INTERNAL PRESSURE

B. Göller, R. Krieg, G. Messemer
Kernforschungszentrum Karlsruhe GmbH
Institut für Reaktorentwicklung
Projekt Nukleare Sicherheit
Postfach 3640
D-7500 Karlsruhe, FRG.

ABSTRACT

It is assumed that the pressure inside the containment is growing monotonically. The response, including the failure of the containment shell at zones located close to reinforced sections must be investigated. For this purpose a computer program has been developed and checked with several membrane experiments. It turns out that membrane failure is controlled by plastic instability. Some shortcomings in modelling the necking regions which occur around reinforced sections still need to be resolved.

1. Introduction

In case of a hypothetical core melt accident the pressure inside the containment is expected to grow beyond the design limit up to containment failure which then will occur at the weakest containment part. This could be the containment shell close to reinforced sections which surround nozzles, locks and other penetrations.

Since the strains in the reinforced sections are rather low, the circumferential strains and consequently the circumferential stresses around the reinforced sections must be low, too. Then, in order to satisfy equilibrium with the internal pressure, the stresses in the meridional direction must be rather high (Fig. 1).

In comparison to this, the corresponding stress components far away from reinforced sections assume equal values which are right between the above ones. However, since the equivalent strain is largely influenced by the maximum strain component, the equivalent strain close to reinforced sections is higher than the corresponding value in a larger distance. In other words, the containment shell close to reinforced sections represents a weak containment part.

Therefore, the failure pressure and the failure mode of the containment shell close to reinforced sections must be investigated.The work done so far is presented in this paper. It belongs

to a more comprehensive program, where other weak parts of spherical PWR-containments are considered, too /1/.

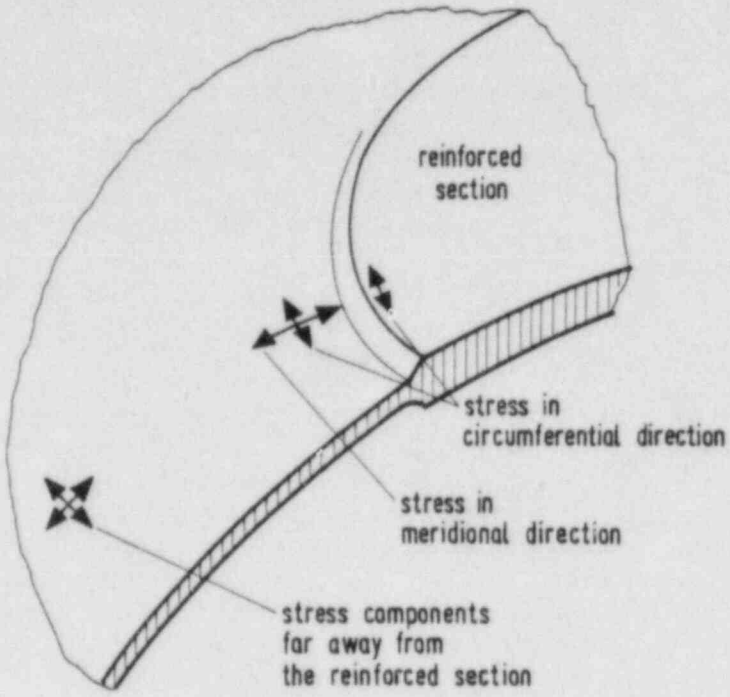

Fig. 1: Stresses in the neighbourhood of reinforced sections

2. Computational Model

The investigation of the mechanical behavior of the containment shell in the neighborhood of reinforced sections will be based on computational models. Therefore the program ROTMEM has been developed /2/. It allows for calculation of the membrane stresses and strains of an axisymmetric shell under axisymmetric pressure loading. Any elastic-plastic material behavior (in the present version without unloading) can be considered. The two-axial state of stresses is treated according to the theory of Hencky (nonlinear relations between stresses and strains) or according to Prandtl-Reuss (nonlinear relations between stress increments and strain increments). Large deformations including changes of shell thickness are considered, i.e. the equilibrium conditions are satisfied at the deformed shell. However, bending and shear stresses are neglected. Whether this is acceptable will be checked by appropriate experiments.

For application of ROTMEM the axes of the reinforced circular sections are used as axes of symmetry. That means, mutual interactions between different nozzles are not considered. This is allowed, since the stress perturbations due to the reinforced sections have a rather local character.

Due to the above simplifications and neglects high computational effort may be spent to the spatial resolution around the reinforced sections, where strong strain gradients are expected. Furthermore many load steps are allowed which is necessary for ferritic steel with a sharp elastic-plastic transition region.

3. Experimental Investigations

Experiments are required to ascertain reliable equations of state (relations between stresses and strains) for the containment material under two-axial stress conditions. Another goal is to get information about the mode of failure, e.g. occurrence of leakages, propagation of cracks, etc. The third goal is to check the computer program ROTMEM.

However, tests on containment models with excessive internal pressures have been found to be unsuitable, since manufacture of several models in correct scale (thin spherical shells) would be very expensive and miniatur weldings with the same quality as the real containment welding would even be impossible.

Instead tests with plane circular membranes loaded by unilateral pressure up to failure have been done. The plates used to manufacture the membranes are the same as those used for PWR-containments (15MnNi63-sheets with a thickness of 38 mm). The manufacture process for the membranes (facing the plates with a lathe) is relatively simple (Fig. 2) and the material properties

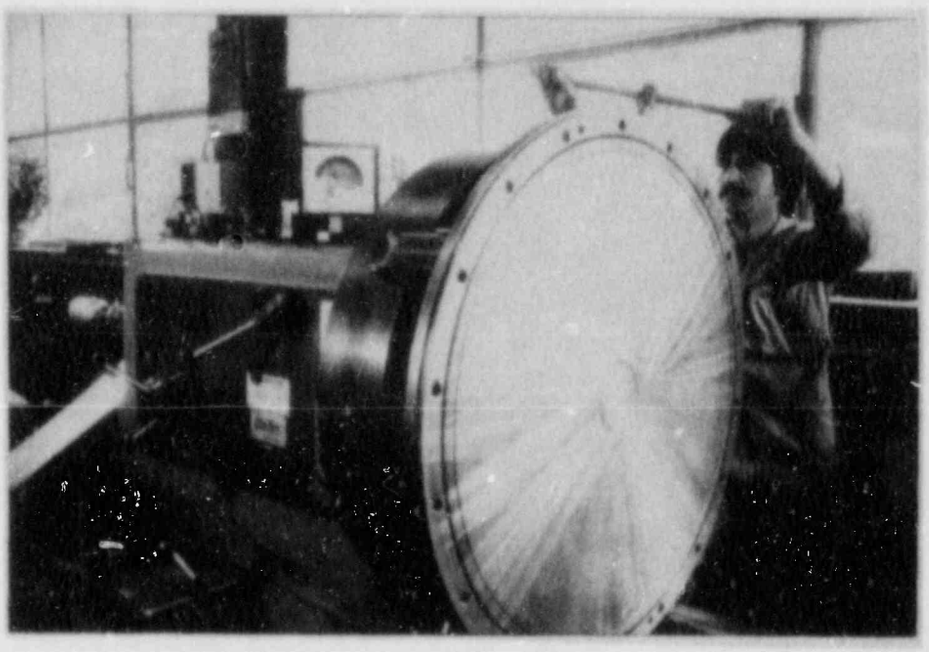

Fig. 2: Manufacture process for the membranes (facing the plates with a lathe)

obtained in this way can be expected to be realistic. The diameter of the membranes used is 800 mm, the thickness is 2 mm with a tolerance of $\pm$0.04 mm. Some membranes are smooth, others contain reinforced sections with a circular or a rectangular shape. For the later case a direct computational model does not exist. But comparing the results with those from the other experiments it can be found out, how to approximate rectangular reinforced sections by circular sections.

The unilateral pressure is applied by an oil-hydraulic system. During the test the pressure is increased in steps of about 5 bar until failure. After each step the displacements of a large number of control points marked on the membrane are measured using a three-coordinate measuring machine (Fig. 3). For the same points also the decreasing thickness of the membrane is determined using an ultrasonic sensor.

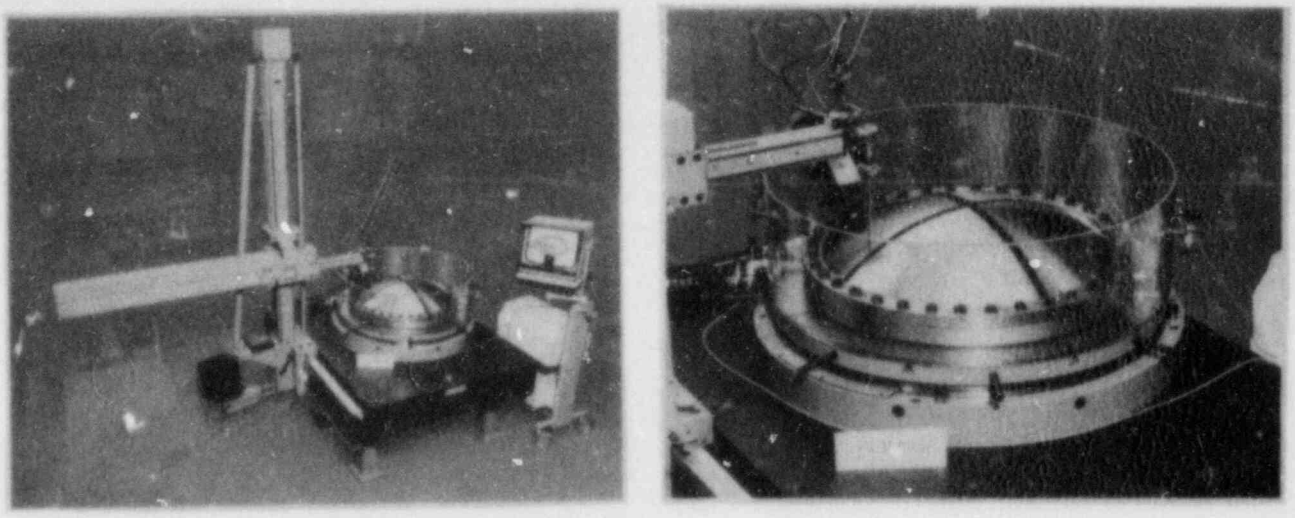

Measuring machine.
Feeler and control points magnified by a television set.

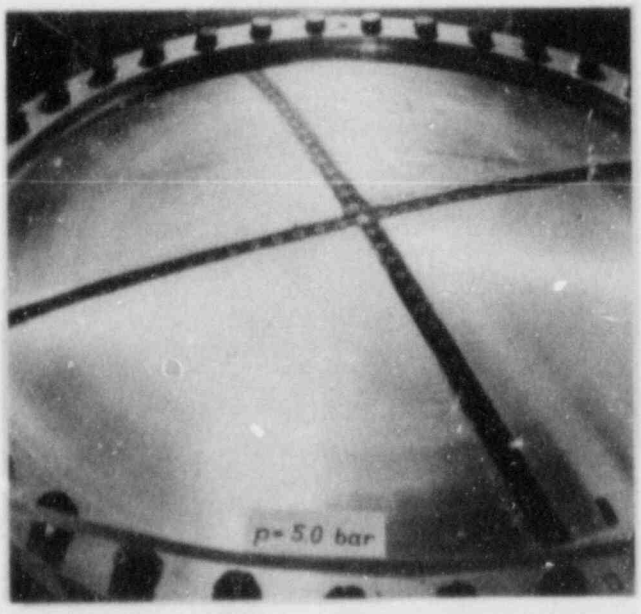

Circular membrane with control points

Fig. 3:
Circular membrane under unilateral pressure.
Investigation by a three-coordinate measuring machine

Based on these data strains can be calculated using simple geometric relations. The meridian stresses can be obtained using the equilibrium condition in axial direction for a cap of the membrane (Fig. 4a) and the circumferential stresses can be obtained using the equilibrium condition in normal direction of the membrane elements (Fig. 4b). From these data the stress-strain relation under two-axial loading conditions can be derived. The failure mode in the experiment may also be extrapolated to the conditions of a containment. If in the experiment where oil is used for pressurization a crack propagates rapidly, then in the containment filled with compressible gases the failure will propagate even faster. Finally, the measured displacements can be compared with the calculated values to assess the efficiency of the program ROTMEM .

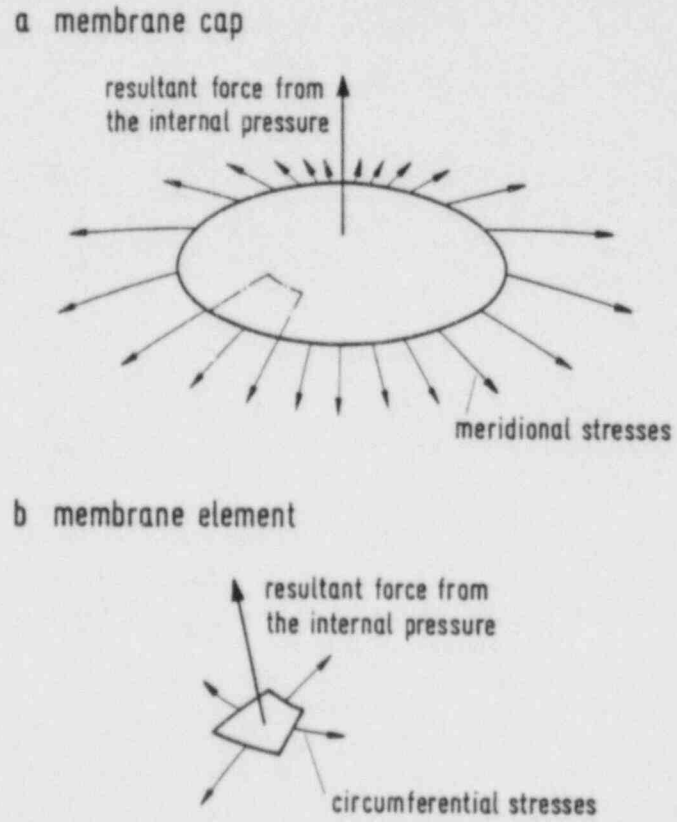

Fig. 4: Equilibrium condition at membrane caps and membrane elements

4. First Results

Membranes with smooth surfaces:

Untill now two smooth circular membranes have been tested and a large number of points describing the stress-strain relation under two-axial conditions have been obtained. In order to compare these results with those from one-axial tensile tests, equivalent stresses and strains are calculated using the v. Mises stress hypothesis. The results show that the stress-strain relations obtained from the two-axial membrane tests differ noticeably from the relation obtained from one-axial tensile tests (Fig. 5). However, it should be mentioned that the membrane tests took hours, and each set of measurement was made some time after the oil supply had been stopped, while the tensile tests were carried out within minutes. A first tensile test, run also over hours, indicates that the different time scales is one reason for the deviations of the stress-strain diagrams. The difference between two- and one-axial loading and the application of the v. Mises stress hypothesis may be other reasons for these deviations.

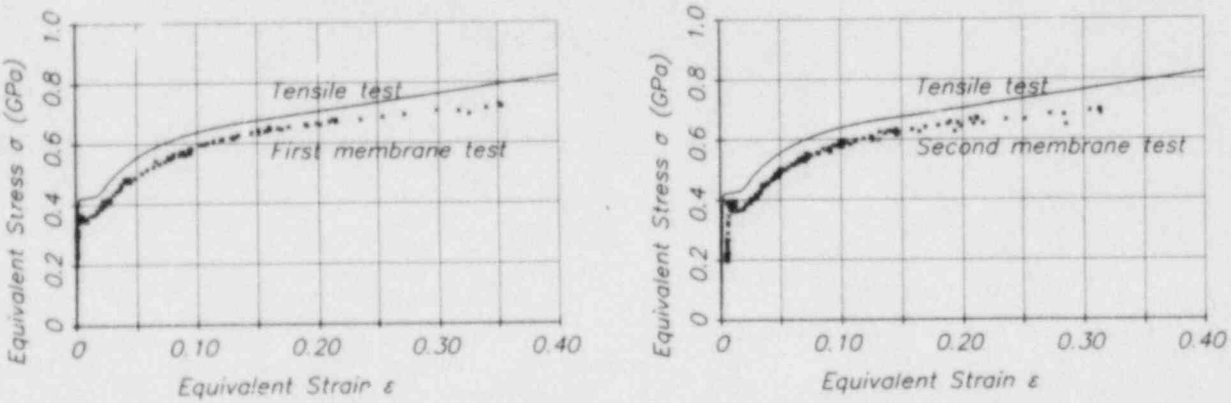

Fig. 5: True stress - true strain relation obtained by membrane tests and tensile tests

It is also interesting to note that for strains in the one-percent-region so-called Lüder-lines could be seen on the surface of the membranes (Fig. 6). This corresponds with the sharp elastic-plastic transition region (different upper and lower yield point) found in the stress-strain diagram.

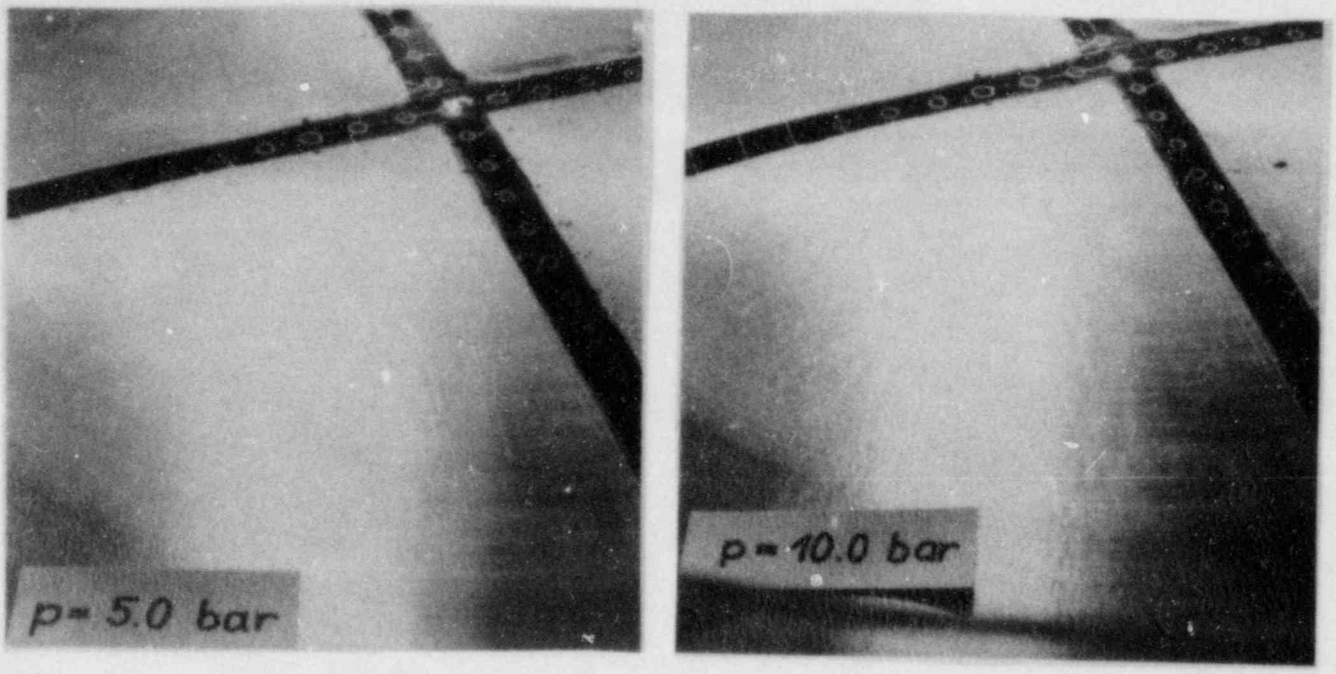

Fig. 6: Lüder-lines at the surface of the membrane

Failure of the membranes occured for rather high equivalent strains in the order of 50 % (in-plane strain components in the order of 25 %). The arising cracks had rather large extensions (Fig. 7). In comparison to this, necking in the tensile tests started with a strain of about 15 % and failure occured for an ultimate strain of about 25 % (Fig. 8).

These results are very interesting, especially if one considers that for pressurized cylindrical and spherical shells usually failure occurs for strains which are much lower than the uniform elongation strains*) and the ultimate strains obtained for tensile tests. The key to understand this is the phenomenon of plastic instability. It means, that a critical state of deformations has been reached, when the load decrease due tc contraction of the cross section exceeds the load increase due to strain hardening. Then under a given constant load, strains start to grow rapidly and rupture occurs immediately. Often these strains will be concentrated in small regions which then become necking regions. However, the failure is controlled by the critical deformations marking the beginning of plastic instability. The strains occurring in these necking regions are of minor interest. On the other hand it is well known that plastic instability depends strongly on the geometry of the given problem /3/. In some

*) strain before necking

cases the critical strains marking the beginning of plastic instability are higher, in other cases these strains are much lower than the uniform elongation strains and ultimate strains for tensile tests. This explaines, why for pressurized membranes the strains before failure may be higher and for pressurized cylindrical and

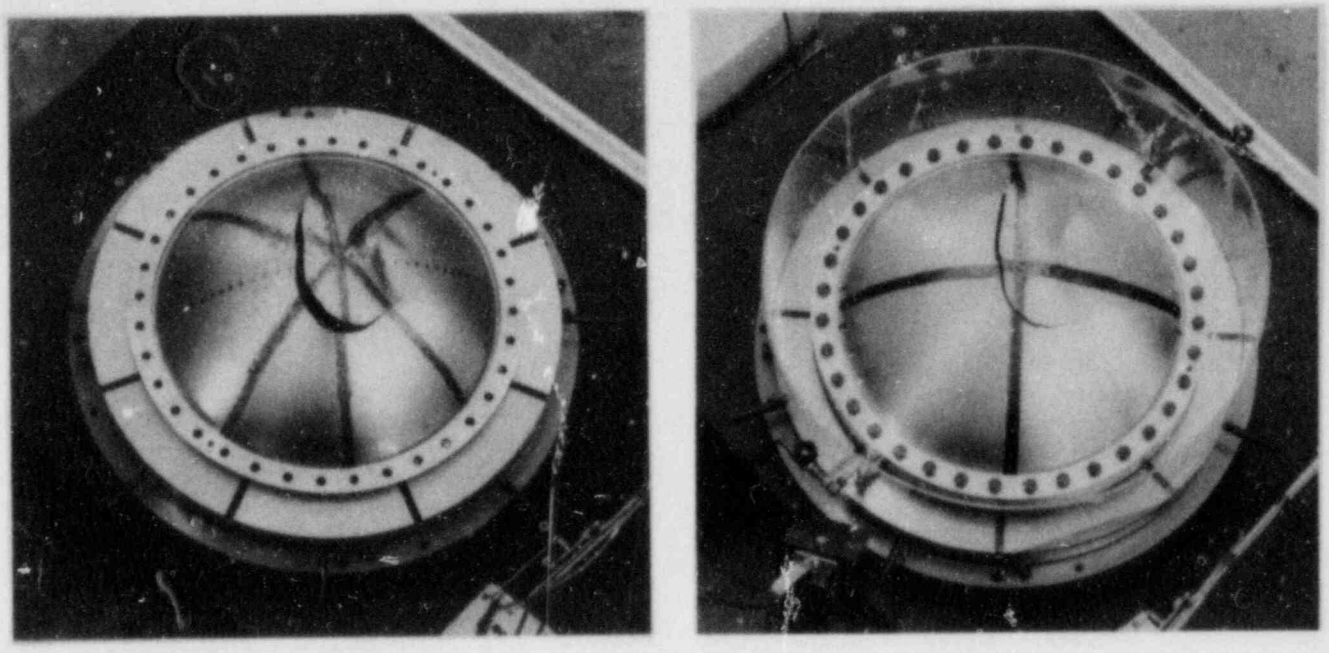

first test second test

Fig. 7: Failure of the membranes with smooth surfaces

spherical shells these strains may be lower than the values obtained for tensile tests.

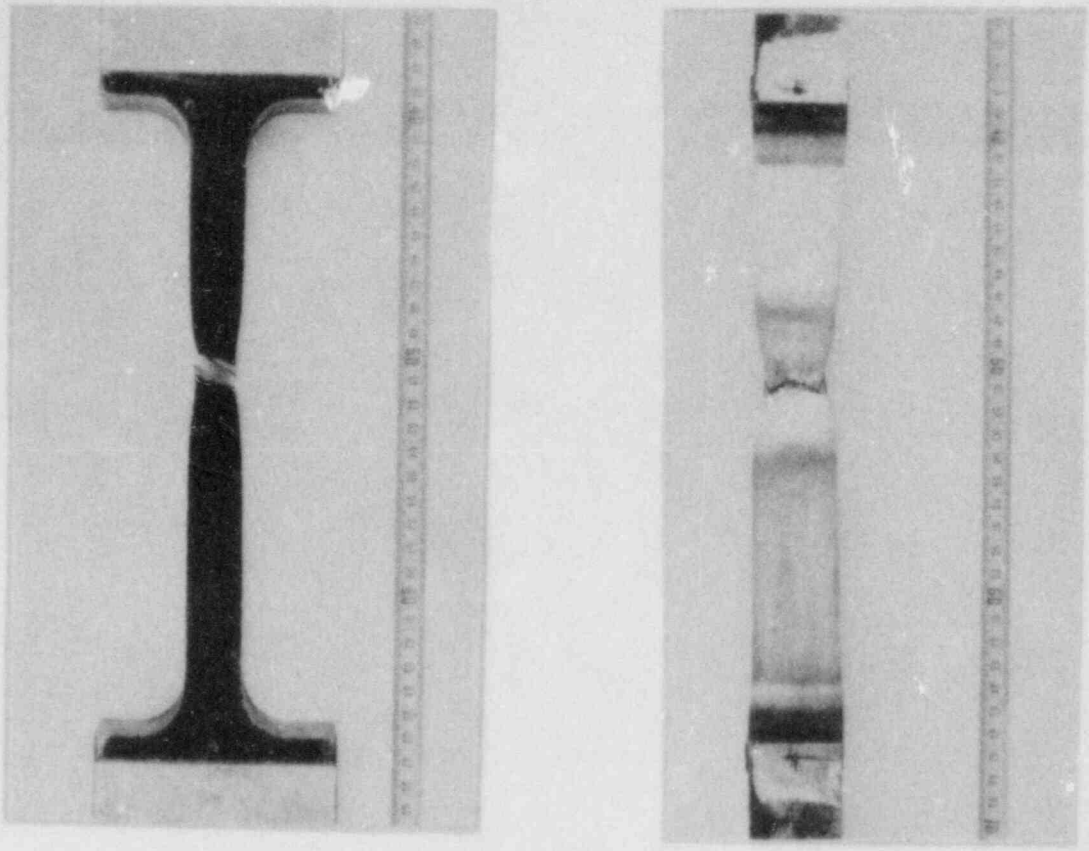

Fig. 8: Necking during a tensile test

That the failure of the tested membranes was indeed controlled by plastic instability has been confirmed by applying the computer program ROTMEM. Here, plastic instability is reached, when the decrease in wall thickness divided by the increase in loading approaches infinity. Considering the measured initial membrane thickness which varies slightly along the membrane radius, the decrease of this thickness as a function of the membrane pressure has been calculated (Fig. 9). Plastic instability has been obtained for a pressure of 45.2 bar (first test) and 45.8 bar (second test). In the experiments failure occured at a pressure of 42.8 bar (both tests).

Two other facts also indicate that failure of the membranes is controlled by plastic instability. Before rupture of the membrane the load increase versus strain increase vanished. After rupture there seemed to be a small necking zone along each side of the crack.

Other data calculated and measured for the deforming membranes are also compared (Figs. 10-12). Since the stress-strain relation from the one-axial tensile tests where the material was

harder than in the membrane tests has been used for the calculations, the displacements have been a little bit underestimated and the stresses overestimated.

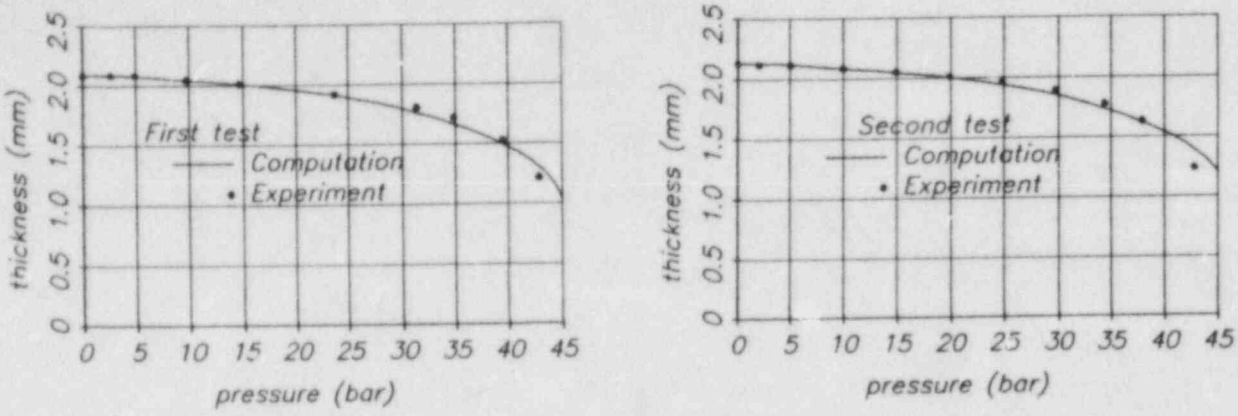

Fig. 9: Decrease of the membrane thickness at the pole as a function of the pressure (membranes with smooth surfaces)

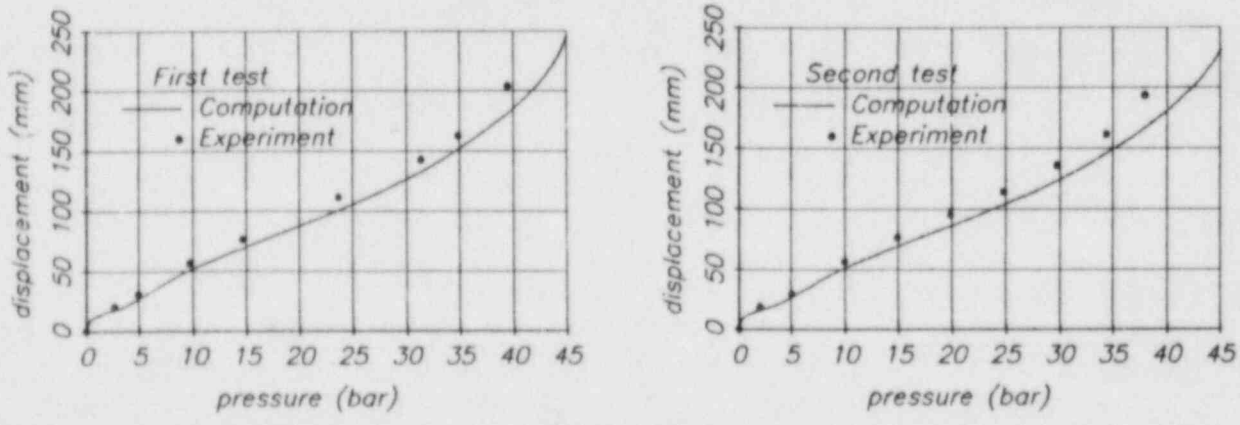

Fig. 10: Vertical displacement of the membrane pole as a function of the pressure (membranes with smooth surfaces)

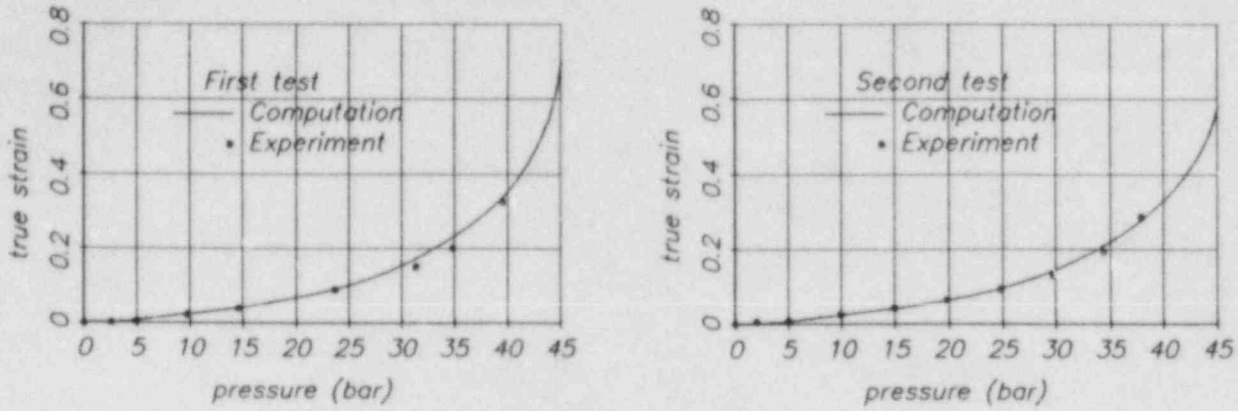

Fig. 11: True strain at the membrane pole as a fuction of the pressure (membranes with smooth surfaces)

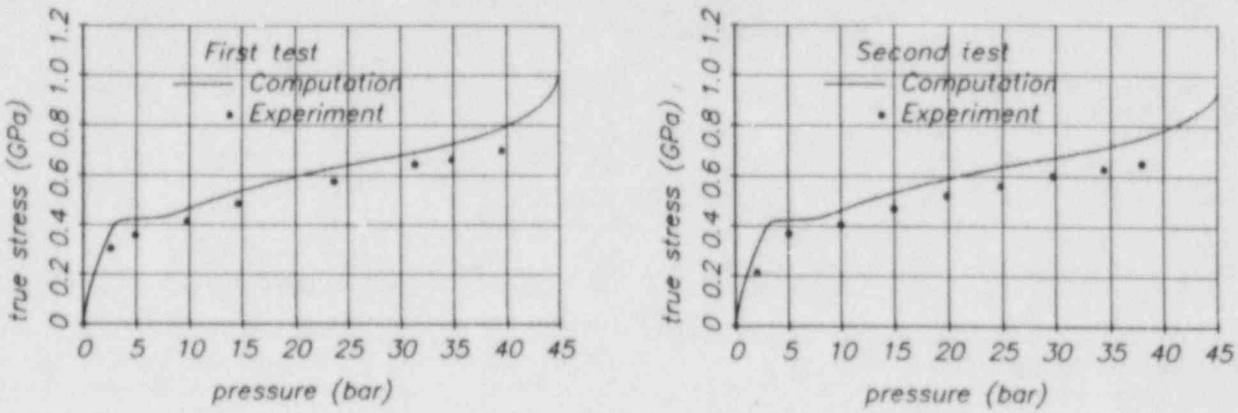

Fig. 12: True stress at the membrane pole as a function of the pressure (membranes with smooth surfaces)

Membranes with a reinforced circular section:

Two membranes with a reinforced circular section have been also tested so far. The dimensions were the same as for the membranes with smooth surfaces, except the central region with a diameter of 132 mm, where the thickness had been increased from 2 mm to 3.2 mm. Of course, sharp notches between the regions of different thicknesses had been avoided.

The stress-strain relation obtained from these tests are almost the same as those from the previous tests. Again, the arising cracks had large extensions. They did not arise directly in the transition region tc the reinforced section rather they propagated in a 2 to 3 mm distance around the reinforced sections (Fig. 13). In one case the crack left this circular path and propagated about 80 mm in straight direction.

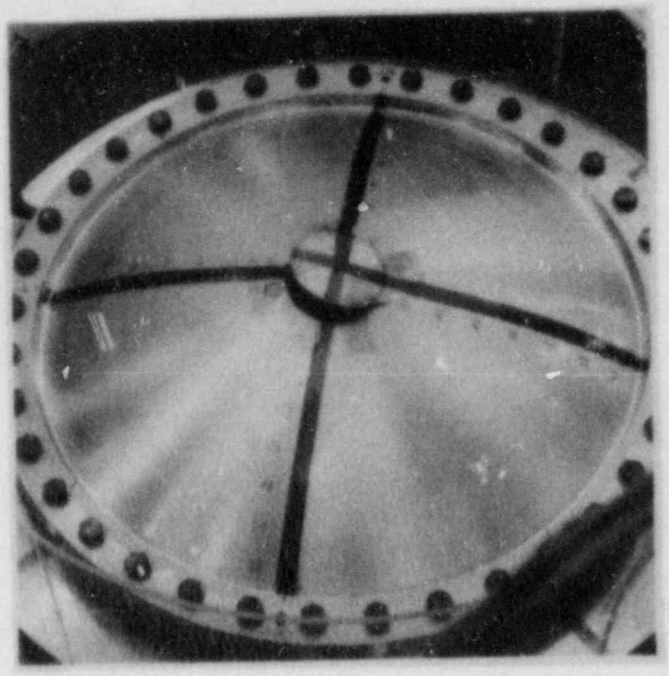

Fig. 13: Failure of a membrane with reinforced circular section

However, the failure pressures were only 28.0 bar and 31.7 bar which is considerably lower than the value of 42.3 bar for the previous tests. This can be explained by the plastic strains which in case of a reinforced section are concentrated in a ring region around this section. In case of a smooth membrane the plastic strains are distributed more uniformly. Consequently in the case of a reinforced section the resulting vertical membrane displacements, the membrane curvatures and therefore also the pressure causing a given maximum membrane stress are smaller than in the case of a smooth membrane.

For the membranes with reinforced sections failure is also con trolled by plastic instability. But now the computational description with the program ROTMEM caused difficulties. Up to a certain loading measurements and calculations were in good agreement. But when the pressure exceeded a value of about 19 bar, the decrease of the membrane thickness started to grow rapidly. At the same time the convergence of the numerical calculations became worse. Then for a pressure approaching a value of 20.3 bar failure by plastic instability could be assumed (Fig. 14). The

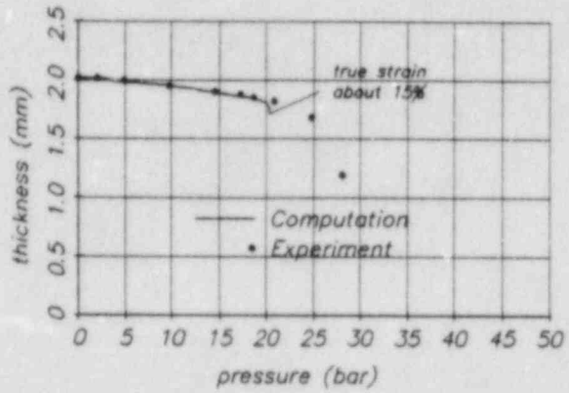

Fig. 14: Decrease of the membrane thickness close to the reinforced section as a function of the pressure

maximum equivalent strain was about 15 %. The same conclusions could be drawn using the simplified graphic technique (Fig. 15) described in /3/. Here the plastic instability was assumed to be a local effect mainly influenced by the meridional stress. Therefore the condition of one-axial tension was assumed to be appropriate. The theoretical results, however, differ considerably from the experimental finding. Similar problems have been described some years ago by Salmon /4/.

We suppose that the reason for this discrepancy may be the neglect of the shear stresses perpendicular to the membrane plane. In the computational model the decrease of the wall thickness within a mesh cell is not influenced by the shear stresses between this cell and the neighbouring cells (Fig. 16). In reality, however, such an influence exists. It smoothes and extends the necking region such, that the overall plastic deformations including the membrane curvature will be increased. Consequently the failure pressure will be also increased in comparison to models where the shear stresses are not considered.

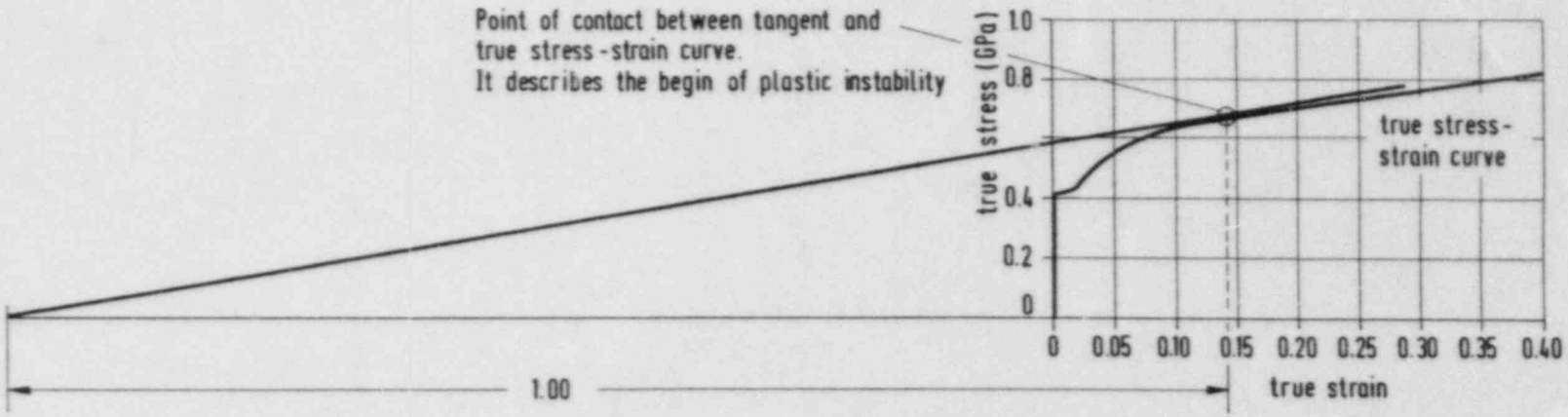

Fig. 15: Graphic technique to describe the begin of plastic instability

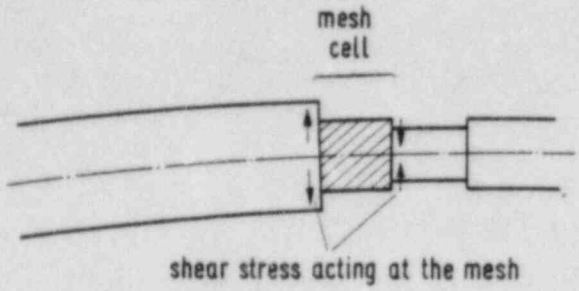

Fig. 16: Shear stresses in the necking region of a shell

Therefore, work has been started to include the shear stress effects into the theoretical model. On the other hand it should be mentioned that for the spherical containment shell the geometric relations are quite different and therefore the influence of the shear stresses can be expected to be smaller.

5. Literature

/1/ R. Krieg et al.: Investigation Program on PWR-Steel-Containment Behavior under Accident Conditions; Kernforschungszentrum Karlsruhe, KfK 3589, Oct. 1983

/2/ B. Göller: Zum Verhalten eines DWR-Containments unter hohem, quasistatischem Innendruck - Grundlagen des Programmes ROTMEM; Internal report

/3/ W. Johnson, P.B. Mellor: Engineering Plasticity; van Nostrand Reinhold Company, 1973

/4/ M.A. Salmon: Studies of Reactor Containment Structures; Final Report, U.S. Atomic Energy Commission, Reactor Development Branch Germantown, Maryland, IITRI-578P22-15, UC-80, TID-4500, June 1966

FAILURE INTERNAL PRESSURE OF SPHERICAL STEEL CONTAINMENTS

G. Sanchez Sarmiento
Empresa Nuclear Argentina de Centrales Electricas S.A.
Av. L.N. Alem 712 (1001) Buenos Aires, Argentina

S. R. Idelsohn, A. Cardona y V. Sonzogni
Instituto de Desarrollo Technologico para la Industria Quimica
(INTEC). Casilla de Correo N° 91 (3000) Santa Fe, Argentina

ABSTRACT

An application of the British CEGB's R-6 Failure Assessment Approach to the determination of failure internal pressure of nuclear power plant spherical steel containments, is presented in this paper. The presence of hypothetical cracks both in the base metal and in the welding material of the containment, with geometrical idealizations according to the ASME Boiler and Pressure Vessel Code (Section XI), was taken into account in order to analyse the sensitivityof the failure assessment with the values of the material fracture properties. The knowledge of this sensitivity is of prime importance in a probabilistic risk assessment of this containment under overpressurization conditions.

Calculations of the elastoplastic collapse load have been performed by means of the Finite Element System SAMCEF. The clean axisymmetric shell (neglecting the influence of nozzles and minor irregularities) and two major penetrations (personnel and emergency locks) have been taken separately into account. Large-strain elastoplastic behaviour of the material was considered in the Code, using lower bounds of true stress-true strain relations obtained by testing a collection of tensile specimens.

For an internal pressure which produce general membrane stress of the entire spherical shell greater than the yield point, it was observed that the clamp and the nozzles have very little influence on the calculated displacement. That means, the elastoplastic collapse pressure does not essentially depend on the mentioned geometrical irregularities.

Assuming the presence of cracks in non perturbed regions, the reserve factor for test pressure and the failure internal pressure have been determined in function of the flaw depth.

1.- INTRODUCTION

Stress analysis of nuclear power plant steel containment under design basis accident (mainly the typical loss of coolant accident), and other design and test load conditions, has reached nowadays [1-7] a high degree of sophistication and reliability since the development of general structural analysis programs running in large-size computers. Nature and origin of loads, and the probability of their occurrence both individually and in combination, are sufficiently known [8] for any given kind of containment.

Core meltdown accidents of the types considered in probabilistic risk assessment (PRA) [9] notwithstanding, have been predicted to lead to environments that are much more severe than those considered for the design basis, and may challenge the integrity of containment structures [10]. As stated by Corradini et al [11], the Reactor Safety Study (WASH-1400) [12] "demonstrated, based on PRA, that core meltdown accidents are the dominant risk contributors to the public frow Light Water Reactor (LWR). One reason for this conclusion, was that containment failure and subsequent radioactivity release was possible given the occurrence of any of a number of physical processes; such as hydrogen combustion, steam explosion, overpressurization of containment, or melt through the containment base-mat".

The quantification of the probability of containment failure due to internal overpressurization is thus of basic importance in any PRA [10]. In order to establish the internal pressure at which the structure will fail, it is necessary to define one or more failure criteria for the structure [9]: a limiting stress, strain, or some other condition. Given to the geometrical complexity of the containments, the definition of failure criteria and the associated failures pressures is far from straightforward. Also, because of uncertainties in the conditions leading to failure, a specific failure pressure cannot be determined. What is needed for a PRA is a density function describing the probability of failure as a function of loading (pressure). The shape of such a density function will vary with the containment design, level of analysis, and knowledge of the details of the actual containment. Tsai and Orr [13] give a general route for performing such a probabilistic failure assessment.

A number of studies to determine the failure pressure of steel containments both in a deterministic or in a probabilistic manner have been published in the available literature [13-17]. For the penetrations in this containments, are also applicable the conclusions arrived in analysis of nozzles of pressure vessels [18-21].

None of the papers cited above have considered the influence of hypothetical cracks preexistent in the structure, in spite that for spherical pressure vessels this problem has been extensively treated [22-23]. Because of the exhaustive examination of the material, cracks are very unlikely to be present in nuclear steel containment. Notwithstanding, for a reliable determination of its

failure pressure, the effects that cracks there produce cannot be disregarded. Such an assessment can be performed by means of the British CEGB's R-6 Failure Assessment Diagram approach [24], briefly described below. This procedure can provide a sensitivity analysis of the failure pressure on the values of the strength and fracture properties both of the base material and of welding metal. Conversely, knowing fixed values of this material parameters, one can determine by means of this approach the reserve factor (both on internal pressure and on the flaw depth) for a given internal pressure, and then, bounds for the failure load.

In this paper, an application of the R-6 approach is presented for the failure assessment of spherical steel containment of characteristics shown in figure 1, commonly used for PWR or PHWR nuclear power plants.

2.- THE CEGB's R-6 FAILURE ASSESSMENT DIAGRAM APPROACH

Steels used in the type of containments as the analysed in this work have in general a great ductility, then plasticity effects play an important role in the failure of such structures when they have preexistent cracks.

After the development of several approaches for dealing elastoplasticity in crack behaviour, Downling and Townley [25] suggested that metal structures containing a flaw could only operate within limits imposed by linear elastic fracture mechanics and plastic limit theory ("two-criteria approach"). Between these limits, some interpolation is necessary to be done for structures operating near the failure condition. This interpolation is provided by the "strip yield model" of Bilby, Cottrell and Swinden [26], and their work was then taken in a form modified by Heald, Spink and Worthington [27]. From this model the resulting expression for failures of finite geometries can be written as [28]:

$$K_{1c}^2 = \frac{8}{\pi^2} Y^2 a \ln \sec \left(\frac{\pi}{2} \frac{\sigma_f}{\sigma_1}\right) \qquad (1)$$

where K_{1c} is the plain strain fracture toughness; Y is the linear elastic compliance factor; a is the flaw depth; σ_f is the applied stress at failure; and σ_1 is the flow stress in the plastic zone. The use of eq. (1) for predicting elastic-plastic failure in a variety of geometries has been validated by a large number of experimental and analytical results presented by Downling and Townley [25], by Chell and Milne [29], by Chell [30] and by Milne [31].

Harrison, Loosemore and Milne [24] reformulated the two-criteria approach of Downling and Townley stating the failure procedure known in the literature as the CEGB's R-6 failure assessment diagram. The coordinates (S_r, K_r) of an assessment point of this diagram (see figure 2) are calculated by:

$$S_r = \frac{\text{Stress (load) applied}}{\text{Plastic collapse stress (load) of cracked structure}} = \frac{\sigma\,(L)}{\sigma_1(L_1(a)}$$

$$K_T = \frac{\text{Stress (load) applied}}{\text{LEFM failure stress (load)}} = \frac{K_1(a,L)}{K_{1c}} \qquad (2)$$

Here, K_1 is the applied stress intensity factor; L is the applied load and $L_1(a)$ is the failure load.

Rearranging eq. (1), it is clear that at failure the points (K_r^f, S_r^f) must verify the expression:

$$K_r^f = S_r^f \left\{ \frac{8}{\pi^2} \ln \sec \left(\frac{\pi}{2} S_r^f\right) \right\}^{-1/2}, \qquad (3)$$

that is plotted as the failure assessment line in figure 2. Points (S_r, K_r) inside this curve indicate that the structure is safe, and the position of these points relative to such a line defines how safe the structure is. The locus of this failure point as a function of load is a straight line through the origin (zero load) to the failure assessment line, so that the reserve factor on load, F_p, is easily evaluated as shown in figure 2. Alternatively, F_p may be calculated from the following formulae [32]:

$$F_p = \frac{2}{\pi S_r} \cos^{-1} \exp \left(-\frac{\pi^2}{8} \frac{S_r^2}{K_r^2} \right) \qquad (4)$$

Other loci, as a function of K_{1c} or flow stress $\bar{\sigma}$, are also straight lines parallel to the S_r and K_r axes respectively, while the locus as a function of flaw size is in general curved [31], as indicated in the same figure. These properties facilitate a sensitivity analysis of the input data on the failure condition. Valuable discussions of the advantageous characteristics of this procedure can be seen in refs. 31, 33-37.

Milne [38-39] and Bloom [40-42] have shown that the R-6 failure assessment approach can be extended to account for stable crack growth (ductile tearing) beyond initiation.

Combined thermal and pressure loads have been also taken into account by Milne in ref. 43.

Bloom has proposed [40] also an extension of the R-6 procedure for the assessment of structural integrity of nuclear pressure vessels, combining this approach with deformation plasticity solutions [44-46] obtained in the U.S. General Electric Company.

3.- CALCULATION OF THE ELASTOPLASTIC COLLAPSE LOAD

The simulation of the elastoplastic behaviour of the structure until its collapse is reached, has been performed taken separately into account the clean axisymmetric shell (neglecting the influence of nozzles and minor irregularities) and two major penetrations (personnel and emergency locks).

The Finite Element System SAMCEF [47-49] was employed, in a version running in the Instituto de Desarrollo Tecnológico para la Industria Química [50].

3.1 Analysis of the clean sphere

The clean axisymmetric shell (figure 3) was idealised by axisymmetric thin shell elements, obtained by degenerating an isoparametric volume element of axisymmetric geometry and quadrangular cross section. The displacement field is linear through its thickness, and of second order along its longitudinal coordinate ϕ. A great densification of the elements was taken in the clamping zone.

The bedding material at the clamping zone (figure 4) was represented by axisymmetric isoparametric volume elements with a quadratic displacement field. A total number of 33 elements of both classes was taken for this modelling.

The following boundary conditions was imposed:

i) Between $\phi = 0°$ and $\phi = 50.72°$, the component of the displacement in the radial direction was constrained, leaving free its meridional component (it is a conservative assumption in the absence of trusty data about the contact friction between the steel shell and the concrete structure).

ii) Between $\phi = 50.72°$ and $\phi = 52.76°$, equal radial displacements of the steel shell and of the elastic bedding was imposed. The second one was assumed fixed to the concrete bed.

iii) At the upper and bottom pole, null radial displacement was assumed.

Minimum true stress-true strain relationship of the sphere material from a collection of tensile specimens was used (figure 5). Elastic isotropy and the Huber-von Mises elastoplasticity theory with isotropic strain-hardening were considered, taking also into account geometrical nonlinearities (large deformations). On the other hand, the elastic bedding material was assumed having the bilinear elasto-plastic behaviour shown in figure 5. Rupture in the circumferential direction (appearance of radial cracks) is assumed to occur when its equivalent strain exceed 10%.

The physical and geometrical data for the calculations are indicated in Table 1. With these data, a non-linear static analysis of the sphere subjected only to internal pressure was performed. The load was increased from zero by several discrete steps. The three former increments was of 0.3 N/mm^2; the fourth is of 0.2 N/mm^2; and then four increments each one of 0.05 N/mm^2 was applied until the elastoplastic collapse be reached.

Material properties	Symbol	Value
Young modulus	E	2.10×10^5 N/mm^2
Poisson ratio	ν	0.3
Yield point	σ_y	544 N/mm^2
Fracture toughness of base metal	K_{1c}	5.6 KN/mm$^{3/2}$
Fracture toughness of welding metal	K_{1c}	3.6 KN/mm$^{3/2}$

Geometrical parameters	Symbol	Value [mm]
Spherical shell:		
- Internal radius	R_i	28000
- Thickness	t	30
Personnel lock:		
- Equivalent internal radius	r_i	1787
- Longitude	L	2375
- Thickness	d	80
- Pad external radius	r_p	2833
- Pad thickness	S_A	50
Emergency lock:		
- Equivalent internal radius	r_i	765
- Longitude	L	1350
- Thickness	d	50
- Pad external radius	r_p	1515
- Pad thickness	S_A	50

TABLE 1: Geometrical and material data.

Dimensionless meridional and hoop stresses at the outside and inside bounding surfaces calculated at the clamping zone and its neighbourhood are shown in figure 6. Both stresses are divided by the asymptotic membrane stress far from irregularities, of value $\sigma_m = P_i R/2t$, where P_i is the internal relative pressure; R is the sphere mean radius; and t is the shell thickness.

The quasi-coincidence of the dimensionless stress for P_i = 0.9 and 1.1 N/mm^2, as shown in figure 6, indicate that the behaviour of the shell is almost linear elastic up to the second value of P_i. On the other hand, the relaxation of the stress concentration and of the bending stress by the plastic behaviour at the clamping zone are manifest in these plots for P_i greater than 1.1 N/mm^2.

For the determination of the plastic analysis-collapse load (internal pressure that produce elasto-plastic collapse), we follow here a procedure discussed by Berman [51] and based on rules of the ASME Boiler and Pressure Vessel Code, Section III, Appendix II [52] for tests for the determination of collapse loads. The load must be plotted against the maximum principal strain or displacement as shown in figure 7 herein. The collapse load is then determined by the intersection of the calculated curve with a line making an angle with the load axis whose tangent is twice the tangent of the angle that makes the linear stage line with the load axis. For the global containment (clean sphere) results in this manner a collapse pressure of P_1 = 1.171 N/mm^2.

3.2 Analysis of the personnel lock

The nozzle of the personnel lock (see basic dimensions in Table 1) has been modelled by the finite element discretization shown in figure 8. Axisymmetric, isoparametric volume elements with a quadratic displacement field have been used for the nozzle and for the pad. From the weld of the pad with the spherical shell, up to an angle of 30° with the nozzle axis, this shell was idealized by axisymmetric thin shell elements as used in the clean sphere.

Boundary conditions of spherical symmetry have been imposed at the edge of the spherical cap: null meridional component of the displacement; rotation constrained; and free radial displacement. The structure was subjected to the same discrete steps of internal pressure as done in the former analysis, and the total force coming from the enclosure of the lock has been circumferentially distributed along the bottom boundary in axial direction.

The calculated equivalent (von Mises) stresses at the outside and inside bounding surfaces of pad and neighbouring spherical shell, are plotted in figure 9 for four values of the internal pressure. Up to P_i = 1.1 N/mm^2, the behaviour is practically linear elastic, but for greater values of this load, large plasticity effects are there appreciated.

At the inside and outside bounding surfaces at the nozzle, the calculated equivalent stresses are as plotted in figure 10,

for the same values of P_i as in figure 9. An (r,Z)-map of the equivalent stress in the welding zone, corresponding to P_i = 1.1 N/mm^2, can be observed in figure 11.

An interesting conclusion can be drawn for the results shown in figures 9, 10 and 11, as follows: In spite of the fact that in the elastic range the maximum equivalent stress appears at the nozzle internal surface, at the plastic range ($P_i \geq 1.05$ N/mm^2) the equivalent stress in the entire nozzle is not greater than the asymptotic membrane stress in the spherical cap $\sigma_m^{as} = P_i R/2t$. At P_i = 1.25 N/mm^2, the value of σ_m^{as} is 584 N/mm^2, while in the nozzle the maximum equivalent stress is of 555 N/mm^2 (see figure 11). The greatest stress concentration appears at the welding between the pad and the spherical shell.

Plotting the displacement of a point in the welding between the nozzle and the pad (see figure 7), it results a collapse pressure of P_i = 1.162 N/mm^2, only a little lower than the value corresponding to the clean sphere. This fact is in agreement with the conclusions obtained in studies of limit pressure of nozzles performed by other authors, such as the refs. 14,15,18-21.

3.3 Analysis of the emergency nozzle

For the nozzle of the emergence lock, the analysis was very similar than that of the former nozzle. In figure 12 a map of the equivalent stress in the welding between this nozzle and the pad is shown, corresponding to an internal pressure of 1.35 N/mm^2.

In figure 7 the determination of the collapse pressure for this nozzle is also indicated. The resulting value is almost the same as in the former case.

4.- FAILURE ASSESSMENT OF CRACKED SPHERICAL SHELL FAR FROM IRREGULARITIES

From the last analysis we can infer that the limit pressure of the containment in the complete absence of cracks is P_i = 1.16 N/mm^2.

The CEGB's R-6 Failure Assessment approach, as described in Section 2, is now applied to the containment analysed with cracks located in regions far from irregularities and not interacting between them. A semielliptical model for the crack has been considered, as indicated in fig. 13, in order to follow the recommendations of the ASME Code, Section XI, Appendix A [53]. We will consider two different ratios of the flaw depth a to the flaw length l: a/l = 0.3 and 0.1. The ratio a/t will be increased from zero by steps of 0.1. Two values of the internal pressure will be taken into account: a) the test pressure of P_i = 0.6 N/mm^2; and b) P_i = 0.85 N/mm^2.

4.1 Material properties of the base and welding metals

From a collection of test data, the following lower bounds result for the material fracture toughness: K_{1c} = 5.6 KN/mm$^{3/2}$ for the base metal and K_{1c} = 3.6 KN/mm$^{3/2}$ for the welding metal. We adopt for the flow stress the value of the pure membrane stress corresponding to the collapse load P_i = 1.171 N/mm^2 calculated for the clean shell:

$$\bar{\sigma} = \frac{RP_i}{2t} = \frac{28015 \times 1.170}{2 \times 30} \text{ N/mm}^2 = 547 \text{ N/mm}^2 \qquad (5)$$

This value is slightly greater than the yield point: σ_{ys} =544 N/mm^2. We suppose that the welding material has the same value of $\bar{\sigma}$.

4.2 Calculation of S_r

For a near uniform stress field the collapse stress $\sigma_1(a/t)$ can be taken [28,31] as $\bar{\sigma}$ (1 - c/w), where $\bar{\sigma}$ is the flow stress adopted in Section 4.1, and the factor (1 - c/w) corrects for the uncracked ligament and contains a flaw ellipticity. The values of c/w were obtained from Milne [28] in terms of a/w and are indicated in Table 2. Thus, for a given internal pressure:

$$S_r = \frac{\sigma_m}{\sigma_1} = \frac{P_i R/2t}{\bar{\sigma}\ (1-c/w} = 0.854\ \frac{P_i}{1-c/w} \qquad (6)$$

4.3 Calculation of K_r

The ASME Code, Section XI [53] provides the expression of K_I for semielliptical flaws in shells or plates subjected to tension and bending. For the present purpose the following expression applies:

$$K_I = \sigma_m M_m \sqrt{\pi}\ \sqrt{a/Q_o} \qquad (7)$$

where Q_o (a/1) is the flaw shape parameter regardless plasticity effects, given by [28]:

$$Q_o = 1 + 4.593\ (a/1)^{1.65}; \qquad (8)$$

and M_m (a/1;a/t) is a correction factor for membrane stress, given by Figure A-3300-3 of ref. 53.

4.4 Failure analysis

Table 2 contains the data and results of the failure analysis corresponding to the internal pressure test, obtained by expressions (2), (6-8). The points (S_r,K_r) determine the loci indicated in figure 13 corresponding to the increment of flaw depth in the welding metal as well as in the base metal for this internal pressure. The loci for any other internal pressure, such as 0.85 N/mm^2 in the diagrams, is directly obtained scaling the former ones.

By means of expression (4) each value of the reserve factor

a/l	Q_o	a/t	a [mm]	M_m	c/w	S_r	Welding metal			Base metal		
							K_r	F_p	P_{crit} [N/mm²]	K_r	F_p	P_{crit} [N/mm²]
		0.1	3	1.12	0.052	0.540	0.255	1.85	1.11	0.164	1.85	1.11
		0.2	6	1.20	0.131	0.589	0.386	1.64	0.982	0.248	1.70	1.02
0.1	1.103	0.3	9	1.32	0.224	0.660	0.520	1.38	0.829	0.334	1 51	0.904
		0.4	12	1.51	0.325	0.758	0.687	1.13	0.678	0.441	1.30	0.778
		0.5	15	1.77	0.422	0.886	0.900	0.908	0.545	0.579	1.09	0.653
		0.1	3	1.10	0.029	0.527	0.206	1.90	1.14	0.132	1.90	1.14
		0.2	6	1.105	0.077	0.555	0.292	1.79	1.07	0.188	1.80	1.08
		0.3	9	1.13	0.151	0.603	0.366	1.62	0.973	0.235	1.66	0.995
0.3	1.630	0.4	12	1.16	0.232	0.667	0.434	1.45	0.868	0.279	1.50	0.899
		0.5	15	1.22	0.317	0.750	0.510	1.27	0.765	0.328	1.33	0.799
		0.6	18	1.27	0.406	0.862	0.582	1.11	0.666	0.374	1.16	0.695
		0.7	21	1.36	0.507	1.039	0.673	0.930	0.558	0.433	0.962	0.577

TABLE 2: Failure analysis data and results for the internal pressure test (0.6 N/mm²).

F_p (on load) included in Table 2 is obtained, as well as the critical internal pressure ($P_{crit} = F_p \times 0.6$ N/mm^2). They are plotted in figure 14, in terms of F_p flaw depth, for both the base and welding metal and for both ratios a/l considered.

References

1.- A.Andersen, S.Bantle and L.M.Habip: "Stability analysis of spherical metal containment vessels". Proceedings of the Fifth International Conference on Structural Mechanics in Reactor Technology, Paper J 6/6, Berlin, 1979.

2.- A.Andersen and S.Bantle: "Optimization of the containment nozzles". Proceedings of the Fifth International Conference on Structural Mechanics in Reactor Technology, Paper J 4/4, Berlin, 1979.

3.- R.Krieg, B.Göller and G.Hailfinger: "Dynamic stresses in spherical containments with pressure suppression system during steam condensation". Nuclear Engineering and Design, Vol. 64, pp. 203-223 (1981).

4.- M.Miksch and A.Mera: "Static and heat transfer analysis of a sphere-cone intersection in a nuclear containment vessel". NASTRAN European User's Forum, Munich, May 1974.

5.- F.G.Weber and W.Elfmann: "Computational approach in the assessment of seismic structural safety for spherical shells with openings analysis of the KWU-PWR containment vessel". Proceedings of the Third International Conference on Structural Mechanics in Reactor Technology, Paper K 6/4, London, 1975.

6.- G.Sánchez Sarmiento, A.N.Bergmann, A.Lotorto and H.Lux Wurm: "Computational techniques for the stress analysis of nuclear steel containments" (in Spanish). Revista de Ingeniería Estructural, Buenos Aires, Argentina, Vol. 1, N°3, pp. 1-19, June 1983.

7.- G.Sánchez Sarmiento and A.N.Bergmann: "Thermal stresses at nozzles of nuclear steel containments under LOCA conditions". To be presented at the Conference on Structural Analysis and Design of Nuclear Power Plants, Porto Alegre, Brasil, October 3-5, 1984.

8.- L.I.Skundric: "Metal containments: nature of loads and behaviour limits". Nuclear Engineering and Design, 46, pp. 409-416 (1978).

9.- Probabilistic Risk Assessment Procedures Guide. NUREG/CR-2300, Vol.1. Office of Nuclear Regulatory Research, U.S. Nuclear Regulatory Commission, Washington D.C.

10.- P.Cybulskis: "On the definition of containment failure". Proceedings of the Workshop on Containment Integrity, Arlington,

Virginia, June 7-9, 1982. NUREG/CP-0033; SAND82 - 1659, Vol. II, pp. 65-76 (1982).

11.- M.L.Corradini, D.V.Swenson, R.L.Woodfin y L.E.Voelker: "An analysis of containment failure by a steam explosion following a postulated core meltdown in a light water reactor". Nuclear Engineering and Design, 66, pp.287-298 (1981).

12.- Reactor Safety Study - WASH - 1400, NUREG-75/0114, Appendix VII, Nuclear Regulatory Commission (October 1975).

13.- J.C.Tsai and R.S.Orr: "Probabilistic failure modes and locations in containments subjected to internal pressurization". Proceedings of the Workshop on Containment Integrity, Arlington, Virginia, June 7-9, 1982. NUREG/CP-0033; SAND82 - 1659, Vol. II, pp. 365-382.

14.- D.S.Horschel and T.E.Blejwas: "An analytical investigation of the response of steel containment models to internal pressurization". Proceedings of the Seventh International Conference on Structural Mechanics in Reactor Technology, Chicago, Illinois, August 22-26, 1983, Paper J 6/3.

15.- T.E.Blejwas and D.S.Horschel: "Analysis of steel containment models". Proceedings of the Workshop on Containment Integrity, Arlington, Virginia, June 7-9, 1982. NUREG/CP-0033; SAND 82-1659, Vol. I, pp. 201-226 (1982).

16.- P.F.Gow and J.E.Love: "Pressure carrying capability of the containment structural system of the MARK III Standard Plant". Proceedings of the Workshop on Containment Integrity, Arlington, Virginia, June 7-9, 1982. NUREG/CP-0033; SAND82-1659, Vol. I, pp. 263-317.

17.- W.Gulden, B.Göller and R.Krieg: "Analysis of the mechanical behaviour of LWR-containments under accident conditions". Proceedings of the Workshop on Containment Integrity, Arlington, Virginia, June 7-9, 1982. NUREG/CP-0033; SAND82-1659, Vol. I, pp. 319-335.

18.- H.Stegmüller, E.Ramm and F.W.Bornscheuer: "Ultimate load analysis of nozzle reinforced reactor containments-A parametric study". Proceedings of the Sixth International Conference on Structural Mechanics in Reactor Technology, Paris, August 1981 - Paper J 5/9.

19.- M.Robinson: "Some problems associated with the behaviour of structures in the plastic range". International Journal of Pressure Vessels and Piping, Vol.10, pp. 409-420 (1982).

20.- J.N.Ashton, H.Mc Intyre and S.S.Gill: "A design procedure based on limit analysis for a pad reinforced nozzle in a spherical pressure vessel". International Journal of Mechanical Science, Vol.20, pp.747-757 (1978).

21.- H.Mc Intyre, J.N.Ashton and S.S.Gill: "Limit analysis of a pad reinforced flush nozzle in a spherical pressure vessel". International Journal of Mechanical Science, Vol.19, pp.399-412 (1977).

22.- F.M.Burdekin and T.E.Taylor: "Fracture in spherical pressure vessels". Journal of Mechanical Engineering Science, Vol. 11, N°5, pp. 486-497 (1969).

23.- I.W.Goodall and J.E.Griffiths: "On the limit analysis of a spherical pressure vessel with fully circumferential defects". International Journal of Mechanical Sciences, Vol. 24, N°10, pp. 635-645 (1982).

24.- R.P.Harrison, K.Loosemore and I. Milne: "Assessment of the integrity of structures containing defects", CEGB Report N° R/H/6, Central Electricity Generating Board (1976).

25.- A.R.Downling and C.H.A.Townley: "The effects of defects on structural failures: A Two-Criteria Approach", International Journal of Pressure Vessels and Piping, Vol. 3, pp.77-107 (1973).

26.- B.A.Bilby, A.H.Cottrell and K.H.Swinden: "The spread of plasticity from a notch". Proceedings of the Royal Society of London, Vol. A272, pp. 304-314 (1963).

27.- P.T.Heald, G.M.Spink and P.J.Worthington: "Post-Yield fracture mechanics". Material Science and Engineering, Vol. 10, p. 129 (1972).

28.- I.Milne, K.Loosemore and R.P.Harrison: "A procedure for assessing the significance of flaws of in pressurized components". I Mech E Conference "Tolerance of Flaws in Pressurized Components", Paper C 106/78, pp. 317-324 (1978).

29.- G.G.Chell and I.Milne: Materials Science and Engineering, Vol. 22, p. 349 (1976).

30.- G.G.Chell: Materials Science and Engineering, Vol. 24, p.233 (1976).

31.- I.Milne: "Failure Assessment". Chapter 8 of "Developments in Fracture Mechanics - 1". Edited by G.G.Chell. Applied-Science Publishers LTD., London (1979).

32.- G.G.Chell and I.Milne: "A simple practical method for determining the ductile instability of cracked structures". Proceedings of CSNI Specialists Meeting on Plastic Tearing Instability. St. Louis, NUREG CP-0010, CSNI Report N°39 (1979).

33.- B.J.L.Darlaston: "The CEGB two-criteria proposal". Chapter 4 of "Developments in Pressure Vessel Technology - 1 (Flaw Analysis)". Edited by R.W.Nichols. Applied Science Publishers Ltd. London, (1979).

34.- A.R.Dowling, R.P.Harrison and I.Milne: "The CEGB approach to the assessment of the integrity of structures containing defects". Fitness for purpose validation of welded constructions, London, 17-19 Nov. 1981, Paper 34.

35.- I.Milne: "Application of the CEGB procedure to the analysis of HSST intermediate vessel tests V5 and V9". Fitness for purpose validation of welded constructions, London, 17-19

Nov. 1981, Paper 35.

36.- J.G.Collier, M.R.Hughes, C.J.Gardner, L.M.Davies and I.Milne: "Fracture assessment of a PWR pressure vessel", International Atomic Energy Agency, IAEA-SM-269/103, pp. 189-209(1983).

37.- G.G.Chell: "Elastic-plastic fracture mechanics". Chapter 3 of "Developments in Fracture Mechanics - 1". Edited by G.G. Chell. Applied Science Publishers Ltd., London (1979).

38.- I.Milne: "Failure analysis in the presence of ductile crack growth", Materials Science and Engineering, Vol. 39, pp.65-79 (1979).

39.- I.Milne: "Calculating the load bearing capacity of a structure failing by ductile crack growth". Advances in fracture research (D.Francois et al, editors), pp. 1751-1758. Pergamon Press (1980).

40.- J.M.Bloom: "A procedure for the assessment of the structural integrity of nuclear pressure vessels". Transactions of the ASME, Journal of Pressure Vessel Technology, Vol. 105, pp. 28-34 (Febr. 1983).

41.- J.M.Bloom: "Prediction of ductile tearing of compact fracture specimens using the R-6 failure assessment diagram". International Journal of Pressure Vessels and Piping, p. 215 (May-June 1980).

42.- J.M.Bloom: "Elastisch-plastische Versagensanalyse (Elastic-plastic failure analysis". 6.MPA Seminar, Staatliche Materialprufungsanstalt - Universitat Stuttgart, Paper N°9, 9/10 (Oct. 1980).

43.- I.Milne: "Assessment of the defect tolerance of structures subjected to combined secondary and primary loads". Central Electricity Generating Board, RD/L/N112/78 (Sept. 1978). Also: SMIRT 5, Berlin, Paper G 1/3 (1979).

44.- C.F.Shih et al: "Methodology for plastic fracture". Final Report to EPRI, Contract N° RP 601-2, NP-1735, General Electric Company, Schenectady, New York, Aug. 1980.

45.- C.F.Shih, V.Kumar and M.D.German: "Studies on the failure assessment diagram using an estimation method and I-controlled crack growth approach", presented at the 2nd. International Symposium on Elastic-Plastic Fracture Mechanics, Philadelphia, Oct. 6-9, 1981, to appear in ASTM STP; see also, Electric Power Research Institute Report NP-1931, July 1981.

46.- C.P.Shih and J.W.Hutchinson: "Fully plastic solutions and large-scale yielding estimate for plane stress crack problems". ASME Journal of Engineering Materials and Technology, Vol. 98, Oct. 1976, p. 289.

47.- SAMCEF - User's Manual. Vol. 1,2 and 3. University of Liege. Liege, Belgium.

48.- S.Idelsohn and G.Sander: "On the deep, shallow or flat shell

finite elements for the analysis of thin shell structures". Computer Methods in Applied Mechanics and Engineering. Vol. 26, N°3, pp. 321-330 (1981).

49.- M.Geradin, S.Idelsohr and M.Hogge: "Nonlinear structural dynamics via Newton and Quasi-Newton Methods". Nuclear Engineering and Design, Vol. 58, pp.339-348 (1980).

50.- S.Idelsohn: "El Sistema SAMCEF y su desarrollo actual en el Instituto de Desarrollo Tecnológico para la Industria Química". Anales del III Congreso Latinoamericano sobre Métodos Computacionales para Ingeniería (Comp. by A.J.Ferrante). Buenos Aires, Argentina, May 1982.

51.- I.Berman: "Inelasticity and the ASME Code". Nuclear Engineering and Design, 46, pp. 335-348 (1978).

52.- Boiler and Pressure Vessel Code. Section III. Nuclear Power Plant Components Division 1. American Society of Mechanical Engineering, 1980 Edition.

53.- Boiler and Pressure Vessel Code. Section XI. Rules for Inservice, Inspection of Nuclear Power Plant Components. Division 1, Appendix A (Analysis of Flaw Indications). American Society of Mechanical Engineering, 1980 Edition.

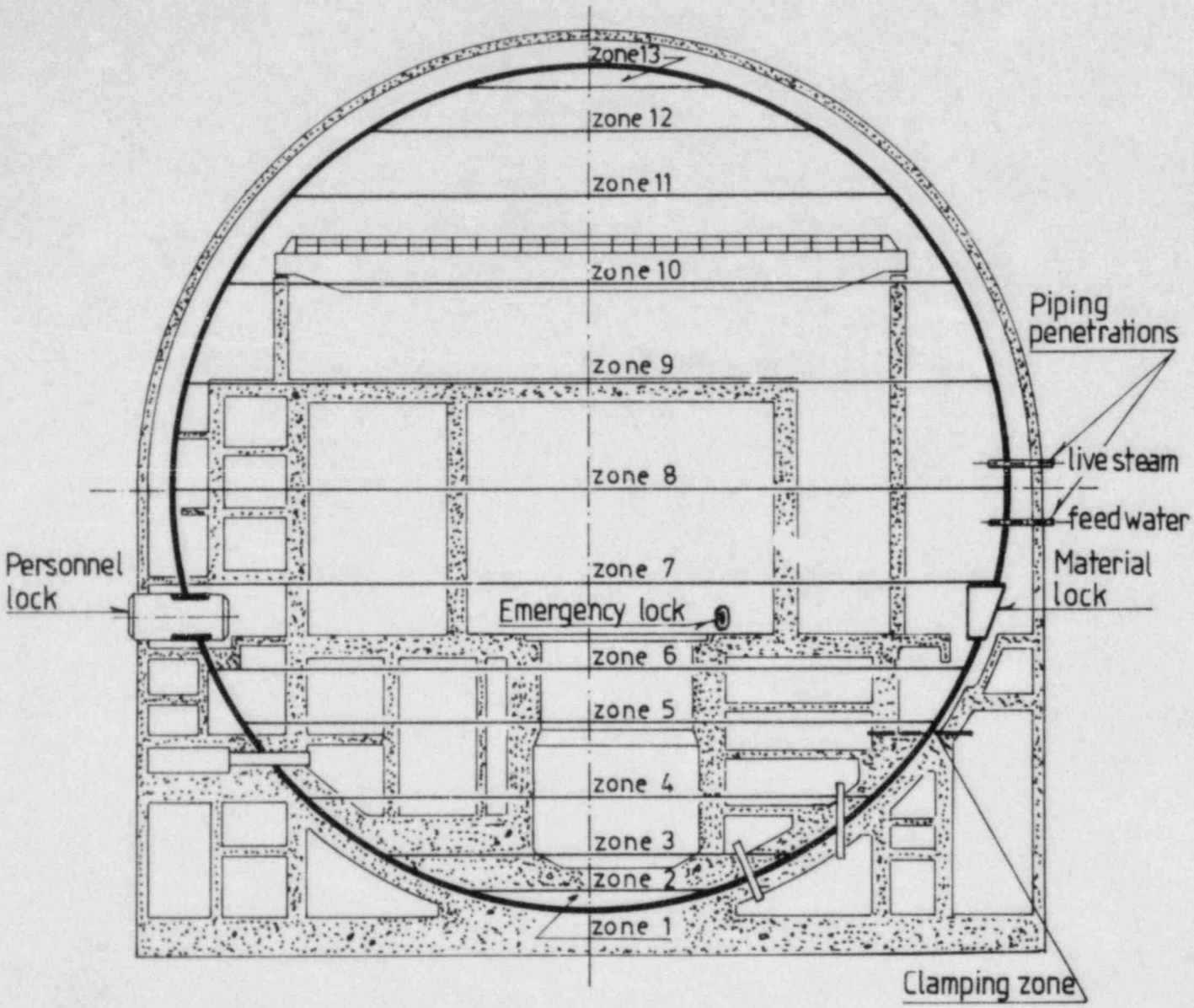

Figure 1. Typical Spherical Steel Containment of a PWR or a PHWR Nuclear Power Plant

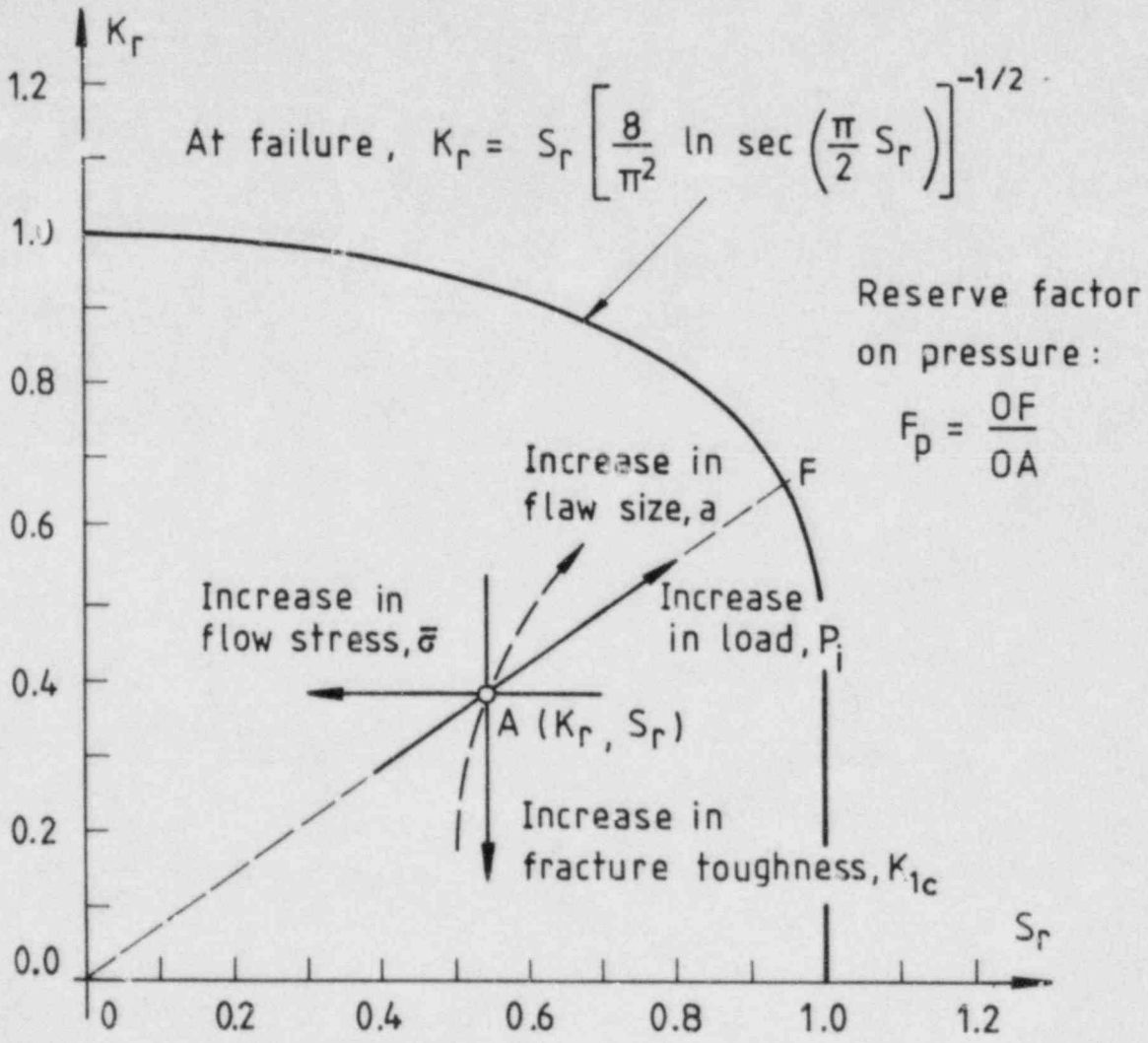

Figure 2. The CEGB's P-6 Failure Assessment Diagram

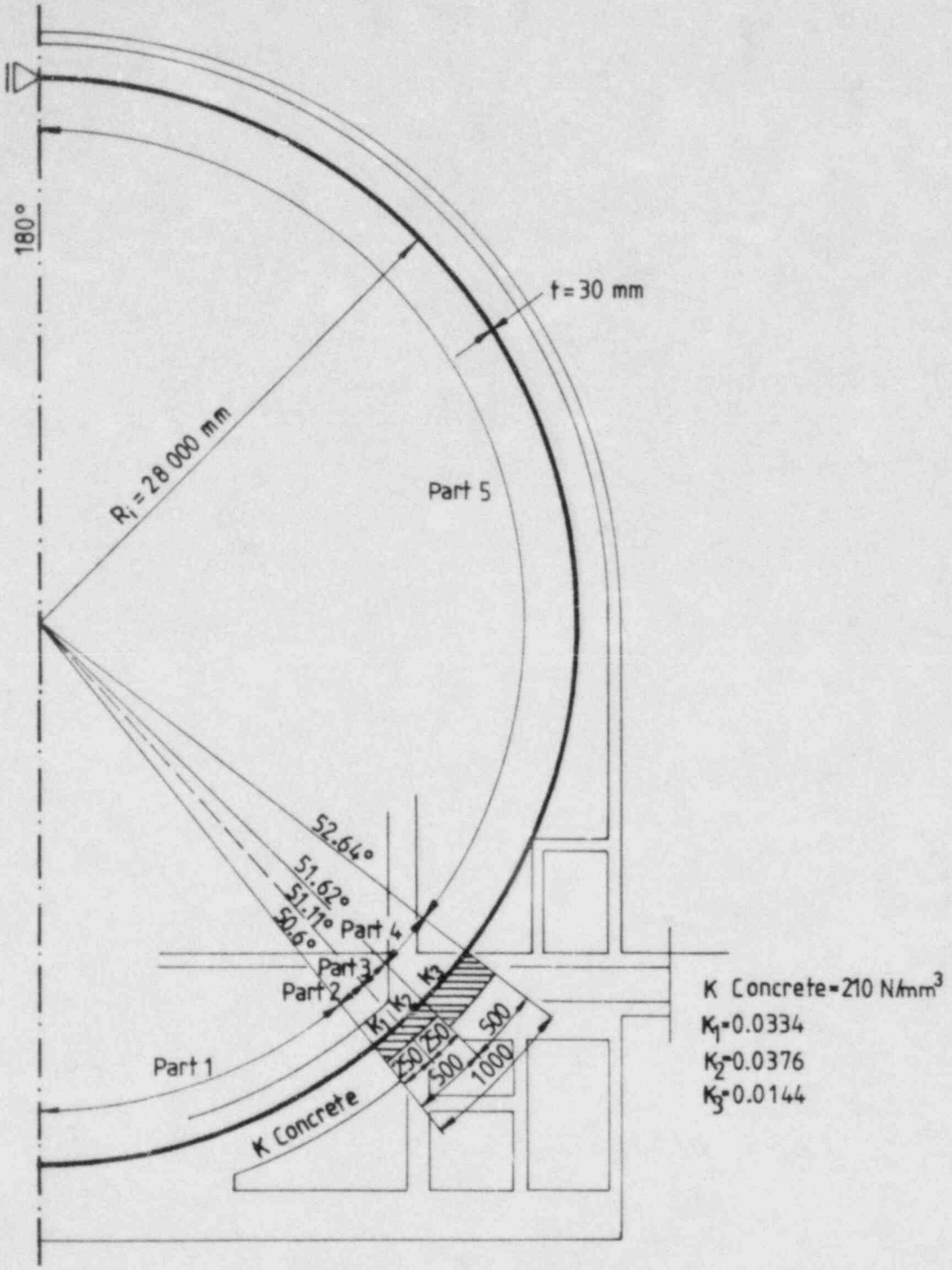

Figure 3. Axisymmetric Thin Shell Model for the Clean Sphere

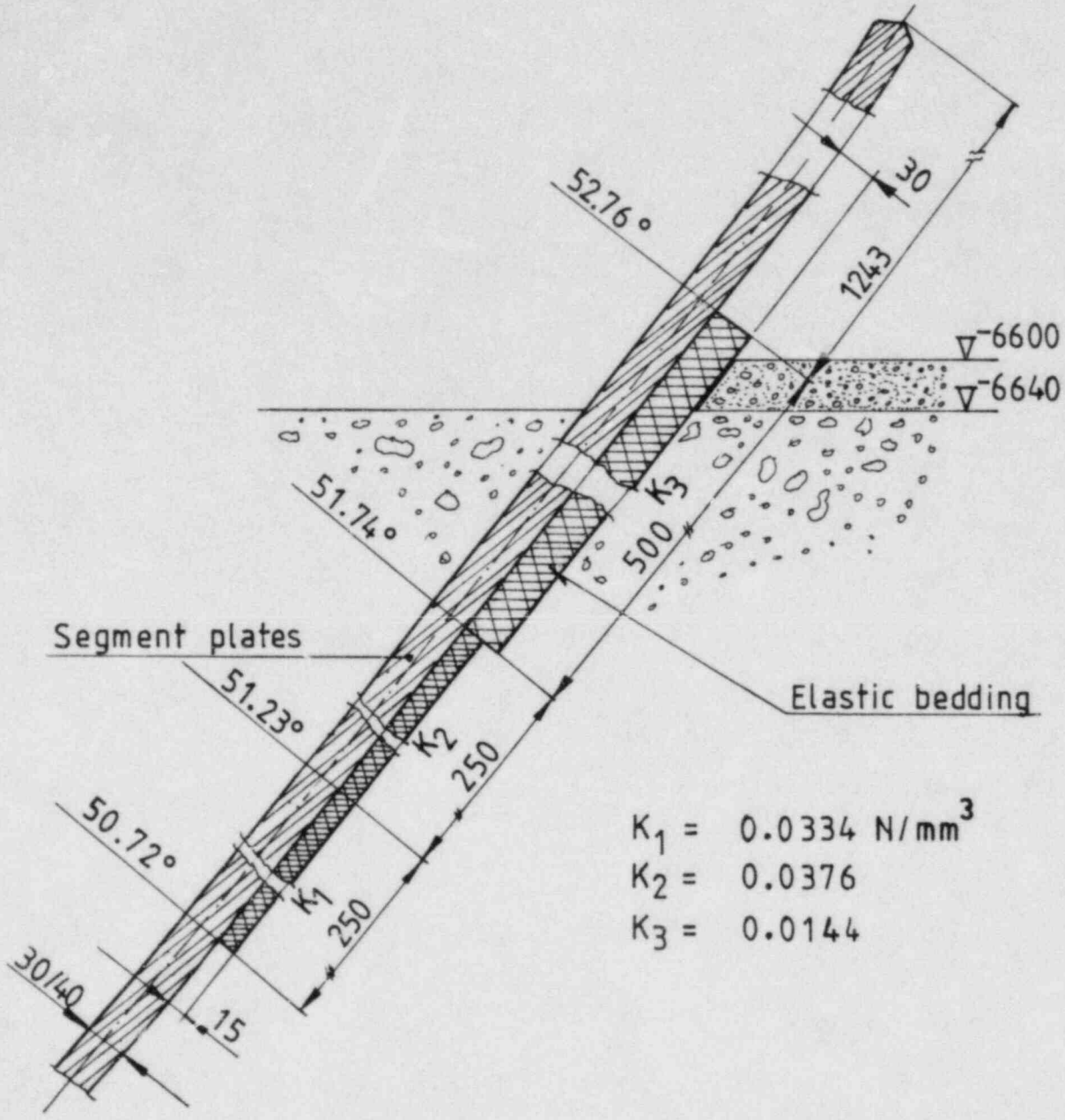

Figure 4. Detail of the Clamping Zone

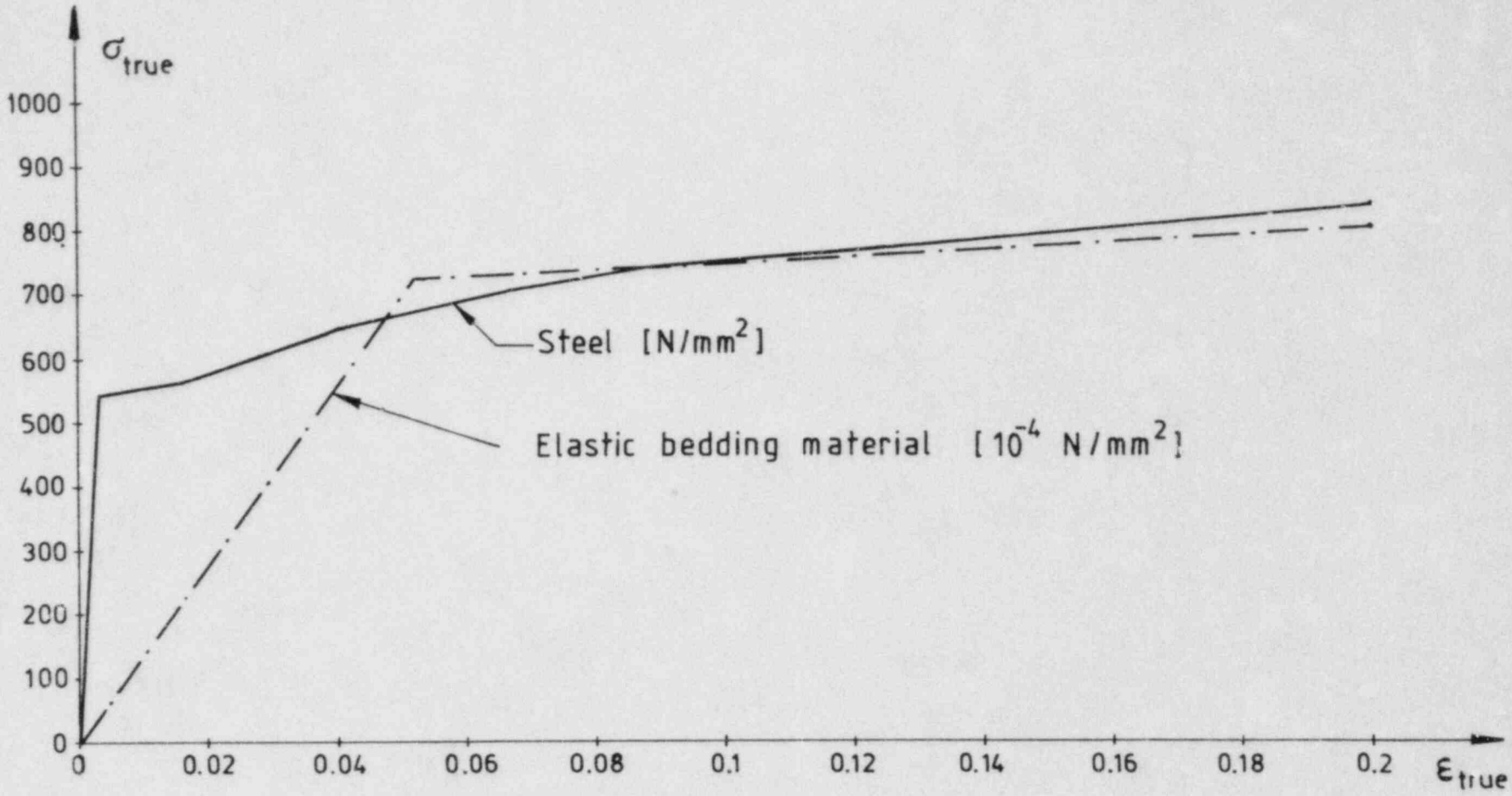

Figure 5. True Stress vs. True Strain Curves of the Containment Steel and of the Elastic Bedding Material Used in the Calculations

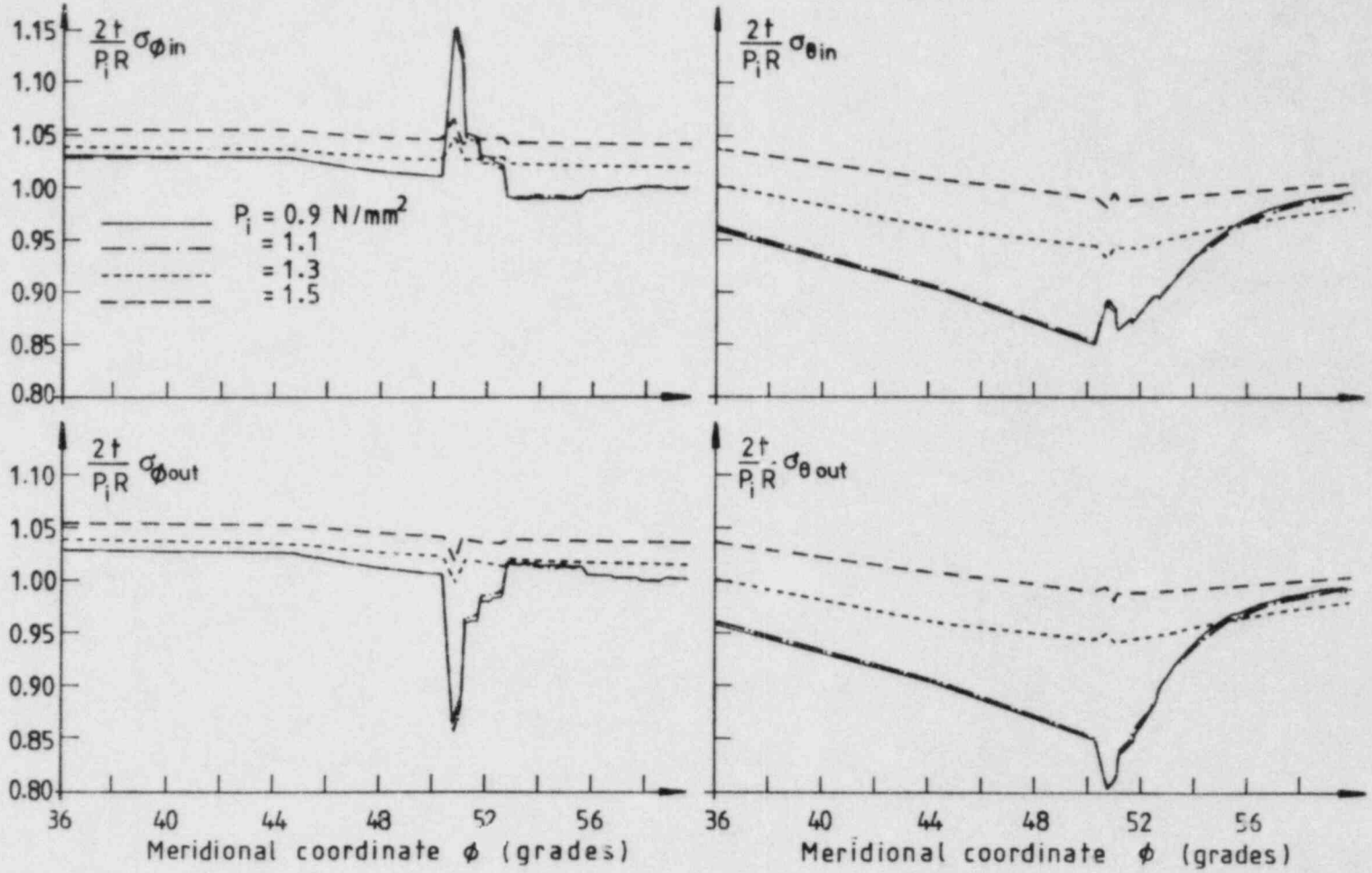

Figure 6. Dimensionless, Meridional and Hoop Stresses at the Outside and Inside Bounding Surfaces of the Spherical Shell Calculated at the Clamping Zone and its Neighborhood Relative to the Membrane Stress of the Free Shell

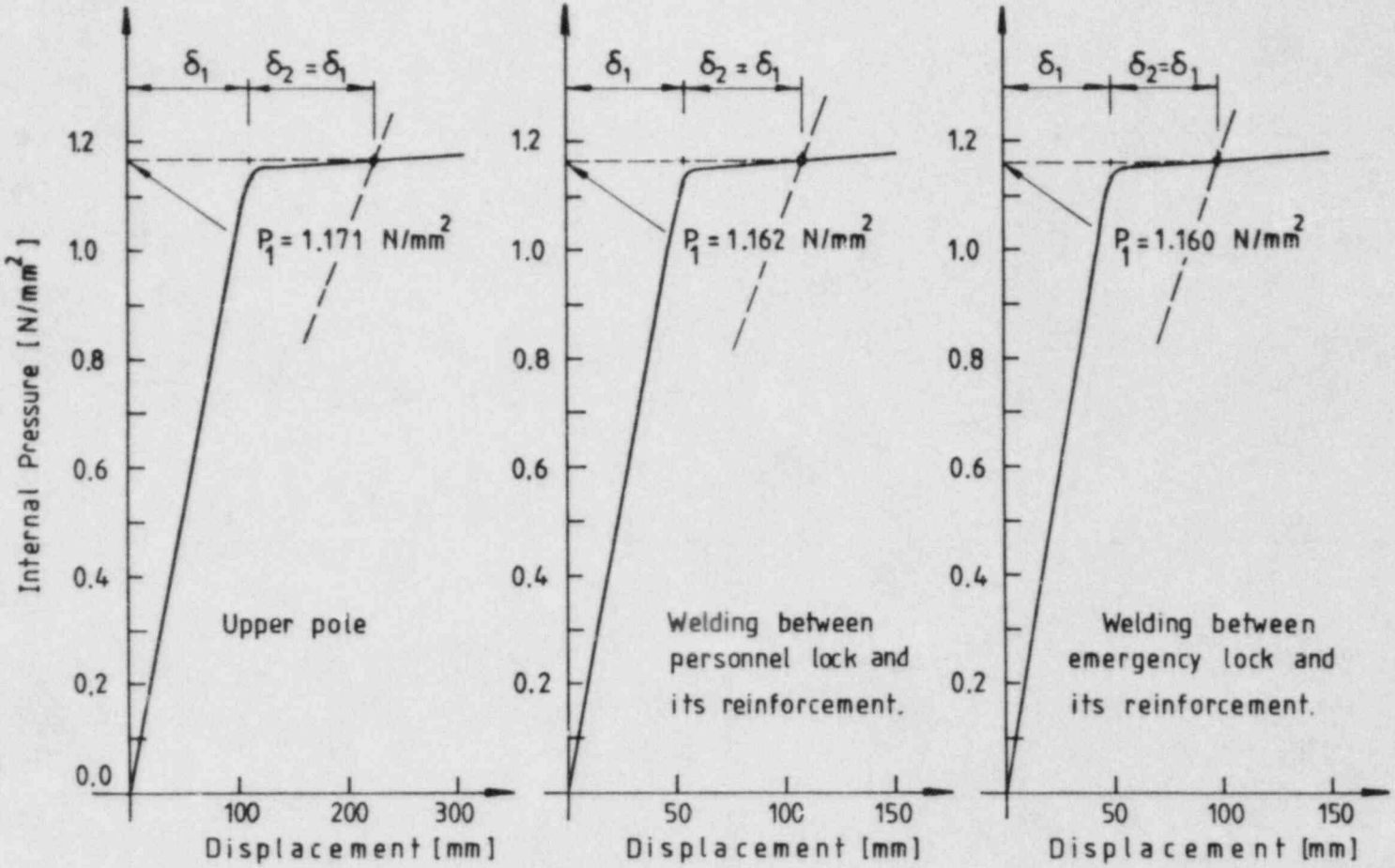

Figure 7. Comparison Between the Calculated Displacements at Three Significant Points and the Respective Collapse Internal Pressure from Them Deduced

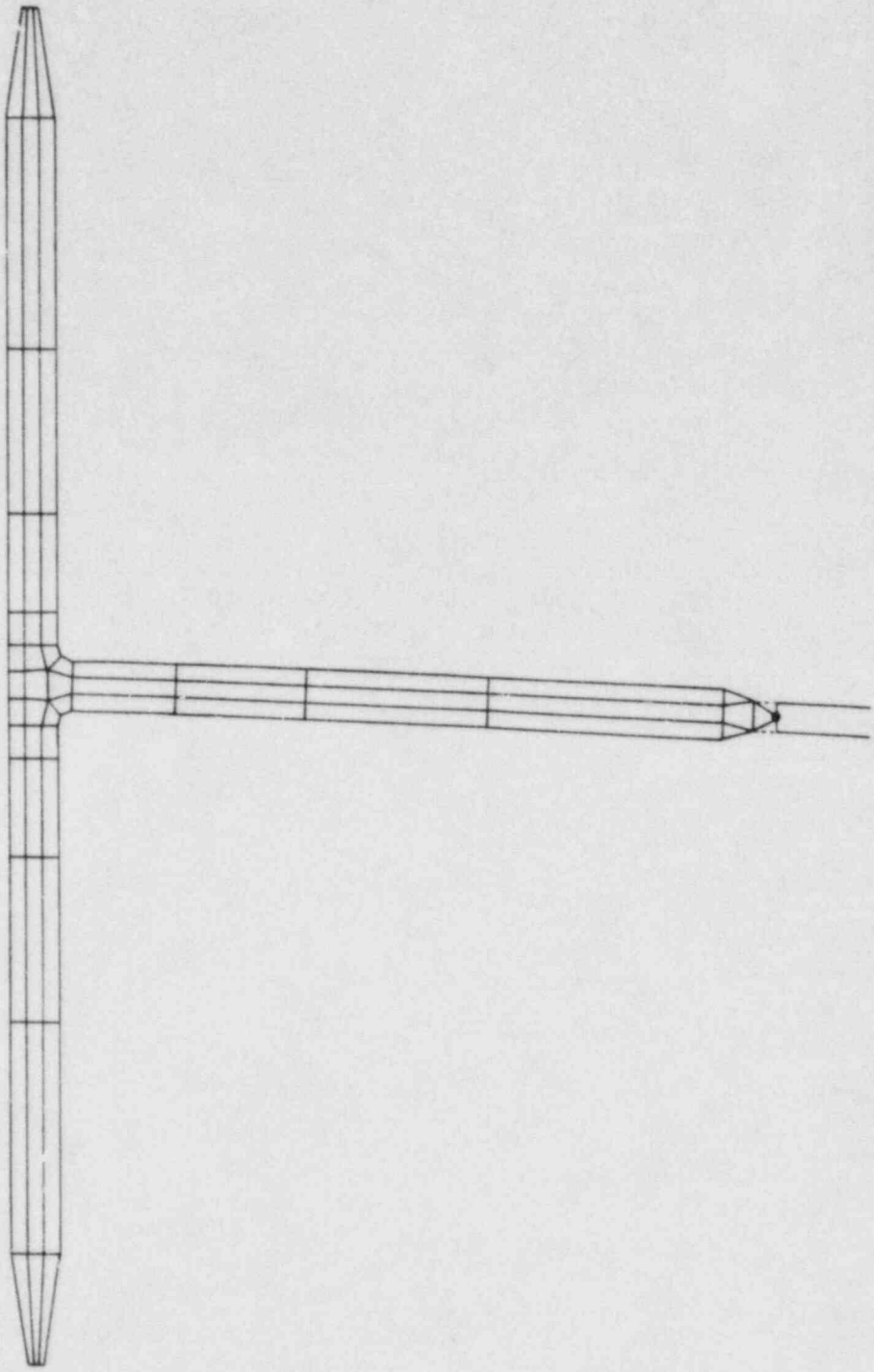

Figure 8. Axisymmetric Finite Element Model of the Emergency Nozzle

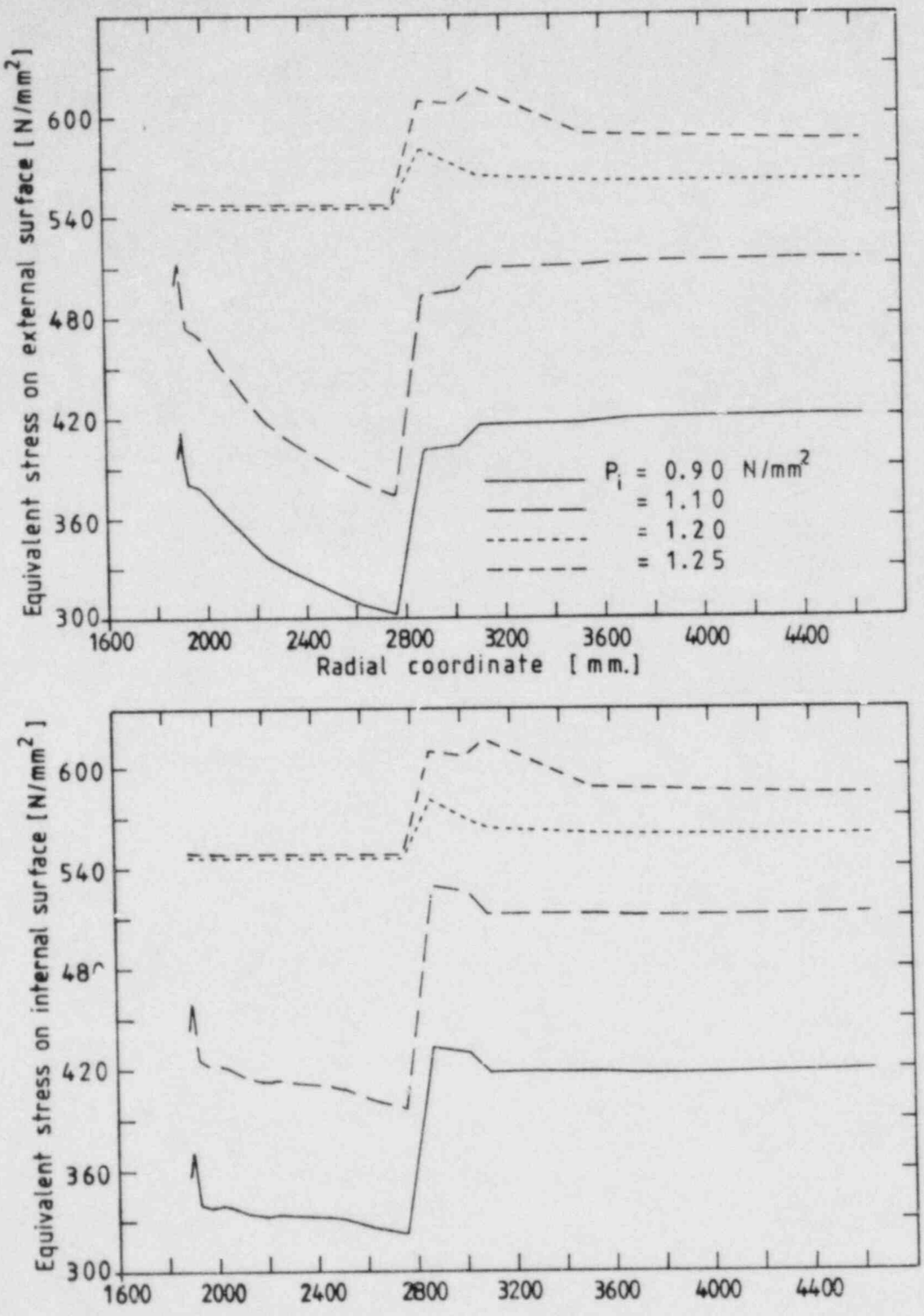

Figure 9. Calculated Equivalent (von Mises) Stresses at the Inside and Outside Bounding Surfaces of the Spherical Shell and of the Pad Besides the Personnel Nozzel

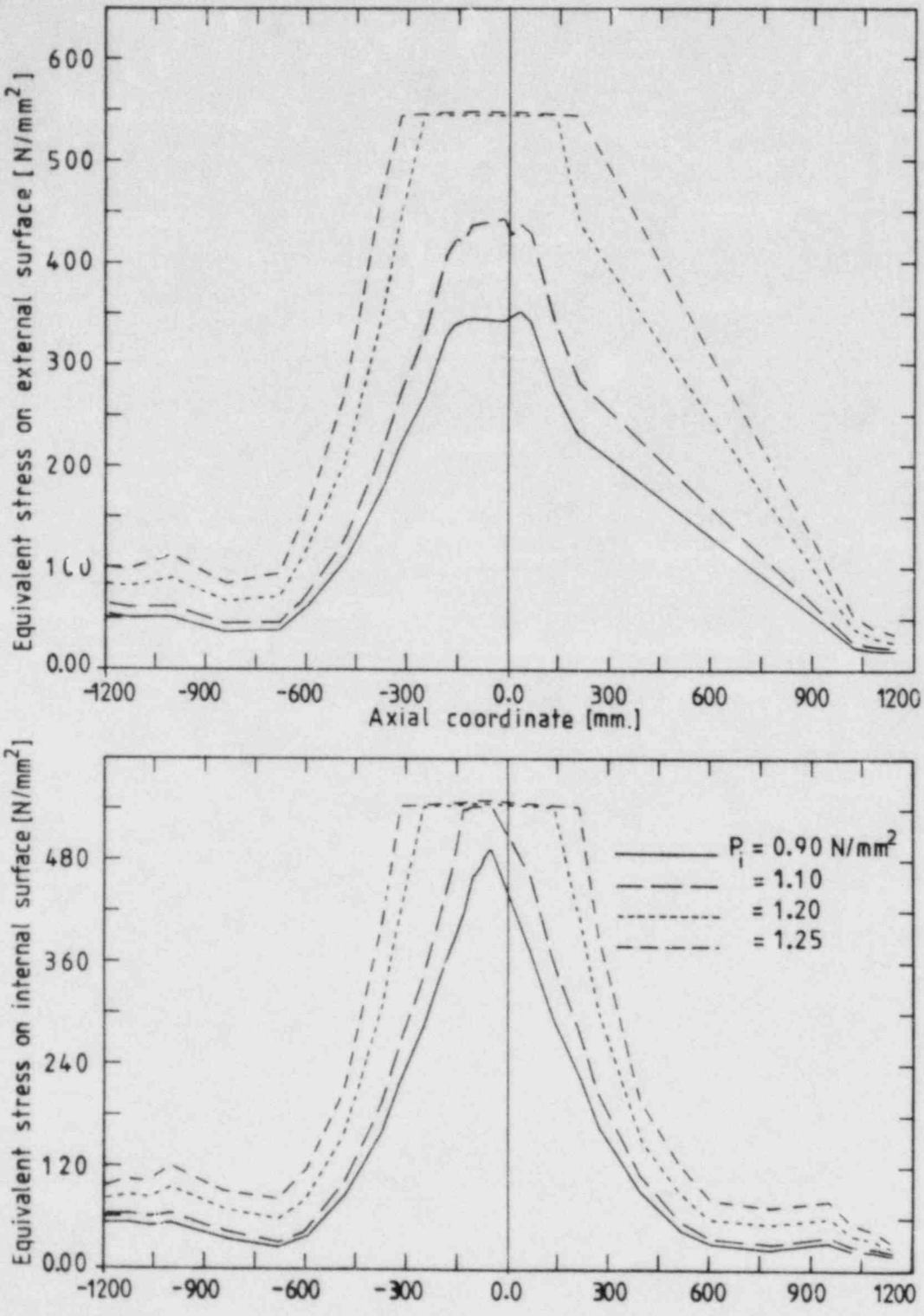

Figure 10. Calculated Equivalent (von Mises) Stresses at the Inside and Outside Bounding Surfaces of the Personnel NOzzle

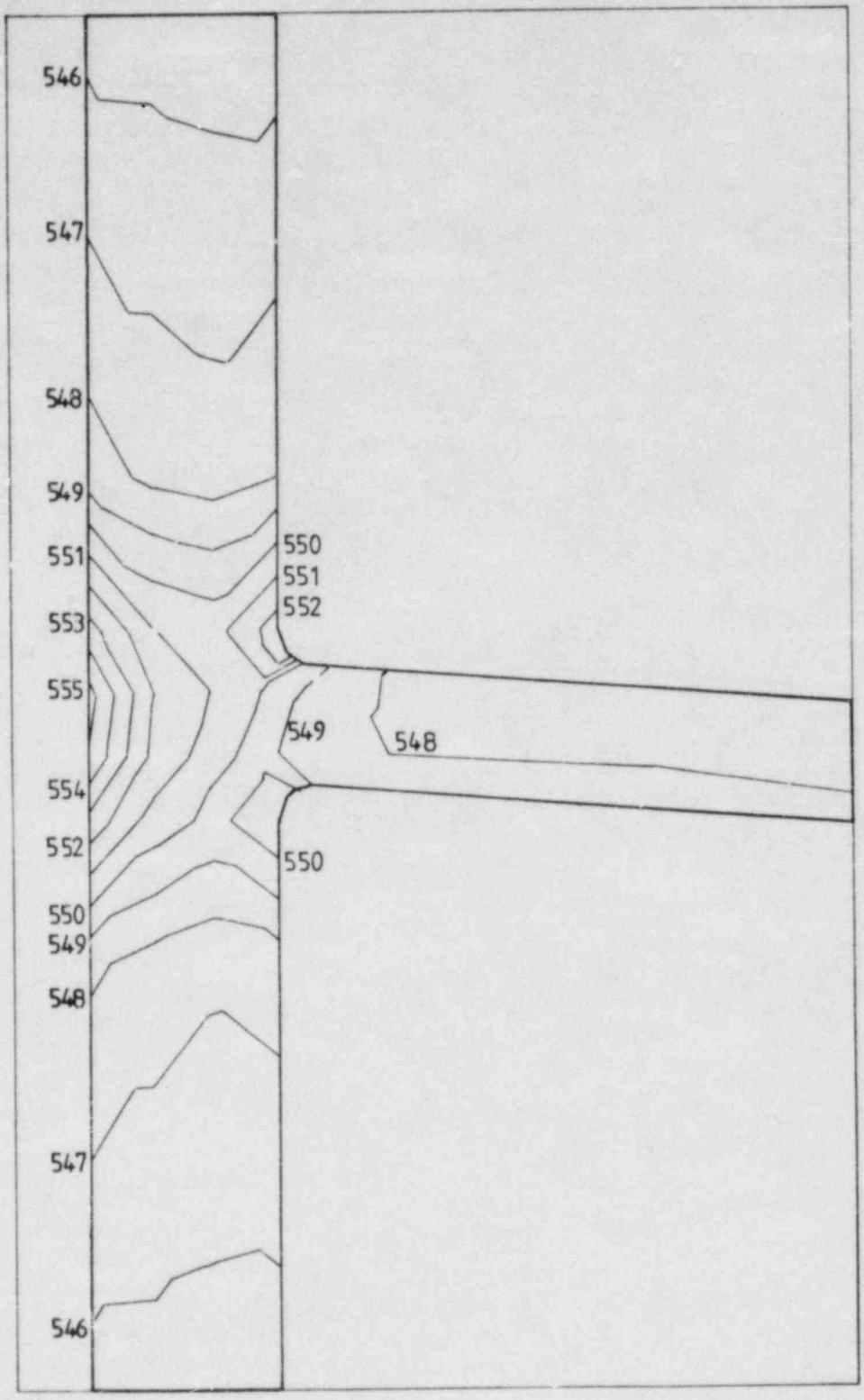

Figure 11. Map of the Equivalent (von Mises) Stress in the Zone of Welding Between the Personnel Nozzle and the Pad of Reinforcement (P_i = 1.25 N/mm^2)

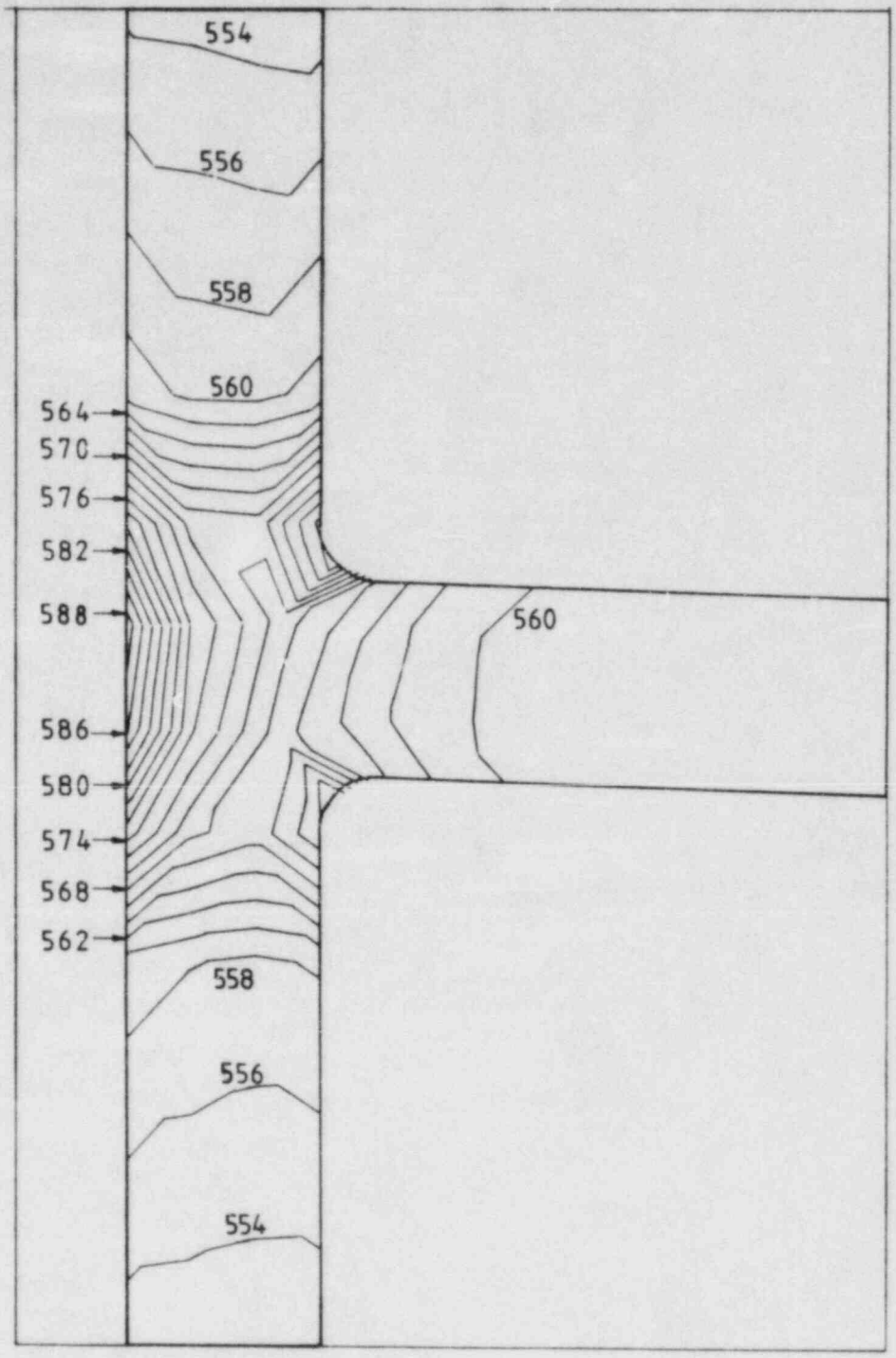

Figure 12. Map of the Equivalent (von Mises) Stress in the Zone of Welding Between the Emergency Nozzle and the Pad of Reinforcement (P_i = 1.35 N/mm^2)

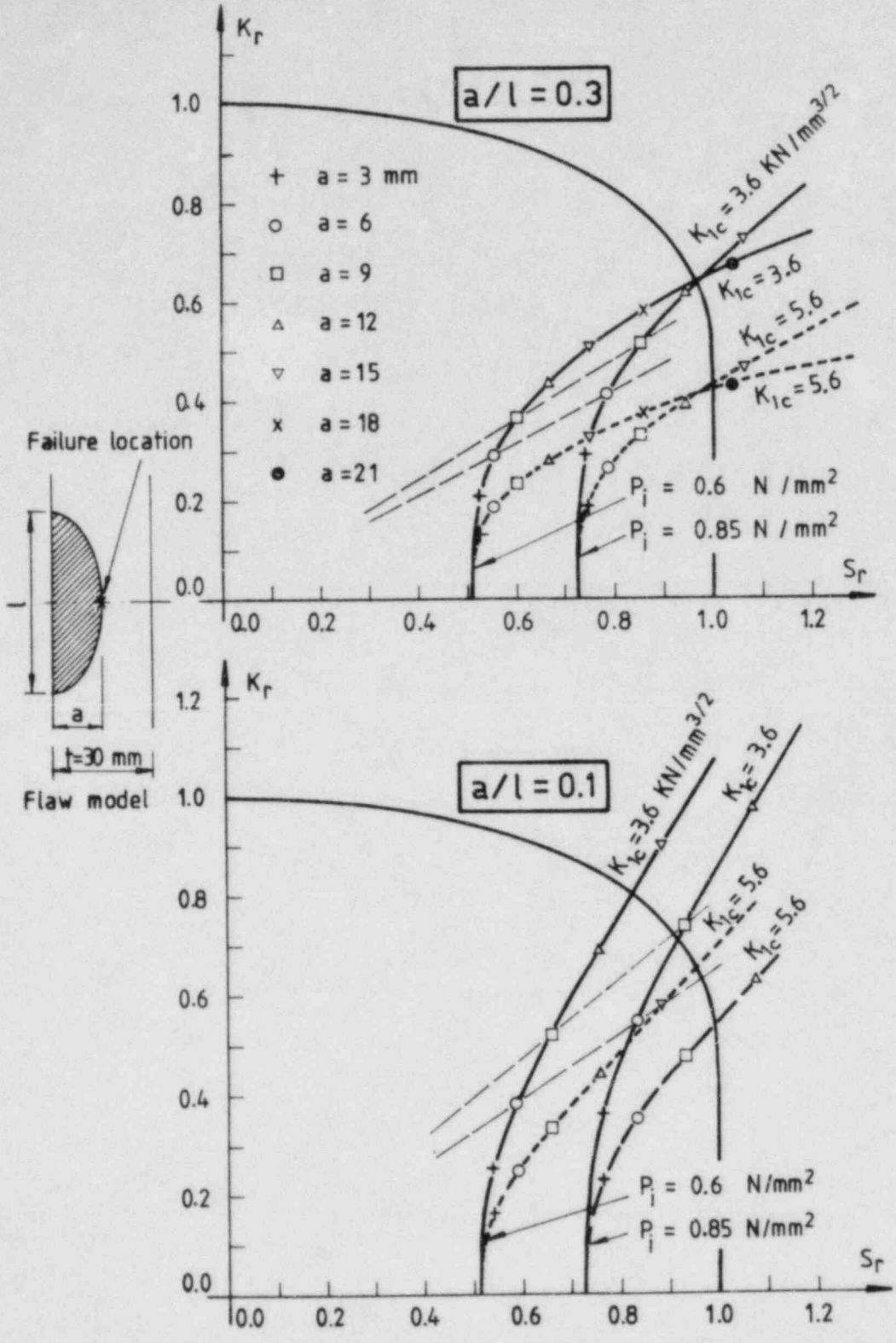

Figure 13. Loci of Assessment Points for Two Idealized Flaw Profiles and Two Different Values of the Internal Pressure, as a Function of the Flaw Depth. The flaw is assumed to be located at the base metal (K_{1c} = 5.6 KN/mm$^{3/2}$) as well as at a weld (K_{1c} = 3.6 KN/mm$^{3/2}$).

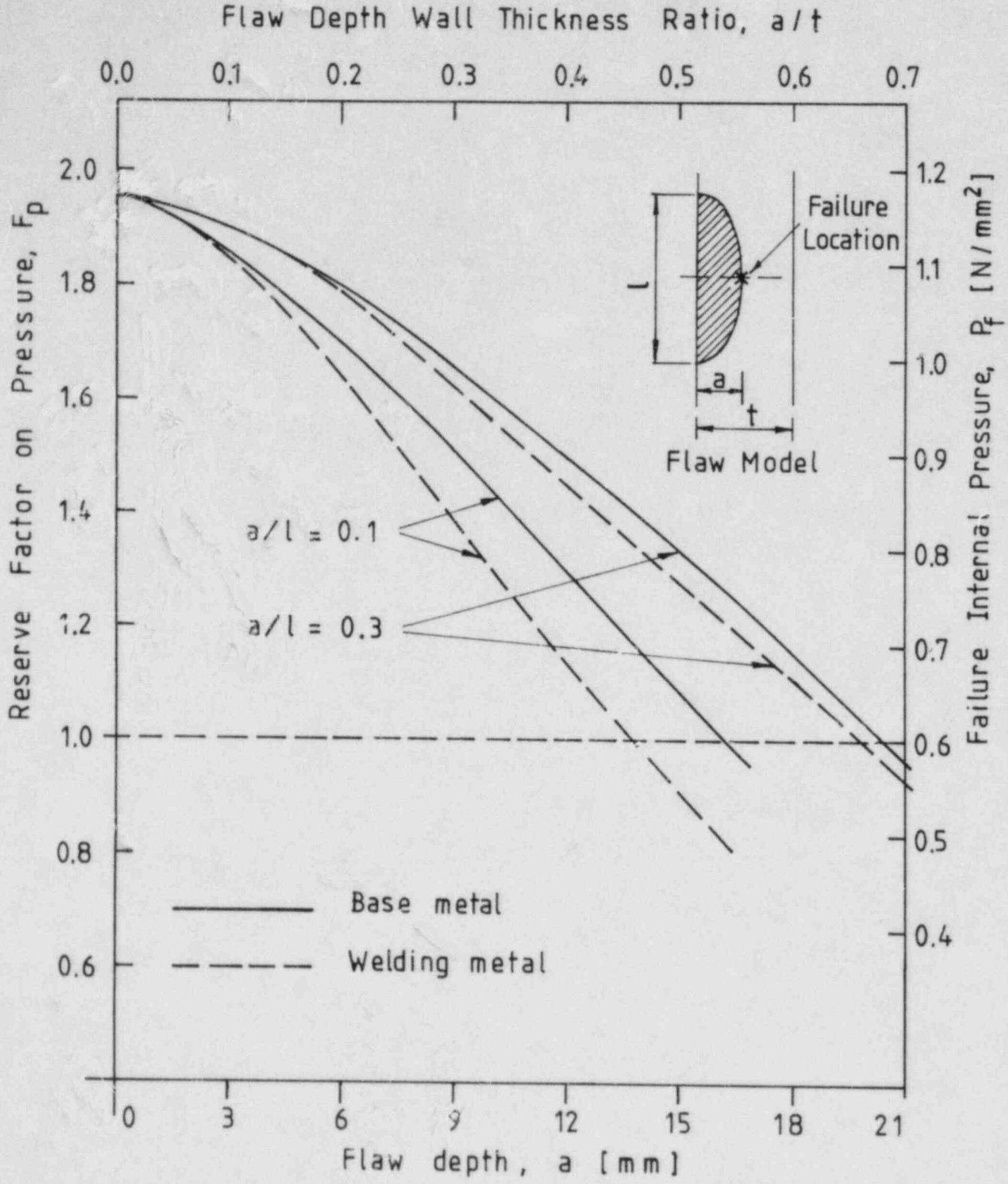

Figure 14. Calculated Reserve Factor and the Failure Internal Pressure as a Function of the Flaw Depth. The flaw is assumed with two idealized profiles and to be located at the base metal as well as at a weld.

EXPERIMENTAL AND ANALYTICAL RESULTS OF STEEL CONTAINMENT TESTS*

Daniel S. Horschel
Sandia National Laboratories
Albuquerque, NM 87185

ABSTRACT

The Containment Integrity Division at Sandia National Laboratories is conducting tests on models of nuclear containment buildings. The tests currently being conducted are on steel containment vessels subjected to quasi-static internal overpressurization. Four 1/32 scale models have been tested by incrementally pressurizing the model until failure or leakage occurs.[2] The testing of the containment models provides both insight and data on the response of containment vessels to overpressurization. The data are used to answer important technical questions that have arisen and to assess the adequacy of analytical methods in predicting containment behavior to accidents more severe than design basis accidents. Some of the details about the tests and the results of the experiments as well as the results of the finite element analyses are presented in this paper. Options selected for the analyses of the containment models accounted for finite strain, elastic-plastic and nonlinear geometric behavior of the containment models. The data obtained during the testing of the models are compared to the analytical results for selected areas.

INTRODUCTION

As part of the Containment Integrity Program [1] various types nuclear containment models are being tested by subjecting the containment models to different loadings. The current phase of the program is concerned with the response of steel containments subjected to internal overpressurization. Future plans and other interrelated NRC sponsored programs are discussed in Reference [1]. The models are tested to gather fundamental insight and a data base on the response of the models to internal pressurization. The data are used to assess and qualify different analytical predictive methods. Several organizations, as well as Sandia, are analyzing the containment models. When the organizations send the results of their analyses to Sandia a draft data report is supplied to them allowing them to assess their predictive analytical capabilities.

*This work is supported by the U.S. Nuclear Regulatory Commission and performed at Sandia National Laboratories which is operated for the U.S. Department of Energy under contract number DE-AC04-76DP00789.

Four 1/32 scale steel models of three configurations were built and tested at Sandia National Laboratories. The first configuration, of which there were two models, was termed a clean shell. Geometrically the clean shell is a right circular cylinder with one end welded to a hemispherical steel dome and the opposite end is welded to a thick base ring which in turn is bolted to a rigid testing fixture. The diameter of the cylinder is about 43 inches (1.1 meters) and has a height of 65 inches (1.65 meters) including the dome. The thickness of the cylinder and dome material is about 0.045 inch (1.15 mm). A basemat was not modeled. The second configuration is termed a ring-stiffened containment which used the clean shell geometry with the addition of ten stiffening rings brazed to the cylinder wall. The third configuration is a penetration model which is also based on the clean shell geometry. Three penetrations are included in the penetration model, which represent two personnel locks and an equipment hatch.

Data Acquisition

The containment models were pressurized incrementally with nitrogen gas. Strain and displacement data were recorded at each pressure increment. Due to the inherent dangers of pneumatic pressurization, testing was performed remotely in an isolated area on Kirtland Air Force Base, Albuquerque, New Mexico. The steel containment models were instrumented with high elongation strain gages [2,3], several displacement gages, pressure transducers and thermocouples to acquire data during the testing of the models. A coordinate determination system, which uses theodolites and the principle of triangulation, was also used to measure large displacements.

Analytical Technique

MARC [4], a general purpose finite element program, was chosen to analyze the containment models. Since the containment models were expected to strain and deform significantly before the model failed, an option which accounts for plastic finite strain and large deformations; i.e., updated Lagrangian formulation, was invoked. The von Mises yield criterion and a full Newton-Raphson iteration technique were used in the analyses of the containment models.

A maximum equivalent plastic strain criterion was used to determine the maximum pressure carrying capability of the models. During an analysis, failure of the model was assumed to occur if the equivalent plastic strain anywhere in the finite element model exceeded the maximum uniaxial strain of the material.

The materials used to fabricate the 1/32 scale steel models are not prototypical of materials used in actual containment construction. The material used is more typical in a draw forming or stamping industry, characterized by its low yield point and carbon content, high ductility and mild strain hardening rate.

CLEAN SHELL EXPERIMENT

Two clean shell models were tested. The first test was used to assess the testing procedures and to provide a check of the entire testing system; i.e., personnel, hardware, and software and the interfacing of these areas. This model was only sparsely instrumented. Problems arose during this test, which did not allow the data taken during the test to be properly saved or accessed.

The first clean shell model at a pressure of 130 psig (896 kPa) is shown in Figure 1. The entire model was painted white prior to testing. As soon as the cylinder began to yield the paint began to peel off the cylindrical portion of the model. As can be seen in Figure 1 nearly the entire cylindrical portion of the model is void of paint and there is significant bulging of the cylinder wall. It is estimated that the strain in the circumferential direction is about 20%. This model failed shortly after the pressure was increased to 135 psig (930 kPa).

The second clean shell model was fully instrumented. Significant yielding of the cylinder was observed when the pressure in the model was increased from 80 to 90 psig (550 to 620 kPa). This model was pressurized incrementally until a small meridional tear at the mid-height of the cylinder occurred at a pressure of 110 psig (760 kPa). Details of the test are reported in Ref. [5]. The maximum residual strain in the model after depressurization was about 6%. The maximum residual radial displacement was about 1.3 inch (33 mm). The second clean shell model was not repaired or tested again.

CLEAN SHELL ANALYSIS

Fifty-nine cubic displacement axisymmetric shell elements were used to model the majority of the cylinder and the hemispherical dome. A group of 16 axisymmetric continuum elements were used to model the cylinder at the attachment of the cylinder to the base ring. The use of continuum elements was necessary due to high shear strains in this area. This axisymmetric finite element model had 336 degrees of freedom. Only the geometry of the second clean shell model was specifically used in the analysis, although the differences between the two clean shell models were slight.

The majority of the cylinder wall was predicted to yield at 95 psig (655 kPa). Failure of the clean shell model was predicted to occur at 132 psig (910 kPa) due to the mid-height portion of the cylinder wall exceeding its strain capabilities.

CLEAN SHELL COMPARISON

Displacements and strains obtained during the experiment as a function of pressure were compared, at several locations on the second clean shell model, to the analytical results. A typical plot is shown in Figure 2. The markers on the plot represent the strain gage data for gages that were located circumferentially

around the cylinder mid-height of the model. The solid line represents the analytical results. The experimental strain data were converted to true (log) strain before plotting to allow a direct comparison with the analytically predicted strain. Although the yield pressure predicted is higher than the pressure that the model actually began to yield, the analytical results are quite similar in overall response to the actual behavior of the model. Figure 3 is the predicted deformed shape of the clean shell model at 130 psig (896 kPa) superimposed over the original shape. The dome apex was both observed and predicted to displace downward. In comparing the predicted shape and actual shape (Figure 1) the correlation is judged to be quite good.

RING STIFFENED MODEL EXPERIMENT

The ring stiffened model was tested to determine the effect that the stiffening rings had on the containment response. The cylinder and stiffening rings began to yield as the internal pressure was increased from 106 to 109 psig (730 to 750 kPa). There was no noticeable difference between the pressure at which the rings and the cylinder wall began to yield. The pressure was incrementally increased to 120 psig (830 kPa), when a small leak was detected. By attempting to apply a slightly higher pressure, the model was able to structurally stabilize at 120 psig (830 kPa). A picture of the model at 120 psig is shown in Figure 4. Upon depressurization and inspection, two very small tears were found in the cylinder material adjacent to the dome near a weld repair in an area that had been thinned when a defective weld was ground away. These areas were repaired in situ along with some other areas that appeared to have been thinned or inadequately welded.

With the model repaired the model was again pressurized. The elapsed time between pressurization was nearly three weeks. The pressure of the model was increased incrementally past 120 psig (830 kPa) with no signs of re-yielding of the model. When the final pressure step, from 135 to 140 psig (930 to 965 kPa), was applied the model began to expand unstably until failure occurred. Before the last pressure increment the model appeared to be responding linearly to the pressure increase; no plastic straining was observed. This was thought to be due to strain aging of the cylinder material.

The material used to fabricate the cylinder was tested for the possibility and extent of the material to strain age. The material was strained past the Lüder's band region (the approximate amount of strain that was achieved in the cylinder wall) of the stress-strain curve and allowed to age at 212° Fahrenheit (100° C) for one hour. The temperature and time were selected to accelerate the strain aging process, and still approximate the ambient conditions and time that the containment was subjected to. Upon reloading the test specimens, the yield stress increased by more than 10% and was within 5% of the ultimate tensile strength of the material. Hall [6] suggests that

it is possible for the yield strength to exceed the ultimate tensile strength of the material due to strain aging.

ANALYSIS OF THE RING STIFFENED MODEL

The ring-stiffened model was analyzed using 89 cubic displacement axisymmetric shell elements to model the dome, stiffening rings and the majority of the cylinder. The remaining portion of the cylinder, which was attached to the base ring, was modeled with 16 axisymmetric continuum elements. The braze material used to join the rings to the cylinder wall was not included in the finite element model. The resulting model had 490 degrees of freedom.

The analysis predicted that ooth the rings and the cylinder would yield at about the same pressure. Although there were some meridional bending strains in the cylinder wall, the bending strains did not increase significantly after the cylinder wall yielded. General yielding of the cylinder was predicted to occur at 110 psig (760 kPa). The analysis was continued until the maximum equivalent strain in the stiffening rings was reached. Failure of the model was predicted to occur at 138 psig (950 kPa) initiated by the failure of the stiffening rings.

RING STIFFENED COMPARISON

A comparison of analytical results to some strain data gathered during the test of the model are shown in Figure 5. The strains gathered during testing of the model were converted to true (log) strain. The solid line represents the analytical results while the markers represent several gages located circumferentially around the mid-height of the cylinder. The gages are located both (meridionally) in between stiffeners and radially behind the stiffeners. The differences between the strains/displacements measured at a pressure level either between or adjacent to stiffeners is indistinguishable in the experimental scatter. Although there was almost a three week break in the test and welding was performed on the model the test was treated as a single test; i.e., the instrumentation was not re-zeroed when the second pressurization of the model began. Note that one gage showed quite a bit of change from the end of the first test to the start of the second test. The predicted deformed shape of the ring stiffened model at 120 psig (827 kPa) plotted with the original shape is shown in Figure 6. The analysis very closely depicted the deformations of the ring stiffened model at this pressure level.

During the second loading of the model there was no plastic flow observed until just prior to failure; therefore, the strains predicted analytically for pressures beyond 120 psig (827 kPa) are more than what was observed due to unanticipated strain aging of the cylinder wall material.

PENETRATION-MODEL EXPERIMENT

The penetration model was tested to determine the effect that simplified major penetrations can have on containment capability. The penetration model had three penetrations that intersected the cylinder wall. Due to the small scale, there were no gaskets or seals of any type; all of the penetrations were of welded construction. The shell wall was not thickened due to the presence of the penetration as is dictated by the ASME area replacement rule. Two penetrations were simple personnel locks. Each personnel lock consisted of a cylindrical sleeve that passed through and was welded to the cylinder wall. The diameter of this sleeve is about 3.1 inches (80 mm) with a height (sleeve length) of 1.1 inches (28 mm). The personnel lock doors were represented by a flat circular plate welded to each end of the cylindrical sleeve.

The third penetration was a model of an equipment hatch. The equipment hatch sleeve was about 7.5 inches (190 mm) in diameter with a height of 1.3 inches (33 mm). The sleeve passed through and was welded to the cylinder wall. The equipment hatch door was a spherical cap with a radius of 7.5 inches (190 mm). The door was fitted into the sleeve and welded in place concave inward.

A snap through buckle of the equipment hatch door was anticipated early during the pressurization of the model. Within seconds after the pressure in the model was increased from 40 to 50 psig (275 to 345 kPa) the equipment hatch door buckled; however, the model did not leak. The majority of the model was determined to be responding linear-elastically.

It was decided to depressurize the model, push the equipment hatch door back to its original position, drill a small hole through the door, and weld a flat circular plate to the equipment hatch sleeve to allow further testing of the other penetrations, the modified equipment hatch and the containment shell. With this accomplished the model was again pressurized. Noticeable plastic straining began to occur at a pressure increase from 80 to 85 psig (550 to 586 kPa). While waiting for the model to stabilize at 120 psig (830 kPa), the model failed suddenly. A picture of the model at 120 psig (830 kPa) is shown in Figure 7. The large circular unpainted area is the metal plate welded to the equipment hatch sleeve. To the right of the equipment hatch the personnel lock can be seen. The maximum strain in the model at this pressure level is over 14.5%. Shortly after this picture was taken the model failed suddenly.

PENETRATION MODEL ANALYSIS

Three-dimensional analyses, using the MARC [4] code were used to analyze the penetration model. A series of analyses were performed to analyze the personnel lock [7]. It was concluded from the analyses, that the personnel lock did not decrease the capacity of the containment. The equipment hatch was modeled in two separate analyses, one to determine the buckling of the equipment hatch, the second to analyze the model with the addition

of the flat circular plate welded to the equipment hatch sleeve. Both of these analyses were performed prior to the containment models being tested.

The finite element model used to determine the buckling pressure of the equipment hatch door included a thirty degree segment of the model. The segment included the entire cylinder height and the dome (Figure 8), with symmetry boundary conditions imposed on the meridional boundaries. The sleeve around the equipment hatch begins to yield at a pressure of 26 psig (180 kPa) due to the high bending strains in the sleeve and the sleeve material's lower yield strength. The analysis was continued to 75 psig (517 kPa) where a buckling calculation was performed. A buckling pressure of 76 psig (524 kPa), using the updated elastic-plastic stiffness matrix, was predicted.

A new finite element mesh was created to reflect the addition of the flat circular plate welded to the equipment hatch sleeve. For this analysis a larger 45 degree segment of the model was used. The mesh used is shown in Figure 9. The sleeve again began to strain plastically very early on in the analysis (22 psig; 152 kPa). Some yielding of the cylinder wall occurred as the pressure was increased from 80 to 85 psig (550 to 590 kPa), while most of the cylinder accumulated some plastic strain at 95 psig (655 kPa). Failure of the model was predicted to occur at 122 psig (840 kPa) due to a small area on the sleeve reaching its maximum plastic strain in the outer fibers caused by high bending strains.

PENETRATION MODEL COMPARISON

The results of the analysis are compared to the results of the experiment in Figure 10. The strain gage data were again converted to true (log) strain. The lines on the graph indicate the major and minor strain at two points in the model. Note that there are four lines representing the minor strains (two experimental and two analytical) and there are four lines representing the major strains (the two analytical curves overlay one another). The strains produced by the finite element analysis were converted to their principal components in the plane of the shell surface. The point chosen for comparison in Figure 10 is about three inches from the three o'clock position of the equipment hatch sleeve in the shell wall. A similar plot, Figure 11, is also shown for an area in the shell wall just below (6 o'clock) the equipment hatch sleeve. There are two lines representing experimental results, one major and one minor strain, and four lines representing analytical results, two major and two minor (which overlay one another). A displaced shape of the model at 120 psig is shown in Figure 12.

CONCLUSIONS

For the geometries investigated, stiffening rings attached to the containment wall increase the pressure at which the majority of the wall yields and the ultimate strength of the vessel. Treating the stiffening rings implicitly, by increasing

the thickness of the cylinder wall by a volume equal to the increase in volume represented by the stiffening rings; i.e., smearing of the rings is a reasonable analytical procedure.

The penetrations in the penetration model did not have a thickened shell area around the penetration sleeves and no gaskets or seals were included in the penetrations. For these simplistic penetration geometries, the penetrations do not significantly decrease the capability of the containment. The tendency of ductile steels to flow plastically mitigates the effect of discontinuities such as penetrations.

In the absence of severe flaws, estimating failure pressure using an equivalent plastic strain criterion does an adequate job for the simple geometries investigated with these analyses.

REFERENCES:

[1] Blejwas, T. E., von Riesemann, W. A. and Costello, J. F. "The NRC Containment Integrity Program ", Transactions of the 7th International Conference on Structural Mechanics in Reactor Technology, Vol. J1/1, August 1983.

[2] Toth, R. P., "In Search of a High Elongation Strain Gage System", NUREG/CR-3222, SAND83-0549, September 1983.

[3] Woodfin, R. L. and Dennis, A. W. "Techniques Used in Static Pneumatic Pressure Experiments on Models of a Generic Steel Containment Building" , Transactions of the 7th International Conference on Structural Mechanics in Reactor Technology, Vol. J6/2, August 1983.

[4] "MARC General Purpose Finite Element Program", Revision J.2, MARC Analysis Research Corporation, Palo Alto, CA, 1981.

[5] Blejwas, T. E. and von Riesemann, W. A. "Pneumatic Pressure Tests of Steel Containment Models-Recent Developments", Nuclear Engineering and Design, accepted for publication.

[6] Hall, E. O., "Yield Point Phenomenon in Metals and Alloys", Plenum Press, New York, 1970.

[7] Derbalian, G., Fowler, G. and Thomas, J., "Three-Dimensional Finite Element Analysis of a Scale Model Nuclear Containment Vessel". FaAA-83-4-5, Failure Analysis Associates, Palo Alto, CA, May 1983.

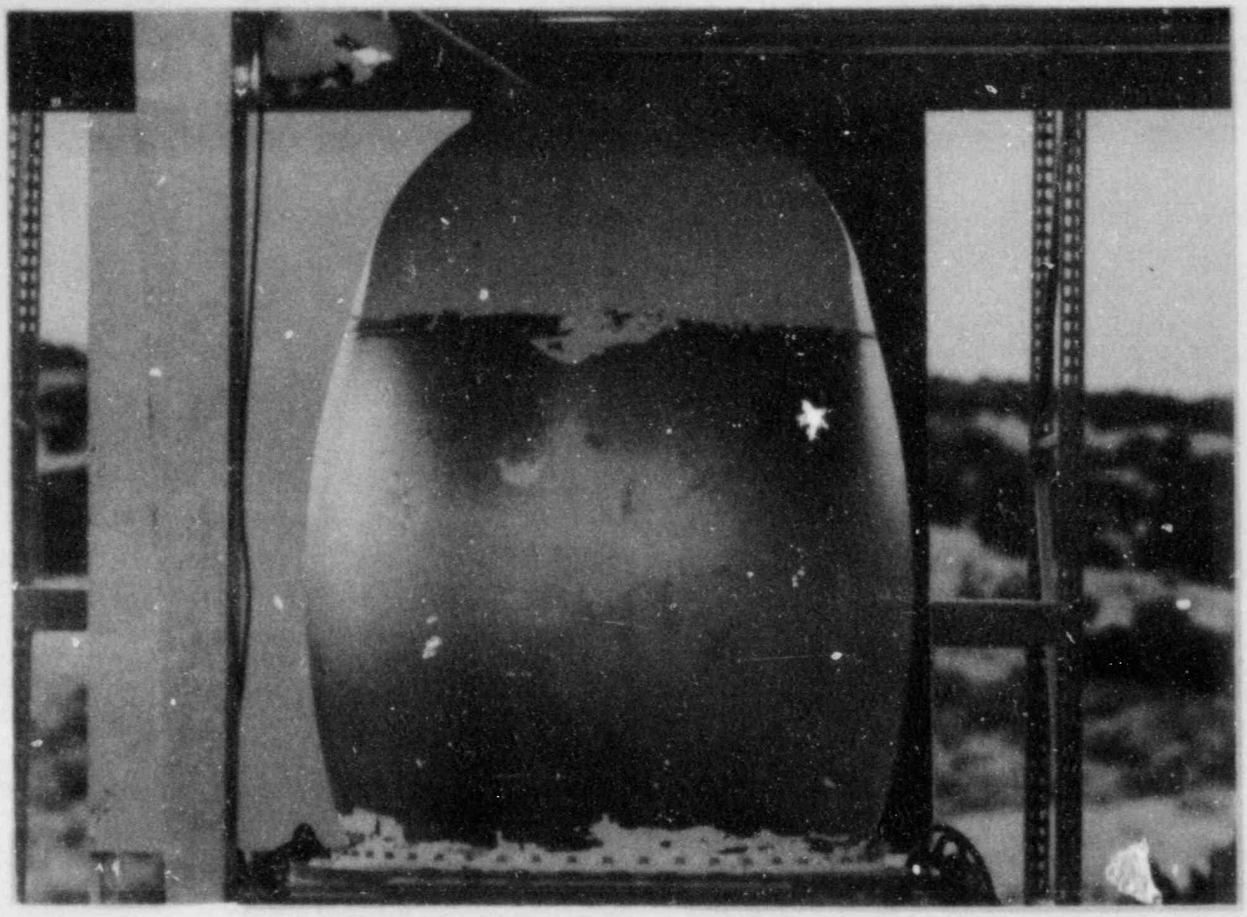

Figure 1
First Clean Shell Model at 130 psig.

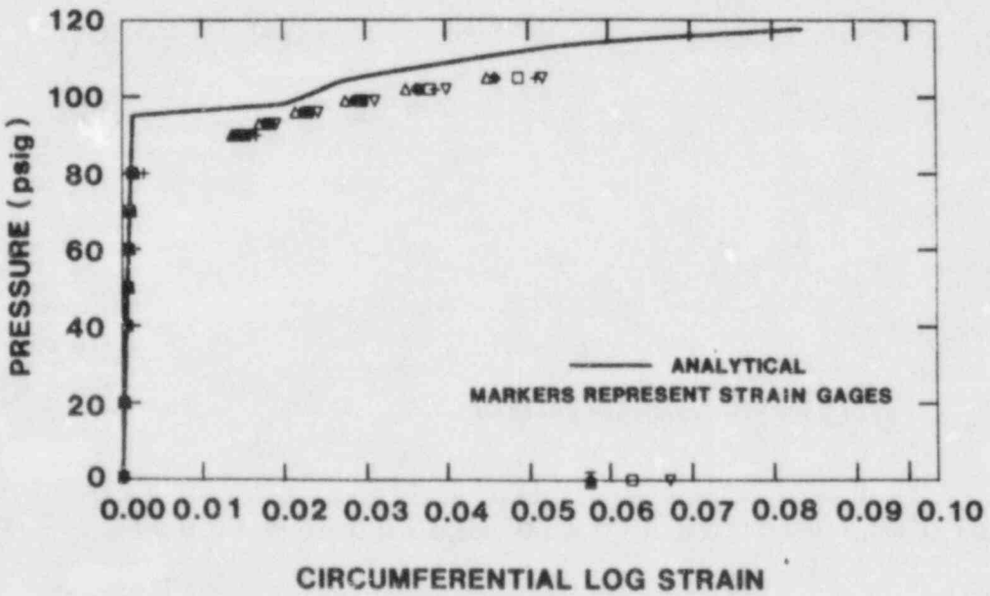

Figure 2
Second Clean Shell Model
Analytical and Experimental Comparison at Cylinder Mid-Height.

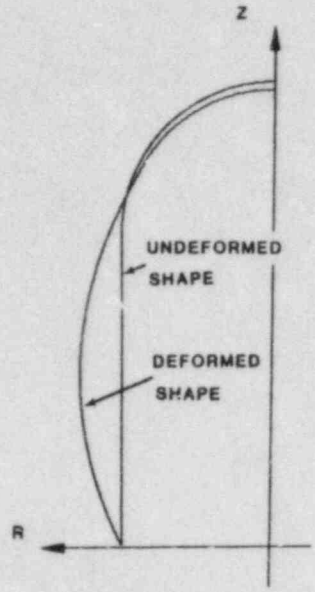

Figure 3
Clean Shell Model
Original and Predicted Deformed Shape, 130 psig.

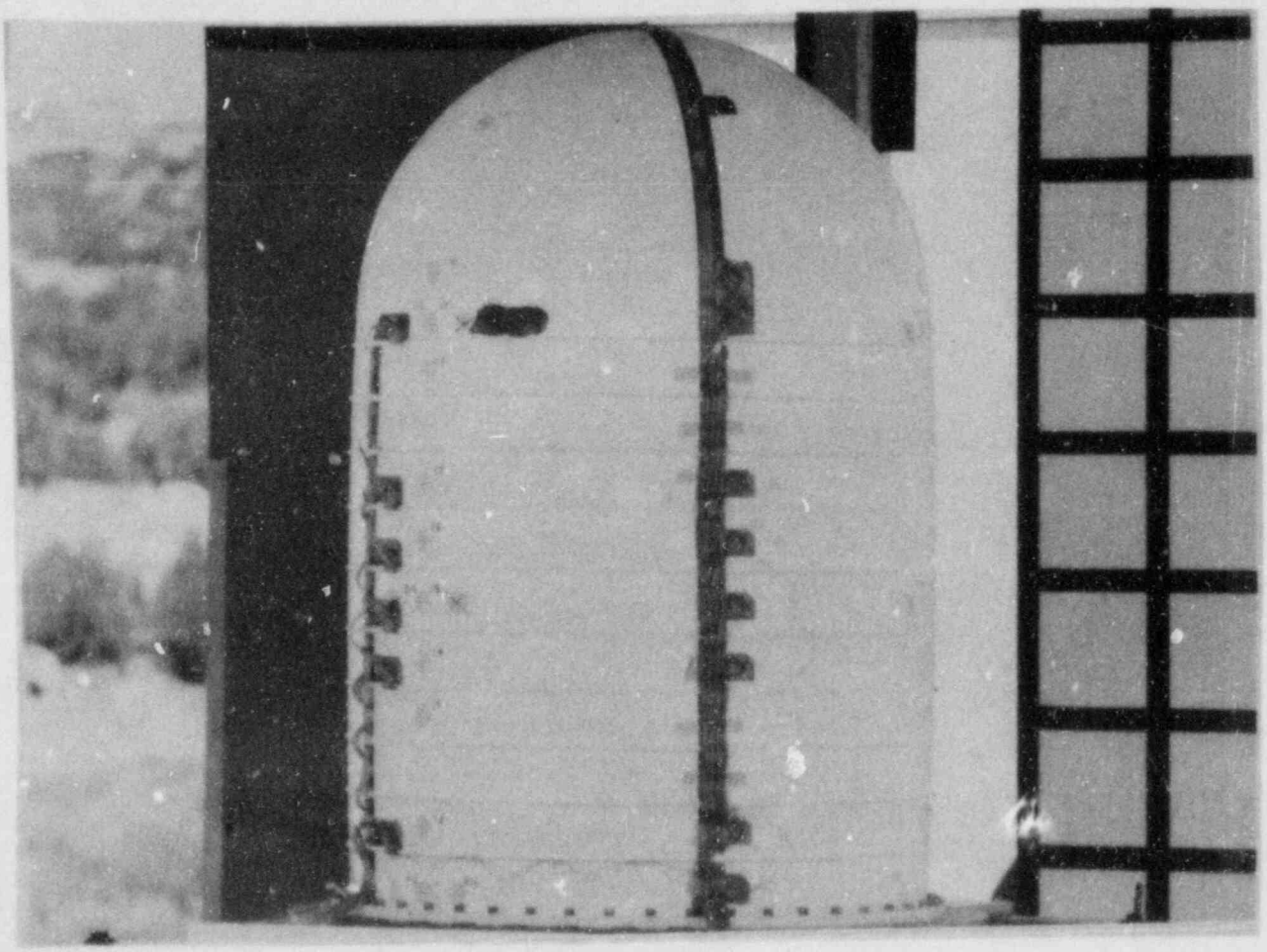

Figure 4
Ring Stiffened Model at 120 psig.

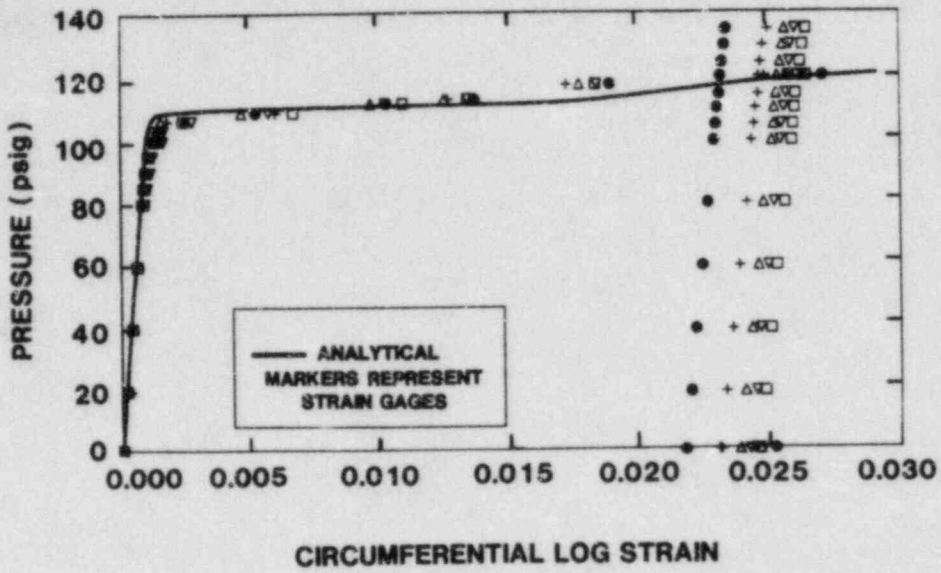

Figure 5
Ring Stiffened Model
Analytical and Experimental Comparison at Cylinder Mid-Height.

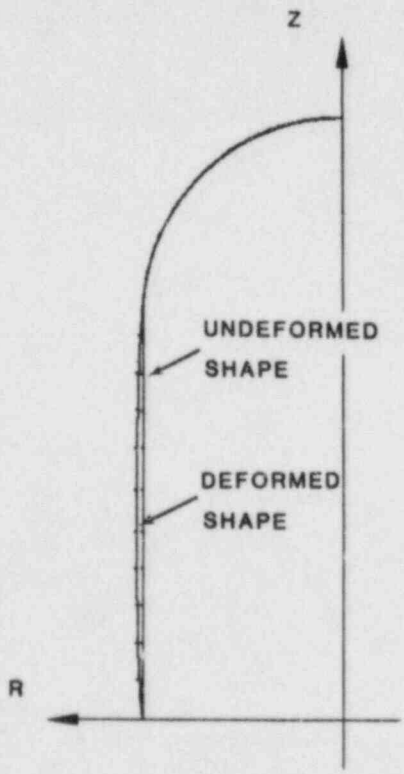

Figure 6
Ring Stiffened Model
Original and Predicted Deformed Shape, 120 psig.

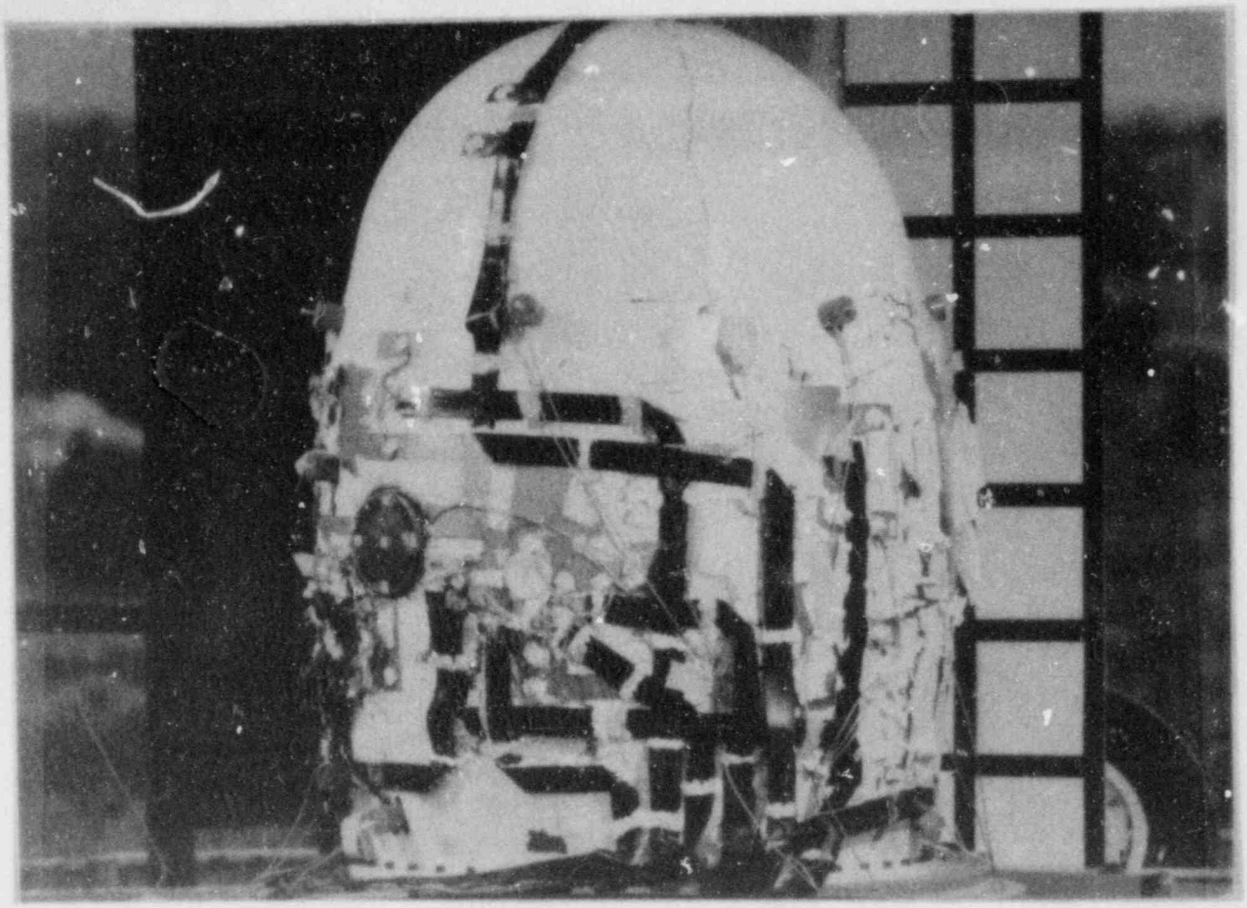

Figure 7
Penetration Model at 120 psig.

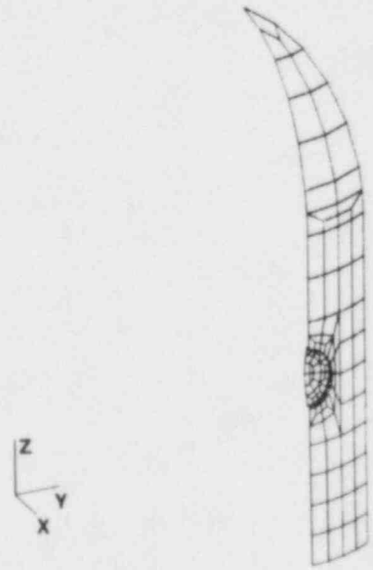

Figure 8
Finite Element Mesh of Equipment Hatch.

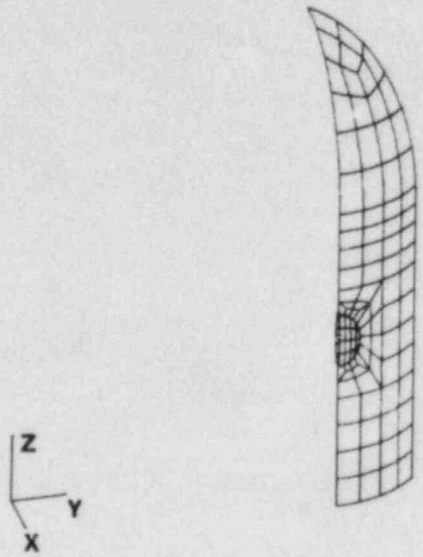

Figure 9
Finite Element Mesh of Reconfigured Penetration Model.

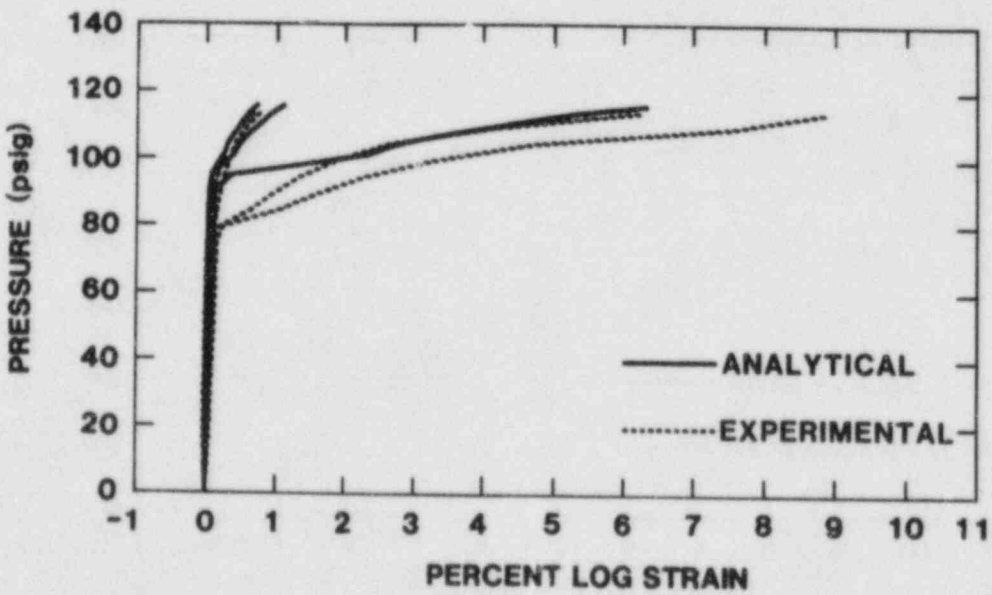

Figure 10
Comparison of Strains Near the Equipment Hatch.

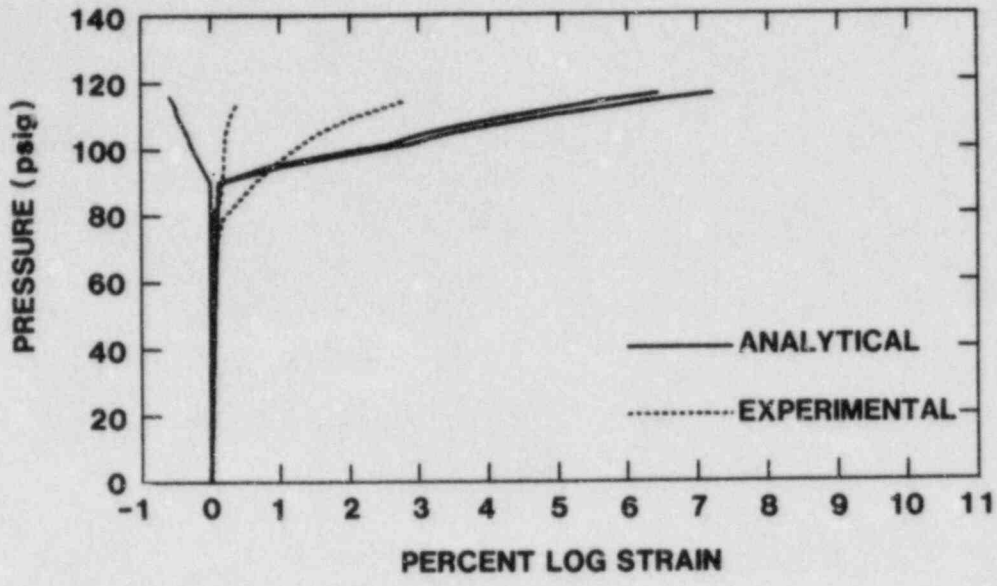

Figure 11
Comparison of Strains Near the Equipment Hatch.

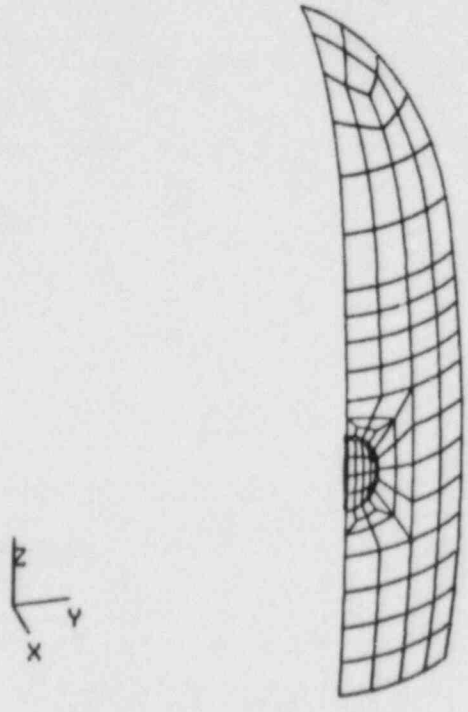

Figure 12
Predicted Deformed Shape at 120 psig.

ANALYSIS OF A 1:8 SCALE STEEL CONTAINMENT MODEL SUBJECT TO INTERNAL STATIC PRESSURIZATION*

David B. Clauss
Sandia National Laboratories
Albuquerque, NM 87185

ABSTRACT

The Containment Integrity Division at Sandia National Laboratories is investigating the response of nuclear containments subjected to loads that could arise during severe accidents. As part of this program, a 1:8 scale steel containment model has been built and will be tested to determine the response due to overpressurization. This experimental model contains several prototypical penetrations including personnel lock representations, operable equipment hatches, a constrained pipe penetration, and other pipe penetrations. Pretest predictions of the response of the experimental model to static overpressurization have been obtained using finite element methods. Analyses of a ring stiffened shell with (1) no penetrations, (2) a personnel lock, (3) an equipment hatch, and (4) a constrained pipe penetration are discussed. Each of the models represents a different circumferential segment of the experimental model. The response of the ring stiffened shell with no penetrations is compared to the response of the ring stiffened shell with penetrations, and conclusions are made regarding the effect of penetrations on containment behavior. Leakage around the 'O' ring seal in the equipment hatch assembly is discussed.

INTRODUCTION

The structural response of nuclear containments during postulated severe accidents has an important effect on the risks and consequences associated with these accidents. The Containment Integrity Division at Sandia National Laboratories is conducting a combined experimental and analytical program to determine the structural capability of LWR containments. As part of this program, a static pressurization test of a 1:8 scale steel containment model will be conducted in the near future.

The response of the model to internal pressurization beyond the design basis has been predicted using finite element methods. Data from the test will be compared to the pretest predictions in order to assess the adequacy of the analytical method. The analytical effort will provide a basis for predicting containment failure (excessive leakage) due to static overpressurization in

* This work is supported by the U.S. Nuclear Regulatory Commission and performed at Sandia National Laboratories which is operated for the U.S. Department of Energy under contract number DE-AC04-76DP00789.

conjunction with the experimental effort. Containment failure is associated either with a gross structural failure, which would result in a sudden venting of the containment, or with large deformations near seals and gaskets, which would result in relatively slow leakage.

The model was designed and constructed by Chicago Bridge and Iron. The design pressure is 40 psig (276 kPa). The model consists of a right circular cylinder which is welded to a hemispherical dome along its top edge and an ellipsoidal base along its bottom edge, as shown in Fig. 1. Twelve stiffening rings are welded to the cylinder wall at equal intervals along the meridian. The ellipsoidal base is much thicker than the cylinder and dome since it is used for fixturing. The model includes operable equipment hatches, personnel lock representations, a constrained pipe penetration, and other pipe penetrations. In general, the penetrations are comprised of cylindrical sleeves that pass through the cylinder and are closed by flat circular plates. The spherical equipment hatch covers are the lone exceptions. The containment wall is reinforced at all intersections with penetration sleeves by plates that are twice the nominal thickness of the cylinder.

The experimental model will be pressurized incrementally with nitrogen gas. High elongation strain gages, displacement gages, pressure transducers and thermocouples will be used to acquire data at each pressure increment. A coordinate determination system which uses theodolites and the principles of triangulation will also be used to determine displacements. In addition, an acoustic emission system and flow meter will be installed to aid in leak detection. The model and test plan are described in detail in [1].

ANALYTICAL METHOD

The J2 version of the MARC finite element code, [4], was used as the primary analysis tool. Finite strain, large displacement, follower force, and nonlinear material behavior capabilities in MARC were invoked. MARC element 72, which is a bilinear, thin shell element, was used almost exclusively. Preliminary stress-strain curves for the cylinder and dome materials are simple bilinear approximations based on the yield and ultimate properties (A516 steel) given in Table 1. The models

Material (True Stress-True Strain)	Yield Stress ksi (MPa)	Ultimate Strain	Ultimate Stress ksi (MPa)
Hemispherical Dome	57.5 (396)	0.212	96.4 (664)
Cylinder and Penetrations	59.1 (407)	0.205	98.2 (677)
Ellipsoidal Base	46.1 (320)	0.243	98.3 (677)

Table 1 Preliminary Material Properties

will be updated as the measured material properties become available.

Structural failure was assumed to occur when the maximum predicted effective strain at a point in the model exceeded the ultimate strain obtained from uniaxial tensile tests. No distinction was made between membrane and bending strains with regard to the application of this failure criterion. Containment failure due to leakage was more difficult to infer from the analysis, since presently no general methodology relating deformations of seals and gaskets to leakage rates is available. However, when the calculated deformations became sufficiently large, leakage was anticipated.

Much of the analysis effort was directed towards predicting the response of and around penetrations. It was assumed that the penetrations could be analyzed individually with little loss of accuracy due to structural interactions. Four three-dimensional finite element analyses of the containment were conducted: one without penetrations, one with a personnel lock, one with an equipment hatch, and one with the constrained pipe penetration. The response of the containment with no penetrations served as a useful reference in evaluating the effect of penetrations.

The ring stiffeners were modeled explicitly only for the analysis of the containment shell without penetrations. Blejwas and Horschel showed that the effect of the ring stiffeners is similar to that of increasing the thickness of the cylinder wall by an amount which accounted for the material volume of the rings in [2]. The ring stiffeners were modeled implicitly for all the analyses involving penetrations using this approach. This involved increasing the cylinder wall thickness from its true value of 0.197" (5.0 mm) to 0.229" (5.8 mm).

ANALYSIS OF THE CONTAINMENT SHELL WITHOUT PENETRATIONS

The response predicted for the containment without penetrations was qualitatively similar to that for the small steel model reported by Horschel and Blejwas in [3]. First yield occurred at the intersection of the cylinder and the ellipsoidal base at 123 psig (847 kPa). General membrane yielding of the cylinder occurred near 185 psig (1275 kPa) at which point the characteristic bulging of the cylinder began to be noticeable. Ultimate strain was exceeded at 255 psig (1756 kPa) near the midheight of the cylinder, and is associated primarily with circumferential membrane stretching.

ANALYSIS OF A PERSONNEL LOCK REPRESENTATION

Personnel lock representations intersect the cylindrical containment wall at two locations: one personnel lock is about two and one-half feet above the intersection of the cylinder with the ellipsoidal base, and the other is near midheight of the

cylinder. Each personnel lock consists of a cylindrical sleeve that is capped by flat, circular plates as shown in Fig. 2. The containment wall is stiffened by a reinforcing plate around the penetration. The construction is all welded, so there are no potential leakage paths associated with these penetrations.

The personnel lock representation near midheight of the cylinder was modeled because the displacement and strain of the containment wall is greatest at this point. A thirty six degree circumferential segment of the containment was included in the finite element model, with one boundary cutting through the center of the penetration. Symmetry conditions (no tangential displacement) were imposed on the edges. Enforcing symmetry on the edge coinciding with the centerline of the penetration is justified solely on geometrical arguments. The perturbation in the axisymmetric state of stress for the containment shell caused by the personnel lock representations is localized. No significant tangential displacement arises at the other edge because it is far enough away so as not to be affected by the penetration.

First yield occurred at 106 psig (730 kPa) in the personnel lock sleeve near its intersection with the reinforcing plate, and was associated primarily with the bending response due to the geometric discontinuity at this point. The maximum effective plastic strain in the model was negligible (less than 0.2%) until the onset of general membrane yielding in the containment cylinder wall, which occurred between 180 and 185 psig (1240 to 1275 kPa). Above 185 psig (1275 kPa), the radial displacement and the midsurface effective plastic strain of the cylinder wall increased rapidly with increasing pressure. The deformation of the model at 230 psig (1585 kPa) is shown in Fig. 3. At 230 psig (1585 kPa) the characteristic bulging shape of the cylinder can be seen clearly. Because the reinforcing plate is thicker than the cylinder, it did not stretch circumferentially as easily. Tangential displacements arose in the cylinder adjacent to the reinforcing plate to compensate for the absence of significant stretching in the reinforcing plate, which resulted in a strain concentration. The midsurface plastic strain contours for the cylinder, reinforcing plate, and personnel lock sleeve at 230 psig (1585 kPa) plotted in Fig. 4 clearly show the strain concentration in the cylinder adjacent to the reinforcing plate. The midsurface plastic strain in the reinforcing plate and cylinder at the elevation of the axis of the personnel lock is plotted as a function of the circumferential angle for several pressure levels in Fig. 5. The ultimate strain was exceeded in the cylinder adjacent to the reinforcing plate at about 226 psig (1557 kPa). The strain in the cylinder approached a constant value at all pressure levels asymptotically with increasing distance from the personnel lock. At 225 psig (1550 kPa), the maximum strain was about 1.75 times the asymptotic value, which represented the strain for the containment without penetrations.

degree circumferential segment of the containment. Tangential displacements are set to zero along both edges.

First yield occurred in the cylinder at its intersection with the ellipsoidal base at a pressure of 118 psig (813 kPa). The deformed shape at 250 psig (1723 kPa) is shown in Fig. 13. The dashed line represents an undeformed outline of the cylinder. As expected, the containment wall was essentially fixed at its intersection with the thru-pipe. The pipe restricted the bulging of the cylinder even at points well away from the penetration, as can be seen from Fig. 14. A strain concentration arose in the cylinder adjacent to the reinforcing plate similar to that predicted for the personnel lock model, although it was not as severe. Ultimate strain was exceeded at this point at 250 psig (1723 kPa), which is only a slight reduction in the capacity predicted for the containment without penetrations. In fact, the strain and displacement at a given pressure for most points on the containment wall were less for the containment with a constrained penetration than for the containment without penetrations.

It is evident from Fig. 14 that the effect of the thru-pipe penetration was not localized. Therefore, the possibility of interaction between the thru-pipe and other penetrations should be considered. A model including both the constrained pipe penetration and the equipment hatch is planned, since the equipment hatch appears to be the most critical penetration.

CONCLUSIONS

Preliminary analyses of the 1:8 scale steel containment model due to overpressurization have been completed. Based on a maximum strain criterion, the results indicated that major penetrations do reduce the structural capacity of the containment. Reinforcing plates can lead to a strain concentration in the cylinder wall if the penetration sleeve is sufficiently stiff. This was the case for the personnel lock representations in the 1:8 scale model, which resulted in a decrease in the capacity of the containment from 255 psig (1757 kPa) without penetrations to 226 psig (1557 kPa). Bending strains in the penetration sleeves at their intersections with the containment wall depended largely on the radius to thickness ratio of the sleeve. If this ratio was large, relatively high bending strains were predicted in the sleeve. The maximum strain in the 1:8 scale model occurred in the equipment hatch sleeve and was due primarily to bending. The ultimate strain was exceeded at 186 psig (1282 kPa) in the sleeve compared to 255 psig (1757 kPa) for the containment without penetrations.

Leakage near seals and gaskets can also result in a containment failure. In the 1:8 scale model, the only potential leakage path not associated with a structural failure is around the 'O' rings in the equipment hatch assembly. Large deformations of the sealing surface occurred because the seals do not

ANALYSIS OF AN EQUIPMENT HATCH (See Note)

The two equipment hatches in the large steel model are both located near midheight of the cylinder and are approximately 90 degrees apart. A schematic representation of an equipment hatch in the large steel model is shown in Fig. 6. The diameter of the equipment hatch sleeve is nearly 2.5 times that of the personnel lock sleeve, which is the next largest penetration. An 'O' ring is used to provide a seal between the sleeve and the supporting ring. Therefore, the possibility of significant leakage prior to a structural failure must be addressed. The spherical cover and the supporting ring were considered to be structurally uncoupled from the sleeve because it was assumed that the 'O' ring transmits only loads parallel to the sleeve's axis of revolution. Therefore, the response of the spherical cover and the supporting ring, and the response of the sleeve and its interaction with the containment shell were considered in separate analyses.

The cover was modeled as a ring supported, shallow spherical shell subject to external pressure. Assuming that the seal can transmit only normal loads, the ring is free to slide radially and to rotate. The threaded rod used to close the hatch was not modeled. Axisymmetric stress and buckling solutions were carried out with MARC. Linear, elastic behavior of the spherical cover and supporting ring is expected at least up to the pressure predicted to cause containment failure. The radial displacement and rotation of the ring were negligible compared to the deformation of the sleeve. The cover in the large steel model is much thicker than normal practice dictates because of the method of attachment. Consequently, the response is probably not representative of that for equipment hatch covers in real containments.

The finite element model used to analyze the interaction of the equipment hatch sleeve and the containment shell included a forty eight degree circumferential segment of the containment. Symmetry boundary conditions were imposed on each edge for reasons similar to those described for the model with the personnel lock representation. The inside edge of the sleeve, where the 'O' ring is found, was not constrained. A uniform line load having a net force equal to that transmitted by the equipment hatch cover due to pressurization was applied to this edge.

First yield occurred in the sleeve near its intersection with the reinforcing plate at a pressure of 41.2 psig (284 kPa). Deformation of the model is shown at 185 psig (1275 kPa) in Fig. 7. The sleeve ovalized in a manner suggestive of an inextensional deformation. Inextensional behavior can be expected to occur when an unrestrained shell is loaded in a non-uniform manner. The classic example is that of an unrestrained cylinder to pinch loads. The equipment hatch sleeve is unrestrained at its ends, and is subject to a non-uniform line load due to its interaction with the containment wall. Large deformations and low strain energies are associated with

inextensional behavior. The change in the sleeve diameter at the sealing surface from 12 to 6 o'clock, and from 3 to 9 o'clock is plotted against pressure in Fig. 8. At approximately 185 psig (1275 kPa), the change in the diameter of the sleeve was twice the thickness of the sleeve at the sealing surface. This would certainly result in excessive leakage, since the displacement of the supporting ring was negligible. In a real containment the cover assembly may be more flexible, and the displacement of the supporting ring could more closely match that of the sleeve. However, the supporting ring displacements were axisymmetric and the sleeve ovalized, which precludes any close matching of the two.

Localized bending deformations arose in the sleeve at its intersection with the reinforcing plate and are naturally associated with large bending strains. Strain contours on the midsurface and for an outer fiber are plotted at 192.5 psig (1326 kPa) in Figs. 9 and 10, respectively. The maximum plastic strain was due to bending in the sleeve at 12 and 6 o'clock near its intersection with the reinforcing plate. Large bending strains were also observed in the personnel lock sleeve, but at considerably higher pressures. The plastic strain vs. pressure curve predicted for a point on the equipment hatch sleeve is compared in Fig 11. to that predicted for a similar location on two other penetrations that have different sleeve radius to thickness (r/t) ratios. A sleeve penetration with $r/t \approx 95$ was analyzed although it is not physically present in the 1:8 scale containment model. The ultimate strain was exceeded at 186 psig (1282 kPa) in the equipment hatch sleeve. The different penetration sleeves exhibited qualitatively similar response. The radius to thickness ratio of the sleeve affected the pressure at which the deformation and strain in the sleeve began to increase rapidly. A high ratio resulted in a low pressure at this point. Decreasing the radius to thickness ratio of a penetration sleeve required a proportional increase in the pressure required to produce a given amount of strain.

As can be seen from Fig. 9, there were strain concentrations in the containment wall immediately above and below the equipment hatch. This behavior is analagous to the elastic stress concentration that arises in a flat plate with a hole for a similar loading condition. It is interesting to contrast this behavior with the response of the cylinder near the personnel locks, which was similar to the response near a rigid inclusion.

ANALYSIS OF A CONSTRAINED PIPE PENETRATION

The cylindrical containment wall is intersected by a thru-pipe at two diametrically opposed points just below midheight of the cylinder, as shown in Fig. 12. This pipe constrains the radial displacement of the wall at its intersection with the pipe to essentially zero. Because of the geometric symmetry, the behavior can be predicted with a model representing a ninety

couple the structural response of the sleeve and cover. It is difficult, if not impossible, to design the cover assembly to match the sleeve deformations without structural coupling because the sleeve does not deform axisymmetrically. Some seal designs do provide some structural coupling, for instance, a tongue and groove seal design. Although no formal method of correlating deformations to leakage rates is presently available, excessive leakage is expected to occur at around 185 psig (1275 kPa) in the 1:8 scale model because the deformations were so large near the 'O' ring sealing surface.

NOTE: An error was found in the analyses of the equipment hatch shortly after the paper was submitted. Corrected analyses indicate qualitatively similar distortions of the sleeve but at pressures approximately 20 psig higher. Complete update results will be published at a later date.

References:

[1] Blejwas,T. E.,"Testing and Analysis of Containment Models", to be presented at the International Meeting on Thermal Nuclear Reactor Safety, Karlsruhe, FRG, September 10-13, 1984.

[2] Blejwas,T. E. and Horschel,D. S., "Analysis of Steel Containment Models", Proceedings of the Workshop on Containment Integrity, NUREG/CP-0033, SAND82-1659 edited by W. Sebrell, October 1982.

[3] Horschel,D. S. and Blejwas, T. E.,"An Analytical Investigation of the Response of Steel Containment Models to Internal Pressurization", Transactions of the 7th International Conference on Structural Mechanics in Reactor Technology, Vol. J6/4, August 1983.

[4] MARC General Purpose Finite Element Program, Revision J.2, MARC Analysis Research Corporation, Palo Alto, CA, 1981.

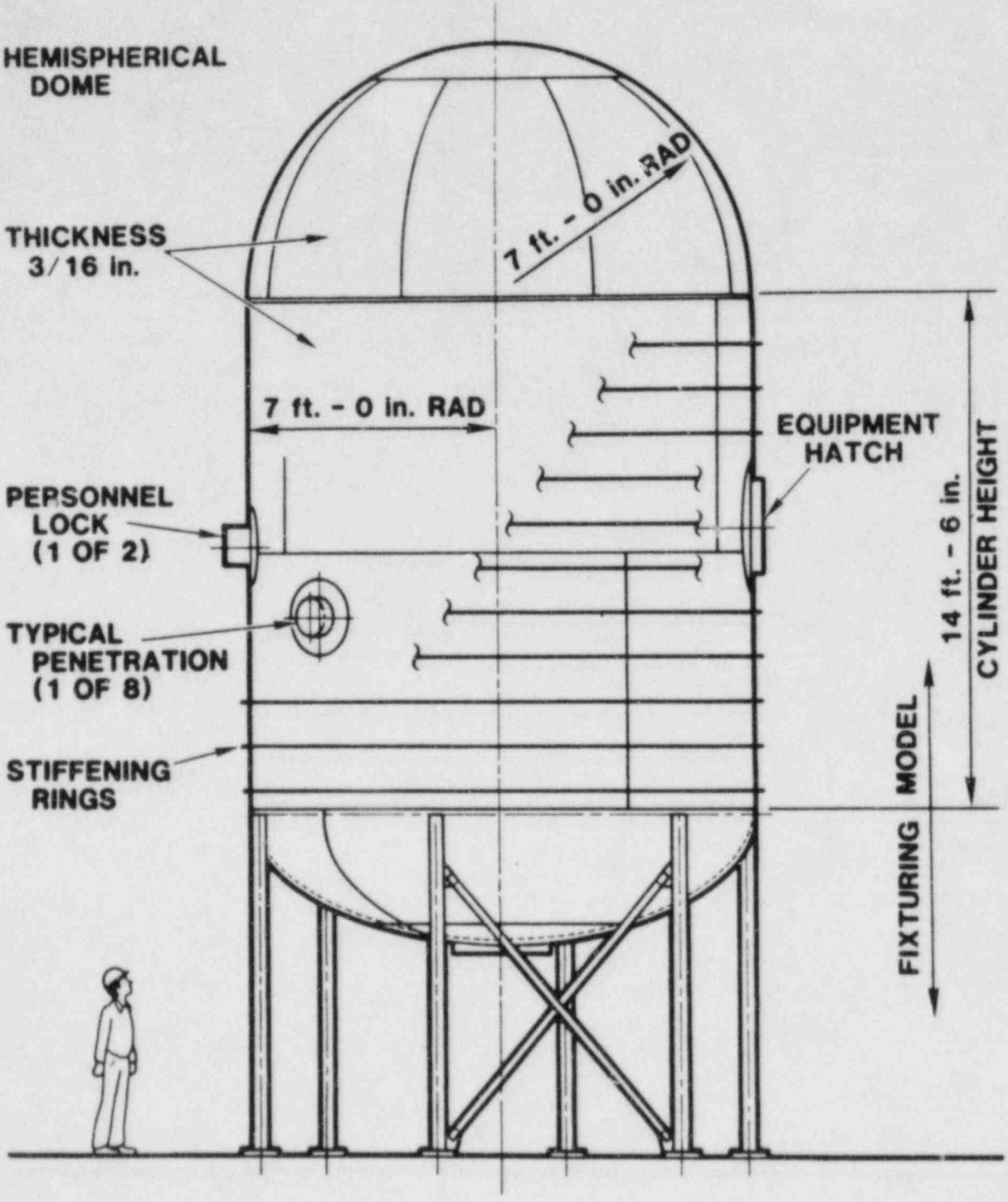

Figure 1. 1:8 Scale Steel Containment Model

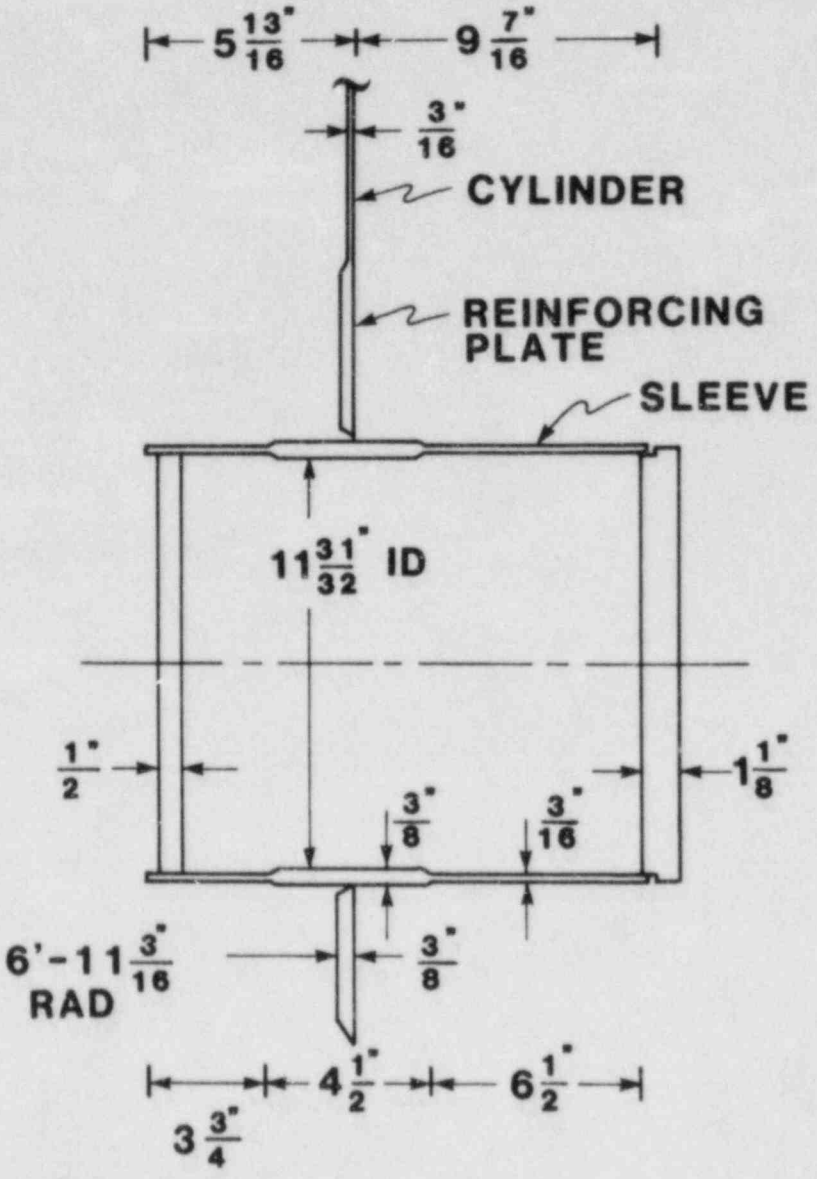

Figure 2. Schematic of a Personnel Lock Representation in the 1:8 Scale Containment Model

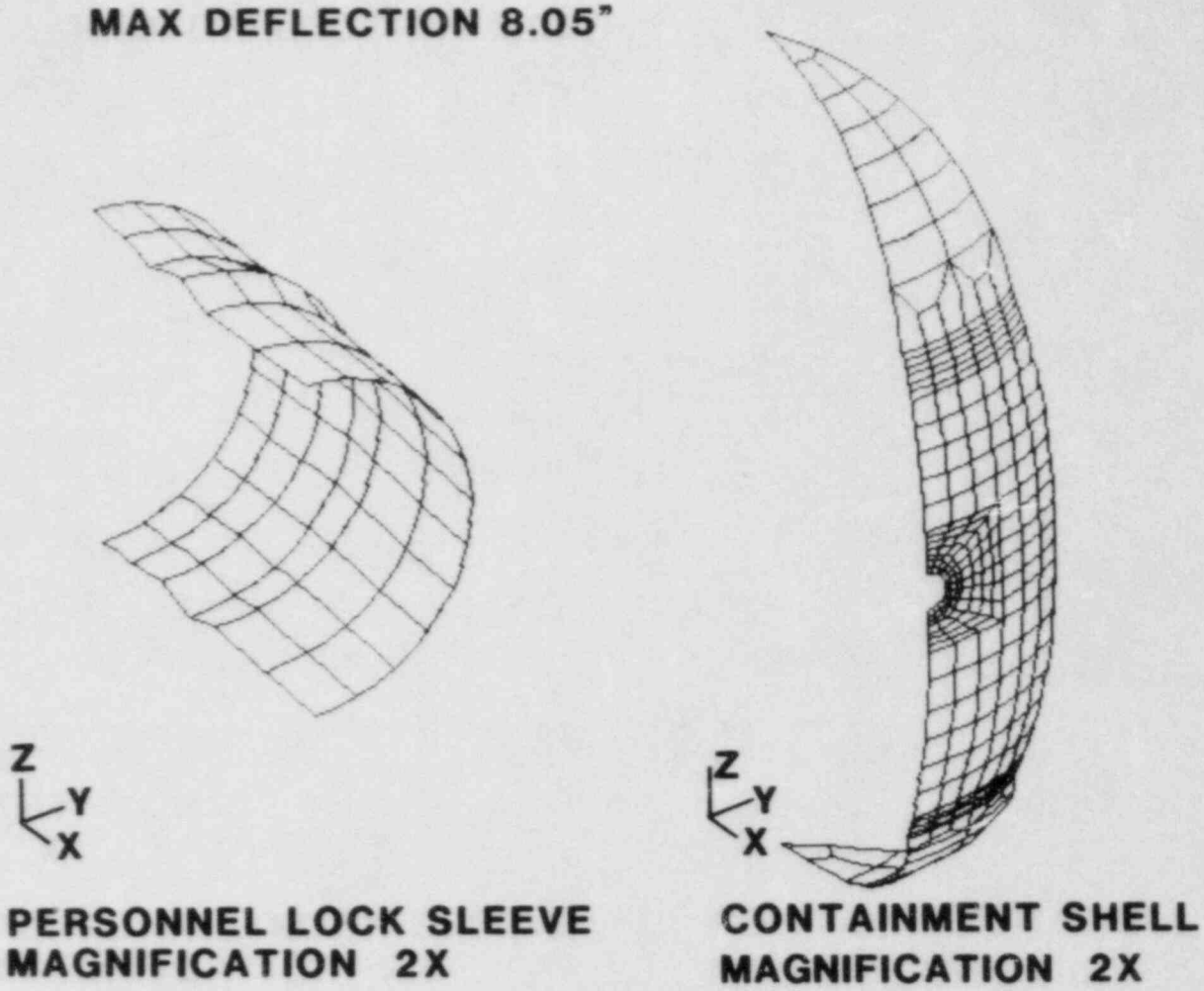

Figure 3. Deformed Shape of the Containment with a Personnel Lock Representation at 230 psig

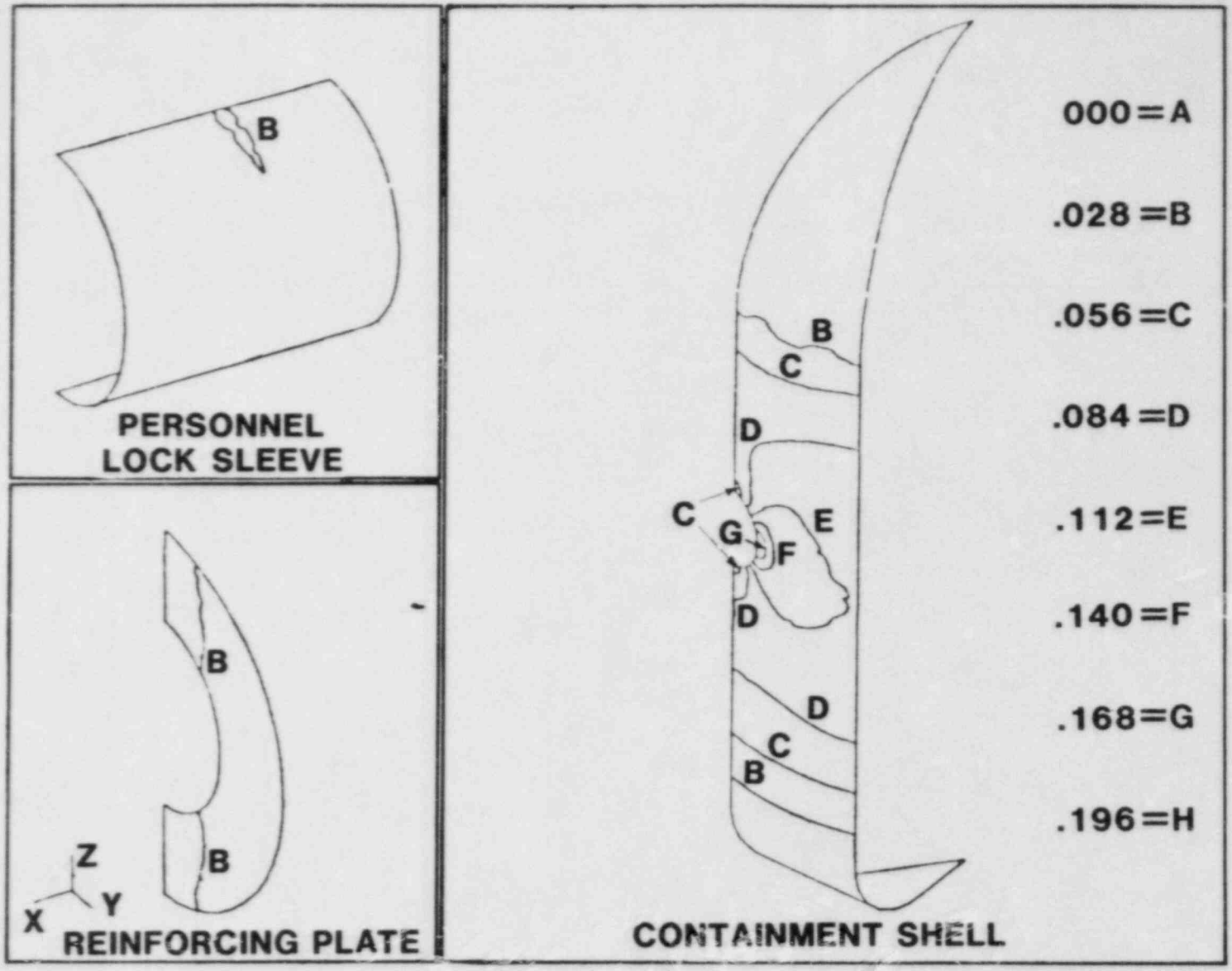

Figure 4. Midsurface Effective Plastic Strain Contours for the Containment with a Personnel Lock Representation at 230 psig

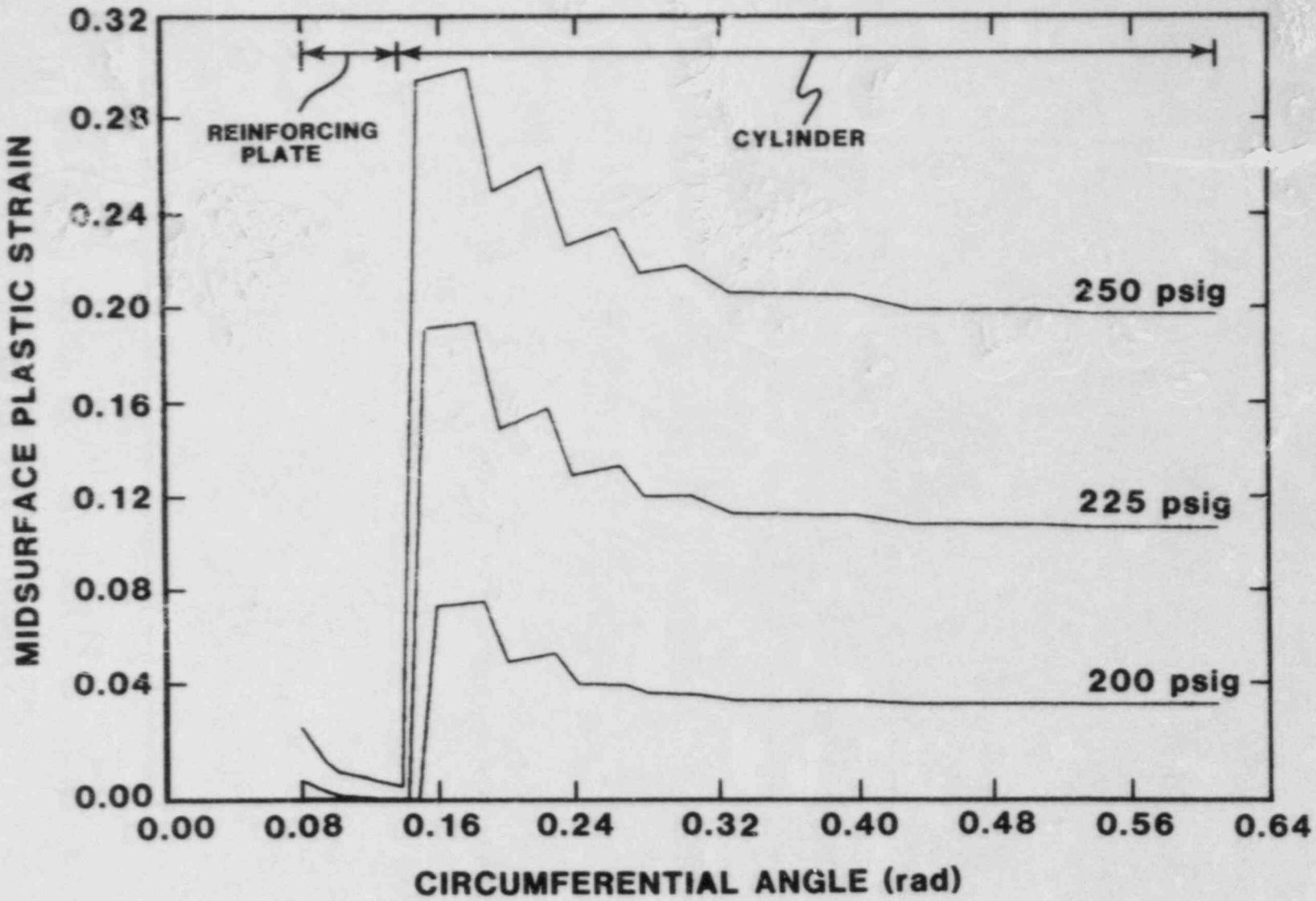

Figure 5. Midsurface Effective Plastic Strain vs. Circumferential Angle at the Elevation of the Personnel Lock Sleeve Axis at 200, 225, and 250 psig

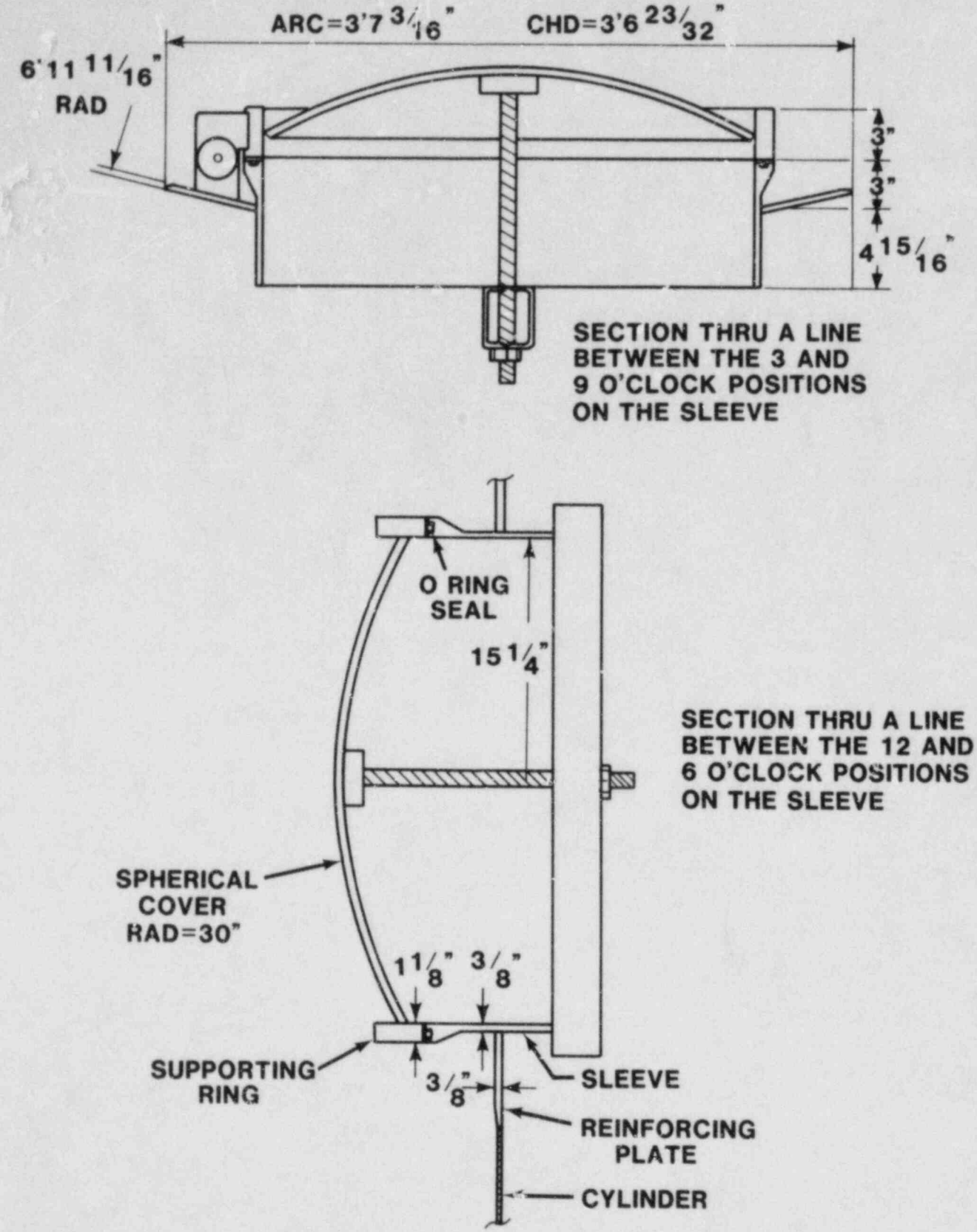

Figure 6. Schematic of an Equipment Hatch in the 1:8 Scale Containment Model

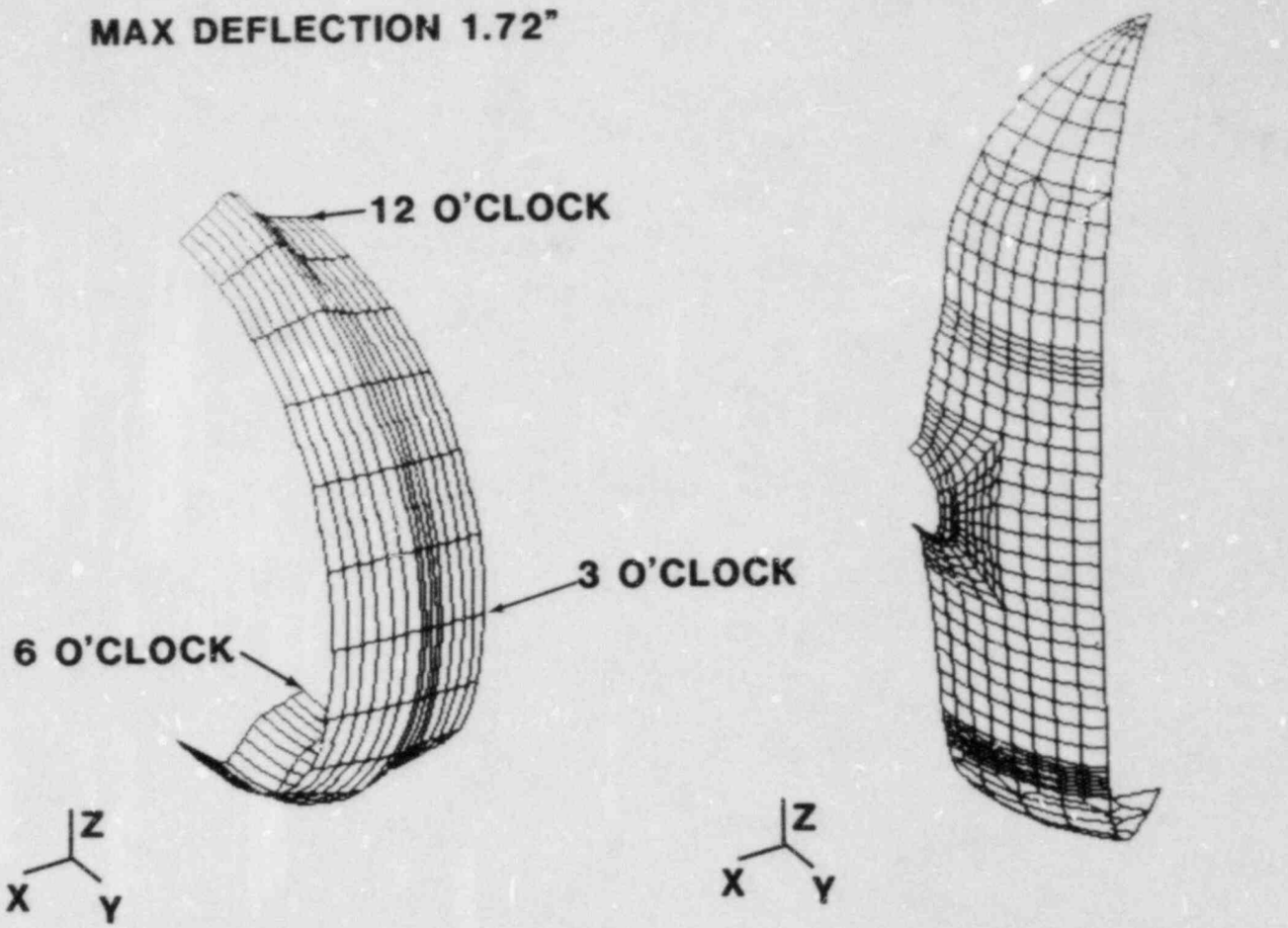

Figure 7. Deformed Shape of the Containment with an Equipment Hatch at 185 psig

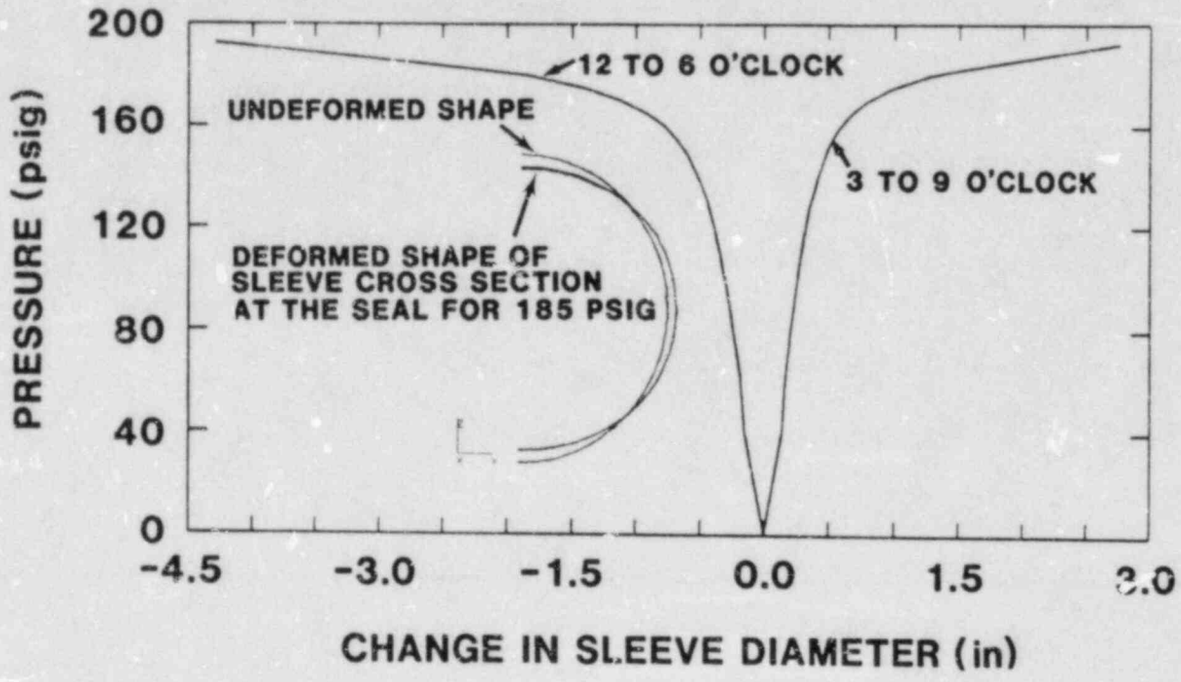

Figure 8. Deformation of the Cross Section of the Equipment Hatch Sleeve Coinciding with the O-Ring Seal

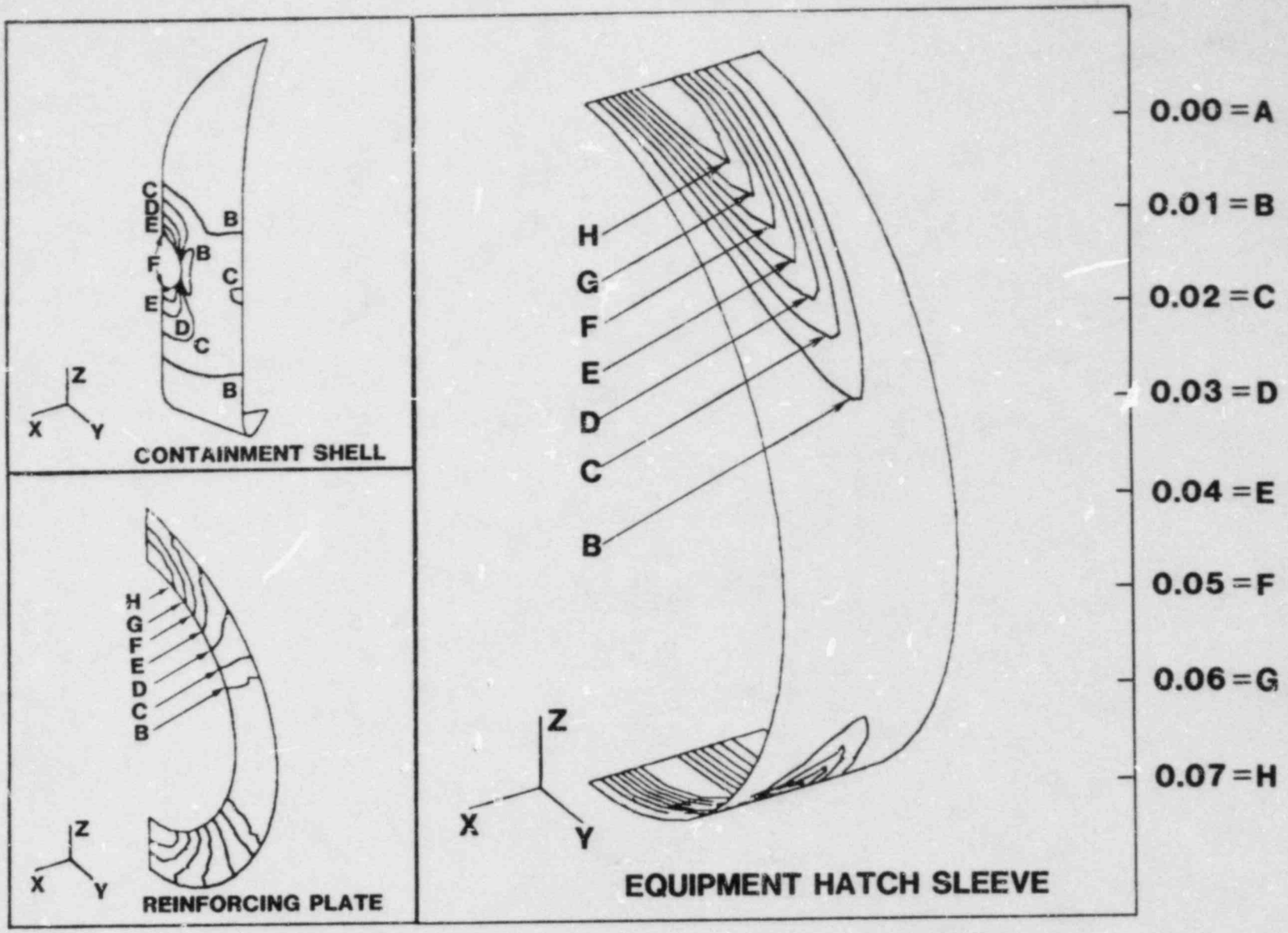

Figure 9. Midsurface Effective Plastic Strain Contours for the Containment with an Equipment Hatch at 192.5 psig

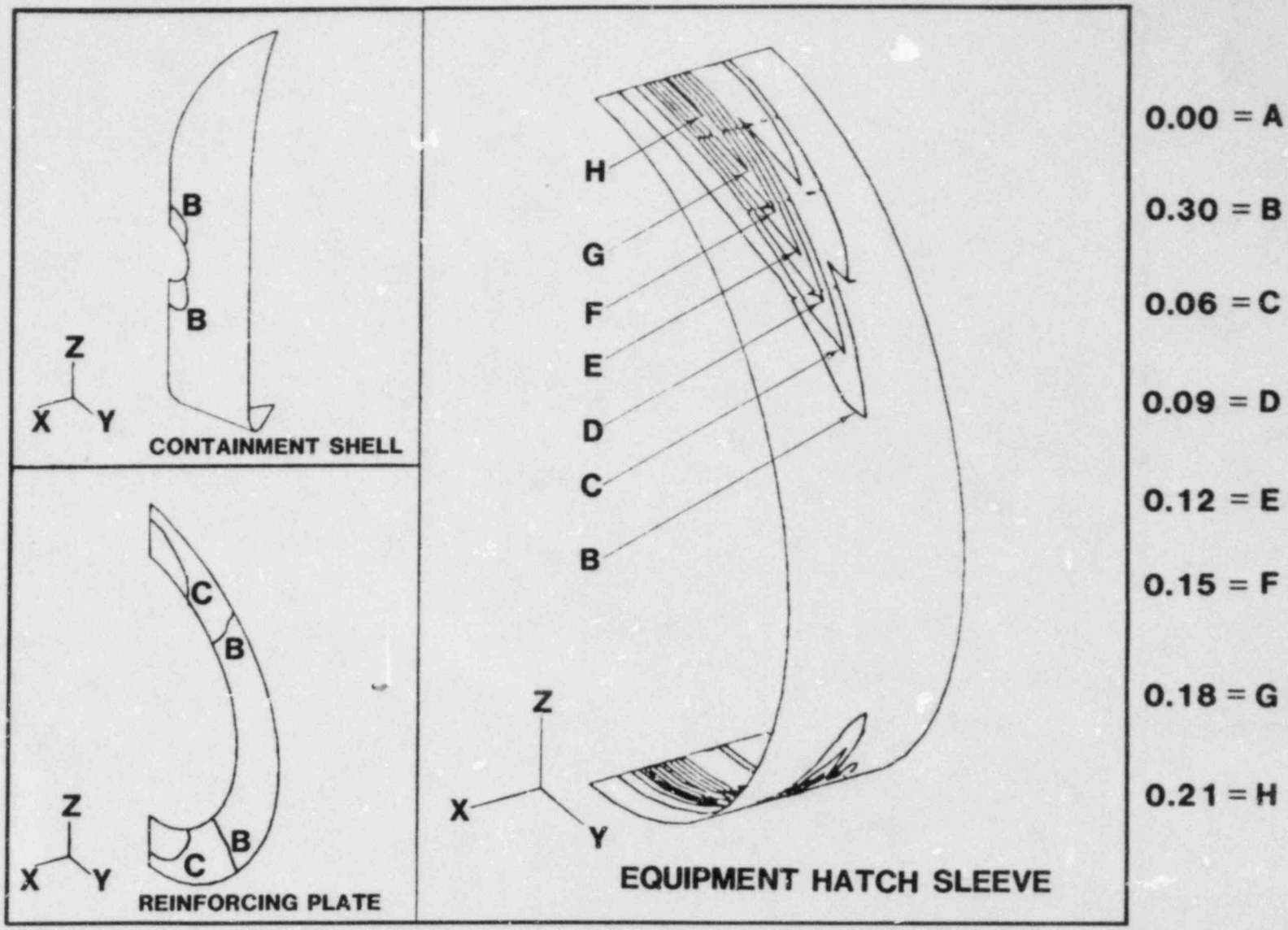

Figure 10. Effective Plastic Strain Contours on an Outer Fiber for the Containment with an Equipment Hatch at 192.5 psig

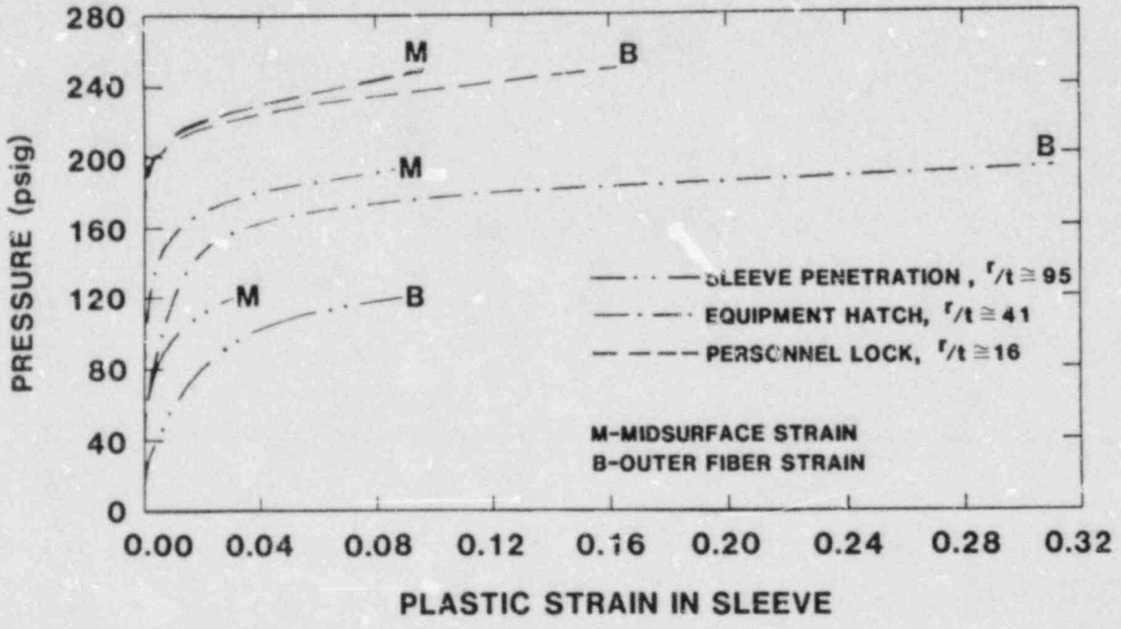

Figure 11. Effective Plastic Strain vs. Pressure for Three Penetration Sleeves at 12 o'clock Near Their Intersections with the Containment Wall

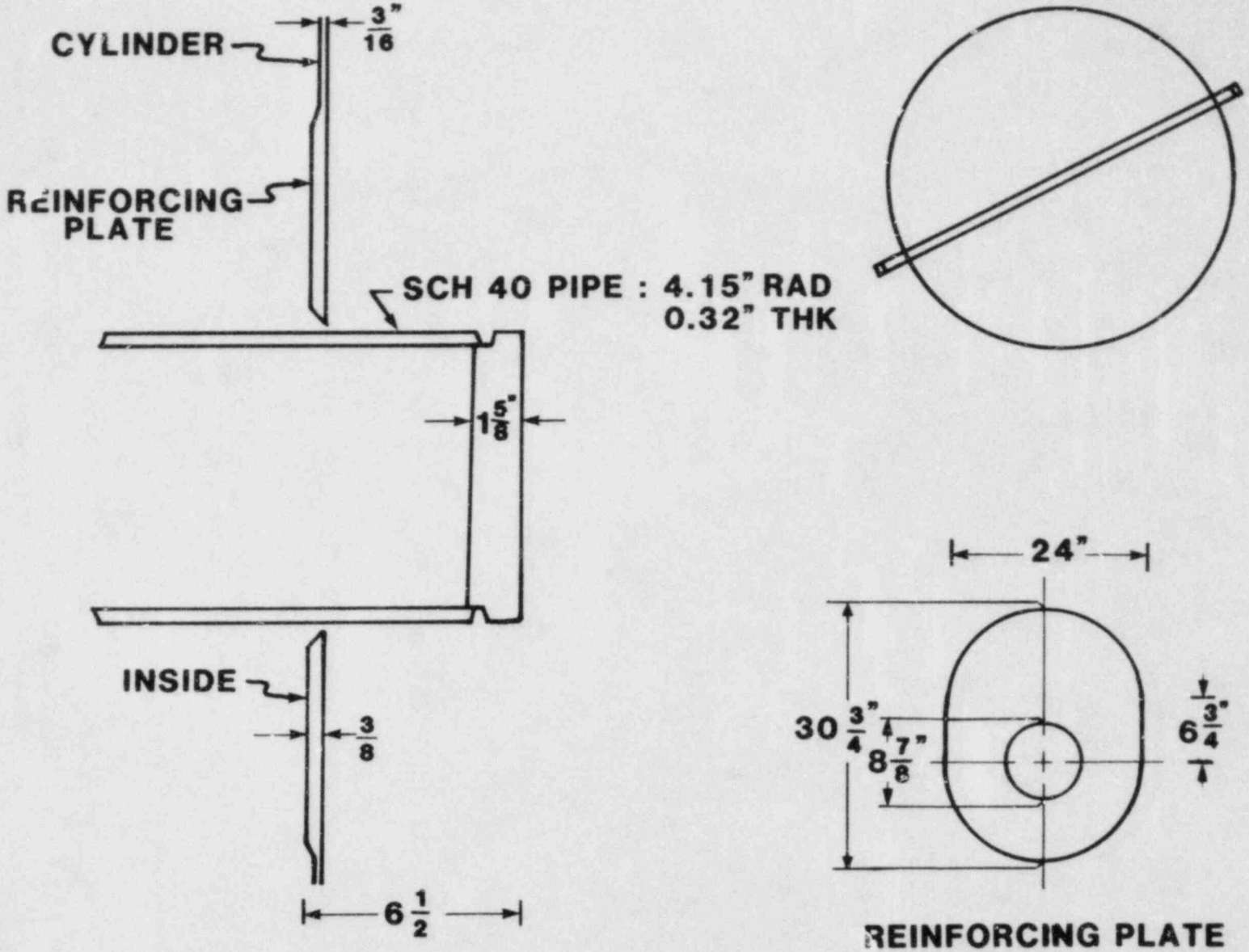

Figure 12. Schematic of the Constrained Pipe Penetrations in the 1:8 Scale Containment Model

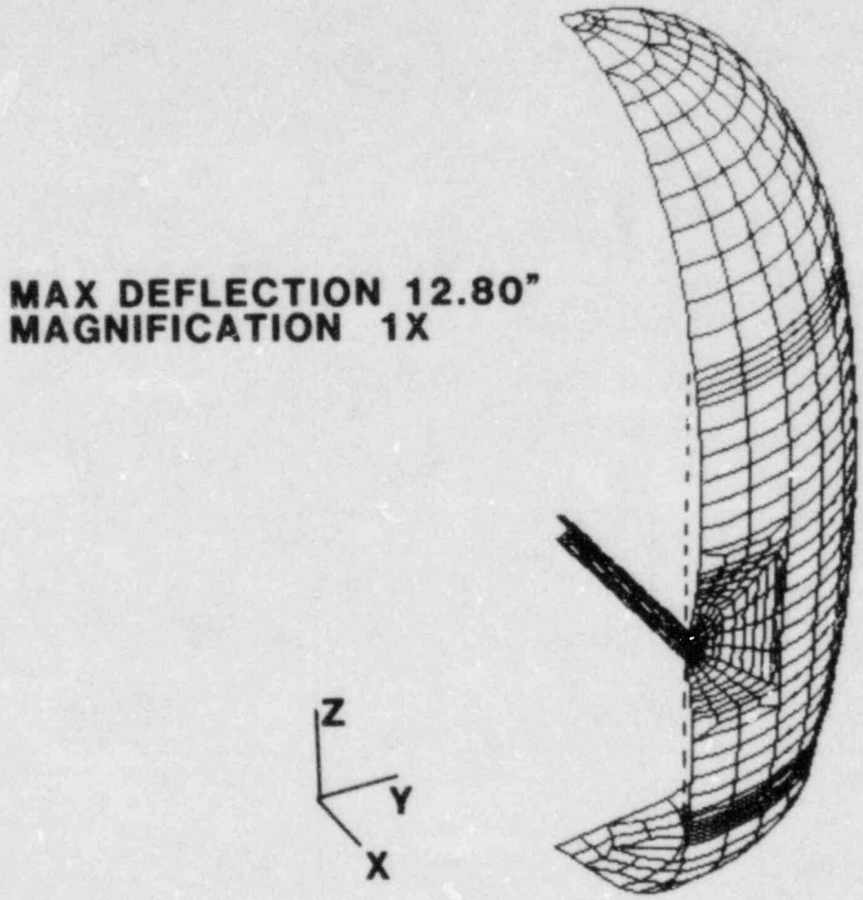

Figure 13. Deformed Shape of the Containment with a Constrained Pipe Penetration at 250 psig

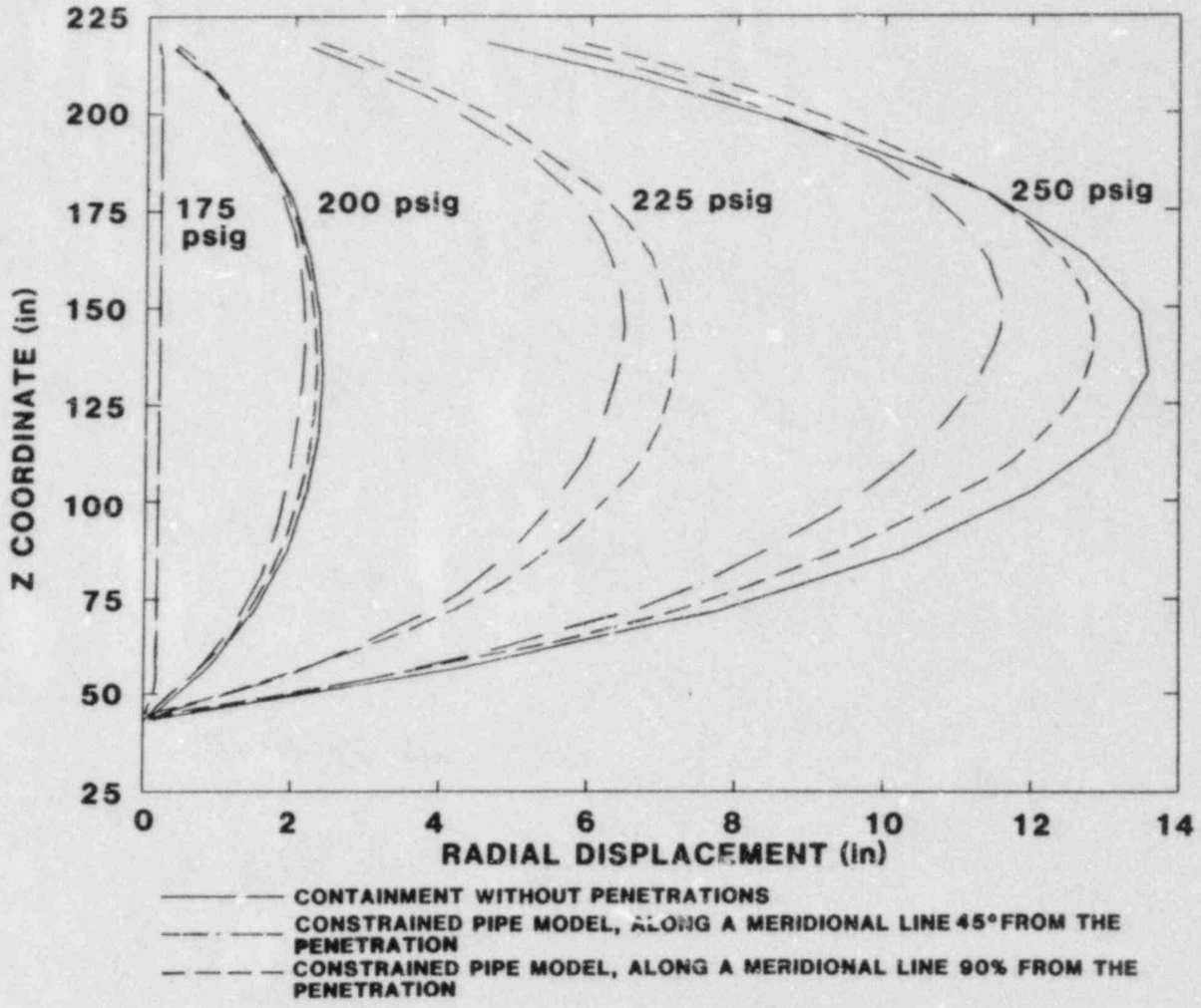

Figure 14. Comparison of Radial Displacement vs. Elevation Along Several Meridional Lines of the Constrained Pipe Penetration Model to That for the Containment Model Without Penetrations

FRAGILITY CURVES FOR STEEL CONTAINMENTS WITH INTERNAL PRESSURE

Fouad Fanous and Lowell Greimann
Ames Laboratory, Iowa State University
Ames, IA

ABSTRACT

Containment structures for nuclear power plants have long been designed for static internal pressure. However, since the Three Mile Island accident there has been heightened interest in the behavior of containments under conditions beyond design, particularly the actual, in-place resistance of containments to static internal pressure. Probabilistic methods are being applied to both the loading and resistance quantities so public risk can be accurately assessed. In this paper, a reliability assessment of a steel containment strength under uniform internal pressure is summarized.

Typically the containment vessel is a stiffened shell structure. Failure modes for this type of structure are identified as general, inter-ring and panel failure. Simplified methods to predict the resistance of the vessel under internal pressure are presented.

The Advanced First Order Second Moment technique is used in conjunction with the simplified methods to construct the cumulative distribution of the containment resistance as a function of pressure. Uncertainty of the basic variables which affects the containment resistance are propagated through the analysis to evaluate the total uncertainty of the system. The resulting distribution considering all possible failure modes is given for a typical Mark III steel containment. Fragility curves for the containment at 95% and 5% certainty are also given.

INTRODUCTION

The function of the containment structure is to prevent the escape to the atmosphere of any radioactivity which may be released within the vessel. In spite of the design procedures to ensure safe operation for accident loadings, leakage of radioactivity still does have a small non-zero probability of occurrence. This has motivated efforts to study the behavior of the containment under different loading conditions. The objective of this paper is to obtain a statistical description of the containment strength due to static internal pressure.

Failure is defined to occur when maximum strains exceed twice the yield strain. (This definition is certainly debatable but that is beyond the scope of this paper. It is sufficient to recognize that the failure criteria does represent a departure beyond "usual" design consideration, i.e., significant inelastic behavior.)

Simplified equations for the static pressure resistance of stiffened shells are formulated. These methods provide the limit pressure, p_o, of stiffened cylindrical shells. This pressure is

considered as a good approximation to the vessel resistance [1,2]. Finite element analyses were used to calibrate these methods.

The resulting reliability problem is analyzed by the Advanced First Order Second Moment method. Uncertainty limits are established.

ANALYSIS OF STIFFENED CYLINDRICAL SHELLS

A stiffened cylindrical shell can be considered as a number of rectangular curved panels framed by a ring sector and a stringer section (see Fig. 1). Failure modes for this type of structure can be identified as: (1) General Failure; (2) Inter-ring Failure; and (3) Panel Failure. The first mode is considered to occur when the entire panel expands in the radial direction uniformly as shown in Fig. 2.a. The inter-ring failure mode occurs when the radial deformation of the vertical stiffeners and the shell skin increase, while the ring stiffener deformation remains small, i.e., within the elastic range (see Fig. 2.b). The third failure type occurs when the shell skin bulges outward while the ring and stringer reinforcement remain in the elastic range.

Basic Equations

For an axisymmetrically loaded cylindrical shell with large deformation, the membrane strain-displacement relationships are [3]

$$\varepsilon_\phi = \frac{du}{dx} + \frac{1}{2}\left(\frac{dw}{dx}\right)^2 ; \qquad \varepsilon_\theta = \frac{w}{r} \tag{1}$$

in which ε_ϕ and ε_θ are the meridional and circumferential membrane strain, respectively, w is the displacement perpendicular to the shell surface; u represents the meridional displacement; r is the shell midsurface radius; and x is the cylinder meridional coordinate. The internal energy, U, dissipated per each panel is written as

$$U = \int_V (f_\phi \varepsilon_\phi + f_\theta \varepsilon_\theta)\, dV + \int_{V_r} f_r\, \varepsilon_\theta\, dV + \int_{V_s} f_s\, \varepsilon_\phi\, dV \tag{2}$$

where f_ϕ and f_θ are the shell meridional and circumferential membrane stresses, while V represents the material volume. The stresses f_r and f_s, respectively, are the ring and longitudinal stiffener stresses, while V_r and V_s are the ring and longitudinal stiffener volumes, respectively. The external work for a uniform internal pressure loading, p, can be expressed as

$$W = \int_A p\, w\, dA \pm 2\pi r\, (N_\phi\, \bar{u} + M_\phi\, \bar{\theta})\Big|_{\text{boundary}} \tag{3}$$

where A is the surface over which the load is applied. The second term indicates the work of the meridional membrane force N_ϕ and the moment M_ϕ at the plastic hinges at the panel boundaries (N_ϕ and M_ϕ are forces per unit length). The quantity $\bar{u}$ denotes

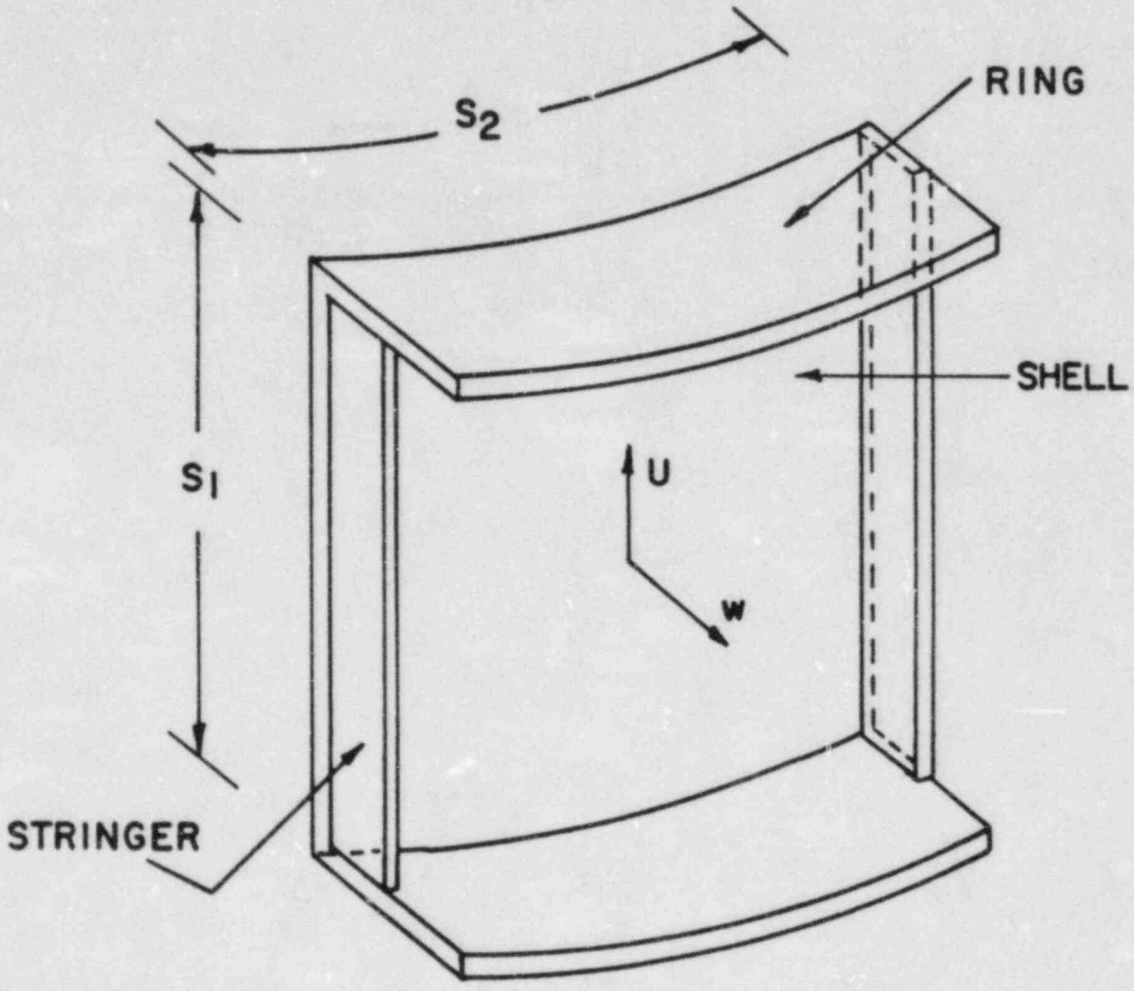

Figure 1 Typical Stiffened Shell Panel

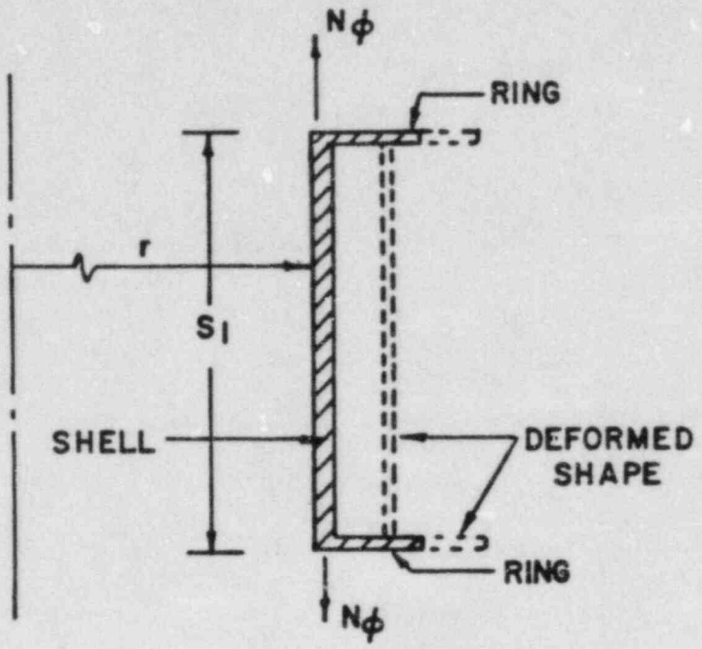

(a) General Failure Mode

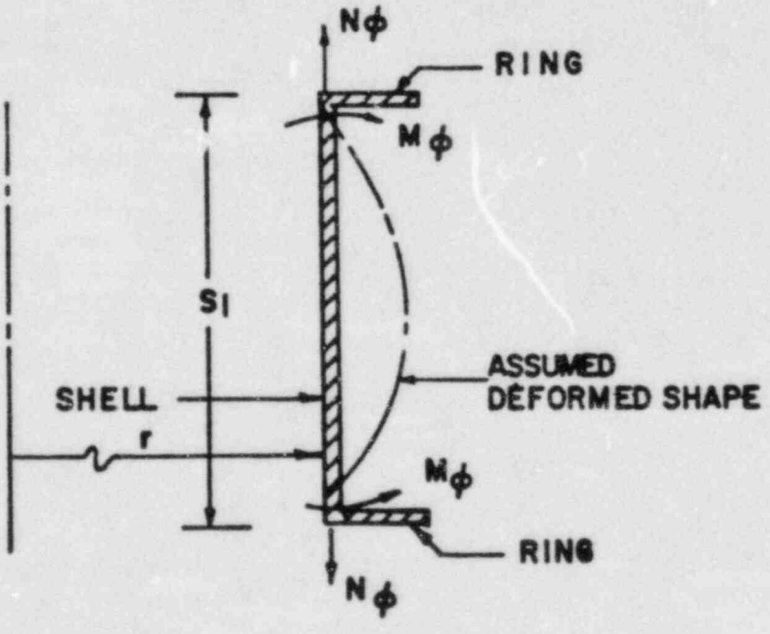

(b) Inter-Ring Failure Mode

Figure 2 Assumed Deformed Shape
(stringer not shown)

the change in the length of the panel and $\bar{\theta}$ is the slope of the deformed shape at the plastic hinges.

The membrane strains are written, according to the deformation strain theory of plasticity [4], as follows

$$\varepsilon_\phi = C(f_\phi - f_\theta/2) \; ; \qquad \varepsilon_\theta = C\,(f_\theta - f_\phi/2) \tag{4}$$

in which C denotes a proportionality constant. The von Mises yield criteria [4] is employed in this work to relate the membrane stresses to the material yield strength, F_y, as

$$f_\theta^2 + f_\phi^2 - f_\theta f_\phi = F_y^2 \tag{5}$$

Analysis of the General Failure Mode

For this case, the circumferential strain is assumed to be constant, while the meridional strain is neglected, or

$$\varepsilon_\theta = e \quad ; \qquad \varepsilon_\phi = 0 \tag{6}$$

where e is the maximum allowable strain. The plasticity conditions of Eqs. (4) and (5) in conjunction with the assumption in Eq. (6) yield the following membrane stresses:

$$f_\phi = \frac{1}{\sqrt{3}} F_y \; ; \qquad f_\theta = \frac{2}{\sqrt{3}} F_y ; \qquad f_r = F_y \tag{7}$$

When the above relationships are substituted into the following minimization principle

$$\frac{\partial U}{\partial e} - \frac{\partial W}{\partial e} = 0 \tag{8}$$

An expression of the limit pressure, p_o, for the general failure mode is found as:

$$p_o = \frac{t\,F_y}{r}\left(\frac{2}{\sqrt{3}} + \frac{A_1}{s_1\,t}\right) \tag{9}$$

in which t represents the containment wall thickness, s_1 and A_1 are the ring stiffener spacing and cross-sectional area, respectively.

Analysis of the Inter-ring Failure Mode

In this case the circumferential strains are assumed to vary parabolically, while the longitudinal strain is assumed negligible, or

$$\varepsilon_\theta = e\left[1 - \left(\frac{2x}{s_1}\right)^2\right] \quad ; \qquad \varepsilon_\phi = 0 \tag{10}$$

where e represents the circumferential strain midway between the rings. Substitution of Eq. (10) into Eq. (1), yields the following radial and meridional displacements:

$$w = er\left[1 - \left(\frac{2x}{s_1}\right)^2\right] \quad ; \quad u = -\frac{32\, e^2 r^2\, x^3}{s_1^4} \tag{11}$$

The rotation, $\bar{\theta}$, at the upper and lower boundaries of the panel, and the change in the panel length, $\bar{u}$ are found as

$$\bar{\theta} = \left.\frac{dw}{dx}\right|_{x = \pm \frac{s_1}{2}} = \pm \frac{4\, er}{s_1} \quad ; \quad \bar{u} = \frac{4e^2 r^2}{3\, s_1} \tag{12}$$

For an elastic-perfectly plastic material, the strain energy, U_e, which is accumulated up to yield strain, ε_y, can be approximated as:

$$U_e \simeq \frac{1}{2}\, U\Big|_{e = \varepsilon_y} \tag{13}$$

Substitution of the above relationships into Eq. (2) and (3) and using a strain ductility limit of two gives a limit pressure for the inter-ring failure modes as

$$p_o = \frac{F_y\, t/r}{\left(1 - \frac{8\, \varepsilon_y r^2}{s_1^2}\right)} \left(\frac{2}{3} + \frac{12\, Zr}{s_1^2\, t}\right) \quad ; \quad Z = \frac{t^2}{4} + \frac{A_2\, c}{s_2} \tag{14}$$

where Z is the plastic section modulus of the shell and stringer per unit circumference, A_2 and s_2 are the stringer cross-sectional area and spacing, and c is the eccentricity and c is the stringer centroid measured from the shell middle surface.

The foregoing equations were verified by comparing the results to finite element analyses accomplished using the ANSYS [5] program. Reference [6] gives a summary for this comparison. The results were found to be sufficiently accurate to define the resistance of a stiffened cylindrical shell structure.

RELIABILITY ASSESSMENT

The purpose of a reliability analysis is to use statistical descriptions of all the basic parameters of a structural system to determine the statistical properties of the structural behavior. In the case of a vessel under internal pressure problem, the containment is described by rather arbitrarily selected basic parameters. Table 1 lists the random parameters used in this study. Sources of uncertainties associated with a containment analysis are explained in Ref. [7]. Lack of information, imperfect data sources and limited sample size are sources of uncertainty in each of these statistical descriptions. Other even more subjective sources, such as human error, data censoring,

extrapolation to future cases and experimental versus actual in-place values, introduce uncertainty.

Table 1 - Basic Parameters

Variable	Type	Standard Deviation	
		Randomness	Uncertainty
Analysis Error	Lognormal	0.12	0.08
F_y (ksi)	Lognormal	3.7	2.00
Radius (in.)	Normal	0.60	0.60
Area (in.^{2})	Normal	0.80	1.00
Thickness (in.)	Normal	0.02	0.04
Ring Spacing (in.)	Normal	0.08	0.08

Since most structural systems are too complex to test or model directly, one should propagate the uncertainty of the basic component variables through the reliability analysis to evaluate the total uncertainty of the system. Several approaches are available to quantify the uncertainty associated with the analysis [8]. One of these methods is to separate the total uncertainty on a variable X into randomness and subjective uncertainty [9], i.e,

$$X = X_R + X_U \tag{15}$$

in which X_R and X_U represent the objective and subjective uncertainty in the variable X, respectively. If perfect knowledge of the randomness of X existed, then X_U would be zero. The distribution of X_R has no uncertainty and is determined by the available data. Table 1 lists the statistical properties which describe the randomness of each parameter. The sources of these properties are presented in [2].

On the other hand, X_U is completely subjective and its variance can be selected with professional judgment. One approach to such a judgment is to take a subjective uncertainty statement such as, "I am ω certain that the true mean of X is greater than a specified value. The distribution of X_U will be taken as normally distributed (a subjective statement). One can use this subjective statement to calculate the standard deviation of X_U as

$$\sigma_{X_U} = \frac{m_X^{\omega} - m_X}{\Phi^{-1}(1 - \omega)} \tag{16}$$

where $\Phi^{-1}(.)$ is the inverse of the standard normal cumulative distribution. The mean of the available data X_R is m_x. For example, if the sample mean of yield srength, m_x, is 51.1 ksi, one could subjectively say, "I am 95% certain that the true mean of the yield strength, (m_x^{ω}), is greater than 45 ksi". Using this subjective statement, the standard deviation of X_U is calculated as:

$$\sigma_{X_U} = \frac{45 - 51.1}{\Phi^{-1}(0.05)} = 3.7 \text{ ksi} \tag{17}$$

The standard deviation of the uncertainty variables for each of the random parameters are similarly determined and listed in Table 1.

RESISTANCE FUNCTION

The structural resistance is defined as the point at which the structural response reaches failure. The reliability assessment of a containment involves the evaluation of structural resistance for many different sets of the structural parameters, X_i. The resistance of each of the 16 failure modes for the containment shown in Fig. 3 are calculated using the simplified methods. Eqs. (9) and (14) are used to analyze the cylindrical portion. The resistance of the containment head is calculated using the following equations [2].

$$\text{Yielding:} \quad p_o = \frac{F_y t}{r}\left(1 + \frac{50\ F_y}{E}\right) \tag{18}$$

$$\text{Buckling:} \quad p_o = 10.4\ F_y \left(\frac{t}{2r}\right)^{1.25} \tag{19}$$

where E is the material Young's modulus. The structure resistance evaluated at the mean value of the basis parameters is

$$m_p = \text{Minimum}\ \{p_{o_j}\ (m_{x_i})\} \tag{20}$$

where j is the number of the failure modes. This was obtained as 99 psi and is controlled by buckling of the ellipsoidal head (caused by circumferential compression introduced in the head by the head/cylinder membrane discontinuity).

Simplified equations are useful for reliability assessments but have several practical limits - principally lack of generality. The mean value analysis (resistance at the mean) can also be performed by general finite element/finite difference techniques, such as , in this case, BOSOR5 [10]. The numerical solution was obtained by increasing the load, tracking the displacement and strain behavior, and checking for bifurcation at each load point. A bifurcation point (inelastic buckling load) occurred at a pressure of 101 psi (see Fig. 4), which compares favorably with the simplified method result. (Buckled shape in Fig. 3.)

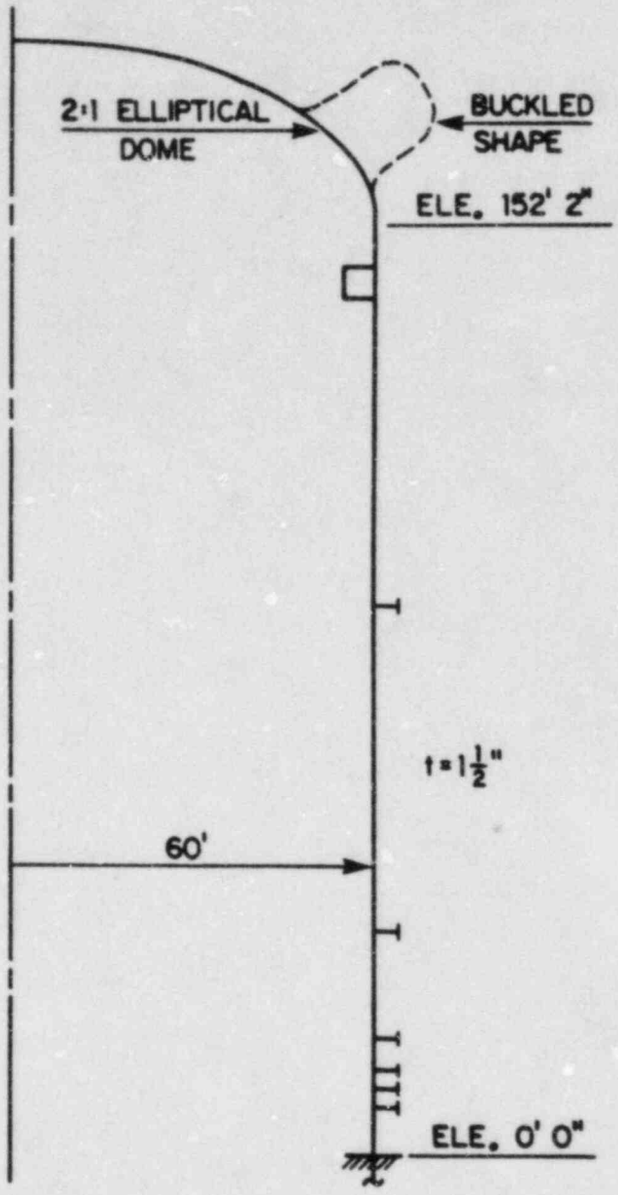

Figure 3 Containment Geometry

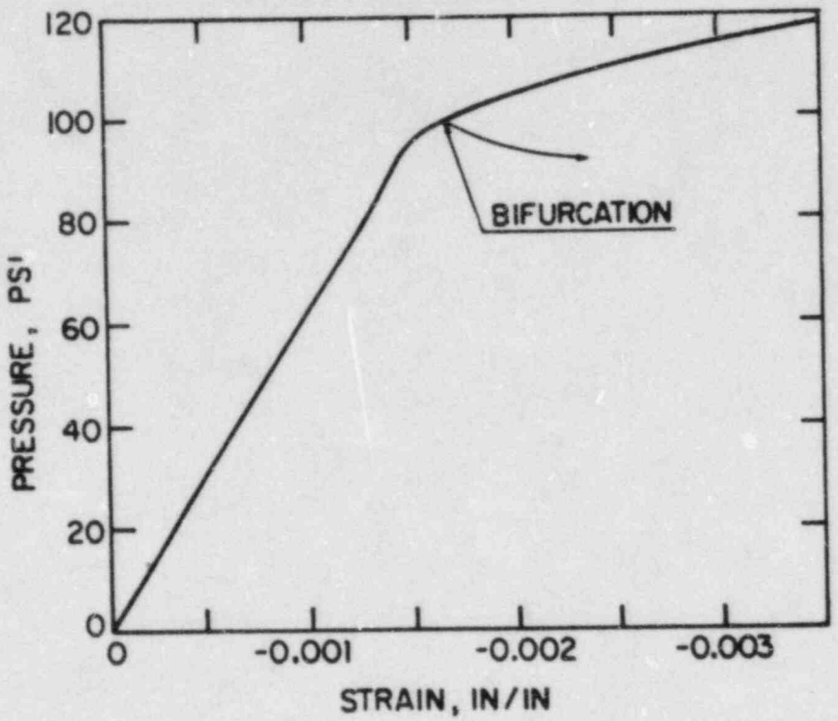

Figure 4 Maximum Circumferential Strain Versus Pressure for the Containment in Fig. 3

RELIABILITY METHOD APPLICATION

The Advanced First Order Second Moment Method (AFSOM) is used as a reliability assessment technique, in conjunction with the simplified equations. Table 1 shows the mean value of X_R as well as the standard deviation of the randomness and uncertainty. The uncertainty propagation requires two applications [8]:

- Randomness only - no uncertainty $\sigma_{X_U} = 0$. This step yields the cumulative distribution of $F_{P_R}(p)$ in Fig. 5.
- Uncertainty only - no randomness ($\sigma_{X_R} = 0$). This step gives the cumulative distribution $F_{P_U}(p - m_p)$ illustrated in Fig. 5.

As explained in [8], the 5% and 95% certainty levels on the containment strength, p , are constructured by:

$$F^{\omega}_{p}(p) = F_{P_R}\left(p - F^{-1}_{P_U}(1 - \omega)\right) \tag{21}$$

where ω is 0.05 and 0.95, respectively. The resulting fragility curves are shown in Fig. 5.

SUMMARY

Simplified approaches were developed for the analysis of stiffened axisymmetric shells under uniform static internal pressure. The methods are based on classical limit analysis theory and take into account the effects of large deformations. These approaches provide the limit pressure for each possible failure mode. For a static uniform internal pressure, the simplified methods give good results when applied to axisymmetric stiffened shells.

The cumulative distribution of the resistance is predicted using the Advanced First Order Second Moment method. The uncertainty is quantified by separating uncertainty into randomness and subjective uncertainty. Fragility curves at 95% and 5% certainty are constructed.

ACKNOWLEDGMENTS

This paper represents a portion of a more complete study conducted at Ames Laboratory, Iowa State University for the Nuclear Regulatory Commission.

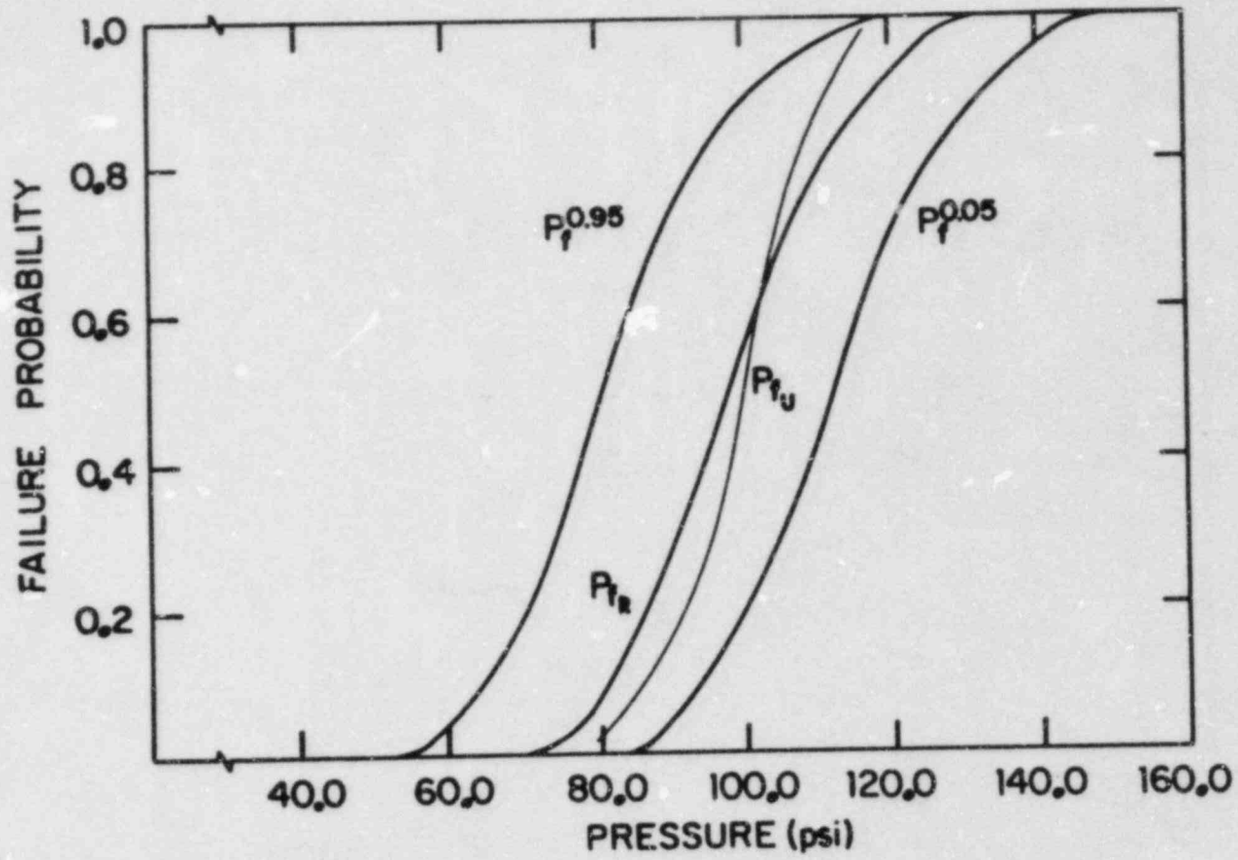

Figure 5 Fragility Curve for the Containment Resistance

REFERENCES

(1) Gerdeen, J.C., "A Critical Evaluation of Plastic Behavior Data and a Unified Definition of Plastic Loads for Pressure Components", Draft of Final Report submitted to Pressure Vessel and Research Committee, Welding Research Council (April 1979).

(2) Greimann, L.F., Fanous, F.S., Wolde-Tinsae, A., Ketelaar, D., Lin, T., Bluhm, D., "Reliability Analysis of Containment Strength", Report to U.S. NRC, NUREG/CR-2442, IS-4753 (Nov. 1981).

(3) Baker, E.H., Cappel, AP.O., Kovalevsky, L., Verehe, R.M., Shell Analysis Manual, Springfield, Virginia: NASA CR-912, Clearinghouse for Federal Scientific and Technical Information, N68-24802, (1968).

(4) Ford, H., Alexander, J.M., Advanced Mechanics of Materials, 2nd ed., New York: John Wiley and Sons, Inc., (1963).

(5) ANSYS, Engineering Analysis System. User's Manual, Houston, PA: Swanson Analysis System, Inc., (1983).

(6) Greimann, L.F., Fanous, F.S., "Simplified Methods for the Inelastic Analysis of Stiffened Shells," Transactions of the 7th International Conference on Structural Mechanics in Reactor Technology, Paper No. J3/2, Chicago, IL, pp. 121-128, August 1983.

(7) Greimann, L., Fanous, F., "On the Uncertainties Associated with Containment Analysis," Paper presented at the Second Workshop on Containment Integrity, Washington, D.C., June 1984.

(8) Greimann, L., Knapp, W., "Propagation of Uncertainty Levels," Paper accepted for publication in the ASCE Journal

(9) PRA Procedures Guide, Office of Nuclear Regulatory Commission, NUREG/CR-2300, Review Draft, September 28, 1981.

(10) Bushnell, D., "BOSOR5 Program for Buckling of Elastic-Plastic Complex Shells of Revoltion Including Large Deflection and Creep," Structural Mechanics Laboratory, Lockheed Missiles and Space, Co., Inc., Palo Alto, CA, 1974.

Distribution:
Division of Technical Information
and Document Control
NRC Distribution Contractor
U.S. Nuclear Regulatory Commission
15700 Crabbs Branch Way
Rockville, MD 20850
425 copies for R1, RD, RM

List of Attendees (130 copies)

Librarian
Earthquake Engineering Res. Ctr. Library
University of California/453 R.F.S.
1301 South 46th St.
Richmond, CA 94804

National Nuclear Corporation Limited
Cambridge Rd., Whetstone
Leicester LE8 3LH
England

Science & Engineering Associates
Suite 610
2500 Louisiana NE
Albuquerque, NM 87110
Attn: Dr. Willard Thomas

Mr. William C. Black
2650 Woodside Road
Bethlehem, PA 18017

Bechtel Power Corp.
777 East Eisenhower Pwy
Ann Arbor, MI 48101
Attn: T. E. Johnson

University of Illinois
Dept. of Civil Engineering
503 W. Michigan
Urbana, IL 61801
Attn: Prof. Mete A. Sozen

Stevenson and Associates
9217 Midwest Ave.
Cleveland, OH 44122
Attn: Dr. John D. Stevenson

Electrical Power Research Institute
3412 Hillview Avenue
P.O. Box 10412
Palo Alto, CA 94304
Attn: Dr. Ian Wall

Dr. Karl F. Kussmaul
Staatliche Materialpruefungsanstalt (MPA)
University of Stuttgart
Pfaffenwaldring 32
D-7000 Stuttgart 80 (Vaihingen)
Federal Republic of Germany

Dr. Ing Helmut Karwat
Technische Universitat Müchen
Forschungsgelände
8046 Garching
Federal Republic of Germany

Dr. R. J. Sutbbs
Health & Safety Exeuctive
Thames House North
Millbank
London SW1 4QJ
United Kingdom

Mr. T. Currie
Health & Safety Executive
Thames House North
Millbank
London SW1 4QJ
United Kingdom

Mr. Norbert J. Krutzik
Kraftwerk Union
Aktiengesellschaft
Berliner Strasse 295-299
Postfach 962
D-6050 Offenbach AM Main
Federal Republic of Germany

Mr. Aksel Anderson
Kraftwerk Union
Aktiengesellschaft
Berliner Strasse 295-299
Postfach 962
D-6050 Offenbach AM Main
Federal Republic of Germany

Mr. Helmut Schulz
Gesellschaft für Reaktorsicherheit (GRS) mbH
Schwertnergasse 1
5000 Köln 1
Federal Republic of Germany

Dr. Alfred Hoefler
Gesellschaft für Reaktorsicherheit (GRS) mbH
Schwertnergasse 1
5000 Köln 1
Federal Republic of Germany

Dr. Carl C. Fleischer
Taylor Woodrow Construction Limited
345 Ruislip Road
Southall, Middlesex UB1 2QX
United Kingdom

Mr. Peter Barr
Atomic Energy Establishment
Winfrith
Dorchester Dorset
DT2 8DH
United Kingdom

Mr. Michel Livolant
C.E.N. Saclay
DEDR/DEMT/DMTS
B.P. #2 91190-Gif-Sur-YVette
France

Dr. G. I. Schuëller
Universitat Innsbruck
Technikerstrabe 13
A-6020 Innsbruck
Austria

Mr. J. L. Jemielewski
Motor Columbus
CH-5401 Baden
Parkstrasse 27
Switzerland

Mr. O. Mercier
Motor Columbus
CH-5401 Baden
Parkstrasse 27
Switzerland

Mr. Kjell O. Johansson
Studsvik Energiteknik AB
S-611 82 Kyköping
Sweden

Dr. Hans-Jürgen Gehrhardt
Bundesministerium des Innern
Abtellung RS
Postfach 170290
5300 Bonn 1
Federal Republic of Germany

Dr. Ing Otto Schad
Kraftwerk Union
Aktiengesellschaft
Berliner Strasse 295-303
P.O. Box 962
D-6050 Offenbach AM Main
Federal Republic of Germany

Dr. Max Hintergräber
Kraftwerk Union
Aktiengesellschaft
Hammerbacherstrasse 12 + 14
D-8520 Erlanger
Federal Republic of Germany

Mr. W. J. Penn
Nuclear Studies and Safety Dept.
Ontario Hydro
700 University Ave.
Toronto, Ontario
M5G 1X6
Canada

National Nuclear Corp. Ltd.
Cambridge Research
Whetstone
Leicester LE8 3LH
United Kingdom
Attn: A. G. Chalmers
R. Crowder

Dr. Yoshio Ando
Dept. of Nuclear Engineering
University of Tokyp
7-3-1, Hongo, Bunkyo-Ku
Tokyo

Teiichi Yoshikawa
Mitsubishi Anmil Power Industries, Inc.
4-1 Shibakouen 2-Chome
Minato-Ku
Tokyo 105
Japan

Dr. Heki Shibata
University of Tokyo
Institute of Industrial Science
22-1, Roppongi 7
Minato-Ku
Tokyo
Japan

Harri Launonen
Institute for Radiation Protection
Kalevankatu 44A
Helsinki 18
Finland

Sandia Distribution:
1523 C. H. Conley
3141 C. M. Ostrander (5)
3151 W. L Garner
6400 A. W. Snyder
6410 J. W. Hickman
6415 J. L. Sprung
6420 J. V. Walker
6425 R. J. Lipinski
6425 W. Frid
6427 M. Berman
6442 T. Molina (35)
8024 M. A. Pound

NRC FORM 335 (2-84) NRCM 1102, 3201, 3202

U.S. NUCLEAR REGULATORY COMMISSION

BIBLIOGRAPHIC DATA SHEET

SEE INSTRUCTIONS ON THE REVERSE

1. REPORT NUMBER (Assigned by TIDC, add Vol. No., if any)
NUREG/CP-0056
SAND84-1514

2. TITLE AND SUBTITLE
PROCEEDINGS OF THE SECOND WORKSHOP ON CONTAINMENT INTEGRITY

3. LEAVE BLANK

4. DATE REPORT COMPLETED
MONTH: August
YEAR: 1984

5. AUTHOR(S)

6. DATE REPORT ISSUED
MONTH
YEAR

7. PERFORMING ORGANIZATION NAME AND MAILING ADDRESS (Include Zip Code)
Sandia National Laboratories
Albuquerque, NM 87185

8. PROJECT/TASK/WORK UNIT NUMBER

9. FIN OR GRANT NUMBER
A1249

10. SPONSORING ORGANIZATION NAME AND MAILING ADDRESS (Include Zip Code)
Division of Engineering Technology
Office of Nuclear Regulatory Research
U.S. Nuclear Regulatory Commission
Washington, DC 20555

11a. TYPE OF REPORT
Workshop Proceedings

b. PERIOD COVERED (Inclusive dates)

12. SUPPLEMENTARY NOTES

13. ABSTRACT (200 words or less)

The Second Workshop on Containment Integrity was held in Crystal City, Virginia, on June 13-15, 1984. The workshop provided a forum for exchanging information on the integrity of containments at nuclear power plants. The behavior of containments during severe accidents was of primary interest to the over 130 participants. Forty-three oral presentations were made at the workshop. Written contributions that correspond to each of the presentations make up the body of this report.

The workshop was hosted by Sandia National Laboratories under the sponsorship of the U.S. Nuclear Regulatory Commission. Principal organizers for the workshop were T. E. Blejwas and W. A. von Riesemann of Sandia, T. D. Molina of Technadyne, and J. F. Costello of the U. S. Nuclear Regulatory Commission.

14. DOCUMENT ANALYSIS - a. KEYWORDS/DESCRIPTORS

b. IDENTIFIERS/OPEN ENDED TERMS

15. AVAILABILITY STATEMENT
NTIS

16. SECURITY CLASSIFICATION
(This page)
Unclassified
(This report)
Unclassified

17. NUMBER OF PAGES
675

18. PRICE

*U.S. GOVERNMENT PRINTING OFFICE: 1984-0-776-027/4368